

Demystifying the Paradox of Biomineralization:  
Mechanisms Regulating Simultaneous Physiologic  
and Pathologic Bone Formation

By

Stephanie Nicole Moore-Lotridge

Dissertation

Submitted to the Faculty of the  
Graduate School of Vanderbilt University  
in partial fulfillment of the requirements

for the degree of

DOCTOR OF PHILOSOPHY

in

Pharmacology

December 15, 2018

Nashville, Tennessee

Approved:

Joey Barnett, Ph.D.

Justin M.M. Cates, M.D. Ph.D

Christine Konradi, Ph.D.

Brain Wadzinski, Ph.D

Jonathan G Schoenecker, M.D. Ph.D

## ACKNOWLEDGEMENTS

---



Hello- My name is Stephanie and you just opened my thesis Dissertation! While my name may be on the cover, this work would not have been possible without the love, support, and assistance of the individuals highlighted below. I am eternally grateful to each and every one of these individuals. Whether it was through scientific support, friendship, mentoring, or a combination of these events, you all are the reason this work was possible. Thank you for picking me up on the hard days, constantly motivating me to be the best version of myself, and helping me to celebrate the little victories. I look at my graduate school years as some of the best of my life, and it is because of you that this was possible. This giant block of written science is for you.

-Love Steph

---



To my amazing husband Corey-

You have been my rock through essentially my entire scientific career. You have been there since the beginning, constantly motivating me to be the best I can be. Your support has meant the world to me and I cannot imagine taking on this journey without you. Thank you for always being patient with me. I know during grant season I can be hectic, but you always find a way to help me relax and laugh. Thank you for reminding me to not take myself so seriously. Coming home to you after a long day makes all my stress disappear and I cannot thank you enough for that.

---

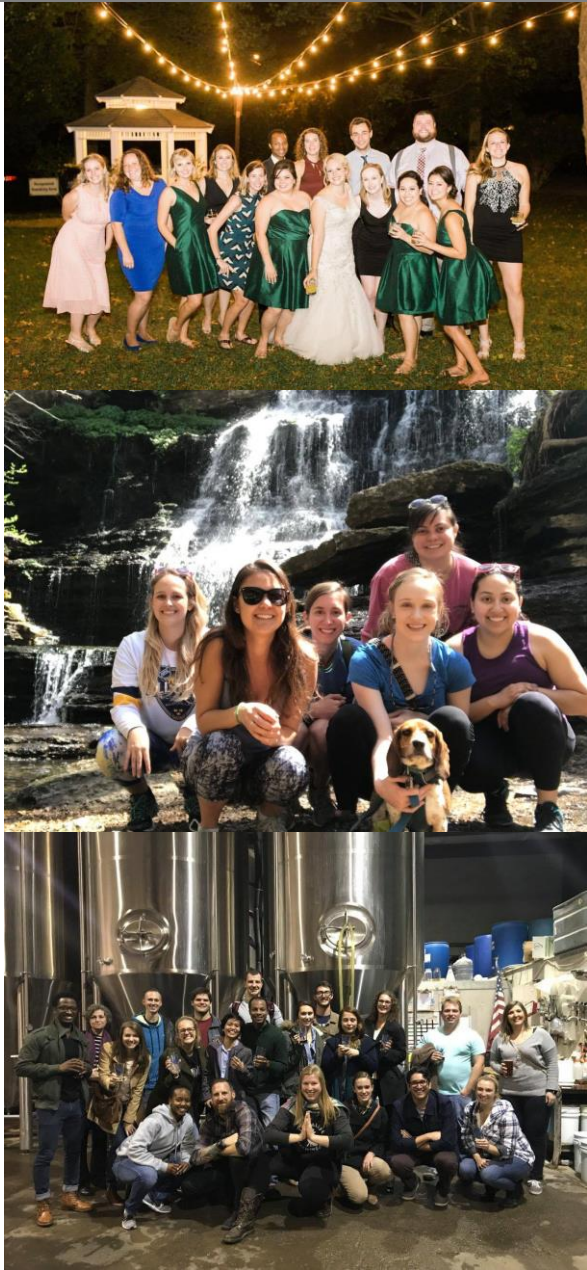
## ACKNOWLEDGEMENTS

---



To my little boy Taco-

You have been such a joy to my life- Thank you for always greeting me with a snuggle and a snort after a long day. Writing this dissertation would have been much less warm and snuggly without you!



To my friends-

Thank you for your friendship and support all these years. Thank you for providing a listening ear and celebrating with me when science finally cooperates! As we each are going through the PhD journey, your camaraderie and understanding of this process has been priceless. Thank you for your patience when you may not see me for a while. Thank you for always being up to grab a drink or dinner together to unwind. Thank you for helping make Nashville my home.

To Caleigh-

Thank you for keeping me sane and always being willing to try out new restaurants around town with me. The time spent exploring Nashville with you have helped keep me grounded and I appreciate your support and friendship so much.

To Diana-

Thank you for reminding me to always be strong and not back down. I am a stronger person for knowing you. Your tenacity and drive is an inspiration.

To Kim-

Thank you for reminding me to have fun! Thank you for sharing your fur babies with me before Taco and always reminding me that life is not just about science. Thank you for helping me to balance.

To Diane-

Thank you for your listening ear and advice as we've jumped the VUMC gap. You have helped me to learn to laugh at the little things I cannot

## ACKNOWLEDGEMENTS

### TASTE OF MUSIC CITY 2016



Caleigh Azumaya and Stephanie Moore

The Nissan Taste of Music City Festival held its 14th annual all-inclusive food tasting event downtown in Nashville's Public Square Park. Attendees enjoyed tastings from some of the area's best restaurants along with some of Nashville's local beverage flavors including Yazoo Brewing, Jack Daniel's, Arrington Vineyards, Hap & Harry's and more.



control. Thank you for always remembering to celebrate with baked good and reminding me that crafting is a valuable life skill.

### To Meredith-

Thank you for giving me faith that becoming a post doc is possible! You are always so calm and calculated, even when chaos ensues. Thank you for teaching me to breath and learn to love hiking and nature. Without you and Diane, I'm not sure I would have ever venture off the path. Thank you for teaching me to take a minute for myself and see the world around me.

### To Kelsey-

I miss you! Even through we live in different states now, you have always found a way to be there when I needed it most. Thank you for being understanding of my crazy life and a spectacular friend. Now that this dissertation is done, I think that mean we get to travel the world again!

### To the ladies and gents of Pharmacology-

You are all spectacular examples of the next generation of scientist- keep that up! I am so proud of the growth I have seen around me these past 5 years. Thank you for being there day to day through this journey and always being a smiling face at journal club or seminar. I appreciate the support, understanding, and motivation I've received from each of you more than I can express. Thank you for making the department a place of fun and support- this environment is so special, never loose that sense of community.

### To the VPs of PhGSA-

You made my time as President so easy. Thank you for being wonderful leaders and role models. Its because of your hard work that the community in the Pharmacology Department is what it is. Keep striving to make your Graduate School experience everything you want it to be.

## ACKNOWLEDGEMENTS

---



### To the Schoenecker Lab-

Thank you for being my home away from home. You took me in in 2013 and I have loved every minute with you guys. Working with each of you has made me a better person, both personally and scientifically. Thank you for motivating me to be the best scientist possible and helping me to grow in both my skills and scientific understanding. Our lab works hard, there's no doubt in that, but you all also help me have so much fun! From dinners out, to games at Soda Parlor, thank you so much for being a wonderful team to tackle our scientific questions and life with.

### To our medical students, past and present (Lou, Deke, Alex, Patton, Shelby, Patrick, Dan, Colby, Josh, Joe, Rivka, Courtney, Emilie, & Tanya)-

Thank you for teaching me and trusting in me to help you! Your belief in me has given me more confidence than I can express to you. Thank you for believing in me as a mentor and helping me learn everyday how become the best mentor possible. Thank you for challenging me and teaching me to speak the language of physicians. You will all make spectacular doctors- Remember to keep asking questions, challenge the status quo, and always always read- because history can teach us so much.



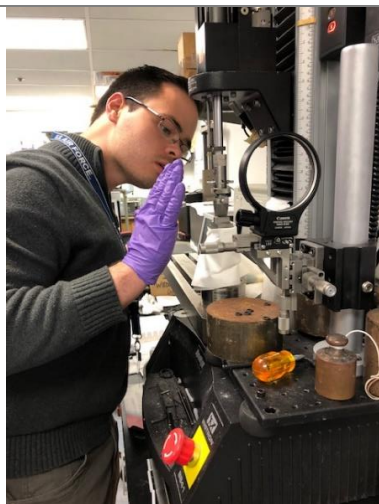
### To the OLD SCHOOL Lab (Masato, Tets, Rick, and Nick)-

Thank you for training me when I joined the laboratory, a naïve 21-year-old, in the field of Orthopaedics. I have learned so much from each of you. Your technical and practical knowledge has helped to set the foundation for my thesis work. Your hard work and motivated natures set the precedent for the lab, and has driven me to emulate your work ethic. Working with each of you has been instrumental to my success. Thank you for being patient with me as I learned and grew. Masato, thank you for teaching me even when I talk a lot and splatter microfill across the lab. Tets, thank you for taking me under your wing and making me believe I could succeed in the lab. Rick and Nick- Thank you for being the big brothers ive never had. I can't wait to work

---

## ACKNOWLEDGEMENTS

---



with each of you more in the future.

### To the NEW SCHOOL lab (Masa, Eggy, Breanne, Sam, Court, Hayes & Greg)-

Thank you for your patience during my thesis writing and preparation of manuscripts of the past few months. Thank you for proof reading, offering critical edits, and helping me overall to become a better scientist and writer. Eggy and Masa- I have and continue to learn so much from each of you. Thank you for being great work partners on projects and always pushing me to be better.

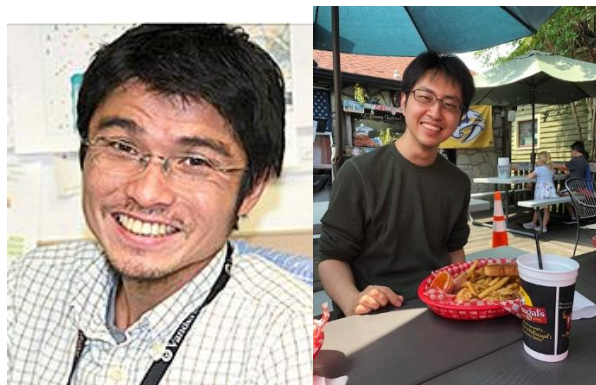
### To my Undergraduates, Zach, Joey, Greg, Yael, & Emilie-

You guys are wonderful! Thank you for understanding my crazy schedule and working with me to solve problems in the laboratory. You all were instrumental to my thesis work. Thank you for scoring x rays and helping me to develop the STiCSS. I know some days were very boring, but you never complained. Thank you for being willing to learn and be excited about science! As each of you go on to bigger and better things, know that I am incredibly proud of each of you! Keep up the hard work and passion for science that you showed me.



### To Breanne-

Thank you for being my partner in crime and fellow graduate student. Being a graduate student in pharmacology can at times be hard, but having you in the laboratory to commiserate with help me get through even the hardest days. Thank you for supporting me through my committee meetings, paper submission, paper rejections, and everything in between. Thank you for celebrating our success with me and picking me back up after rejections. Your friendship means to world to me.



### To Jon, my mentor-

Thank you for believing in me. Thank you for always pushing me to reach the next level. While you know that I am my own harshest critic, you have taught me how to turn my mistakes in the victories, how to fall forward and not back when science fails. You have

## ACKNOWLEDGEMENTS

---



taught me how to turn my criticisms into learning points and motivation. While you have taught me so many lessons, I think this the most important.

Thank you for believing in work life balance and helping me to achieve a better balance in my own life. Susan and yourself are such an inspiration. Thank you for welcoming me into the lab and your life. I have loved getting to know your family, clinical colleagues, and our collaborators. Thank you for making me always feel like a valuable part of the Lab Team, even from the very beginning.

Thank you for giving me the opportunity to be a mentor to the medical students. Thank you for believing in my ability to lead even when I was young and inexperienced. Thank you for teaching me how to be a mentor, and continuing to work with me to develop my own mentoring style. You have never told me I could not do something because of my stage in my career-Thank you for allowing me to help with grants, head up project, take charge of manuscripts, and build my strength and confidence. Thank you for always pushing me to be better.



### To my parents-

Thank you for instilling the love of science in me from a young age.

Mom, thank you for teaching me compassion and how to work with others. Without you, I would not be the person I am today.

Dad, thank you for always being willing to dissect gross things in the yard with me. You instilled not only a strong work ethic in me but also a love of discover and exploration. Thank you for always helping me find opportunities to explore and learn new things. Thank you for supporting me on the journey. Without you, these last 5 years would have been much more stressful.

## ACKNOWLEDGEMENTS

---



To my new parents, Marsha and Chris-  
You, like Corey, have been here since the beginning of my college journey. Thank you for the constant support, love, and understanding. Thank you for never asking “when will you be done with school” but instead offering your support in any way possible. Marsha, thank you for proof-reading my dissertation! It was so helpful!



Finally, to my extended family-

While some are close and others farther away, each of you have been instrumental to me through these last 5 years. Thank you for the warm wishes, texts of encouragement, and random cards in the mail to say hello and that you love me. Those little gestures have meant so much, and always seem to arrive when I needed them the most. I love you all.

---



	Page
ACKNOWLEDGMENTS .....	ii
LIST OF TABLES .....	xii
LIST OF FIGURES .....	xiv
ABBREVIATIONS .....	xx
SCIENTIFIC CONTRIBUTIONS .....	xxvi
CHAPTER OVERVIEW .....	xxxvi
CHAPTER 1:	
Foundations of Bone Biology and Mineralization.....	1
Biom mineralization .....	1
Favorable Biom mineralization: Skeletal System.....	1
Bone Formation .....	2
Endochondral Ossification During Bone Development .....	2
Intramembranous Ossification During Bone Development .....	8
Bone Resorption and Remodeling .....	9
Application of The Foundations of Bone Biology to Fracture Repair.....	9
Article 1: The Unifying Theory of Fracture Healing- Clinical and Scientific Implications .....	12
Article 2: The Size of Intramedullary Device Affects Endochondral Mediated Angiogenesis During Fracture Repair.....	55
Application of The Foundations of Bone Biology: Promoting Bone Formation to Improve Spinal Fusion.....	86
Article 3: Autologous Chondrocyte Grafting Promotes Bone Formation in The Posterolateral Spine .....	86
Your Body’s Response to Injury: The Acute Phase Response and Related Complications .....	106
Article 4: C-Reactive Protein Predicts Risk of Venous Thromboembolism in Pediatric Musculoskeletal Infection .....	106

Article 5: Should Catheter and Non-Catheter Related Deep Vein Thrombosis Cohorts Be Mixed for Risk Assessment?.....	124
Chapter 1 Summary .....	142

CHAPTER 2:

Pathologic Biomineralization of Soft Tissues .....	144
Article 6: Plasmin Prevents Dystrophic Calcification After Muscle Injury.....	149
Article 7: Validation of a Radiography-Based Quantification Designed to Longitudinally Monitor Soft Tissue Calcification in Skeletal Muscle.....	154
Building Upon Plasmin: A Critical Reparative Protease.....	218
Article 8: Unexpected Timely Fracture Union in Matrix Metalloproteinase 9 Deficient Mice.....	220
Article 9: Novel Preclinical Murine Model of Trauma-Induced Elbow Stiffness .....	242
Regulation and Fate of Dystrophic Calcification Found Within Damaged Tissues- Is Dystrophic Calcification Sufficient to Form Heterotopic Ossification?.....	264
Application of A High Phosphate Diet Predisposes Skeletal Muscle to Dystrophic Calcification .....	265
Soft Tissue Protection Mechanisms .....	272
Article 10: Trauma-Induced Nanohydroxyapatite Deposition in Skeletal Muscle is Sufficient to Drive Heterotopic Ossification.....	278
Chapter 2 Summary.....	309

CHAPTER 3:

Therapeutic Modulation of Trauma-Induced Heterotopic Ossification.....	311
Current Practice .....	311
Bisphosphonate Treatment for The Prevention of Heterotopic Ossification .....	312
Article 11: Temporal-Spatial Localization of Bisphosphonates in a Combined Musculoskeletal Injury Model .....	337

Section Summary: Bisphosphonates .....	364
Bmp Antagonists for The Treatment of Heterotopic Ossification.....	365
Therapeutic Modulation of Plasmin to Prevent Heterotopic Ossification .....	366
Chapter 3 Summary .....	372
CHAPTER 4:	
Future Directions .....	373
Physiologic Bone Formation: Fracture Repair .....	373
Bone Grafting .....	375
Pathologic Bone Formation: Drilling Down on the Macrophage .....	376
The Transition of Dystrophic Calcification to Heterotopic Ossification .....	378
Within the Sarcomere- How Is Dystrophic Calcification Born?.....	380
What Do These Findings Meaning Clinically?.....	382
APPENDIX I:	
Article 12: Necrotizing Fasciitis: Coagulopathy, Adrenal Insufficiency, and Nosocomial Transmission.....	388
REFERENCES .....	423

## LIST OF TABLES

<b>Table</b>	<b>Page</b>
Table 1: CRP Values Per Cohort	115
Table 2: Effect of Peak CRP on Predicted Probability of VTE	117
Table 3: Demographic Characteristics of DVT Patients Aged 0-18 by Catheter Status	131
Table 4: Difference in CRP value by Catheter Status and Congenital Heart Disease	134
Table 5: Difference in CRP value by Catheter Status Stratified by Congenital Heart Disease	134
Table 6: Differences in CRP value by Congenital Heart Disease Stratified by Catheter Status	137
Table 7: Differences in CRP Values by Catheter Status Stratified by Congenital Heart Disease	138
Table 8: Cost, Time, and Radiation Exposure Analysis	156
Table 9: Intra-observer analysis of Post-Image Processing	169
Table 10: Intra-observer Error on STiCSS	170
Table 11: Inter-observer Analysis of the STiCSS	171
Table 12: Spearman Correlation of the STiCSS and $\mu$ CT measurements	173
Table 13: Sample Size Calculator for the STiCSS	175
Table 14: <i>In vivo</i> Effectiveness of Plasminogen Knockdown by ASO Injection	193
Table 15: Statistical Analysis of STC Score in Plasminogen Deficient Mice After CTX-induced Muscle Injury	194
Table 16: Statistical Analysis of STC Score in Mice treated with Plasminogen ASO after CTX induced Muscle injury	196
Table 17: Statistical Analysis of STC Score Demonstrating that Knockdown of the Plasmin Inhibitor $\alpha$ 2AP Prevents Soft Tissue Calcification Independent of Fibrinogen	213
Table 18: Interobserver Agreement of Upper Extremity Radiographic Assessment	252

Table 19: Statistical Analysis of STiCSS Values of Mice fed different diets at 28 Days Post Injury	269
Table 20: Human Diseases Associated with Mutations in the Pyrophosphate Pump that Result in Aberrant Mineralization	277
Table 21: Quantification of Skeletal Muscle Calcification in ABCC6 Deficient Mice at 7DPI	292
Table 22: Histological Quantification of Skeletal Muscle Calcification and Regeneration at 7 and 28 DPI	295
Table 23: Review of Bisphosphonate Use for Treatment of HO	314
Table 24: Literature Review of Bisphosphonate use in Fracture Healing	320
Table 25: Analysis of inter-observer variation between 7 independent observers	345
Table 26: Y-Scale Statistical Analysis	353
Table 27: STiCSS Score Statistical Analysis	354
Table 28: Y-Scale Statistical Analysis	363
Table 29: STiCSS Score Statistical Analysis	363
Table 30: Quantitation of percent $\alpha$ 2AP mRNA knockdown in the livers of WT mice after receiving 100mg/kg/week of the respective ASO for 2 weeks	366

## LIST OF FIGURES

<b>Figure</b>	<b>Page</b>
Figure 1: Physal Biology: Chondrocytes are the Foundation of Endochondral Ossification	3
Figure 2: Hypertrophic Chondrocyte-Mediated Mechanisms of Bone Formation	7
Figure 3: The Body's Response to Fracture Injury: The Acute Phase Response (APR)	16
Figure 4: Fibrin must be removed following fracture injury for revascularization and subsequent ossification to occur	23
Figure 5: Visual representation of the evolution of matrices at the fracture site	25
Figure 6: Meet the Cellular Heroes of Bone Formation.	26
Figure 7: Cellular Heroes at Work in the Fracture Callus	28
Figure 8: Origin of the Osteoblast: Transdifferentiation or direct from the pericyte- a matter of strain and hypoxia?	31
Figure 9: Intramembranous Ossification in Fracture Healing.	33
Figure 10: Secondary Bone Repair- Endochondral Ossificaiton in Fracture Healing	35
Figure 11: Historical vascularity models	39
Figure 12: Temporal-spatial fracture repair and angiogenesis	42
Figure 13: Radiographs depicting a healing femur fracture in a young adult treated with open reduction and internal fixation with plate and screws.	44
Figure 14: Fracture Fixation Methods	49
Figure 15: Estimation of intramedullary fracture strain between 23G and 30 G pins	65
Figure 16: Comparison of intramedullary vascular disruption between 23G and 30G pins.	67
Figure 17: Radiographic, macroscopic, and histologic characteristics of fracture calluses at 10 DPF	69
Figure 18: Quantitative analysis of histology and mRNA expression in the fracture callus at 10 DPF	71

Figure 19: Macroscopic and histologic characteristics of fracture calluses at 14 DPF	73
Figure 20: The quantitative analysis of histology and mRNA expression in the fracture callus at 14 DPF	75
Figure 21: Comparison of fracture callus angiogenesis at 14 DPF	77
Figure 22: Correlation of callus vascularization with histomorphometric features at 14 DPF	78
Figure 23: Time course of fracture healing following fixation allowing for varying interfragmentary strain	79
Figure 24: Delayed fracture remodeling observe din femurs fixed with smaller 30G pins	81
Figure 25: Experimental Design- Use of FCCG as compared to ICBG for promoting bone formation in the posterolateral spine	88
Figure 26: Optimal Timing for FCCG Isolation	90
Figure 27: Murine Posterolateral Spinal Fusion Model	92
Figure 28: Radiological Quantification of Bone Formation between Transverse Processes	94
Figure 29: Implantation of hypertrophic chondrocytes promotes bone formation	99
Figure 30: Flow diagram of pediatric MSKI patient selection	111
Figure 31: Cumulative and peak CRP for pediatric MSKI patients	114
Figure 32: Predictive Models of CRP for VTE in MSKI	116
Figure 33: CONSORT flow diagram of patient study population	130
Figure 34: Distribution of CRP values (mg/L) by catheter status	133
Figure 35: Stratified analysis of interaction effect between CRP, catheter status, and CHD	136
Figure 36: Operational Definitions of Soft Tissue Calcification	147
Figure 37: Flow Diagram of Post-Image Processing	162
Figure 38: Soft Tissue Calcification Scoring System (STiCSS)	163

Figure 39: Comparison of STiCSS Score and Mineral Volume Determined by ex vivo $\mu$ CT	172
Figure 40: Radiographic Analysis and Quantification of Soft Tissue Calcification Following Burn/CTX Injury	174
Figure 41: Dystrophic Calcification and Heterotopic Ossification Are Histologically Distinct Yet Radiographically Equivalent	176
Figure 42: Continuous Muscle Injury in the Setting of Plasminogen Deficiency Results in Soft Tissue Calcification	186
Figure 43: Soft tissue calcification in mdx/Plg $\pm$ mice	188
Figure 44: Continuous and Acute Plasminogen Deficiency Results in Muscle Calcification After Acute Muscle Injury	191
Figure 45: Crush Injury Model of HO	195
Figure 46: Partial Plasminogen Deficiency and Muscle Injury Results in Poor Muscle Regeneration, Persistent Dystrophic Calcification, Diminished Macrophage Invasion and Endochondral Ossification	199
Figure 47: Histologic Quantitation of Muscle Healing in WT and Plg $\pm$ mice	201
Figure 48: Injured Plg $\pm$ Mice Undergo Endochondral Ossification	204
Figure 49: Characterization of Heterotopic Ossification after Muscle Injury and Plasminogen Deficiency	205
Figure 50: Increasing Plasmin Activity Prevents Soft Tissue Calcification and Rescues Muscle Regeneration Independent of Fibrinolysis	208
Figure 51: Soft Tissue Calcification in Continuous Muscle Injury and Plasminogen Deficiency Can Be Rescued by Increasing Plasmin Activity with $\alpha$ 2-Antiplasmin ASO	210
Figure 52: Histological Analysis and Quantification of Muscle Healing in Plg $\pm$ Mice Treated with either Control ASO or $\alpha$ 2-Antiplasmin ASO	211
Figure 53: Radiographic Quantification of Fracture Healing	228
Figure 54: Radiographic Quantification Score Sheet	229
Figure 55: Skeletal Healing of Stabilized Femur Fracture in MMP-9 Deficient Mice	230
Figure 56: MMP-9 is Not Required for Endochondral Fracture Healing	232



Figure 57: Sample Histology of WT and MMP-9 Deficient Mice Following Fracture Injury	234
Figure 58: Revascularization of the Fracture is Unaffected by a Loss of MMP-9	236
Figure 59: Vascular Quantification of Healing Fractures of WT and MMP-9 Deficient Mice	237
Figure 60: Preclinical Model of Upper Extremity Injury	247
Figure 61: Quantification of muscle calcification by radiographic analysis	251
Figure 62: Upper extremity functional assessment following per-elbow soft tissue injury	254
Figure 63: Histological analysis of frontal and transverse sections of injured peri-elbow soft tissues 28 DPI	256
Figure 64: Characterization of skeletal muscle calcification following peri-elbow injury	259
Figure 65: High Phosphate Diet Alone is Sufficient to Predispose Skeletal Muscle to Dystrophic Calcification Following Focal Injury	268
Figure 66: Microcomputed tomography Assessment of Dystrophic Calcification at 28 DPI	270
Figure 67: Diet-induced Dystrophic Calcification Impairs Sarcomere Regeneration and Promotes Fibrosis	271
Figure 68: Protein components of the Pyrophosphate Pump	276
Figure 69: Loss of ABCC6 Predisposes Skeletal Muscle to Nanohydroxyapatite deposition at 7DPI	291
Figure 70: Nanohydroxyapatite deposition in ABCC6 Deficient Mice is Degraded Over 28 DPI	294
Figure 71: Macrophage-mediated Resolution of Nanohydroxyapatite Prevents Maturation to HO	297
Figure 72: Quantification of F4/80+ Staining in Damaged Skeletal Muscle at 7 & 28 Days Post Injury	298
Figure 73: Histological sampling of <i>Abcc6</i> Heterozygous mice treated with control (PBS-filled) Liposomes	300

Figure 74: Histological sampling of <i>Abcc6</i> heterozygous mice treated with clodronate filled Liposomes	301
Figure 75: The “Two Hit” Mechanism of HO Formation	303
Figure 76: Bisphosphonate Treatment Prevents Soft Tissue Calcification in the Setting of Plasmin Deficiency and Muscle Injury	324
Figure 77: Bisphosphonate administration of zoledronic acid prior to injury minimally reduces soft tissue calcification by 7 DPI	326
Figure 78: Bisphosphonate Administration Stabilized Dystrophic Calcification and Impedes Regression	328
Figure 79: Burn-induced Skeletal Muscle Calcification Model	329
Figure 80: Following burn injury, mice experience detectable burn induced osteoporosis within 3 days post injury	331
Figure 81: Bisphosphonate administration prior to burn injury effectively reduced skeletal muscle calcification present at 7 DPI	333
Figure 82: Administration of bisphosphonates improved the osteoporotic phenotype observed in mice following a burn injury to levels comparable of non-burned animals	335
Figure 83: Standard Fracture Healing and Soft Tissue Calcification in murine combined injury model	341
Figure 84: Modified Soft Tissue Calcification Scoring System for use in Quadriceps	343
Figure 85: $\mu$ CT-FEA of Fracture Callus on femur mid-shaft	348
Figure 86: Temporal Assessment of Bisphosphonate Localization Following Combined Fracture and Skeletal Muscle Injury	350
Figure 87: Continuous Bisphosphonate Dosing Following Combined Fracture and Skeletal Muscle Injury Delays Fracture Repair and Regression of Soft Tissue Calcification	352
Figure 88: Histological analysis of injured quadriceps at 42 DPI	354
Figure 89: Structural and Biomechanical Properties of Healing Fractures Following Continuous Bisphosphonate Dosing	357
Figure 90: Two Dimensional Images of Fracture Femur at 42 DPI	359

Figure 91: Single Dose Bisphosphonate Dosing Following Combined Fracture and Skeletal Muscle Injury	361
Figure 92: Enhancement of Plasmin Activity Prior to Injury Prevents Dystrophic Calcification	368
Figure 93: Enhancement of Macrophages Reduces Dystrophic Calcification at 7 DPI	371
Figure 94: Patient 1's right upper extremity	393
Figure 95: Patient 1 Laboratory Values	395
Figure 96: Patient 2 Laboratory Values	399
Figure 97: Plasmin Activation	404
Figure 98: Containment of Bacteria by DNA Webs	405
Figure 99: Fascial Spreading	406
Figure 100: Release of Superantigens	408
Figure 101: Development of Toxic Shock	410
Figure 102: Diffuse Intravascular Coagulation (DIC) Following Necrotizing Fasciitis	411
Figure 103: Critical-Illness Related Corticosteroid Insufficiency (CIRCI) Following Necrotizing Fasciitis	416
Figure 104: Summary of Necrotizing Fasciitis Pathophysiology	421

## ABBREVIATIONS

μCT	Microcomputed Tomography
3D	3 Dimensional
a2AP	Alpha-2 Antiplasmin
ABCC6	ATP binding Cassette Subfamily C Member 6
ACTH	Adrenocorticotropic Hormone
ALP	Alkaline Phosphatase
ALT	Alanine Aminotransferase
AMP	Adenosine Monophosphate
ANCOVA	Analysis of the Covariance
ANK	ANKH inorganic pyrophosphate transport regulator
ANOVA	Analysis of Variance
AP	Anterior- Posterior
APR	Acute Phase Response
ARDS	Acute Respiratory Distress Syndrome
ASO	Antisense Oligonucleotide
AST	Aspartate Aminotransferase
ATP	Adenosine Triphosphate
AUC	Area under the Curve
BI	Brain Injury
BMP	Bone Morphogenic Protein
BMPR	Bone Morphogenic Protein Receptor
Bppi	Bisphosphonate

BSA	Bovine Serum Albumin
BV/TV	Bone Volume/Tissue Volume
CD39	Cluster of Differentiation 39
CD73	Cluster of Differentiation 73
cDNA	Complimentary DNA
CHD	Congenital Heart Disease
CI	Confidence Interval
CIRCI	Critical Illness Related Corticosteroid Insufficiency
CL	Component Labeling
CO <sub>2</sub>	Carbon Dioxide (Gas)
CPPD	Calcium Pyrophosphate Deposition
CRP	C-Reactive Protein
CRT	Catheter Related Thrombosis
CT	Computed Tomography
CTX	Cardiotoxin
DIC	Disseminated Intravascular Coagulation
DPF	Days Post Fracture
DPI	Days Post Injury
DVT	Deep Vein Thrombosis
EC	Endochondral
EDS	Energy Dispersive X ray
ELISA	Enzyme-Linked Immunosorbent Assay
ENPP1	Ectonucleotide Pyrophosphatase/Phosphodiesterase 1

Fbg	Fibrinogen
FCCG	Fracture Callus Bone Graft
FEA	Finite Element Analysis
FGF-2	Fibroblast Growth Factor
FOP	Fibrodysplasia Ossificans Progressiva
G	Gauge
GACI	Generalized arterial calcification of infancy
GAS	Group A Streptococcus
H/E	Hematoxylin and Eosin
Hif-1 $\alpha$	hypoxia-inducible factor 1 $\alpha$
HO	Heterotopic Ossificaiton
HPA	Hypothalamic Pituitary Adrenal
HPO4	High phosphate
HRP	Horseradish Peroxidase
IACUC	Institutional Animal Care and Use Committee
ICBG	Illiac Crest Bone Graft
IHC	Immunohistochemistry
IM	Intramembranous
LISS	Less invasive Stabilization System
LR	Lactated Ringers
MAPK	Mitogen-Activated Protein Kinase
MDX	Duchenne's Muscular Dystrophy
Mef2	Monocyte enhancer factor-2

ML	Medial- Lateral
MMP-9	Matrix metalloproteinase 9
MOF	Multiorgan Failure
MPLA	Monophosphoryl Lipid A
MRI	Magnetic Resonance Imaging
mRNA	Messenger ribonucleic acid
MSB	Martius Scarlet Blue
MSC	Mesenchymal Stem Cells
MSKI	Musculoskeletal Infection
NCRT	Non-Catheter Related Thrombosis
NIR	Near-infrared
NSAID	Non-steroidal Anti-inflammatory Drugs
O <sub>2</sub>	Oxygen (gas)
OPN	Osteopontin
OR	Odds Ratio
OR	Operating Room
Osx	Osterix
PDGF	Platelet Derived Growth Factor
PE	Pulmonary Embolism
Pecam1	Platelet and endothelial cell adhesion molecule 1
Pi	Phosphate
Pit-1/2	Na Dependent Phosphate transporter 1 or 2
PLG	Plasminogen

pMOI	Polar Moment of Inertia
PPi	Pyrophosphate
PXE	Pseudoxanthoma Elasticum
RCT	Randomized Control Trial
RNA	Ribonucleic acid
ROC	Receiver Operator Curve
RQ	Radiograph Quantification
RT	Room temperature
RT-PCR	Reverse Transcription-Polymerase Chain Reaction
SCI	Spinal Cord Injury
SD	Synthetic Derivative
SD	Standard Deviation
SEM	Standard Error of the Mean
SIRS	Systemic Inflammatory Response
SOX-9	SRY-box 9
STiCSS	Soft Tissue Calcification Scoring System
Tb. N.	Trabecular Number
Tb. Sp.	Trabecular Space
Tb. Th.	Trabecular Thickness
TBS	Tris Buffered Saline
THR	Total Hip Replacement
TMD	Tissue Mineral Density
TOI	Time of Injury



tPA	Tissue Plasminogen Activator
TRAP	Tartate-Resistant Acid Phosphate
uPA	Urokinase Plasminogen Activator
UV	Ultra Violet
VEGFA	Vascular Endothelial Growth Factor A
VEGF-R	Vascular Endothelial Growth Factor Receptor
VOI	Volume of Interest
VTE	Venous Thromboembolism

## SCIENTIFIC CONTRIBUTIONS

### Article 1: The Unifying Theory of Fracture Healing- Clinical and Scientific Implications

Through the development of this review article I drafted components of the manuscript text, developed the figures with Dr. Schoenecker, formatted the article for submission, prepared supplementary materials necessary for manuscript submission, and conducted the submission process. Once reviews were obtained, I assisted in substantial manuscript revisions, editing of figures, and preparation of the response to reviewer documents. Finally, I oversaw the resubmission of this article.

### Article 2: The Size of Intramedullary Device Affects Endochondral Mediated Angiogenesis During Fracture Repair

For this article, I was responsible for drafting the initial manuscript, guided by the data generated from Drs. Masato Yuasa and Masanori Saito. I assisted in data analysis and validation, as well as data generation to assess and quantify strain across our fracture model. Furthermore, I assisted Dr. Yuasa with figure development, data presentation, and statistical analysis throughout the manuscript. As we obtain review of this work, I will be responsible for critical revisions and resubmission of this manuscript.

### Article 3: Autologous Chondrocyte Grafting Promotes Bone Formation in The Posterolateral Spine

For this article, I was responsible for drafting the initial manuscript, guided by the data generated from Drs. Alexander Sielatycki, Masanori Saito, and Masato Yuasa. I assisted in data analysis, statistical assessments, model validation, data presentation, and figure preparation. For example, I assisted in developing and validating a radiographic quantification method around the spine to

assess boney formation between the transverse processes. Furthermore, prior to these studies, in developing this novel model with Drs. Sielatycki and Yuasa, I was responsible for prepared the animal protocols and gaining institutional approval to conduct the following studies. Once reviews were obtained, I assisted in substantial manuscript revisions, editing of figures, and preparation of the response to reviewer documents. Finally, I oversaw the resubmission and proofs of this article which was published in the inaugural issue of Journal of Orthopaedic Research: Spine.

Article 4: C-Reactive Protein Predicts Risk of Venous Thromboembolism in Pediatric Musculoskeletal Infection

This article was once of my first experiences guiding a team of medical student to conduct a research study. With Dr. Schoenecker's guidance, I worked with Drs. Amaro, Marvi, and Posey to develop the study, collect retrospective patient data, visualize the data, statistically analyze the data, prepare figures, and prepare the initial manuscript for submission. When reviews were returned, I assisted in substantial manuscript revisions, editing of figures, and preparation of the response to reviewer documents. Finally, I oversaw the resubmission and proofs of this article which was published in the Journal of Pediatric Orthopaedics

Article 5: Should Catheter and Non-Catheter Related DVT Cohorts Be Mixed for Risk Assessment?

For this article I assisted our team of medical students with project design, setting up the synthetic derivative database for data collection, and assisted in writing and critically reviewing the manuscript prior to submission. When reviews were returned, I have assisted with critical

revisions prior to overseeing resubmission.

Article 6: Plasmin Prevents Dystrophic Calcification After Muscle Injury

For this article, I helped generate critical data, worked with the Department of Biostatistics to conducted statistical analyses, designed figures and tables, and assisted with data presentation throughout the manuscript. Furthermore, I assisted with drafting of the initial manuscript, offered critical revisions, and assisted with the initial manuscript submission. When reviews were returned, I assisted with data generation, manuscript revisions, and preparation of the response to reviewer documents prior to resubmission.

Article 7: Validation of a Radiography-Based Quantification Designed to Longitudinally Monitor Soft Tissue Calcification in Skeletal Muscle

For this article, I was responsible for study design, data generation, data analysis and validation of new experimental tools, performed statistical analysis, and produced the accompanying training videos. Furthermore, I was responsible for drafting the initial manuscript, designing the figures and tables, collecting and implementing critical revisions, formatting the article for submission, preparing supplementary materials necessary for manuscript submission, and conducting the submission process. When reviews were returned, I was responsible for revising the manuscript and preparing the response to reviewer documents prior to resubmission. Finally, once approved for publication I oversaw the proofs of this article which was published in PLoS One.

#### Article 8: Unexpected Timely Fracture Union in Matrix Metalloproteinase 9 Deficient Mice

For this article, I was responsible for drafting the initial manuscript, guided by the data generated from Drs. Masato Yuasa and Masanori Saito. I assisted in data analysis and validation, statistical analysis, figure and table development, and data presentation throughout the manuscript. Following internal review, I was responsible for intercalating revisions, formatting the article for submission, preparing supplementary materials necessary for manuscript submission, and conducting the submission process. When reviews were returned, I was responsible for revising the manuscript and preparing the response to reviewer documents prior to resubmission. Finally, once approved for publication I oversaw the proofs of this article which was published in PLoS One.

#### Article 9: Novel Preclinical Murine Model of Trauma-Induced Elbow Stiffness

In collaboration with Dr. William Oelsner, for this article I was responsible for data collection, data analysis and validation, statistical analysis, figure development, and data presentation throughout the manuscript. Furthermore, I was responsible for drafting the initial manuscript, collecting and intercalating internal revisions, formatting the article for submission, preparing supplementary materials necessary for manuscript submission, and conducting the submission process. When reviews were returned, I was responsible for revising the manuscript and preparing the response to reviewer documents prior to resubmission. Finally, once approved for publication I oversaw the proofs of this article which was published in Journal of Experimental Orthopaedics.

Article 10: Trauma-Induced Nanohydroxyapatite Deposition in Skeletal Muscle is Sufficient to Drive Heterotopic Ossification

For this article I was responsible for study design, data collection, data analysis and validation, statistical analysis, figure development, and data presentation throughout the manuscript. In collaboration with Thomas Jefferson University, I helped to obtain the mice necessary for this study, amended the animal protocols, and conducted both the pilot studies and main experiments of this manuscript. Furthermore, I was responsible for drafting the initial manuscript, collecting and intercalating internal revisions, formatting the article for submission, preparing supplementary materials necessary for manuscript submission, and conducting the submission process. When reviews were returned, I was responsible for revising the manuscript and preparing the response to reviewer documents prior to resubmission.

Article 11: Temporal-Spatial Localization of Bisphosphonates in a Combined Musculoskeletal Injury Model

In collaboration with Dr. Masanori Saito, for this article I was responsible for data collection, data analysis and validation, statistical analysis, figure development, and data presentation throughout the manuscript. Furthermore, I was responsible for drafting the initial manuscript, collecting and intercalating internal revisions, formatting the article for submission, preparing supplementary materials necessary for manuscript submission, and conducting the submission process.

## Article 12: Necrotizing Fasciitis: Coagulopathy, Adrenal Insufficiency, and Nosocomial Transmission

In collaboration with a spectacular team of medical students, for this article I assisted with retrospective data collection and analysis, figure development, drafting of the initial manuscript, formatting the article for submission, preparing supplementary materials necessary for manuscript submission, and conducting the submission process.

In addition to the articles presented in whole within my thesis work, I have also prepared the following manuscripts and abstracts for publication and/or presentation at local or national meeting.

### Manuscripts

- Stephanie N Moore, S Bobo Tanner & Jonathan G Schoenecker (2015) Bisphosphonates: from softening water to treating PXE. 2015. *Cell Cycle*, 14:9, 1354-1355, DOI: 10.1080/15384101.2015.1024585
- Howard, AW., Moore, SN., Schoenecker JG, authors. *Medical Therapy in Pediatric Orthopaedics*. Rosemont, IL American Academy of Orthopaedic Surgeons; c2016. 107-119 p. (Martus, JE, editor. *Orthopaedic Knowledge Update Series; Pediatrics 5*).

### Abstracts

- Moore, SN., Ohba, T., Cates, JMM., Cole, H., Mignemi, NA., Ichikawa, J., Hirota, H., Schwartz, HS., Schoenecker, JG. 2015. Fibrinogen Regulates MMP-9 Processing of VEGF-induced Angiogenesis and Tumor Growth in Osteosarcoma. Abstract for Oral Presentation, 2015 Experimental Biology Meeting, Boston, MA, April 2015. \*Abstract was selected as a Finalist in the Graduate Platform Award Competition.

- Moore, SN. Combined Therapeutic Targeting of Matrix Metalloproteinase-9 and VEGF in Osteosarcoma. Oral Presentation, Vanderbilt Center for Bone Biology Seminar, Nashville, TN. September 11th, 2015
- Moore, SN., Ohba, T., Cole, H., McIntyre JO., Cates, JMM., Schoenecker, JG. 2016. Fibrin(ogen) is a Novel Negative Regulator of Angiogenesis. Poster Presentation, 2016 Gordon Research Conference- Plasminogen and Plasmin Activators, Ventura, CA. February, 2016.
- Moore, SN. TNAP, Pyrophosphate, and the Effect on Bone: A look into Hypophosphatasia Mechanism of Action, Basic Science Advancements, and Current Clinical Therapies. Oral Presentation, Vanderbilt Center for Bone Biology Seminar, Nashville, TN. May 2016
- Moore, SN. Investigation of the Multifactorial Nature of Trauma-Induced Soft Tissue Calcification and Potential Therapeutic Approaches. Oral Presentation, Vanderbilt Center for Bone Biology Seminar, Nashville, TN. August 2016
- Moore, SN., Schoenecker, JG. Trauma-Induced Skeletal Muscle Calcification and Potential Therapeutic Approaches. Invited Oral Presentation, 2016 PXE International Conference, Thomas Jefferson University, Philadelphia, PA. September 2016
- Moore, SN., Gibson, BHY., Amaro, E., Schoenecker, JG. Role of the Acute Phase Response in Soft Tissue and Bone Targeted Malignancies. Oral Presentation and Journal Club Discussion, Vanderbilt Department of Orthopaedics and Rehabilitation, Nashville, TN. November, 9th 2016.
- Baker CE, Moore SN, Yuasa M, et al. "Osteopontin deficiency contributes to heterotopic ossification." Gordon Research Seminar: Plasminogen and Extracellular Proteolysis,



February 2016, Ventura CA. Poster

- Amaro, EJ., Moore-Lotridge, SN., Gibson, BHY., Schoenecker, JG. Role of the Acute Phase Response in Soft Tissue and Bone Malignancies. Vanderbilt Department of Orthopaedics and Rehabilitation, Nashville, TN. 2016. Oral Presentation
- Saito, M., Moore-Lotridge, SN., Ihejirike, Y., Gibson, BHY., Schoenecker, JG. 2016. Bisphosphonates Prevent the Regression of Fracture Associated Muscle Calcification. Abstract and Poster Presentation, 2017 ORS National Conference San Diego, CA. March, 2017.
- Moore-Lotridge, SN., Hawley, GD., Gibson, BHY., Martin, JT., Tannouri, S., Li, Q., Uitto, J., Schoenecker, JG. 2017. Traumatic Soft Tissue Calcification: A Tale of Pyrophosphate and Phosphate Balance, Abstract and Poster Presentation, 2017 ORS Conference, San Diego, CA. March, 2017.
- Moore-Lotridge, SN and Schoenecker, JG. Trauma-Induced Skeletal Muscle Calcification and Potential Therapeutic Approaches. Oral Presentation, Langman Graduate Student Platform Presentation, 2017 Experimental Biology and the American Association of Anatomists Annual Meeting, Chicago, IL. April 2017 \*2nd Place Award for Best Scientific platform presentation by a Graduate Student at AAA's Annual Meeting/EB 2017
- Amaro, E., Mignemi, NA., Moore-Lotridge, SN., Gibson, BHY., Baker, CE., Hawley, GD., Ihejirika, RC., Bohannon, JK., Oelsner, WK., Wallace, CS., Luang, L., Sherwood, ER., Schoenecker, JG. April 2017. Severe Injury Leads to Plasmin Consumption Below a Critical Threshold Required to Heal Soft Tissue Injury. Abstract. Plastic and Reconstructive Surgery Conference.

- Benvenuti, M., Amaro, EJ., Moore-Lotridge, SN., An, TJ., Johnson, ME., Martus, J., Schoenecker, JG. The Total Acute Phase Response Predicts Complications in Children with Musculoskeletal Infection. American Academy of Pediatrics National Conference and Exhibition, Chicago, IL. 2017. Oral Presentation.
- Saito M, Yuasa M, Moore SN, Benvenuti MA, Schwartz HS, Nyman JS, Schoenecker JG. Unexpected Dispensable role of MMP-9 in Murine Fracture Repair. Orthopaedic Research Society National Meeting, New Orleans, LA. 2018. Poster
- Hawley GD, Cole HA, Moore-Lotridge SN, Jacobson R, Ohba T, Yuasa M, Schoenecker JG. Reduction of Fibrinogen, Not Interleukin-6, Rescues Skeletal Development Phenotypes of Plasminogen Deficiency. Orthopaedic Research Society National Meeting, New Orleans, LA. 2018. Poster
- Moore-Lotridge SN, Gibson BHY, Martin JT, Hawley GD, Arnold TH, Saito M, Schwartz HS, Schoenecker JG. Macrophages Protect Skeletal Muscle from Trauma-Induced Heterotopic Ossification by Regulating Dystrophic Calcification. Gordon Research Conference: Bone and Teeth. Galveston, TX. 2018. Poster. \*Best Poster Award\*, LA. 2018. Poster
- Saito M, Yuasa M, Moore SN, Benvenuti MA, Schwartz HS, Nyman JS, Schoenecker JG. Unexpected Dispensable role of MMP-9 in Murine Fracture Repair. Orthopaedic Research Society National Meeting, New Orleans
- Posey, SL., Gibson, BH., Hawley, GD., Ihejirika, R., Moore-Lotridge, SN., Schoenecker, JG. Burn-induced Osteoporosis and Muscle Calcification: Are These Related Complications?. Southern Orthopaedic Association Annual Meeting. Palm Springs, FL. July 2018. Oral Presentation.

- Hysong, AA., Posey, SL., Moore-Lotridge, SN., Engstrom, SM., Polkowski, GG., Schoenecker, JG. Anti-fibrinolytics are Dosed Inappropriately in Joint Replacement Surgery. Southern Orthopaedic Association Annual Meeting. Palm Springs, FL. July 2018. Oral Presentation.
- Osteoporosis and Muscle Calcification: Are These Related Complications?. Southern Orthopaedic Association Annual Meeting. Palm Springs, FL. July 2018. Oral Presentation.
- Hysong, AA., Posey, SL., Moore-Lotridge, SN., Engstrom, SM., Polkowski, GG., Schoenecker, JG. Anti-fibrinolytics are Dosed Inappropriately in Joint Replacement Surgery. Southern Orthopaedic Association Annual Meeting. Palm Springs, FL. July 2018. Oral Presentation.
- Benvenuti, M., Amaro, E., Moore-Lotridge, SN., An, TA., Johnson, ME., Martus, J., Schoenecker, JG., The Total Acute Phase Response Predicts Complications in Children with Musculoskeletal Infection. American Academy of Pediatrics Meeting. May 2018.

## **CHAPTER SUMMARIES**

In chapter 1, you will find the information and discussion surrounding our work into physiologic mineralization. Specifically, this chapter will cover how the body responds to injury and processes through which new bone is formed following a fracture within the skeleton. In chapter 2, we will transition our discussion to pathologic mineralization of soft tissue following injury, highlighting novel murine models that have helped us defined new pathophysiologic mechanisms behind these conditions. In chapter 3, we will build upon the discussions of chapter 2 and discuss therapeutics aimed at preventing soft tissue calcification and their effect of physiologic bone, both at a resting state and following injury such as a fracture. In chapter 4, we will discuss the future directions of this work, the implication on both physiology and pathologic mineralization, and what these findings may mean clinically.

## CHAPTER 1:

### Foundations of Bone Biology and Biomineralization

#### Biomineralization

Biomineralization is broadly defined as the precipitation of inorganic substances into an organic matrix. This process is widely applied in all 6 taxonomic kingdoms, from algae to vertebrates, in which living organisms produce and use minerals to harden tissues or form shells. In vertebrates, mineralization is an essential process, tightly balanced throughout the body, to support the formation of bones and teeth. In humans, the regulation of mineralization is critical to sustain life, such that while necessary for the proper formation of bones and teeth, mineralization of soft tissues is pathologic and significantly impacts patient morbidity and mortality. Through my thesis work, I have explored the biological mechanisms by which the body regulates biomineralization, the pathologic consequences aberrant mineralization has in skeletal muscle, and novel pharmacologics that can be applied to regulate mineralization-- directing them in conditions where more mineralization is needed or preventing mineralization of soft tissues.

#### Favorable Biomineralization: Skeletal System

In vertebrates, mineralization of the skeleton is necessary for proper function as it provides the strength and rigidity required for structural support, protection of internal organs, and movement of the body. Mineralization of the skeleton begins *in utero*, heightens during skeletal development, and is actively maintained throughout life as bone is a highly dynamic organ, continually undergoing remodeling and repair. Calcium and phosphate are two essential elements

that make up the main mineral found in bone, hydroxyapatite ( $\text{Ca}_{10}(\text{PO}_4)_6(\text{OH})_2$ ). These elemental building blocks continually circulate in the blood at near saturating concentrations, establishing an environment ideal for maintaining the integrity of bone. To begin, we will discuss the process of normal bone formation, the key cellular mediators, and highlight the cellular and acellular mediated mechanisms of mineralization. The biological mechanisms responsible for preventing mineralization in adjacent soft tissues will be discussed in further detail beginning in Chapter 2.

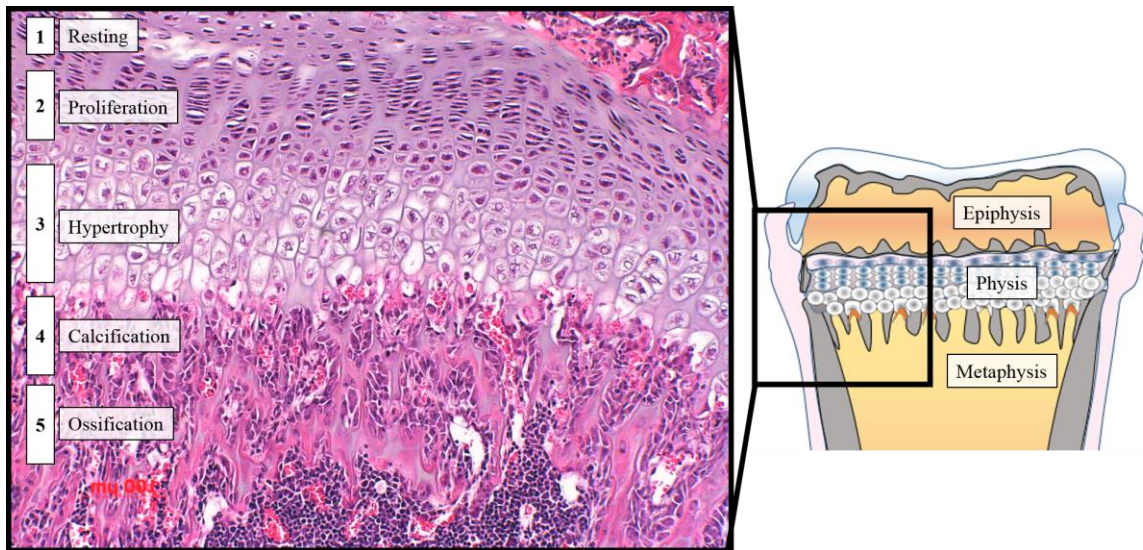
### Bone Formation

Bone is a highly dynamic, vascular organ comprised of both organic (collagen, proteoglycans, and matrix proteins) and inorganic components (mainly hydroxyapatite), with more than 99% of the body's calcium being stored in hydroxyapatite. Formation of bone, either during development or following a bone injury, is a tightly regulated process involving 1) the production of a collagenous extracellular matrix, 2) coordinated intracellular and extracellular mineralization, and 3) vascularization. These events occur in vertebrates through two distinct processes of bone formation: endochondral ossification involving a cartilage precursor or direct intramembranous ossification.

#### *Endochondral Ossification During Bone Development*

At the heart of endochondral ossification lays the chondrocyte- the main cellular component of cartilage. Chondrocytes play an essential role in endochondral bone formation as they secrete collagenous extracellular matrix, assist directly in mineralization, and alter the tissue environment to favor bone formation. The function of chondrocytes within the physis (or growth

plate) relates strongly to their location such that chondrocytes organize and develop through 5 distinct zones: the resting zone, the zone of proliferation, the zone of hypertrophy, the zone of calcification, and the zone of ossification (Figure 1).



**Figure 1: Physeal Biology: Chondrocytes are the Foundation of Endochondral Ossification.**

1) The resting zone is comprised of chondrocytes that serve as the germinal layer of the developing physis, but remain in a relatively quiescent state. In this zone, chondrocytes are irregularly scattered throughout a greater ratio of extracellular matrix to cell volume. Finally, if injured, loss of resting chondrocytes can result in cessation of physis and subsequently inhibited growth. 2) The zone of proliferation is comprised of actively dividing chondrocytes, responsible ultimately for the length of bone developed. Cells in this region possess a flattened appearance and are organized into columns as they progress to the hypertrophic zone. 3) While no active growth occurs in the zone of hypertrophy, chondrocytes actively undergo terminal differentiation, ultimately resulting in cell death and release of the intracellular components (discussed in detail below), two processes necessary for endochondral bone formation. Cells in

the hypertrophy region have an enlarged swollen appearance, making this region the structurally weakest portion of the physis. 4) Following chondrocyte hypertrophy, the contents of the dead cell assist in the formation of provisional calcification, serving as a template for osteoblastic-mediated bone formation in the 5) zone of ossification.

While the majority of bone is highly vascularized, the region of the physis is a relatively hypoxic environment in which chondrocytes thrive. Within the resting and proliferation zones, nutrients are provided by the epiphyseal vasculature, allowing the cells to rapidly divide and produce collagenous extracellular matrix comprised of collagen type II, IX, and XI and proteoglycans. This specialized extracellular matrix possesses ample tensile and shear strength to facilitate compression across the physis[1-3]. Yet, as the chondrocytes progress away from the epiphyseal vascular supply, they enter areas of greater hypoxia where they transition to a hypertrophic state. These hypertrophic chondrocytes are the critical cellular mediators of bone formation, possessing unique phenotypic traits not observed in other populations of immature chondrocytes. As such, hypertrophic chondrocytes produce extracellular matrix comprised on collagen type II and X that will serve as the foundation for provisional mineralization and the subsequent template for osteoblastic bone formation. Furthermore, hypertrophic chondrocytes regulate the surrounding microenvironment to favor calcification described in further detail below.

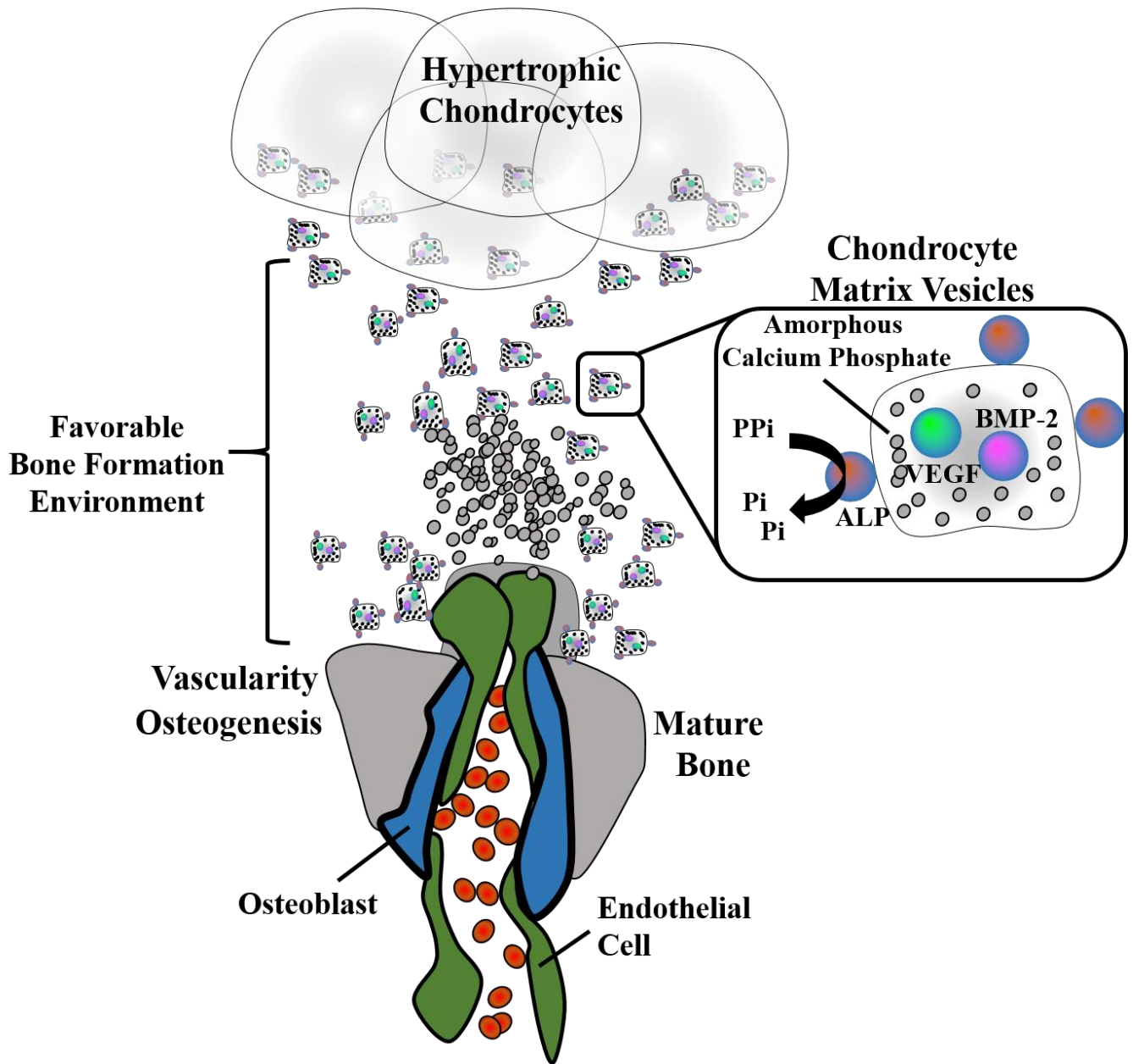
Hypertrophic chondrocytes promote mineralization of the collagenous extracellular matrix using cell-mediated mechanisms through which they package and regulate amorphous calcium and phosphate into matrix vesicles. When exported from the cell, matrix vesicles rupture in the extracellular environment, delivering immature apatite (nanohydroxyapatite) to the collagenous



extracellular matrix where it acts as a nidus for further deposition and maturation of nano-hydroxyapatite. Yet, until recently the origin of the amorphous calcium phosphate residing in the matrix vesicles and the mechanism by which it accumulated was unclear. While previous reports demonstrated that matrix vesicles bud from the plasma membrane and accumulate nano-hydroxyapatite [4], Boonrungsiman *et. al.* demonstrated in 2012 that calcium-phosphate containing vesicles also form intracellularly. Through the use of specialized microscopy, Boonrungsiman *et. al.* established that amorphous calcium phosphate can be stored in the mitochondria as dense granules, transported to intracellular matrix vesicles, and exported to the extracellular matrix where the calcium phosphate is converted to more crystalline nano-hydroxyapatite capable of propagating mineralization [5]. Taken together, these mechanisms of matrix vesicle accumulation of calcium phosphate and formation of nano-hydroxyapatite are a critical step in bone formation.

In addition to packaging amorphous calcium and phosphate into matrix vesicles, hypertrophic chondrocytes simultaneously package proteins for release that modulate the microenvironment to favor mineralization and subsequent ossification [6] (Figure 2). Specifically, hypertrophic chondrocytes produce alkaline phosphatase (ALP), a potent enzyme that cleaves phosphate groups. ALP activity supports mineralization by providing an additional source of inorganic phosphate while simultaneously neutralizing pyrophosphate (PPi), a potent anti-mineralization molecule. In addition to ALP, hypertrophic chondrocytes also produce and package concentrated amounts of vascular endothelial growth factor (VEGF) and bone morphogenic protein 2 (BMP-2), two essential factors that drive vascularity and ossification, respectively. While hypertrophic chondrocytes can survive in areas of relative hypoxia, bone forming cells known as osteoblasts

cannot. For example, if the vascular supply to bone is lost due to injury resulting in the formation of a hypoxic zone, osteoblasts can only survive for approximately 24 hours [7]. To provide oxygen and nutrients to the developing bone, hypertrophic chondrocytes assist in the invasion of the vascular supply by secreting VEGF. Once a vascular supply is established, osteoblasts can enter in association with the vascular supply, thrive, and begin to utilize the provisional zone of calcification established by the hypertrophic chondrocyte as a template for mature bone formation.



**Figure 2: Hypertrophic Chondrocyte-Mediated Mechanisms of Bone Formation.**

Following chondrocyte hypertrophy and release of their intracellular components to establish a favorable bone formation environment, the primary responsibility of bone formation is handed off to the osteoblasts. Within the zone of ossification, osteoblasts utilize the provisional calcification upon the collagen X matrix as a template for osteoblastic bone formation. During this process, the extracellular matrix is remodeled and the majority of collagen X is replaced by

collagen I. Furthermore, upon this new matrix nanohydroxyapatite progressively mineralizes to form mature hydroxyapatite, the main mineral found in bone. Like chondrocytes, osteoblasts have been demonstrated to release matrix vesicle containing both additional nanohydroxyapatite and ALP, to support ossification [8, 9]. While some osteoblasts will remain on the bone surface, others will be surrounded in bony matrix, effectively trapping the cell in a space known as a lacunae [10]. Once encapsulated, osteoblasts become less active and are then referred to as osteocytes. Though trapped, osteocytes maintain communication with surrounding cells through a network of small channels in the bone matrix known as the canaliculi. As bone is a highly dynamic organ, these communication channels are essential during homeostasis to signal remodeling and following an injury to direct bone and nerve regeneration [10].

#### *Intramembranous Ossification During Bone Development*

Intramembranous ossification, like endochondral, is a cellular mediated process of bone formation employed during both skeletal development and regeneration of bone following injury such as a fracture; yet this process does not utilize a chondrocyte intermediate. Rather, intramembranous ossification occurs when mesenchymal stem cells proliferate and differentiate directly into an osteoprogenitor cell. Eventually, these cells develop into osteoblasts, begin to secrete collagenous extracellular matrix, and undergo ossification to form new mature bone.

Intramembranous ossification occurs in regions with little to no strain. While chondrocyte found in endochondral ossification have the ability to resolve strain and protect the newly forming vasculature from disruption, intramembranous bone formation allows for no such buffering capacity. Therefore, intramembranous ossification occurs during development primarily in the flat bones (such as the skull, mandible, and clavicle) or on the subperiosteal surface on long bone

were strain is substantially reduced.

### Bone Resorption and Remodeling

While osteoblasts are the primary cells responsible for bone formation during endochondral and intramembranous ossification, osteoclasts are the antagonists of this process as they are the specialized cell type responsible for bone resorption and remodeling. Osteoclasts are large multinucleated cells localized on the surface of bone, which when activated, utilize enzymes to create an acidic environment to dissolve bony matrix. Given that bone is the primary store of calcium (~99%), in response to hypocalcemia, the process of bone resorption is essential for the release of stored calcium into circulation[9]. Furthermore, bone remodeling allows for the removal of micro-damaged bone to maintain the integrity of the skeleton, yet it is critical that bone remodeling and formation be in balance. Imbalances of these processes can result in skeletal pathologies such as osteoporosis (decreased in bone formation) or osteopetrosis, a genetic condition where bone formation is enhanced, resulting in denser bone which is prone to fractures [11, 12].

### **Application of the Foundations of Bone Biology to Fracture Repair**

Above, I have described in detail the process by which bone is formed during skeletal development. Many of these same processes are likewise utilized to form bone following a fracture injury. Yet, unlike during bone development, in addition to the need to form new bone and vascularity, fractures also create additional problems as they are injuries resulting in the breach of tissue compartments. Specifically, fractures create five principal problems: bleeding,

susceptibility to infection due to a breach in compartments, excessive intramedullary strain at the fracture site, tissue hypoxia, and inability to bear weight. The body's acute phase response (APR) responds to the stimuli generated by the injury (cytokines, hypoxia, uncontrolled strain) by first acting to contain bleeding and infection, and subsequently by synthesizing a temporary stabilization lattice of chondroid soft tissue callus to control strain. Once strain across the fracture site is appropriately controlled, chondrocytes direct vascular ingrowth to restore vascular union and eliminate hypoxia in the injury site. Having reestablished vascular continuity across the fracture site, osteoblasts can now fill in the defect and create an immature hard callus that can bear weight, albeit inefficiently. Finally, the initial hard callus is remodeled based on repetitive load bearing into a structurally and metabolically efficient construct.

Summarized below is our laboratory's unified model of fracture healing. Over the last 100 years, there has been enormous growth in the scientific understanding of fracture healing, including work from our own lab which was fundamental for my understanding foundation into bone biology. Through the following work, I learned not only the fundamentals of bone biology, but applied this knowledge to both fracture repair and spine fusion studies outlined below. Within this chapter, I will cover our recent review article on the unifying models of fracture repair (Article 1), our recent study investigating the impact of intramedullary strain on fracture biology, specifically vascularity (Article 2), illustrate how we can apply fundamental mechanisms of bone formation to promote spinal fusion (Article 3), and finally two retrospective patient studies which highlight the APR (the body's injury response system), and demonstrate how markers can be predictive of serious complications, primarily deep vein thromboses (DVT) (Article 4 & Article 5). Building upon this foundation of physiologic bone formation and the fundamentals of

bone biology, we will next discuss pathologic biomineralization of soft tissue beginning in Chapter 2.

Article 1: The Unifying Theory of Fracture Healing – Clinical and Scientific Implications

Courtney E. Baker, MD<sup>8</sup>, **Stephanie N. Moore-Lotridge, BS<sup>1,4</sup>**, Alexander A. Hysong, BA<sup>5</sup>, Samuel L. Posey, BS<sup>5</sup>, J.Patton Robinette, BS<sup>5</sup>, Deke Blum, BS<sup>5</sup>, Michael A. Benvenuti, MD<sup>1</sup>, Heather A. Cole, MD<sup>1</sup>, Satoru Egawa, MD PhD<sup>1,7</sup>, Masanori Saito, MD PhD<sup>1,7</sup>, Masato Yuasa, MD PhD<sup>1,7</sup>, Atsushi Okawa, MD PhD<sup>7</sup>, Jason McCarthy, PhD<sup>10</sup>, Jeffrey S. Nyman, PhD<sup>1,6,9</sup>, & Jonathan G. Schoenecker, MD PhD<sup>1,2,3,4,\*</sup>

Vanderbilt University Medical Center, <sup>1</sup>Department of Orthopaedics and Rehabilitation, <sup>2</sup>Department of Pathology, Microbiology, and Immunology, and <sup>3</sup>Department of Pediatrics  
Vanderbilt University <sup>4</sup>Department of Pharmacology, <sup>5</sup>School of Medicine, and <sup>6</sup>Department of Biomedical Engineering

Tokyo Medical and Dental University, <sup>7</sup>Department of Orthopaedic Surgery

Mayo Clinic, <sup>8</sup>Department of Orthopaedics

Tennessee Valley Health Care System, <sup>9</sup>Department of Veterans Affairs

<sup>10</sup>Masonic Research Institute

\*To whom correspondence should be directed

Submitted for publication September 2018 in the *Journal of Bone and Mineral Metabolism*

*Significance: The Need for a Complete Understanding of Fracture Healing in Orthopaedics*

Each year, more than 16 million fractures are treated in the United States [13, 14]. Up to 10% of these cases are complicated by delayed- or non-unions, which result in significant patient



morbidity and impose an economic burden to our healthcare system [13, 14]. Critical to addressing this public-health concern is understanding both the clinical interventions and physiological processes involved in bone repair.

Over the last 100 years, there has been enormous growth in the scientific understanding of fracture healing. This has led to advances in clinical practice and technology that have improved patient outcomes. However, with this rapid expansion came a large body of knowledge that has been difficult to synthesize into a modern, comprehensive theory of fracture healing.

The goal of this review is to integrate the most significant advancements in fracture healing and management over the last 100+ years to create a coherent and unified theory of fracture healing. To do so, this review focuses on the primary problems created by a fracture and relates each one of these problems to specific, well recognized, complications. Next, it provides a thorough explanation of the body's biological response to resolve these problems and prevent complications. Finally, it uses what is currently known about the biology of fracture healing to explain when and how clinicians should intervene to improve patient outcomes.

## *Introduction*

### *The Primary Problems Created by Fractures*

Fractures create five primary problems: bleeding, susceptibility to infection, interfragmentary strain, bone hypoxia, and an inability to bear weight (Figure 3). First, bleeding is seen clinically with the ubiquitous fracture hematomas that accompany all fractures. These occur because bone employs an open vascular system, which makes rapid hemostasis a challenge following

disruption. Second, infection is a common concern in fractures as every fracture causes disruption of the body's protective anatomical compartments. In particular, open fractures, which expose bone to the outside environment have a high rate of infection. Third, strain, defined as the change in length of a structure upon loading relative to its overall length when unloaded, is immediately apparent after long bone fractures. Internal and external fixators provide stability to fractures by reducing interfragmentary strain, making strain the most intuitive problem of fracture healing in orthopaedics. Fourth, hypoxia, while less obvious, is of nearly equal importance to stability. A fracture creates both bony and vascular discontinuity—leaving a large area of under perfused, hypoxic tissue. Finally, inability to bear a load is the last problem to be resolved before a fracture is considered healed. In order return to pre-injury function, a bone must not only physically bridge the fracture gap, but also be able to transmit force across it. Ideally, the fractured bone can return to weight bearing without altered joint mechanics.

In order to address these problems, the body activates the Acute Phase Response (APR). The APR is the body's complex hormonal system for surviving injury and repairing itself following any trauma, including a fracture (Figure 3A).

#### *Acute Phase Response—The Heroes*

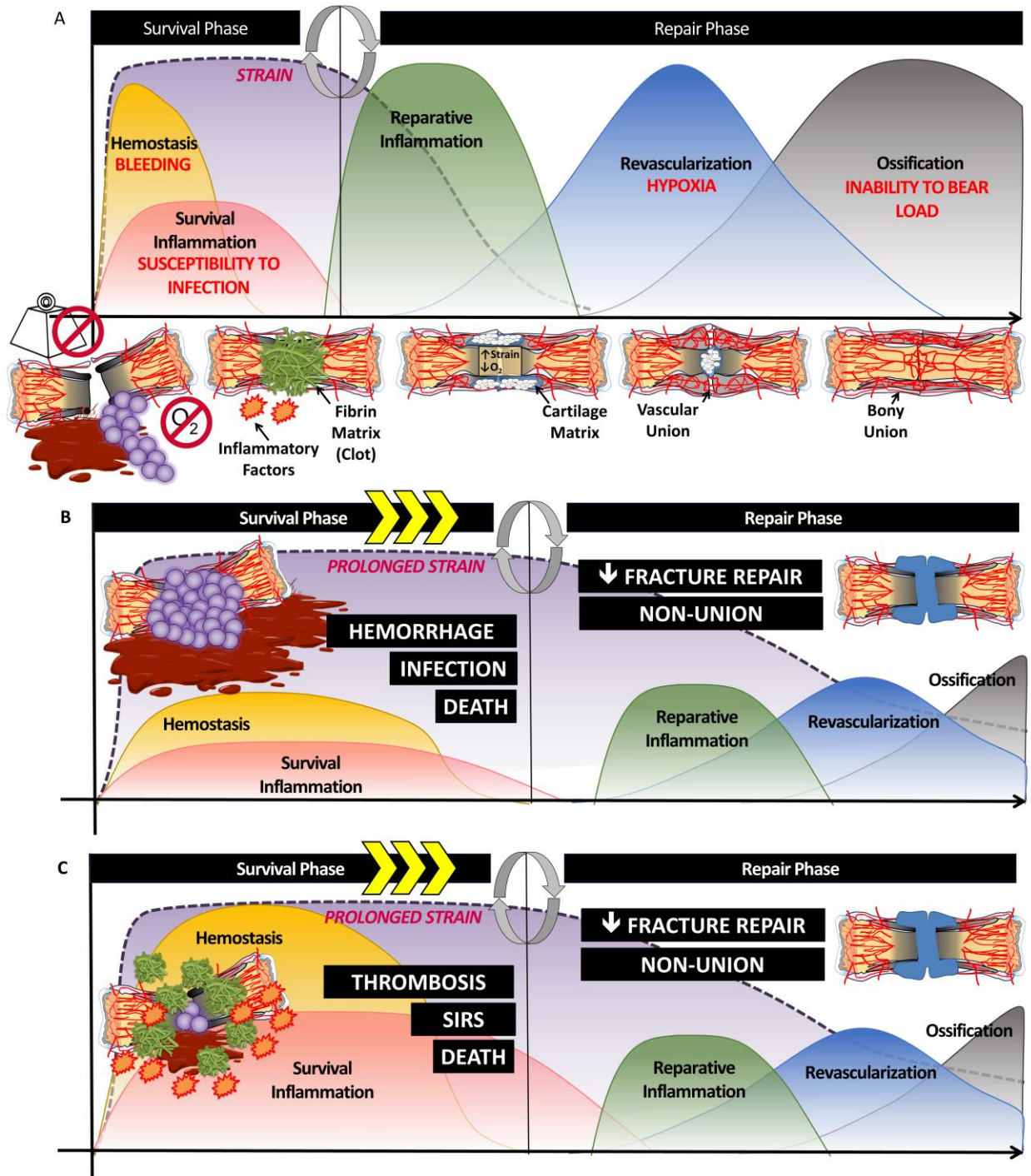
There are many problems and complications that result from fractures, but the body has evolved over millennia to heal broken bones in an orderly fashion, collectively termed the APR. As such, the APR is divided into two distinct phases-- survival and repair.

First, the APR's "survival" phase contains the injury: utilizing coagulation and inflammation to

achieve hemostasis and prevent of infection. These are the most lethal threats of a fracture and must be addressed immediately. Once the body has “survived” these two hurdles, it proceeds to the APR’s “repair” phase, which aims to recreate functional anatomy. The “repair” phase minimizes excessive strain at the fracture site, restores vascular unity, and finally returns the bone to a load-bearing status. Understanding these ordered and distinct “survival” and “repair” phases determines when and how clinicians should intervene.

### *Complications of Fracture Repair—The “Villains”*

Like many biological processes, these five problems are not ends in and of themselves, but rather they are drivers of the APR. If stimulated appropriately, the APR heals a fracture without incident. If the APR is insufficient (Figure 3B) or inappropriately exuberant (Figure 3C), these problems can cause significant complications, or “villains”, of fracture repair: hemorrhage, thrombosis, systemic inflammatory response syndrome (SIRS), infection, death, and/or impaired fracture healing.



**Figure 3: The Body's Response to Fracture Injury: The Acute Phase Response (APR).**

Primary Objective- Save the Day and Prevent the “Villains”. A) Following a fracture, the body must resolve 5 primary problems: bleeding, susceptibility to infection, strain, hypoxia, and inability to bear weight. The APR is the body's response system to injury. The APR regulates

biologic factors in a temporal fashion, first resolving lethal problems such as bleeding and susceptibility to infection, thereby working to preserve life in the “survival” phase. Activation of the coagulation cascade and fibrin deposition at the fracture injury site helps to stop bleeding (hemostasis), and also provides a temporary fibrin sealant to reduce the susceptibility to infection. Once these two survival phase problems have been managed, the APR can transition to the “repair” phase. In this phase, strain is reduced by cellular and acellular factors (ie cartilage matrix). Once strain has been minimized, the fragile new vasculature can begin to extend across the fracture site, reducing bone hypoxia, and leading to vascular union. As vascularity begins, cooperation with cellular and chemical mediators allows for ossification to ensue, leading to bony union and reestablishing the bone’s strength and ability to bear load. B) However, if the APR is insufficient or C) inappropriately exuberant, complications or “villains” arise, such as hemorrhage, infection/sepsis, thrombotic complications such as a deep vein thrombosis (DVT), SIRS, and in severe cases death. In addition, complications that prolong the survival phase will delay the initiation of repair. Delayed reduction of interfragmentary strain, revascularization, and subsequently ossification can result in impaired healing, such as atrophic non-union, fibrous non-union or the development of pseudoarthrosis. Ultimately, these lead to a persistent inability for the bone to bear a load.

Villains of fracture healing occur either in the survival phase (bleeding, thrombosis, SIRS, infection, death) or repair phase (impaired fracture healing) of the APR. Bleeding from a major bone (femur, pelvis, etc.) can quickly lead to vital sign instability due to unchecked hemorrhage. The thigh and lower abdomen are known to accommodate several liters of a patient's blood before tamponade takes effect. This extreme hemorrhage is a significant risk factor for death

from hypovolemic shock. Thrombosis and SIRS are the result of an overstimulated inflammatory response to injury. Any ongoing tissue damage acts as a stimulant for activating the body's inflammatory response. If the scope of injury related to a fracture is not controlled soon after the injury, the systemic inflammatory response may become pathologically uncontrollable. Infection is a predictable complication after any fracture because – a fracture causes previously distinct and well-contained areas in the body to be disrupted, thereby becoming susceptible to contamination and spread of infection from one area to another. This is especially true with open fractures, in which the bone and its rich vascular system are exposed to superficial bacteria. The most common and virulent bone and soft tissue infectious agents have specifically evolved to hijack and attack the musculoskeletal system and its response to infection [15, 16]. Death is very uncommon in most instances but may result from any of the above serious complications: hemorrhage, thrombosis, SIRS, or infection.

As the APR occurs in a sequential manner, complications that prolong the survival phase will inevitably delay the initiation of repair. In addition to problems encountered during the survival APR, impaired fracture healing also is rooted in situations isolated to the repair APR. For example, either too exuberant, or too little, interfragmentary strain interferes with proper endochondral ossification. Excessive, unresolved, interfragmentary strain can prevent vascular and bone union, observed as a hypertrophic non-union. On the other hand, surgeon induced resolution of interfragmentary strain with overly rigid constructs can remove the stimulus for endochondral ossification, observed as an oligotrophic or atrophic non-union. Atrophic non-union also occurs from a paucity of progenitor cells and/or insufficient vascularity. Therefore, it is important to consider that a dysfunctional survival APR, inappropriate interfragmentary strain,

insufficient progenitor cells, and/or impaired revascularization all result in the same pathology-- impaired fracture healing.

In order to resolve problems of fracture healing, the cause of the pathophysiology must first be determined. This requires an extensive understanding of all aspects of the fracture-induced APR. Specifically, impaired fracture healing can result from not only deficient ossification, but also a dysfunctional survival APR, inappropriate interfragmentary strain, insufficient progenitor cells, and/or impaired revascularization. Without a comprehensive understanding of the many the pathologic causes of impaired fracture healing, the cause cannot be identified and the a potentially inappropriate treatment applied. A common example of this is the ubiquitous use of BMP. Ossification is the most common measure of fracture repair given the availability of radiography, leading most surgeons to conclude that the primary problem of impaired fracture healing is a deficiency of ossification. Under this assumption, the application of BMP (with the intent to promote ossification) should resolve the problem. However, fracture healing can halt secondary to other problems at many steps before ossification ever becomes biologically necessary. What is necessary are measurements besides radiography that signal deficiencies critical to the fracture healing process. Such outputs would include direct measures for strain, vascularity, and cellular activity. With a complete understanding in mind and an array of measurements in hand, impaired fracture healing could be addressed through more directed treatment beyond targeting ossification. Interventions such as altering the survival APR, changing the rigidity of fixation, promoting pericyte proliferation, or simulating angiogenesis would become a menu of targeted treatment options to address compromised fracture healing. The purpose of this review is to present a unified model of fracture repair and provide the

stimulus for research development of such clinical tools.

*The Acute Phase Response: Survival Phase- Contain the Injury*

The human body is organized into discrete functional anatomical compartments. When a fracture occurs, the normal architecture and vasculature of the bone, periosteum, and surrounding soft tissue are disrupted, breaching at least three anatomical compartments.[17-19] When the boundaries between these compartments are disrupted, the damaged cells release cytokines which travel to hepatocytes and stimulate thousands of gene transcripts to jump-start the APR. The APR upregulates coagulation, inflammation, tissue repair, and angiogenesis to address the principal problems of injury. The first component of this response is “survival” of the most life-threatening complications of tissue damage: hemorrhage and infection.

Bone is a highly vascular organ receiving roughly 10-15% of the heart’s total cardiac output via a combination of metaphyseal/epiphyseal, diaphyseal, and periosteal arteries. These arteries contribute to the open-sinusoidal vascular network that supplies both the cortical and medullary bone [20, 21]. As such, disruption of these vessels poses a serious bleeding risk. This is seen with the significant internal hemorrhage that often accompanies traumatic pelvic and femur fractures. In fact, several studies estimate that blood loss from an isolated closed femoral shaft fracture can exceed one liter, and a combination of these fractures poses the risk of hypovolemic shock.[22, 23]

In addition to hemorrhage, the disruption of protective tissue barriers (i.e. skin) that occurs secondary to a fracture, puts patients at risk for developing serious and potentially life-



threatening infections. Skin, a major component of the body's innate immune system, is often breached in traumatic long bone fractures. This allows for direct inoculation of the fracture site with bacteria, which greatly increases the risk of infection.[24] Some studies report an infection rate of over 30% following surgically treated open tibial fractures.[25] Even with closed fractures, patients can develop infection through hematogenous seeding. This is because the bacteria that commonly cause orthopaedic infections exhibit tropism for damaged and repairing musculoskeletal tissue.[15] Until an infection is completely eradicated, the body is exposed to a state of continuous tissue damage resulting in hyperinflammation. If severe enough, infection can lead to devastating complications such as thromboembolism, sepsis, disseminated intravascular coagulopathy, and multiple organ failure.[16] Therefore, surgeons take steps such as irrigation, debridement of necrotic tissue, administration of parenteral and local antibiotics, and minimization of soft tissue stripping to reduce the risk of infection.

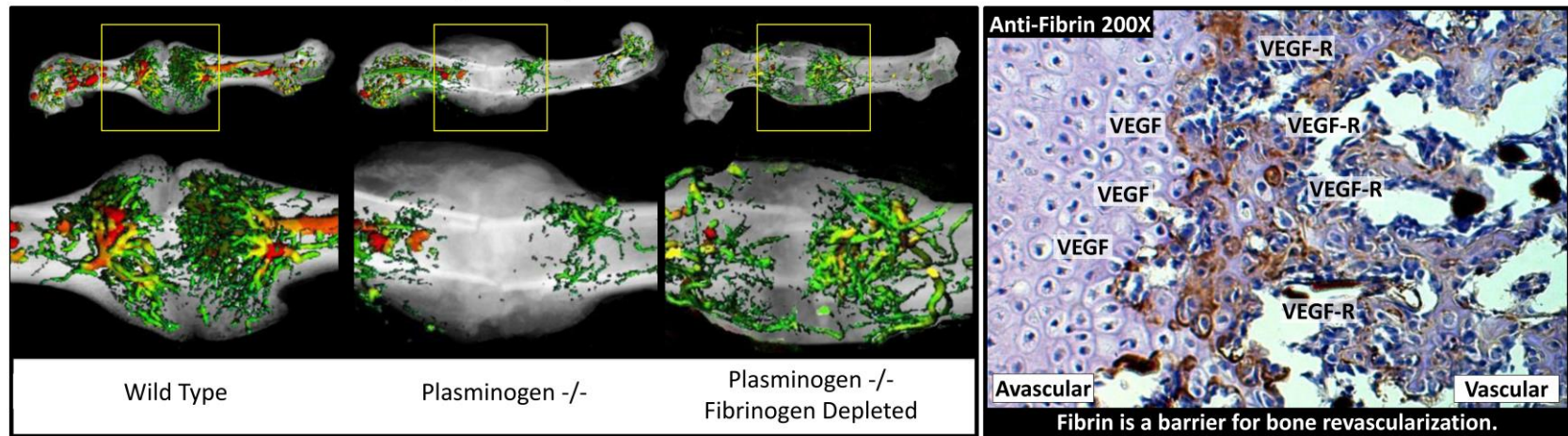
In the setting of a fractured bone, the body's first goal is to achieve hemostasis. Thus, the survival portion of the acute phase response in bone healing begins with reactive contraction of arterioles and activation of coagulation. Activation of the coagulation cascade, secondary to exposure of subendothelial collagen, results in the formation of a platelet and fibrin rich meshwork both intravascularly and extravascularly.[17, 26, 27] This meshwork, more commonly known as the fracture hematoma, acts to resolve bleeding at the fracture site. [28, 29] In addition to providing hemostasis, the fracture hematoma serves to contain and help eliminate potential sources of infection.[15] Specifically, the fibrin itself has been shown to physically trap bacterial pathogens at site of tissue damage, preventing their dissemination.[15, 16, 30] Furthermore, chemotactic factors released from platelets, complement factors, proinflammatory cytokine

release from necrotic tissue, and integrin expression on fibrin itself all act together to attract inflammatory cells to the fracture.[15-17, 31] In the first 24 hours following a fracture, neutrophils are the predominant inflammatory cell that arrive, which further contain and destroy the trapped pathogens.[15-17]

### *Repair Phase- Reconstruct the Bone*

Once the problems of bleeding and susceptibility to infection have been resolved, the APR shifts from “survival” to “repair”. At this time, both the coagulation and inflammatory systems change their functions and act to remove the provisional fibrin matrix and necrotic tissues that comprise the fracture hematoma. This process prepares the bone for vascular invasion and ossification [15-17]. With regards to coagulation, plasminogen is activated into the protease plasmin, which acts to degrade fibrin polymers [29]. With regards to inflammation, the neutrophils that are present in the fracture attract the second wave of inflammatory cells, macrophages [17, 32]. These macrophages consume the necrotic tissue and fibrin split products that are contained within the fracture site. Additionally, macrophages secrete chemotactic factors that promote the recruitment of mesenchymal stem cells and osteoprogenitor cells to the fracture to begin tissue regeneration [17-19]. Failure to effectively remove fibrin from the fracture site can impede angiogenesis, thus preventing the formation of bone (Figure 4) [29, 33]. This exemplifies one central tenet of the APR: in order for proper tissue healing to occur, the body must successfully complete one phase before it can transition to the next [15].

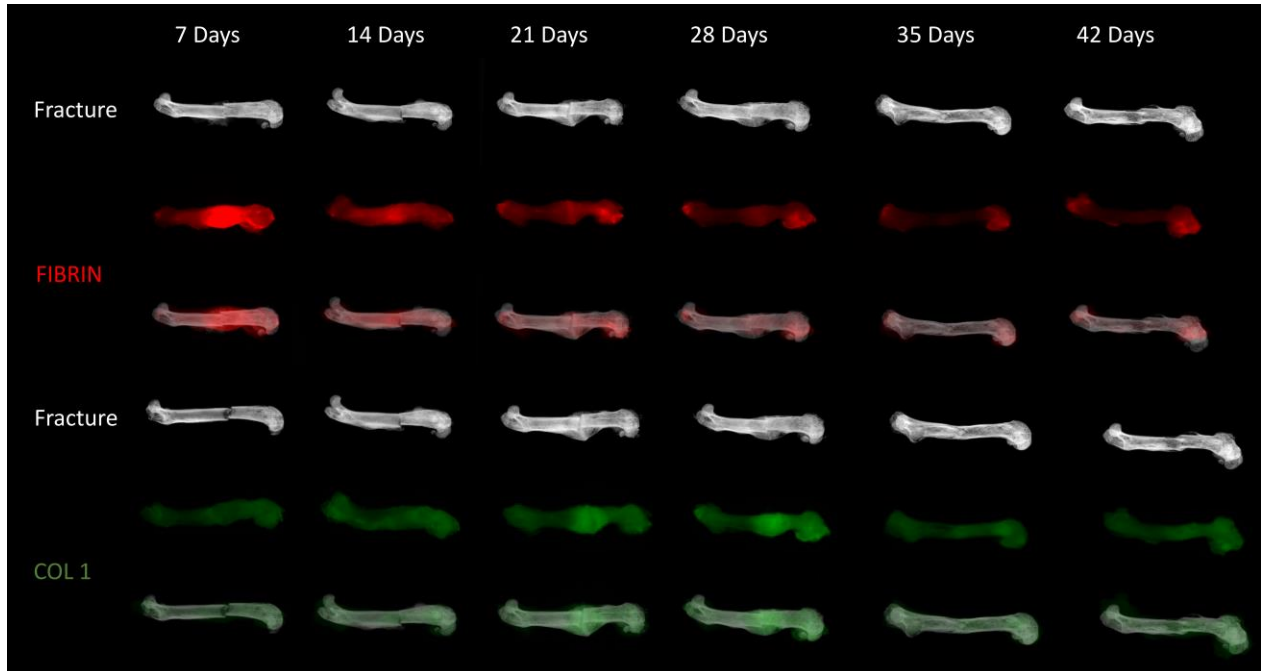
Fracture Vascularity at 14 Days Post Fracture



**Figure 4: Fibrin must be removed following fracture injury for revascularization and subsequent ossification to occur.** Wild type mice exhibit robust vascularity at the fracture site 14 days post fracture. In plasminogen knockout mice, however, fibrin cannot be removed, and angiogenesis is significantly inhibited. Interestingly, when fibrinogen was depleted in plasminogen knockout mice, angiogenesis is largely restored. This demonstrates the importance of plasminogen-mediated fibrinolysis in fracture healing. If present, fibrin acts as a barrier for bone revascularization, preventing VEGF produced by the hypertrophic chondrocytes from effectively reaching the VEGF-R upon the endothelial cells. Because vascularity is not completely restored with fibrinogen depletion, plasmin likely promotes angiogenesis by other means in addition to fibrinolysis.

Next, the fracture site faces the three remaining problems: unresolved strain, hypoxia, and an inability to bear weight. The resolution of each problem occurs in a chronological and co-dependent manner. First, excessive interfragmentary strain is resolved. In most fractures this occurs through the synthesis of a chondroid soft tissue callus. Once strain is reduced to a sufficient degree, the chondrocytes promote vascular growth into the soft callus. Vascularity provides nutrients and osteoprogenitor cells that form bone thus restoring the bone's ability to bear weight (Figure 3A).

In a sense, fracture healing can be considered an evolution of matrices. While the predominant matrix of the survival phase is fibrin, the ultimate goal of repair is to first remove the temporary fibrin matrix, promote vascular invasion, and allow for ossification of collagen 1 (Figure 5). While each of these processes must occur in series, they are not independent of one another, such that the cells that mediate each step are specifically designed to promote the next phase of healing. A thorough understanding of these cells and their respective roles, as discussed next, will ideally help clinicians prevent complications and facilitate timely fracture repair in their patient

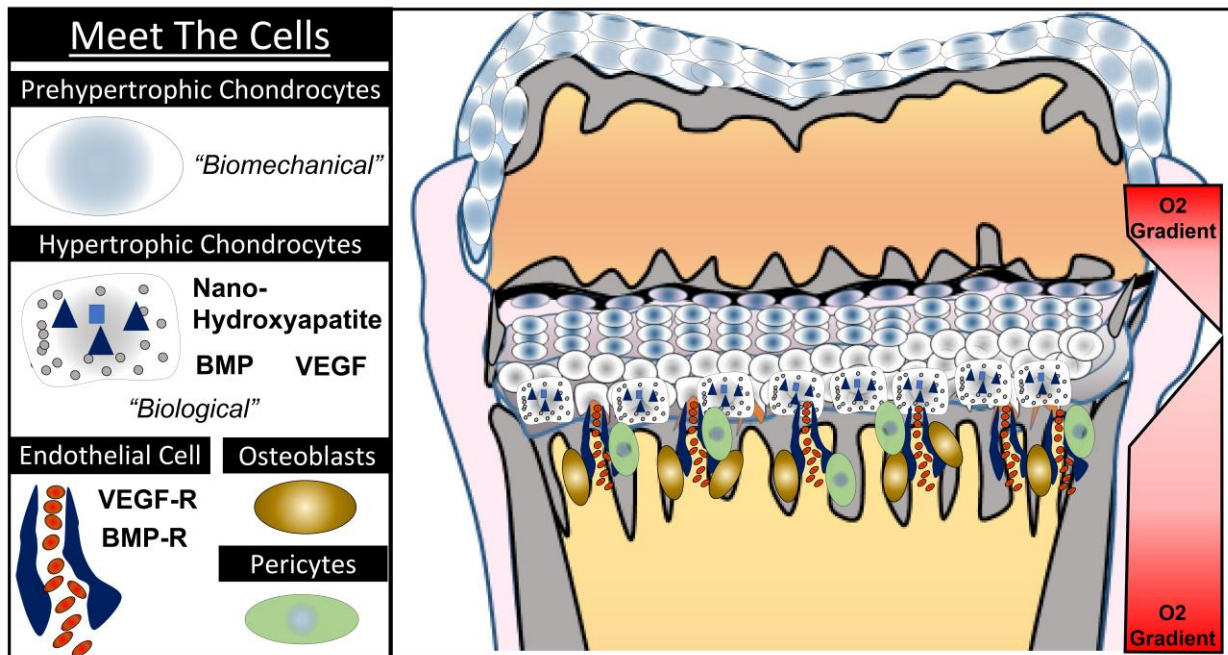


**Figure 5: Visual representation of the evolution of matrices at the fracture site.** Utilizing fluorescently labeled fibrin (red) and collagen 1 (green) targeting probes, the evolution of matrices was assessed in a murine model of a transverse femur fracture with fixation. Here, we observed at 7 days post fracture, abundant fibrin deposition at the fracture site. By 14 days post fracture, the fibrin matrix (red) has begun to be cleared and collagen II and collagen X (not pictured fluorescently) begin to form at the fracture site. By 21 days post fracture, the presence of collagen I (green) is pronounced at the site of fracture healing in the form of hard callus. As remodeling of the hard callus occurs through 42 days post fracture, we observed a decrease in observable collagen 1 signal (green).

#### *Coordinated Teams of Cells in The Repair Phase- Heroes Working Together*

Following removal of the provisional fibrin matrix, the “repair” phase of the APR is characterized by teams of cells that work to address strain, hypoxia and inability to bear weight following a fracture. Depending on the microenvironment of the fracture, these teams of

cells “fix” fractures using intramembranous and/or endochondral ossification, two processes previously described above. [34] As previously discussed, understanding the differences between these processes starts with distinguishing the major cell types at work: pericytes, prehypertrophic chondrocytes, hypertrophic chondrocytes, endothelial cells, osteoblasts, and osteoclasts (Figure 6).

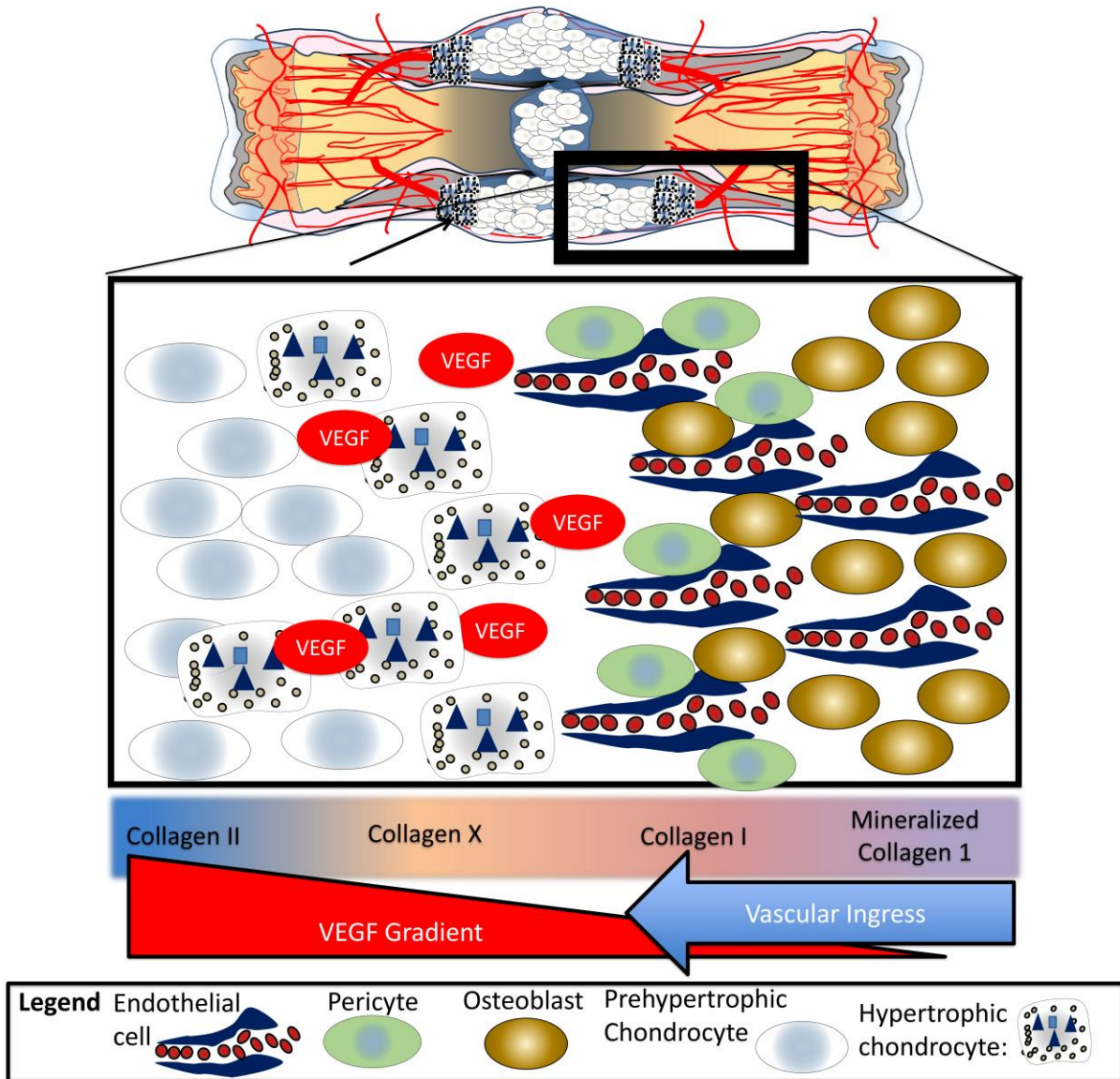


**Figure 6: Meet the Cellular Heroes of Bone Formation.** The cellular heroes of bone formation after a fracture are the same cells that develop bone within the physis. Within the physis (pictured right) prehypertrophic chondrocytes can survive and proliferate in areas of relative hypoxia (low O<sub>2</sub>), where they function to resolve strain and provide cushion at the articular surface. As chondrocytes proliferate and transition to areas of even lower O<sub>2</sub> level, prehypertrophic chondrocytes transition into hypertrophic chondrocytes. These specialized cells do not possess the same capacity to resolve strain as their prehypertrophic counterparts but do produce the building blocks to induce ossification: nanohydroxyapatite, bone morphogenic protein (BMP), and vascular endothelial growth factor (VEGF). Once an endothelial cell comes

into contact with a hypertrophic chondrocyte, the chondrocyte lyses, releasing its contents to the microenvironment, priming the area for further revascularization and subsequent ossification. Pericytes in conjunction with endothelial cells form fenestrated capillaries that bridge the fracture site as it is revascularized. When pericytes come into the microenvironment created by the hypertrophic chondrocytes, they transition into osteoblasts and begin the process of ossification, utilizing the materials provided by the hypertrophic chondrocyte to form new bone.

The pericyte is the “stem cell” that gives rise to much of new tissue required to bridge a fracture. At rest, pericytes form part of the boundary of blood vessels in bone. [35] When a vessel is damaged as a result of fracture, pericytes are activated and begin to proliferate. [36] Once activated, pericytes differentiate into osteoblasts or chondrocytes depending on the local microenvironment. [35] The most significant source of pericytes during fracture healing is the vasculature of the periosteum and endosteum. [37]

Derived from pericytes, chondrocytes are a unique cell, as they thrive in the hypoxic environments and play a critical role in fracture healing by providing both biological and biomechanical properties to support the resolution of strain and subsequent ossification. [38, 39] the differentiation of chondrocytes from mesenchymal stem cells (MSCs) is regulated by both the chemical and mechanical environment, with compressive loading promoting chondrocyte differentiation. [40] Chondrocytes play both biomechanical and biological roles in fracture healing to first resolve strain and subsequently direct vascular ingress into the fracture callus culminating in vascular union of the fracture (Figure 7).



**Figure 7: Cellular Heroes at Work in the Fracture Callus.** Following a fracture, prehypertrophic chondrocytes function to resolve strain by producing a biomechanical matrix composed of cellular and acellular materials, primarily collagen II. Once the prehypertrophic chondrocytes have sufficiently minimized strain, they move away from the intact vascular supply. They begin to hypertrophy, leading to the formation of the hypertrophic chondrocyte, which will provide angiogenic factors to pull in endothelial cells and the raw products to promote ossification with the help of osteoblasts.



The main function of the prehypertrophic chondrocyte is biomechanical. Specifically, they resolve the strain generated within the fracture by producing a shock absorbing matrix. [41, 42] These chondrocytes proliferate in response to strain and create an organized extracellular matrix composed predominately of type II collagen. Cell proliferation and matrix production continues until strain is reduced to a degree that allows fracture healing to progress. [28, 43] Interestingly, these same prehypertrophic chondrocytes are also present in healthy articular cartilage, a physiologically hypoxic environment, where they function similarly to absorb shock at the joint surface (Figure 5). [44]

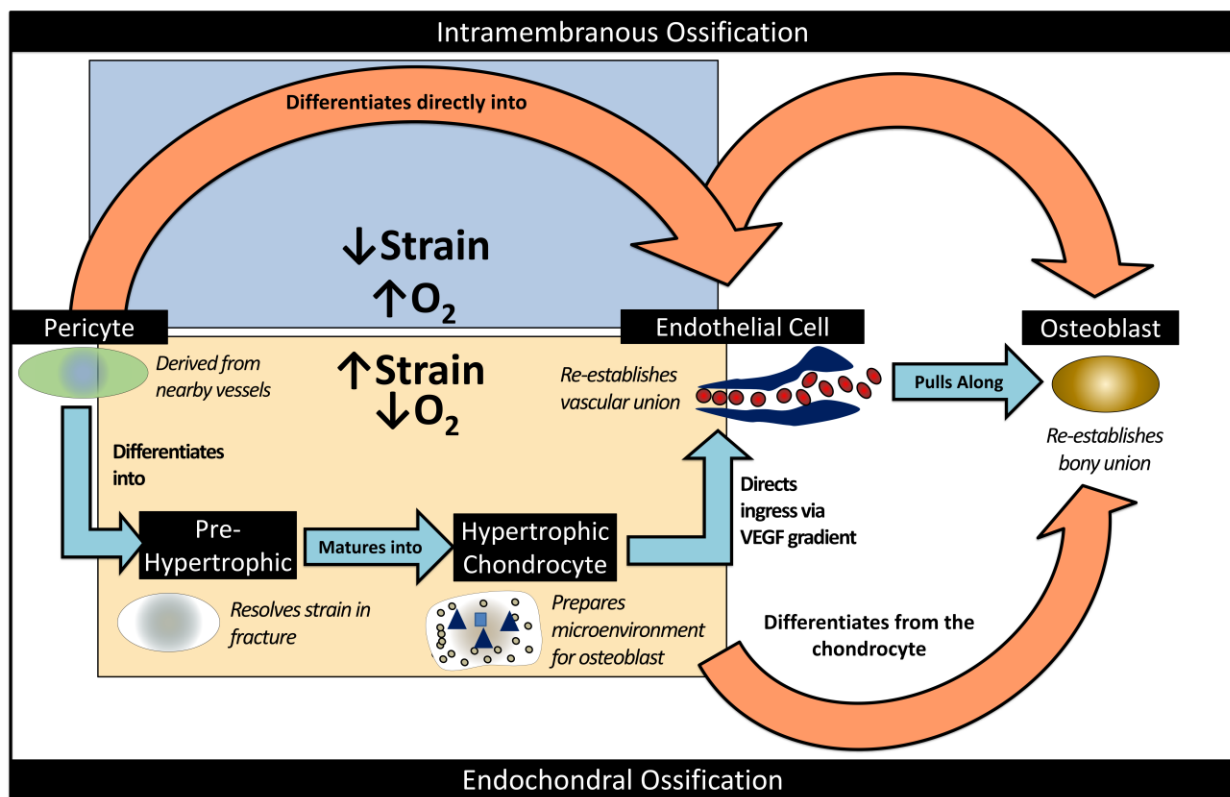
Once prehypertrophic chondrocytes have sufficiently reduced interfragmentary strain they hypertrophy and progress to their second form: the hypertrophic chondrocyte, whose main function is now to promote vascularity and create a supportive environment for osteoblasts. As described above during the process of bone formation at the physes during development, hypertrophic chondrocytes, having created the extracellular matrix to minimize strain are free to produce cytokines, growth factors, and raw products for vascular ingress and bone growth. As described during development, the most recent literature proposes that these cells release microvesicles coated with ALP to counteract PPI, the principle inhibitor of hydroxyapatite formation. These microvesicles are filled with nano-hydroxyapatite, a potent seed crystal for full, micro-hydroxyapatite.[5, 45] Together with type X collagen, these elements promote calcified cartilage, an important precursor of bone. In addition, microvesicles produced by the hypertrophic chondrocytes promote angiogenesis and osteogenesis by carrying concentrated VEGF and BMP-2, respectively (Figure 7) [28, 46].

Endothelial cells manage the transition from chondroid soft tissue callus to a hard tissue callus. Similar to hypertrophic chondrocytes, endothelial cells either found at the physis are those bridging a fracture site, are not suited to withstand excessive amounts of strain. Unlike vasculature found in the rest of the body, they do not possess smooth muscle, and are particularly susceptible to shear stress. Thus, they rely on the biomechanical nature of prehypertrophic chondrocytes to resolve strain prior to their arrival. Once strain is resolved, endothelial cells are drawn into the soft tissue callus by the VEGF produced by the hypertrophic chondrocytes (Figure 7) [47, 48].

Osteoblasts develop from pericytes (i.e. MSCs present in the microenvironment) found in conjunction with endothelial cells as they migrated into the soft tissue callus. Once within a bone forming microenvironment, the pericyte differentiates into an osteoblast, capable of producing collagen 1, hydroxyapatite, BMP and additional VEGF, encouraging further revascularization. [49, 50] The osteoblast advances the ossification initiated by the hypertrophic chondrocyte by promoting the formation and deposition of micro-hydroxyapatite on collagen I. This process continues until the osteoblast has surrounded itself with hydroxyapatite and becomes an osteocyte or undergoes apoptosis.

Decades of histologic evaluation have shown that the appearance of osteoblasts was temporally and spatially associated with the invasion of blood vessels and disappearance of chondrocytes in areas of endochondral ossification. Therefore, it was classically taught that osteoblasts develop from primary pericyte mesenchymal precursors brought in with new vessels to replace the apoptotic chondrocytes [51-53]. Recently, advanced animal models and cell-lineage tracking

methodologies have challenged this theory. Current literature suggests that osteoblasts can also develop directly from chondrocytes through a process of transdifferentiation promoted by endothelial factors [54, 55]. While transdifferentiation is an exciting new concept, it remains consistent with the classic theory that the development of osteoblasts in a fracture is spatially and temporarily predicated on vascular invasion, and reinforces hypoxic signaling and vascularity as essential elements for fracture healing (Figure 8).

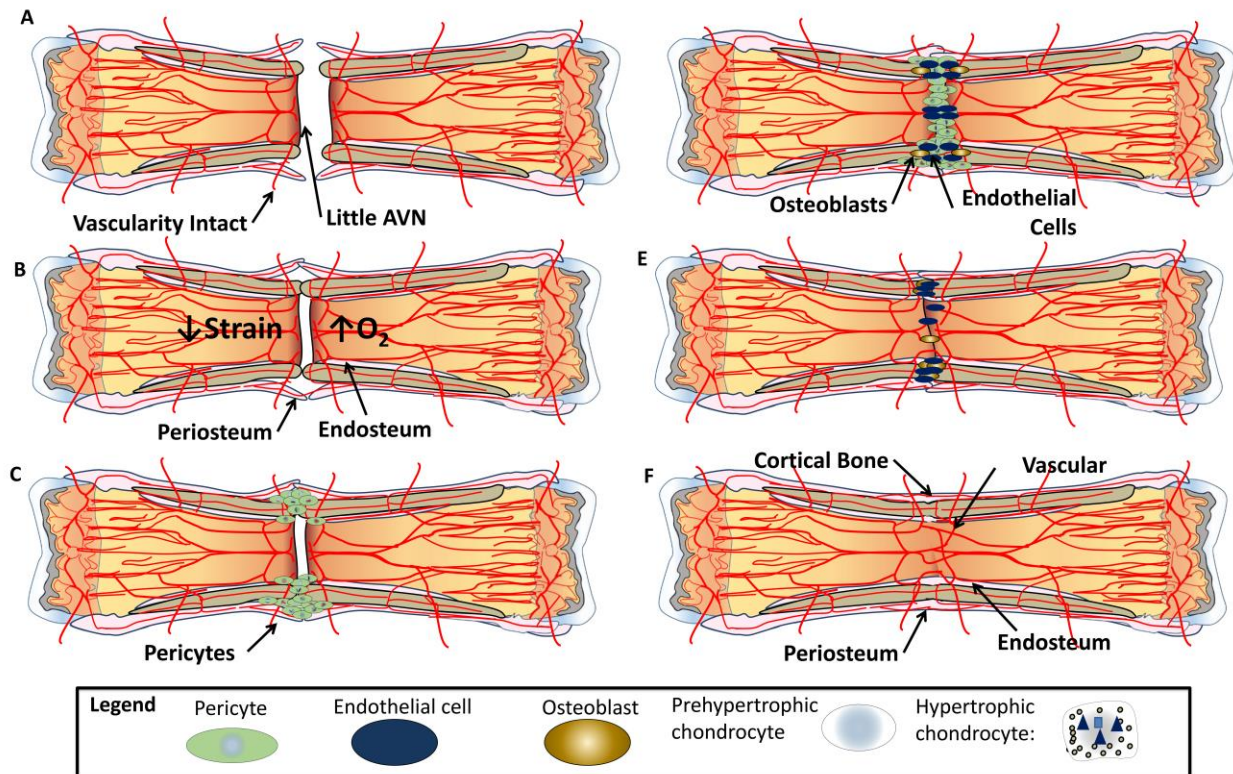


**Figure 8: Origin of the Osteoblast: Transdifferentiation or direct from the pericyte- a matter of strain and hypoxia?** Over the past several decades of fracture research, it has been well described that the appearance of osteoblasts was spatially and temporally associated with newly formed vascularization. This observation aligns with Dr. Arthur Hamm’s observations that osteoblasts, unlike chondrocytes that thrive in areas hypoxia, cannot survive more the 200um

from a vascular supply. Therefore, it has long been taught that osteoblasts develop from pericyte mesenchymal precursors brought in with new vessels to replace the apoptotic chondrocytes. Yet advances in animal models and cell-lineage tracking methodologies have expanded upon this theory and suggest that osteoblasts can also develop directly from chondrocytes through a process of transdifferentiation promoted by endothelial factors. These two proposed theories highlight the importance of vascularity for a healing fracture. The fact that strain and hypoxia can modulate the method of bone formation (either endochondral or intramembranous) suggests that strain and/or the level of hypoxia may also alter the origin of the osteoblast during fracture repair.

*The Ossification Processes—Strain, Vascularity, and the Significance of a Chondrocyte Intermediate*

There are two methods of bone formation: intramembranous and endochondral ossification. Intramembranous ossification (Figure 9) is the formation of bone without a cartilage intermediary and occurs when osteoblasts (derived from pericytes) lay down bone into an existing connective tissue matrix. Endochondral ossification (Figure 10) is bone formation through a cartilage intermediary.



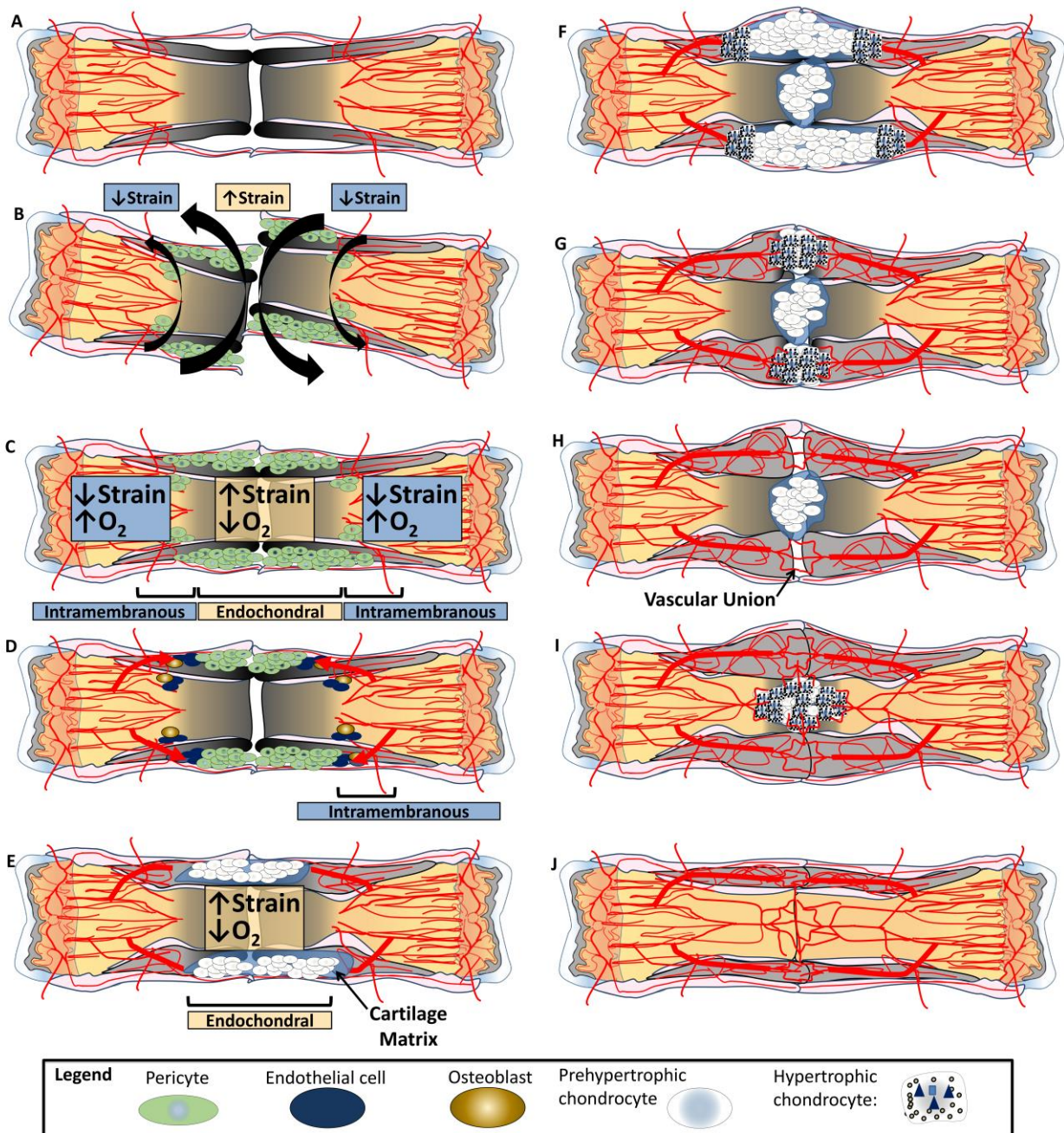
**Figure 9: Intramembranous Ossification in Fracture Healing.** In fractures with (A) intact vascularity, little avascular necrosis, (B) low strain, good oxygenation, and healthy periosteum and endosteum, intramembranous ossification is possible. Through intramembranous ossification, or primary bone healing, (C) pericytes that are capable of invade the fracture site. They are followed by (D) endothelial cells and the pericytes transition into osteoblasts. The osteoblasts (E) gradually achieve bony union that includes (F) union of cortical bone, intramedullary vascularity, periosteum, and endosteum.

As described above, the purpose of the cartilage intermediate is to resolve strain (prehypertrophic chondrocyte) and provide a stimulus for vascular ingrowth and subsequent ossification (hypertrophic chondrocytes). Fractures that have a significant amount of interfragmentary strain

and disruption of vascularity will require some component of endochondral ossification (Figure 10). Fractures that are stable, with limited to no vascular disruption may skip the cartilage intermediate and proceed directly to intramembranous ossification by direct osteoblast infiltration (Figure 9).

Primary bone healing is another name for fracture repair that occurs exclusively by intramembranous ossification. This process requires a setting with intact vascularity near the fracture site and minimal subsequent avascular necrosis. The healthy adjacent periosteum and endosteum provide sufficient levels of oxygenation. Rigid fixation (absolute stability) creates an environment with low strain. In this environment of minimal hypoxia and low strain, pericytes differentiate directly into osteoblasts. [56] These osteoblasts, tethered to the invading endothelial cells, release the components required for ossification (hydroxyapatite, collagen 1, and BMP). Osteoblasts also release VEGF, which acts as a positive feedback loop, promoting further revascularization and ensuring that endothelial cells remain in close proximity. [57, 58] This process mimics the remodeling that occurs in healthy bone (Figure 8 & Figure 9).

Secondary bone healing occurs when a combination of endochondral AND intramembranous ossification is employed to heal a fracture. Generally, these are situations with insufficient vascularity and/or low-to-medium interfragmentary strain. Typically, endochondral ossification is utilized centrally where the osseous deficit and vascular discontinuity exists, and intramembranous ossification occurs at the periphery of the fracture site where vascularity and periosteum remain intact (Figure 10).



**Figure 10: Secondary Bone Repair- Endochondral Ossification in Fracture Healing.** In the majority of fractures, the structural integrity of the bone and the vascular supply to the fracture site are commonly disrupted, leading to (A) hypoxia and the potential for interfracture

motion. Under these conditions, (B) pericytes are drawn to the fracture site and begin the reparative process. Depending on the conditions of strain and oxygen tension that the pericytes are subject to, either (C) intramembranous or endochondral ossification will ensue. (D) At the periphery of the fracture (relatively preserved oxygen supply and low strain) pericytes in close association with the bone's intact blood supply differentiates into osteoblasts and begin the process of intramembranous ossification. Within the center of the fracture site (high strain and low oxygen tension) (E), the pericytes develop into prehypertrophic chondrocytes, which thrive in the hypoxic environment, proliferate in response to strain, and resolve strain by forming a shock-absorbing biomechanical extracellular matrix. When strain is sufficiently resolved, (F) these chondrocytes undergo hypertrophy and become hypertrophic chondrocytes, whose main function is to act as an angiogenesis and osteogenesis machine. (G) Hypertrophic chondrocytes promote vascular invasion and osteogenesis by releasing BMP, VEGF, and hydroxyapatite. (H) Vascular union always precedes bony union in a fracture site as the endothelial cells are necessary for ossification. (I) With bony union of the fracture callus, the fracture is stabilized, and the remaining chondrocytes become hypertrophic. (J) The fracture is now healed and remodeling proceeds as in a healthy bone to make it more biomechanically efficient.

In theory, certain fractures in specific locations (i.e., the pelvis) that are perfectly realigned with rigid fixation may heal entirely from primary bone healing. It is uncommon to observe fracture callus indicative of secondary bone healing after pelvis fracture fixation. At the other end of the spectrum, a fracture with a large defect usually requires a significant cartilage intermediate and will heal almost entirely through endochondral ossification. In reality, the majority of fractures will fall between these ossification extremes and employ a combination of intramembranous and



endochondral ossification. Even in the best approximated fracture, there is an area of avascular necrosis and micromotion which stimulates chondrocyte development resulting in some degree of endochondral ossification. And even in a widely displaced fracture, there will be intramembranous bone forms the hard collar at the periphery of the fracture ends.

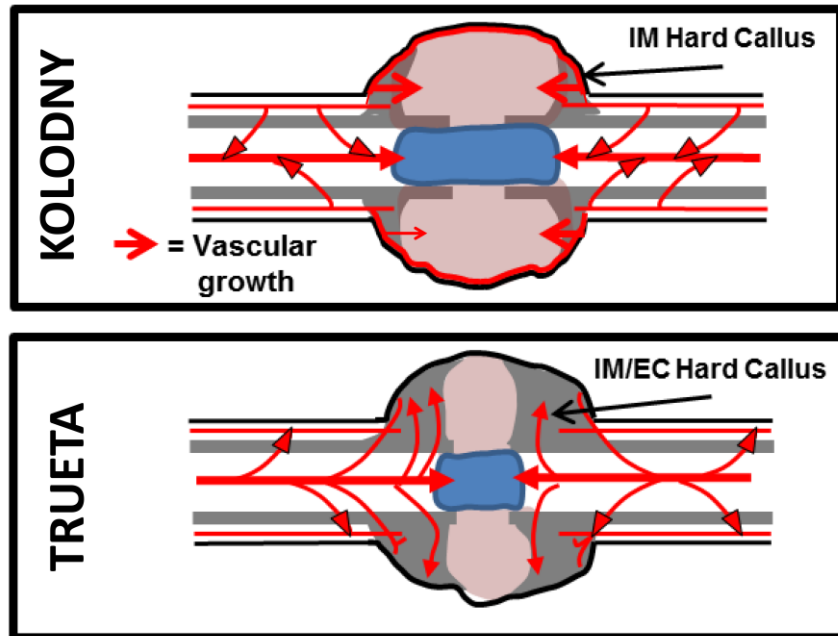
Often, there is inappropriate status given to primary bone healing over secondary bone healing—the belief that in some way achieve minimal strain across a fracture and inducing intramembranous ossification alone is superior to a combination of intramembranous and endochondral ossification. However, it is clear that attempting to force primary bone healing in areas that vascularity cannot support it is not superior, but in fact worse than allowing a soft tissue callus to form, draw vascularity into the fracture site, and then form a hard tissue callus. In normal biology, there is no superiority of primary bone healing over secondary bone healing. They are merely two different tools tailored for different fracture situations. Ideally, an orthopedic construct would harmonize with the type of ossification that is most appropriate to the fracture type.

### *Vascularity in Fracture Healing*

As described above, vascularity is a primary driving force behind both intramembranous and endochondral ossification. Consideration of the disrupted vasculature caused by a fracture is critical, as revascularization precedes bony union. Knowledge of the patterns of revascularization is required to understand how an orthopaedic construct can affect the remaining vascularity during fracture repair.

### *Historical Perspectives on Vascularity*

The revascularization pattern of a healing fracture was debated throughout the 20<sup>th</sup> century by physician-scientists, with particular focus on the relative contribution of periosteal and intramedullary vessels. The first theory was presented by Kolodny in 1923, who suggested the periosteum was the dominant supply of vascularity in fracture healing. [59] This "centripetal model" was challenged by Trueta after his experiments demonstrated the intramedullary blood supply was essential in fracture revascularization—leading to the centrifugal model (Figure 11). [60-63] Resolution of these discordant theories occurred in the 1960s when Rhinelander displayed that revascularization was dependent on the type of fracture model used. [64-66] In non-displaced fractures, the intramedullary vascularity was re-established relatively early, as Trueta claimed, without developing a significant periosteal component. A different pattern, however, was recognized in displaced fractures. After a fracture with significant displacement, even in the setting of subsequent reduction and fixation, revascularization began with new periosteal vasculature (as claimed by Kolodny) and was followed by subsequent intramedullary revascularization. This work was the first to describe how fracture type and fixation method directly affect the pattern of revascularization.



**Figure 11: Historical vascularity models.** The Kolodny model showed that fracture healing depended on periosteal vascularity (arrows demonstrate centripetal vascular growth) leading to intramembranous (IM) ossification. Trueta later showed that that “forcibly nailing a fracture” with a Küntscher nail could disrupt the intramedullary vessels and compromise the cortex. This suggested that development was intra-medullary dominant (arrows demonstrate centrifugal vascular growth) leading to a combination of intramembranous (IM) and endochondral (EC) ossification. Years later, Rhinelander synthesized the two models by demonstrating that in displaced fractures, periosteal revascularization dominates, while in minimally displaced and well approximated fractures, intramedullary revascularization dominates.

### *Applying Physeal Biology to Fracture Healing*

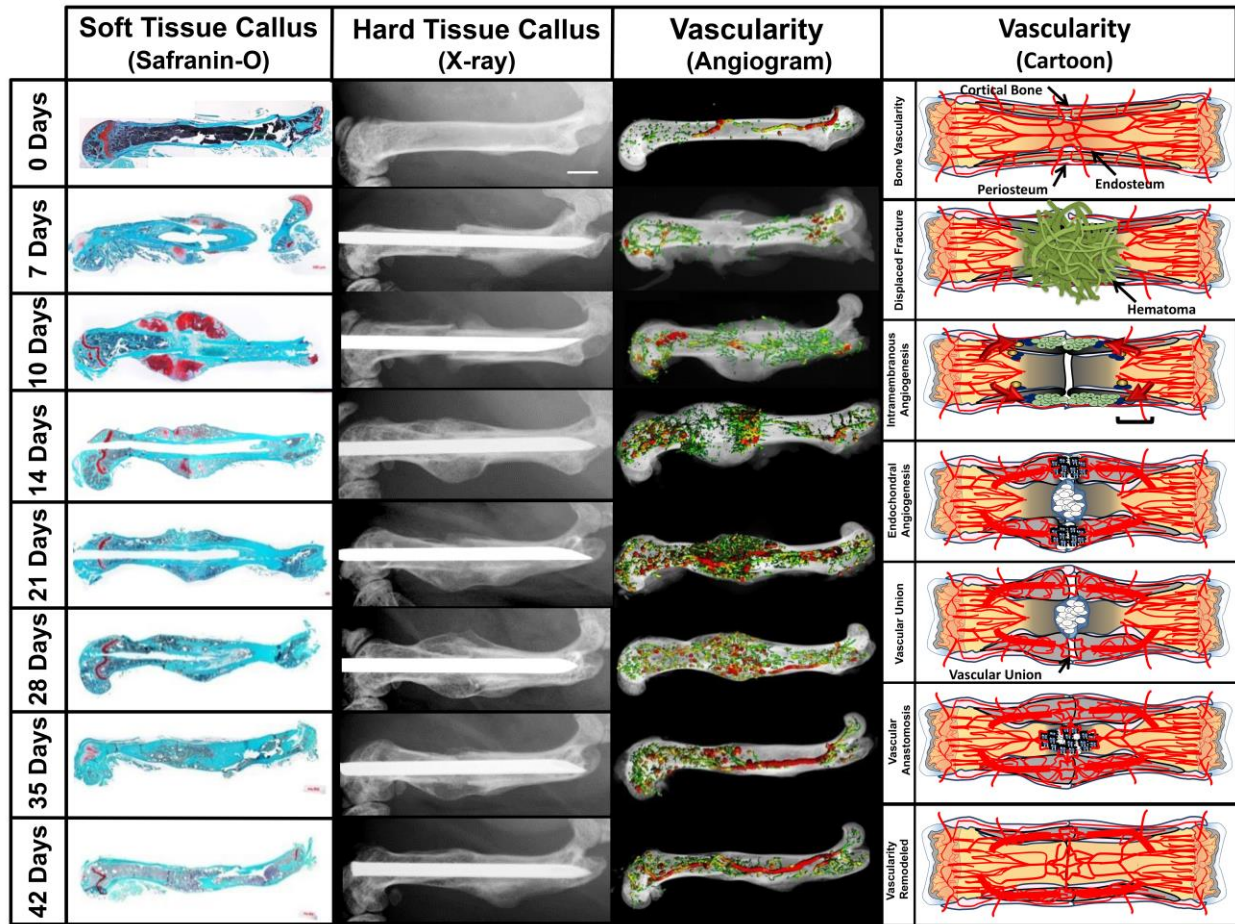
To understand the basic science tenets of vascularity in a healing fracture it is important to be familiar with physeal development highlighted in Figure 5 and prior in Chapter 1. The same biologic machinery that drives growth during physeal development is also employed to heal a

fracture. As a reminder, in the growth plate, chondrocytes proliferate and organize into prodigious columns until they outgrow the diffusion capacity of the epiphyseal blood supply. Hypoxia was shown to promote chondrocytic commitment of mesenchymal cells and cartilaginous matrix synthesis primarily through p38 MAPK pathways. [39] The transcription factor Sox-9 is also critical for the development, early differentiation, and maintenance of columnar proliferation as well as the prevention of osteoblastic differentiation of chondrocytes within a hypoxic environment. [38, 67, 68] Loss of Sox-9 expression leads to early columnar cell growth arrest, prehypertrophy and osteoblastic regulation through upregulation of Runx2, Osx, and Mef2c production and b-catenin signaling. [38]

With modern molecular imaging techniques, Gerber *et. al.* built on this vascular work to show that once chondrocytes become hypertrophic, they release VEGF, an essential stimulant of vascular growth and invasion of the cartilage template. [47] Both endothelial cells and osteoblasts express VEGF receptors 1 and 2 on their surface and are highly responsive to VEGF gradients. [69] Gerber *et. al.* found that without chondrocytic VEGF signaling, metaphyseal blood vessels become disorganized and dilated rather than being organized neatly into parallel chondrocyte columns. The net effect of blocked VEGF signaling is an expanded zone of viable hypertrophic chondrocytes without bone elongation—similar to the results in Trueta's experiments blocking the metaphyseal blood supply. Thus, a chondrocyte-derived VEGF gradient directs endothelial cells into the hypoxic cartilage matrix, drawing with it the osteoblasts, and nutrients necessary for bone formation, while also signaling retirement for the hypertrophic chondrocytes.

Wang *et. al.* further solidified the intimate relationship between osteogenesis and angiogenesis with their work on the hif-1 $\alpha$  transcription protein. [70] Hif-1 $\alpha$  is normally broken down by proteosomal ubiquitination, but in the setting of hypoxia, it is stabilized and resists degradation to stimulate gene transcription. Wang *et. al.* showed that continuous hif-1 $\alpha$  stabilization within osteoblasts during development led to increased bone development with robust vascularity, whereas genetic knockout of hif-1 $\alpha$  led to narrow, less vascularized bone. [70] Hif-1 $\alpha$ 's control of early bone growth was mediated through VEGF signaling and preferentially affected bones that develop through endochondral ossification.

During the entire fracture healing process, the production and resolution of soft tissue callus, hard tissue callus, and vascularity are highly correlated with one another (Figure 12). Specifically, soft tissue callus volume expands rapidly soon after a fracture to promote initial stabilization; however, this matrix diminishes at the same rate that hard tissue callus and blood vessel volume expand. Hard tissue callus and vessel volume expand until union occurs and then they too begin to diminish during the remodeling phase towards pre-injury levels. This dynamic relationship between soft tissue callus, hard tissue callus and vessel growth enables reexamination of fracture x-rays as inferred angiograms, not just evidence of osteogenesis (Figure 13) [28].



**Figure 12: Temporal-spatial fracture repair and angiogenesis.** During the fracture healing process, the production and resolution of soft tissue callus, hard tissue callus, and vascularity are highly correlated with one another. Safranin-O-staining, radiographs, and angiograms of fractured femurs demonstrate the temporal and spatial development of the fracture callus and associated vasculature. Seven days post-fracture (7 DPF), the diaphyseal intramedullary vasculature remains disrupted by regional hematoma, resulting in an avascular femoral segment flanked proximally and distally by intact intramedullary vasculature and shunting blood to the periosteum. Radiographic and histopathologic examination shows formation of a cartilaginous soft tissue callus without evidence of osteoid formation within this avascular zone. The soft tissue callus rapidly enlarges to its maximal size by 10-DPF. Simultaneously, hard tissue callus is

initially formed via intramembranous ossification at the extreme proximal and distal aspects of the fracture site, where the periosteum inserts on unaffected adjacent cortical bone. This process occurs in conjunction with the formation of small highly branching extramedullary vessels recruited by cells in the periosteum expressing VEGFA (10 DPF). As hard tissue callus replaces soft tissue callus (14 DPF), it is accompanied by an expansion of newly formed vasculature. Spatially, the regions of vascular expansion begin at the proximal and distal aspects of the fracture site and migrate centrally toward the soft tissue callus, directed by the ordered release of VEGF by hypertrophic chondrocytes. Vascular ingrowth continues until anastomoses are developed, coinciding with complete dissolution of soft tissue callus and formation of bridging hard tissue callus (21 DPF). Following a vascular anastomosis and bridging of hard callus across the fracture site, the fracture callus remodels back to within the original cortices coinciding with the vasculature returning to larger vessels with reduced branching (28–42 DPF).



**Figure 13: Radiographs depicting a healing femur fracture in a young adult treated with open reduction and internal fixation with plate and screws.** The hardware provides greater stabilization on the ipsilateral side of the fracture. As such, more chondroid soft tissue callus is required on the contralateral fracture side for equivalent stabilization. The lack of motion on the side of the plate coupled with the compression of the periosteum, even with a limited contact plate, prevents callus formation. The hazy soft tissue callus become radiopaque as it is replaced by hard tissue, which is definitive evidence of vascular ingress to the area.

*The Unified Model of Fracture Healing- Summary*

When an initial trauma causes a fracture, there are five principle problems that must be resolved: bleeding, risk of infection, uncontrolled strain, hypoxia and inability to bear weight. The body's APR responds to the stimuli generated by the injury (cytokines, hypoxia, uncontrolled strain) by first acting to contain bleeding and infection, and subsequently by synthesizing a temporary stabilization lattice of chondroid soft tissue callus to control strain. Once strain across the



fracture site is appropriately controlled, chondrocytes direct vascular ingrowth to restore vascular union and eliminate hypoxia in the injury site. Having reestablished vascular continuity across the fracture site, osteoblasts can now fill in the defect and create an immature hard callus that can bear weight, albeit inefficiently. Finally, the initial hard callus is remodeled based on repetitive load bearing into a structurally and metabolically efficient construct.

#### *Applied Fracture Fixation Principles: Considering the Ossification Type*

Besides aiding in hemostasis to prevent hemorrhage and irrigating/debriding fractures to prevent infection, the primary way that orthopaedic surgeons treat fractures is through the modulation of strain with fixation devices. For thousands of years, external fixation was the only method for treating a fracture. External casting was able to reasonably approximate fracture ends, align joints, restore length and alleviate pain. This remains true for external fixators today. Modern internal constructs—intramedullary nails, plates and their various application techniques—allow for a more nuanced approach to fracture fixation. A complete understanding of the “unified theory of fracture healing,” particularly the roles of vascularity and strain, will aid surgeons as they decide on how to best fix each fracture they encounter.

The strain experienced by a fracture is highly dependent on the fracture pattern. The amount and type of strain within a fracture site dictates the cellular fate of mesenchymal progenitor cells at the fracture. If strain is too high (>100%) then there will be no granulation tissue at all as cells cannot survive such distortion [71]. However, at levels below 100% but above 10%, then secondary healing via chondrocytes may be possible [72-74]. Strain of less than 10% permits vascular ingress and the production of woven bone while even less strain (<2%) is necessary for

the direct production of lamellar bone and primary healing.

As knowledge of the physiologic mechanisms and surgical outcomes in fracture healing has increased, so too have the approaches to modulating strain. [75, 76] Numerous studies have been performed examining the effect of strain on fracture healing, including clinical studies, animal model studies, and finite element studies based on rules developed from prior experimental data. The type of strain has an important effect on bone healing. Interfragmentary compression is widely known to promote bony healing. [77-79] However, the timing of the load is important as early compression and excessive compressive forces can inhibit healing.[77] On the other hand, tensile loads are more likely to prevent fracture healing and high tensile loads can even lead to cortical resorption. However, low tensile loads, like other types of strain may actually promote callus formation.[72] The role of shear strain in fracture healing is more controversial. While it is difficult to precisely compare tissue strain across studies, it appears that shear strain in general inhibits bony healing [80, 81], however some studies suggest that low levels of shear strain may be beneficial [82] especially in conjunction with compression. Regardless of the type of strain, increased strain at the fracture site necessitates increased callus size to stabilize the fracture and enable bony healing as discussed above. Studies employing fixation with less rigidity have shown that both a larger soft and hard tissue callus is the end result. [83]

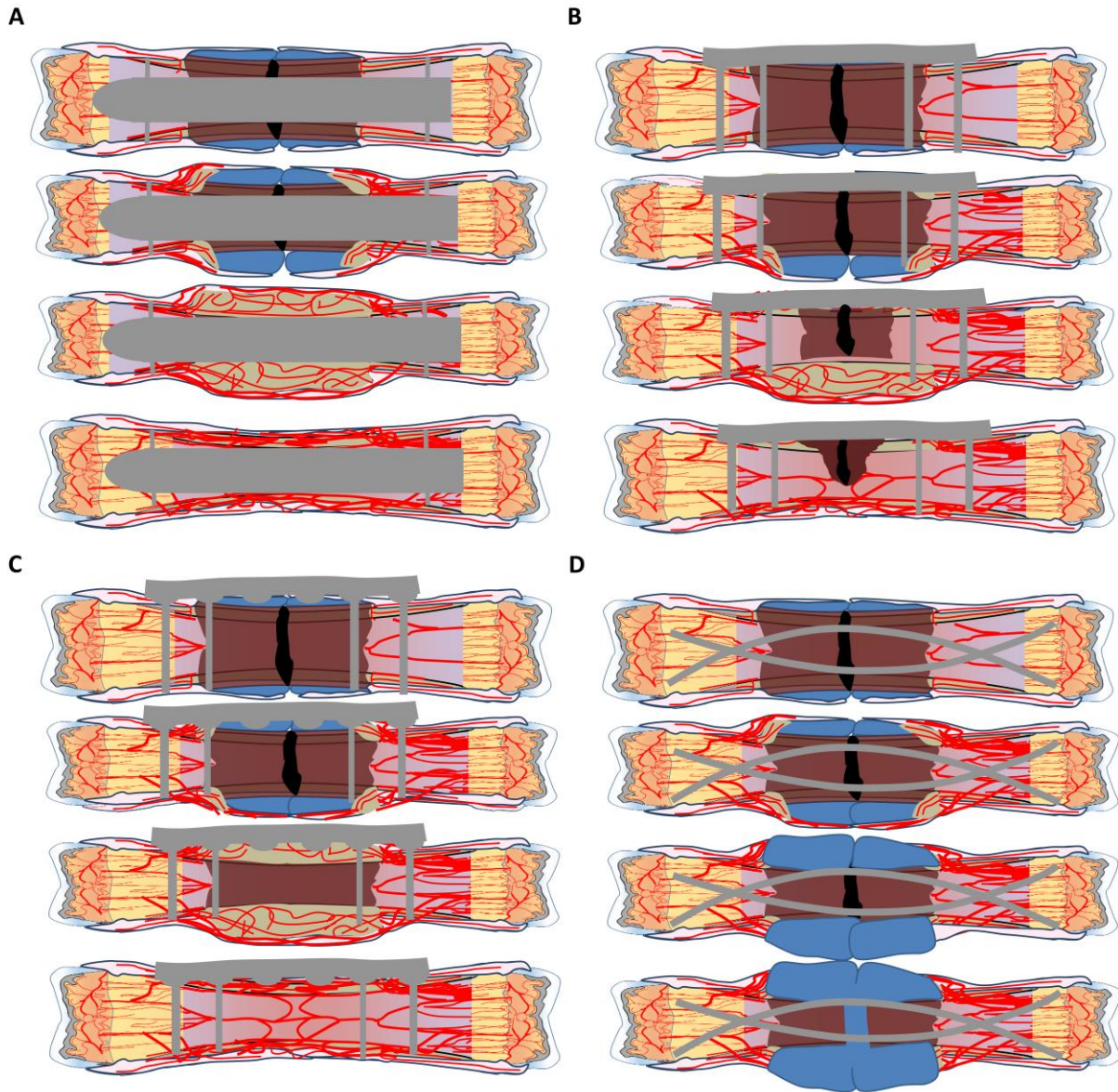
As reviewed earlier, where primary bone healing is desired, a surgeon may plate with the goal of absolute stability. This can be accomplished by using plates and screws in a manner that generates compression across the fracture site, minimizing strain. Fractures fixed in this way heal through intramembranous ossification in the absence of a chondrocyte-derived callus, as the

drivers of endochondral ossification (strain and avascular segments) are not present. Technical pearls, like bending a plate before application to generate compression across the far cortex, are used to further promote primary bone healing across the fracture site.

On the other hand, there are settings where absolute stability and primary bone healing are not feasible or desired. Specifically, absolute stability increases the risk of nonunion if i) reduction is not achieved ii) the fracture has significant avascular segments or iii) the application of the plate creates significant avascularity. [74, 84] These three situations require endochondral ossification which is stimulated primarily by strain. Therefore, rigid plate fixation should be avoided in these situations.

Ideally, a surgeon would have measures of strain and vascularity to help determine if absolute stability is possible. However, this technology is not available and therefore the determination must be predicated by other factors. Severe comminution, extensive soft tissue injury, or a fracture in poorly vascularized regions of bone, commonly renders a fracture healing environment hypoxic regardless of fixation method. In these cases, one or both of the requirements for primary bone healing (low strain and high vascularity) are absent. In such instances, a surgeon can still promote successful bony union by creating an optimal environment for secondary ossification (i.e. an environment that promotes chondrocyte differentiation). Understanding how to create this environment through the thoughtful application of implants is critical in fracture care. For example, Perren described the concept of ‘biological plating’ where surgeons use internal plates to bridge segments of comminuted bone instead of attempting perfect reduction. In this way he decreased rigidity across the fracture site permitting increased

micromotion and promoting chondrocyte development and callus formation. [85] Importantly, while soft tissue callus forms in response to strain, motion that exceeds the stabilizing ability of the callus will not allow prehypertrophic chondrocytes to develop into hypertrophic chondrocytes, thus preventing eventual vascular and bony union. Conversely, overly rigid fracture fixation in this hypoxic setting will not provide enough stimulus for pericytes to differentiate, which can prevent callus formation entirely and delay bone healing (Figure 14). [86] Thus both overly rigid and exceedingly flexible constructs can lead to nonunion. [87]



**Figure 14: Fracture Fixation Methods.** A) Intramedullary nailing disrupts the medullary vasculature yet leaves periosteal vessels intact. It also provides slightly flexible fixation, promoting chondrocyte proliferation. This combination enables robust callus formation that is highly vascular. B) Plate and screw fixation of fractures provides rigid fixation, limiting callus formation and causing little disruption of the intramedullary vasculature. However, the compression of the plate against bone disrupts extramedullary vasculature and can cause hypoxia

under the plate. C) Limited contact plating aims to provide rigid fixation, leaving remaining intramedullary vasculature intact while also causing as little disruption of extramedullary vasculature as possible. This theoretically enables improved fracture healing with limited callus formation compared to full contact plating. D) When fixation is inadequate, as is often the case of flexible nailing of an adult fracture, chondrocytes proliferate to try to reduce the strain that has not been adequately treated. However, the strain and motion may be too great for the chondrocytes to stabilize, preventing chondrocyte hypertrophy and bony union, leading to pseudarthrosis.

### *Plating*

When plating, close attention must be paid to preserving the vascularized soft tissues and periosteum at the level of the fracture. Preserving the periosteum, a source of stem cells and growth factors for fracture healing, is a critical technical consideration. Preserving the periosteum allows surgeons to limit avascularity and to preserve an important mediator of subsequent revascularization. [88-90] These concepts have been instrumental in implant development, and modern plates reflect this focus on respecting the soft tissues and periosteum. Limited contact plates employ reefing to preserve underlying periosteum, with bony contact occurring only in the area surrounding screw holes. [91] Percutaneous plating systems, such as the Less Invasive Stabilization System (LISS), have been designed to limit dissection to only what is needed for plate application, thus maximally preserving the vascularity to the tissue surrounding a fracture. [92] A number of other implants have been developed with this aim, and all emphasize the importance of preserving vascularity and soft tissues while providing appropriate stability (Figure 14).

### *Intramedullary Nailing*

Intramedullary nailing is an effective treatment for many diaphyseal fractures and promotes many of the previously discussed elements of fracture healing. Nails are often used as load-sharing devices that provide relative, as opposed to absolute, stability. Permitting micromotion within the fracture encourages chondrocyte development and subsequent endochondral ossification. Additionally, nailing prevents iatrogenic devitalization of the periosteum near the fracture.

However, the effect of reaming on a bone's vascularity is an important consideration when inserting an intramedullary nail. While reaming is done at a cost to the endosteum, this deleterious effect is limited and compensated for by the periosteal blood supply. Cortical ischemia and necrosis caused by reaming is followed by both reconstitution of the medullary blood supply and reversal of the centripetal flow to centrifugal from the intact periosteum. Understanding this relationship is important, because an insult to both the endosteal and periosteal blood supply (e.g., open reduction and nailing), would be expected to cause a more significant vascular insult at the level of the fracture and a commensurate increase in the time to revascularization and bony union. Similarly, a larger diameter nail made possible with reaming is more rigid and improves stability, but may devitalize more cortical bone and prolong the regeneration of the medullary blood supply. [93] One must balance the need for stability with devitalization of a bone's vasculature when choosing the size of an intramedullary nail.

Numerous clinical studies have attempted to optimize fracture healing through modification of one or more of the parameters that impact the stability and initial soft tissue insult of a nail

construct (nail size, locking, nail composition, or pre-reaming) with varying results. [94-101] It is the authors' opinion that the ideal nail, here termed the "biological nail," is likely a dynamic one where stability can be altered during the course of a fracture healing to promote each desired biological process of healing. For example, it could permit relatively more micromotion during the development of the soft tissue callus thus bolstering mesenchymal cell differentiation into prehypertrophic chondrocytes. [17-19] Once sufficient soft callus has formed, increasing the nail's stability would allow for the large number of chondrocytes to hypertrophy, release VEGF, and promote robust vascular ingress and subsequent ossification. As an example, one study created rudimentary "biological nails" by using sequential magnetic compression of the nail to heal humerus fractures at risk for non-union. The study reported excellent rates of healing all with the formation of large fracture calluses.[101] While studies like these are promising, further research and innovation is required to determine which mode of dynamization best supports the biomechanical and biological needs of every fracture.

### *Conclusions*

Despite advances in orthopaedic care, fractures remain an important public health concern with frequent and serious consequences. With this review of fracture healing, we emphasize the five problems that accompany every fracture (bleeding, susceptibility to infection, strain, hypoxia, and inability to bear weight), their associated complications, and the body's stepwise approach to resolve them (the APR). To do so, we synthesized both the modern and historic scientific discoveries and put forth a unified, rule based, working model of fracture repair with two goals in mind.



Goal 1: First, this model provides scientists with essential variables to control or monitor—matrix production, cellular activity, strain, and vascularity—in any basic or translational science endeavor exploring fracture repair. Ideally, monitoring of these variables in the lab would translate into menu of clinical tools that can be applied in the OR and the recovery process to monitor fracture repair and dictate when and how to intervene. Gone are the days of a “silver bullet” solution for all impaired fracture healing. Future discovery can be used to expand upon and improve our working model while simultaneously developing novel methods to treat fractures.

Goal 2: Second, this model informs clinicians of the essential principles for fracture management. Specifically, fracture repair is a chronological process, and appropriate healing requires resolution of one step before transitioning to the next. The insertion of any orthopaedic construct has both immediate and long-term biological consequences, and these consequences are directly related to the construct’s biomechanical properties. Thus, in order to improve patient outcomes, surgeons must select interventions that promote the appropriate ossification processes for fracture healing, resisting the urge to go for rigid compression of every fracture.

Hopefully, innovative efforts will lead to the development of devices capable of creating the perfect biological and biomechanical environment for every fracture. Maybe one day, even in the most severe of cases, perfect fracture healing will become an expectation.

Paralleling this comprehensive review of the basics of bone biology and fracture repair, I have also participated in numerous studies in the laboratory aimed at defining the mechanism of

fracture repair utilizing small animals models as previously discussed. An essential component to consider when assessing a healing fracture is the intramedullary strain. Strain must be considered on a biological level as it dictates the form of bone formation to take place (intramembranous vs endochondral ossification), yet also by orthopaedic surgeons at an application levels as too little or too much strain implemented by a fixation device can negatively impact patient morbidity and fracture site repair.

Through this next article, we investigated on a biological level how altering the intramedullary strain of a transverse femur fracture can impact fracture biology, primary fracture revascularization and union. To modulate the intramedullary strain, we fixed the transverse femur fracture with two varying gauges of pins that allow for varying degrees of displacement. Through this work, I expanded my knowledge on the biomechanical properties of fracture repair, the impact of strain on fracture healing and bone biology, and expanded my thinking to future investigations aimed at identifying the ideal intramedullary fixation device for promoting fracture healing and revascularization. My future goals are discussed in detail in Chapter 4.

Article 2: The Size of Intramedullary Device Affects Endochondral Mediated Angiogenesis  
During Fracture Repair

Masato Yuasa MD, PhD<sup>a,b</sup>, Masanori Saito MD<sup>a,b</sup>, Deke M. Blum BS<sup>h</sup>, Alexander A. Hysong BA<sup>h</sup>, Satoru Egawa, MD<sup>a,b</sup>, Sasidhar Uppuganti, MS<sup>a</sup>, Toshitaka Yoshii MD, PhD<sup>b</sup>, Atsushi Okawa, MD, PhD<sup>b</sup>, Herbert S. Schwartz MD<sup>a</sup>, Stephanie N. Moore-Lotridge BS<sup>a,g</sup>, Jeffrey S. Nyman PhD<sup>a,c,d,e</sup>, and Jonathan G. Schoenecker MD, PhD<sup>a,f,g,i\*</sup>

<sup>a</sup>Department of Orthopaedics and Rehabilitation, Vanderbilt University Medical Center.

<sup>b</sup>Department of Orthopaedic Surgery, Tokyo Medical and Dental University

<sup>c</sup>Department of Biomedical Engineering, Vanderbilt University

<sup>d</sup>Center for Bone Biology, Vanderbilt University Medical Center

<sup>e</sup>Department of Veterans Affairs, Tennessee Valley Health Care System

<sup>f</sup>Department of Pathology, Microbiology, and Immunology, Vanderbilt University Medical Center.

<sup>g</sup>Department of Pharmacology, Vanderbilt University

<sup>h</sup>Vanderbilt University School of Medicine

<sup>i</sup>Department of Pediatrics, Vanderbilt University Medical Center

\*To whom correspondence should be directed

*Submitted September 2018 to the Journal of Orthopaedic Trauma for Publication*

## *Abstract*

### *Objectives*

Formerly considered only for their biomechanical properties, intramedullary nails are now understood to have important biological consequences during fracture healing, namely the presence and size of a fracture callus. Determining the ideal nail to promote union mandates a comprehensive understanding of the relationship between biomechanics and fracture biology. The purpose of this study was to explore the effect of intramedullary pin size on the biology of a healing fracture, specifically endochondral angiogenesis. We hypothesized that fracture fixation with a smaller pin would permit greater interfragmentary strain resulting in the formation of a larger fracture callus, increased the total amount of VEGF within the callus, and greater angiogenesis compared to fixation with a larger pin.

### *Methods*

Transverse mid-shaft femur fractures in 8-week old mice were fixed with either a 23 gauge (G) or 30G pin. Differences in interfragmentary strain at the fracture site were estimated between cohorts. A combination of histology, gene expression, serial radiography, and micro-computed tomography with and without vascular contrast agent were utilized to assess fracture healing and vascularity for each cohort.

### *Results*

Larger soft tissue callus formation, increased VEGF-A expression, and a corresponding increase in vascular volume was observed in the higher strain, 30G cohort. Radiographic analysis demonstrated earlier hard callus formation with greater initial interfragmentary strain, similar

rates of union between pin size cohorts, yet delayed callus remodeling in mice with the larger pin size.

### *Conclusions*

These findings suggest that the stability conferred by an intramedullary nail influences endochondral angiogenesis at the fracture.

### *Introduction*

Approximately 18 million fractures occur annually in the United States, and up to 1.8 million of these fractures are complicated by delayed or non-union. [102-104] Morbidity associated with these complications is common and includes prolonged pain, functional disability, extended hospital stays, and reoperation. [104] Additionally, medical costs of non-unions are substantial. For example, the direct cost of one tibial non-union can reach up to \$25,000. [105] Vascularity is a pre-request for fracture healing and as such insufficient vascularity is a primary cause of delayed or non-unions, with the rate of impaired healing as high as 46% in patients who have concomitant vascular injuries. [29, 106, 107] Thus, developing interventions that optimize fracture healing are imperative in orthopaedics.

Formerly, intramedullary nails were strictly considered for their biomechanical properties and surgeons sought to insert nails that would provide the most stability and thus lowest strain to permit early mobilization. [108] More recently, it is understood that the stability of any fixation construct has important biological consequences, namely the presence and size of a fracture callus. [109-112] Studies assessing the four major parameters that govern intramedullary nail

stability (size of the nail, composition of the nail, locking of the nail, and pre-reaming of the canal prior to nail insertion) have been conducted to elucidate a construct that optimizes union. Understandably, there have been variable results. [101, 108, 113-116] Determining the ideal nail to promote union mandates a comprehensive understanding of the relationship between biomechanics and biology in fracture healing.

When a fracture occurs, the architecture and vasculature of the bone, periosteum, and surrounding soft tissues are disrupted, resulting in interfragmentary strain and hypoxia. [112, 117] In displaced fractures with disrupted vasculature, resolution of interfragmentary strain and hypoxia occurs predominantly through endochondral processes, mediated by chondrocytes. [28, 118, 119] As the strain is reduced by the biomechanical function of the soft tissue callus, the chondrocytes hypertrophy. [28, 118-121] Hypertrophic chondrocytes assume a biological, as opposed to biomechanical function, to synthesize angiogenic factors, like vascular endothelial growth factor (VEGF), that are essential for stimulating the growth of vasculature into the cartilaginous callus. [28, 120, 121] Previous studies have established that the total amount of soft tissue callus formed is inversely proportional to the amount of interfragmentary strain at the fracture site. [43, 110-112] There have been few studies examining if the increased chondrogenesis in less stabilized fractures also causes a proportional increase in VEGF and endochondral angiogenesis during healing.

The purpose of this study was to modulate fracture stability conferred by an intramedullary device through altering one parameter (pin size) to further examine the impact of strain on the biology of fracture healing, specifically endochondral angiogenesis. Beyond recapitulating prior

studies, we hypothesized that greater initial interfragmentary strain would lead to a subsequent increase total VEGF-A expression and subsequently increased endochondral angiogenesis at the fracture site. To test this hypothesis, we utilized two pins of varying gauges (30G and 23G) in a femur fracture model and assessed fracture repair longitudinally.

## *Materials & Methods*

### *Murine Femur Fracture Model*

All animal procedures were approved by the Institutional Animal Care and Use Committee (IACUC) at Vanderbilt University Medical Center (M1600231). Following adequate anesthesia, a transverse mid-shaft femur fracture was made in the right femur at the mid diaphysis of 8-week-old, male, C57BL/6J mice (Jackson Laboratory, Bar Harbor, Maine) as previously described<sup>7</sup>. Transversely fractured femurs were pre-reamed with a 25G needle before either a 23G pin (0.6414 mm) or 30G pin (0.3112 mm) was inserted. A sub set of mice from each experimental group were sacrificed at 10 DPF (n=5 (23G), n=6 (30G)), 14 (n=11 (23G), n=15 (30G)) and 42 DPF (n=13 (23G), n=10 (30G)) to quantify soft tissue callus formation and composition, fracture vascularity, and fracture union. Pins were obtained from Becton, Dickinson and Company (BD Medical - Medical Surgical Systems).

### *Assessment of Strain*

Initial Interfragmentary strain in the fracture was estimated ex vivo in both the anterior-posterior (AP) and the medial-lateral (ML) directions. Total strain in the AP and ML planes was estimated as the maximal (fracture displacement/ the cortical diameter) + the yield strain of the pin = total

reported strain. Maximal fracture displacement and the cortical diameter were measured by radiographic analysis (4 sec at 35kV) and quantified using ImageJ (NIH).

#### *Biomechanical Test of Fixation Pins*

After measuring the nominal outer diameter of the pin with calipers, a standard Birmingham Wire Gauge was used to determine the nominal inner diameter and wall thickness of both pin sizes. The pins were loaded in a three-point bend fatigue testing controller (Instron DynaMight 8800) at 3 mm/min until failure. The span was twenty times the outer diameter, 12.83 mm (23 G) and 6.23 mm (30 G). The yield point was identified by the 0.2% offset method, and strain estimated by  $12 \times \text{displacement} \times \text{radius} / \text{span}^2$  where radius is the outer diameter / 2.

#### *Imaging and Quantification: Radiographic Analysis*

Fracture healing was assessed longitudinally with a Faxitron X-ray system (Lincolnshire, IL) (4 seconds at 35kV) as previously described. [29] Radiographs were obtained in both the ML and AP views, though AP radiographs were not taken at 7 DPF to avoid disrupting fixation. All X-rays were quantified by two independent examiners to assess fracture healing as previously described. [122]

#### *Microfil Injection and Angiography*

In a subset of mice sacrificed at 10 and 14 DPF (n=11 (23G), n=15 (30G), vessels were perfused with Microfil (MV-122; Flow Tech Inc., Carver, MA) immediately after euthanasia as previously described, to assess fracture vascularity. [29] Perfused femurs were assessed radiographically then placed in 0.5M EDTA, pH 7.4, for 4 days to decalcify. After



decalcification, macroscopic photos were taken. In the mice that were sacrificed at 14 DPF, samples were scanned by  $\mu$ CT, and 3D reconstructions of the vascularity were overlaid onto radiographs of the undecalcified femurs. Vessel volume ( $\text{mm}^3$ ) was measured as quantified as previously described. [29, 122] Additionally, the total area of vascularity in the callus was measured in both the ML and AP planes through  $\mu$ CT images and quantification using ImageJ software (NIH).

#### *Micro-Computed Tomography ( $\mu$ CT)*

The soft tissue surrounding the fracture was removed before  $\mu$ CT ( $\mu$ CT40, Scanco medical AG, Bassersdorf, Switzerland) analysis. Femurs (42 DPF (n=13 (23G), n=10 (30G))) were scanned at 55kVp, 145uA, 200ms integration, 1000 projections per 360° rotation, with a 20 $\mu$ m isotropic voxel size. Microfil vascular contrast (14 DPF, n=11 (23G), n=15 (30G)) was imaged at 20 $\mu$ m isotropic voxel size with following scan parameters: 55kVp, 145uA, 200ms integration, and 1000 projections per 360° rotation. To analyze bone healing at 42 DPF, 100 proximal and 100 distal slices above and below the level of the fracture site were defined the region of interest and bone volume, bone area (callus cross sectional area), polar moment of inertia (pMOI), connective density, tissue mineral density (TMD), and degree of anisotropy were measured using a global threshold of 150 permille and standard Scanco evaluation scripts.

#### *Gross Morphology of The Fractured Femur*

Photographs were taken of 10 and 14 DPF samples using a dissecting microscope and digital camera. A subset of the previously perfused and decalcified samples were dissected sagittally to assess the center of the fracture callus.

### *Histological Analysis*

At 10, 14, and 42 DPF (after  $\mu$ CT), fractured femurs were fixed in 10% neutral buffered formalin, decalcified in 0.5M EDTA (pH7.4), processed and embedded in paraffin prior to sectioning. 5 micron sagittal sections were produced for staining. A subset of slides per mouse were stained with Safranin-O/Fast Green per standard protocols. [123] Immunohistochemistry for platelet and endothelial cell adhesion molecule-1 (Pecam1) was performed per standard protocols (Pecam1 Antibody, R&D System, AF3628). Horseradish peroxidase (HRP) was amplified using a TSA Biotin System kit (Perkin Elmer, NEL700A001KT). HRP was then visualized using DAB (SK-4100, VECTOR laboratories, Burlingame, CA). Immunofluorescent staining was utilized to visualize VEGF-A and VEGFR1. Following deparaffinization, antigen retrieval was performed using 0.1M citric acid/0.1 M sodium citrate buffer followed by a Tris-buffer saline wash. Slides were blocked (5% BSA/10% goat serum solution) and immunostained for VEGF-A (1:200, Abcam 46154, Cambridge, MA), and VEGFR1 (1:100, Abcam 32152) overnight at 4°C. Alexa Fluor 647 labeled secondary (10ug/mL, Life Technologies 792514, Grand Island, NY) and DAPI were used to visualize proteins of interest and nuclei, respectively, prior to adding a coverslip with an aqueous mounting media. Slides incubated without primary antibodies served as negative controls. All histological images were obtained on an Axio Imager.A1 polarized light microscope (Carl Zeiss AG, Carl-Zeiss-Straße 22, 73447 Oberkochen, Germany). Total callus area, cartilage area, and mineralized area were assessed by analyzing serial histologic sections of fracture calluses taken from a subset of mice (n=5 per cohort) at 10 and 14 DPF and stained with Safranin-O. Mineralized area was assessed by identifying the primary spongiosa area in each section. All measurements were obtained using ImageJ Software (NIH) and an average value per mouse was reported.

### *RNA Isolation And Quantitative Real-Time PCR*

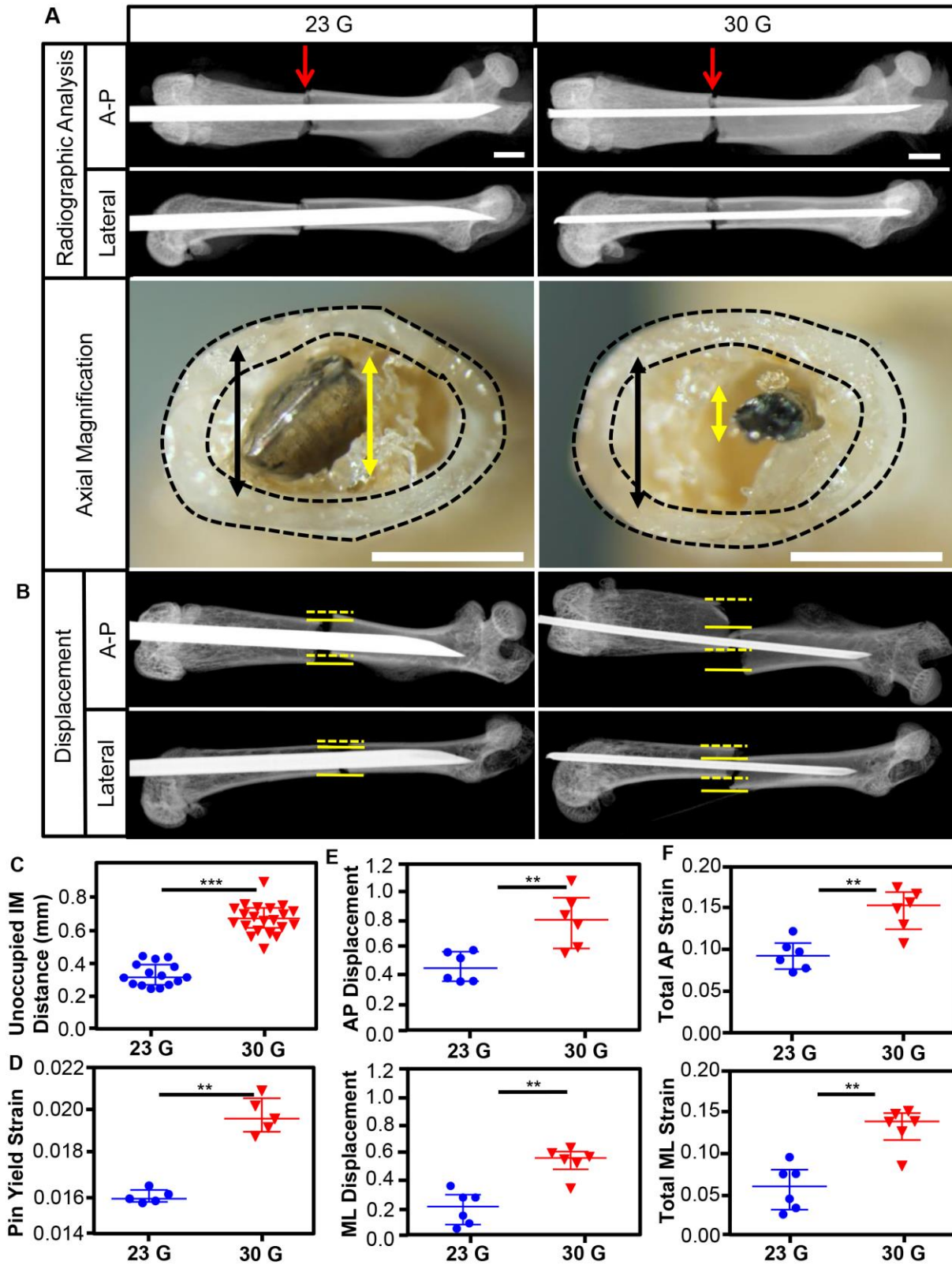
Total RNA was extracted from fracture calluses using Trizol (Invitrogen, Carlesbad, CA) at 10 and 14 DPF. Fracture calluses from mice (n=4 per cohort per time point) were carefully excised from the lower limb and individually prepared for subsequent mRNA analysis. Specimens were placed in Trizol, flash-frozen in liquid nitrogen, homogenized, and their RNA was extracted according to the manufacturer's protocol. cDNA was synthesized from 2 $\mu$ g total RNA using SuperScript III™ First-Strand Synthesis System for RT-PCR (Invitrogen). RT-PCR was performed in a 7900HT Fast RT-PCR system using TaqMan probes for Pecam1: Mm01242584\_m1, VEGFA: Mm01281449\_m1, Flt1 (VEGF Receptor1): Mm00438980\_m1 with the Taqman gene expression master mix (Applied Biosystems). 18S (Mm99999901\_s1) was used as an endogenous control gene for all TaqMan-based RT-PCR analyses.

### *Statistical Analysis*

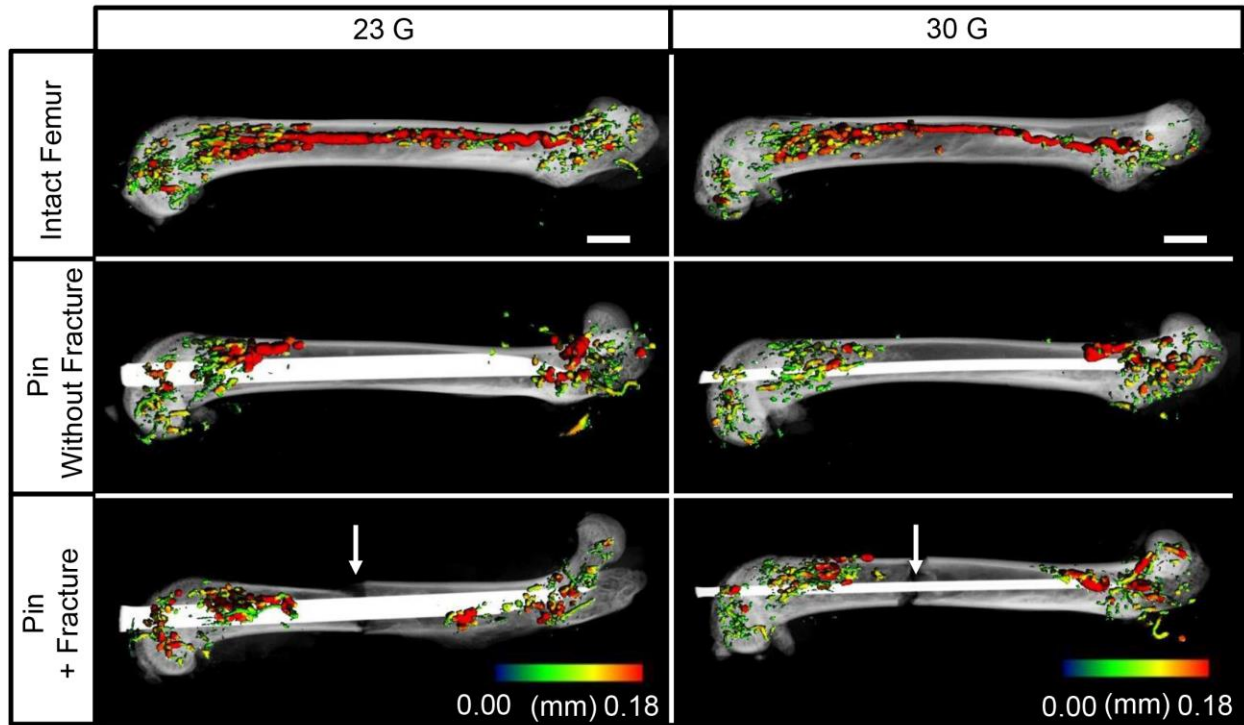
Appropriate sample size ( $\beta=80\%$ ,  $\alpha=5\%$ ) was previously determined. [124] The non-parametric Mann-Whitney test (two-tailed) was used to determine whether differences between the two pin sizes were significant ( $p<0.05$ ) for calculation of strain and each fracture parameter-DPF. Correlation between fracture vascularity and various fracture properties was assessed by non-parametric Spearman correlation. Each analysis performed was assessed for normality using the D'Agostino & Pearson normality test. Given that not all data passes the normality test, non-parametric assessments have been utilized throughout. Statistical significance is indicated by P values as \*  $P<0.05$ , \*\*  $P<0.01$ , \*\*\*  $P<0.001$ . Analyses were performed using GraphPad Prism V7.04 (College Station, TX).

*Results: Functional Differences Between 23 G And 30 G Intramedullary Pins:*

The 23G pin occupied almost twice the intramedullary space as the 30G pin (Figure 15A&C). Coupled with the lower pin yield strain (Figure 15D), the estimated interfragmentary strain at the fracture site was significantly lower in both the AP and ML direction for the 23G than for 30G cohort (Figure 15B, E, & F). For several additional mice, we performed angiography immediately after the reaming of the canal with a 25G pin and then inserted either the 23G or 30G pin, with and without a fracture, to display equivalent vascular disruption between the two cohorts (Figure 16).



**Figure 15: Estimation of intramedullary fracture strain between 23G and 30 G pins.** A) Representative X-rays and macroscopic photographs of murine femur fractures (red arrows) fixed with 23 G and 30 G pins. Yellow double headed arrows indicate pin diameter, and black double headed arrows indicate the diameter of intramedullary space. Both radiographic and gross imaging reveal that the 30G pin occupies less intramedullary space than the 23G pin and that the 23G pin has near inner cortical contact at the fracture site. Scale bar; 1mm. Quantification in panel C. B) Maximal fracture displacement in the AP and ML planes. Area between dotted and solid yellow lines represents displacement between cortices. C) Quantification of intramedullary space occupied by each pin.  $n \geq 15$  each. \*\*\*,  $P < 0.001$ . D) Pin yield strain calculated for each gauge.  $N = 5$ . \*\*,  $P < 0.01$ . E) Quantification of fracture displacement in both the AP and ML plane visualized in panel B.  $N \geq 5$ . \*\*,  $P < 0.01$ . F) Estimation of total strain at the fracture site. Calculated as (fracture displacement/bone diameter) + pin yield strain = total strain in either the ML or AP plane.  $N \geq 5$ . \*\*,  $P < 0.01$ .  $P < 0.05$  analyzed with non-parametric t-tested (Mann-Whitney).



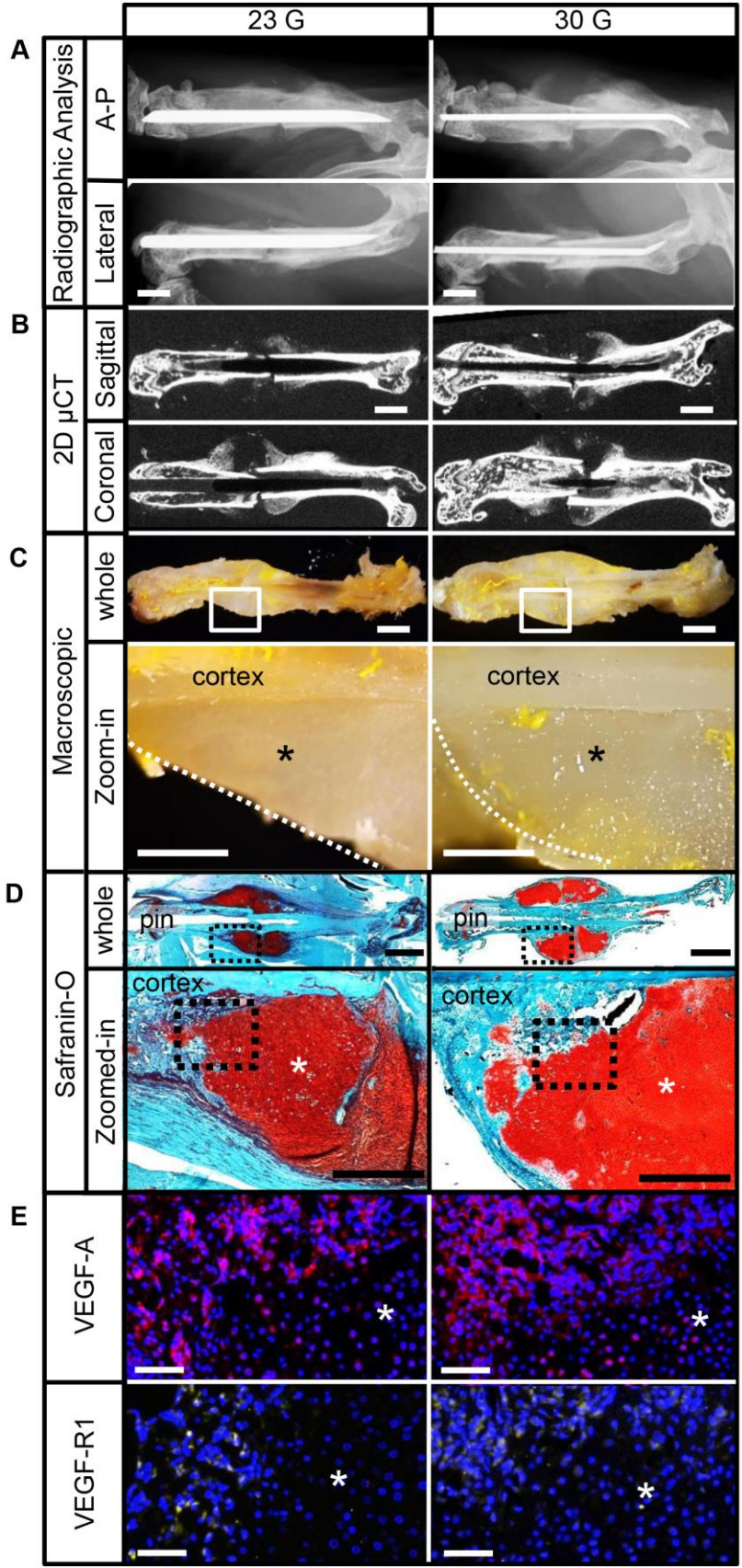
**Figure 16: Comparison of intramedullary vascular disruption between 23G and 30G pins.** Representative images of intramedullary vascularity within intact femurs, pre-reamed, and pinned unfractured femurs, and pre-reamed, and pinned fractured femurs. White arrows indicate the fracture site. The lack of angiographic signal within the intramedullary canal of pinned femurs (both fractured and unfractured) indicates similar vascular disruption independent of gauge. Vessel diameter demarcated by color (0.00 and 0.18 mm). Scale bar; 1 mm

*Greater Initial Interfragmentary Strain Results in a Larger Soft Tissue Callus and Greater Expression of Angiogenic Markers At 10 DPF.*

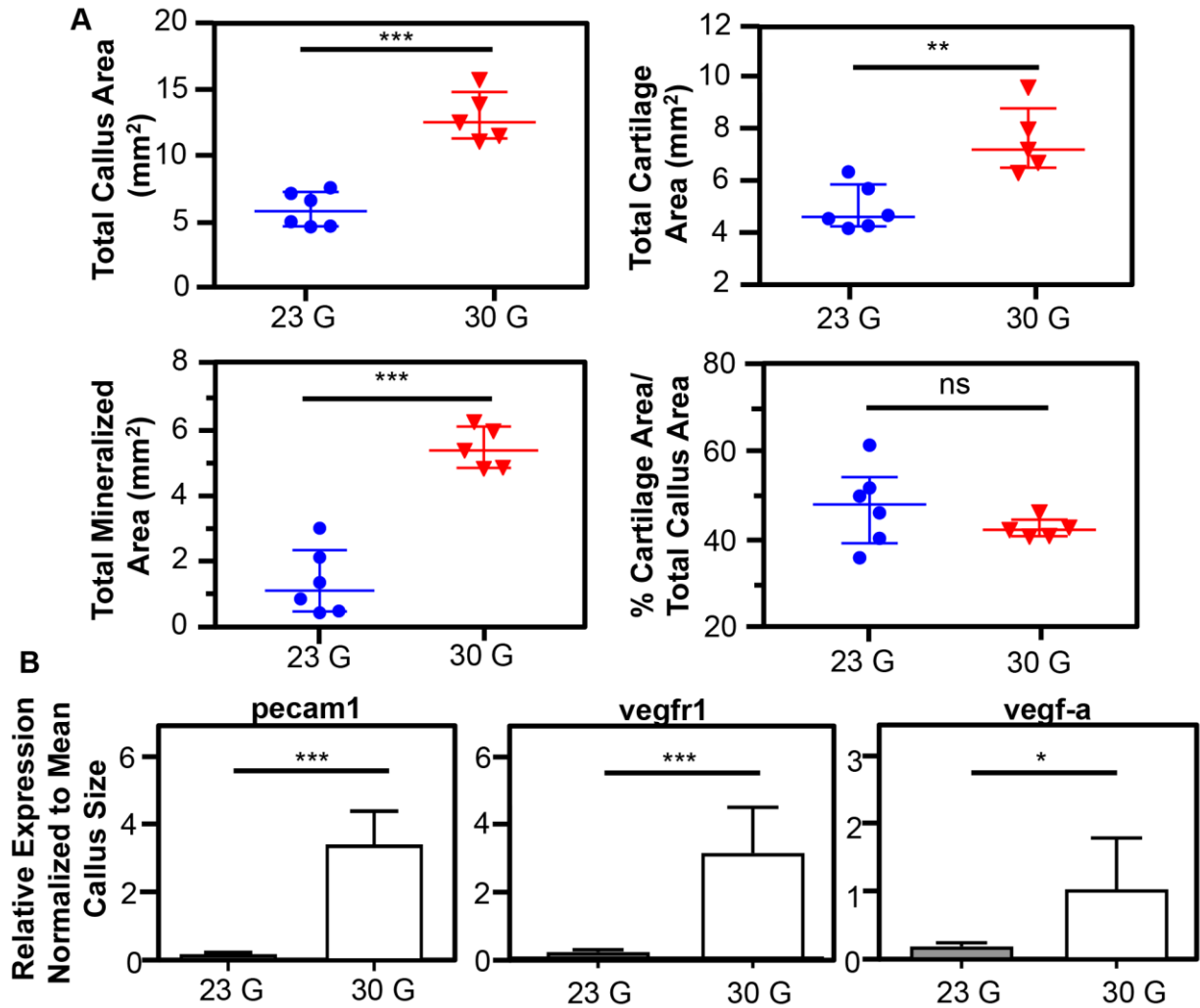
In agreement with prior studies, we observed that at 10 DPF both cohorts displayed large radiolucent zones in the middle of the callus, with limited vascular invasion and minimal hard tissue callus formation (Figure 17A-C). [28] Histological assessment of Safranin-O stained sections of callus demonstrated significantly greater soft tissue callus size, total cartilage area,

and total mineralized area in fractures with greater interfragmentary strain compared those with lesser strain (Figure 17D, Figure 18A). Immunofluorescent analysis and RT-PCR quantification of soft tissue calluses normalized to the mean soft tissue callus size demonstrated significantly greater *Pecam1*, *VEGF-A*, and *VEGFR1* expression in chondrocytes juxtaposed to the primary spongiosa of fractures with greater interfragmentary strain (Figure 17E, Figure 18B).





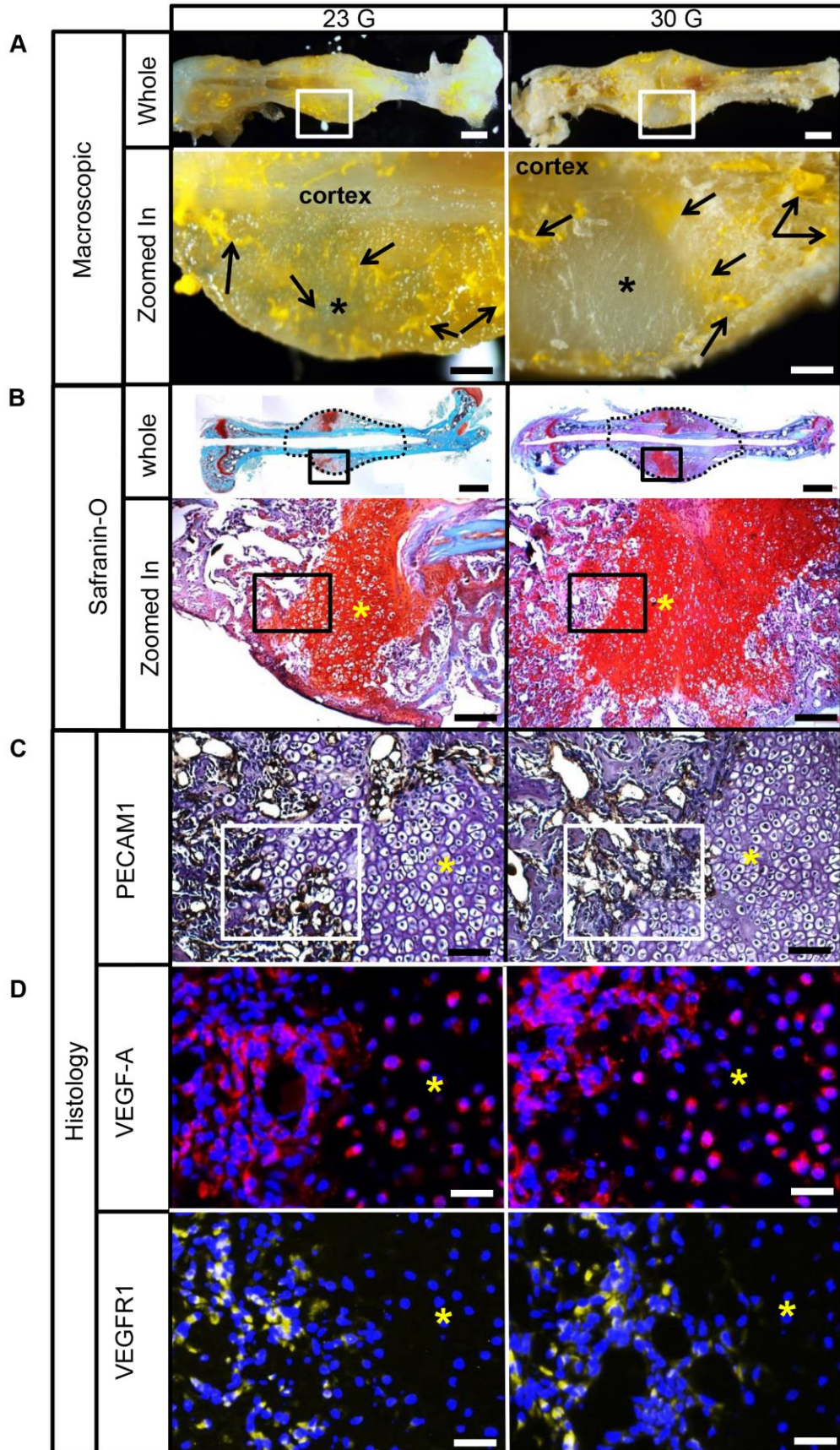
**Figure 17: Radiographic, macroscopic, and histologic characteristics of fracture calluses at 10 DPF.** A) Lateral and AP X-ray views of pinned fractured femurs. B) Sagittal and coronal two-dimensional micro-CT views of pinned fractured femurs. Radiolucency within the fracture calluses demonstrates primarily cartilaginous composition. C) Macroscopic photographs of sagittally cut fracture calluses. Black asterisks indicate avascular area. Peripheral yellow microfil indicates limited vascular invasion of the fracture calluses. Gross examination reveals larger fracture callus formation under greater initial interfragmentary strain. D) Sagittal histologic sections of fracture calluses stained with fast green/safranin-O. Red stain indicates cartilage (white asterisks), demonstrating cartilage predominance within the fracture calluses. E) Immunofluorescence of area indicated by black dotted square in section D (stained for VEGF-A and VEGFR1). Red fluorescence indicates cells expressing VEGF-A and yellow fluorescence indicates cells expressing VEGFR1. White asterisks indicate cartilage zone. Scale bar=1 mm (A-D), 500  $\mu$ m (C&D “zoomed in”), 100  $\mu$ m (E).



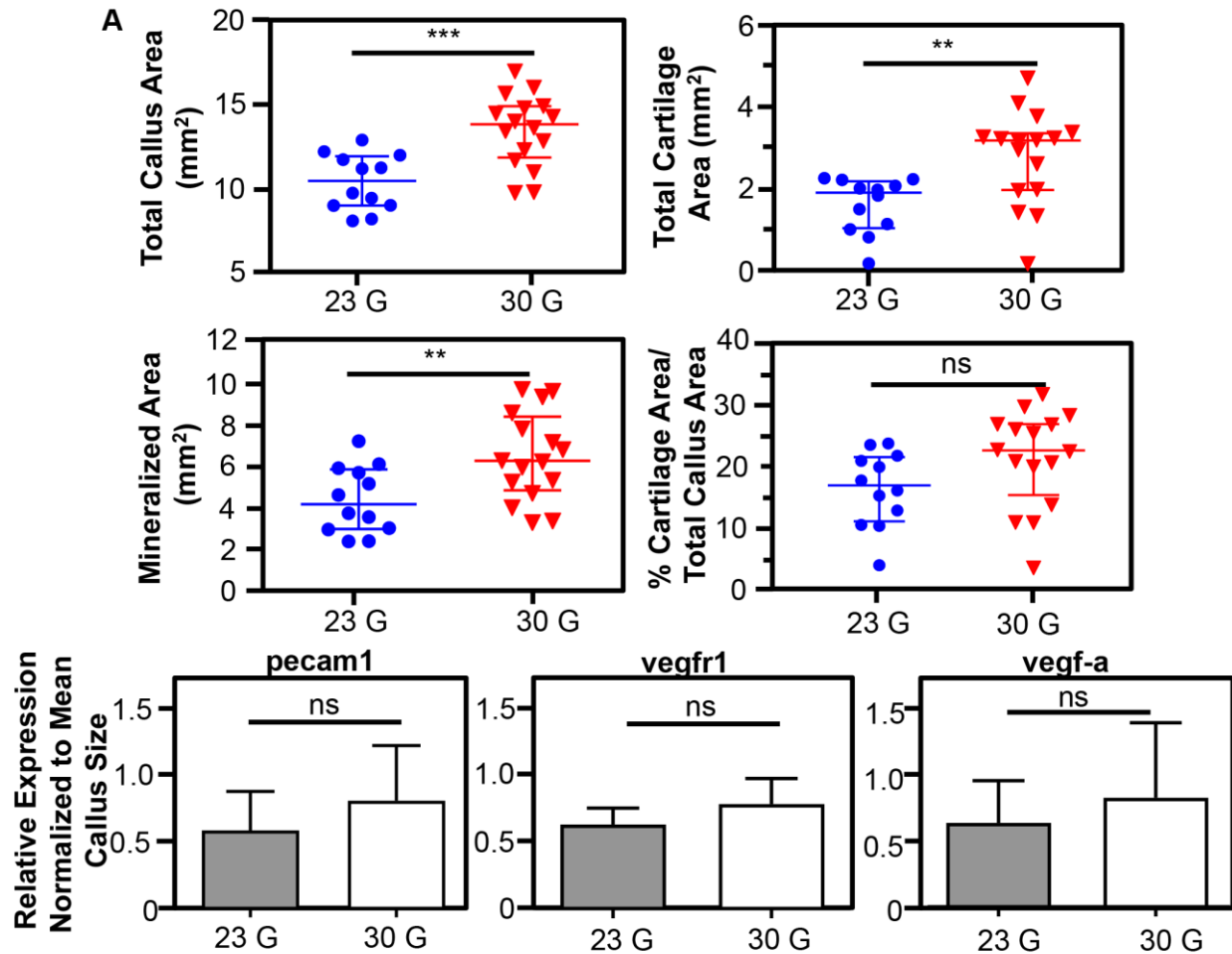
**Figure 18: Quantitative analysis of histology and mRNA expression in the fracture callus at 10 DPF.** A) Total callus area, total cartilage area, total mineralized area, and ratio of cartilage to total callus area between 23G and 30G pin fixation. B) Quantified mRNA expression of pecam1, vegf-a, and vegfr1 normalized to mean cartilage area per cohorts between 23G and 30G pin fixation. Results represent median  $\pm$  interquartile range (error bars) of  $n \geq 5$ . \*\*\*  $P < 0.001$ , \*\*  $P < 0.01$ , \*  $P < 0.05$  analyzed with non-parametric t-tested (Mann-Whitney).

*Greater Initial Interfragmentary Strain Results in a Larger Soft Callus, Yet Comparable Expression of Angiogenic Markers at 14 DPF*

At 14 DPF, histology demonstrated persistently larger total callus area, total cartilage area, and mineralized area in fractures with greater initial interfragmentary strain (Figure 19A&B, Figure 20A). Histological analysis for PECAM1 (endothelial cells marker) demonstrated marked expression at the boundary between the vascularized cartilage anlage and the areas of avascular cartilage in both cohorts of mice (Figure 19C). When quantified by RT-PCR and normalized to the mean soft tissue callus size, no significant difference in Pecam1, VEGFR1, or VEGF-A expression was observed, though levels still trended higher in fractures with greater initial interfragmentary strain (Figure 19D, Figure 20B).



**Figure 19: Macroscopic and histologic characteristics of fracture calluses at 14 DPF.** A) Representative macroscopic cross sections of fracture calluses. Black arrows indicate microfil compound in the callus (representative of vasculature). Black asterisks indicate areas without microfil (avascular cartilage). Scale bar= 1mm (whole) and 200  $\mu$ m (zoomed in). B) Histologic sections of femurs stained with Safranin-O. Black dotted lines specify the fracture calluses. Black square on the “zoomed in” images represent area shown in section. Red staining represents cartilage. Scale bar= 1mm (whole) and 200  $\mu$ m (zoomed in). C) Immunohistochemical staining for PECAM1. White squares represent the area of the callus shown in section D. Yellow asterisks indicate avascular hypertrophic chondrocytes. Scale bar=100  $\mu$ m. D) Immunofluorescent staining for VEGF-A and VEGFR1. Red fluorescence indicates cells expressing VEGF-A and yellow fluorescence indicates cells expressing VEGF-R1. Yellow asterisks indicate avascular cartilage. Scale bar= 50  $\mu$ m.

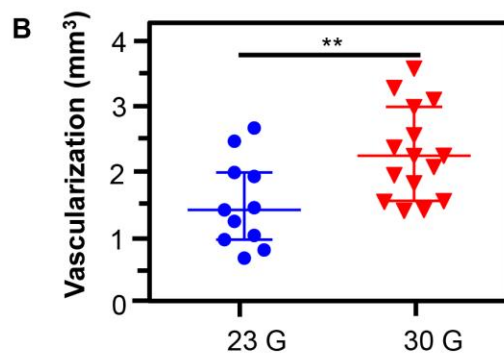
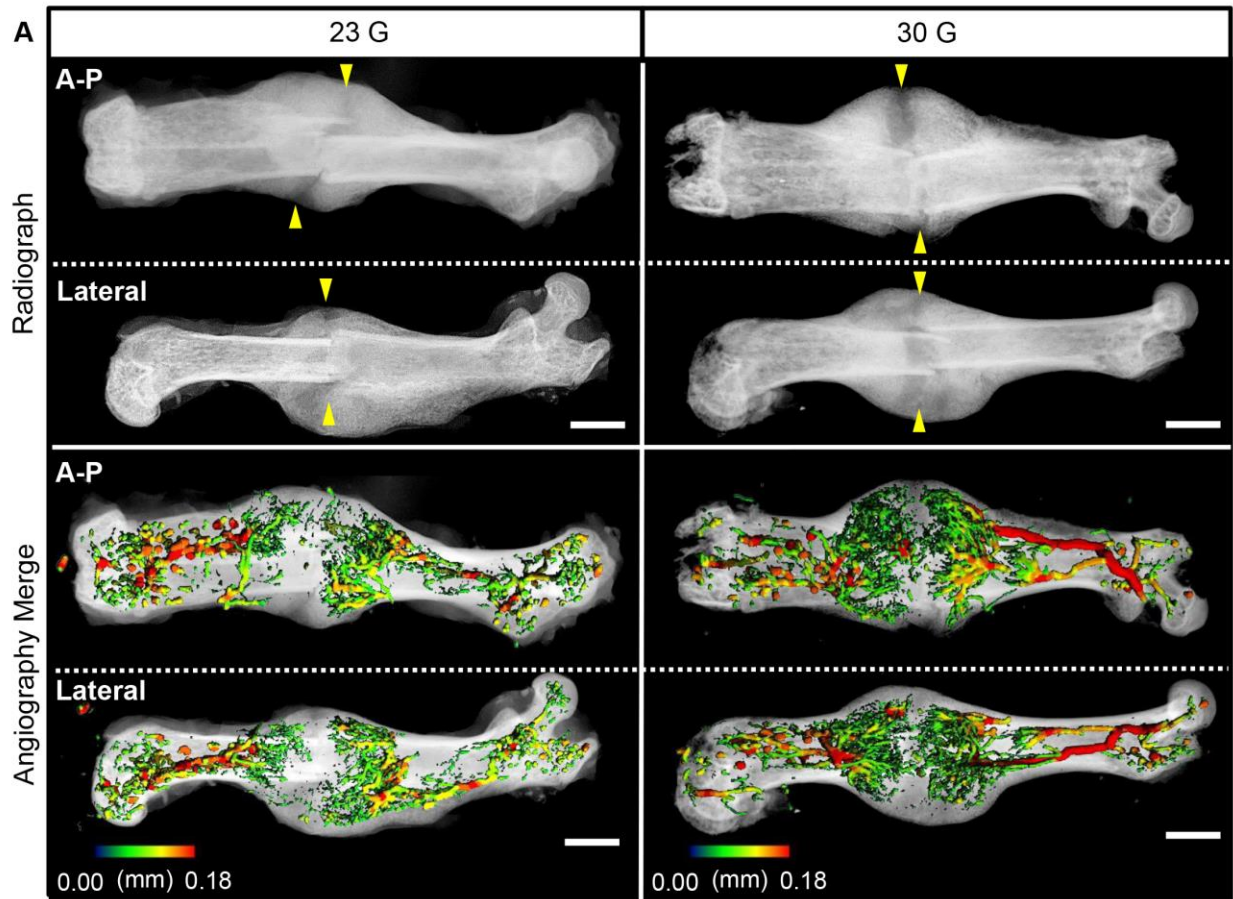


**Figure 20: The quantitative analysis of histology and mRNA expression in the fracture callus at 14 DPF.** A) Total callus area, total cartilage area, total mineralized area, and ratio of cartilage to total callus area between 23G and 30G pin fixation.  $n \geq 12$ . B) Quantified mRNA expression of *pecam1*, *vegf-a*, and *vegfr1* normalized to mean cartilage area per cohorts between 23G and 30G pin fixation. Results represent median  $\pm$  interquartile range (error bars) of  $n \geq 5$ . \*\*\*  $P < 0.001$ , \*\*  $P < 0.01$ , \*  $P < 0.05$  analyzed with non-parametric t-tested (Mann-Whitney).

*Greater Initial Interfragmentary Strain Results in Increased Fracture Revascularization At 14 DPF*

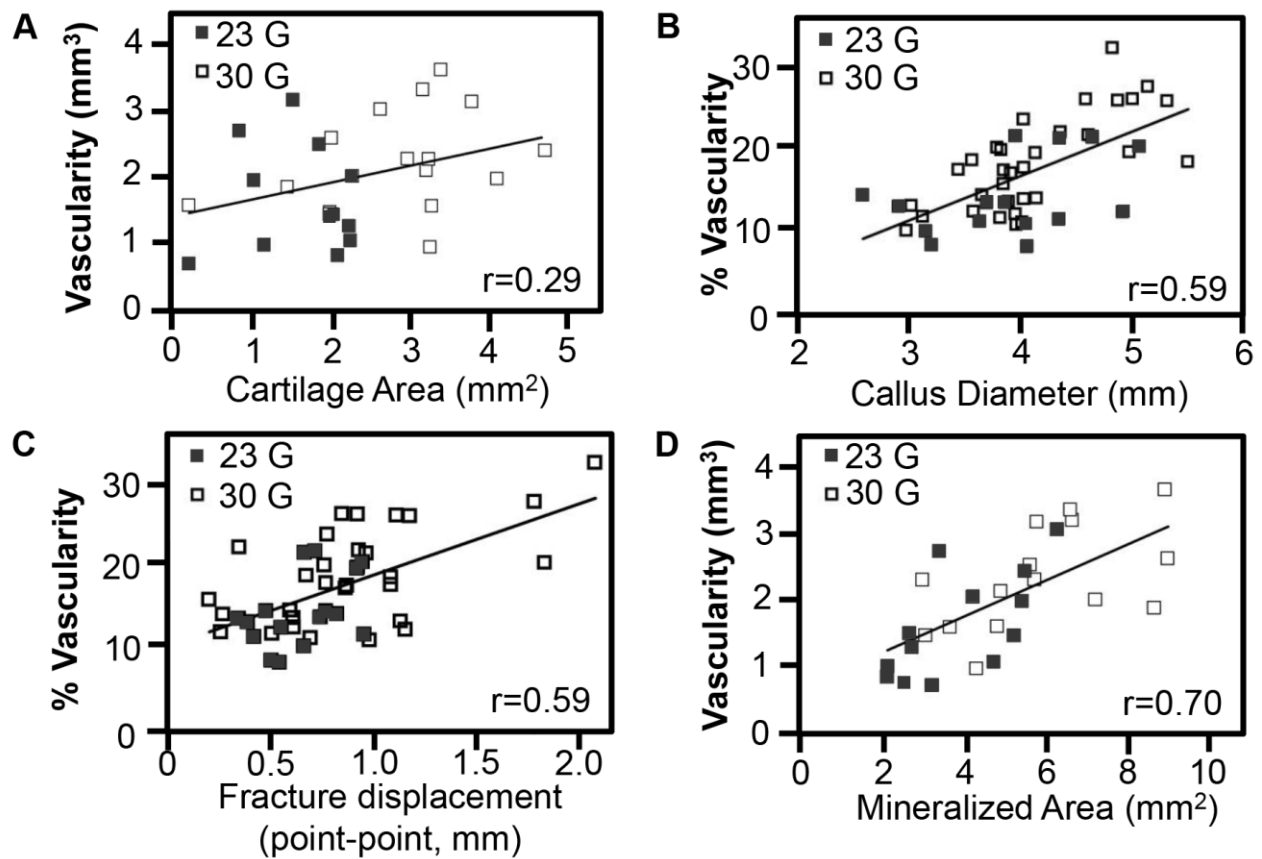
Given the observed increase in expression of angiogenic factors (PECAM, VEGF-A, and VEGFR1) in the higher strain cohort, we next assessed if expression of these factors correlated with increased fracture angiogenesis at 14 DPF. Through  $\mu$ CT angiography, we observed that fractures with greater initial strain developed significantly more fracture revascularization than those with less initial strain (Figure 21A&B). Furthermore, we observed a positive correlation between fracture revascularization and cartilage area, callus diameter, and fracture displacement; three parameters which are each significantly greater in the higher strain cohort (Figure 22A-C). Finally, as fracture vascularity is a requisite for mineralization and subsequent fracture healing, we also observed a strong correlation between fracture vascularity and mineralization of the fracture callus (Figure 22D), with the higher initial strain cohort exhibiting earlier bone formation following injury (Figure 23A&B). [28]



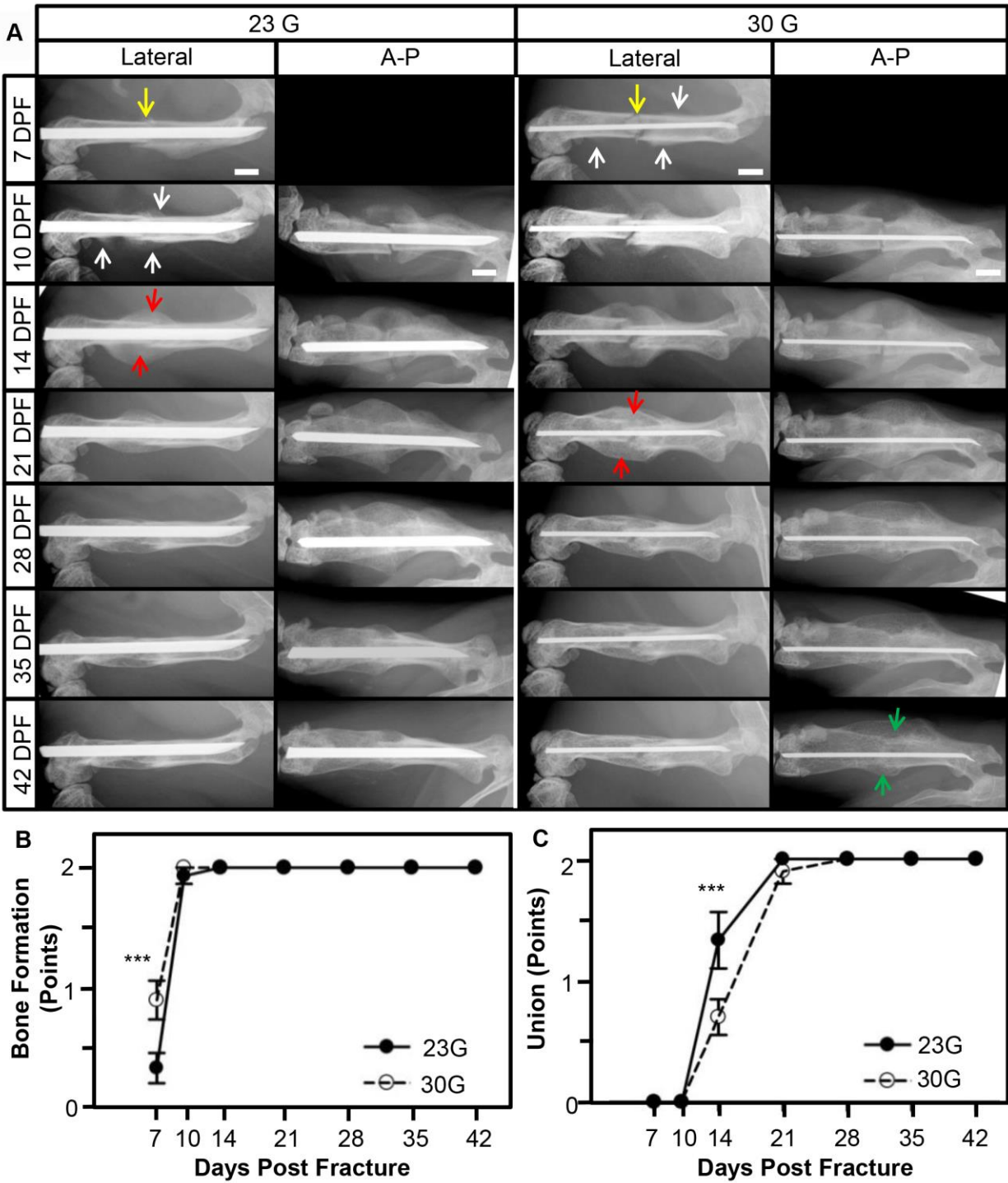


**Figure 21: Comparison of fracture callus angiogenesis at 14 DPF.** A) Representative lateral and A-P X-rays of pinned fractured femurs, with overlying 3D reconstructions of  $\mu$ CT angiograms. Yellow arrow heads indicate apparent fracture gap in the callus. Angiogram reconstructed images show the robust vascularity in the fracture callus both distally and proximally. Vessel diameter demarcated by color (0.00 and 0.18 mm). Scale bar; 1 mm. B)

Quantified revascularization between 23G and 30G pin fixation. \*\* P<0.01 analyzed with non-parametric t-test (Mann-Whitney) n=11 (23G) and n=15 (30G).



**Figure 22: Correlation of callus vascularization with histomorphometric features at 14 DPF.** Overall, there was a positive correlation between callus vascularity and A) cartilage area, B) callus diameter, C) fracture displacement, and D) mineralized area. Callus vascular volume (mm<sup>3</sup>) and callus vascular area (%vascularity of total callus area) was measured using  $\mu$ CT. n $\geq$ 11 per cohort.

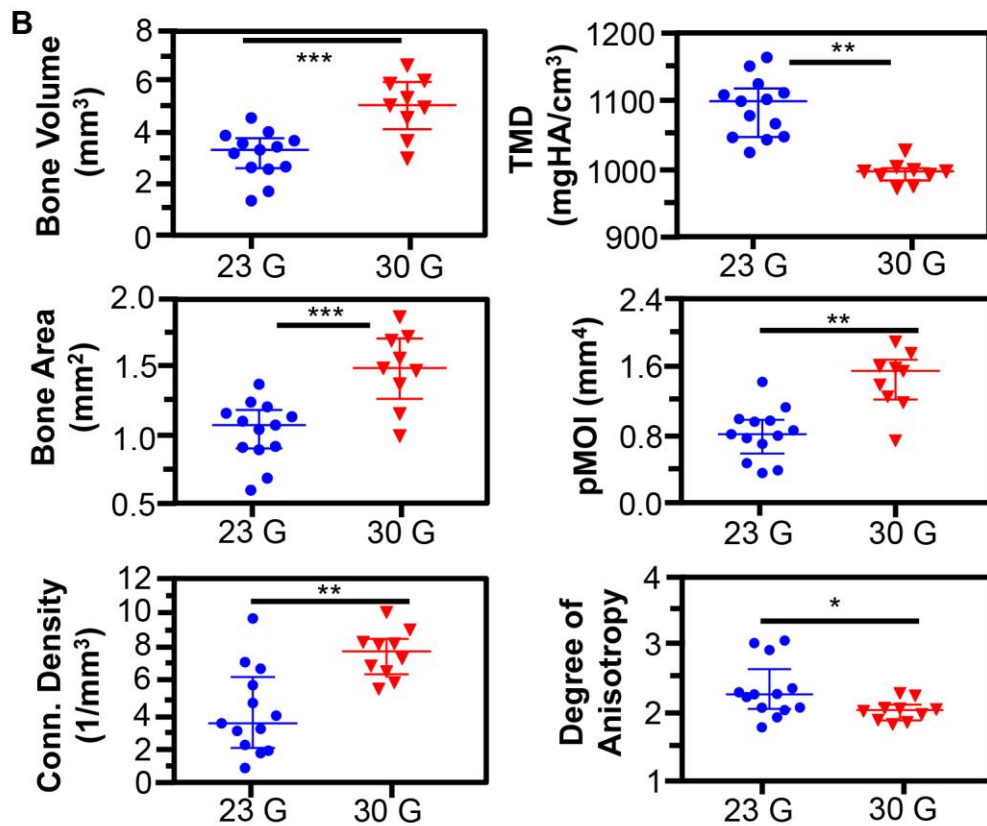
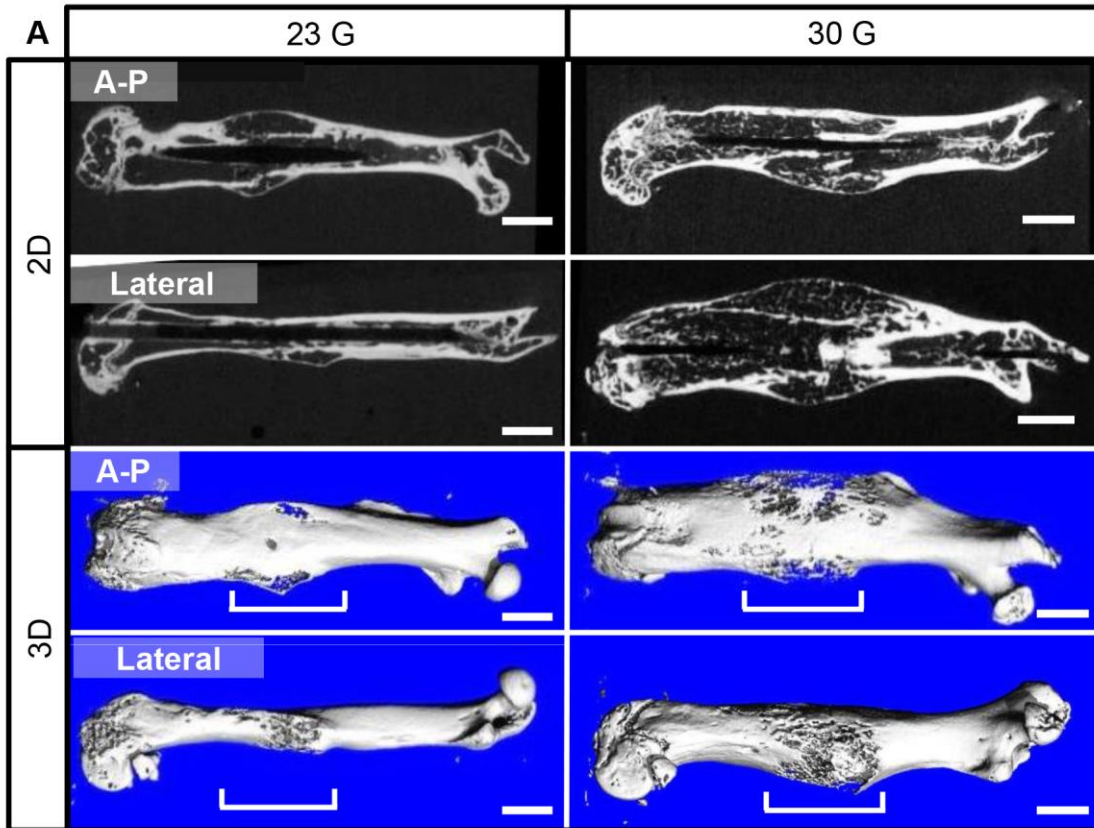


**Figure 23: Time course of fracture healing following fixation allowing for varying interfragmentary strain.** A) Sequential x-rays of both lateral and AP views from 7 DPF to 42 DPF. Yellow arrows indicate fracture site, white arrows indicate hard tissue callus, red arrows

indicated fracture union, and green arrows indicate remaining fracture callus in AP view. Scale bar; 1 mm. B) Quantified bone formation analyzed from 7 DPF to 42 DPF. Score of 1 indicates bone formation in either the AP or lateral views. Score of 2 indicates bone formation in both AP and lateral views. n= 15 (23G) and n= 20 (30G). C) Quantified fracture healing using radiograph grading system in both 23 G and 30G analyzed from 7 DPF to 42 DPF. Score of 1 indicates union in either the AP or lateral views. Score of 2 indicates union in both AP and lateral views. n= 15 (23G) and n= 20 (30G). Error bars represent mean+ SEM. \*\*\*, P<0.001.

#### *Differences in Initial Interfragmentary Strain Altered Fracture Remodeling But Not Union at 42 DPF*

Throughout fracture healing, we observed hard tissue callus formation earlier in the fractures with greater initial strain, yet comparable hard tissue bridging and time-to-union between the two cohorts (Figures 23 & 24). Through AP radiographs and  $\mu$ CT analysis, we observed a larger hard callus remaining at 42 DPF in the high strain cohort (Figure 24A). Moreover,  $\mu$ CT analysis demonstrated a delay in fracture remodeling with greater initial strain as indicated by increased bone volume, bone area, connective density, and polar moment of inertia (Figure 24B).



**Figure 24: Delayed fracture remodeling observe din femurs fixed with smaller 30G pins.** A) Representative 2D and 3D  $\mu$ CT reconstructions at 42 DPF. White brackets indicate fracture callus. Scale bar; 1 mm. B) Quantification of the structural properties of the fracture calluses derived from  $\mu$ CT analysis at 42 DPF. Bone volume, Tissue mineral density (TMD), bone area, polar moment of inertia (pMOI), connective tissue density (Conn. Density), and degree of anisotropy were assessed in each cohort.  $n \geq 10$  per cohort. \*  $P < 0.05$ , \*\*  $P < 0.01$ , \*\*\*  $P < 0.001$ . Error bars represent median  $\pm$  interquartile range.

### *Discussion*

This study unveils another biological consequence of a surgeon's choice of fracture fixation, namely the link among size of intramedullary fixation, strain, and endochondral angiogenesis. Akin to Perren's concept of "biological plating", here we demonstrate the potential for "biological nailing" in which an intramedullary nail can be modified to influence the biology of fracture healing, specifically angiogenesis, through alteration of strain. [74, 84] Building upon this foundational study, endochondral angiogenesis may be used in addition to other known variables (i.e. fracture callus size) in future investigations exploring "biological nailing" and the optimal environment for fracture healing.

It is widely established that angiogenesis is critical for successful fracture repair. [18, 19] The effect of the mechanical environment of a fracture on chondrogenesis and soft callus production has also been described in previous studies. [43, 110-112] However, to our knowledge there have been few studies examining if the increased chondrogenesis that occurs for fractures subjected to greater initial strain results in a proportional increase in endochondral angiogenesis during

healing. This study provides insight into the link between the initial biomechanical environment of the fixed fracture, its effect on chondrocytes, and subsequently the development of vascularity within a fracture callus.

It is known that mechanical stress stimulates chondrocytes to produce, maintain, and remodel cartilage. [112] Consequently, during secondary healing the size of the cartilaginous soft callus is proportional to the degree of initial strain within at the fracture. [111, 117] Similarly, we observed a significantly larger callus in 30G fixation compared to 23G. Furthermore, we observed a link between the initial amount of strain, callus size, expression of angiogenic factors, and amount of revascularization. This suggests that modifying chondrocyte function early in fracture healing (i.e. by permitting greater strain) imparts longer lasting changes that can be observed as they mature into hypertrophic chondrocytes. Here, we observed a significant increase in the expression Pecam1, VEGF-A, and VEGFR1 in fractures with greater initial strain 10 DPF. Subsequently we observed a significant increase in the total vasculature of the healing fractures as evidenced by  $\mu$ CT angiography at 14 DPF. This study suggests a link between the mechanical stability fracture fixation, chondrogenesis, and subsequently fracture vascularity. As such, the effect of strain on subsequent fracture angiogenesis should be considered when designing or comparing fracture studies.

Limitations of this study include that we did not directly measure the interfragmentary strain of the fracture fixation construct in-situ. As a surrogate, we measured the intramedullary space that each pin filled along with the pin's bending rigidity and used these to estimate strain within the initial fracture hematoma. Furthermore, these examinations were conducted using 8-week-old

male mice, therefore representing a juvenile model of healing as to not introduce confounding variables of sex and aging. Future studies will be necessary to determine if these same results can be extrapolated to conditions of less optimal bone biology such as aging and chronic conditions such as diabetes.

In the 1990s, Dr. Stephen Perren revolutionized orthopaedic practice by modulating interfragmentary strain when he developed “biological plating”. [74, 84] When treating comminuted diaphyseal fractures, Perren found that it was more effective to use plates that “bridged” the bony fragments, instead of perfectly reducing them. In this way, he destruction of local vasculature and allowed for an acceptable degree of motion at the fracture. This led to rapid healing through secondary ossification. Importantly, Perren found that this mode of fixation was not beneficial for all fracture types. Specifically, bridge plating of simple transverse diaphyseal fractures with small fracture gaps permitted too much strain, resulting in delayed or non-unions. [74, 84] Perren’s discoveries highlight that increasing strain within a fracture does not always improve healing, and excessive strain is a risk factor for impaired healing. The amount of strain must be tailored to a degree that optimizes the desired biological processes of fracture healing without interfering with union. [34, 84, 125]

Similar to Perren’s work, numerous clinical studies have attempted to optimize intramedullary nailing through modification of one or more of the parameters that impact their stability, and thus strain (nail size, locking, nail composition, or pre-reaming) with varying results. [97, 99, 101, 108, 114, 116] The ideal fixation construct is likely a dynamic one that can specifically modify strain throughout the course of a healing fracture to promote each desired biological process.



From this foundation, I have begun, under the guidance of Dr. Schoenecker, further lines of investigation into the ideal biological nature of the intramedullary nail to best promote fracture repair. Through using a murine model of fracture repair, we have the ability to measure beyond ossification, in that we can visualize fracture revascularization, the composition of the soft tissue callus, and estimate interfragmentary strain of varying constructs. Currently, as highlighted in Article 1, these measurements cannot yet be conducted in human patients, thereby leading orthopaedic surgeons to rely primarily upon measures of ossification which only paint a portion of the picture. Through future work in small animal models, we will possess the ability to examine each of these factors that individually can influence bone biology, thereby allows us to examine new intramedullary constructs in a controlled and highly informative manner for multiple aspects of bone biology

In the next article, we will discuss a fundamental study that I assisted a very talented resident, Dr. Alex Sielatycki, and two of our talented postdoctoral fellows, Drs. Masanori Saito and Masato Yuasas, on completing. This study highlights the power of harnessing ones knowledge of bone biology to promote bone formation in an area where it is greatly needed, but not normally found: spinal fusion. Through this work, I not only further expanded my knowledge and application of bone biology in a new basic science model, but also learned about a significant area of orthopaedic practice, spine care and fusion. Through working with Dr. Sielatycki, I learned the basics of spine structure and function, the process of a spinal fusion, as well as the “villains” that can arise such as pseudarthrosis. With this training, I was able to play an integral part of this study highlighted in Article 3 and apply these findings to new grant applications!

## **Application of The Fundamental of Bone Biology: Promoting Bone Formation To Improve Spinal Fusion**

### Article 3: Autologous Chondrocyte Grafting Promotes Bone Formation in The Posterolateral Spine

J. Alexander Sielatycki<sup>a,^</sup>, Masanori Saito<sup>a,b,^</sup>, Masato Yuasa<sup>a,b</sup>, **Stephanie N. Moore-Lotridge<sup>a,g</sup>**, Sasidhar Uppuganti<sup>a</sup>, Juan M. Colazo<sup>h</sup>, Alexander A Hysong<sup>h</sup>, J. Patton Robinette<sup>h</sup>, Atsushi Okawa<sup>b</sup>, Toshitaka Yoshii<sup>b</sup>, Herbert S. Schwartz<sup>a</sup>, Jeffrey S. Nyman<sup>a,c,d,e</sup>, & Jonathan G. Schoenecker<sup>a,f,g,I,\*</sup>

Vanderbilt University Medical Center, <sup>a</sup>Department of Orthopaedics and Rehabilitation, <sup>d</sup>Center for Bone Biology, <sup>f</sup>Department of Pathology, Microbiology, and Immunology, and <sup>i</sup>Department of Pediatrics

Vanderbilt University, <sup>g</sup>Department of Pharmacology, <sup>h</sup>School of Medicine, and <sup>e</sup>Department of Biomedical Engineering

Tennessee Valley Health Care System, <sup>c</sup>Department of Veterans Affairs

Tokyo Medical and Dental University, <sup>b</sup>Department of Orthopaedic Surgery,

<sup>^</sup> Indicates that authors contributed equally

<sup>\*</sup>To whom correspondence should be directed

*Accepted March 2018 to the Journal of Orthopaedic Research: Spine*

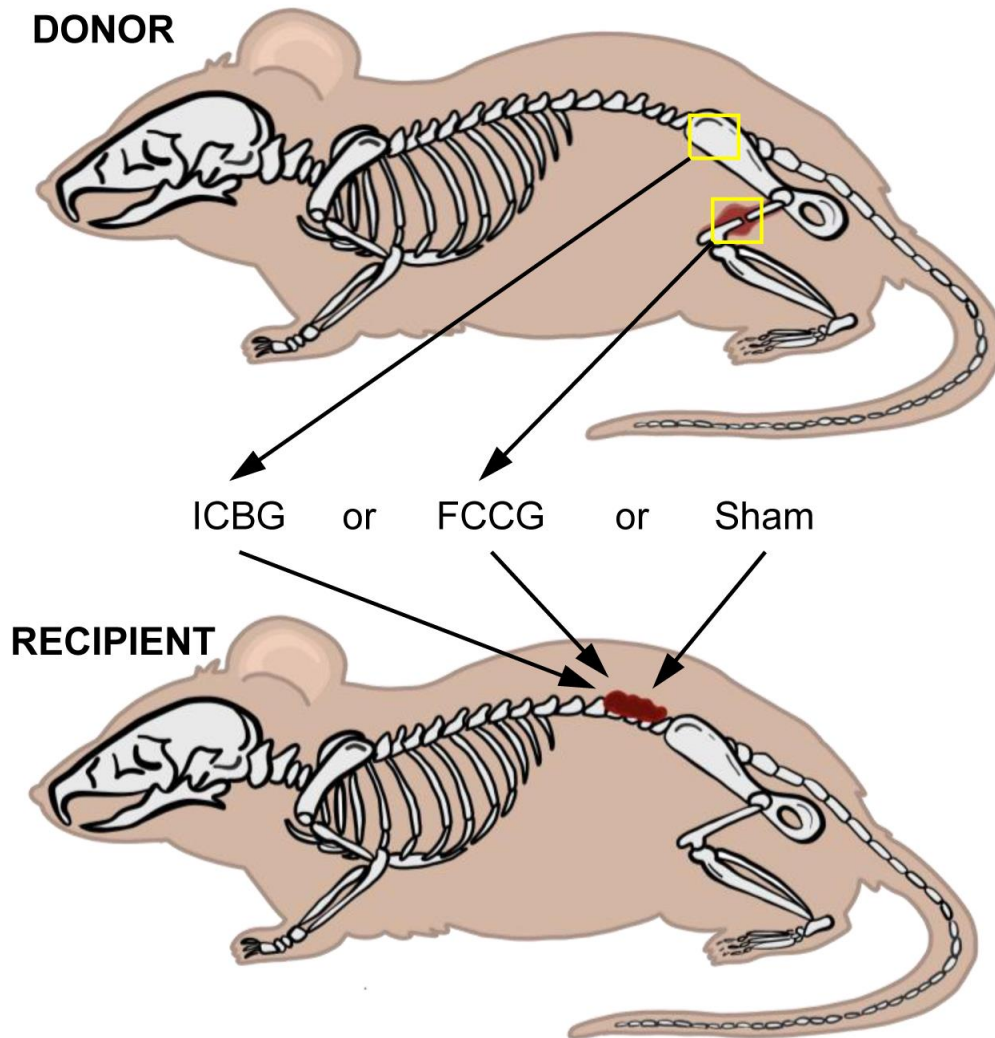
<https://doi.org/10.1002/jsp2.1001>

## *Introduction*

When a patient necessitates a spinal fusion, the primary goal of the procedure is to provide stability across two or more levels of vertebrae to reduce pain and compression at the site in the spine. To provide stability, implants such as plates, screws, or cages are placed in conjunction with bone grafts to promote boney fusion across the affected vertebrae. Bone grafts can be isolated directly from the patient (autograft) from the iliac crest, from donors (allografts), or from synthetic bone substitutes. Given that the rate of spinal fusions is increasing over the past 10 year [126, 127], and that current iliac crest bone graft (ICBG) method are hampered by donor site morbidity and limited supply, particularly for multi-level fusion [128-130], novel bone graft alternatives that can be clinically available in large quantities and provide ample bone formation with limited side effects are needed.

In spinal fusion, new bone formation has been previously described to occur via intramembranous and endochondral ossification—processes similar to long bone development and fracture healing. [129, 131-135] As discussed in Article 1, the key cellular mediator of endochondral ossification is the hypertrophic chondrocyte. Along with their unique ability to survive in hypoxia, hypertrophic chondrocytes induce neovascularization and ossification through the release of VEGF, vesicles of hydroxyapatite, and BMP. [28, 136-138] For these reasons, we examined the hypothesis that hypertrophic chondrocytes offer a potential graft alternative for promoting spinal fusion. To test this hypothesis, hypertrophic chondrocytes were harvested from a soft fracture callus at day 10 post fracture and surgically implanted into the posterolateral spinal gutters of a genetically identical mouse recipient. Following implantation, the ability of these fracture callus chondrocyte grafts (FCCGs) to drive posterolateral bone

formation was assessed and compared with either standard ICBG or a sham implantation surgery control group (Figure 25)

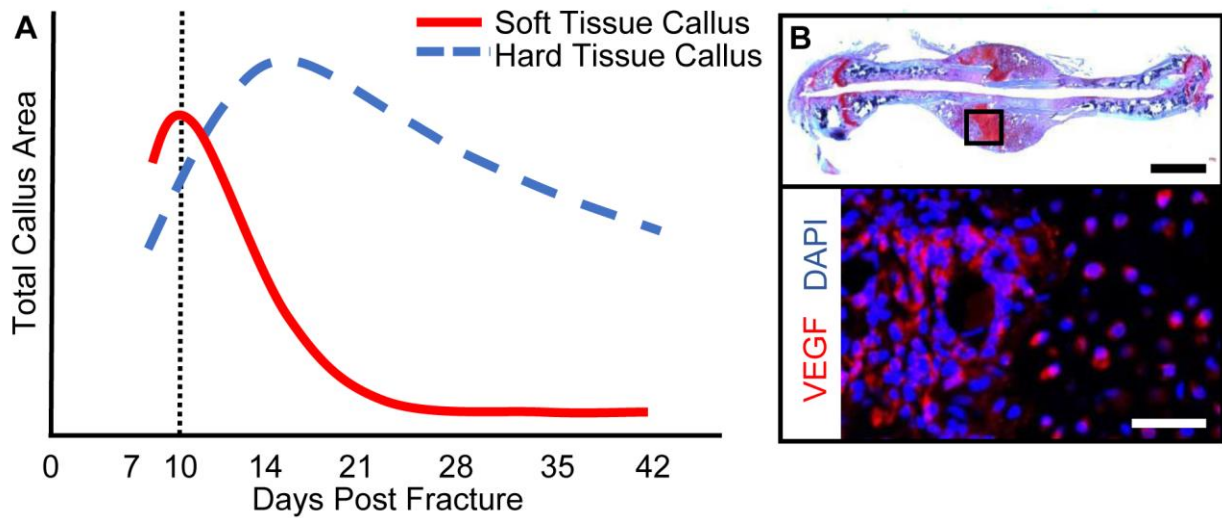


**Figure 25: Experimental Design- Use of FCCG as compared to ICBG for promoting bone formation in the posterolateral spine.** To test the hypothesis, ICBG and FCCG were harvested from a single donor mouse. Grafts were then individually transplanted into the posterolateral gutters of a genetically identical recipient mouse. A sham surgery with no graft implantation was used as a control. N=10 per experimental group.

*Study Specific Methods: Graft Harvesting (FCCG AND ICBG)*

All animal procedures were reviewed and approved by the Institutional Animal Care and Use Committee (IACUC) of Vanderbilt University Medical Center (M1600140).

Male C57BL/6J mice were purchased from Jackson Laboratory and housed at Vanderbilt University in a 12-hour light/dark cycle with food and water provided *ad libitum*. At 8 weeks of age, an open femur fracture model, previously developed by our lab [28, 29], was performed. Following adequate anesthesia and analgesia, a 10-12 mm long medial incision was made to expose the mid-shaft of the femur. The femur was then fractured in a controlled manner by scoring the bone with a beaver blade before inducing a clean break. The transverse fracture was stabilized with the intramedullary placement of a 30 gauge needle, to induce a larger soft-tissue fracture callus, as compared with needles of a larger size (23G) with more stiffness; thereby allowing for a more efficient harvest. The incision was then closed using 5-0 nylon sutures. Mice received analgesics every 12 hours for three days following the fracture procedure to minimize pain and discomfort. Ten days following the fracture, when the soft-tissue callus was largest and amply expressing VEGF (Figure 26), the mice were sacrificed by CO<sub>2</sub> inhalation. At this time, the FCCG was harvested, along with an ICBG, for the subsequent transplantation into the posterolateral spine of syngeneic mice. Harvested grafts were standardized by volume and a 2x2x2 mm section was obtained for implantation.

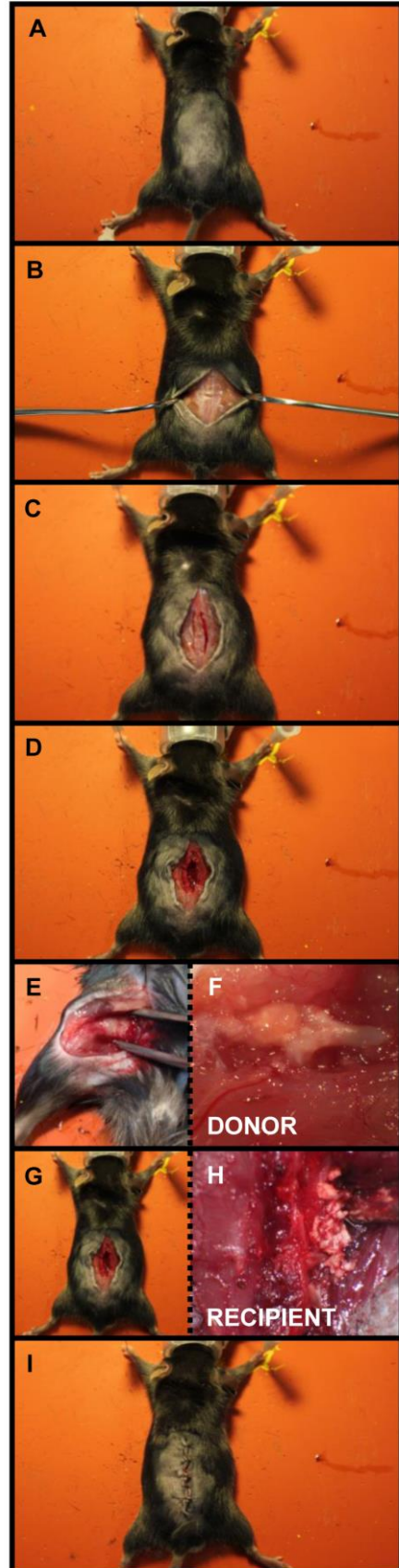


**Figure 26: Optimal Timing for FCCG Isolation.** Previous longitudinal investigations of fracture callus size and composition<sup>20</sup> have demonstrated a) maximal soft tissue callus volume at 10 days post fracture (red line) and maximal hard tissue callus between 14 and 21 days post fracture (blue dashed line). b) At 10 days post injury, hypertrophic chondrocytes found within the soft tissue callus are producing VEGF-A. Top Panel: Scale Bar = 1mm. Bottom panel: Scale Bar = 200µm

#### *Murine Posterolateral Spinal Bone Formation Model*

The purpose of this surgery model was to determine the capacity of FCCG or ICBG to promote bone formation following implantation to the posterolateral lumbar spine. Immediately following FCCG and ICBG harvesting, posterolateral lumbar surgeries were performed on separate, yet genetically identical, male C57BL/6J mice from Jackson Laboratory at 8 weeks of age (Figure 27). Following adequate anesthesia and analgesic, the dorsal fur was removed (Figure 27A) and a midline incision was made through the skin and dorsolumbar fascia to expose the peri-spinal musculature (Figure 27 B&C). Sub-periosteal dissection was carried out using a beaver blade to expose the transverse processes of the L3 to L5 vertebrae prior to decortication (Figure 27D).

The laminae and spinous processes were then decorticated with a beaver blade. The previously harvested FCCG or ICBG was then transplanted into the posterolateral gutters (Figure 27E-H). Following this, the internal fascia was closed with absorbable monofilament suture while the skin was closed with 5-0 nylon suture in a simple interrupted fashion (Figure 27I). Mice were then transferred to their respective cages and monitored until they regained normal ambulation. Analgesic was administered every 12 hours for three days following surgery to minimize pain and discomfort.



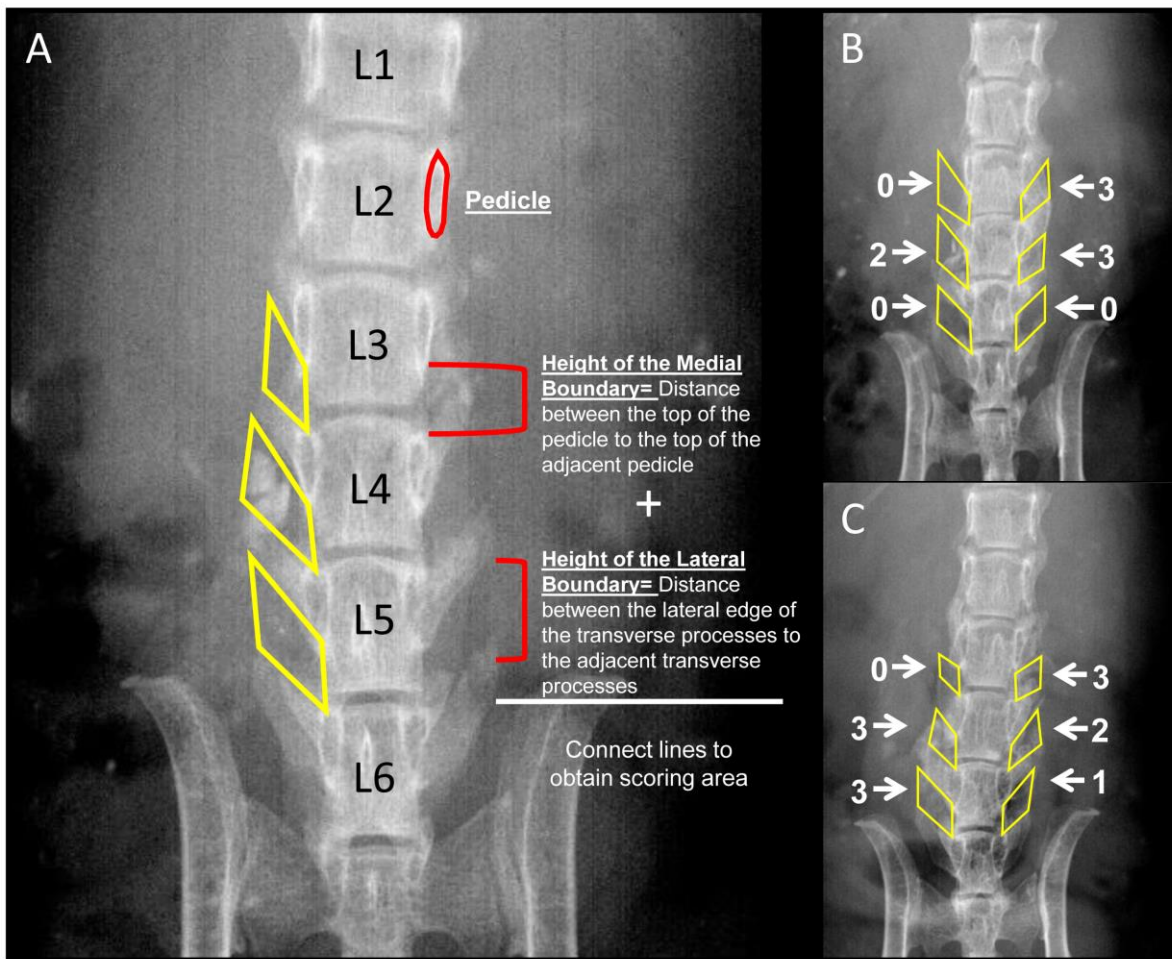


**Figure 27: Murine Posterolateral Spinal Fusion Model.** A) Removal of dorsal hair to prepare incision site. B&C) Midline incision followed by exposure of the dorsolumbar fascia and peri-spinal musculature. D) Sub periosteal dissection to expose the transverse processes of the L3 to L5 vertebrae. E) Isolation of FCCG from donor mouse. F) Magnified view of a soft-tissue fracture callus for hypertrophic chondrocyte collection. G&H) Transplantation of graft (FCCG or ICBG) into the posterolateral gutters of recipient mouse. I) Incision closure.

*Assessment of Posterolateral Bone Formation: Radiographical Assessment and Quantification*

To assess the development of bone formation between the transverse processes, digital radiographs were obtained longitudinally (4 seconds, 35 kV) beginning day one post-surgery and then weekly until 6 weeks post-surgery (Faxitron, Tuscon ZA). Mice were placed in the prone position, aligning the spine vertically within the imaging plane. Images were used to quantify the amount of bone formation by three blinded independent observers. For each image, the area surrounding the transverse processes of vertebrae L3 through L5 was selected (Figure 28). The 6 selected areas were then scored for the amount of calcification present, with a score of “0” representing  $\leq 25\%$  of the total area becoming calcified, a score of “1” representing 26-50% of the total area becoming calcified, a score of “2” representing 51-75% of the total area becoming calcified, and a score of “3” representing  $>75\%$  of the total area becoming calcified. The sum of the 6 boxes was then recorded per observer per mouse (Figure 28 B&C). Inter- and intra-observer error was assessed through the use of kappa statistics. On average, observers were found to be in fair to moderate agreement (kappa =0.255-0.489) per the Landis and Koch criteria. Additionally, when rescored with more than 7 days between analyses, intra-observer variability was found to be moderate with observers being in slight to moderate agreement (kappa= 0.087-

0.481). Further assessment of individual observer scores over time (i.e. the slope of the line) were found to have no statistical difference between observers for any experimental group as measured by the analysis of the covariance (ANCOVA). FCCG-  $F= 0.072$ ,  $DF =2$ ,  $p=0.930$ ; ICBG-  $F= 0.021$ ,  $DF= 2$ ,  $p=0.979$ ; Sham surgery-  $F=0.283$ ,  $DF= 2$ ,  $p=0.754$ .



**Figure 28: Radiological Quantification of Bone Formation between Transverse Processes.**

A) To assess the amount of newly formed bone between the transverse processes, the areas between L3, L4, and L5 vertebrae processes were delineated. First, the pedicle for each vertebra was identified. Second, a vertical line was drawn between the top of the proximal pedicle to the top of the adjacent pedicle to delineate the height of the medial boundary. Third, the height of the

lateral boundary was delineated as the distance between the lateral edges of the transverse processes to the adjacent transverse processes. Finally, these two vertical lines were connected to form the analysis area. B&C) Example images with subsequent scores for each delineated section.

#### *In Vivo Fluorescent Imaging of Bone Formation*

To assess new bone formation, OsteoSense 800 (NEV11105, PerkinElmer, Shelton, CT), an NIR-labeled, targeted fluorescent bisphosphonate was used to visualize areas of new calcification. 24 hours before imaging, a representative mouse per group was injected intraperitoneally with 2nmols of OsteoSense 800 in a total volume of 100uL. A Pearl small animal imaging system and image studio software (LI-COR Biotechnology, Lincoln, NE) were utilized to measure in vivo fluorescence at an excitation wavelength of 780 nm and an emission wavelength of 805nm.

#### *Micro-computed Tomography ( $\mu$ CT) Analysis*

To further assess bone formation qualitatively, mice were sacrificed 6 weeks post-surgery and 3D renderings of the posterior lumbar region were generated using microcomputed tomography ( $\mu$ CT 40, Scanco Medical AG, Bassersdorf Switzerland).  $\mu$ CT images of the spine from the thoracic to the sacral region were acquired using a polychromatic x-ray source with peak beam voltage at 55 kVp and tube current of 145  $\mu$ A. The sample acquisition settings were as follows, 1024 samples per 500 projections per 180 degree rotation of the sample tube holder and each projection lasting 232 ms i.e. integration time. The raw image slices, with an isotropic voxel size of 20  $\mu$ m, were reconstructed using Scanco OpenVMS software (v8.4). Post re-construction, the

volume of interest containing the posterior elements of L3-L5 was contoured by transecting the pedicles within a 5.93 mm diameter tube. The calcified tissue was segmented from the soft tissue using a relatively low global threshold of 150 per mille of the x-ray attenuation coefficient without a Gaussian noise filter. The Scanco evaluation software v6.6 also provided Component labeling (CL) function with rank 1 to 1 in order to remove any small noisy speckles that were not connected to the main structure. The CL ranked, segmented image file was used to represent a 3D rendering of the L3-L5 spine using Scanco 3D viewer v4.0-4.

### *Histological Analysis*

To assess the fracture calluses isolated from the donor mouse a subset of femurs were isolated, decalcified, processed, and embedded in paraffin prior to sectioning at 10 days following fracture injury, when the soft tissue callus was largest. Histological sections through the fracture callus were stained for the presence of VEGF.

### *Immunofluorescent Staining of VEGF*

Following deparaffinization, slides were hydrated and processed for antigen retrieval using a solution of 0.1M citric acid and 0.1M sodium citrate. Slides were then heated for 2 minutes, cooled to room temperature, and washed with Tris-buffer saline before blocking with a solution of 5% BSA and 10% goat serum. Immunostaining was performed with anti-mouse VEGF-A (1:200, Abcam 46154, Cambridge, MA) antibody overnight at 4°C. Slides were then washed, incubated with 10ug/ML AlexaFluor-647 anti-rabbit secondary antibody (Life technologies 792514, Grand Island, NY) in blocking buffer for 1 hour at room temperature, and counterstained with DAPI. All microscopic images were obtained on a Zeiss Axio Imager A.1

(ZEISS, Oberkochen, Germany).

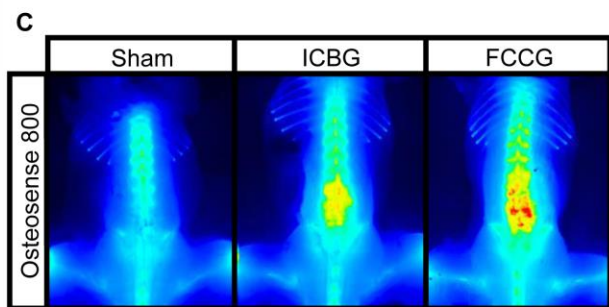
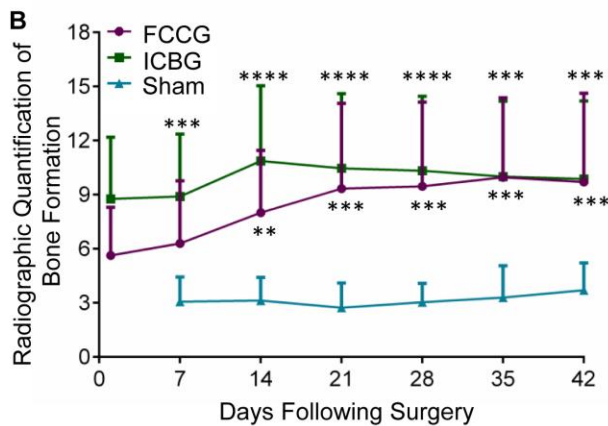
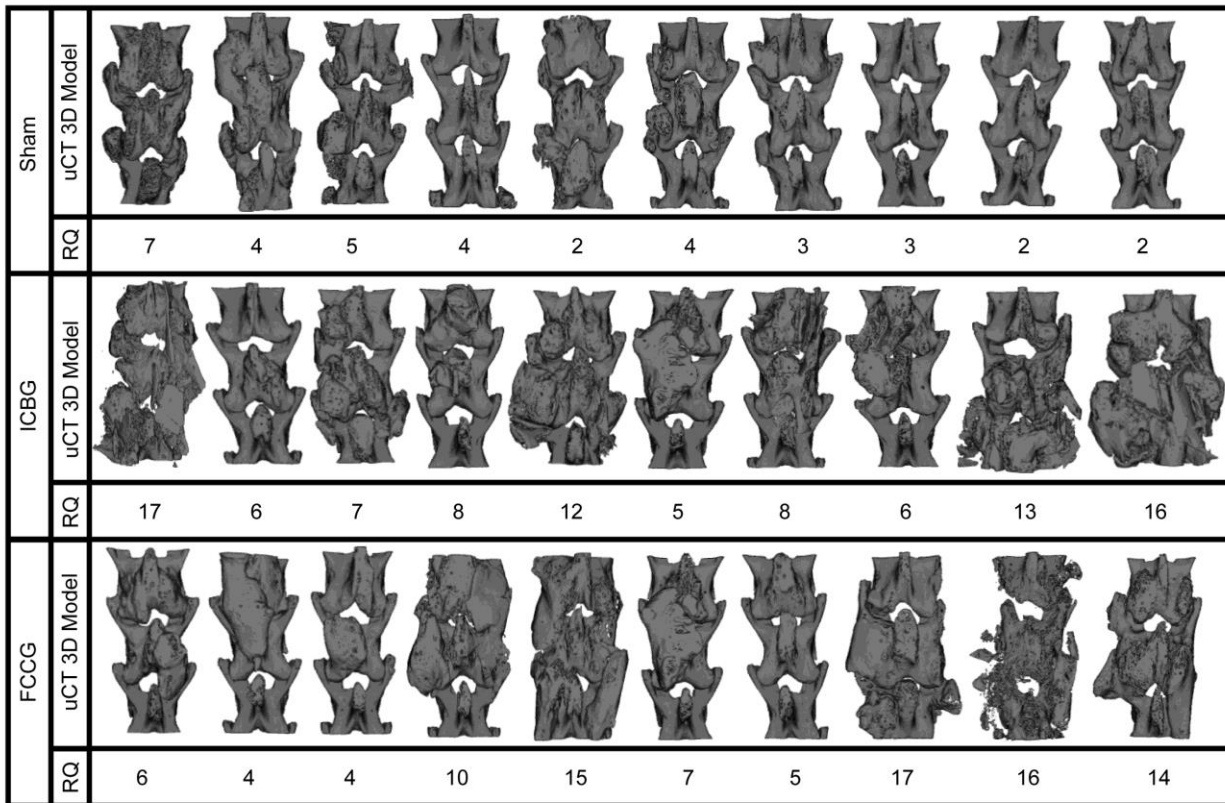
### *Statistical Analysis*

Inter- and intra-observer variability, for quantification of calcification surrounding the transverse processes, was assessed using kappa statistics and interpreted with the Landis and Koch criteria. [139] Variability in the score over time between observers was assessed through an analysis of the covariance (ANCOVA). Analysis of bone formation between groups at each time point was assessed by a non-parametric two-way ANOVA, corrected for multiple comparisons. Statistical analysis was conducted in GraphPrism V6 (La Jolla, CA) or STATA V14.2 (College Station, TX).

### *Results: Implantation of Posterolateral Hypertrophic Chondrocytes (FCCG) Promotes Bone Formation*

3D renderings of L3-L5 spinal levels by  $\mu$ CT revealed that both FCCG and ICBG increased bone formation at 6 weeks post-surgery to equivalent levels as compared to the sham control group (Figure 29A). Additionally, the median radiographic quantification scores per mouse (RQ) at 42 days post-implantation correlated visually with the amount of bone present (Figure 29A and Figure 29). As opposed to ICBG, in which bone was observed without changes in quantity over time, FCCG bone formation developed substantially over time and equaled that of ICBG by 21 days post-implantation (Figure 29B). Furthermore, sensitive assessment of bone formation at 42 days post-implantation demonstrated marked increases in newly formed bone, with the greatest amounts seen in mice receiving a FCCG (Figure 29C).

While the primary objective of this study was to assess the ability of hypertrophic chondrocytes to promote bone formation in the posterolateral spine, we also observed by  $\mu$ CT analysis successful bony union of the laminae/transverse processes as well as a longitudinal bony bridge across vertebrae, indicative of fusion in a subset of animals from both the FCCG and ICBG group. Taken together, these results support the hypothesis that FCCG can promote bone formation to comparable to ICBG, and therefore warrants further investigation as a potential graft alternative in spinal fusion.



**Figure 29: Implantation of hypertrophic chondrocytes promotes bone formation.** A) 3D  $\mu$ CT reconstructions of the posterior spine (L3-L5) following sham surgery, implantation of ICBG, or implantation of FCCG. Median radiograph quantification (RQ) per mouse correlates visually with the amount of bone formation. B) Longitudinal RQ of bone formation via blinded scoring of digital radiographs (Figure 28). Points represent mean score between three reviewers per mouse  $\pm$  SD. N=10 mice per experimental group. \* represent statistical significance

between ICBG or FCCG and Sham. \*\* =  $p < 0.01$ , \*\*\* =  $p < 0.001$ , \*\*\*\* =  $p < 0.0001$ . Alpha=0.05. No statistical difference between experimental groups was detected at any time point. C) *In vivo* fluorescent imaging of bone deposition using Osteosense 800.

### *Discussion*

To our knowledge, this is the first proof-of-concept study investigating the use of hypertrophic chondrocytes in promoting bone formation in the posterolateral spine. Ultimately, these findings support the hypothesis that hypertrophic chondrocytes have the capacity to drive posterolateral bone formation, with equal or greater efficacy as compared to ICBGs. Furthermore, while not a primary focus of this work, we observed successful bony bridging across vertebrae by  $\mu$ CT analysis, despite the lack of mechanical stabilization. Therefore, this work provides the foundation for future studies aimed at 1) assessing spinal fusion following implantation of hypertrophic chondrocytes and 2) producing ample and clinically feasible sources of hypertrophic chondrocytes for testing in larger rodent and small animal studies. In order to one day translate these findings to clinical use, such studies are necessary.

During fracture healing and spinal fusion, new bone formation takes place both by intramembranous and endochondral ossification. [132, 134] Current strategies to promote vascularized bone regeneration have largely focused on the process of direct intramembranous bone formation while stimulating angiogenesis through the local application of growth factors. [129, 132, 140, 141] VEGF [142], fibroblast growth factor (FGF-2) [143], platelet-derived growth factor (PDGF) [138], hydroxyapatite, BMP [133, 141] and other factors are currently applied therapeutically. The problem with this direct intramembranous approach is that it is not



very efficient at promoting neovascularization and/or successful graft incorporation, frequently resulting in early graft failure. [134, 144, 145] Boden et. al. showed that endochondral ossification occurs in the central/hypoxic zone of the fusion bed, which is also where pseudarthroses occur. Thus, strategies aimed at augmenting intramembranous bone formation may not be addressing the problem area in the fusion bed. Furthermore, Arthur Ham's work has demonstrated that osteoblasts cannot survive more than 200 micrometers from an oxygen source (vascular capillary). [7] Thus, augmentation strategies that rely on the influx of osteoblasts into a relatively hypoxic fusion bed, like the direct intramembranous approach, are inherently limited.

In contrast, endochondral ossification forms new bone indirectly through a cartilaginous intermediary known to survive hypoxia, while simultaneously inducing angiogenesis. During long bone development, as well as fracture repair, neovascularized bone forms from a cartilage anlage under the direction of hypertrophic chondrocytes. [55, 131, 135, 146] This process has the advantage of being highly angiogenic [28, 145, 147], while taking place through a progression of mesenchymal stem cell differentiation, vascularization, and mineralization. At the site of fracture healing, pluripotent stem cells differentiate into hypertrophic chondrocytes and recapitulate the developing physis in order to bridge the fracture gap with vascularized bone. [28, 146] Importantly, hypertrophic chondrocytes have been shown to survive and proliferate in relative hypoxia (as compared to osteoblasts) while releasing required growth factors in proper temporal and spatial patterns as discussed in Article 1. [137] Conveniently, these hypertrophic chondrocytes, for the sake of analogy, can be considered a versatile "bone bomb", containing all the necessary factors (i.e. VEGF, BMP, and hydroxyapatite) to promote new bone formation in an area of relative hypoxia. In the present study, our findings suggest that hypertrophic

chondrocytes may be used to induce bone formation in the spine.

Recently, rat studies have established the feasibility and efficacy of hypertrophic chondrocytes to induce new bone formation in tibial defects. Bahney *et. al.* showed that cartilage, isolated from a healing fracture callus, was effective at inducing vascularized bone formation in 2mm defects of the tibia – confirmed by micro-CT and histology. [147] The cartilage grafts in this previous study were shown to be equally as effective as the autograft, and superior to the allograft, in terms of both fusion rate and fusion strength. In this current study, a similar hypothesis was employed, and we found that hypertrophic chondrocytes augmented paraspinous bone formation comparable to standard ICBG. While this purpose of this study was not to assess the mechanism of bone formation (intramembranous vs endochondral ossification), use of this model in future studies in combination with lineage tracing experiments may prove insightful.

Although the findings of the current study provide a foundation for advancement in bone graft biologics, they are not without limitation. Primarily, the murine model utilized here is not directly applicable to human anatomy and/or physiology, and thus, directly extrapolating these results to human spinal fusion is not plausible. Rather, the findings here serve to establish the proof-of-concept foundation for potential transition to small and larger animal studies. Secondly, use of a murine model preclude the use of pedicle screws or surgical stabilization to immobilized vertebral segments; yet even in an unstabilized setting, we did observe cortical bridging between vertebrae. Therefore, future studies in larger animal models, where pedicle screws/surgical stabilization can be employed, are warranted and should investigate the effects of mechanical stimulation of hypertrophic chondrocyte maturation and ossification. Lastly, while

this study establishes that hypertrophic chondrocytes may effectively augment bone formation in the posterolateral spine, soft-tissue fracture calluses are not a feasible harvest source in clinical practice. Thus, this study provides the foundation for future work aimed at procuring abundant hypertrophic chondrocytes in a clinically feasible and safe manner. Despite these limitations, we believe that the findings presented here provide proof-of-concept and establish a new paradigm in bone graft alternatives that will drive future research in larger animal models, and ultimately if successful, humans

### *Future Directions*

Given the overall success of the above proof- of-concept study demonstrating that hypertrophic chondrocytes can be utilized as a successful bone graft, we aim to tackle one of the biggest hurdles for application of this method clinically: where are the hypertrophic chondrocytes going to come from? Rather than take the approach of expanding autologous chondrocyte in culture to a mass suitable for transplantation, we will take an alternate approach by manufacturing synthetic analogs of chondrocyte microvesicles that harness the majority of the cellular machinery required for ossification while concomitantly protecting the required proteins from the biological milieu. Going forward we will test the specific hypothesis that manufactured chondrocyte microvesicle mimetics (MCMM) are equally as effective at forcing ossification in muscle as autologous cellular transplants via ICBG and fracture callus cartilage graft (FCCG).

### *Summary*

To this point, we have discussed extensively the molecular mechanisms through which bone is formed both during development at the physis and following injury (Article 1 & 2). Furthermore,

we have discussed how application of bone biology fundamental can be applied to promote spine fusion in a novel way (Article 3). From this point, I will transition our conversation to the problems of fracture repair, beyond loss of bone and ability to bear load. As a reminder, the body has evolved over millennia to heal injured tissues in an orderly fashion, collectively termed the acute phase response (APR). As such, the APR is divided into two distinct phases-- survival and repair.

First, the APR's "survival" phase contains the injury: utilizing coagulation and inflammation to achieve hemostasis and prevent of infection. These are the most lethal threats of an injury and must be addressed immediately. Once the body has "survived" these two hurdles, it proceeds to the APR's "repair" phase, which aims to recreate functional anatomy (i.e. bone healing). However, like many biological processes, the primary problems experienced following injury (bleeding, susceptibility to infection, tissue hypoxia, and tissue dysfunction) are also drivers of the APR. As such if stimulated inappropriately, an over activated or insufficient acute phase response can result in complications such as hemorrhage, thrombosis, systemic inflammatory response syndrome (SIRS), infection, death, and/or impaired tissue healing.

Therefore, our laboratory, in addition to studying the repair phase, as has been interested in examining the APR and how dysregulations in the APR can be predictive or potentially causative of complications. The overarching goal of these studies is to identify characteristic of the APR, both in pattern and in molecular mechanism, that we can intervene to reduce complications. In the next two articles (Article 4 and 5), I will highlight to prospective studies that has been focused on characterizing the APR for risk of vascular complications, primarily DVT. These

studies were conducted in pediatric patient populations, many of which were diagnosed with an infection driving their APR. Infection is a significant complicator of tissue repair, such that if a patient is infected, they can become stuck in the “survival” phase of the APR, thereby limiting their transition to the tissue repair phase, and simultaneously putting them at risk for “survival” phase complications such as thromboses. Therefore, identification of specific APR markers and patterns associated with complications is extremely advantageous clinically to identify at risk patients, track a patient’s status over time, and also identify points of intervention that may be beneficial.

## **Your Body's Response to Injury: The Acute Phase Response and Related Complications**

### Article 4: C-Reactive Protein Predicts Risk of Venous Thromboembolism in Pediatric Musculoskeletal Infection

Emilie Amaro, MD<sup>1^</sup>, Tanya K. Marvi, MD<sup>1^</sup>, Samuel L. Posey, BS<sup>1</sup>, Michael A. Benvenuti, MD<sup>1</sup>, Thomas J. An, MD<sup>1</sup>, Kevin M. Dale, MD<sup>3</sup>, Steven A. Lovejoy, MD<sup>3,5</sup>, Jeffrey E. Martus, MD<sup>3,5</sup>, Megan E. Johnson, MD<sup>3,5</sup>, Gregory A. Mencio, MD<sup>3,5</sup>, Stephanie N. Moore-Lotridge, BS<sup>2,3</sup>, Isaac P. Thomsen, MD MSCI<sup>5,6</sup>, Jonathan G. Schoenecker, MD PhD<sup>2,3,4,5\*</sup>

Vanderbilt University, Nashville, Tennessee USA

1) School of Medicine

2) Department of Pharmacology

Vanderbilt University Medical Center, Nashville, Tennessee USA

3) Department of Orthopaedics and Rehabilitation

4) Department of Pathology Microbiology and Immunology

5) Department of Pediatrics

6) Division of Infectious Diseases

^ Indicates authors contributed equally

\* To whom correspondence should be referred.

*Accepted August 2018 to the Journal of Pediatric Orthopaedics*

## *Abstract*

### *Background*

The rate of venous thromboembolism (VTE) in children with musculoskeletal infections (MSKI) is markedly elevated compared to hospitalized children in general. Predictive biomarkers to identify high risk patients are needed to prevent the significant morbidity and rare mortality associated with thrombotic complications. We hypothesize that over-activation of the acute phase response (APR) is associated with the development of pathologic thrombi and we aim to determine whether elevations in C- reactive protein (CRP) are associated with increased rates of thrombosis in pediatric patients with MSKI.

### *Methods*

A retrospective cohort study measuring CRP in pediatric MSKI patients with or without thrombotic complications.

### *Results*

The magnitude and duration of elevation in CRP values correlated with the severity of infection and the development of pathologic thrombosis. In multivariable logistic regression, every 20 mg/L increase in Peak CRP was associated with a 29% increased risk of thrombosis ( $p < 0.001$ ). Peak and Total CRP were strong predictors of thrombosis with area under the ROC curve of 0.90 and 0.92, respectively.

### *Conclusions*

Future prospective studies are warranted to further define the discriminatory power of CRP in

predicting infection-provoked thrombosis. Pharmacologic prophylaxis and increased surveillance should be strongly considered in patients with MSKI, particularly those with disseminated disease and marked elevation of CRP.

### *Introduction*

Vascular thrombosis results in significant morbidity and mortality. In a systematic review, Kim *et. al.* found that in patients with deep venous thrombosis (DVT), 15% developed a pulmonary embolus (PE), 16% recurred, and 8% resulted in death. [148] Furthermore, the rate of vascular complications are increasing in hospitalized pediatric patients. [149] A multicenter analysis of up to forty tertiary care hospitals cited a 70% increase in the annual rate of venous thromboembolism (VTE) over a 7-year span. [150]

Infection has been identified as a significant risk factor for pathologic thrombosis. [148, 151] Pediatric patients with musculoskeletal infections (MSKI) develop thrombotic complications at significantly higher rates than those of the general inpatient pediatric population. In a systematic review, Mantadakis *et. al.* reported that 9% of patients with MSKI developed a DVT and a subset of this population sustained significant systemic sequelae including respiratory distress, multi-organ failure, and even death. [152, 153] Furthermore, the potentially lethal triad of osteomyelitis, DVT, and septic thromboembolism has been described in multiple reports. [154, 155] Despite the growing body of literature describing the association between MSKI and thrombosis, few studies have defined specific clinical predictors.

The acute phase response (APR) is the body's hormonal response to injury that resolves



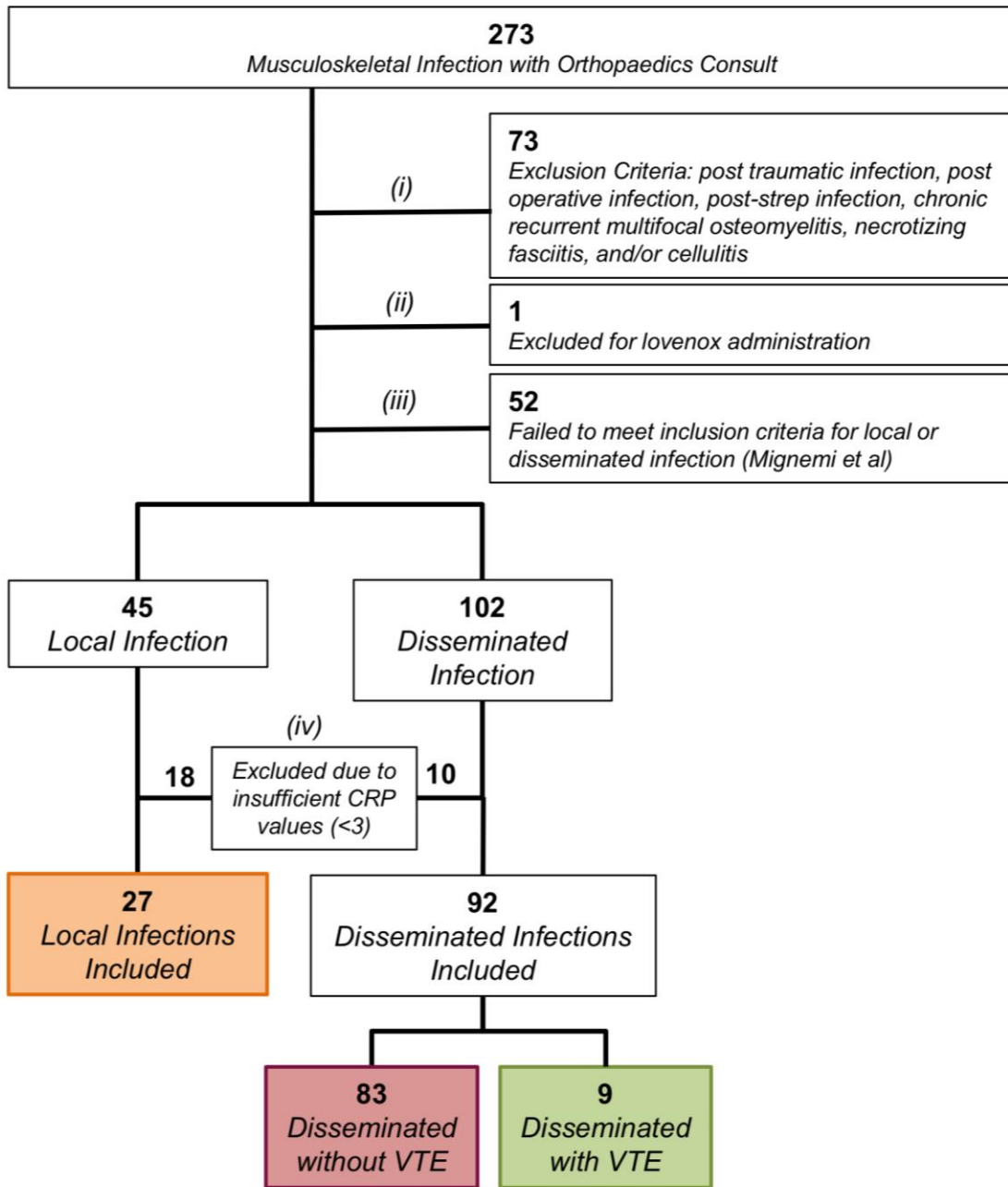
bleeding, susceptibility to infection, hypoxia, and tissue dysfunction (Figure 3). The initial phase of the APR involves activation of the coagulation system to form fibrin and platelet webs that stop bleeding, contain damaged tissue, and prevent hematogenous spread of pathogens. [15, 156-158] CRP, for example, is a well-known acute phase reactant with established pro-inflammatory as well as pro-coagulant effects through its induction of tissue factor and plasminogen activator inhibitor-1. [156, 159] While the APR is essential for survival and repair following tissue injury, extreme or prolonged activation of the APR in the setting of malignancy, polytrauma, and infection has been linked to vascular complications including thrombosis, endothelial dysfunction, and disseminated intravascular coagulation (Figure 3). [160] Thus, we hypothesize that the magnitude and duration of the APR, as measured by CRP, correlates with the severity of infection and can be used to predict thrombotic complications in pediatric MSKI.

#### *Methods:*

##### *Study Design*

This retrospective review was approved by the Vanderbilt University Medical Center IRB. Patients included were ages 0 to 18 years who had an orthopaedic consult placed for MSKI from 2008-2013 at a single institution. Demographic, diagnostic, and complication data were extracted from the medical record. CRP values were collected from the time of admission until CRP normalization (CRP <10.0 mg/L). Exclusion criteria included post-traumatic infection, post-operative infection, post-streptococcal disease, chronic recurrent multifocal osteomyelitis, necrotizing fasciitis, cellulitis, and thrombotic prophylaxis with enoxaparin (Figure 30i and 1ii). Inclusion in the study required confirmed local or disseminated infection as described by Mignemi et. al. [161] Classification as local infection required confirmed superficial abscess,

septic arthritis, pyomyositis, or osteomyelitis in one anatomic site by imaging, positive local culture (including PCR positive) or fluid/tissue consistent with infection (grossly purulent, cell count >50,000). Patients with involvement of two distinct anatomic sites by imaging or fluid/tissue analysis as above, two or more positive blood cultures, and/or VTE were classified as having disseminated infection (Figure 30iii). Patients with less than three CRP values were excluded from the study (Figure 3iv). Venous thromboembolic complications (VTE) were defined as DVT, pulmonary emboli, or septic pulmonary emboli confirmed by imaging. While most providers independently identified DVT, septic pulmonary emboli were included in the criteria for VTE due to its association with DVT. Due to varying clinical presentations, indicators for imaging for thrombotic complications included clinical symptoms (hypoxia, ischemia, pain, persistently positive blood cultures despite proper antibiotics and debridement), incidental findings, and imaging orders due to high clinical associations (i.e. high association of VTE with osteomyelitis). Thrombotic complications were identified with various modalities including MRI, CT, or Doppler imaging. The rate of pathologic thrombosis in this patient set was previously reported. [16]



**Figure 30: Flow diagram of pediatric MSKI patient selection.**

### *Statistical Analysis*

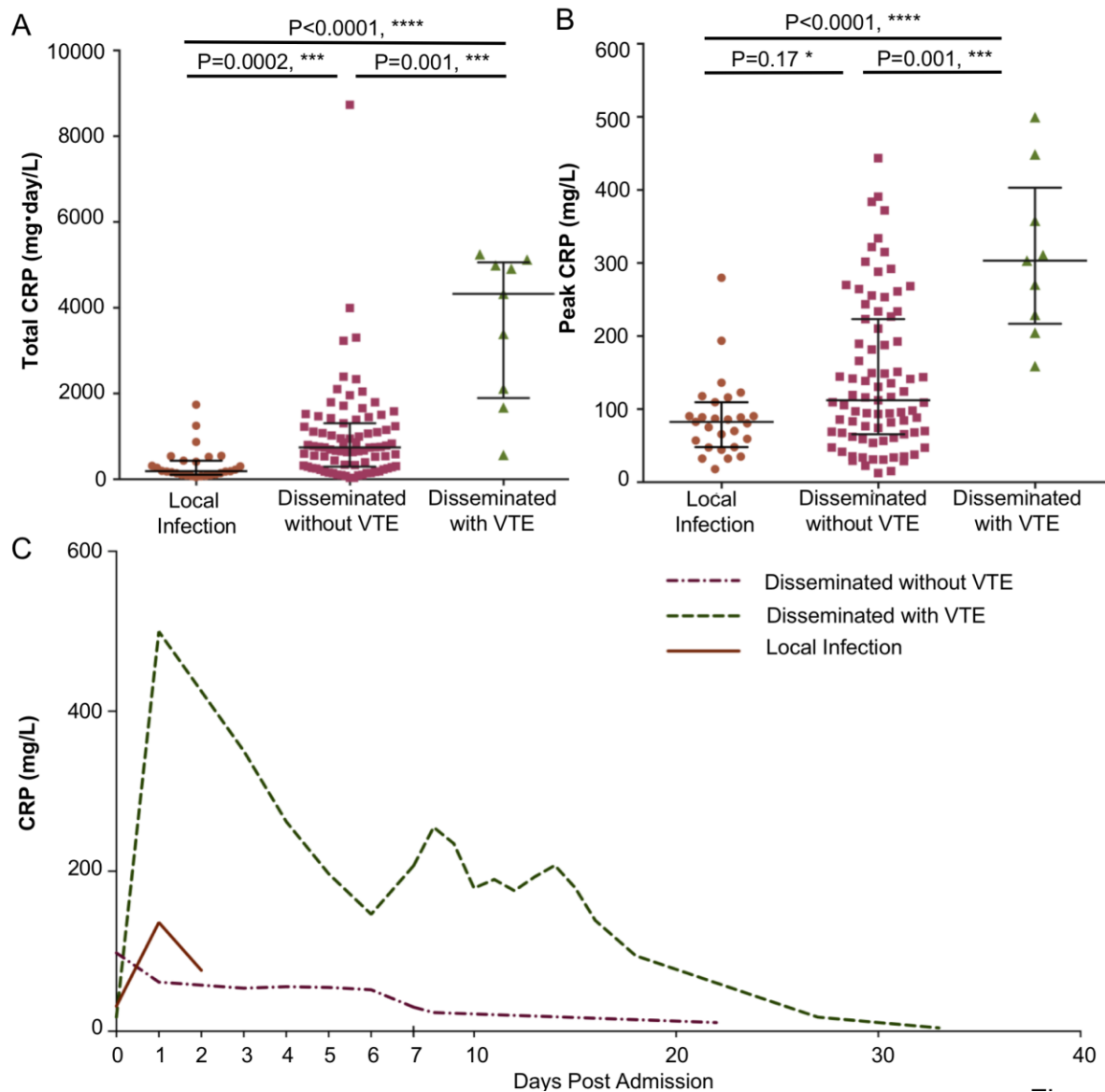
A two-sample t-test was used to compare the mean age between patients with and without vascular thrombosis. Peak CRP was defined as the maximum CRP from time of admission to

CRP normalization. Total CRP was defined as the area under the CRP curve calculated by trapezoidal numerical integration in MATLAB (Natick, MA). Peak and Total CRP were compared between cohorts by non-parametric ANOVA (Kruskall-Wallis Test) followed by a Dunn's post-hoc multiple comparison test to adjust the p-values for multiple comparisons. A multivariable binary logistic regression and predictive margins for each level of CRP was performed in Stata (Stata15.0, StataCorp LP; College Station, TX). Age and gender were selected for inclusion in the model a priori. Receiver operator curves (ROC) were utilized to determine the discriminatory power of peak and total CRP to predict thrombosis with calculations of area under the ROC curve to determine probability of correct prediction.

### *Results*

Overall, 273 pediatric patients with suspected MSKI were identified. Of these, 119 patients met criteria for stratification into either local infection (N=27), disseminated infection without VTE (N=83), or disseminated infection with VTE (N=9) as shown in the CONSORT flow diagram (Figure 30). No patients in the local infection cohort sustained a thrombotic complication. All patients who sustained a thrombotic complication presented with osteomyelitis plus a concomitant infection of the MSK system including septic joint, myositis, and pyomyositis. The mean age for local infection was 4.4 years (67% of patients were male), and the mean age for disseminated infection without VTE was 6.8 years (58% male). Disseminated infection with VTE was diagnosed in 9 patients (7.6%), all of whom were male. The mean age of patients with VTE (9.3 years) was significantly greater than that of patients without VTE (6.2 years,  $p=0.022$ ). The rate of thromboembolism has previously been reported within a subset of this cohort with proven *S aureus* MSKI at 9.9%. [16]

CRP levels between cohorts were measured as both Total (area under the curve) and Peak values. While Peak CRP measures the magnitude of the acute phase response at a single time point, Total CRP elevation measures the overall exposure to an activated APR by capturing the magnitude and duration of elevation (Figure 31C). Total CRP differed significantly between the three cohorts and increased with infection severity as follows: local, disseminated without VTE, and disseminated with VTE (Local vs Disseminated without VTE,  $p=0.0002$ ; Local vs Disseminated with VTE,  $p<0.0001$ ; Disseminated without VTE vs disseminated with VTE,  $p=0.001$ ) (Figure 31 & Table 1). Likewise, Peak CRP was significantly greater in patients with VTE compared to those with local infection or dissemination infection without VTE ( $p<0.001$  and  $p=0.001$  respectively). Furthermore, in patients without VTE, Peak CRP was greater in disseminated infection compared to local infection, although this difference did not reach statistical significance ( $p=0.17$ ).

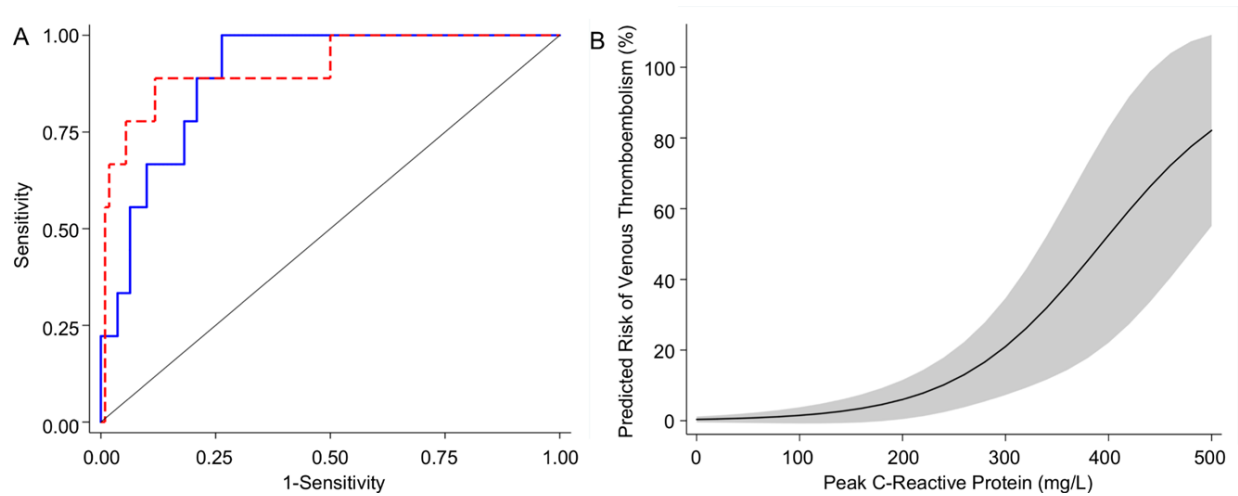


**Figure 31: Cumulative and peak CRP for pediatric MSKI patients.** A) Total CRP as measured by AUC. B) Peak CRP values. C) Representative CRP time course of the median patient per cohort as determined by AUC. Statistical comparison per group conducted with a non-parametric ANOVA with correction for Dunn’s multiple comparisons test. P values reported are adjusted for multiplicity. Alpha=0.05.

**Table 1: CRP Values Per Cohort**

	<b>Median AUC CRP (mg*d/L)</b>	<b>Median Peak CRP (mg/L)</b>
<i>Local</i>	190.1	82.5
<i>Disseminated w/o VTE</i>	742.4	112.1
<i>Disseminated w/ VTE</i>	4324	303.4

Overall, Peak CRP elevation was strongly correlated with risk of VTE. ROC for Peak and Total CRP had similar discriminatory power (Figure 33A). Area under the ROC was 0.90 for Peak CRP and 0.92 for Total CRP (95% CI: 0.83 - 0.97; 0.81-1.0, respectively). Increasing Peak CRP was associated with the development of VTE independent of patient age (OR for a 20mg/L increase: 1.29, confidence interval (CI): 1.12 - 1.48,  $p < 0.001$ ). Thus, a 20 mg/L increase in Peak CRP conferred a 28% increased risk of VTE by logistic regression (Figure 32B). The predicted probabilities of VTE for each level of CRP are shown in Table 2 and Figure 32B (model  $p < 0.0001$ ). Age was not significantly associated with VTE in univariate analysis or in the multivariable model with Peak and Total CRP ( $p = 0.05$ ,  $p = 0.59$ ,  $p = 0.52$ , respectively). All patients with VTE were male; therefore, patient sex could not be included in the model.



**Figure 32: Predictive Models of CRP for VTE in MSKI.** A) Receiver operator curves [149] for Peak (blue, solid line) and Total CRP (red, dashed line). Area under the ROC curve is similar for Peak and Total CRP (Peak CRP: 0.90; Total CRP: 0.92). Increased discriminatory power of Total CRP is likely conferred by its ability to include the duration of elevation in the prediction. B) Predicted probability of VTE by CRP level. The predicted probabilities of VTE with increasing CRP are represented by the black solid line. Shaded gray areas represent the 95% CI for prediction.



**Table 2: Effect of Peak CRP on Predicted Probability of VTE**

<b>CRP (mg/L)</b>	<b>Predicted Probability (%)</b>	<b>P-value</b>	<b>CI (%)</b>	
0	0.5	0.337	-0.6	1.6
20	0.7	0.305	-0.6	2.0
40	0.9	0.271	-0.7	2.4
60	1.1	0.235	-0.7	3.0
80	1.4	0.199	-0.8	3.7
100	1.9	0.162	-0.7	4.5
120	2.4	0.126	-0.7	5.4
140	3.0	0.094	-0.5	6.6
160	3.9	0.065	-0.2	8.0
<b>180</b>	<b>4.9</b>	<b>0.042</b>	<b>0.2</b>	<b>9.7</b>
<b>200</b>	<b>6.2</b>	<b>0.026</b>	<b>0.8</b>	<b>11.7</b>
<b>220</b>	<b>7.9</b>	<b>0.015</b>	<b>1.5</b>	<b>14.2</b>
<b>240</b>	<b>9.9</b>	<b>0.009</b>	<b>2.4</b>	<b>17.3</b>
<b>260</b>	<b>12.4</b>	<b>0.006</b>	<b>3.5</b>	<b>21.2</b>
<b>280</b>	<b>15.3</b>	<b>0.005</b>	<b>4.6</b>	<b>26.1</b>
<b>300</b>	<b>18.9</b>	<b>0.005</b>	<b>5.7</b>	<b>32.0</b>
<b>320</b>	<b>23.0</b>	<b>0.005</b>	<b>6.8</b>	<b>39.2</b>
<b>340</b>	<b>27.7</b>	<b>0.006</b>	<b>7.9</b>	<b>47.5</b>
<b>360</b>	<b>32.9</b>	<b>0.007</b>	<b>9.1</b>	<b>56.7</b>
<b>380</b>	<b>38.6</b>	<b>0.007</b>	<b>10.7</b>	<b>66.5</b>
<b>400</b>	<b>44.7</b>	<b>0.006</b>	<b>12.9</b>	<b>76.4</b>
<b>420</b>	<b>50.9</b>	<b>0.004</b>	<b>15.9</b>	<b>85.9</b>
<b>440</b>	<b>57.0</b>	<b>0.003</b>	<b>19.7</b>	<b>94.3</b>
<b>460</b>	<b>63.0</b>	<b>0.001</b>	<b>24.6</b>	<b>101.4</b>
<b>480</b>	<b>68.6</b>	<b>0.000</b>	<b>30.3</b>	<b>106.8</b>
<b>500</b>	<b>73.7</b>	<b>0.000</b>	<b>36.8</b>	<b>110.6</b>

*Model p-value <0.001, statistically significant values are bolded*

*CI: 95% confidence interval*

## *Discussion*

This retrospective study demonstrates that the peak level and duration of CRP elevation are associated with both the severity of infection and risk of thrombotic complications in children with musculoskeletal infection (Figure 31C). Multiple studies have identified systemic infection as a risk factor for the development of DVT, and this study shows that CRP may be a prognostic biomarker which can be used to further risk-stratify patients. [148, 151] Serial CRP measurement may therefore be a diagnostic and prognostic tool that allows for real-time tracking of the APR.

CRP levels rise within 4-6 hours of tissue damage and rapidly fall following acute tissue injury, making CRP a nonspecific diagnostic tool following any tissue injury. [162] However, CRP values have been shown to be sensitive in the diagnosis of pediatric MSKI. For example, Unkila-Kallio et al demonstrated that CRP values are elevated in 98% of cases of acute hematogenous osteomyelitis. [163] Furthermore, in patients with septic arthritis superimposed on hematogenous osteomyelitis, CRP levels were further elevated and remain elevated for a longer duration than in patients with osteomyelitis alone. [163] More recently, measurement of the APR has been utilized to stratify patients and predict clinical outcomes. CRP at presentation, 48 hours, and 96 hours from admission have been shown to be associated with prolonged hospitalization in pediatric patients with hematogenous osteomyelitis. [164] Martin *et. al.* demonstrated that cases of complicated osteomyelitis, defined as multifocal disease or osteomyelitis requiring a surgical procedure or resulting in readmission to the hospital within 6 months, were associated with an elevated CRP at presentation and an increased duration of CRP elevation, supporting the use of CRP as both a diagnostic and prognostic tool in MSKI. [165]

Beyond its diagnostic and prognostic value, serial CRP measurement may guide therapeutic intervention by identifying high risk patients for targeted DVT prophylaxis. Rudolf Virchow was among the first to recognize that derangements in systemic factors can contribute to vascular dysfunction and described three elements that contribute to venous thrombosis: stasis, endothelial damage, and a hypercoagulable state. [166] Thus, mechanical, biochemical, and anatomic disturbances underlie vascular thrombosis. While congenital coagulopathies, pregnancy, and malignancy are well-known hypercoagulable states, it is important to recognize that the body's natural response following significant injury, such as disseminated infection, similarly leads to a systemic dysfunction of the vasculature. [167-169] The intricate relationship between inflammation and coagulation has been well defined in injury models such as total joint arthroplasty and sepsis, leading to the use of prophylactic antithrombotic agents. [170, 171] For example, prior to the routine use of prophylaxis in adult total joint arthroplasty, VTE occurred in up to 40-60% of patients. With routine administration of post-operative low molecular weight heparin these rates have dropped to 15.4%. [170, 172] MSKI similarly places patients at a high risk for derangements in the APR that could lead to vascular complications and therefore prospective studies to evaluate pharmacologic prophylaxis are warranted.

This study had several strengths and limitations that influence the interpretation of the results. Strengths of this study include the longitudinal collection of laboratory data in well-characterized patients. CRP was treated as a continuous variable, which allowed us to estimate thresholds of CRP that predispose patients to VTE while avoiding arbitrarily stratifying patients into low and high-risk CRP groups as has been done in prior studies. Additionally, the rates of VTE in this cohort were similar to those reported in the literature, suggesting that it is a representative

sample<sup>5</sup>. While most thrombotic complications in the literature are reported in patients with osteomyelitis, all patients in this study with thrombotic complications presented with concomitant infections of the MSK system (septic arthritis, myositis, pyomyositis, abscesses, etc.). At our institution, it is common for patients to present with fulminant and complicated infections. Thus, in order to account for all patients with infections provoking a severe inflammatory response with subsequent complications, all patients with MSK infections were included.

While data was collected longitudinally, one limitation of this study was the irregular timing of laboratory measurements which may have prevented the capture of Peak CRP values and influenced the calculation of the Total CRP. For example, changes in the frequency of measurement would impact the total CRP depending on the trend of the measurement. Therefore, if every peak and trough is captured by the data, the total CRP would reflect the true AUC. Given this limitation and the retrospective nature of this study, the calculations made throughout only utilized values obtained in the EMR and did not account for unknown and unmeasured CRP values.

Furthermore, while CRP measurements are commonly used to evaluate MSK infection, no standardize protocol currently exists and therefore data is obtained at the discretion of the individual providers. Therefore, until a standardized measurement protocol used by all physicians is implemented, retrospective studies of this type will be limited by the data available. As such, we hope that the findings from the study will provide the impetus for future prospective studies assessing the value of more frequent CRP trending and identification of the ideal interval

to gather meaningful data in a cost-effective manner.

Finally, a proportion of patients were excluded from this study for insufficient CRP measurements. In patients who met criteria for a local infection, those who were excluded had significantly lower admission CRP values (Kruskall-Wallis Test,  $p=0.014$ ). This suggests that a disproportionate number of patients excluded from the study had less severe infections, which likely weakened our ability to discern significant difference in CRP values between groups based on severity of disease.

While infection represents one model of tissue injury that can lead to an exuberant or prolonged APR, this overarching theory can be applied to various other mechanisms of injury including trauma, burns, surgical procedures, and malignancy. Neoplastic cells, for example, lead to significant tissue injury as they invade and destroy native tissue. Malignancy is therefore a form of continuous tissue injury that persists until chemotherapy or surgical resection treats the underlying malignancy. While “hypercoagulability of malignancy” is a well-defined pathologic state [168], measuring the acute phase response is an underutilized tool that may allow clinicians to integrate multiple possible predictors to quantify the risk of complications. [168] In a prospective study of adult patients with cancer, Kroger et al. found that CRP was the only variable in multivariable analysis to be associated with increased risk of VTE. [173] Therefore, monitoring CRP to evaluate for complications may be widely applicable across disease states and patient populations.

### *Summary*

In conclusion, pediatric patients with musculoskeletal infections develop thromboses at markedly increased rates compared to the general inpatient population. The magnitude (peak) and duration (total) of APR activation are associated with both the severity of infection and the development of VTE. These data support the need for enhanced monitoring and consideration of prophylaxis for VTE in pediatric patients with infection, especially those with disseminated infection and markedly elevated or prolonged CRP elevations. Though future prospective studies are needed to determine absolute CRP thresholds and in order to define the efficacy of CRP-guided VTE risk stratification.

This study selected and stratified patients based on their infection and DVT status, and then assessed their CRP values. Next, we conducted another retrospective study where we removed the variable of infection, and instead look at our pediatric population for DVT and an associated CRP at the time of the complication, independent of the inciting factor. Building upon the findings in Article 4, we hypothesized that, independent of the injury experience by the child, CRP values could be predictive of a DVT.

This data was collected utilizing the synthetic derivative database at Vanderbilt University. Through analyzing the de-identified patient database, we began to observe a dichotomy in the patients selected. Specifically, when collecting records for pediatric DVTs, we observed two cohort of patients: 1) very young (>1 year old) patients with congenital heart disease (CHD), who has received a line that experienced a DVT, or 2) older patients, many of which had an infection, did not receive a line and experience a DVT. This dichotomous observation was very

interesting, both from a biological as well as a clinical guidelines perspective.

Currently, the best practice guidelines established for preventing DVTs and other thrombotic event in pediatric patients, encompasses both of the cohorts we observed into the same guidelines. These guidelines are set by a group of physicians that take into consideration the current best practices and data available, synthesize their recommendations, which are passed onto the hospitals to implement. Given the rarity of pediatric DVTs as a whole, many previous studies have necessitated grouping these two cohort together to reach statistical significance. However, our observations led us to question whether, instead of being consider equivalent, these populations were indeed dichotomous and therefore, should be separated when considering prophylaxis as well as monitoring regimes. To answer this question, we conducted the following study (Article 5) with the help of a wonderful biostatistician, Abigale Henry.

Article 5: Should Catheter and Non-Catheter Related DVT Cohorts Be Mixed for Risk Assessment?

Daniel Y. Hong<sup>a</sup>, BA, Samuel L. Posey<sup>a</sup>, BS, Abigail L. Henry<sup>c</sup>, MPH, Stephanie N. Moore-Lotridge<sup>b,c</sup>, BS, Jonathan G. Schoenecker<sup>b,c,d,e,\*</sup>, MD PhD

Vanderbilt University, Nashville, TN

<sup>a</sup>School of Medicine

<sup>b</sup>Department of Pharmacology

Vanderbilt University Medical Center, Nashville, TN

<sup>c</sup>Department of Orthopaedics and Rehabilitation

<sup>d</sup>Department of Pediatrics

<sup>e</sup>Department of Pathology

\*indicated corresponding author

*Submitted September 2018 for Publication*



## *Abstract*

### *Objective*

Deep vein thromboses (DVT) can be categorized as catheter related (CRT) or non-catheter related thromboses (NCRT). This study compared known risk factors for pediatric DVT between CRT and NCRT. We believe that differences in risk profiles of these groups demand differentiated risk assessment and prophylaxis studies, something not currently done due to the rarity of pediatric DVT.

### *Methods*

Case-control study. Inclusion criteria were patients under 18 years with ICD-9 code for DVT, CPT code for ultrasound, and C-reactive protein (CRP) lab value within one week prior to ultrasound. Patients without confirmed DVT, without CRP lab value within one week prior to ultrasound report, or on extra-corporeal membrane oxygenation were excluded. Patients were stratified upon presence of catheter within vessel of thrombosis.

### *Results*

NCRT had higher average pre-thrombosis CRP (132.4 mg/L +/- 90.2) than CRT (48.9 mg/L +/- 63.2),  $p < 0.0001$ . Average age of NCRT (4.27 years) was higher than that of CRT (1.65 years),  $p < 0.0001$ . CRT had a higher proportion of congenital heart disease (CHD) than NCRT (52% vs 18%),  $p < 0.001$ . Odds of having CRT, as opposed to NCRT, increased with lower CRP (OR=0.99,  $p < 0.001$ ) and with presence of CHD (OR= 3.09,  $p = 0.04$ ).

### *Conclusions*

Our results demonstrate differences in catheter status, age, CHD, and inflammation in children with thrombosis. CRP levels preceding CRT are lower than that of NCRT. Concurrent CHD affects catheter status's relationship with CRP. Therefore, we suggest that CRT and NCRT are dichotomous populations and should not be combined in studies of risk and prophylaxis.

### *Introduction*

Venous thromboembolism (VTE) is a rare yet serious complication in pediatric patients. VTE encompasses pulmonary embolism, cerebral sinus venous thrombosis and deep vein thrombosis (DVT).[174] DVT is the predominant phenotype of pediatric VTE and has multiple risk factors, as initially established by Virchow.[175] Although guidelines for DVT prophylaxis in hospitalized adults were established decades ago, similar guidelines have only recently been proposed for hospitalized children.[176]

An important categorization of pediatric DVT is catheter related thrombosis (CRT) and non-catheter related thrombosis (NCRT).[177, 178] Risk factors besides venous catheter include cardiac pathology, systemic inflammation from cancer or infection, and coagulation abnormalities.[179] Importantly, each variable increases the risk for developing a DVT to a different degree, complicating combined risk assessment across variables. For example, when creating cohorts to determine DVT risk assessment, prior investigations have separated children and adults, as it is well established that their risk patterns for DVT differ significantly.[180] Furthermore, the efficacy of mechanical or pharmacologic DVT prophylaxis also varies according to the number and nature of the variables present.[181] For example, although low

molecular weight heparin is efficacious at preventing DVT in an adult patient undergoing an elective orthopaedic surgery, it is less efficacious in a pediatric patient undergoing surgery and chemotherapy for a tumor.[182]

Another problem in creating study cohorts to help determine risk and efficacious prophylaxis guidelines in children is that pediatric DVT are rare occurrences. To overcome this obstacle, many study cohorts combine CRT and NCRT cases together to increase sample size.[183, 184] This practice, while providing greater statistical power, runs the risk of combining dissimilar cohorts, leading to conclusions that may be applicable to one cohort but not the other, or mask results altogether.[176] Specifically, pediatric CRT occurs at a rate of 8:1 as compared to NCRT.[185-187] Thus, the combined cohorts created to determine risk and therapeutic prophylaxis of pediatric DVT are typically biased towards pathologic variables associated with CRT. Here, we tested the hypothesis that pediatric patients with CRT are significantly different from NCRT in other variables known to predispose to thrombosis: age, systemic inflammation, and known congenital heart disease history.[185-187] If found to be distinct conditions, this may indicate CRT and NCRT as separate conditions and thereby provide the basis for future studies to delineate NCRT from CRT for determining prophylaxis guidelines.

## *Methods*

### *Study Design*

Utilizing a de-identified database from a single institution, referent to as the Synthetic Derivative (SD), we selected patients aged 0 to 18 years with an ICD-9 code for a DVT, independent of location, and at least one CRP laboratory value. The SD is a de-identified copy of medical record

databases created for research purposes and contains over 1.5 million electronic records. Datasets contain no HIPAA identifiers and are exported directly from the system into a statistical/analysis program.

Patient were excluded from the study if they were placed on extra-corporeal membrane oxygenation (ECMO) during the hospitalization of thrombosis discovery, lacked confirmation of the DVT on ultrasound report, or lacked a CRP value within a week prior to ultrasound report. Prior to exclusion criteria, 489 patients were identified, 323 were excluded due to ECMO (n=101), insufficient conformation by imaging (n=103), or insufficient CRP measurements within 1 week prior to event detection (n=119), leaving 166 patients. The included population was then stratified by the presence (n=133; CRT) or absence (n=33; NCRT) of a venous catheter within the vessel of the DVT as determined by ultrasound report. Patients who previously had a catheter within the vessel of the DVT that was then removed within one week prior to the ultrasound report were included in the CRT group. The etiology for hospital admission was determined for each patient via chart review.

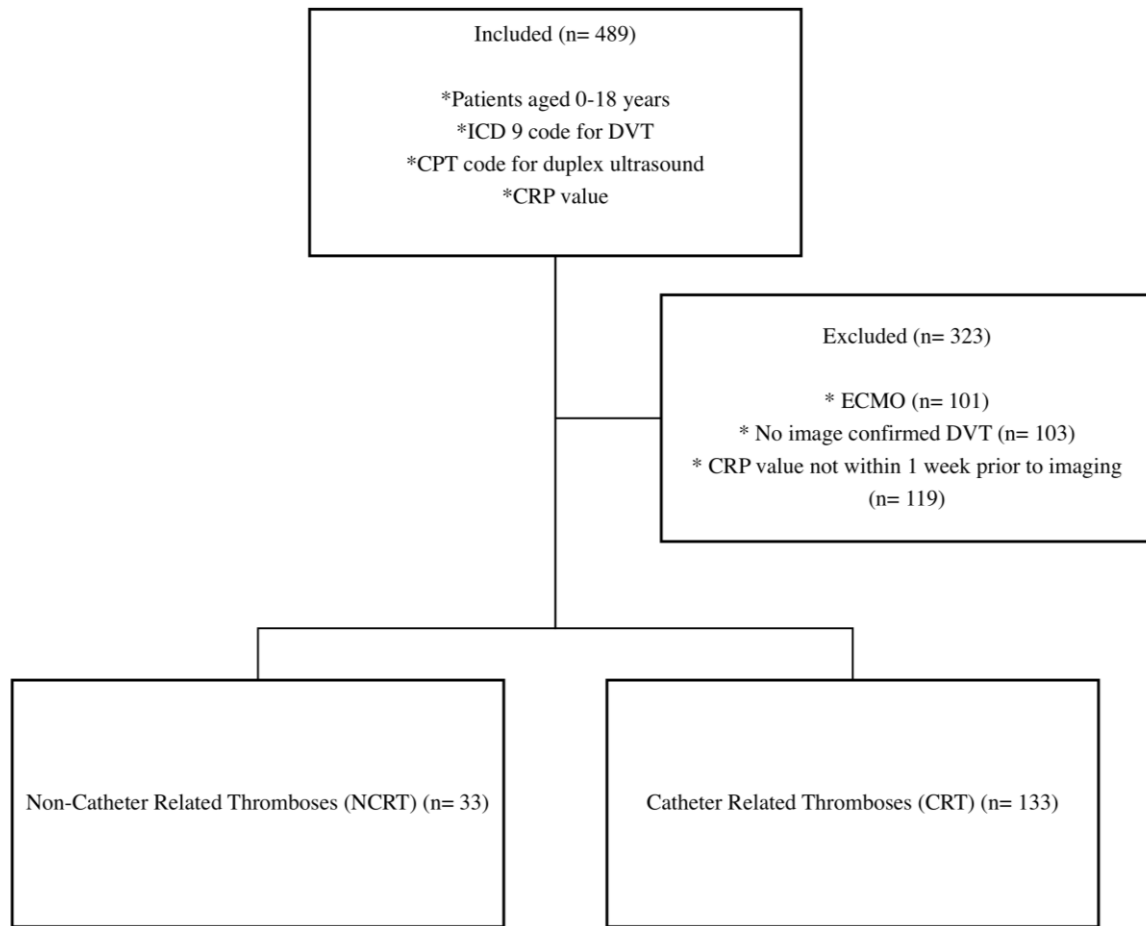
### *Statistical Analysis*

Mann-Whitney U tests were used to compare the average age, CRP value, and selected patient characteristics between the CRT and NCRT cohorts. Pearson's chi-square tests were used to examine the relationships between catheter thrombosis association, CHD, death, and age group. A logistic regression analysis was conducted to predict catheter thrombosis association with CRP, age, and CHD. Stratified Mann-Whitney U analyses were conducted to assess the effect of CHD and catheter status on CRP levels. Kruskal-Wallis and Mann-Whitney U tests were

conducted to test for differences among a 4-level interaction variable and CRP level. A correlation coefficient (r) was calculated for the effect size. The interpretation of effect size was determined using the following intervals: 0.1 to 0.3 for small effect, 0.3 to 0.5 for medium effect, and greater than 0.5 for large effect size. Effect sizes greater than or equal to 0.3 were considered to be meaningful.[188]

*Results: Pediatric Patients with CRT Are Younger Than Those with NCRT*

Among the 166 patients included in this study (Figure 33), we observed that the CRT group (n=133) possessed a significantly higher proportion of patients under the age of 1 year (77%) compared to the NCRT (n=33) group (45%,  $p < 0.001$ ). The proportion of male to female patients (CRT- 53%, NCRT- 52%,  $p = 0.91$ ) was comparable between the cohorts, as was racial composition ( $p = 0.42$ ). (Table 3)



**Figure 33: CONSORT flow diagram of patient study population**

**Table 3: Demographic Characteristics of DVT Patients Aged 0-18 by Catheter Status**

Characteristics	CRT (n = 133)	NCRT (n = 33)	p <sup>a</sup>
	n (%)	n (%)	
Sex			0.91
Male	70 (53)	17 (52)	
Female	63 (47)	16 (48)	
Race and/or ethnicity			0.42 <sup>b</sup>
Caucasian	86 (65)	25 (76)	
African American	22 (17)	5 (15)	
Hispanic or Latino	13 (10)	2 (6)	
Asian or Pacific Islander	2 (2)	1 (3)	
Unknown	10 (8)	0	
Age			<0.001
< 1 year	102 (77)	15 (45)	
≥ 1 year	31 (23)	18 (55)	
Deceased			0.11
No	105 (79)	30 (91)	
Yes	28 (21)	3 (9)	
Congenital Heart Disease			<0.001
No	64 (48)	27 (82)	
Yes	69 (52)	6 (18)	
Reason for Admission			<0.001
CHD	69 (52)	6 (18)	
Infection	26 (20)	20 (61)	
Other	38 (29)	7 (21)	
CRP, mg/L			<0.001 <sup>c</sup>
Median, IQR	22.4 58.3	148.3 136.9	

IQR, Interquartile range

<sup>a</sup> Pearson Chi-Square, except where noted.<sup>b</sup> Fisher's Exact Test.<sup>c</sup> Mann-Whitney U.*Congenital Heart Disease Is More Prevalent in Patients with CRT Than Patients With NCRT*

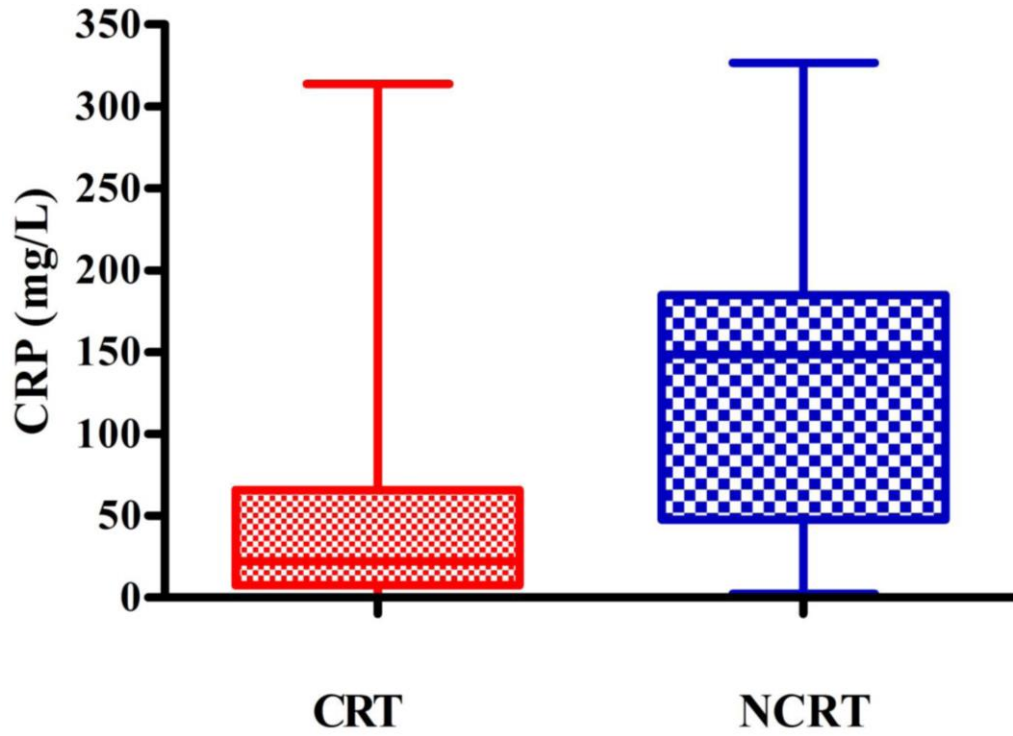
Etiology for admission varied between the two cohorts. Among patients with CRT, CHD and associated procedures was the predominant admission diagnosis (52%) with infection second (20%) (Table 3). In patients with NCRT, infection was the predominant reason for admission (61%), while congenital heart disease was less common (18%,  $p < 0.001$ ). There was a significant relationship between the two groups and CHD status ( $p < 0.001$ ) (Table 3). In total, 75 patients were identified with CHD (Table 3). Less common etiologies associated with CRT and NCRT

included trauma, auto-immune conditions, and inherited hypercoagulable conditions.

*Catheter Status, But Not CHD, Significantly Affects CRP Levels In Patients With Venous Thrombosis*

CRP levels in each cohort were determined as the value closest to the date of the ultrasound report of venous thrombosis as to best reflect the inflammatory state responsible for the generation of the thrombosis seen on ultrasound. The median CRP level differed significantly between patients with NCRT (148.3, IQR = 47.8 – 184.7) compared to CRT (22.4, IQR = 7.5 – 65.8,  $p < 0.001$ ) (Figure 34). A medium effect size between catheter status and CRP ( $r = 0.38$ ) was detected, thereby further establishing the difference in CRP between cohorts as statistically meaningful (Table 4). In contrast, there was no significant association between CHD and CRP; the median CRP levels in patients with CHD (26.1) were lower than in patients without CHD (41.0, IQR = 6.7 – 135.3,  $p = 0.41$ ). There is also a small effect size between CHD groups and CRP ( $r = 0.06$ ), suggesting that this comparison is not statistically meaningful (Table 4).





**Figure 34: Distribution of CRP values (mg/L) by catheter status.** The median, upper, and lower quartile, and range are depicted

**Table 4: Difference in CRP value by Catheter Status and Congenital Heart Disease**

	n	Median	IQR	Z	r <sup>a</sup>	p <sup>b</sup>
<b>Catheter Status</b>						
NCRT	33	148.3	136.9	-4.95	0.38	<0.001
CRT	133	22.4	58.3			
<b>Congenital Heart Disease</b>						
No	91	41.0	128.6	-0.83	0.06	0.41
Yes	75	26.1	63.5			

IQR, Interquartile range

<sup>a</sup> Measure of effect size.<sup>b</sup> Mann-Whitney U.

*In Pediatric Patients with Venous Thrombosis, Odds of the Thrombosis Being Catheter Associated Increase with Decreasing CRP and Presence Of Congenital Heart Disease*

To assess the odds of CRT occurring, a multivariate logistic regression model with age, CHD, and CRP as independent variables was performed. Among all of our patients, as CRP decreases, the odds of the patient having a catheter related thrombosis increased (OR=0.99, p<0.001). Similarly, patients with CHD have increasing odds of having a catheter related thrombosis (OR=3.09, p=0.04). Age was not a significant predictor of catheter status (OR=0.94, p=0.15) (Table 5).

**Table 5: Difference in CRP value by Catheter Status Stratified by Congenital Heart Disease**

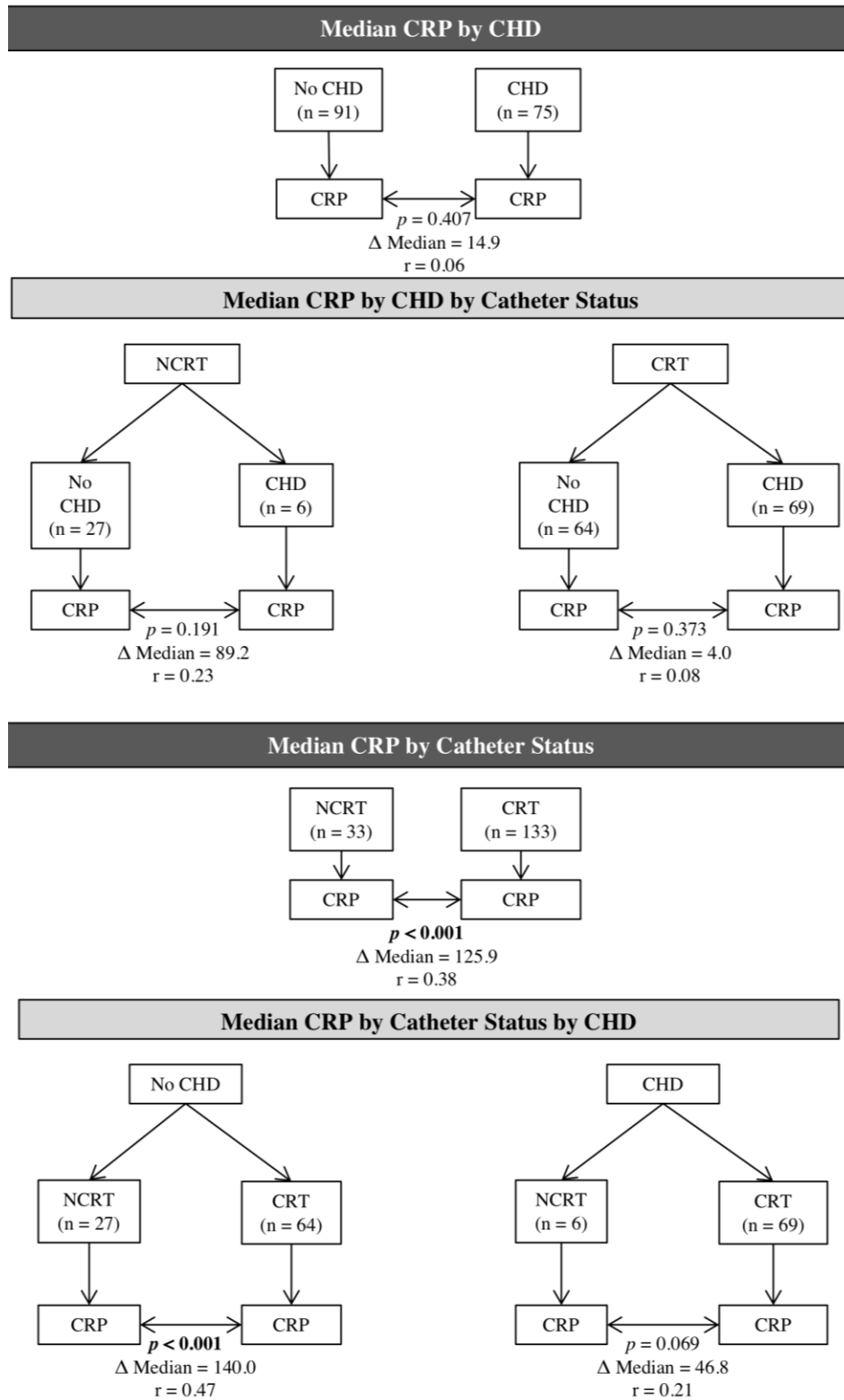
	$\beta$	OR	95% CI		p
			Lower	Upper	
CRP, mg/L	-0.01	0.99	0.98	0.99	<0.001
Congenital Heart Disease	1.13	3.09	1.05	9.12	0.04
Age, y	-0.06	0.94	0.86	1.02	0.15

OR, odds ratio; CI, confidence Interval

<sup>a</sup>  $\chi^2(3) = 38.44, p < 0.001, R^2 = 0.327$

*CHD Interacts with Catheter Status on CRP Levels in Patients With Venous Thrombosis*

Since CHD was a significant predictor of catheter status, a Kruskal Wallis test was run to test for differences in CRP by a four-level variable that combined catheter status and CHD (CRT\*CHD, CRT\*No CHD, NCRT\*CHD, NCRT\*No CHD), with the results being statistically significant ( $p < 0.001$ ). To better understand this effect, a stratified analysis was performed to assess if catheter status had an effect on the association between CRP and CHD (Figure 35). Among patients with NCRT, there is no statistical difference in CRP between patients with CHD or without CHD ( $p = 0.19$ ). The small effect size also suggests that the difference in level of CRP by CHD group among patients with NCRT is not statistically meaningful ( $r = 0.23$ ) (Table 6). Conversely, among patients with CRT, there is also no statistical difference in CRP levels between patients with CHD and those without ( $p = 0.37$ ). The small effect size also suggests that there is not a statistically meaningful difference in CRP level between patients with and without CHD ( $r = 0.08$ ) (Table 6).



**Figure 35: Stratified analysis of interaction effect between CRP, catheter status, and CHD**

**Table 6: Differences in CRP value by Congenital Heart Disease Stratified by Catheter Status**

	n	Median	IQR	Z	r <sup>a</sup>	p <sup>b</sup>
Congenital Heart Disease (CHD) By Catheter Status						
NCRT						
No CHD	27	160.4	146.0	-1.31	0.23	0.19
CHD	6	71.2	83.6			
CRT						
No CHD	64	20.5	45.1	-0.89	0.08	0.37
CHD	69	24.4	60.7			

IQR, Interquartile range

<sup>a</sup> Measure of effect size.

<sup>b</sup> Mann-Whitney U.

A second stratified analysis was conducted to test if CHD status had an effect on the association between CRP and catheter status. Among patients without CHD, median CRP levels were significantly lower in patients with CRT (20.5, IQR = 5.2 – 50.3) compared to those with NCRT (160.4, IQR = 51.6 – 197.6,  $p < 0.001$ ). This relationship is also statistically meaningful as evident by the medium effect size ( $r = 0.47$ ) (Table 7). Conversely, among patients with CHD, median CRP levels were not significantly different in patients with CRT (24.4, IQR = 8.5 – 69.2) compared to those with NCRT (71.2, IQR = 37.2 – 120.8,  $p = 0.07$ ). Additionally, the effect size is small ( $r = 0.21$ ), further suggesting that the difference between level of CRP by catheter status among patients with CHD is not statistically meaningful (Table 7).

**Table 7: Differences in CRP Values by Catheter Status Stratified by Congenital Heart Disease**

	n	Median	IQR	Z	r <sup>a</sup>	p <sup>b</sup>
Catheter Status By Congenital Heart Disease (CHD)						
No CHD						
NCRT	27	160.4	146.0	-4.44	0.47	<0.001
CRT	64	20.5	45.1			
CHD				-1.82	0.21	0.07
NCRT	6	71.2	83.6			
CRT	69	24.4	60.7			

IQR, Interquartile range

<sup>a</sup> Measure of effect size.

<sup>b</sup> Mann-Whitney U.

### *Discussion*

Our results identified a greater amount of CRT than NCRT in pediatric patients with venous thrombosis, as described by literature. In addition, we found 3 other major variables to be different in the largest series of CRT vs NCRT to date: age, CHD, and inflammatory status. These differences support our hypothesis that CRT and NCRT are dichotomous pediatric populations, thereby providing rationale for why these cohorts should not be combined in future studies on pediatric venous thrombosis risk assessment or prophylactic measures.

The literature supporting the differences of these variables between groups is quite variable; for starters, differences in age between CRT and NCRT has been well established. Jaffray *et al.* demonstrated in a literature review that CRT was more likely to occur in neonates whereas NCRT was more common in adolescents.[179] Similar to Jaffray’s findings, Takemoto *et al.* demonstrated that central venous catheter associated thromboses occurred most commonly in infants under the age of 1.[189] The age disparity between CRT and NCRT points to different underlying pathophysiology of thrombosis given the well-established phenomenon of

developmental hemostasis.[190, 191]

Another factor supporting this divergence in pathophysiology is the difference in underlying pathology, namely CHD, in our patients. In this model, the odds of being CRT also increased if the patient had congenital heart disease; conversely, age was not a significant predictor of CRT. This data aligns with the previous principle KIDCAT study, which examined 90 children who had a short term venous catheter placed in their upper extremities.[192] Of these, 95% of these children had CHD, and the remainder had acquired heart disease. The incidence of CRT in the KIDCAT study was 28%, which was concordant with other studies of CRT in children with malignancies and long-term catheters.<sup>21</sup> CHD and malignancy, among other diseases such as sickle cell disease, were risk factors for CRT in other studies.[179]

Median CRP values, as a marker of the inflammatory status, were significantly lower in pediatric patients with CRT compared to those with NCRT. Furthermore, logistic modeling demonstrated that as CRP increased, the odds of being CRT decreased and that of being NCRT increased; this relationship held with and without CHD and age in the model. While previous studies have suggested inflammation's modulatory role in venous thrombosis formation, CRP and other inflammatory markers have not been well studied in the context of venous catheters and thrombosis.[193] Our results potentially suggest that the endothelial damage caused by the catheter lowers the threshold of inflammatory insult necessary to drive a thrombosis, thereby supporting such an idea and the potential utility of CRP in DVT risk prediction. Thus, further studies establishing the predicative capability of inflammatory markers in DVT risk prediction are warranted.

An additional novel aspect of our study was the discovery of an interaction between CHD and catheter status on CRP levels in pediatric patients with a DVT. To our knowledge, no prior studies have highlighted such an interaction. Given our hypothesis that a venous catheter causes endothelial damage that decreases the amount of pre-thrombosis inflammation necessary to generate a DVT, it can be surmised how concurrent congenital heart disease may further drop this threshold, as it and associated corrective procedures are known risk factors for thrombosis generation.[194-196] The large variability in effect sizes within our subgroup analyses suggest that a larger study would be further necessary to fully investigate this relationship between CHD, venous catheters, and pre-thrombosis inflammation.

The demographic data obtained in this study aligns with previous reports of deep vein thromboses in children. The novel KIDCAT study, published in *Pediatrics* in 2008, determined the incidence of thrombosis in children with CHD and central venous catheters to be 28%. [192] Here, we report the prevalence of CHD in children with CRT compared to those with NCRT. The selection bias of infants with CHD in the CRT group is clinically correlative, as these infants likely required venous catheters during their hospitalization for correction of cardiac defects. While the incidence of pediatric CRT is still lower than that of adults, our analysis suggests that children who develop CRT are more likely to be infants and have congenital heart disease than those who develop NCRT.[150]

In summative, these results suggest a difference in baseline venous thrombosis risk between the CRT and NCRT groups. This is most likely due to the studied effects that infantile age and CHD have on the coagulation system.[197] With a still-developing coagulation system that is further



impacted by the demands of cardiac defects, it is arguable that these children have a different coagulation pattern than those who are older and lack such medical history. Related, Vidal *et. al.* conducted a review of 10 studies and did not find evidence that heparin-bonded catheter, unfractionated heparin, low molecular weight heparin, warfarin, antithrombin concentrate or nitroglycerin reduced risk for patients with CRT.[198] Other studies have similarly found lack of efficacy in traditional venous thrombosis prophylaxis regimens in preventing pediatric CRT.[191] While not directly studied here, we believe that further studies of different prophylactic regimens between children with central venous catheters and those without may be necessary to improve clinical guidelines in the future.

### *Strengths and Limitations*

Strengths of this study include the temporal relationship of CRP values to well-established diagnoses of deep vein thromboses. Dual use of ICD codes as well as manual chart review of ultrasound reports established clear demonstration of outcome of interest. Search of the literature suggests that this is one of the largest cohorts of children with catheter related thrombosis studied as well. Demographic data was similar to that reported in literature, suggesting that this is a representative sample.[179, 180] Although there is biologic plausibility that the endothelial damage from the catheter is responsible for the diminished inflammatory response and corresponding CRP value, only one target variable was examined and further studies are necessary to look at other markers. The study was conducted at a single institution; although the results match that of literature, further studies would need to be conducted to confirm results at other institutions. Patients without a CRP value within 1 week prior to DVT were excluded, which may skew the representation of our cohorts.

### *Summary*

Through this study, we compared age, CHD status, and inflammatory profiles between pediatric patients with CRT and NCRT. These differences of age, underlying pathology, and inflammation are all known to affect the development of venous thrombosis. Because of these findings, we suggest that the two cohorts of CRT and NCRT are distinct and should not be combined in future studies that evaluate pediatric VTE prophylaxis.

Through understanding the premise of the APR and harnessing critical marker and patterns of complication, Article 4 & 5 demonstrate the potential clinical impact of such lines of investigation. Through measuring CRP, one acute phase reactant, we have effectively provided a foundation for better patient monitoring and potentially prophylactic intervention. Furthermore, this data has been used to define unique populations, thereby calling into question whether the prophylactic strategies currently applied across both cohorts are truly appropriate. It is important to note that while CRP is a single APR reactant, there are hundreds more markers available to be tested. Going forward, through analysis of these markers, it may become possible to construct “APR fingerprints” of diseases and complications to better assess patients, guide physician treatment, and ultimately get in front of serious complications before they begin.

### Chapter 1 Summary

Through Chapter 1, I have highlighted to you the fundamentals of bone biology, the mechanisms of physiologic bone formation both at a physis during development and following injury, and the body’s main injury response system, the APR. Taken together, these studies highlight integral aspects of both the “survival” and “repair” stages of the APR that are critical following an injury

such as a fracture. During the repair phase, to this point, we have solely discussed the processes of normal physiologic bone formation, necessary to heal a fracture. However, following traumatic injuries, it has been well demonstrated that biomineralization can become dysregulated, resulting in loss of mineral from the skeleton and a simultaneous gain of mineralization in soft tissue. This relocation of mineral into soft tissue parallels much of what a person experiences during aging. Thus, soft tissue mineralization is an overarching pathology experienced by many individuals, not just the seriously injured. Therefore, building upon this foundation of physiologic bone formation and the fundamentals of bone biology covered in Chapter 1, the next stage of my thesis work was to elucidate the mechanisms of pathologic biomineralization of soft tissue, specifically skeletal muscle. The overarching goal of this work is to identify the pathologic mechanisms through which mineral is deposited in the soft tissue and identify therapeutics aimed at re-establishing the balance of biomineralization: keep mineralization in bone, and prevent it in soft tissues. These studies will be covered in Chapter 2.

## **CHAPTER 2:**

### **Pathologic Biomineralization of Soft Tissues**

Calcium and phosphorous, in the form of phosphate, are essential elements in many biological processes. Not only are they required for proper cellular function and signaling, but they also combine to make biological crystals; most notably, hydroxyapatite found in bone. Because of their essential nature, calcium and phosphate's anatomic distribution is tightly regulated with 10,000 times more calcium and phosphate circulating in the extracellular space, as opposed to the intracellular microenvironment. As discussed above, this biological gradient is ideal for maintaining the integrity of bone; however, this also means that soft tissues such as blood vessels, skin, and skeletal muscle, are simultaneously exposed to these near saturating concentrations. Given that calcium phosphate crystals can begin to form spontaneously at micromolar concentrations, yet the circulating concentrations of these ions are greater (in the millimolar range), all soft tissues should spontaneously mineralize if a nucleating matrix is available. Yet this is not the case as the body has developed specialized anti-mineralization mechanisms aimed at protecting soft tissues while antagonistic mechanisms simultaneously allow mineralization to occur in the adjacent bone [199].

However, as you age, these tightly regulated processes of biomineralization can become distorted, resulting in both the loss of mineral from bone where it is needed (i.e. osteoporosis) yet the simultaneous gain of mineralization in soft tissue, such as the cardiovascular system. This dichotomy of biomineralization is well described by Dr. Atul Gawande, in his book entitled

*Being Mortal*. [200] Within he quotes the following:

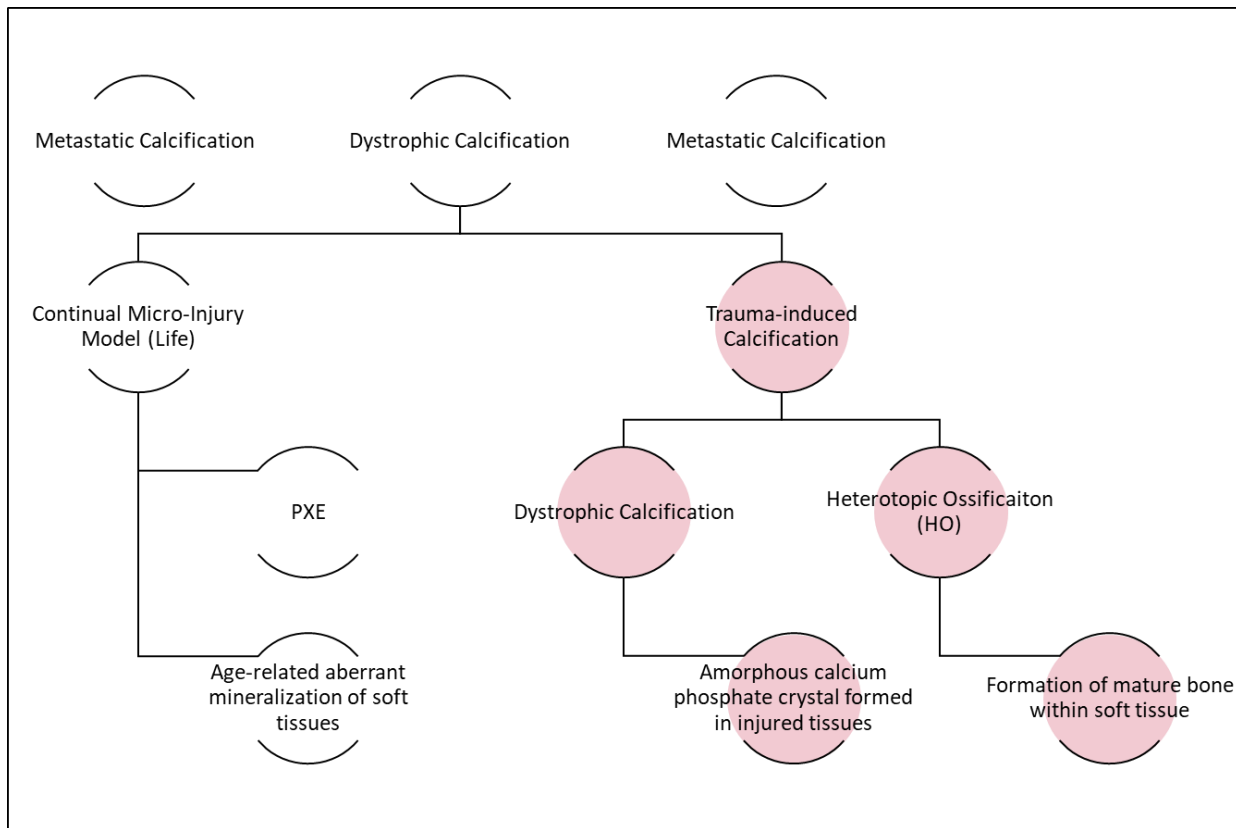
*“In the course of a normal lifetime, the muscles of the jaw lose about 40 percent of their mass and the bone of the mandible loose about 20 percent, becoming porous and weak. The ability to chew declines, and people shift to softer food.....Even as our bones and teeth soften, the rest of our body hardens. Blood vessels, joints, the muscle and valves of the heart, and even the lungs pick up substantial deposits of calcium and turn stiff. Under a microscope, the vessels and soft tissue display the same form of calcium that you would find in the bone. When you reach inside an elderly patient during surgery, the aorta and other major vessels can feel crunchy under your fingers. Research has found that loss of bone density may be an even better predictor of death from atherosclerotic disease than cholesterol levels. As we age, it is as if the calcium seeps out of our skeleton and into our tissues.”*

The acquisition of calcium within soft tissue is a hallmark of aging. Yet, similar pathologic mineral deposition is observed following traumatic injuries such as burns, blasts, spinal cord injuries, and larger orthopaedic procedures. The formation of mineral deposits within soft tissues, such as the skin, cardiovascular system, and skeletal muscle, greatly impacts the overall tissue function, resulting in pain, tissue deformation, chronic inflammation, loss of mobility, and in severe cases may necessitate the surgical excision of the affected tissue [201]. As such, pathologic mineralization of soft tissue as a product of aging or following a traumatic injury, greatly impact patient morbidity and mortality. Yet, few mechanisms utilized locally by soft tissues to prevent mineralization have been elucidated and the molecular pathogenesis of trauma-induced calcification remains unknown.

Therefore, the overarching goal of Chapter 2, building upon previous observations from our laboratory and a strong foundation in physiologic bone formation, is to define the specific mechanisms which protect skeletal muscle from trauma-induced calcification, in aim of elucidating the molecular pathogenesis of the disease, to guide the development of novel therapeutics to regulate biomineralization. As the balance in biomineralization is essential, we aim to i) prevent aberrant mineralization of soft tissue yet, identify therapeutic means to ii) promote of preserve mineralization where it is necessary in the skeleton.

Throughout this introduction and subsequent Articles, we will utilize the following operational definitions in order to improve clarity across fields, of the form of mineralization being discussed (Figure 36). As the main focus of my thesis work is on trauma-induced calcification, these working definitions were developed to aligns with the foundational work conducted by Dr. John Chalmers, an orthopaedic surgeon and expert in the field of soft tissue calcification. In 1975, Chalmers suggested that all injury induced calcification formed as a result of 1) an inducing stimulus (or trauma) 2) the presence of osteogenic precursor cells, and 3) the presence of an osteoinductive tissue environment capable of supporting aberrant mineralization [202]. Considering Chalmers' theory of trauma-induced calcification, many previous studies have focused on the inappropriate cellular transformation of mesenchymal cells to an osteogenic lineage, thereby promoting trauma-induced calcification by providing cells capable of bone formation (such as osteoblasts and chondrocytes) to areas of damaged tissues. Indeed, this pathologic mechanism has been defined in a genetic form of HO known as fibrodysplasia ossifican progressive (FOP), where specific mutations in the genes encoding osteoinductive signaling factors, such as BMP, are up regulated resulting in mesenchymal cell transformation to

a chondrocyte lineage capable of supporting bone formation [203]. Despite the clear genetic etiology of FOP, mutations in BMP signaling pathways have not been observed in patients with trauma-induced HO [204]. Therefore, my investigations will instead focus on the osteoinductive tissue environment and the capacity of this environment to promote cellular transformation favoring an osteogenic lineage and subsequent trauma-induced calcification.



**Figure 36: Operational Definitions of Soft Tissue Calcification.** Tier 1: Clinically, soft tissue calcification as a whole can be divided into three main categories: metastatic calcification, dystrophic calcification, and calcinosis. Within, we will focus our discussions primarily on dystrophic calcification (DC), broadly defined clinically by the radiology community as mineralization that occurs follow tissue damage [205]. It is important to note that aging is a form of continual injury, as micro injuries are sustained over many years of life. Tier 2: Pathologies

within the classification of DC range from pseudoxanthoma elasticum (PXE), a genetic disorder in which mineralization forms in the skin and cardiovascular system as a result of tissue damage sustained due to daily life, to calcification formed in soft tissues as a result of direct traumatic damage such as a burn, blunt force trauma, spinal cord and traumatic brain injuries, or large orthopaedic procedures such as a total joint arthroplasty. Therefore, to further clarify the composition of pathologies under the overarching term dystrophic calcification (Tier 1) highlighted in this thesis, we will refer to these pathologies collectively as trauma-induced calcification. Tier 3: In order to better describe the physical state of the mineral found in damaged tissues following traumatic injury, we will separate trauma-induced calcification into two subcategories: dystrophic calcification (DC), or the deposition of amorphous calcium phosphate crystals within damaged tissue, and heterotopic ossification (HO), more specifically characterized by the formation of organized, mature bone tissue, comprised of both organic and inorganic components. We will use these definitions going forward to describe the state of calcification and our pathology of interest clearly.

As an outline for Chapter 2, I will cover our investigations identifying protection mechanisms essential for preventing soft tissue from mineralization (Article 6, 9, & 10), highlight novel methodology advancements that streamlined this work (Article 7), and cover a manuscript drilling down upon a potential molecular target for one such protection mechanism, plasmin (Article 8). Following these articles, in Chapter 3 we will discuss therapeutic modulation of the identified protection mechanism in Chapter 2, as a means to inhibit trauma-induced calcification yet preserve mineralization in bone.



Article 6: Plasmin Prevents Dystrophic Calcification After Muscle Injury

N.A. Mignemi<sup>1†</sup>, M. Yuasa<sup>1,5†</sup>, C.E. Baker<sup>1,2†</sup>, **S.N. Moore**<sup>1,3</sup>, R.C. Ihejirika<sup>2</sup>, W.K. Oelsner<sup>1,2</sup>, C.S. Wallace<sup>2</sup>, T. Yoshii<sup>5</sup>, A. Okawa<sup>5</sup>, A.S. Revenko<sup>7</sup>, A.F MacLeod<sup>7</sup>, G. Bhattacharjee<sup>7</sup>, J.V. Barnett<sup>2,3</sup>, H.S. Schwartz<sup>1</sup>, J.L. Degen<sup>6</sup>, M.J. Flick<sup>6</sup>, J.M. Cates<sup>4</sup>, & J.G. Schoenecker<sup>1,3,4,8,9</sup> \*

†These authors contributed equally

Affiliations:

Vanderbilt University Medical Center

<sup>1</sup>Department of Orthopaedics and Rehabilitation, <sup>2</sup>School of Medicine, <sup>3</sup>Department of Pharmacology, <sup>4</sup>Department of Pathology, Microbiology, and Immunology, <sup>8</sup>Department of Pediatrics, and <sup>9</sup>Vanderbilt Center for Bone Biology

Tokyo Medical Dental University

<sup>5</sup>Department of Orthopaedics.

Cincinnati Children's Hospital

<sup>6</sup>Department of Experimental Hematology.

<sup>7</sup>Ionis Pharmaceuticals

\*Corresponding Author

Accepted for publication August 2016 in the *Journal of Bone and Mineral Research*

<https://doi.org/10.1002/jbmr.2973>

### *Study Objective & Background*

This first article is focused on answering the question, what protects skeletal muscle from calcification? What are the critical mechanism that when lost, lead muscle to form either dystrophic calcification or HO following injury? Building upon Chalmer's theory, we wanted to investigate the hypothesis that an osteoinductive tissue environment, beyond alterations to the BMP pathway, has the capacity to promote cellular transformation, favoring an osteogenic lineage, and subsequent trauma-induced calcification.

As previously highlighted, circulating levels of calcium and phosphates are close to their solubility coefficient during normal physiology, and rapidly form biological crystals (most notably hydroxyapatite) if stimulated by a nucleating factor [206]. Therefore, we hypothesize that following injury, exposure of potential nucleating matrices to saturating concentrations of calcium and phosphate, may predisposes damaged tissues to crystal aggregation [206-209]. Given that previous reports had demonstrate that the presence of calcium phosphate deposits within soft tissues can then initiate osteogenesis [210-212], it follows that trauma-induced HO may result from the initial formation of DC within damaged tissue in response to the loss of one or more protective factors that normally prevent the formation.

However, the molecular mechanisms that protect skeletal muscle from dystrophic calcification after injury are unclear. Therefore, we built this line of investigation off of previous findings in our fracture model that plasmin, the primary fibrinolytic protease, when loss imposes major deficits in fracture repair, but also induces HO of adjacent

musculature [29]. Therefore, through this present study in Article 6, we aimed to examine in an independent skeletal muscle injury model, whether plasmin, or its precursor plasminogen, was a critical skeletal muscle protection mechanism to soft tissue calcification. To test this hypothesis, we genetically or pharmacologically manipulated plasmin in our murine model of focal skeletal muscle injury, and analyzed the resulting trauma-induced calcification and its fate through skeletal muscle repair.

### *Materials and Methods*

#### *Animal Models And In Vivo Pharmacological Manipulation:*

All animal procedures in this protocol were approved by the Institutional Animal Care and Use Committee at Vanderbilt University. Mice were housed within Vanderbilt University under a 12-hour light dark cycle with free access to food and water. Welfare related assessments were carried out prior to and during the experiments by the authors and veterinary staff at Vanderbilt University.

#### *Cardiotoxin-Induced Muscle Injury Model:*

Skeletal muscle injury was induced by intramuscular injection of 40 $\mu$ L of 10nM Cardiotoxin (CTX, Accurate Chemical and Scientific Corp; Westbury, NY) into the posterior compartments of the lower extremities of male C57/B6 mice. Briefly, following anesthetization with isoflurane, CTX was injected from lateral to medial in the posterior compartment using a 28.5G, 0.5cc insulin syringe. CTX induces massive local myocyte depolarization, leading to myocyte death. However, muscle resident stem cells are unaffected by the CTX, thereby allowing for muscle regeneration following injury.

### *Crush Injury Model*

Mice were anesthetized with isoflurane. Once appropriately sedated, a sterile incision was made on the posterior hindlimb of a mouse in the prone position. The gastrocnemius was separated from underlying tissue using blunt dissection beginning anterior to the Achilles tendon and proceeding superiorly along the anterior gastrocnemius. Once the muscle had been freed, a needle driver was clamped around the muscle at its maximum diameter in the axial plane for 30 seconds and released. The incision was then closed with 4-0 monofilament suture.

### *Antisense Oligonucleotide (ASO) Injections*

All ASOs used in this study were developed in collaboration with Ionis Pharmaceuticals (Carlsbad, CA). Plasminogen (Plg) (AGTGATGGTCTATTGTCACA),  $\alpha$ 2-antiplasmin ( $\alpha$ 2AP) (CACTGGTGATGGTCCTTCCG), Fibrinogen (Fbg) (GCTTTGATCAGTTCTTTGGC), and control ASOs (CCTTCCCTGAAGGTTCTCC) were all administered subcutaneously in the abdomen every week beginning two weeks prior to injury and continuing through the term of the study. All ASO treatments were dosed at 330mg/kg/week, unless otherwise noted in Figure Legends. The ASOs used in this investigation were chemically modified with a phosphorothioate backbone, 2' O methoxyethyl on the wings with a central deoxynucleotide gap. ASOs targeted hepatic translation of their targeted protein. ASOs were synthesized using an Applied Biosystems 380B automated DNA synthesizer (Applied Biosystems) and purified as described previously [213]. In order to identify the most potent fibrinogen ASOs for animal testing, ASOs were designed and tested in primary mouse hepatocytes for their ability to suppress

mRNA levels of the respective targets.

*Output Analysis and Quantification Of Heterotopic Ossification: Radiographic Imaging*

Radiographic imaging was performed following adequate anesthesia, beginning at 7 days post injury. Digital radiographs (Faxitron, Tucson, AZ) were collected at an exposure of 4 sec at 35kV. Mice were placed in the prone position with hips in abduction, allowing for external rotation of the leg placing the tibia in a reproducible lateral position.

*Radiographic Analysis and Quantification of Soft Tissue Calcification:*

In order to assess trauma-induced skeletal muscle calcification longitudinally, we designed and validated a method using plain radiographic techniques and an ordinal scoring system. This method was published in PLoS in 2016 (**Article 7**) and is highlighted in detail below.

Article 7: Validation of a Radiography-Based Quantification Designed to Longitudinally Monitor Soft Tissue Calcification in Skeletal Muscle

**Stephanie N. Moore**<sup>1,2</sup>, Gregory D. Hawley<sup>2</sup>, Emily N. Smith<sup>2</sup>, Nicholas A. Mignemi<sup>2</sup>, Rivka C. Ihejirika<sup>2</sup>, Masato Yuasa<sup>2</sup>, Justin M.M. Cates<sup>4</sup>, Xulei Liu<sup>5</sup>, Jonathan G. Schoenecker<sup>1,2,3,4,6\*</sup>

Vanderbilt University Medical Center

Department of <sup>1</sup>Pharmacology, <sup>2</sup>Orthopaedics, <sup>3</sup>Center for Bone Biology, <sup>4</sup>Pathology, Microbiology, and Immunology, <sup>5</sup>Biostatistics, and <sup>6</sup>Pediatrics.

\*To whom correspondence should be directed

Accepted for publication July 2016 in *PLoS One*

<https://doi.org/10.1371/journal.pone.0159624>

*Study Goal:*

When I join the Schoenecker laboratory in Spring of 2014, the laboratory had recently begun to investigate pathological soft tissue calcification and was utilizing radiographic analysis to assess calcification longitudinally. However, at this point the only validated way to quantify the amount of soft tissue calcification was by uCT or histological analysis, both of which necessitated sacrifice of the mouse thereby precluding longitudinal measurement from the same animals. Given this block, my first project in the laboratory focused on developing a reliable methods to quantify the relative amount of calcification

by radiographic imaging, thereby allow for longitudinally analysis. The cumulation of this project was the creation of the Soft Tissue Calcification Scoring System (STiCSS) which is now commonly employed by our laboratory and has been used in multiple studies since its validation. This project, not only allowed me to develop, design, test, and validate a method from its inception, but also provided me the ability to take ownership of my first project. Through this manuscript I learned much about statistical analysis, working with different departments to gather results and data, and the importance of reproducibility in ones work to allow it to be transferred to other scientists. The foundation and results of the study in full are detailed below.

#### *Study Rational & Background*

Preclinical models of trauma-induced soft tissue calcification are integral for both elucidating the molecular mechanisms behind trauma-induced calcification, and the development of novel therapeutics [214-216]. However, most methods used to quantify the extent of soft tissue calcification, such as histologic analysis or ex vivo micro-computed tomography ( $\mu$ CT), require sacrifice of the animal. Because of the variability between samples and endpoint output measurements, a large number of animals are typically necessary for adequate statistical power to determine the effect of an experimental interventions (i.e., genetic or pharmacologic manipulation) or molecular mechanism involved in trauma-induced calcificaiton. Therefore, longitudinal quantification of soft tissue calcification would be advantageous in reducing the number of animals required for these types of studies as well as to allow for evaluation of therapeutic intervention of already established soft tissue calcification.

In vivo  $\mu$ CT has been used to quantify heterotopic ossification over time in a murine burn/Achilles tenotomy model [216, 217]. The advantage of *in vivo*  $\mu$ CT over radiographic imaging in this setting is the increased spatial resolution. Since, soft tissue calcifications in this model are juxtaposed to the tibia, three dimensional imaging (i.e.  $\mu$ CT) is required to delineate the pathologic areas of mineralization from adjacent bone. Despite the potential utility of this method *in vivo*  $\mu$ CT is more expensive, time consuming, and exposes mice to markedly more radiation than single plane radiography (Table 8) [218].

**Table 8: Cost, Time, and Radiation Exposure Analysis**

	<i>In Vivo</i> $\mu$ CT	Plain Radiography
Cost Per Image <sup>1</sup>	\$130/Hour	\$50/Hour
Time Per Image <sup>2</sup>	~1200 Seconds/ Leg	4 Seconds/ Leg
Radiation Per Image	171-500 mGy <sup>3</sup>	1.4-16.5 mGy <sup>4</sup>

<sup>1</sup>Institutional cost at Vanderbilt University as of May 2016

<sup>2</sup>Scan time necessary to image a single leg of a ~20g mouse

<sup>3</sup>Approximate radiation exposure for a 48 micro resolution image. Variation based on the exact scanning settings and instrument used.

<sup>4</sup>Average radiation exposure measured from two independent Faxitron LX-60 cabinets, 20.9cm from x-ray source, 4 seconds at 35 kV, May 2016

As an alternative to the Achilles tenotomy injury, in which injury to muscle is caused by unopposed contracture leading to muscle migration and ischemia [216], other investigators have used cardiotoxin (CTX) to induce muscle injury. CTX instigates muscle fiber depolarization that leads to skeletal muscle death; however, muscle resident stem cells are unaffected, thereby allowing for muscle regeneration following injury [217-219]. Finally, like the Achilles tenotomy injury, CTX-induced muscle injury has also been demonstrated to reliably results in soft tissue calcification [219, 220].



Here, we demonstrate that CTX injection into the posterior compartment of the lower extremity results in formation of soft tissue calcification away from adjacent bones, which allows for serial detection using single plane radiography. Subsequently, we developed and validated a novel, ordinal Soft Tissue Calcification Scoring System (STiCSS) by which the extent of soft tissue calcification can be reliably quantified from digital radiographic images without necessitating the sacrifice of the animal.

#### *Methods Pertaining to Model Development and Validation*

All animal procedures in this protocol were approved by the Vanderbilt Institutional Animal Care and Use Committee (M1600231 and M/15/024).

#### *Murine Models of Soft Tissue Calcification*

As previously described in Article 6, a cardiotoxin-mediated muscle injury into the posterior compartment of the lower leg with a lateral approach was utilized to induced skeletal muscle calcification following injury. The lower leg of a mouse is divided into two anatomic compartments: the superficial compartment and the deep tissue compartment. Injections were administered primarily in the superficial compartment and within the gastrocnemius and soleus muscles. For validating this quantification method, both the right and left posterior compartment muscles of the lower extremity were injured.

#### *Cardiotoxin-Induced Muscle Injury in Mice Following a Burn Injury*

The burn/Achilles tenotomy model previously reported [216] was modified by replacing

the tenotomy injury with a CTX injection as described above. All burn studies were conducted in 6-week-old male wild-type C57B6J mice (Jackson Lab, Bar Harbor, ME), with no genetic or ASO-induced predisposition for developing soft tissue calcification, weighing 20–25g as previously described [221, 222]. Briefly, prior to adequate anesthesia with Isoflurane, mice received a subcutaneous injection of buprenorphine (0.5-mg/kg) 30 minutes prior to the burn procedure. Following adequate anesthesia with Isoflurane, muscle injury was accomplished by intramuscular injection of CTX into the posterior compartment of the lower extremity as described above. Dorsal hair was then removed and 1ml of saline was injected subcutaneously along the posterior elements of the spine to create a physical buffer from the burn in order to prevent spinal cord injury. The mouse was then placed in a heat-resistant template with the exposed dorsum positioned in the cutout of the template. The template was partially submerged in a 100°C water bath for 10 seconds to create a full-thickness cutaneous burn covering 30% of the body surface area. The mouse was then dried with absorbent bench paper and given 2ml of intraperitoneal resuscitation with lactated Ringer's solution. Negative control mice received CTX muscle injury without concomitant burn injury.

#### *Animal Care and Welfare*

Humane endpoints were in place to euthanize any animal that was in pain, unable to eat or drink, experiences wound dehiscence or infection, or lost > 20% of its original body weight. Throughout all investigations, no animals became ill or necessitated sacrifice prior to the designated experimental endpoint.

### *Methods for Monitoring Animals*

The physical condition of the mice was monitored continuously following all procedures in which mice were placed under anesthesia until recovery as defined by awakening of the animal, observation of normal movement, and returning to normal eating and drinking behavior.

Mice that underwent a cardiotoxin injury were monitored for visible signs of discomfort or pain once per day for three days following injury. After the first three days, mice were then monitored weekly and weighed at the time of radiographic analysis. Weight measurements were obtained to confirm that mice were not losing >20% of their original body weight, thereby necessitating sacrifice and removal from the study. Mice that underwent a burn injury with or without a cardiotoxin muscle injury were monitored for visible signs of discomfort or pain twice daily for the first 48 hours after cutaneous burn. After the first 48 hours, mice were monitored daily and weighed weekly at the time of radiographic analysis to confirm that mice were not losing >20% of their original body weight, thereby necessitating sacrifice and removal from the study.

### *Methods to Minimize Potential Suffering*

All mice in the study were injured under the influence of an anesthetic (isoflurane). Mice that received a cardiotoxin injury alone did not receive any additional analgesia following injury. Mice that were burned with or without a cardiotoxin muscle injury were administered Buprenorphine at 0.05-0.1 mg/kg of body weight subcutaneously 30 minutes prior to the burn and every 12 hours after the burn for 48 hours. Following the first 48

hours, if a mouse was found to be in visible discomfort or pain following the burn injury, additional Buprenorphine was administered as needed.

#### *Methods of Euthanasia*

All mice in this study were euthanized by carbon dioxide inhalation followed by cervical dislocation.

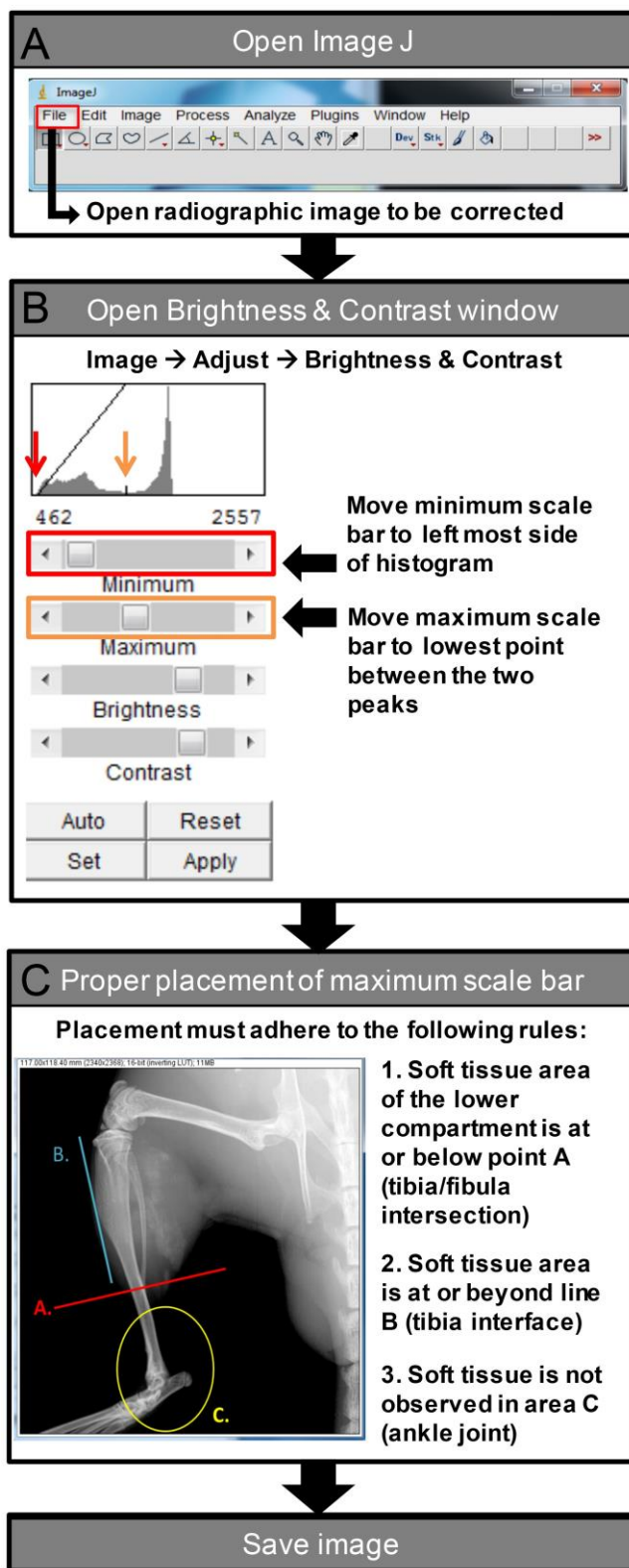
#### *Analysis of Soft Tissue Calcification Following Injury: Radiographic Imaging*

As described previously, beginning 7 days following muscle injury, digital radiographs of the lower extremity were acquired. Following adequate anesthesia, mice were placed in the prone position with hips in abduction, allowing for external rotation of the leg by placing the tibia in a reproducible lateral position. Single plane lateral radiographic images were collected at an exposure of 4 seconds at 35 kV and saved as a DICOM (.dcm) files for image processing.

#### *Post-Image Processing*

Prior to quantification, all digital radiographs underwent post-image processing to ensure appropriate resolution and contrast settings to allow for comparisons between images. DICOM files were adjusted using ImageJ software (National Institute of Health; <http://imagej.nih.gov/ij/>) (Figure 37A). Minimum and maximum scale bars were adjusted using the Brightness & Contrast editing tool. The minimum scale cursor was then moved to the leftmost edge of the displayed histogram (Figure 37B) while the maximum scale position was determined following the “ABC” rules (defined in Figure 37C). Proper

placement of the maximum scale bar was achieved when the soft tissue area of the lower compartment was at or below line A, at or beyond line B, and was not observed in area C. After the maximum scale bar was properly set, the radiographic image was saved for subsequent scoring.




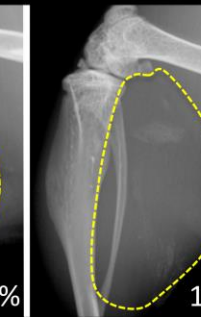
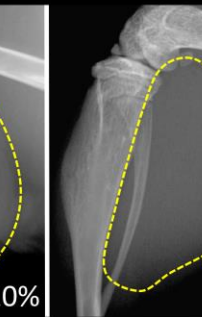


**Figure 37: Flow Diagram of Post-Image Processing.** Prior to quantification, all digital

radiographs underwent post-image processing to ensure appropriate resolution and contrast settings to allow for comparisons between images. The flow diagram demonstrates the stepwise procedure for processing images with ImageJ.

*Soft Tissue Calcification Scoring System (STiCSS):*

Processed digital radiographs were randomized and blinded for quantification. To quantify and statistically evaluate the extent of soft tissue calcification observed in digital radiographs, an ordinal scale (0-4) was formulated according to the varying degrees of soft tissue calcification. The operational definitions of each score are based on the percentage area of soft tissue calcification observed in the posterior compartment of the lower extremity: 0 (0%), 1 (1-25%), 2 (25-49%), 3 (50-75%) and 4 (>75%) (Figure 38).

Radiographic Images					
Score	4	3	2	1	0
Operational Definition	Greater than 75% mineralization of Gastrocnemius	50-74% mineralization of Gastrocnemius	25-49% mineralization of Gastrocnemius	Less than 25% mineralization of Gastrocnemius	No mineralization of Gastrocnemius

**Figure 38: Soft Tissue Calcification Scoring System (STiCSS).** STiCSS is an ordinal scale (0-4) developed for quantifying the varying degrees of soft tissue calcification from radiographic images of the lower extremity. Representative images of each STiCSS score

are provided along with the operational definition designated to each score. Yellow dotted lines outline the area of interest for soft tissue calcification (the posterior compartment of the lower extremity), while the listed percentages correlate to the extent of soft tissue calcification within each sample image

#### *Ex Vivo $\mu$ CT Quantification of Soft Tissue Calcification*

$\mu$ CT images were acquired ( $\mu$ CT40, Scanco Medical AG, Bassersdorf, Switzerland) of injured hindlimbs at 55kVp, 145uA, 200ms integration, 500 projections per 180o rotation, with a 20 $\mu$ m isotropic voxel size following sacrifice. After reconstruction, a volume of interest (VOI) was selected comprising the region of soft tissue calcification within the posterior compartment of the lower extremity. Mineralized tissue within the VOI was segmented from soft tissue using a threshold of 220 per thousand (or 450.7mgHA/cm<sup>3</sup>), a Gaussian noise filter of 0.2, and support of 1. Mineral volume was calculated using the Scanco evaluation software.

#### *Statistical Analysis*

To determine the precision and reproducibility of this method, multiple individuals served as adjusters (individual who performed the post-imaging processing; N=4) and/or observers (individuals who scored previously processed radiographic images using the STiCSS; N=6).

#### *Precision Analysis of Post-Image Processing and Scoring with the STiCSS*

For all precision analysis, weighted kappa statistics were calculated for both intra-observer



and inter-observer analyses. Kappa values were interpreted using the Landis and Koch criteria as follows:  $\kappa < 0$ , less than chance agreement; 0.01-0.20, slight agreement; 0.21-0.40, fair agreement; 0.41-0.60, moderate agreement; 0.61-0.80, substantial agreement; and 0.81-0.99, almost perfect agreement [223]. All kappa statistics were calculated with SAS for Windows 9.4 (SAS Institute, Cary, NC).

*Intra-Observer Error Analysis of Post-Image Processing:*

To assess the variability of digital radiographic post-image processing, four adjusters were trained as outlined above to process the same set of 40 blinded images with varying degrees of soft tissue calcification within the posterior compartment of the lower extremity following CTX muscle injury. Six individual scorers then evaluated all 160 radiographic images obtained from the four adjusters (i.e. each original image was scored four times, reporting one replicate per adjuster) and the intra-observer agreement between adjusters was assessed.

*Intra-Observer Error Analysis of Image Scoring with the STiCSS*

To assess intra-observer variability in the STiCSS, six researchers scored the same set of 40 blinded images twice, with more than one month between scoring sessions. Scores for each image were collected and analyzed using kappa statistics.

*Inter-Observer Error Analysis of Image Scoring with the STiCSS*

To assess inter-observer variability in the STiCSS, 160 total images were scored by six individual scorers. Scores for each image were collected and analyzed using kappa

statistics.

#### *Statistical Correlation of STiCSS Scores and Ex Vivo $\mu$ CT Quantification*

To validate our method as a robust tool for quantifying soft tissue calcification, we compared STiCSS scores to mineral volume measurements obtained from ex vivo  $\mu$ CT analysis (threshold 450.7mgHA/cm<sup>3</sup>) as described above. Twenty-eight images with varying degrees of soft tissue calcification were analyzed by both quantitative  $\mu$ CT and the STiCSS to determine the correlation between these two quantification modalities. Correlation was evaluated using a non-parametric Spearman correlation coefficient. Statistical analyses were performed with GraphPad Prism (v6, GraphPad Software, La Jolla, CA)

#### *Statistical Evaluation of STiCSS Results*

Radiographs were quantified using the STiCSS and scores were individually plotted for each leg with the median and interquartile range. Differences between study groups were assessed using a proportional odds model with random effect. This statistical model takes into account the correlation between the left and the right legs of a single mouse, thereby statistically allowing for inclusion of both legs in our analysis. However, if the number of mice was low or if some of the ordinal categories had very few frequencies, the proportional odds model with random effect failed to fit the data well. Under these circumstances, the Mann-Whitney Rank Test (i.e. a Wilcoxon Rank Sum Test) was used with the understanding that this method fails to account for within-mouse correlation.

### *Sample Size Calculation for The Cardiotoxin-Induced Muscle Injury In Mice With A Burn Injury*

The required sample sizes necessary to discern a 25%, 50%, 75%, and 100% differences in soft tissue calcification, as measured by the mean STiCSS score in the Burn/CTX-induced muscle injury models of soft tissue calcification, were determined given  $\beta=0.80$  and  $\alpha=0.05$ . While the STiCSS is an ordinal variable, for analysis of the sample size, we used this score as a continuous response variable from matched pairs of study subjects for determination of sample size. All sample size calculations analyses have been by conducted with the PS Power and Sample Size Calculation Program (v3.0, Vanderbilt University, Nashville, TN)

### *Histological Analysis and Staining Procedures*

Injured hind limbs were fixed in 10% Neutral buffered formalin for 24 to 72 hours. All samples were processed in graded series of ethanol, cleared, and embedded in paraffin prior to sectioning. 6 $\mu$ m sections were cut and stained as described below.

**Hematoxylin and Eosin (H&E):** Deparaffinized sections were stained in Gills 3 hematoxylin solution for 5 minutes. Slides were then rinsed in tap water for 10 minutes followed by eosin staining for 2 minutes. Finally, slides were dehydrated and cleared in xylene before mounting with Permount. **Von Kossa:** Deparaffinized sections were rinsed with distilled water and exposed to 1% silver nitrate solution under ultraviolet light for 30 minutes to develop black staining of mineralization. Slides were then counterstained with Fast green for 5 minutes, dehydrated, and cleared in xylene before mounting with

Permount.

## *Results*

### *Precision Analysis of Post-Image Processing*

Intra-observer error analysis of post-image process indicated that there were no significant differences among the adjusters performing the post-image processing. Adjusters were in moderate to almost perfect agreement (weighted  $\kappa$  0.78 to 0.96) when images were scored by 6 individual observers, indicating that the post-image processing method was reliable (Table 9). Additionally, of the 40 individual images that underwent post-image processing, 39/40 (97.5%) demonstrated no significant difference in STiCSS score (as measured by ANOVA), thereby further demonstrating good agreement between adjusters. Together, these findings indicated that the post-image processing method reliably standardizes digital radiographic images for subsequent scoring without significant differences.

**Table 9: Intra-observer analysis of Post-Image Processing**

<i>Observer A</i>				<b>Weighted Kappa Range</b>
Adjuster	B	C	D	<b>Observer A</b>
A	0.89 (0.81, 0.98)	0.96 (0.91, 1.00)	0.96 (0.91, 1.00)	0.89 - 0.96
B		0.89 (0.80, 0.98)	0.93 (0.86, 0.99)	
C			0.96 (0.91, 1.00)	
<i>Observer B</i>				<b>Observer B</b>
Adjuster	B	C	D	<b>Observer B</b>
A	0.92 (0.85, 0.99)	0.85 (0.75, 0.96)	0.90 (0.82, 0.98)	0.82 - 0.92
B		0.84 (0.74, 0.93)	0.88 (0.80, 0.97)	
C			0.82 (0.71, 0.93)	
<i>Observer C</i>				<b>Observer C</b>
Adjuster	B	C	D	<b>Observer C</b>
A	0.95 (0.89, 1.00)	0.89 (0.81, 0.98)	0.93 (0.86, 0.99)	0.89 - 0.95
B		0.95 (0.89, 1.00)	0.95 (0.89, 1.00)	
C			0.93 (0.86, 0.99)	
<i>Observer D</i>				<b>Observer D</b>
Adjuster	B	C	D	<b>Observer D</b>
A	0.78 (0.67, 0.90)	0.81 (0.70, 0.92)	0.82 (0.72, 0.93)	0.78 - 0.88
B		0.84 (0.75, 0.94)	0.86 (0.76, 0.95)	
C			0.88 (0.79, 0.98)	
<i>Observer E</i>				<b>Observer E</b>
Adjuster	B	C	D	<b>Observer E</b>
A	0.85 (0.75, 0.95)	0.93 (0.87, 0.99)	0.85 (0.75, 0.94)	0.83 - 0.93
B		0.92 (0.83, 1.00)	0.83 (0.71, 0.96)	
C			0.88 (0.80, 0.97)	
<i>Observer F</i>				<b>Observer F</b>
Adjuster	B	C	D	<b>Observer F</b>
A	0.94 (0.88, 1.00)	0.92 (0.85, 0.99)	0.92 (0.85, 0.99)	0.92 - 0.94
B		0.94 (0.88, 1.00)	0.94 (0.88, 1.00)	
C			0.92 (0.85, 0.99)	

N= 40 images per Adjusters

*Precision Analysis of the STiCSS:*

When the same set of 38 blinded radiographic images was scored by the same observer with more than one month between scoring sessions, weighted kappa statistics ranged from 0.88-0.93, showing substantial to almost perfect intra-observer agreement between the two

scoring sessions. These results indicated that the variation in soft tissue calcification scoring by each individual observer was minimal (Table 10).

**Table 10: Intra-observer Error on STiCSS**

Observer	Weighted Kappa	95% CI
A	0.92	0.84, 0.99
B	0.91	0.94, 0.99
C	0.93	0.86, 0.99
D	0.88	0.79, 0.96
E	0.91	0.83, 0.99
F	0.90	0.82, 0.98

N=38 individual blinded images

Given the minimal intra-observer error, we then determined the agreement between 6 individual observers to assess the inter-observer variability in the STiCSS. When 160 blinded images were scored, weight kappa statistics ranged from 0.73 to 0.90, thereby demonstrating moderate to almost perfect agreement between observers (Table 11). This demonstrates that the STiCSS is a statistically valid and reproducible method for scoring soft tissue calcification within the posterior compartment of the lower extremity following CTX muscle injury without necessitating the sacrifice of the animal.

**Table 11: Inter-observer Analysis of the STiCSS**

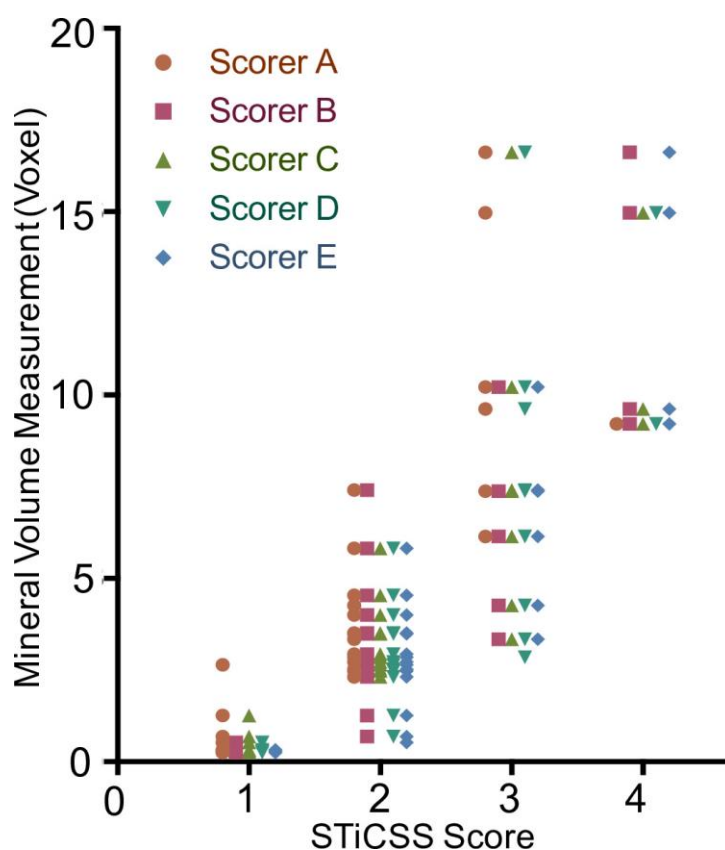
<i>Adjuster A</i>							<b>Weighted Kappa Range</b>
Observer	A	B	C	D	E	F	<b>Adjuster A</b>
A		0.78	0.84	0.74	0.86	0.74	0.74 - 0.88
B			0.86	0.80	0.78	0.83	
C				0.86	0.88	0.86	
D					0.84	0.82	
E						0.77	
F							
<i>Adjuster B</i>							<b>Adjuster B</b>
Observer	A	B	C	D	E	F	
A		0.77	0.89	0.73	0.78	0.74	0.73 - 0.89
B			0.83	0.81	0.79	0.75	
C				0.76	0.78	0.81	
D					0.76	0.83	
E						0.80	
F							
<i>Adjuster C</i>							<b>Adjuster C</b>
Observer	A	B	C	D	E	F	
A		0.76	0.84	0.76	0.83	0.80	0.76 - 0.85
B			0.82	0.77	0.80	0.77	
C				0.78	0.85	0.82	
D					0.80	0.77	
E						0.84	
F							
<i>Adjuster D</i>							<b>Adjuster D</b>
Observer	A	B	C	D	E	F	
A		0.77	0.84	0.77	0.77	0.73	0.73 - 0.90
B			0.90	0.79	0.90	0.82	
C				0.76	0.86	0.82	
D					0.83	0.78	
E						0.79	
F							

N=160 images scored per Observer (40 per Adjuster)

*Correlation of the STiCSSto ex vivo  $\mu$ CT Quantification*

Many previous investigations have relied upon  $\mu$ CT to accurately quantify soft tissue calcification. We found that the STiCSS scores among 5 scorers and mineral volume

measurements from  $\mu$ CT (threshold 450.7 mgHA/cm<sup>3</sup>) were strongly correlated (Spearman's  $r = 0.83$  to  $0.89$ ,  $p < 0.0001$ ) (Figure 39 and Table 12). Therefore, the STiCSS scoring is consistent with soft tissue calcification quantification by end-point  $\mu$ CT analysis at a threshold of 450.7 mgHA/cm<sup>3</sup>, and thereby represents an affordable, alternative, non-endpoint analysis for quantification of soft tissue calcification within the posterior compartment of the lower extremity.



**Figure 39: Comparison of STiCSS Score and Mineral Volume Determined by ex vivo  $\mu$ CT.** STiCSS scores correlated with mineral volume measurement determined by ex vivo  $\mu$ CT at a threshold of 450.7mgHA/cm<sup>3</sup>. Correlation was examined using scores from 5 independent observers (A-E) who individually scored 28 images using the STiCSS scale. Scores were then individually plotted against mineral volume measurements obtained by



ex vivo  $\mu$ CT from the same samples.

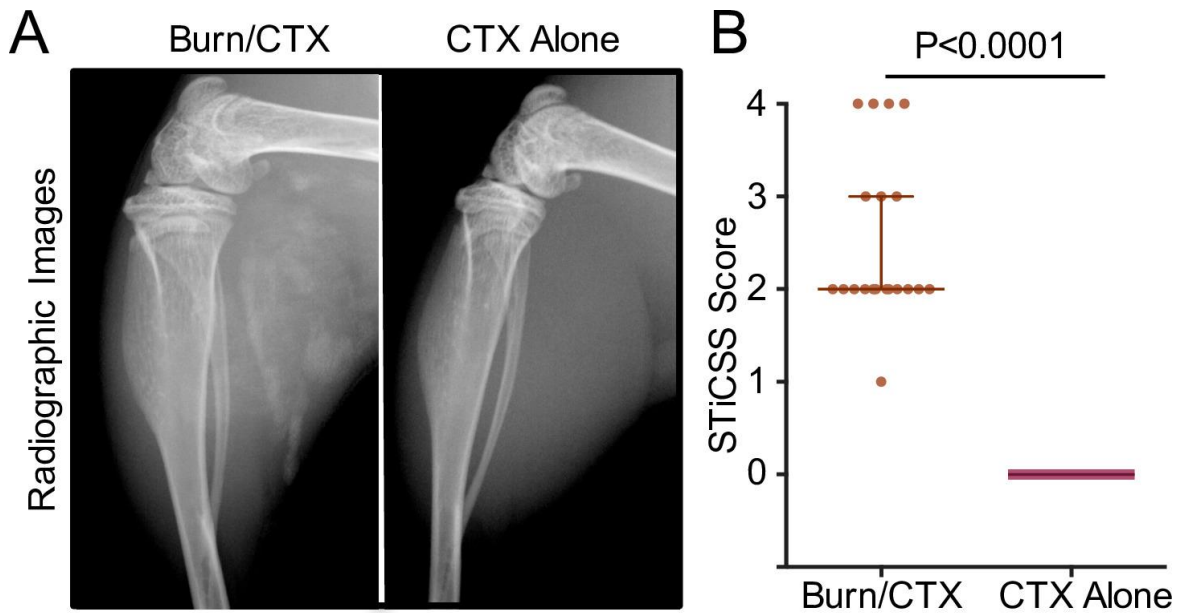
**Table 12: Spearman Correlation of the STiCSS and  $\mu$ CT measurements**

Observer	R	95% CI	P
A	0.88	0.76 to 0.95	<0.0001
B	0.84	0.68 to 0.93	<0.0001
C	0.89	0.78 to 0.95	<0.0001
D	0.83	0.66 to 0.92	<0.0001
E	0.86	0.72 to 0.94	<0.0001

N= 28 XY pairs per scorer

*Quantification of Soft Tissue Calcification in the Murine Burn/CTX-Induced Soft Tissue Calcification Model with the STiCSS*

CTX-induced muscle injury followed by a 30% body surface area, full thickness cutaneous burn resulted in soft tissue calcification separate from the tibia and fibula, thereby allowing for detection by single plane radiography (Figure 40A). Separation from anatomical bone allowed for soft tissue calcification to be detected in radiographic images and be quantified with the STiCSS (Figure 40B). Together, these findings demonstrate that we successfully validated the methodology required to quantify soft tissue calcification in a CTX injury model, without sacrifice, using an ordinal scoring system.



**Figure 40: Radiographic Analysis and Quantification of Soft Tissue Calcification Following Burn/CTX Injury.** A) Radiographic images of C57BL6 mice that either received a CTX injury alone (N=8 mice, 16 samples) or a burn injury with a CTX injection (N=10 mice, 20 samples). B) Graphical representation of radiographic images quantified using the STiCSS. Data represents both the left and right leg of each individual animal. Median and interquartile ranges are shown. Mann-Whitney rank test ( $p < 0.0001$ , \*\*\*\*) demonstrated significant differences between control (CTX injury alone) and the burn injury group (CTX/Burn Injury).

*Sample Size Calculation:*

Sample size calculations for the number of mice needed per group necessary to discriminate 25%, 50%, 75%, and 100% differences in STiCSS scores 7 days following burn/CTX-induced muscle injury are shown in Table 13.

**Table 13: Sample Size Calculator for the STiCSS**

---

Burn/CTX Injury

---

Mean	2.50
SD	0.889

---

Sample Size Calculations:

---

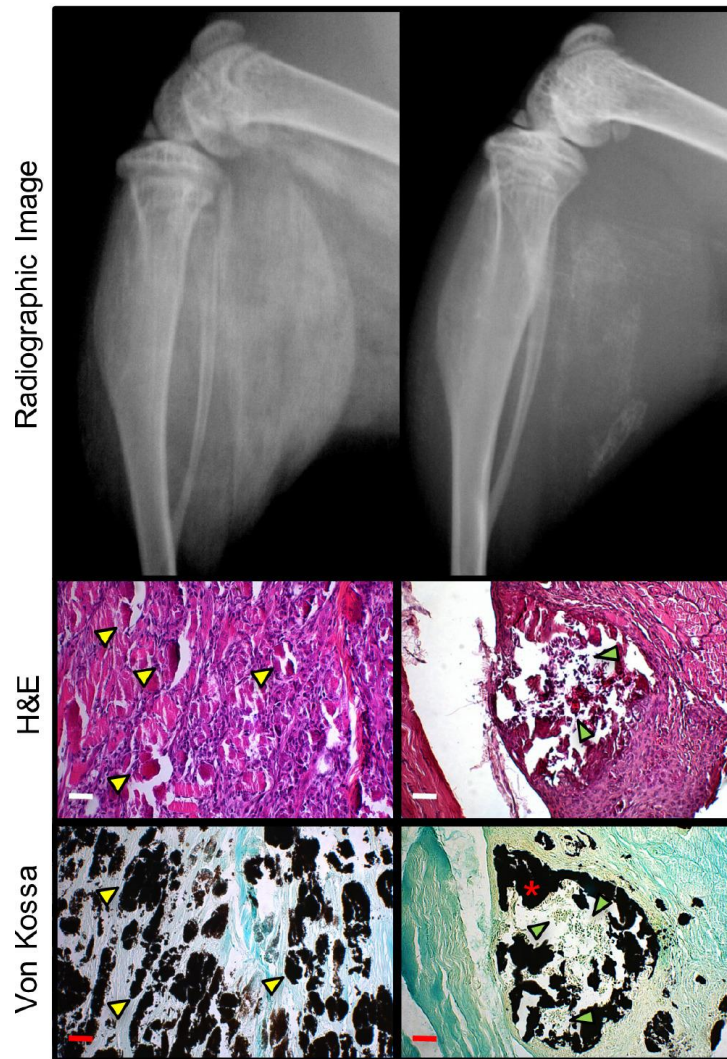
25% Difference	18 mice per group
50% Difference	6 mice per group
75% Difference	4 mice per group
100% Difference	3 mice per group

*Use of STiCSS In Quantifying Dystrophic Calcification And Heterotopic Ossification:*

Soft tissue calcification includes dystrophic calcification and heterotopic ossification. Although these processes are histologically distinct, they are radiographically equivalent by STiCSS (Figure 41). The STiCSS represented a reliable method for quantifying the amount of either histological form of soft tissue calcification, but cannot discriminate between them.

## Soft Tissue Calcification

Dystrophic Calcification    Heterotopic Ossification



**Figure 41: Dystrophic Calcification and Heterotopic Ossification Are Histologically Distinct Yet Radiographically Equivalent.** Radiographic and histological images of mice that received a CTX muscle injury and developed dystrophic calcification or heterotopic ossification within the posterior compartment of the lower extremity. Radiographically, dystrophic calcification and heterotopic ossification, two states of soft tissue calcification, are indistinguishable. Nevertheless, the STiCSS can be applied to both processes even though the precise state of mineralization cannot be determined. Histologically, dystrophic

calcification and heterotopic ossification can be easily discriminated by their distinct histological characteristics apparent by H&E and Von Kossa (stain for mineralized tissue) staining. Dystrophic calcification is defined histologically by the presence of amorphous, unorganized, calcium phosphate crystals interspersed with necrotic debris at the site of tissue injury (yellow arrow heads). Heterotopic ossification is characterized by mineralized mature bone (red asterisk), which may be associated with a central medullary cavity with intratrabecular hematopoiesis (green arrow heads).

### *Discussion*

The focus of this study was to develop a time and cost effective, reproducible method to quantify soft tissue calcification within skeletal muscle following a CTX injury. Through the induction of a localized muscular injury with CTX injection of the posterior compartment of lower extremity, we were able to provoke consistent soft tissue calcifications away from anatomical bones, thereby allowing for detection by single plane radiography. We then validated a post-image processing method and the STiCSS scoring method for quantifying soft tissue calcification in this model. These methods, unlike other end-point analyses for soft tissue calcification (i.e. *ex vivo*  $\mu$ CT and histological analysis), does not necessitate sacrifice of the animal, thus permitting longitudinal quantification and reduction of the cost of in vivo studies. As a means to further lower the costs of this method, all post-image processing methods were performed using freely available software maintained by the National Institute of Health. Thus, radiographic imaging and the STiCSS represent a new, cost-effective, high-throughput, alternative method for longitudinal quantification of soft tissue calcification.

Although *in vivo*  $\mu$ CT can be employed to quantify soft tissue calcification in longitudinal study designs, our methods are relatively inexpensive, less time-consuming, and can be applied more universally in the field of soft tissue calcification, since radiographic imaging is a more widely available imaging platform (Table 8). In addition to the aforementioned considerations, when selecting a method for longitudinal quantification of soft tissue calcification, the amount of radiation exposure during the imaging process is potentially an unknown confounding variable. Numerous clinical reports have supported the use of radiation as a treatment for reducing soft tissue calcification, specifically heterotopic ossification [224-227]. Consequently, repeated use of this imaging modality may potentially and unknowingly alter the biological processes of soft tissue calcification and experimental results when measured repeatedly. Though the dose of radiation obtained through therapy is much greater than either imaging modality, currently it remains unclear what effect radiation obtained by *in vivo*  $\mu$ CT, if any, may have on soft tissue calcification [228]. Therefore, we proposed that use of radiographic imaging and the STiCSS may be a preferred method for longitudinal soft tissue calcification quantification as the radiation exposure is markedly less (Table 8).

While the STiCSS provides many advantages for longitudinal quantification of soft tissue calcification, one drawback of these methods is the inability of single plane radiography to distinguish between the state of soft tissue calcification, specifically dystrophic calcification and heterotopic ossification. Histologically, dystrophic calcification and heterotopic ossification can be easily distinguished: whereas the former is characterized by

islands of disorganized calcium phosphate crystals interspersed with necrotic debris, the latter shows mature bone tissue. Thus,  $\mu$ CT (either ex vivo or in vivo analysis) or histological analysis on a subset of samples is still necessary to assess the pathological state of soft tissue calcification. Given the pathologic complexity, variable fates of mineralization, and the dynamic nature of this process, murine models which phenocopy the different states of soft tissue calcification following injury and longitudinal quantification methods are both essential. Together, clinically relevant models and validate longitudinal quantification method can be used to delineate the molecular mechanisms resulting in the development and maturation of soft tissue calcifications, as well as to develop and test novel therapeutic strategies. The STiCSS has been demonstrated to reliably quantify the extent of soft tissue calcification, independent of the histopathological state of the mineralization. Therefore, we propose the STiCSS as an effective method to measure various forms of soft tissue calcification.

Due to the ordinal nature of data obtained from the STiCSS as compared to continuous data obtained through  $\mu$ CT quantification, some clustering of the data points is anticipated (Figure 39), since one ordinal score will cover a range of continuous values. Nevertheless, all observers who employed the STiCSS to quantify radiographic images were in good correlation with the values obtained from  $\mu$ CT (Table 12) and were able to reliably score images resulting in substantial agreement with minimal intra/inter observer error.

While this method by no means replaces the use of  $\mu$ CT or histological analysis for determining the pathological state of soft tissue calcification, it does provide an alternative,

cost-effective method for longitudinal soft tissue calcification quantification other than in vivo  $\mu$ CT. Finally, while the STiCSS is validated for detection of soft tissue calcification in the posterior compartment of the lower extremity, we surmise that due to the robustness of our precision analysis, these methods will be translatable to other trauma-induced soft tissue calcification models as well as other anatomical sites.

*(Article 6 Continued) Output Analysis and Quantification of Heterotopic Ossification*

With the validated Soft Tissue Calcification Scoring System (STiCSS) in hand, the extent of soft tissue calcification was quantified at 7 days post injury (DPI). Images underwent post-image standardization and were semi-quantitatively assessed by a blinded observer

*Histological Analysis and Quantification*

Injured hind limbs were fixed in 4% paraformaldehyde overnight. Samples for which mineral deposition was not examined were decalcified in 0.5M EDTA (pH 8.0) for approximately 5 days prior to processing. All samples were processed in graded series of ethanol, cleared, and embedded in paraffin prior to sectioning. 6 $\mu$ m sections were cut and stained as described below.

**Hematoxylin and Eosin (H&E):** Deparaffinized sections were stained in Gills 3 hematoxylin solution for 5 minutes. Slides were then rinsed in tap water for 10 minutes followed by eosin staining. Finally, slides were dehydrated and cleared in xylene before cover slipping with Permount.

**Safranin-O/ Fast Green Stains (Safranin-O):** Deparaffinized sections were rehydrated and



placed in freshly filtered working Weigert's hematoxylin for 10 minutes. Slides were then immediately washed in running tap water for 10 minutes followed by staining with 0.1% Fast green solution for 5 minutes. Slides were then rinsed quickly in 1% acetic acid for no more than 10-15 seconds and then placed in 0.1% Safranin O solution for 5 minutes. Finally, slides were dehydrated through two changes of 95% EtOH and 100% EtOH for 3 minutes each and cleared in two changes of xylene for 5 minutes. Slides were then cover slipped with Permount.

TRAP staining: Deparaffinized sections were stained in a fast Garnet GBC, naphthol –AS-Bi Phosphate solution containing acetate and tartrate for 10 minutes. Slides were then placed in deionized water to stop the reaction and cover slipped using aqueous mounting medium.

Von Kossa staining: Deparaffinized sections were stained in 1% aqueous silver nitrate solution for 60 mins under a UV lamp. Sections were then washed in distilled water for 1 minute followed by fast green staining for 10 minutes. Finally, slides were dehydrated and cleared in xylene before cover slipping with Permount.

#### *Immunohistochemical Staining*

Deparaffinized and rehydrated samples were processed for antigen retrieval by heating for 2 minutes in 0.1M citric acid and 0.1M sodium citrate. Subsequently, endogenous peroxide was quenched with 3% H<sub>2</sub>O<sub>2</sub> for 15 minutes. Slides were then gently washed with PBS (5min × 3), and then blocked for 30 minutes using Blocking Solution (TSA kit Perkin

Elmer; Waltham, MA). Slides were then immunostained using a rat anti-mouse F4/80 antibody (MCA497 AbD Serptec; Raleigh, NC) at 1:100 dilution in the provided blocking solution overnight at 4°C. Slides were then washed with TNT wash buffer (5min × 3). A biotin conjugated goat anti-rat secondary antibody (BD Pharmigen, 559286 BD Bioscience; San Jose, CA) was diluted 1:100 with blocking buffer and incubated with the slides for 60 minutes. Following TSA signal amplification, the Dako Envision+ HRP/DAB System (Catalog # K4007, Dako; Carpinteria, CA) was used to visualize antibody staining. Slides were counterstained with Mayer's hematoxylin and cover slipped with an aqueous mounting medium.

#### *Immunofluorescent Staining*

Slides were deparaffinized, rehydrated, and processed for antigen retrieval as previously described. Slides were then gently washed with tris-buffered saline (TBS) and blocked with a 5% BSA solution containing 10% goat serum. Following blocking, slides were immunostained with a rabbit anti-mouse fibrin(ogen) (1:1000) antibody [229] overnight at 4°C. Slides were then washed with TBS and incubated with 10µg/mL of Alexa Fluor 647-labeled anti-rabbit antibody (Life Technologies 792514, Grand Island, NY) in blocking buffer for 1 hour at room temperature. Finally, slides were counterstained with DAPI and coverslipped using an aqueous mounting solution (PolySciences Warrington, PA).

#### *Histological Quantification: Measurement of Regenerating and Degenerating Muscle By H&E*

Muscle regeneration and degeneration was assessed by light microscopy of H&E stained

muscle at 200× magnification (Axio imager a1, ZEISS; Oberkochen, Germany). Skeletal muscle regeneration was evaluated by counting the number of centrally nucleated muscle fibers present within each individual 200× field. Skeletal muscle degeneration was evaluated by counting necrotic sarcomeres (identified by hypereosinophilic, hyalinized cytoplasm and absence of nuclei). Counts of regenerating and degenerating myocytes were expressed as a percentage of total muscle fibers (including all necrotic, regenerating, and uninjured sarcomeres within a 200× magnified field). A minimum of 2 mice per group were analyzed.

#### *Histologic Quantitation of PLG<sup>+/-</sup> Mice 28 Days Post Injury*

The presence of bone formation (identified by the presence of woven bone) and the necrotic muscle (identified by the presence of hypereosinophilic, hyalinized cytoplasm and absence of nuclei) were determined by light microscopy of H&E stained muscle at 200x magnification. Sides were scored in a binary method for either the presence or absence of bone and necrotic muscle. The ratio of the positive samples to the ratio of negative samples was then expressed in a table.

#### *Fibrin(ogen) Deposition Analysis by Immunofluorescent Staining*

Each section was exposed for 2 sec using Cy5 filter at 200× magnification. Images were obtained and area of fibrin(ogen), either full fibrinogen or fibrin polymer, immunolocalization was quantified using ImageJ (National Institute of Health, <http://imagej.nih.gov/ij/>). Results were expressed as number of fluorescent pixels per image.

### *Macrophage Migration Measurement by Immunohistochemical Staining*

The number of anti-F4/80-positive cells were quantified in 200× magnification using quantified using ImageJ (National Institute of Health, <http://imagej.nih.gov/ij/>). Each treatment group consisted of 4 mice. Individual fields of injured skeletal muscle were analyzed and results were averaged per experimental group.

### *Quantification of Plasminogen and Plasmin Activity*

Plasminogen Level: Circulating plasminogen levels were determined using a commercial sandwich ELISA (Molecular Innovations; Novi, MI) from murine citrated plasma obtained by cardiac puncture at the time of sacrifice.

### *Statistical Analysis*

Soft Tissue Calcification Score: Statistical comparisons between groups were conducted using the Mann-Whitney rank test. (\*  $P < 0.05$ ; \*\*  $P < 0.001$ ). To further strengthen the analysis, a proportional odds model with random effects was also performed using SAS software (Cary, NC). This test takes into account intra-individual correlations between paired samples (right and left legs) from a single mouse. However, this model cannot be applied when the number of mice in a group is limited or when ordinal scores are relatively homogeneous within groups. Thus, results from the Mann-Whitney rank test are reported for all figures and the proportional odds model is reported when statistically appropriate. All Mann-Whitney rank test calculations were performed using GraphPad Prism version 6 (La Jolla, CA).

### *Histological Quantification*

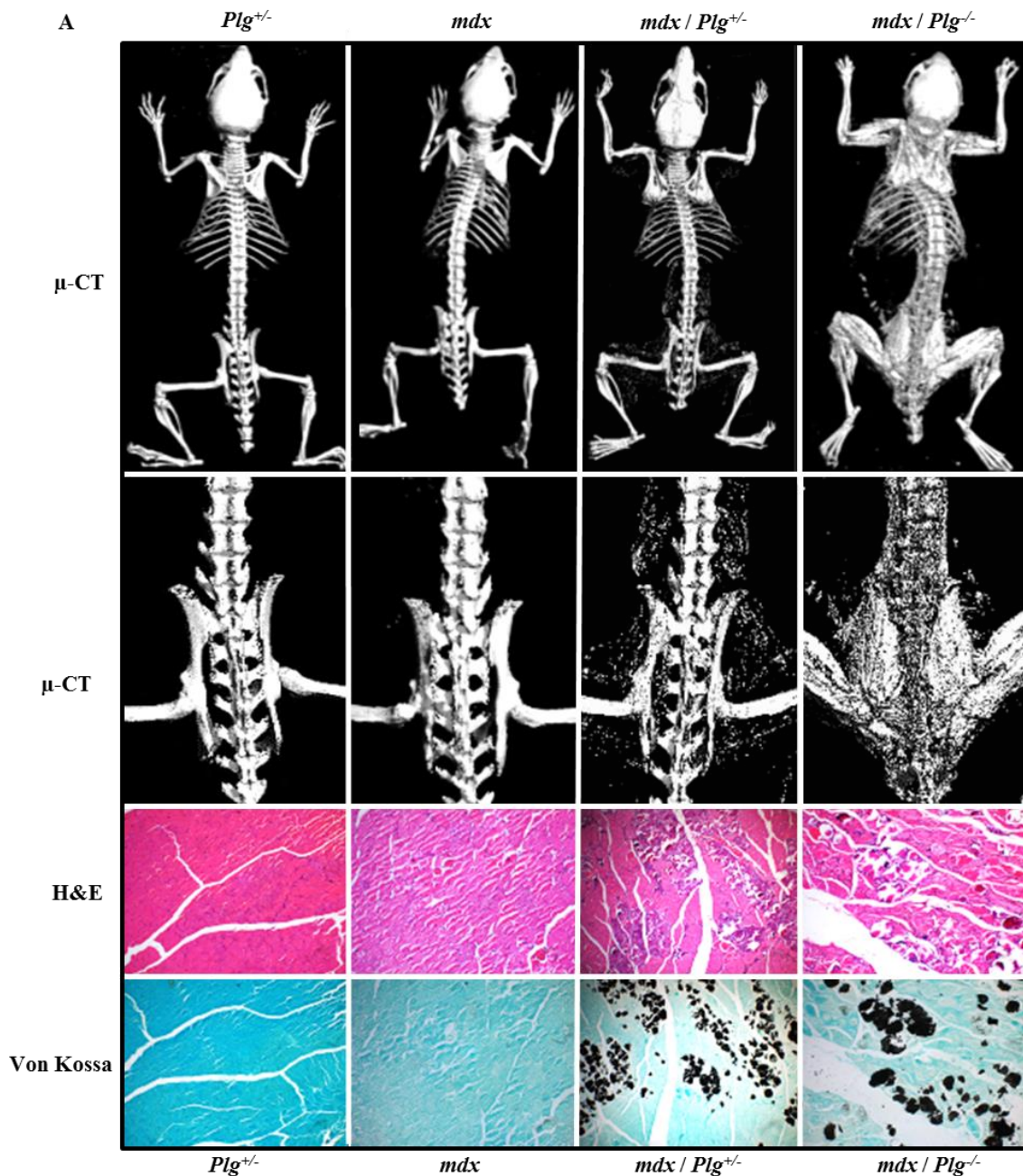
Statistical significance was calculated using a Mann-Whitney Rank test. *P* values and sample sizes are denoted within Figure Legends. Significance of bone formation and muscle necrosis 28 DPI were analyzed using a two tailed Fisher's exact test. *P* < 0.05 was considered significant.

### *Results*

#### *Plasminogen Prevents Soft Tissue Calcification in Muscle Genetically Predisposed to Injury*

To determine whether loss of the plasminogen zymogen or plasmin protease activity establishes an osteoinductive microenvironment in the context of muscle injury, heterozygous (Plg+/-) or homozygous (Plg-/-) plasminogen deficiency was genetically imposed on Duchenne muscular dystrophy (mdx) mice. Mdx mice sustain continuous muscle injury due to the lack of the muscle cytoskeletal protein, dystrophin [230].  $\mu$ CT analysis of mice with singular deficiencies in either plasminogen or dystrophin demonstrated no soft tissue calcification. In contrast, soft tissue calcification was observed in skeletal muscle of mice with combined dystrophin/plasminogen deficiency (mdx/Plg+/- and mdx/Plg-/- mice) (Figures 42 & 43). The degree of soft tissue calcification appeared proportional to the level of genetic plasminogen deficiency. These findings indicate that deficiency in plasmin(ogen), either the plasminogen zymogen or plasmin protease, is sufficient to cause soft tissue calcification in the setting of chronic muscle injury— even without associated bone fracture or major trauma. Histologic analysis determined the specific type of soft tissue calcification observed in mdx/Plg+/- and mdx/Plg-/- mice to be

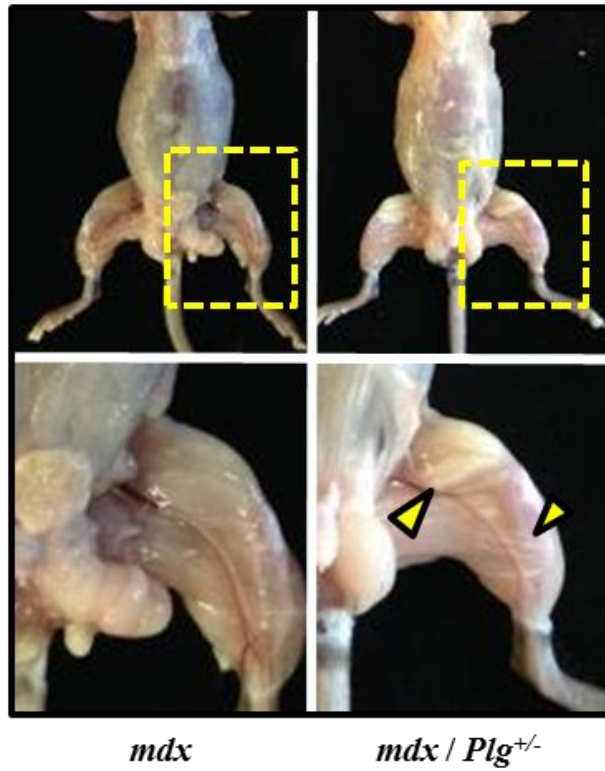
dystrophic calcification of necrotic sarcomeres (Figure 42). These data complement and extend previous findings that soft tissue calcification is sporadically observed in *mdx* mice lacking urokinase-type plasminogen activator [231] and imply that plasmin activity, not the plasminogen zymogen, is key in preventing soft tissue calcification in muscle.



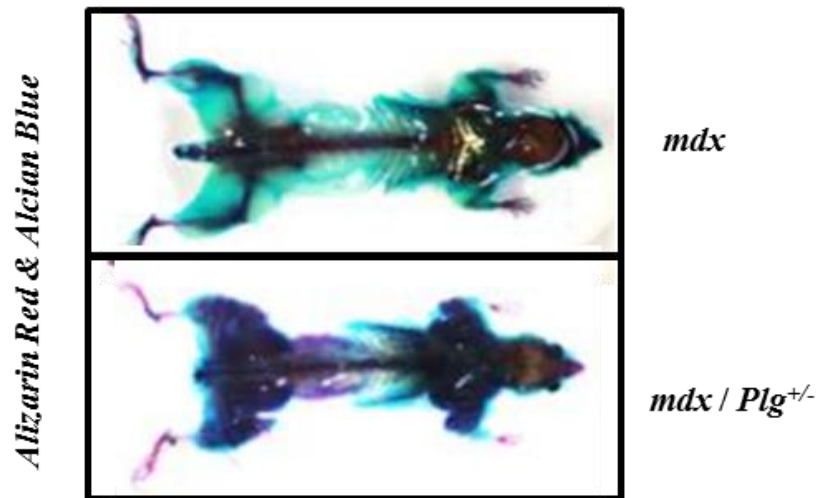
**Figure 42: Continuous Muscle Injury in the Setting of Plasminogen Deficiency**

**Results in Soft Tissue Calcification.** Full body  $\mu$ CT reconstruction of Plg<sup>+/-</sup>, mdx, mdx/Plg<sup>+/-</sup> and mdx/Plg<sup>-/-</sup> mice with focused magnification of paraspinal and pelvic musculature. Plg<sup>+/-</sup> mice without muscle injury showed no apparent calcification within skeletal muscle. Similarly, plasminogen-competent, mdx mice suffering continuous, chronic muscle injury also showed no muscle calcification. In contrast, mdx mice with either a partial (mdx/Plg<sup>+/-</sup>) or complete plasminogen deficiency (mdx/Plg<sup>-/-</sup>) showed calcification within all major skeletal muscle groups. H&E of Plg<sup>+/-</sup> mice revealed unremarkable, uninjured sarcomeres with peripherally located nuclei, whereas mdx, mdx/Plg<sup>+/-</sup>, and mdx/Plg<sup>-/-</sup> mice demonstrated interspersed necrotic (glossy, hypereosinophilic with absent nuclei) and regenerating (centrally located nuclei) sarcomeres. Von Kossa stain demonstrates no calcifications in Plg<sup>+/-</sup> and mdx mice, but marked dystrophic calcifications within necrotic sarcomeres of mdx/Plg<sup>+/-</sup> and mdx/Plg<sup>-/-</sup> mice.

A



B



**Figure 43: Soft tissue calcification in *mdx/Plg<sup>+/-</sup>* mice.** A) Macroscopic images of 8-week-old *mdx* and *mdx/Plg<sup>+/-</sup>* mice following gross dissection showed white calcifications within the muscles of *mdx/Plg<sup>+/-</sup>* mice. Magnified images demonstrated the presence of calcifications (yellow triangles) in the leg musculature of *mdx/Plg<sup>+/-</sup>* mice, but not in *mdx*



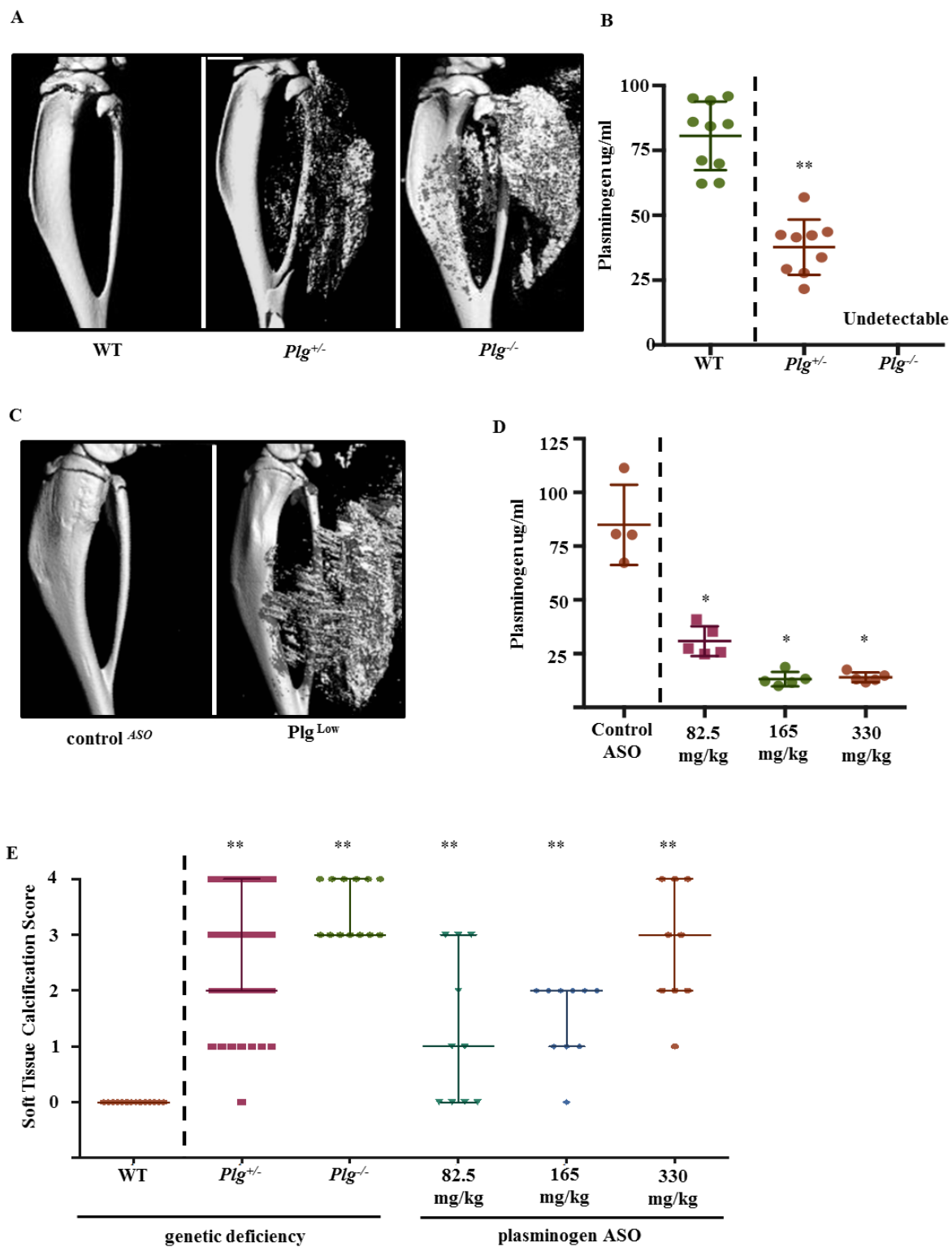
mice. B) Alizarin red and alcian blue whole mount staining of mdx and mdx/Plg<sup>+/-</sup> mice demonstrated the presence of abundant calcification (red staining) within skeletal muscle of mdx/Plg<sup>+/-</sup> mice.

#### *Plasminogen Prevents Soft Tissue Calcification in Muscle After Traumatic Injury*

Skeletal muscle injury in *mdx/Plg<sup>+/-</sup>* mice is continuous but temporally and spatially heterogeneous, complicating assessment of soft tissue calcification in the muscles of these mice. Therefore, we evaluated the impact of congenital plasminogen deficiency on localized, acute muscle injury induced by cardiotoxin (CTX) injection to specifically target the site of myocyte damage [232]. As in the continuous muscle injury model, acute muscle injury in the context of plasminogen deficiency resulted in dramatic soft tissue calcification at the site of injury (Figure 44A). Reduced circulating plasminogen levels were confirmed in genetically deficient murine models (Figure 44B). Importantly, soft tissue calcification was not restricted to CTX-induced muscular injury, as similar findings were observed in a tissue crush injury model (Figure 45). Thus, congenital plasminogen deficiency combined with focal, acute muscle injury is sufficient to cause soft tissue calcification of skeletal muscle.

Because congenital plasminogen deficiency is associated with accelerated skeletal degeneration and impaired tissue regeneration [233, 234], we next examined the impact of transient knockdown of plasminogen expression using a specific plasminogen antisense oligonucleotide “gapmer” (ASO). Wild-type mice treated with plasminogen ASO (Plg<sup>Low</sup>) achieved a 95% transient knockdown of hepatic plasminogen mRNA when dosed prior to

and during CTX injury (Table 14). Following CTX-induced muscle injury,  $\text{Plg}^{\text{Low}}$  mice also manifested soft tissue calcification within skeletal muscle indistinguishable from that observed in congenital plasminogen deficiency (Figure 44C). Reduced circulating plasminogen levels were confirmed in  $\text{Plg}^{\text{Low}}$  mice receiving varying plasminogen ASO doses (Figure 44D). The severity of soft tissue calcification after injury increased with greater genetic plasminogen deficiency and higher plasminogen ASO dosing (Figure 44E, Table 15 & 16). Together these data establish that soft tissue calcification of skeletal muscle in mice with congenital plasminogen deficiency is not secondary to developmental defects and that muscle injury and hypoplasminogenemia are fundamental determinants of soft tissue calcification in skeletal muscle.



**Figure 44: Continuous and Acute Plasminogen Deficiency Results in Muscle Calcification After Acute Muscle Injury.** A)  $\mu$ CT reconstructions of the lower leg of

WT, Plg<sup>+/-</sup> and Plg<sup>-/-</sup> mice 7 days following CTX injury; note the moderate to severe muscle calcification in mice with plasminogen deficits. B) Plasminogen ELISA on murine plasma confirmed reduced circulating levels according to plasminogen genotype. (N $\geq$ 8; \*\* P $<$  0.001; Mann-Whitney test vs. WT) C) Pharmacologic reduction of plasminogen in WT mice with a plasminogen ASO prior to injury led to a Plg<sup>Low</sup> phenotype and markedly more muscle calcification 7 days post injury (DPI) than controlASO-treated WT mice, indicating that plasminogen prevents muscle calcification independent of the method of plasminogen reduction. D) Plasminogen ELISA on murine plasma confirmed reduced circulating levels with increasing plasminogen ASO dosing (N $\geq$ 4; \* P $<$  0.05; Mann-Whitney test vs. Control ASO) E) The extent of soft tissue calcification in these models was scored using plain radiographs and a semi-quantitative scoring method similar to the Brooker classification system for HO [235]. Graphical summary of Soft Tissue Calcification Scores in various experimental cohorts at 7 DPI using this semi-quantitative method showed increasing calcification scores, as measured by the STiCSS, with reduced circulating plasminogen levels. Medians and interquartile ranges are denoted (N $\geq$ 9; \*\* P $<$  0.001; Mann-Whitney test vs. WT). See Tables 14 & 15 for further statistical evaluation.

**Table 14: *In vivo* Effectiveness of Plasminogen Knockdown by ASO Injection.**

Quantitation of percent plasminogen knockdown in the livers of WT mice after receiving 100mg/kg/week of the respective ASO for 2 weeks. Since hepatotoxicity can negatively affect hepatic protein synthesis, AST and ALT levels (U/L) were also determined (normal range of mouse AST, 54-298 U/L; ALT, 17-77 U/L).

<b>Antisense Oligonucleotide</b>	<b>Percent Hepatic mRNA Knockdown</b>	<b>AST</b>	<b>ALT</b>
<b>Plasminogen</b>	95% (+/-1.2%)	192.8 (+/- 52.0)	139.3 (+/- 28.69)

**Table 15: Statistical Analysis of STC Score in Plasminogen Deficient Mice After CTX-induced Muscle Injury.** (Top) Tabular values reported represent the percent incidence of STC scores in each genotype and number of mice per genotype examined. (Middle) *P* values determined by proportional odds model (N/A, proportional odds model was not statistically applicable to data). (Bottom) *P* values determined by the Mann-Whitney Rank test.

<b>Percent Incidence of Score</b>				
<b>Soft Tissue Calcification Score</b>	<b>WT</b>	<b><i>Plg</i><sup>+/-</sup></b>	<b><i>Plg</i><sup>-/-</sup></b>	
<b>0</b>	100%	2%	0%	
<b>1</b>	0%	17%	0%	
<b>2</b>	0%	33%	0%	
<b>3</b>	0%	22%	54%	
<b>4</b>	0%	26%	46%	
<b>N=</b>	16	42	13	
<b>Proportional Odds Model</b>				
<b>Genotype</b>	<b>WT</b>	<b><i>Plg</i><sup>+/-</sup></b>	<b><i>Plg</i><sup>-/-</sup></b>	
<b>WT</b>	-	N/A	N/A	
<b><i>Plg</i><sup>+/-</sup></b>	N/A	-	0.0573	
<b><i>Plg</i><sup>-/-</sup></b>	N/A	0.0573	-	
<b>Mann-Whitney Rank Test</b>				
<b>Genotype</b>	<b>WT</b>	<b><i>Plg</i><sup>+/-</sup></b>	<b><i>Plg</i><sup>-/-</sup></b>	
<b>WT</b>	-	P<0.001	P<0.001	
<b><i>Plg</i><sup>+/-</sup></b>	P<0.001	-	P=0.007	
<b><i>Plg</i><sup>-/-</sup></b>	P<0.001	P=0.007	-	



**Figure 45: Crush Injury Model of HO.** Plain radiographs obtained 28 days after acute crush injury to the posterior compartment of the lower leg in WT, *Plg*<sup>+/-</sup>, and *Plg*<sup>-/-</sup> mice demonstrated that HO formation is not dependent on the mechanism of muscle injury.

**Table 16: Statistical Analysis of STC Score in Mice treated with Plasminogen ASO after CTX induced Muscle injury.** (Top) Tabular values reported represent the percent incidence of STC scores in each treatment group and number of mice per treatment. (Middle) *P* values determined by the proportional odds model (N/A, proportional odds model was not statistically applicable to data). (Bottom) *P* values determined by the Mann-Whitney Rank test.

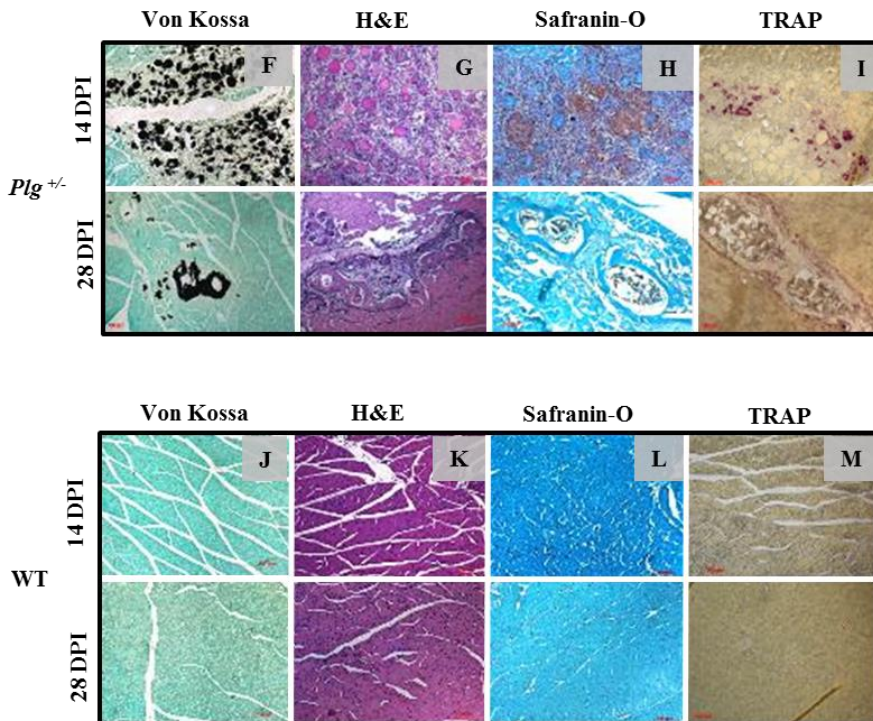
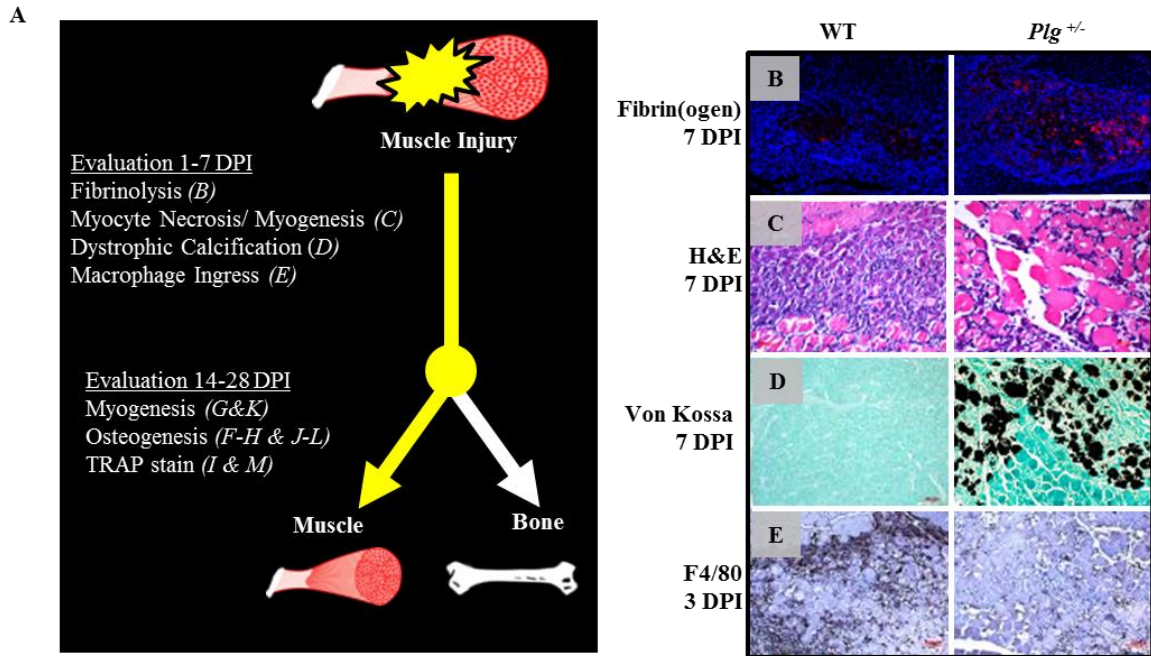
<b>Percent Incidence of Score</b>				
<b>Soft Tissue Calcification n Score</b>	<b>WT</b>	<b>Dose Plasminogen ASO</b>		
		<b>82.5 mg/kg</b>	<b>165 mg/kg</b>	<b>330 mg/kg</b>
<b>0</b>	100%	40%	10%	0%
<b>1</b>	0%	20%	30%	11%
<b>2</b>	0%	10%	60%	33%
<b>3</b>	0%	30%	0%	22%
<b>4</b>	0%	0%	0%	34%
<b>N=</b>	16	10	10	9
<b>Proportional Odds Model</b>				
<b>Dose</b>	<b>WT</b>	<b>82.5 mg/kg</b>	<b>165 mg/kg</b>	<b>330 mg/kg</b>
<b>WT</b>	-	N/A	N/A	N/A
<b>82.5 mg/kg</b>	N/A	-	P=0.893	P=0.126
<b>165 mg/kg</b>	N/A	P=0.893	-	P=0.084
<b>330 mg/kg</b>	N/A	P=0.126	P=0.084	-
<b>Mann-Whitney Rank Test</b>				
<b>Genotype</b>	<b>WT</b>	<b>82.5 mg/kg</b>	<b>165 mg/kg</b>	<b>330 mg/kg</b>
<b>WT</b>	-	P<0.001	P<0.001	P<0.001
<b>82.5 mg/kg</b>	P<0.001	-	P=0.661	P=0.031
<b>165 mg/kg</b>	P<0.001	P=0.661	-	P=0.016
<b>330 mg/kg</b>	P<0.001	P=0.031	P=0.016	-



*Plasminogen Deficiency and Muscle Injury Are Associated with Dystrophic Calcification and Subsequent Endochondral Ossification*

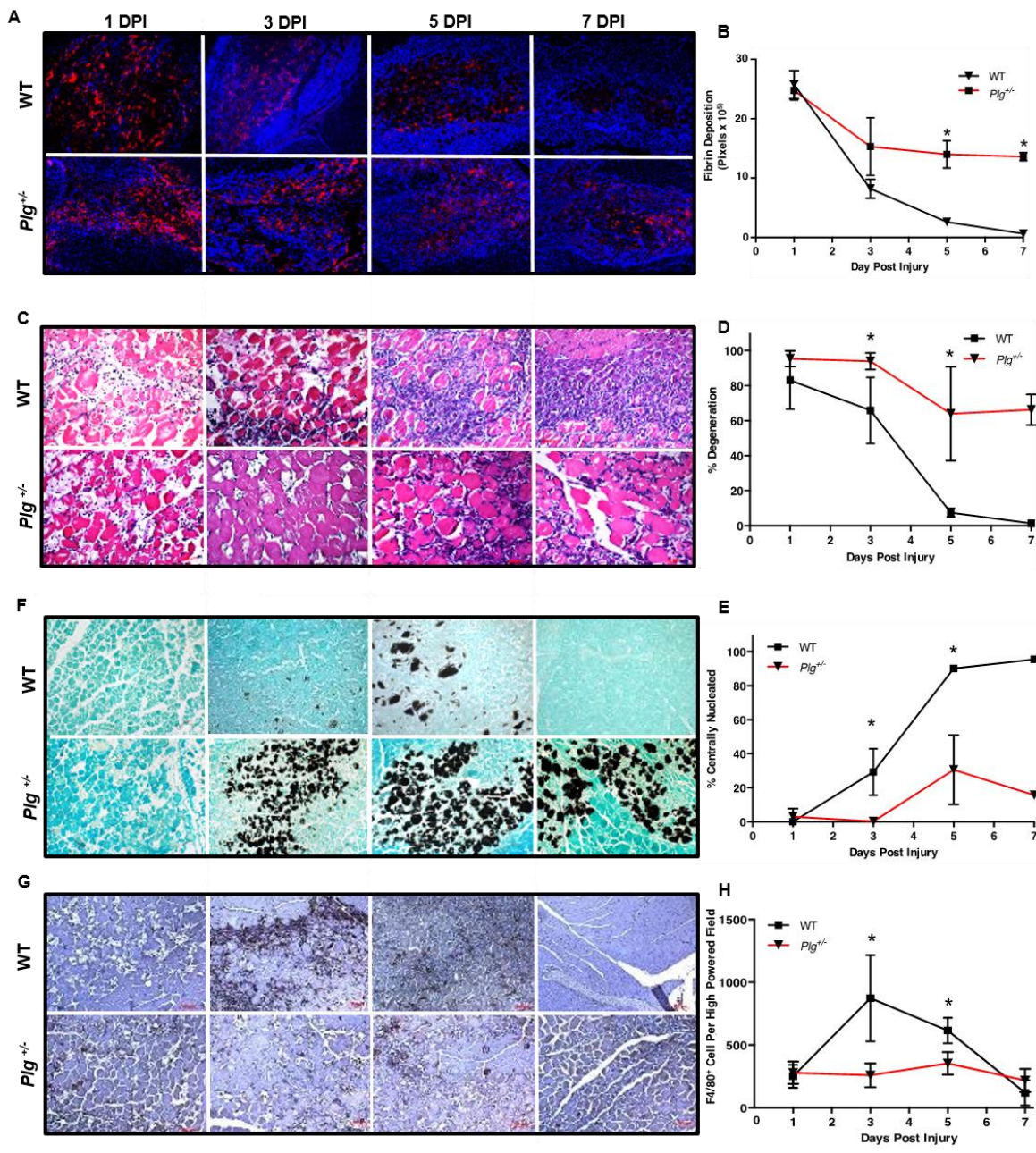
To further define the initial pathophysiological processes that result in soft tissue calcification, we examined sites of CTX-induced muscle injury histologically over the acute (1-7 DPI) post-injury period for evidence of fibrinolysis, myocyte necrosis, myogenesis, dystrophic calcification, and macrophage infiltration (Figure 46A). WT mice cleared fibrin deposits from the site of injury faster than *Plg*<sup>+/-</sup> mice, which supports the assumption that extravascular plasmin activity is reduced in *Plg*<sup>+/-</sup> mice (Figure 12B, Figure 46A&B). In accordance with other findings that plasminogen is essential for skeletal muscle regeneration [236, 237], we also observed that necrotic myocytes persisted at the injury site for at least 28 days in *Plg*<sup>+/-</sup> mice. Additionally, significantly fewer regenerating myocytes were seen in *Plg*<sup>+/-</sup> mice compared to WT mice (Figure 46C, Figure 46C-E). Von Kossa stains for calcium revealed that WT mice developed a limited amount of dystrophic calcification that was completely resorbed by 5 DPI (Figure 46D, Figure 46F). In contrast, exuberant dystrophic calcifications were seen in *Plg*<sup>+/-</sup> mice up to 14 DPI (Figure 46D, Figure 47F). These data indicate that plasmin(ogen) prevents crystallization and/or promotes resorption of dystrophic calcifications within necrotic muscle in the acute post injury period. Efficient fibrin clearance was temporally associated with infiltration of the injury site by monocytes/macrophages in WT mice. Conversely, both fibrin clearance and macrophage infiltration were diminished in *Plg*<sup>+/-</sup> mice. Whereas infiltration of F4/80-positive cells peaked 3 DPI in WT mice, this influx of monocyte/macrophages was not observed in injured muscles from *Plg*<sup>+/-</sup> mice (Figure 46E, Figure 47G&H). These findings demonstrate that dystrophic calcifications form

contemporaneously with delayed monocyte/macrophage infiltration and delayed muscle regeneration in the setting of acute muscle injury and plasmin(ogen) deficiency.



**Figure 46: Partial Plasminogen Deficiency and Muscle Injury Results in Poor Muscle Regeneration, Persistent Dystrophic Calcification, Diminished Macrophage Invasion**

**and Endochondral Ossification.** A) Schematic and key of histologic analyses performed in early and late post-injury periods. B) Fibrin(ogen) (red) clearance 7 DPI is delayed in Plg<sup>+/-</sup> compared to WT mice (DAPI blue counterstain). C) H&E stain 7 DPI demonstrated more regenerating myocytes (central nuclei) in WT compared to persistent necrotic myocytes and reduced inflammatory infiltrates in Plg<sup>+/-</sup> mice. D) Calcium stain (Von Kossa-black) 7 DPI highlighted exuberant dystrophic calcifications in Plg<sup>+/-</sup> mice relative to WT. E) Immunohistochemical staining for F4/80 showed delayed macrophage/monocyte infiltration in Plg<sup>+/-</sup> mice compared to WT 3 DPI. F-I) Endochondral ossification in Plg<sup>+/-</sup> mice 14DPI: Von Kossa stains revealed the presence of dystrophic calcifications and H&E stain revealed persistence of necrotic myofibers and islands of chondroid matrix (confirmed by Safranin-O stain (red)) intermixed with persistent dystrophic calcifications and TRAP-positive cells (purple). This histologic pattern is consistent with early endochondral ossification. Endochondral ossification in Plg<sup>+/-</sup> mice 28 DPI: Von Kossa and H&E stains showed mineralized woven bone with hematopoietic marrow and rimming osteoblasts. Safranin-O stains confirmed the removal of the chondroid matrix and TRAP staining revealed the presence of TRAP-positive cells surrounding woven bone. This histologic pattern is indicative of late endochondral ossification. J-M) WT muscle regeneration 14 and 28 DPI: Von Kossa stains revealed no evidence of persistent calcifications. H&E staining showed muscle regeneration (maturing myocytes with intact sarcomeric structures and central nuclei that become eccentrically located by 28 DPI). Unremarkable Safranin-O and TRAP stains disclosed no evidence of endochondral ossification or osteoclast-like multinucleated giant cells. (200x magnification in Figures B, D-M; 400x magnification in Figure C).



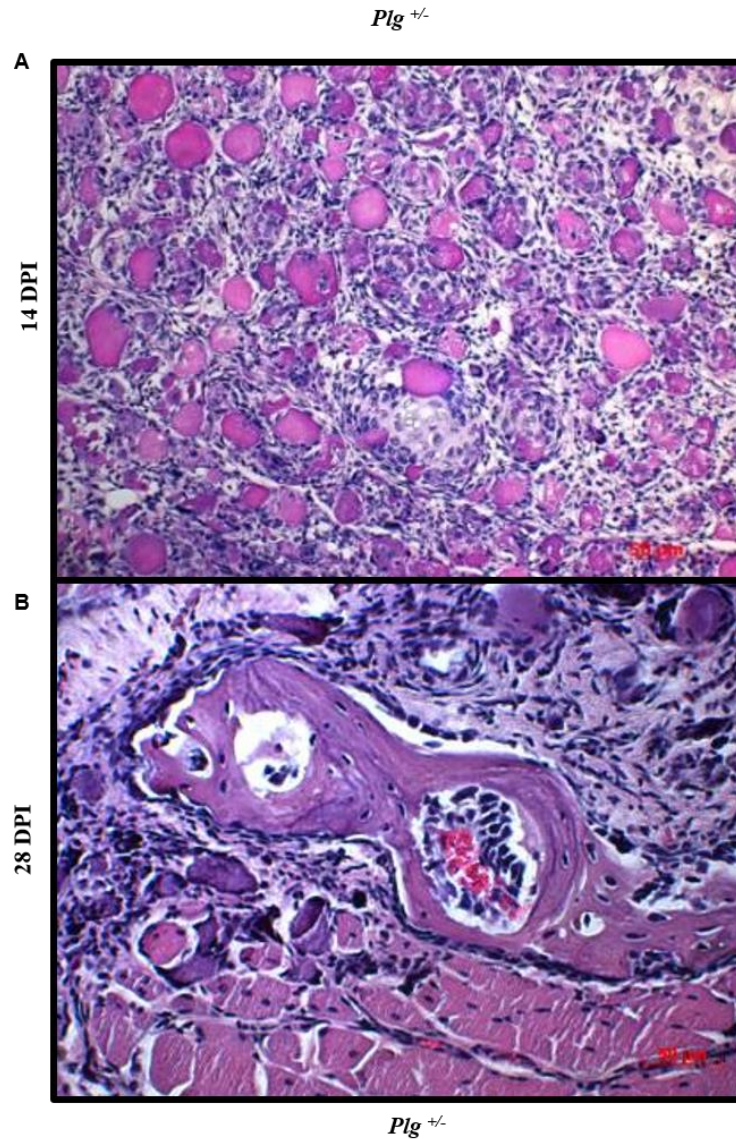
**Figure 47: Histologic Quantitation of Muscle Healing in WT and Plg<sup>+/-</sup> mice.** A) The extensive fibrin(ogen) staining (red) seen 1 DPI in WT injured muscle was cleared by 7 DPI. In contrast, fibrin(ogen) immunostaining persisted through 7 DPI in Plg<sup>+/-</sup> injured muscle (original magnification 200x). B) Quantitation of fibrin(ogen) deposition 1, 3, 5, and 7 DPI in injured muscles served as a surrogate marker of plasmin protease activity

within damaged muscle. Plg<sup>+/-</sup> mice had significantly delayed fibrin clearance compared to WT mice, indicative of decreased plasmin activity. Error bars represent standard deviation (N=4; \* P< 0.05; Mann-Whitney test comparing WT mice to Plg<sup>+/-</sup> mice). C) H&E sections of CTX-injured WT mice demonstrated an early inflammatory infiltrate which peaked 3-5 DPI and small regenerating myofibers with central nuclei by 7 DPI. Comparatively, infiltration of inflammatory cells and muscle regeneration was impaired in Plg<sup>+/-</sup> mice; instead, hypereosinophilic, necrotic sarcomeres persisted through 7 DPI (original magnification, 400x) D) Histologic quantitation of degenerated myocytes WT mice and Plg<sup>+/-</sup> mice expressed as percentage of necrotic myocytes per 400x magnification field 1, 3, 5, and 7 DPI. Plg<sup>+/-</sup> mice showed significantly more necrotic myocytes compared to WT mice. Error bars represent standard deviation (N≥2 for each time point; P< 0.05; Mann-Whitney test comparing WT and Plg<sup>+/-</sup> mice). E) Quantitation of regenerating myocytes expressed as percentage myocytes with centrally located nuclei per 400x magnification field 1, 3, 5, and 7 DPI. WT mice exhibited significantly more muscle regeneration compared to Plg<sup>+/-</sup> mice. Error bars represent standard deviation (N≥2 for each time point; \* P< 0.05; Mann-Whitney test comparing WT to Plg<sup>+/-</sup> mice). F) Von Kossa staining of injured WT muscle showed sparse mineralization 3 DPI (black) and several non-uniform calcium deposits in dead myocytes 5 DPI that were resorbed by 7 DPI. In contrast, injured Plg<sup>+/-</sup> muscle showed numerous calcified deposits within necrotic myocytes 3 DPI that persist until at least 7 DPI. (original magnification, 400x) G) Immunohistochemical stains revealed influx of F4/80-positive cells (brown) into the site of muscle injury in WT mice, peaking 3 DPI and resolving 7 DPI. In contrast, limited numbers of F4/80-positive cells were seen over 7 DPI in injured muscles from Plg<sup>+/-</sup> mice.

(original magnification, 200x). H) Quantitation of F4/80-positive cells in WT and *Plg*<sup>+/-</sup> mice. Significant increased numbers of F4/80-positive cells were observed in injured muscle from WT mice 3 DPI, which returned to baseline levels by 7 DPI. In contrast, influx of F4/80-positive cells in *Plg*<sup>+/-</sup> mice was profoundly blunted. Error bars represent standard deviation (N=5 at each time point; \* P < 0.05; Mann-Whitney test comparing WT and *Plg*<sup>+/-</sup> mice).

The evolution of dystrophic calcifications into HO was also evaluated histologically. Dystrophic calcifications, islands of hyaline chondroid matrix with chondrocytes, and TRAP-positive multinucleated giant cells were intermixed within injured muscle tissue of *Plg*<sup>+/-</sup> mice 14 DPI (Figure 46F-I, Figure 48). Two weeks later (28 DPI), mature woven bone with rimming osteoblasts and intertrabecular hematopoiesis was observed in *Plg*<sup>+/-</sup> injury sites (Figure 46G, Figure 48B). The transition from a primitive chondroid matrix to mature woven bone is consistent with endochondral ossification, a histologic hallmark of HO [238]. In contrast, injury sites in WT mice showed maturing striated muscle 28 DPI, consistent with effective tissue regeneration, without evidence of HO (Figure 49J-M). Histologic evaluation of HO at 28 DPI in *Plg*<sup>+/-</sup> mice demonstrated woven bone entirely contained within the posterior muscle compartment and distinct from the tibia and fibula (Figure 49A). Two dimensional  $\mu$ CT showed the presence of circular condensed calcifications morphologically consistent with HO surrounded by disorganized calcifications consistent with dystrophic calcifications (Figure 49B). Both abnormal findings were distinct from the cortex of nearby tibia and fibula. This data indicates that muscle injury in the setting of partial plasminogen deficiency is associated with persistent

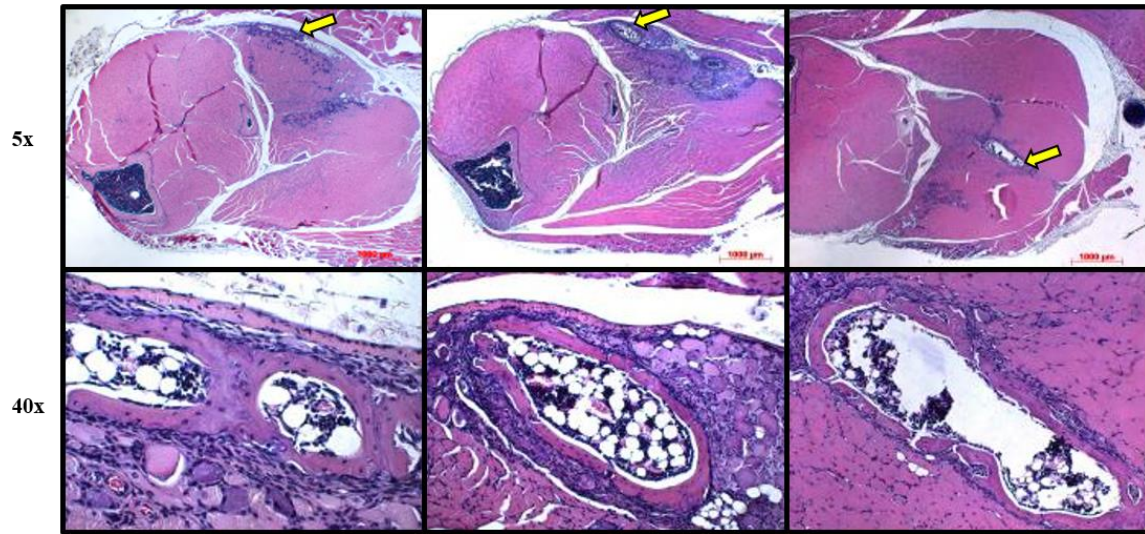
dystrophic calcification, and that persistent dystrophic calcifications are associated with subsequent development of HO within the injured muscle.



**Figure 48: Injured *Plg<sup>+/-</sup>* Mice Undergo Endochondral Ossification. A)** Enlarged H&E of injured *Plg<sup>+/-</sup>* muscle 14 DPI showing islands of cells embedded within extracellular matrix interspersed with glossy hypereosinophilic deposits. **B)** Enlarged H&E of injured *Plg<sup>+/-</sup>* muscle 28 DPI showing woven bone with central hematopoiesis and rimming osteoblast



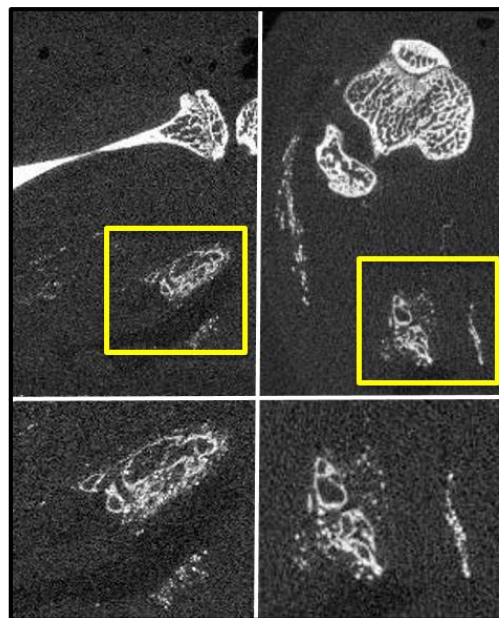
A



B

Coronal 2D  $\mu$ CT

Axial 2D  $\mu$ CT



**Figure 49: Characterization of Heterotopic Ossification after Muscle Injury and Plasminogen Deficiency.** A) Representative H&E (5x magnification) showed woven bone forms exclusively within the posterior muscle compartment, separated by an intact fascial plane and distinct from the tibia and fibula 28 DPI in *Plg*<sup>+/-</sup> mice. Persistent dystrophic calcifications are scattered around the woven bone within the posterior muscle

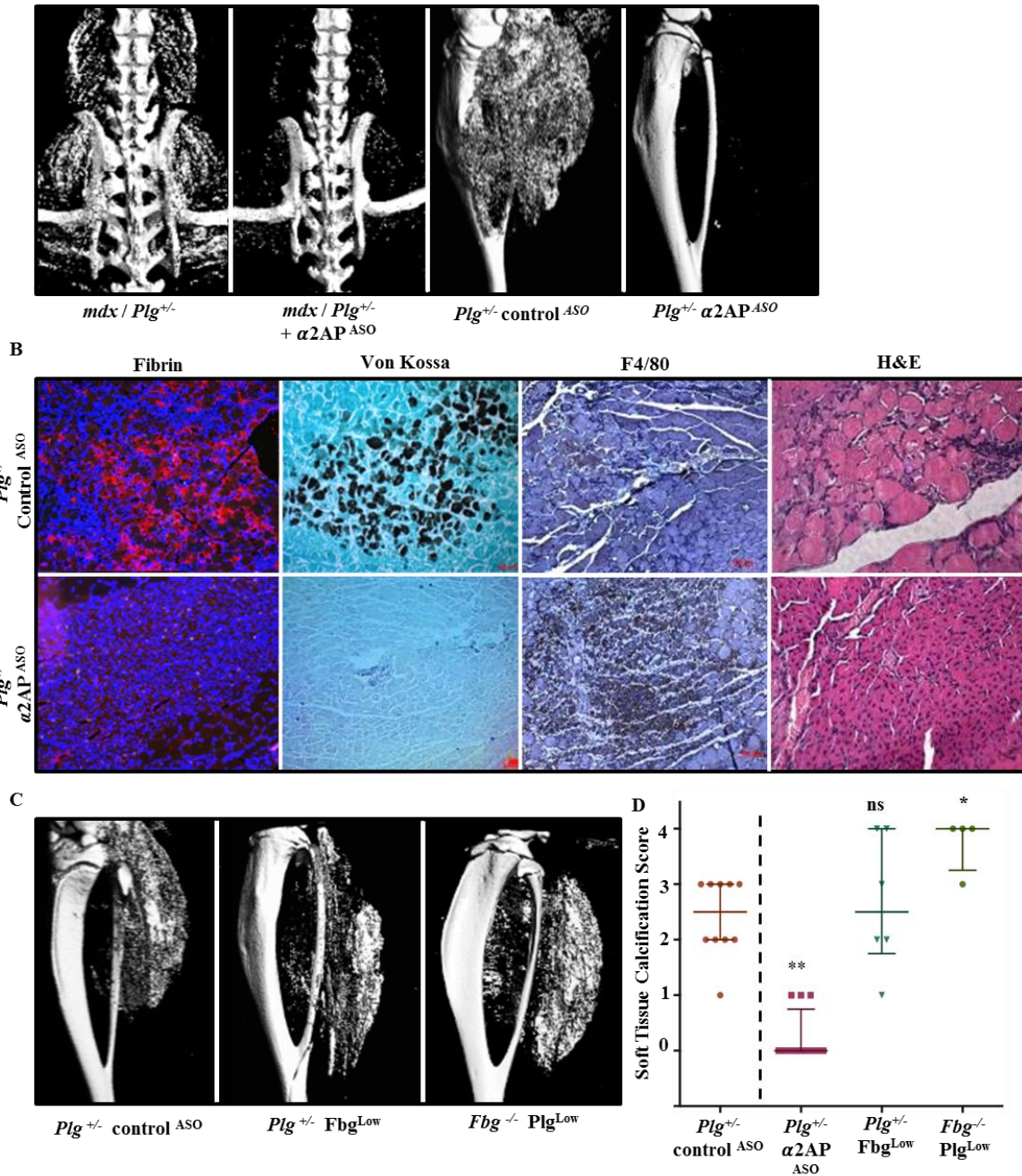
compartment. 40x magnification of the same section confirms woven bone with central hematopoiesis and rimming osteoblasts. B) 2D cross sectional and axial  $\mu$ CT images demonstrated organized calcifications within the posterior muscle compartment distinct from, but morphologically consistent with the nearby tibia and fibula 28 DPI in  $Plg^{+/-}$  mice. Adjacent to organized soft tissue calcifications are disorganized calcifications consistent with persistent dystrophic calcifications that surround HO histologically.

*Plasmin Protease Activity Inhibits Deposition of Dystrophic Calcifications Within Injured Muscle and Promotes Muscle Regeneration*

To test the hypothesis that soft tissue calcifications that form after traumatic injury are specifically attributable to a deficit in plasmin protease activity, and not some other biological activity associated with reduced plasminogen zymogen, we experimentally increased plasmin activity *in vivo* in the setting of global plasminogen reduction ( $Plg^{+/-}$  mice) by targeting the primary inhibitor of plasmin protease activity—  $\alpha$ 2-antiplasmin ( $\alpha$ 2AP). Administration of  $\alpha$ 2AP ASO ( $\alpha$ 2AP<sup>ASO</sup>) resulted in an 85% reduction of hepatic  $\alpha$ 2AP mRNA (Table 14). Treatment of  $mdx/Plg^{+/-}$  mice with  $\alpha$ 2AP<sup>ASO</sup> resulted in a marked reduction in soft tissue calcification compared to control ASO (control<sup>ASO</sup>) treated  $mdx/Plg^{+/-}$  mice (Figure 50A & Figure 51), indicating that plasmin protease activity is a determinant of soft tissue calcification after myocyte injury.

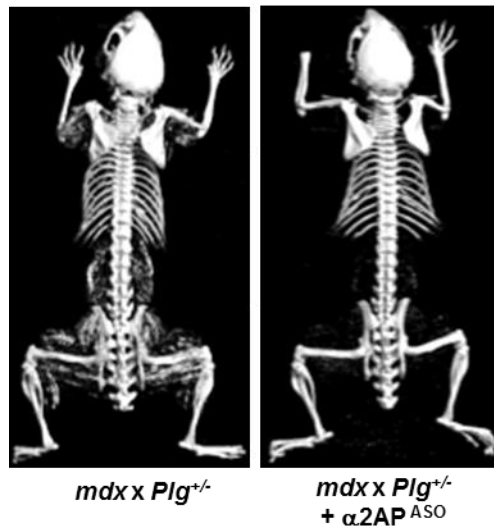
To provide further insight regarding the molecular mechanisms by which plasmin protease activity prevents soft tissue calcification, we studied the effects of increasing plasmin activity on the injury microenvironment in  $Plg^{+/-}$  mice after acute CTX-induced muscle

injury. Treatment of *Plg<sup>+/-</sup>* mice with  $\alpha 2AP^{ASO}$  again resulted in a marked reduction in soft tissue mineralization compared to control ASO (control<sup>ASO</sup>) treatment (Figure 50A). Comparative studies of local fibrin deposition following acute muscle injury confirmed that plasmin activity was a primary determinant of fibrin clearance (fibrinolysis) (Figure 50B & Figure 49A). Histologic analysis showed that  $\alpha 2AP^{ASO}$  treatment limited the degree of dystrophic calcification within necrotic skeletal muscle (Figure 50B). In addition, enhanced plasmin activity promoted monocyte/macrophage infiltration into the site of injury and significantly increased myofiber regeneration (Figures 49B & Figure 52). Together these data indicate that plasmin protease activity promotes local fibrinolysis, monocyte/macrophage infiltration, and muscle regeneration, in addition to inhibiting deposition of dystrophic calcifications.



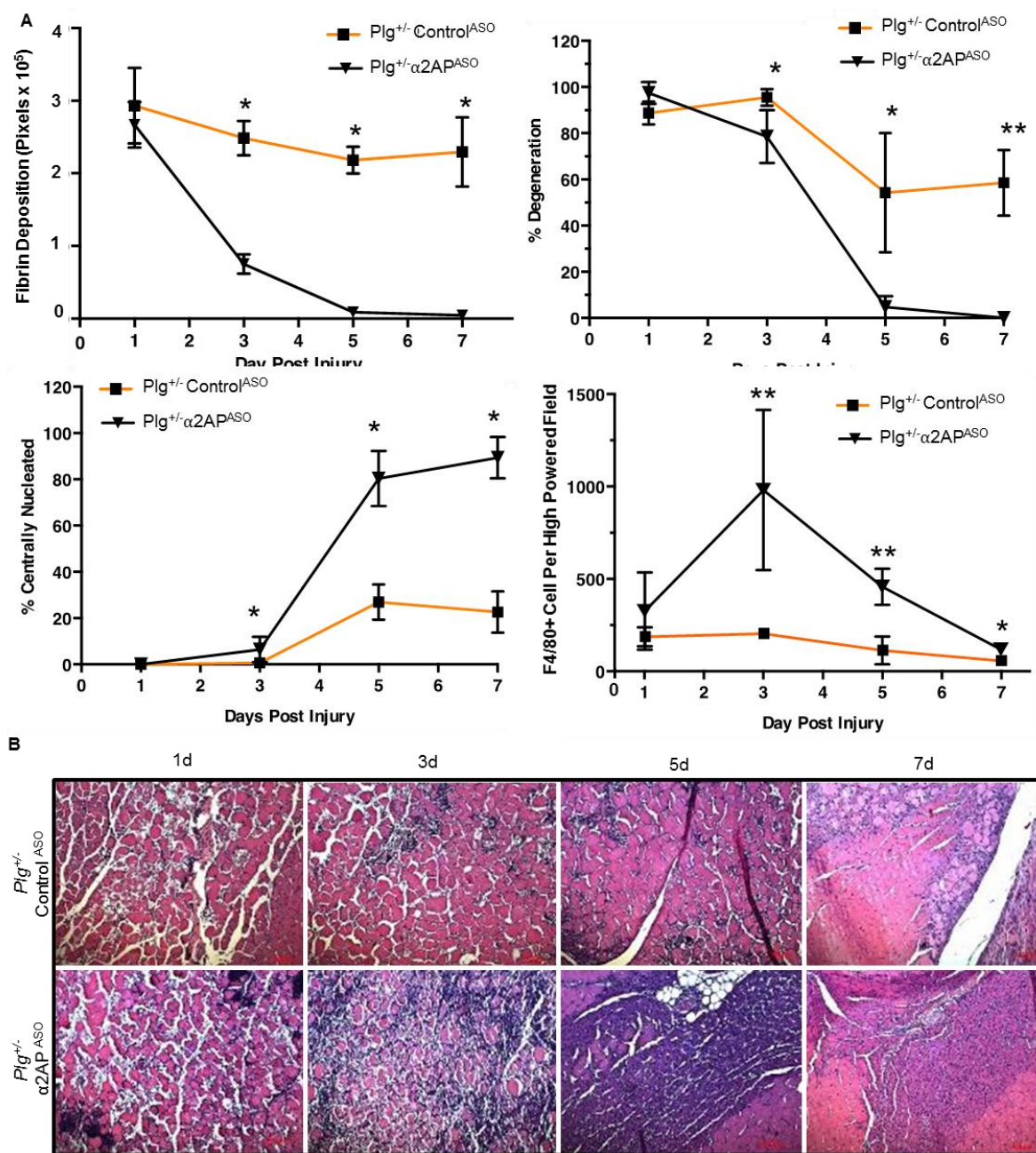
**Figure 50: Increasing Plasmin Activity Prevents Soft Tissue Calcification and Rescues Muscle Regeneration Independent of Fibrinolysis.** A)  $\mu$ CT reconstructions of *mdx/Plg<sup>+/-</sup>* mice treated with  $\alpha$ 2APASO showed markedly reduced soft tissue calcification compared to control *mdx/Plg<sup>+/-</sup>* mice. Similar reductions in soft tissue calcification were noted in CTX-injured *Plg<sup>+/-</sup>* mice treated with  $\alpha$ 2APASO relative to controlASO. B)

Representative histologic images of CTX-injured Plg<sup>+/-</sup> mice treated with controlASO or  $\alpha$ 2APASO.  $\alpha$ 2APASO treatment, but not controlASO, promoted fibrin(ogen) clearance (fibrin-red/DAPI-blue, 7 DPI), prevented dystrophic calcification (Von Kossa-black, 7 DPI), restored macrophage/monocyte cell infiltrate (F4/80, 3 DPI) and restored muscle regeneration (H&E, 7 DPI). These data indicate that plasmin protease activity is essential for limiting dystrophic calcification and promoting muscle regeneration. C)  $\mu$ CT reconstructions of CTX-injured Plg<sup>+/-</sup> mice treated with controlASO (Plg<sup>+/-</sup> controlASO) or fibrinogenASO (Plg<sup>+/-</sup> FbgLow) revealed marked soft tissue calcification formation 7 DPI. Mice genetically deficient in fibrinogen also developed HO when treated with a plasminogenASO (Fbg<sup>-/-</sup> PlgLow). D) Soft Tissue Calcification Score (7-DPI): depleting the plasmin inhibitor  $\alpha$ 2AP ( $\alpha$ 2APASO), but not fibrinogen (Plg<sup>+/-</sup> FbgLow and Fbg<sup>-/-</sup> PlgLow) prevented soft tissue calcification. Medians and interquartile ranges are shown (N $\geq$ 4; \* P< .05; Mann-Whitney test vs. Plg<sup>+/-</sup> controlASO mice)



**Figure 51: Soft Tissue Calcification in Continuous Muscle Injury and Plasminogen Deficiency Can Be Rescued by Increasing Plasmin Activity with  $\alpha 2$ -Antiplasmin ASO.**

Full body  $\mu$ CT reconstructions of *mdx/Plg<sup>+/-</sup>* and *mdx/Plg<sup>+/-</sup>* treated with  $\alpha 2AP^{ASO}$  showed marked reduction in HO in all major muscle groups with  $\alpha 2AP^{ASO}$  treatment.



**Figure 52: Histological Analysis and Quantification of Muscle Healing in Plg<sup>+/-</sup> Mice Treated with either Control ASO or α<sub>2</sub>-Antiplasmin ASO.** A) Treatment of Plg<sup>+/-</sup> mice with α<sub>2</sub>APASO resulted in faster fibrin(ogen) clearance, fewer degenerating myocytes, more regenerating myocytes with central nuclei, and a significant increase in F4/80-positive cells at 3 DPI compared to controlASO-treated Plg<sup>+/-</sup> mice. Error bars represent

standard deviation ( $N \geq 3$ ; \*  $P < 0.05$ , \*\*  $P < 0.01$ ; Mann-Whitney test). B) H&E-stained sections of injured muscles of  $Plg^{+/-}$  mice treated with controlASO or  $\alpha 2APASO$  1, 3, 5 and 7 DPI demonstrated necrotic myocytes in both groups 1 DPI. At 3 DPI,  $\alpha 2APASO$ -treated mice showed an intense inflammatory infiltrate not observed in controlASO-treated mice. At 5 and 7 DPI, numerous myocytes in  $\alpha 2APASO$ -treated mice had centrally located nuclei, consistent with muscle regeneration, whereas in controlASO-treated mice the muscle fibers were hypereosinophilic and necrotic (original magnification, 200x).

#### *Plasmin Regulates Dystrophic Calcification Independent of its Canonical Fibrinolytic Function*

Reduction in plasmin activity may promote dystrophic calcification and subsequent HO through multiple molecular mechanisms. For example, insufficient fibrin clearance (hypofibrinolysis) might result in a persistent fibrin scaffold that could act as a nucleating agent for calcium phosphate precipitation [239]. However, we found that knock-down of fibrinogen expression using a fibrinogen-directed ASO ( $Fbg^{ASO}$ ) failed to prevent soft tissue calcification in  $Plg^{+/-}$  mice following muscle injury (Figure 50 C&D, Table 17). To further exclude a possible role of fibrin and fibrinolysis in soft tissue calcification, complete genetic fibrinogen knockout mice ( $Fbg^{-/-}$  mice) were treated with  $Plg^{ASO}$ . In these fibrinogen/plasminogen-deficient mice, robust soft tissue calcification was observed similar to that seen in animals deficient in plasminogen alone (Figure 50 C&D, Table 17). Thus, the prevention of soft tissue calcification after injury appears to depend upon a plasmin function outside of fibrin cleavage.



**Table 17: Statistical Analysis of STC Score Demonstrating that Knockdown of the Plasmin Inhibitor  $\alpha$ 2AP Prevents Soft Tissue Calcification Independent of Fibrinogen.** (Top) Tabular values reported represent the percent incidence of HO scale scores in each treatment group or genotype and the number of mice per group. (Middle) *P* values determined by the proportional odds model (N/A, proportional odds model was not statistically applicable to data). (Bottom) *P* values determined by the Mann-Whitney Rank test.

<b>Percent Incidence of Score</b>				
<b>Soft Tissue Calcification Score</b>	<b><i>Plg</i><sup>+/-</sup> Control<sup>ASO</sup></b>	<b><i>Plg</i><sup>+/-</sup> <math>\alpha</math>2AP<sup>ASO</sup></b>	<b><i>Plg</i><sup>+/-</sup> + Fbg<sup>Low</sup></b>	<b><i>Fbg</i><sup>+/-</sup> + <i>Plg</i><sup>Low</sup></b>
<b>0</b>	0%	75%	0%	0%
<b>1</b>	10%	25%	17%	0%
<b>2</b>	40%	0%	33%	0%
<b>3</b>	50%	0%	17%	25%
<b>4</b>	0%	0%	33%	75%
<b>N=</b>	<b>10</b>	<b>12</b>	<b>6</b>	<b>4</b>
<b>Proportional Odds Model</b>				
<b>Genotype</b>	<b><i>Plg</i><sup>+/-</sup> Control<sup>ASO</sup></b>	<b><i>Plg</i><sup>+/-</sup> <math>\alpha</math>2AP<sup>ASO</sup></b>	<b><i>Plg</i><sup>+/-</sup> + Fbg<sup>Low</sup></b>	<b><i>Fbg</i><sup>+/-</sup> + <i>Plg</i><sup>Low</sup></b>
<b><i>Plg</i><sup>+/-</sup> Control<sup>ASO</sup></b>	-	N/A	P=0.644	N/A
<b><i>Plg</i><sup>+/-</sup> <math>\alpha</math>2AP<sup>ASO</sup></b>	N/A	-	N/A	N/A
<b><i>Plg</i><sup>+/-</sup> + Fbg<sup>Low</sup></b>	P=0.644	N/A	-	P=0.429
<b><i>Fbg</i><sup>+/-</sup> + <i>Plg</i><sup>Low</sup></b>	N/A	N/A	P=0.429	-
<b>Mann-Whitney Rank Test</b>				
<b>Genotype</b>	<b><i>Plg</i><sup>+/-</sup> Control<sup>ASO</sup></b>	<b><i>Plg</i><sup>+/-</sup> <math>\alpha</math>2AP<sup>ASO</sup></b>	<b><i>Plg</i><sup>+/-</sup> + Fbg<sup>Low</sup></b>	<b><i>Fbg</i><sup>+/-</sup> + <i>Plg</i><sup>Low</sup></b>
<b><i>Plg</i><sup>+/-</sup> Control<sup>ASO</sup></b>	-	P<0.001	P=0.775	P=0.010
<b><i>Plg</i><sup>+/-</sup> <math>\alpha</math>2AP<sup>ASO</sup></b>	P<0.001	-	P<0.001	P<0.001
<b><i>Plg</i><sup>+/-</sup> + Fbg<sup>Low</sup></b>	P=0.775	P<0.001	-	P=0.167
<b><i>Fbg</i><sup>+/-</sup> + <i>Plg</i><sup>Low</sup></b>	P=0.010	P<0.001	P=0.167	-

### *Dystrophic Calcification Is A Determinant of HO*

Histologic analysis of the muscle injury site during the acute phase of injury (1-7 DPI) demonstrated that early soft tissue calcification is principally attributable to formation of dystrophic calcifications within necrotic myocytes (Figure 46). By 14 DPI, chondroid matrix is observed interspersed with persistent dystrophic calcifications. By 28 DPI, these deposits are replaced by woven bone. As dystrophic calcifications precede endochondral ossification, are spatially interspersed with foci of chondroid matrix, and disappear with formation of woven bone at the injury site, persistent dystrophic calcifications represent a potential osteoinductive mechanism for HO.

Deficient plasmin activity caused a number of aberrations during the acute phase of muscle injury: persistent dystrophic calcification and necrotic debris, deficient macrophage infiltration, and deficient myocyte regeneration (Figure 46 B-E). HO was a delayed complication of this disturbed healing microenvironment and could be a result of all or a subset of these pathogenetic factors. Specific inhibition of dystrophic calcification with pyrophosphate analogue prevented HO, but did not promote removal of necrotic debris, macrophage infiltration, or myocyte regeneration. Thus, of all the effects seen in plasmin-deficient muscle injury, persistent dystrophic calcification seems to be a unique mechanism for development of traumatic HO.

### *Discussion*

The present studies disclose an unexpected and new role for plasmin-mediated proteolysis in trauma-induced soft tissue calcification distinct from its classic role in fibrinolysis.

Specifically, a critical threshold of plasmin activity is essential for prevention of dystrophic calcification following muscle injury. Furthermore, we observed that dystrophic calcifications formed in the setting of deficient plasmin activity was sufficient to promote endochondral ossification and HO. These results establish the central role of plasmin, and thereby the plasminogen activation system, in promoting muscle regeneration and protecting against soft tissue calcification in injured skeletal muscle.

One of the major findings of this work is that plasmin activity protects injured muscle from persistent dystrophic calcification independent of its canonical role in fibrinolysis. Extravascular fibrin deposition is a universal feature of muscle injury and fibrin accumulation is a key pathogenic mechanism in a number of phenotypes associated with plasmin deficiency [234, 240, 241]. However, fibrinogen depletion failed to prevent soft tissue calcification associated with plasmin deficiency, indicating that one or more plasmin substrates other than fibrin protect against soft tissue calcification. Plasmin is a promiscuous serine protease, and multiple other plasmin targets may be responsible for its protective effects, such as growth factors, extracellular matrix proteins, or other protease zymogens [242-246]. Defining the plasmin substrates(s) that inhibit soft tissue calcification will be instrumental in fully resolving the pathogenic mechanism(s) involved. However, exclusion of a fibrin-dependent mechanism provides a key foundation for further studies in this regard. Article 8 will highlight one such study where we investigated a potential plasmin substrate, matrix metalloproteinase 9, during fracture healing.

Finally, current and proposed treatments for HO, including anti-inflammatory agents,

pyrophosphate analogues, ionizing radiation therapy, BMP antagonists, and retinoic acid receptor agonists all have the undesirable adverse effect of disrupting systemic bone homeostasis and inhibiting fracture repair [247-252]. In stark contrast to these current or proposed therapies, we have previously reported that plasmin activity is essential for fracture repair and bone homeostasis[29, 253]. Taken together with the results outline in Article 6, these findings suggest that targeting plasmin activity represent one such therapeutic that would, in theory, be beneficial to prevent HO yet simultaneous support physiologic bone formation. These therapeutic studies are covered in more detail in Chapter 3

### *Summary*

These findings amend the long-standing and prevailing view that HO principally develops primarily from aberrant “gain of function” activation of bone-related growth factor signaling pathways, such as BMP. Instead, we propose a “loss of function” mechanism in which HO can result from a deficiency of plasmin’s protective effects that normally serve to limit deposition of dystrophic calcifications within injured muscle tissue. There is also substantial clinical evidence that hypofibrinolysis (a reduction in plasmin activity) occurs in traumatic injuries associated with HO, including burn and spinal cord injuries [254-257]. Future studies are necessary to establish the clinical physiology of acquired plasmin deficiency in both acute traumatic injuries associated with HO as well as chronic inflammation associated with soft tissue calcification (atherosclerosis, tumoral calcinosis, renal calcinosis, etc.). Still, these findings have significant implications for patients at risk for trauma-induced HO.

Aligning with the overall hypothesis of this Chapter, these results are the first to demonstrate that changes to the tissue microenvironment (development of DC) are capable of supporting HO formation. Specifically, we observed here that plasmin deficient animals developed robust DC within damaged tissues that was persistent at the injury site and stimulated endochondral ossification. Importantly, these results were obtained without experimental manipulation of the BMP signaling pathway. As BMP expression is required for all endochondral ossification processes (biologic or pathologic), BMP signaling is likely upregulated in this HO model as well. However, we postulate its effect would be to promote ossification downstream of the initiating effects of decreased plasmin activity and dystrophic calcification, and not the primary pathogenetic mechanism in formation of soft tissue calcification.

While dystrophic calcification was found to be persistent in plasminogen deficient animals, plasmin-competent animals in this study did develop brief flashes of dystrophic calcification that was resorbed during repair. Furthermore, resorption of dystrophic calcifications and rapid clearance of necrotic myocytes in plasmin-competent mice correlated with infiltration of the injury site by monocytes/macrophages. This observation indicates that dystrophic calcification in damaged muscle can be transient, thereby inhibiting the downstream formation of HO. However, this hypothesis cannot be examined in this current study given that plasmin, in addition to protecting skeletal muscle from DC, can also promote monocyte/macrophage migration and phagocytosis [258, 259]. Therefore, to independently examine the hypothesis that DC formation within damaged tissues is sufficient to support an osteoinductive microenvironment capable of forming HO

following injury, we necessitated an alternative preclinical model that develops DC in injured muscle, independent of changes in macrophage/monocyte function. This work is discussed in Article 10

### **Building Upon Plasmin: A Critical Reparative Protease**

In the next two articles, I will briefly step away from our investigations of the capacity of DC in injured muscle to promote HO formation (restarted in Article 10), to highlight two manuscript that develop out of our identification of plasmin as a critical reparative protease for both muscle and bone healing.

First, in Article 8, you will find the story of investigations into the protein target of plasminogen during tissue repair, beyond its primary fibrinolytic function. As previously highlighted, depilation of fibrinogen either in our fracture or skeletal muscle injury model was insufficient to completely rescue the phenotype. Therefore, as plasmin is a protease, we hypothesize that it possessed alternative protein targets that likewise impact tissue repair and regeneration. As we began to investigate potential target, we came across an interesting manuscript from 2003 stating the MMP-9 was essential for fracture repair [260]. As plasmin had been previously described to be able to convert pro-MMP9 to activated MMP-9 we hypothesized that MMP-9 may be a critical plasmin target during repair, beyond fibrin. These experiments and our surprising findings are discussed further in Article 8.

Next, in Article 9, you will find the story of how we applied our previous findings of plasmin role in healing skeletal muscle of the lower extremity to the peri-elbow architecture to develop a mouse model of post traumatic elbow stiffness. Post-Traumatic elbow stiffness and loss of motion is a debilitating condition, precluding patients from performing activities from daily living. Elbow stiffness can occur from osseous malunion or nonunion and/or from pathological healing of soft tissues. Given that plasmin activity is significantly reduced following traumatic injuries, many times associated with elbow stiffness, we hypothesize that plasmin is a single modifiable factor that regulates muscle regeneration and therefore may impact elbow stiffness. Through applying these findings to the upper extremity, we developed the first murine model of post-traumatic elbow stiffness which recapitulates many of the phenotypes observed clinically: heterotopic ossification, capsule thickening, tissue inflammation, and functional deficits. These studies are outlined in Article 9.

Article 8: Unexpected Timely Fracture Union in Matrix Metalloproteinase 9 Deficient Mice

Masato Yuasa<sup>1,2</sup>, Masanori Saito<sup>1,2</sup>, Cesar Molina<sup>1</sup>, **Stephanie N. Moore-Lotridge**<sup>1,7</sup>, Michael Benvenuti<sup>1</sup>, Nicholas A. Mignemi<sup>1,6</sup>, Atsushi Okawa<sup>2</sup>, Toshitaka Yoshii<sup>2</sup>, Herbert S. Schwartz<sup>1</sup>, Jeffrey S. Nyman<sup>1,3,4,5</sup> & Jonathan G. Schoenecker<sup>1,6,7,8,\*</sup>

<sup>1</sup>Department of Orthopaedics and Rehabilitation, Vanderbilt University Medical Center, Nashville, Tennessee, USA

<sup>2</sup>Department of Orthopaedic Surgery, Tokyo Medical and Dental University, Tokyo, Japan

<sup>3</sup>Department of Biomedical Engineering, Vanderbilt University, Nashville, Tennessee

<sup>4</sup>Center for Bone Biology, Vanderbilt University Medical Center, Nashville, Tennessee,

<sup>5</sup>Department of Veterans Affairs, Tennessee Valley Health Care System, Nashville, Tennessee

<sup>6</sup>Department of Pathology, Microbiology, and Immunology, Vanderbilt University Medical Center, Nashville, Tennessee

<sup>7</sup>Department of Pharmacology, Vanderbilt University, Nashville, Tennessee

<sup>8</sup>Department of Pediatrics, Vanderbilt University Medical Center, Nashville, Tennessee

\*To whom correspondence should be directed

*Accepted for Publication in May 2018 in PLoS One*

<https://doi.org/10.1371/journal.pone.0198088>



### *Study Overview*

Here in Article 8, I will highlight our investigations into MMP-9 as a potential plasmin target for tissue repair. Immediately following a fracture, a fibrin laden hematoma is formed to prevent bleeding and infection. Subsequently, the organized removal of fibrin, via the protease plasmin, is essential to permit fracture repair through angiogenesis and ossification. Yet, when plasmin activity is lost, the depletion of fibrin alone is insufficient to fully restore fracture repair, suggesting the existence of additional plasmin targets important for fracture repair. Previously, activated matrix metalloproteinase 9 (MMP-9) was demonstrated to function in fracture repair by promoting angiogenesis. Given that MMP-9 is a defined plasmin target, it was hypothesized that pro-MMP-9, following plasmin activation, promotes fracture repair. This hypothesis was tested in a fixed murine femur fracture model with serial assessment of fracture healing. However, contrary to previous findings, in our studies a complete genetic loss of MMP-9 failed to affect fracture healing and union through 28 days post injury. This surprising finding brought us back to the original article, where we observed a miscalculation of the data presented within, and through this error the conclusion that MMP-9 was essential for fracture healing was born. This prior paper has currently been sighted over 300 times by other laboratories as foundational evidence for MMP-9's essential role in fracture repair. Given this observation, we moved to publish our results to help correct the record and potentially guide future studies away from MMP-9 as a target in fracture repair. Here, our results demonstrated that MMP-9 is dispensable for timely fracture union and cartilage transition to bone in fixed femur fractures. Pro-MMP-9 is therefore not a significant target of plasmin in fracture repair and future studies assessing additional plasmin targets associated with angiogenesis

are still warranted.

This manuscript was highly beneficial to my training as it opened my eyes to the importance of understanding basic bone biology in order to appropriately analyze data obtained during fracture repair, but also illustrated the importance of reviewing article closely. Initially, we, like many other laboratories, took the conclusions from this prior work at face value; however, through our own investigations and a secondary retrospective review, we deciphered that a misanalysis of the data had occurred previously. This experience demonstrated to me the importance of critical peer review, as well as reproducibility of data. I was surprised to see how far this mispropagation of data has been taken (300+ references over 15 years), and has since changed my practice on reviewing literature and including reference within my own work. Below is a detailed account of the experiments performed, demonstrating the MMP-9 is dispensable for fracture repair.

### *Introduction*

Fracture of a bone presents four principle problems; bleeding, susceptibility to infection, bone avascularity, and biomechanical dysfunction (Article 1) [261]. The acute phase response is the injury response system that resolves these problems in a precise temporal sequence over the course of approximately six weeks divided into a survival phase and reparative phase [28]. The survival phase occurs immediately following fracture and includes activation of the coagulation and inflammatory cascades which together provide hemostasis and prevent infection [262]. Once hemostasis is achieved and infection has been avoided, the reparative phase is initiated prompting robust angiogenesis and

osteogenesis which resolve bone avascularity and biomechanical dysfunction [28, 262].

Molecularly, during the survival phase of the acute phase response, the pro-polymer fibrinogen is converted to the crosslinked polymer fibrin which is essential to control bleeding and prevent infection by trapping bacteria and recruiting leukocytes [35]. Once perceived to promote the reparative phase of fracture, we recently determined that, if not removed, fibrin is a barrier to fracture angiogenesis, and therefore resolution of both bone avascularity and biomechanical dysfunction leading to non-union [262]. Thus, the serine protease plasmin, the principal protease that degrades fibrin during the transition from the survival phase to the reparative phase of fracture repair, plays an essential role in fracture repair [262].

Initially it was postulated that the singular role of plasmin in a fracture acute phase response was to remove fibrin at the transition of survival and repair. However, depletion of fibrin alone was not sufficient to fully restore the fracture reparative phase in plasminogen deficient mice, suggesting additional plasmin targets may be integral for proper fracture repair [3]. Given that both a deficiency of plasmin and matrix metalloproteinase 9 (MMP-9) have been reported to inhibit fracture repair resulting in delayed bone union [260, 262], and that plasmin activates pro-MMP-9 to active MMP-9 [263] we hypothesize that plasmin activated MMP-9 promotes fracture repair and bony union. To test this hypothesis, we employed our fixed murine femur fracture model to serially assess fracture healing.

## *Materials and Methods*

### *Animals*

Pro-MMP-9 deficient mice on a C57BL/6J background (JAX stock #007084) [264] and wild-type littermates were bred and housed in the animal facility of Vanderbilt University with a 12-hour light/dark cycle where water and food was provided *ad libitum*. To avoid sex-related confounding effects on developmental bone growth and fracture repair, only male mice were used in this study. All mice were 8 weeks of age at the time of fracture. Sample size calculations for assessing fracture healing were determined previously [265].

### *Fixed Femur Fracture Model*

An open femur fracture model previously validated by our lab [28] was performed when mice were 8 weeks of age as described in Chapter 1. Briefly, following adequate anesthetization and analgesia to minimize suffering, a 10-12mm long, medial incision was performed to expose the mid-shaft of the femur. The femur was then fractured in a controlled manner by scoring the bone and inducing a clean, transverse break with a beaver blade. Finally, the femur was then stabilized with the retrograde placement of a 23-gauge intramedullary pin, and the incision was closed using nylon sutures. Fracture repair was followed radiographically weekly, and mice were sacrificed at varying time points (7, 10, 14, 21, or 28) to allow for histologic, angiographic, and microcomputed tomography ( $\mu$ CT) analysis as described below. All animal protocols were reviewed and approved by the Institutional Animal Care and Use Committee (IACUC) of Vanderbilt University Medical Center (M1600231-00). Humane endpoints were in place to euthanize any animal that was in pain, unable to eat or drink, experienced wound dehiscence or infection, or lost > 20% of

its original body weight. Mice were monitored every 12 hours for the first three days and then weekly until the point of sacrifice. Throughout these experiments no animals died or necessitated sacrifice prior to their designated endpoint. All mice in this study were euthanized by carbon dioxide inhalation followed by cervical dislocation.

#### *Fracture Model Output Measurement- X-Ray*

Radiographic imaging was performed longitudinally to assess fracture healing. Mice were placed in the prone position and imaged 4 seconds at 35kV with a Faxitron LX-60 (Tucson, AZ). Radiographic images were then individually quantified for fracture healing by three independent observers assessing the following 3 criteria: 1. Bone formation, 2. Bone union, and 3. Bone remodeling [262]. Each criterion was scored as either “0” which means “does not meet the criteria” (i.e. not present/visible on the radiograph) or “1” which indicated that the criteria was met and is present by radiographic analysis. Operational definitions for each criteria point are as follows: 1) *Bone Formation*; 0 point: no apparent hard tissue callus formation, 1 point: apparent hard tissue callus formation. Yellow arrow indicates apparent hard tissue callus in x-ray and histology (Figure 53). 2) *Bone Union*; 0: an existence of no mineralization between hard tissue calluses, 1: continuity of mineralization. A red arrow head indicates apparent radiolucent zone (x-ray) (Figure 53- Middle Panel). 3) *Bone Remodeling*; 0: no apparent shrinkage in the size of hard tissue callus compared to maximum size of hard tissue callus, 1: apparent shrinkage in the size of hard tissue callus compared to maximum size of hard tissue callus. Yellow arrows indicate dynamic change of hard tissue callus from larger callus to smaller callus in the same mouse (x-ray) (Figure 53- Bottom Panel). This scoring criterion was employed for both the superior (area 1) and

inferior sides (area 2) of the femur resulting in a maximum score of 6 and a minimum score of 0 per image (Figure 54).

### *Angiography*

Perfusion with microfil vascular contrast (MV-122 Flow Tech Inc., Carver, MA) was conducted as previously described [262]. Due to similarity between density of bone and microfil contrast, all fracture samples that were perfused were decalcified in 0.5 M EDTA, pH 8, prior to  $\mu$ CT imaging (microCT40, Scanco Medical AG, Bassersdorf, Switzerland). 3D vascular reconstructions were then merged onto previously obtained X-ray images to further depict vascular progression using Adobe Photoshop software (San Jose, CA) [123, 262].

### *Micro-Computed Tomography ( $\mu$ CT)*

$\mu$ CT images to visualize angiography were acquired as previously described [3]. Briefly, following specimen harvest, microfil filled femurs were imaged at 55-kVp, 145-uA, 200-ms integration, 500 projections per 360 degrees of rotation, with a 20  $\mu$ m isotropic voxel size. The microfil compound was segmented from soft tissues using a threshold of 220 per thousand (or 450.7mgHA/cm<sup>3</sup>), a Gaussian noise filter of 0.2 with a support of 1. Quantification of fracture vascularity was assessed by vascular volume (mm<sup>3</sup>) and vessel thickness of 100 slices on either side of the fracture.

### *Histological Analysis*

Specimens removed for histological analysis were fixed in 10% neutral buffered formalin

and decalcified in 0.5M EDTA (pH 8.0) for a minimum of 5 days. Tissues were then dehydrated in graded series of ethanol, cleared, embedded in paraffin, and sectioned sagittally at 6 $\mu$ m for subsequent staining. Safranin orange/fast green staining (Safranin-O) was performed following deparaffinization and rehydration. Briefly, slides were placed in freshly filtered working Wiegert's hematoxylin for 10 minutes and immediately washed in running tap water for 10 minutes. Slides were then placed in 0.1% fast green solution for 5 minutes and rinsed quickly in 1% acetic acid for 10 seconds. Slides were then placed in a 0.1% safranin-O solution for 5 minutes and dehydrated prior to mounting with permount. Total callus size and soft tissue callus size was quantified as previously described [28].

#### *Statistical Analysis*

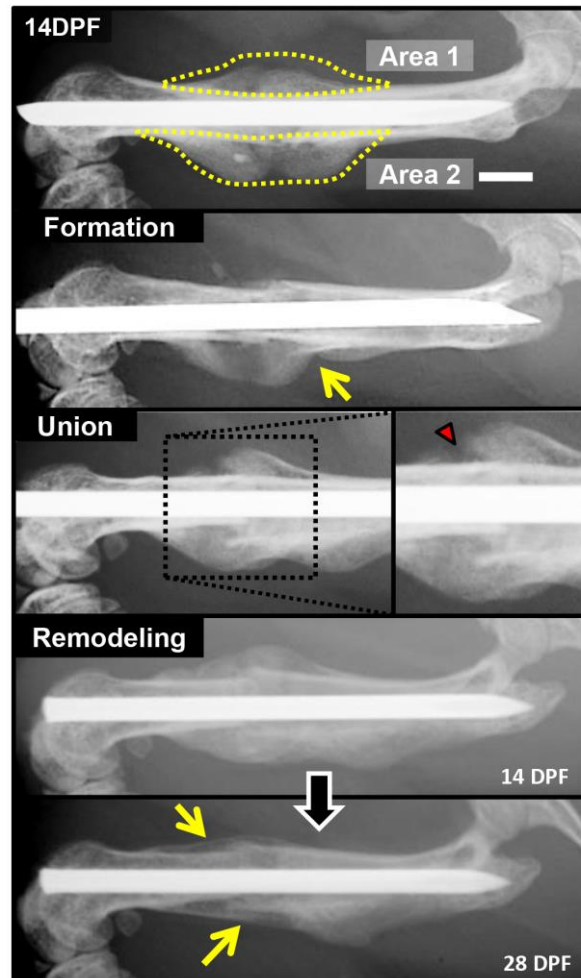
Analysis between MMP-9 deficient mice and wild-type littermates was conducted with a non-parametric t-test (Mann Whitney). Alpha=0.05. Analysis was conducted in GraphPad V6 (La Jolla, CA).

#### *Results*

##### *MMP-9 Is Not Essential For Timely Fracture Healing In An Internally Fixed Femur Fracture Model*

Serial radiographs were performed at 1, 7, 10, 14, 21, and 28 days post fracture (DPF) to monitor development and remodeling of the hard tissue callus and subsequent fracture healing (Figure 53 & 54). The hard tissue callus was clearly evident both proximal and distal to the fracture site in WT and *Mmp9*<sup>-/-</sup> mice starting at day 10 DPF and remodeled over the next two weeks (Figure 55A), resulting in comparable fracture union between

groups at 14 DPF (Figure 56B). In comparison to WT littermates, mice lacking MMP-9 showed no qualitative or quantitative differences in the timing, growth, and remodeling of the hard tissue callus, or bone union. These results indicated that MMP-9 is not essential for fracture healing and contrary to previous reports [260], loss of MMP-9 does not lead to non-unions or delayed unions.



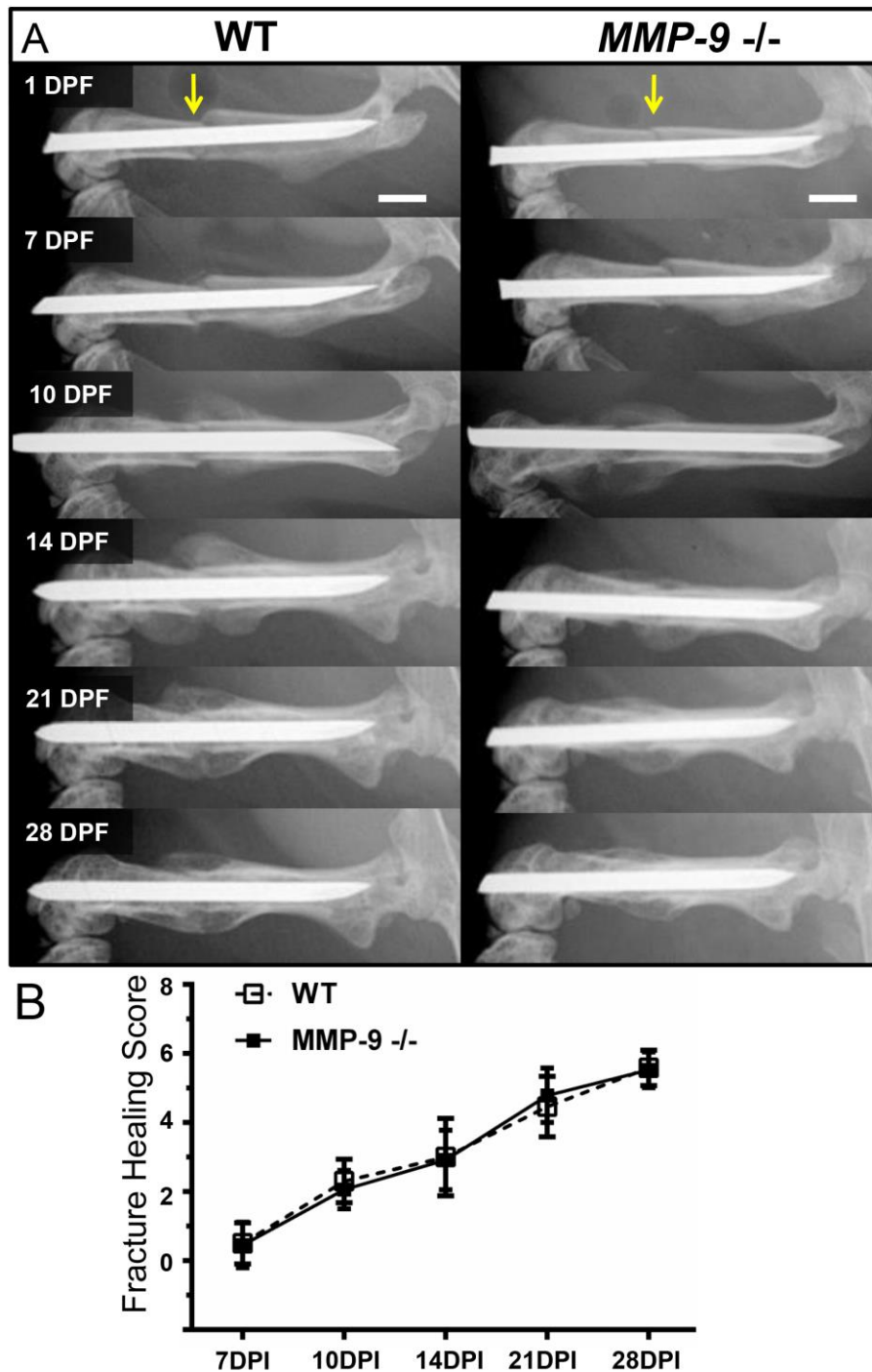
**Figure 53: Radiographic Quantification of Fracture Healing.** Fracture repair was quantified by three criteria: 1) bone formation, 2) bone union, and 3) bone remodeling. The anterior (area 1) and posterior (area 2) sides of the fracture callus were quantified



individually a total score per femur was reported.

	Area1	Area2	Score
	Yes/ No	Yes/ No	
<b>Bone Formation</b>	1/0	1/0	0-2
<b>Bone Union</b>	1/0	1/0	0-2
<b>Bone Remodeling</b>	1/0	1/0	0-2
<b>Combined</b>	<b>(Top)+(Bottom)</b>		<b>0-6</b>

**Figure 54: Radiographic Quantification Score Sheet.** Meets criteria (Yes) = score of 1. Does not meet criteria = score of 0. Maximum score per femur = 6. All radiographic images were assessed in a blinded manner by 3 individual observers from 1 to 4 weeks after fracture.

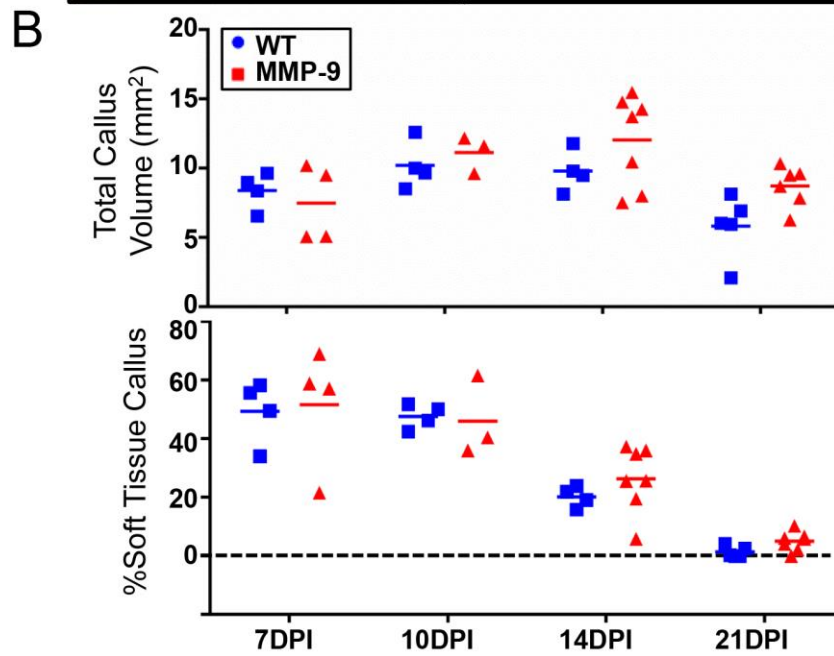
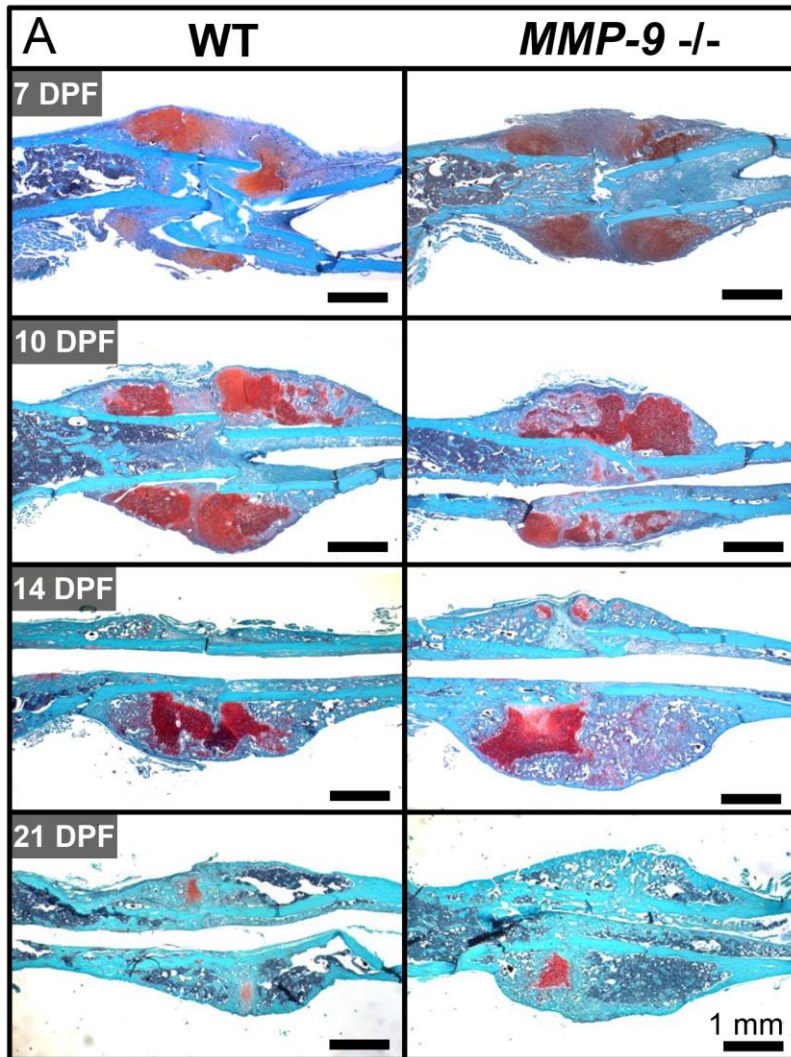


**Figure 55: Skeletal Healing of Stabilized Femur Fracture in MMP-9 Deficient Mice.**

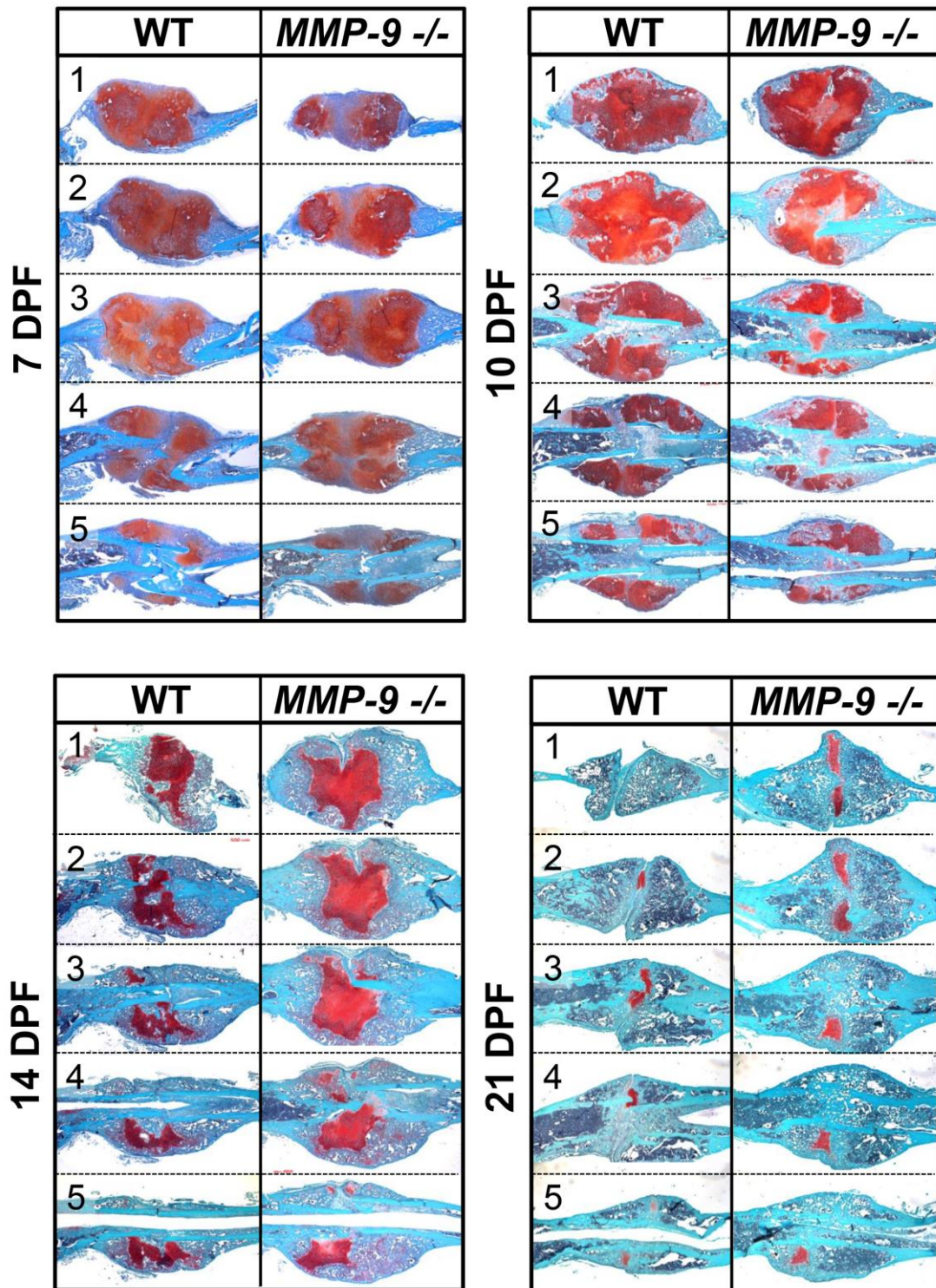
An open femur fracture model with stabilization by a 23-gauge intramedullary pin was used to compare key aspects of fracture healing in mice with and without MMP-9. To assess temporal development and subsequent remodeling of the hard tissue callus, we

performed A) serial x-rays of the fractured femurs (yellow arrow indicates fracture site. Hard tissue callus is evident by X-ray proximal and distal to the fracture in mice with or without MMP-9 by 10 DPF. From 14 to 21 DPF, the proximal and distal hard tissue callus expands and coalesces at the fracture. At this point the hard tissue callus is at its maximum size and subsequently it starts remodeling through day 28. B) *Mmp-9*<sup>-/-</sup> mice did not demonstrate any significant differences in fracture healing compared to WT littermates, based on scores of the bone formation, bone union, and bone remodeling. Data displayed represent the mean  $\pm$  SD. Statistical significance between groups at each time point was determined using a non-parametric Mann-Whitney Test. Number of mice per genotype: 7DPF: WT- 22, MMP-9 KO- 35; 10d: WT-13, MMP-9 KO- 17; 14DPF: WT- 17, MMP-9 KO- 25; 21DPF: WT- 13, MMP-9 KO- 19; 28DPF: WT- 12, MMP-9 KO- 17

To verify complete transition from early soft tissue callus, predominated by chondrocytes, into hard tissue callus, predominated by osteoblasts, osteoclasts, and endothelial cells, we prepared histological sections and stained with Safranin-O. Histologic evaluation of the fracture callus at 7, 10, 14, and 21 DPF revealed a central avascular chondroid matrix in both MMP-9 deficient and WT littermates at both 7 and 10 DPF, which then remodeled to hard callus by 21 DPF (Fig 2A and S2 Fig). Consistent with previous radiographic results, quantitative assessment of the soft tissue callus and total callus volume showed no statistical difference between WT and *Mmp-9*<sup>-/-</sup> mice at any time point assessed (Fig 2B).



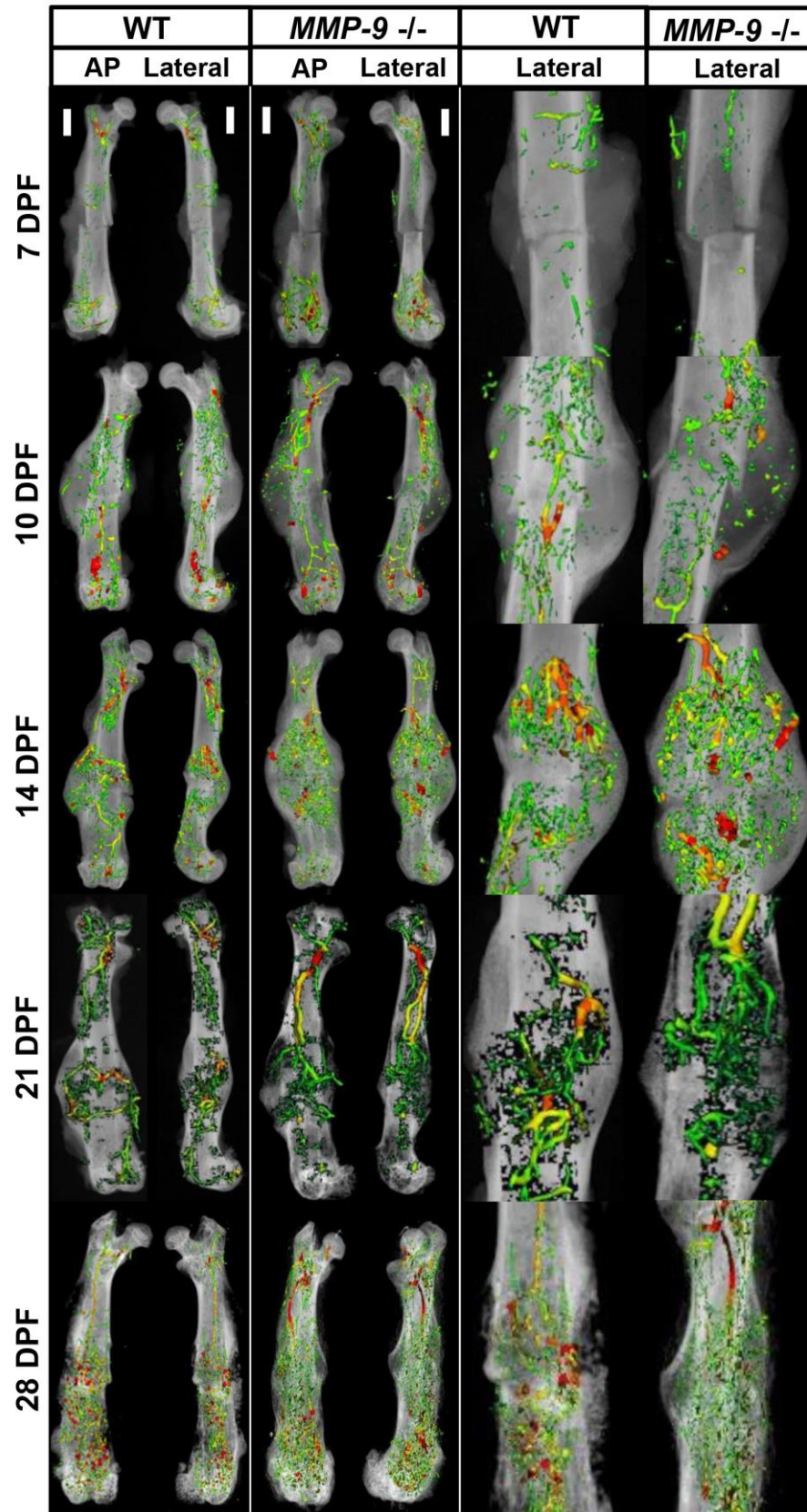
**Figure 56: MMP-9 is Not Required for Endochondral Fracture Healing.** A) Both MMP-9 deficient and WT littermates possessed abundant soft cartilage at 7 and 10 DPF. At 21 DPF, hard tissue callus dominated in MMP-9 deficient and WT littermates. B) Quantification of the total callus volume and % soft tissue fracture callus demonstrated that there was no significant difference between MMP-9 deficient mice and WT littermates at any time assessed. While the % soft tissue callus area appears to trend higher in MMP-9 deficient mice at 14 DPI as previously described [5], there is marked variability between MMP-9 deficient mice.



**Figure 57: Sample Histology of WT and MMP-9 Deficient Mice Following Fracture Injury.** Histological samples from representative fractured femurs of WT and MMP-9 deficient mice at 7, 10, 14, and 21 DPF. Sections 1-5 represent slices 200uM apart,

beginning with the first full slice with callus and ending with a medial slide identified by the pin space. At 7 DPF we observed abundant soft tissue callus that gradually bridged and was replaced by hard callus from day 10 to 21 DPF. We observed no statistical difference in soft tissue callus percentage between WT and MMP-9 deficient mice at any time point (Figure 56).

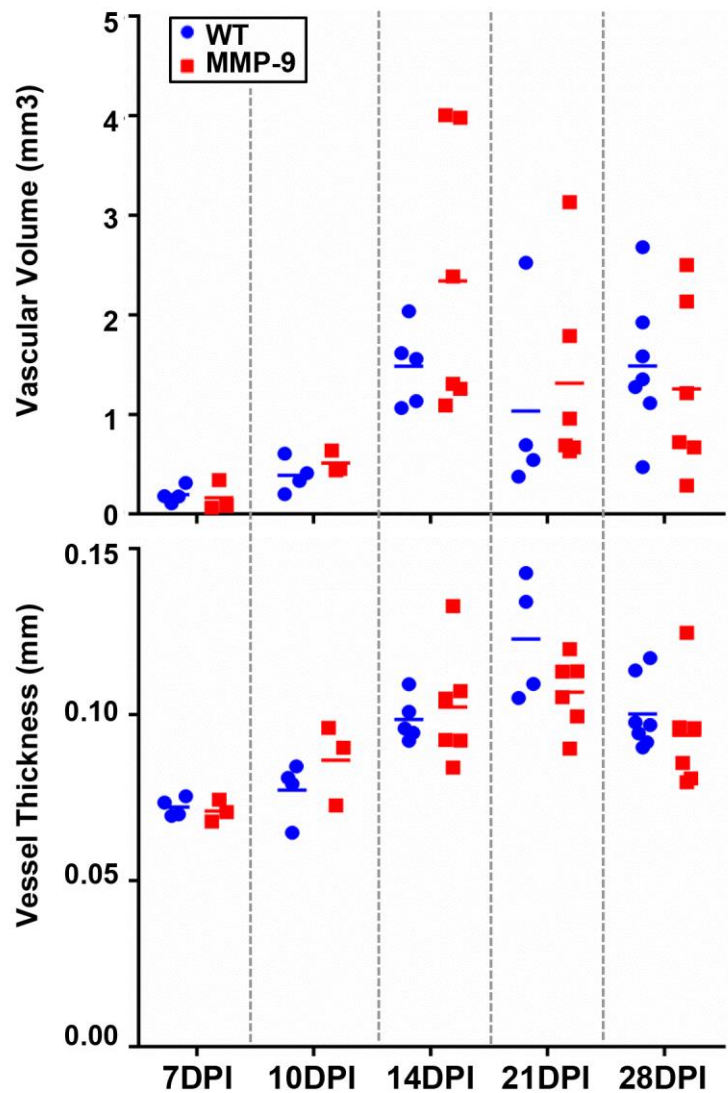
To further assess fracture repair, we comprehensively assess the vascularity throughout the fracture callus, given that clinically, fracture revascularization is essential for bony union. X-rays of the fractured femurs merged with 3D  $\mu$ CT reconstructions of microfil perfused femurs identified a loss of vascularity in both wild-type and MMP-9 deficient mice at 7 DPF. However, by day 21 DPF, dense vascularity bridging the fracture site is observed in both groups. The vascularity then continued to coalesce and remodel through 28 DPF, such that no visible difference was observed between genotype (Figure 58). Through quantitative assessment, we were unable to detect differences in vascular volume or vessel thickness between wild-type and MMP-9 deficient mice (Figure 59).





**Figure 58: Revascularization of the Fracture is Unaffected by a Loss of MMP-9.**

Visual representation of microfil based angiography overlaid with radiographic images. No differences in vascularity were observed between wild type and MMP-9 deficient mice at any time point.



**Figure 59: Vascular Quantification of Healing Fractures of WT and MMP-9 Deficient Mice.** Quantitative assessment of microfil based angiography surrounding the healing fracture. No statistical differences in vascularity were identified between wild type and

MMP-9 deficient mice at any time point for either vascular volume (mm<sup>3</sup>) or vessel thickness (mm). 7d- WT: N=4, MMP-9: N=3; 10d- WT: N=4, MMP-9: N=3; 14d- WT: N=5, MMP-9: N=6; 21d- WT: N=4, MMP-9: N=6; 28d- WT: N=7, MMP-9: N=6. Individual time points were assessed by non-parametric t-tests. Alpha =0.05.

### *Discussion*

We conclude that a deficiency of MMP-9 does not result in a delay or failure of angiogenesis or bone union during fracture repair. Specifically, the loss of MMP-9 resulted in no deficiencies of secondary fracture repair (intramembranous or endochondral ossification), including the development of the soft tissue callus, subsequent angiogenesis, or the formation and union of the hard tissue callus in an internally stabilized femur fracture model. Therefore, pro-MMP-9 can be eliminated as a potential plasmin target affecting timely fracture healing.

Additionally, while these results appear dichotomous to the conclusion of the previous report [260], “that *Mmp9*<sup>-/-</sup> mice have non-unions and delayed unions of their fractures caused by persistent cartilage at the injury site” we would like to note that Colnot *et. al.* results noted that “by 19 days post fracture, the maximum force at failure was equivalent in WT and MMP-9 deficient calluses, demonstrating that the MMP-9 defect around the onset of bone remodeling was resolved” [260]. This data aligns with our findings that MMP-9 deficient mice underwent effective fracture healing with appropriate bony union, contrary to the conclusions previously drawn.

While assessment of the data alone suggests similar findings in regards to bone union, the previous report did observe a difference in cartilage remodeling in an unfixed tibial fracture model and ‘pathologic’ endochondral ossification in a fixed tibial fracture model. In this regard, we would like to note three main possible differences between these present findings and previous reports: 1) technical differences in the mode of fracture stabilization or 2) difference in the vascularity of the femur as opposed to the tibia, or 3) differences in the age/growth phase of the experimental animals.

It has been well described that interfragmentary strain, and therefore fracture stabilization, affects the type (primary or secondary) and timing of fracture repair [266-269]. Likewise, delaying stabilization during the early phases of fracture healing promotes secondary fracture repair characterized by a greater amount of endochondral ossification than strictly primary repair [270]. The great majority of the results from the previous report were derived from an un-fixed tibial fracture model [260, 271], whereas we employed internal fixation of femur fractures with a 23-gauge needle. As such, the differences in the timing of remodeling of the cartilage intermediate may simply be a consequence of the two different models. Along these lines, in the previous report, finding in the fixed tibial fracture model indicated ‘pathologic’ endochondral ossification in the setting of an MMP-9 deficiency as compared to the absence of endochondral ossification in wild type mice. However, it is well recognized that, although stabilization reduces the interfragmentary strain, due to both residual interfragmentary strain and hypoxic segments, the pin stabilization tibial fracture model does repair through secondary fracture repair the includes both intramembranous and endochondral ossification [272].

Secondly, these studies differ in location of the fracture with previous reports assessing the tibia and our reports assessing the femur. While both long bones, these locations differ by the rich vascular supply of the femoral shaft when compared to the watershed areas with low blood flow seen in the tibia; thereby suggesting that MMP-9 may perform different functions in a fracture with poor vascular supply [273, 274]. In addition to a change in anatomical fracture location, the mechanism by which the fracture was induced was different across studies. The current study utilizes an open osteotomy model, whereas the prior study employed a closed 3 point bending fracture jig method [260]. The closed fracture jig likely led to more soft tissue trauma and potentially further decreased perfusion of the tibial fractures. Additionally, given that most diaphyseal fractures are treated with intramedullary nailing resulting in endochondral ossification, we believe that internal needle fixation best represents current clinical practice [275, 276].

Finally, in this study, we utilized 8-week-old, male mice which, though sexually mature, are still undergoing appendicular and axial skeletal growth at the time of fracture repair. Prior studies utilized mice that were 12-20 weeks old and therefore skeletally mature. Previously, Lu *et. al.* has demonstrated that *Mmp-9* expression and angiogenic capacity of a healing tibial fracture is elevated in skeletally immature (juvenile) mice as compared to skeletally mature (adult) counterparts [277]. These findings would suggest that genetic loss of MMP-9 may impact fracture healing of skeletally immature mice to a greater extent than their adult counterparts. Therefore, this present study utilizing 8-week-old animals was designed to detect the greatest changes in fracture healing, yet no differences between

groups was identified.

Though these present studies were aimed at assessing pro-MMP-9 as a target of plasmin essential for fracture healing, when applied to our stabilized femur fracture model. We did not detect any difference in fracture healing or bony union as previous reported. Therefore, pro-MMP-9 can be eliminated as a potential plasmin target affecting timely fracture healing. Future studies assessing additional plasmin targets associated with angiogenesis, such as VEGF-A, are warranted [278].

Article 9: Novel Preclinical Murine Model of Trauma-Induced Elbow Stiffness

**Stephanie N. Moore-Lotridge** <sup>BS<sup>1,4,^</sup></sup>, William K. Oelsner <sup>BS<sup>1,^</sup></sup>, Yael Ihejirika<sup>1</sup>, Mihir J. Desai <sup>MD<sup>1</sup></sup>, Sandra S. Gebhart <sup>MD<sup>1</sup></sup>, & Jonathan G. Schoenecker <sup>MD PhD<sup>1,2,3,4,\*</sup></sup>

Vanderbilt University Medical Center, <sup>1</sup>Department of Orthopaedics and Rehabilitation,  
<sup>2</sup>Department of Pathology Microbiology and Immunology, and <sup>3</sup>Department of Pediatrics

Vanderbilt University, <sup>4</sup>Department of Pharmacology

<sup>^</sup> Indicates authors that contributed equally

<sup>\*</sup>To whom correspondence should be directed

Accepted for publication August 2018 in the *Journal of Experimental Orthopaedics*

<https://doi.org/10.1186/s40634-018-0155-3>

### *Overview*

As stated above, in Article 9, you will find the story of how we applied our previous findings of plasmin's role in healing skeletal muscle of the lower extremity, to the peri-elbow musculature in order to develop a mouse model of post traumatic elbow stiffness. Given that plasmin activity is significantly reduced following traumatic injuries (such as those associated with elbow stiffness), we hypothesize that plasmin is a single modifiable factor that regulates muscle regeneration and therefore may impact elbow stiffness. Through applying these findings to the upper extremity, we developed the first murine model of post-traumatic elbow stiffness which recapitulates many of the phenotypes observed clinically: heterotopic ossification, capsule thickening, tissue inflammation, and functional deficits.

### *Abstract*

#### *Background*

Peri-articular injury may result in functional deficits and pain. In particular, post-traumatic elbow stiffness is a debilitating condition, precluding patients from performing activities of daily living. As such, clinicians and basic scientists alike, aim to develop novel therapeutic interventions to prevent and treat elbow stiffness; thereby reducing patient morbidity. Yet, there is a paucity of pre-clinical models of peri-articular stiffness, especially of the upper extremity, necessary to develop and test the efficacy of therapeutics. We set out to develop a pre-clinical murine model of elbow stiffness, resulting from soft tissue injury, with features characteristic of pathology observed in these patients.

### *Methods*

A soft tissue peri-elbow injury was inflicted in mice using cardiotoxin. Pathologic tissue repair was induced by creating an investigator-imposed deficiency of plasminogen, a protease essential for musculoskeletal tissue repair. Functional testing was conducted through analysis of grip strength and gait. Radiography, microcomputed tomography, and histological analyses were employed to quantify development of heterotopic ossification.

### *Results*

Animals with peri-elbow soft tissues injury in conjunction with an investigator-imposed plasminogen deficiency, developed a significant loss of elbow function measured by grip strength ( $2.387 \pm 0.136$  N vs  $1.921 \pm 0.157$  N, \*\*\*\*,  $p < 0.0001$ ) and gait analysis ( $35.05 \pm 2.775$  mm vs  $29.87 \pm 2.075$  mm, \*\*\*,  $p < 0.0002$ ). Additionally, plasminogen deficient animals developed capsule thickening, delayed skeletal muscle repair, fibrosis, chronic inflammation, and heterotopic ossification; all features characteristic of pathology observed in patients with trauma-induced elbow stiffness.

### *Conclusion*

A soft tissue injury to the peri-elbow soft tissue with a concomitant deficiency in plasminogen, instigates elbow stiffness and pathologic features similar to those observed in humans. This pre-clinical model is valuable for translational studies designed to investigate the contributions of pathologic features to elbow stiffness or as a high-throughput model for testing therapeutic strategies designed to prevent and treat trauma-induced elbow stiffness.



### *Introduction & Background*

Elbow stiffness following peri-articular injury is a debilitating condition, precluding patients from performing activities from daily living. In order for individuals to perform 90% of their daily activities, such as bathing and eating independently, an arc of elbow motion of 100 degrees (30° extension to 130° flexion; 50° pronation to 50° supination) is necessary [279]. Furthermore, it has been reported that a decrease in arc of elbow motion of only 50%, results in an 80% loss of elbow function [280]. As such, clinicians and basic scientists alike, aim to develop novel therapeutic interventions to prevent and treat elbow stiffness; thereby reducing patient morbidity. However, to date, no murine models have been developed which recapitulate the soft tissue pathology (fibrosis, capsular thickening, or heterotopic ossification) or the functional deficits (elbow stiffness) seen in patients clinically.

Elbow stiffness can arise following either a local trauma to the elbow [281-283] or in conjunction with an anatomically remote severe trauma such as burns or head injuries [284-287]. Correspondingly, for more than 200 years it has been recognized that severe trauma provokes systemic changes throughout the body. One such response to severe trauma is the dysregulation of plasmin, the main protease of the fibrinolytic system. As such, severely injured patients can experience both over exuberant generation of plasmin, leading to hyperfibrinolysis that portends to death from bleeding, or prolonged deficit of plasmin activity or hypofibrinolysis, associated with thrombosis [288-290].

Recent investigations have demonstrated that plasmin, in addition to its canonical role of

degrading fibrin, is also essential for musculoskeletal tissue repair [237, 245, 291-293]. The purpose of this work was to develop and validate a pre-clinical murine model of elbow stiffness, resulting from peri-elbow soft tissue injury, with features characteristic of pathology observed in patients. Given that both the degree of elbow stiffness [284, 294, 295] and plasmin activity reduction [296, 297] have been related to the severity of injury, we examined if a focal peri-elbow soft tissue injury, in conjunction with an investigator-imposed plasminogen deficiency, was sufficient to model trauma-induced elbow stiffness.

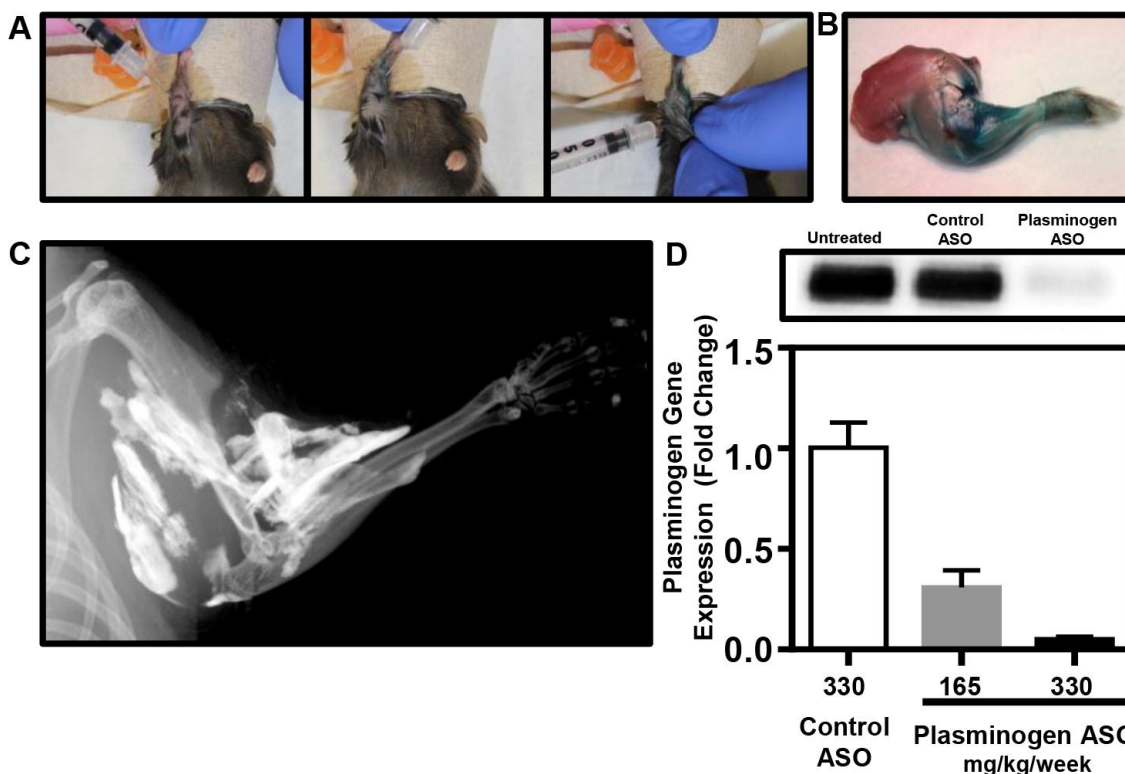
#### *Novel Murine Model of Peri-Elbow Muscle Injury*

All animal procedures were approved by the Vanderbilt University Institutional Animal Care and Use Committee (M1600225) and carried out in strict accordance with the recommendation in the Guide for the Care and Use of Laboratory Animals of the National Institutes of Health. All skeletal muscle injuries were performed under anesthesia, and all efforts were made to minimize suffering.

Male C57BL/6J mice were purchased from Jackson Laboratory and housed at Vanderbilt University in a 12-hour light/dark cycle with food and water provided *ad libitum*. At 6 weeks of age, a cardiotoxin-induced injury was administered to the soft tissues surrounding the elbow [292, 298, 299]. Following anesthetization with Isoflurane, mice were placed in the Trendelenburg position, supinating the forearm, while flexing the forearm over the surface of the nose cone (Figure 60A). From this position, 20 $\mu$ L of 10 $\mu$ M cardiotoxin was injected with a 28.5 G 0.5mL insulin syringe into the posterior compartment of the arm to infiltrate the elbow extensors (triceps), the lateral compartment of the arm/forearm to

infiltrate the elbow flexors (brachialis) and mobile wad (brachioradialis), and the medial aspect of the proximal forearm (pronosupinators and hand extrinsics), resulting in a total of three injection regions (20 $\mu$ L each) surrounding the elbow joint (Figure 60B and C). Both the left and right upper limbs were injured.

To induce an investigator-imposed plasminogen deficiency, a plasminogen specific antisense oligonucleotide (ASO) or a non-targeting control ASO was injected subcutaneously (330mg/kg/week) beginning two weeks before injury and continuing through the duration of the study (Figure 60D) [292]. All antisense oligonucleotides used in this study were developed in collaboration with Ionis Pharmaceuticals (Carlsbad, CA).



**Figure 60: Preclinical Model of Upper Extremity Injury.** A) To reliably induce muscle injury around the elbow, three cardiotoxin injections were applied to the triceps,

brachialis/brachioradialis, and the pronosupinators/hand extrinsics. B) Injection of either blue dye or C) barium sulfate solution with subsequent radiographic analysis demonstrated well dispersed injection areas, fully surrounding the elbow joint. D) Investigator induce plasminogen deficiency is attained by the time of upper extremity injury on both a protein (inset box) and RNA level following weekly administration of plasminogen ASO (330mg/kg/wk) beginning two weeks before injury. Graphical representation of mean +/- SD.

#### *Quantification of Elbow Function Following Injury*

To assess changes in elbow function following peri-articular injury, grip strength and gait analysis were performed 28 days following injury. Grip strength was assessed with an animal grip strength system force meter (San Diego Instruments, San Diego, CA). Briefly, a mouse is placed on the wire grid and allowed to grab on with its forepaws. Once secure, the mouse's tail is gently pulled backwards and the maximum force of the grip is recorded in Newtons. This test was performed three times per mouse with 5-10 minutes of rest between measurements. The data from each trial is then averaged before the final analysis between experimental groups. Gait analysis was assessed with a Treadscan System (Clever Sys Inc. Reston, VA) to evaluate changes in gait disturbances. Briefly, mice were placed in a clear acrylic box above a treadmill monitored by a high-speed camera. The treadmill was then equilibrated to a speed of 13.7 cm/s and a 20 second video of the mouse's walking pattern was obtained. Treadscan Software was then utilized to assess active range of motion in the longitudinal direction per limb. Results are presented as a mean step distance (mm) per animal.

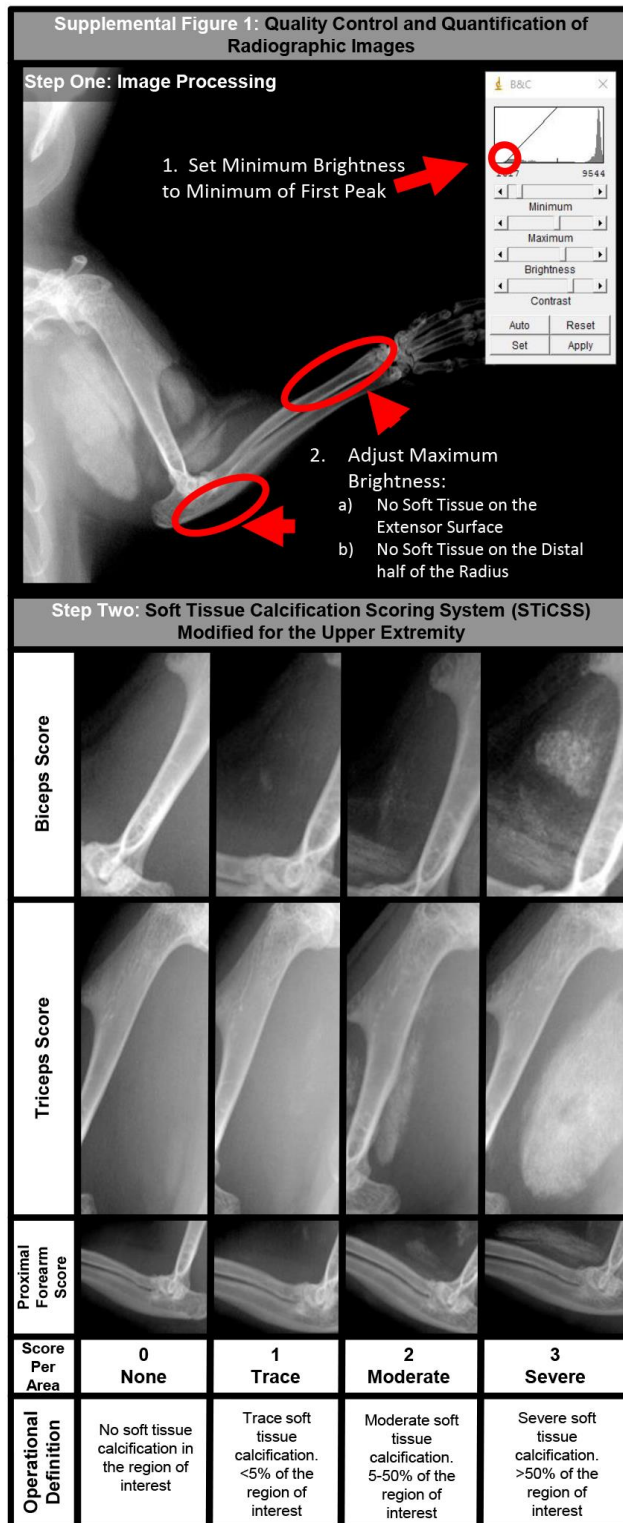
### *Histological Analysis*

Following sacrifice at 28 days post peri-articular injury, the upper extremity was disarticulated at the glenohumeral joint, fixed in 10% neutral buffered formalin, decalcified in 0.5M EDTA for one week, processed, and embedded in paraffin prior to frontal or transverse sectioning. Six micron frontal section of the upper extremity were produced and stained with hematoxylin and eosin (H/E) and Martius Scarlet Blue (MSB). Additionally, at the time of sacrifice, the triceps were dissected, fixed in 10% Neutral buffered formalin, processed, and embedded in paraffin prior to transverse sectioning. Six micron sections were then stained with H/E, MSB, or Von Kossa to visualize deposits of calcification. Additionally, immunofluorescence and immunohistochemistry were performed to detect the presence of fibrin or F4/80+ cells within damaged tissues, respectively. Whole slide imaging of frontal sections was performed in the Digital Histology Shared Resource at Vanderbilt University.

Hematoxylin and Eosin (H/E) staining was performed according to standard protocols to assess tissue morphology as previously described[292, 298]. Martius Scarlet Blue (MSB) staining was performed according to standard protocols to assess for the presence of fibrin and collagen deposits within damaged tissues. Von Kossa staining to assess calcific deposits was performed according to standard protocols as previously described.[292, 298] Immunohistochemical staining of F/480+ cells were performed according to standard protocols by the Vanderbilt University Medical Center Tissue Pathology Shared Resource. Immunofluorescent staining for the presence of fibrin was performed as previously described.[253]

### *Quantification of Muscle Calcification*

Longitudinal radiographic analysis was performed weekly following injury to visualize and quantify heterotopic ossification within the injured tissues of the upper extremity. Briefly, following adequate anesthesia, digital radiographs (Faxitron LX60, Tucson, AZ) were collected weekly at an exposure of 35kV for 4 seconds. Digital radiographs were standardized and the extent of muscle calcification was quantified using a modified version of the Soft Tissue Calcification Scoring System (STiCSS) for the upper extremity (Figure 61) [298]. All radiographic images were scored in a blinded manner by three independent observers found to be in substantial to almost perfect agreement ( $\text{Kappa}=0.706\text{-}0.901$ , Table 18) per the Landis and Koch criteria [188]. As such, results reported represent the total score for a single limb (either left or right) as scored by a single observer.



**Figure 61: Quantification of muscle calcification by radiographic analysis.** To quantify muscle calcification, digital radiographs were first standardized using ImageJ (Step 1:

Image Processing) by adjusting the minimum and maximum brightness of the image so that no soft tissue is visible on the extensor surface or the distal half of the radius. Next, processed digital radiographs are scored by an ordinal scale of 0-3 representing varying degrees of calcification with a score of “0” indicating no visible calcification, “1” indicating trace amounts of calcification with <10% of the region of interest being calcified, “2” indicating moderate calcification with 10-50% of the region of interest being calcified, and “3” indicating severe soft tissue calcification with >50% of the region of interest being calcified. Given the multiple muscle belly injury method, we assess the development of calcification in three distinct anatomical locations (the biceps, triceps, and proximal forearm), assigned a score to each area, and reported the final score per animal as a sum of the individual scores. Therefore, the highest possible score is 9.

**Table 18: Interobserver Agreement of Upper Extremity Radiographic Assessment**

	A	B	C
A		0.901	0.706
B			0.756
C			

In addition to radiographic analysis, microcomputed tomography ( $\mu$ CT) was utilized to visualize the formation of muscle calcification around the elbow joint.  $\mu$ CT images were acquired ( $\mu$ CT 40, Scanco Medical AG, Bassersdorf Switzerland) of injured forelimbs at 55kVp, a45uA, 200ms integration, 500 projections per 180-degree rotation with a 20 micron isotropic voxel size. After scanning, the volume of interest containing the entire forelimb was selected the calcified tissues were segmented from soft tissues using a threshold of 220 per thousand (or 450.7mgHA/cm<sup>3</sup>), a Gaussian noise filter of 0.2, and



support of 1.

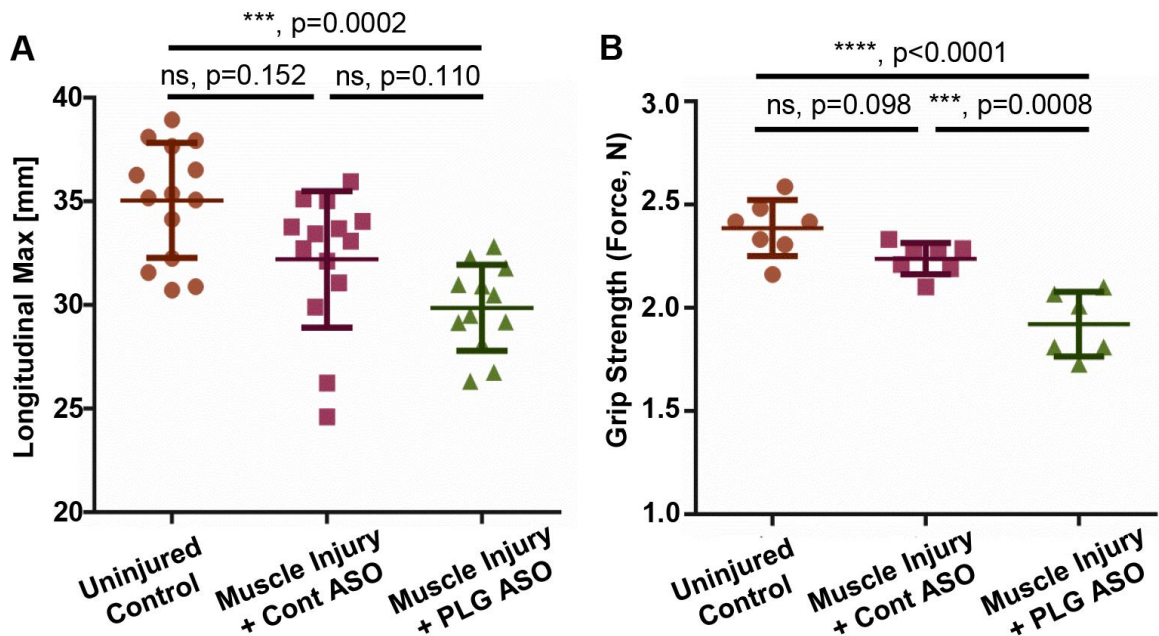
### *Statistical Analysis*

Statistical analyses of functional changes between groups were evaluated using an ordinary two-way ANOVA with a multiple comparison test. P values reported are adjusted for multiplicity. STiCSS upper extremity scores were statistically evaluated between groups using a non-parametric Mann-Whitney test. For all analysis, alpha = 0.05.

### *Study Results*

#### *Peri-Elbow Soft Tissue Injury, In Conjunction with an Investigator-Imposed Plasminogen Deficiency, Results in a Significant Loss of Elbow Function*

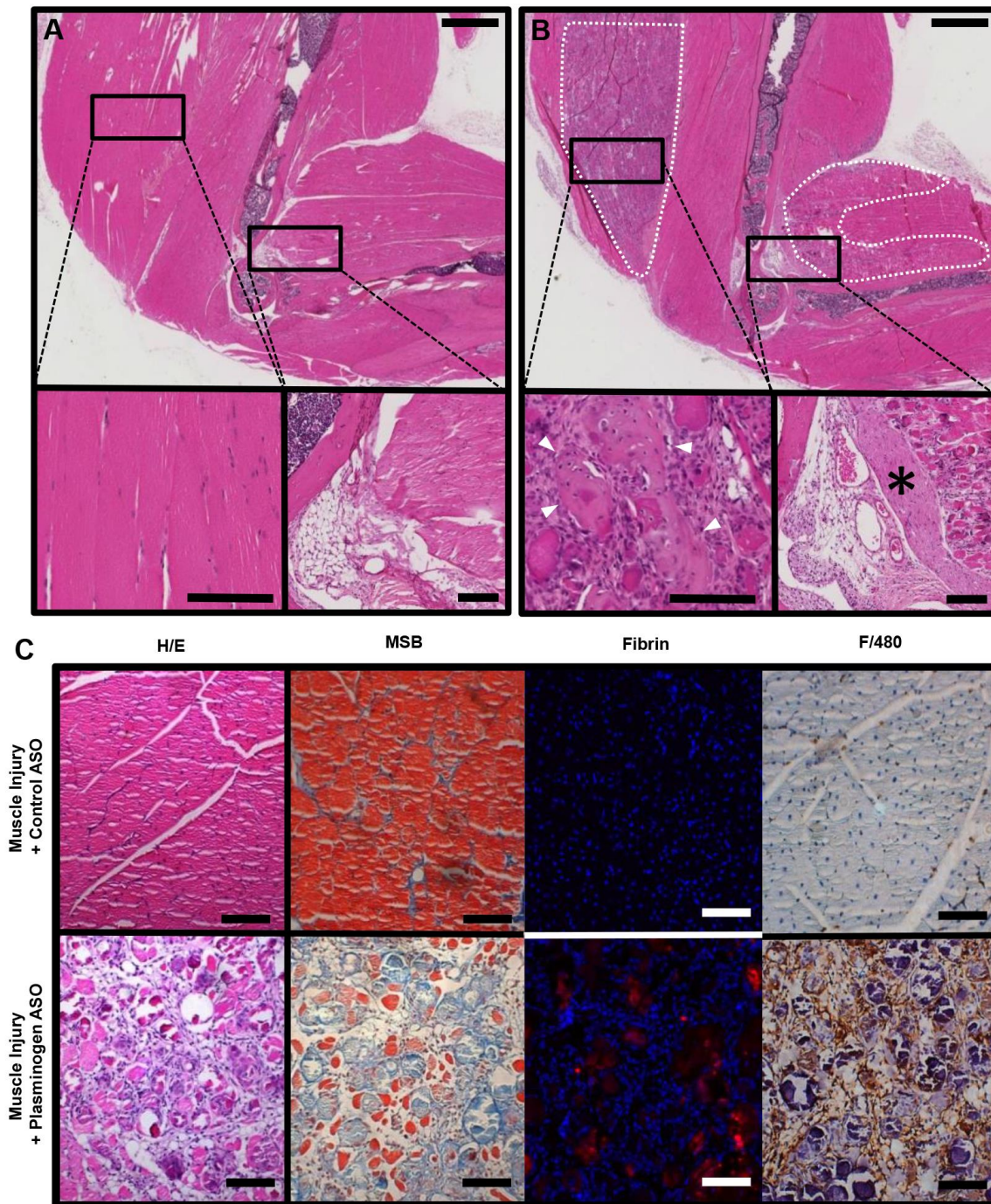
Given that functional deficits following a peri-articular injury are a life altering event, we first assessed in our murine model if following a peri-elbow injury, in conjunction with an investigator-induced plasminogen deficiency, we could detect a change in upper extremity function. At 28 days post injury (DPI), we observed marked functional changes for both active longitudinal motion (Figure 62A) and grip strength (Figure 62B) in plasminogen deficient animals as compared to either uninjured mice or injured + control ASO treated animals. Interestingly, we also observed marked functional changes between uninjured control and injured + control ASO treated animals, indicating that peri-elbow injury alone, independent of plasminogen deficiency, was sufficient to impact elbow function. Taken together, these results demonstrated that an investigator-induced plasminogen deficiency, in conjunction with a focal peri-elbow soft tissue injury, is sufficient to impact elbow function.



**Figure 62: Upper extremity functional assessment following per-elbow soft tissue injury.** To assess changes in upper extremity function in our model following injury with or without an investigator induce plasminogen (PLG) deficiency, A) Treadscan analysis was utilized to measure active motion in longitudinal direction. Points (n) represent individual limbs, left and right per mouse. N= 7; uninjured controls, 7; Injury + Control ASO, 7; Injury + PLG ASO. n=14 points per group. Mean  $\pm$  SD: Uninjured control- 35.05  $\pm$  2.776; Muscle Injury + Control ASO- 32.20  $\pm$  3.294; Muscle Injury + PLG ASO- 29.87  $\pm$  2.075. B) Grip strength analysis plotted as an average per mouse. N= 7; uninjured controls, 7; Injury + Control ASO, 7; Injury + PLG ASO. Total of 7 data points per group. Mean  $\pm$  SD: Uninjured control- 2.387  $\pm$  0.136; Muscle Injury + Control ASO- 2.238  $\pm$  0.076; Muscle Injury + PLG ASO- 1.921  $\pm$  0.157. Data represented in all plots as mean  $\pm$  SD. Statistical difference was assessed by an ordinary two-way ANOVA with a Tukey's multiple comparison test. P values reported are adjusted for multiplicity.

*Peri-Elbow Soft Tissue Injury, in Conjunction with an Investigator-Imposed Plasminogen Deficiency, Results In Delayed Muscle Repair, Fibrosis, and Chronic Inflammation*

To assess soft tissue healing following peri-elbow injury, in conjunction with an investigator-imposed plasminogen deficiency, the upper extremity was isolated at 28 DPI and sectioned in either the frontal and transverse plain for histological analysis. Hematoxylin and eosin (H/E) staining of frontal sections from control ASO (Figure 63) treated animals demonstrated normal skeletal muscle regeneration and soft tissue architecture. Alternatively, mice with an investigator-imposed plasminogen deficiency (PLG ASO treated) (Figure 63B), possessed substantial areas of disorganized necrotic sarcomeres characterized by hypereosinophilic staining, hyalinized cytoplasm, and absent nuclei (see white dashed outline). Additionally, plasminogen deficient animals also possessed marked thickening of the capsule immediately adjacent to the capitulum and radial head (Figure 63B- black asterisk) as well as chondrocyte laden lesions, characteristic of early heterotopic ossification (Figure 63B- white arrow).



**Figure 63: Histological analysis of frontal and transverse sections of injured peri-elbow soft tissues 28 DPI.** H/E staining of frontal sections from A) Control ASO or B) plasminogen ASO treated animals. Gross morphology of whole limb at 1x, scale bar represents 1mm. Zoomed in sections of the injured triceps muscle or capsule immediately

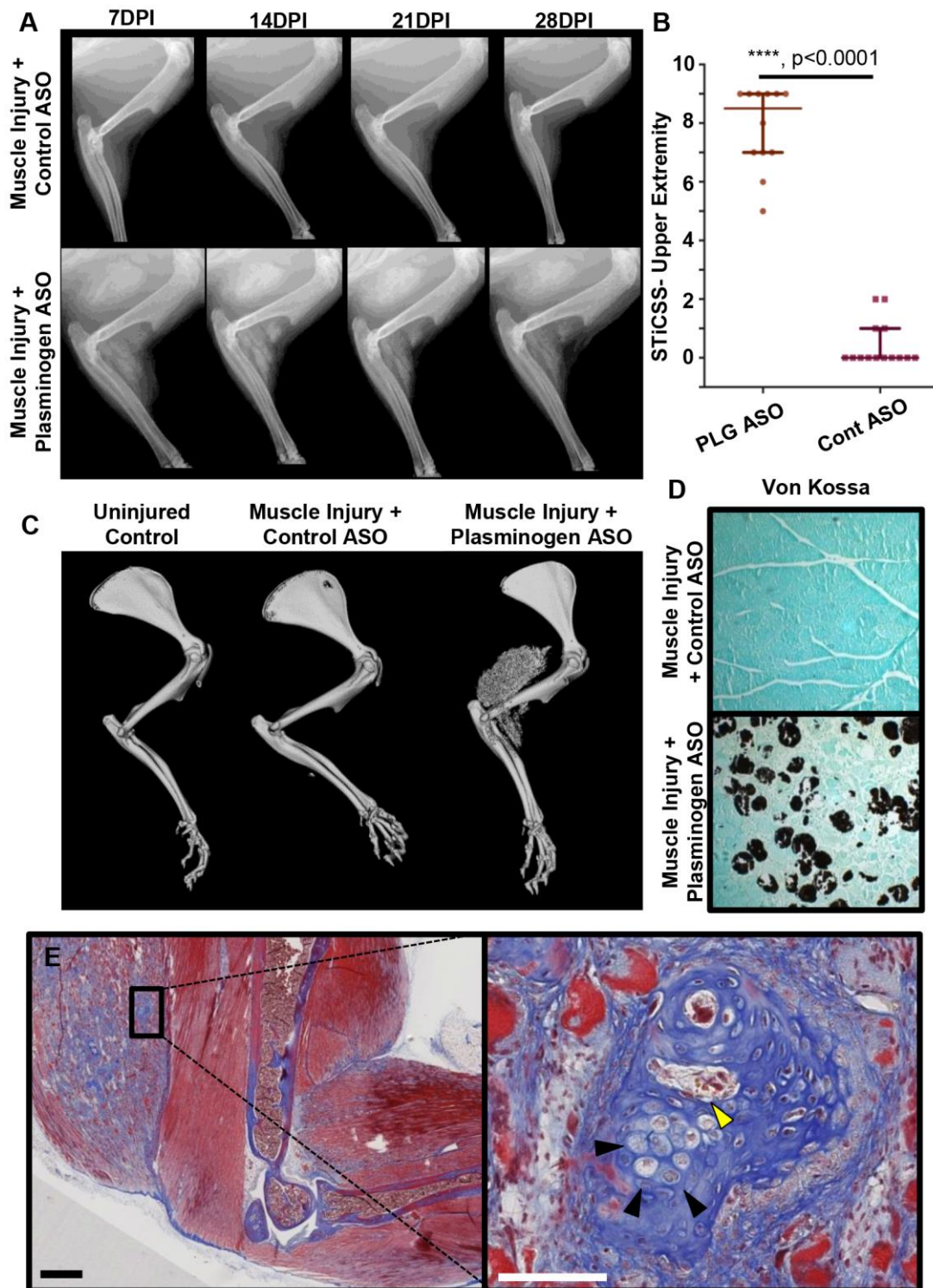
adjacent to the capitulum and radial head (20x and 10x respectively, scale bar represents 100  $\mu\text{m}$ ). Black asterisk indicates thickening of the capsule observed in plasminogen ASO treated animals. White arrows indicate focal chondrocytic lesions indicative of heterotopic ossification formation. C) Transverse sections from control ASO or plasminogen ASO treated animals, stained with H/E, MSB, immunofluorescent staining for fibrin(ogen), or immunohistochemical staining for F4/80+ cells (macrophage/monocytes). All transverse images 20x magnification, scale bar represents 100  $\mu\text{m}$ .

Further histological analysis of transverse sections (Figure 63C) demonstrated substantial deposits of connective tissues or fibrosis, as demonstrated by MSB staining, while immunofluorescent staining for fibrin(ogen) demonstrated marked co-localization to areas of necrotic sarcomeres in plasminogen deficient animals. Furthermore, immunohistochemical staining detected substantial F4/80+ cellular infiltrate surrounding necrotic sarcomeres in plasminogen deficient animals, but limited F4/80+ cells within regenerated sarcomeres of control ASO treated animals. Taken together, these results indicated that following peri-elbow injury, an investigator-induced plasminogen deficiency, is sufficient to induce characteristically similar impaired soft tissue healing seen clinically in patients following traumatic elbow injuries.

*Peri-Elbow Soft Tissue Injury, in Conjunction with an Investigator-Induced Plasminogen Deficiency, Results in Heterotopic Ossification Surrounding the Elbow*

Next, we further assessed the formation of heterotopic ossification following peri-elbow injury, in conjunction with an investigator-imposed plasminogen deficiency, at 28 DPI.

Longitudinal radiographic,  $\mu$ CT analysis, and 3D reconstruction demonstrated significantly greater amounts of heterotopic ossification surrounding the elbow of plasminogen ASO treated animals compared to control ASO treated animals (Figure 64A-C). Furthermore, detailed histological analysis of the injured skeletal muscle stained positive for the presence of calcium as indicated by black coloration (Figure 64D) and possessed regions with distinctive patterning of heterotopic ossification inducing the presence of hypertrophic chondrocytes (Figure 64E- black arrows) and early hematopoiesis, as indicated by yellow stained erythrocytes (Figure 64E- yellow arrow). Taken together, these results indicate that an investigator-imposed plasminogen deficiency, in combination with a peri-elbow soft tissue injury, results in the development of heterotopic bone that progresses through endochondral ossification.



**Figure 64: Characterization of skeletal muscle calcification following peri-elbow injury.** A) Longitudinal radiographic analysis of control ASO or plasminogen (PLG) ASO

treated mice at 7, 14, 21, and 28 DPI. B) Quantification of the soft tissue calcification within the triceps and muscle of the forearm as scored by the modified STiCSS for upper extremity. Error bar represent median and interquartile range. Statistical analyses between groups were analyzed by a non-parametric Mann-Whitney test. \*\*\*\*,  $p < 0.0001$ . C)  $\mu$ CT analysis and 3D reconstruction of uninjured and injured upper extremities treated with control ASO or plasminogen ASO. D) Von kossa staining of transvers sections of injured triceps 28 days post injury. E) Gross morphology of PLG ASO treated animals at 1x (scale bar represents 1mm) stained with MSB. B) Zoomed in section of the injury triceps (20x, scale bar represents 100  $\mu$ m). Black arrow heads indicate hypertrophic chondrocytes. Yellow arrow heads indicate erythrocytes.

### *Discussion & Conclusion*

Through this study, we successfully developed and validated a novel murine model which, following a peri-elbow tissue injury in conjunction with an investigator-imposed reduction of plasminogen, recapitulates features characteristic of pathology observed in patients clinically. This model fills a necessary gap for basic science and translational studies to investigate trauma-induced elbow stiffness. Specifically, this model will be valuable for assessing novel pharmacologic treatments, given that current therapeutics including anti-inflammatory agents, pyrophosphate analogues, ionizing radiation therapy, BMP antagonists, and retinoic acid receptor agonists [281], have been demonstrated to possess negative side effects, in particular to fracture healing. Given that many times elbow stiffness occurs in combination with other traumatic injuries, current therapeutic measures effectively sacrifice the healing of one tissue (bone) for proper healing of the other (soft



tissues/skeletal muscle). With this new model, we now can assess novel therapeutics aimed at preventing trauma-induced elbow stiffness, while simultaneously working to preserve bone formation and regeneration.

Previous investigations have demonstrated the plasmin is an essential reparative protease, which in addition to its canonical function of degrading fibrin, also acts on growth factors, extracellular matrix proteins, and other protease zymogens [242-246, 300]. Following severe injury, it has been well demonstrated independently that plasmin activity is reduced and elbow stiffness can develop. Furthermore, both the degree of elbow stiffness [284, 294, 295] and reduction of plasmin activity [296, 297] have been individually related to the severity of injury. However, to date it has yet to be determined clinically if these two events are related. Through the development of this model, we observed that a focal peri-elbow soft tissue injury, in conjunction with an investigator-imposed plasminogen deficiency, was sufficient to model trauma-induced elbow stiffness. Importantly, unlike genetically plasminogen deficient mice that possess impaired growth, develop rectal prolapses, and die prematurely [301], use of a plasminogen-targeted ASO permits temporally-controlled reduction of plasminogen, thereby allowing mice to develop normally and avoid premature death. While no adverse side effects have been observed by our laboratory following the administration of plasminogen ASO [29, 292, 298], given that the ASOs developed primarily target the liver where plasminogen is produced, high dose administration of ASOs can result in liver toxicity and should be considered when designing similar studies. Taken together, these results support the hypothesis that plasmin may play a role in peri-elbow tissue repair and elbow function. Strengthened by the

availability of critical experimental tools (i.e. plasminogen-targeted ASO) and a novel murine model, this manuscript provides the foundation for further studies assessing i) the molecular mechanisms of plasminogen as it relates trauma-induced elbow stiffness and ii) the clinical correlations between changes in plasmin activity following injury and resulting elbow stiffness.

Akin to our findings within, recently a rat model of post-traumatic elbow contracture was developed and demonstrated to possess persistent joint motion loss and increased capsule thickening. This model, which utilizes focal peri-elbow soft tissue damage and subsequent immobilization to induce elbow stiffness is, to our knowledge, the only other small animal model of elbow stiffness currently reported [302-304]. Here, in our murine model, we observed loss of joint function and capsule thickening (as reported in the rat model above), as well as tissue scarring, fibrosis, and of the formation of heterotopic ossification; all pathologies suggested clinically to impact elbow stiffness. Yet, this model is not without limitations. Specifically, the cardiotoxin injury method cannot localize the injury to a single type of soft tissue, therefore we cannot partition plasmin's role in skin, tendon, skeletal muscle, and capsule healing individually as they pertain to elbow stiffness. Additionally, this study did not utilize post-operative immobilization of the affected limb, yet this current model could be utilized to examine such a hypothesis. Finally, while the elbow is highly susceptible to impaired function and stiffness following traumatic injury, we hypothesize that this model has the potential to be translated to other joints, such as the knee, hip, or shoulder, given that each of these joints have been found clinically to be susceptible to pathologic calcification, fibrosis, and impaired soft tissue healing following

injury.

### *Summary*

Through this study, I was able to apply my previous experience with model development and validation (Article 7) to create and validate a new murine model of peri-elbow injury that phenocopies the pathologic findings of patients clinically. Through this work I was fortunate to work with a new group of attendings who specialize in hand surgery. This project not only allowed me to work directly with residents, such as Dr. Sandra Gebhart, but exposed me to an additional area of Orthopaedics I was not previously familiar with. Through this work and many discussions with this research team, I learned about the “villains” of hand surgery and was able to effectively conduct this new study to recapitulate the phenotype observed clinically.

## **Regulation and Fate of Dystrophic Calcification Found Within Damaged Tissues- Is Dystrophic Calcification Sufficient to Form HO?**

Coming back to the results discussed in Article 6, in which plasminogen deficient mice developed injury-induced dystrophic calcification that persisted and matured to form HO over 28 DPI, we aimed to further investigate this novel pathophysiology of HO formation. While previous reports have segregate dystrophic calcification and HO into individual pathologies, the results in Article 6 rather suggest that dystrophic calcification and HO may be part of the same pathologic continuum. As such, we hypothesized that the development of dystrophic calcification within damaged tissues is sufficient to support an osteoinductive microenvironment capable of forming HO following injury.

However, as previously eluded to, plasmin has many different targets during tissue repair, include the activation of additional proteases (MMP-9), growth factors such as VEGF, and activation of cells such as macrophages and monocytes. In plasminogen deficient mice, while we observed the development of persistent dystrophic calcification that progressed to HO, we also observed marked macrophage inhibition and limited migration into areas of damage. Given that we observed flashes of dystrophic calcification in wild type animals that regressed, we hypothesized that macrophages may play a role in modulating dystrophic calcification within injury tissues. Therefore, to effectively test the hypothesis that dystrophic calcification within damaged tissues is sufficient to support an osteoinductive microenvironment capable of forming HO, we necessitated a model of trauma-induced calcification, prone to the development of dystrophic calcification, yet

possessing unaltered macrophage/monocyte function.

As a reminder, calcium and phosphate circulate at near saturating concentrations. While this concentration is ideal for maintaining bone integrity, these levels of calcium and phosphate have the potential to aggregate in soft tissue such as muscle, skin, and blood vessels, especially in the presence of a nucleating factor, such as collagen. The fact that most soft tissues are free of aberrant mineralization indicates that there are specialized biological protection mechanisms in place to prevent aberrant mineralization. This balance of promoting factors (calcium and phosphate) to prevent mechanisms is essential, such that distortion to either side of the balance can predispose soft tissue to aberrant calcification. As such we first investigated whether a change in diet, specifically to a high phosphate chow, would be sufficient to shift the balance in favor of dystrophic calcification following a focal skeletal muscle injury

#### Application of a High Phosphate Diet Predisposes Skeletal Muscle to Dystrophic Calcification

Through numerous preclinical studies, it has been well defined that dietary alteration of phosphate can promote the formation of dystrophic calcification within soft tissues, yet the application for promoting dystrophic calcification in skeletal muscle following injury was unknown. Previously, these diets have been utilized in preclinical studies to drive soft tissue calcification pathologies in the skin and cardiovascular system, thereby shortening the time needed to conduct studies and making the pathology more detectable for

researchers. Given the large amount of studies utilizing these methods, we aimed to assess the effect of a high phosphate diet on our murine model of skeletal muscle injury. We hypothesized that like previous reports, feeding mice a high phosphate diet would shift the balance in favor of dystrophic calcification formation and predispose skeletal muscle dystrophic calcification following injury; thereby providing us a model to test our larger hypothesis.

### *Brief Methods*

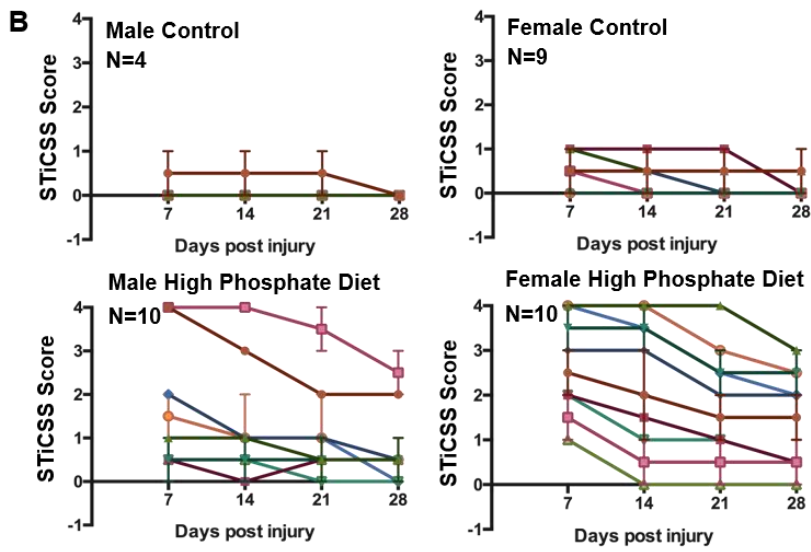
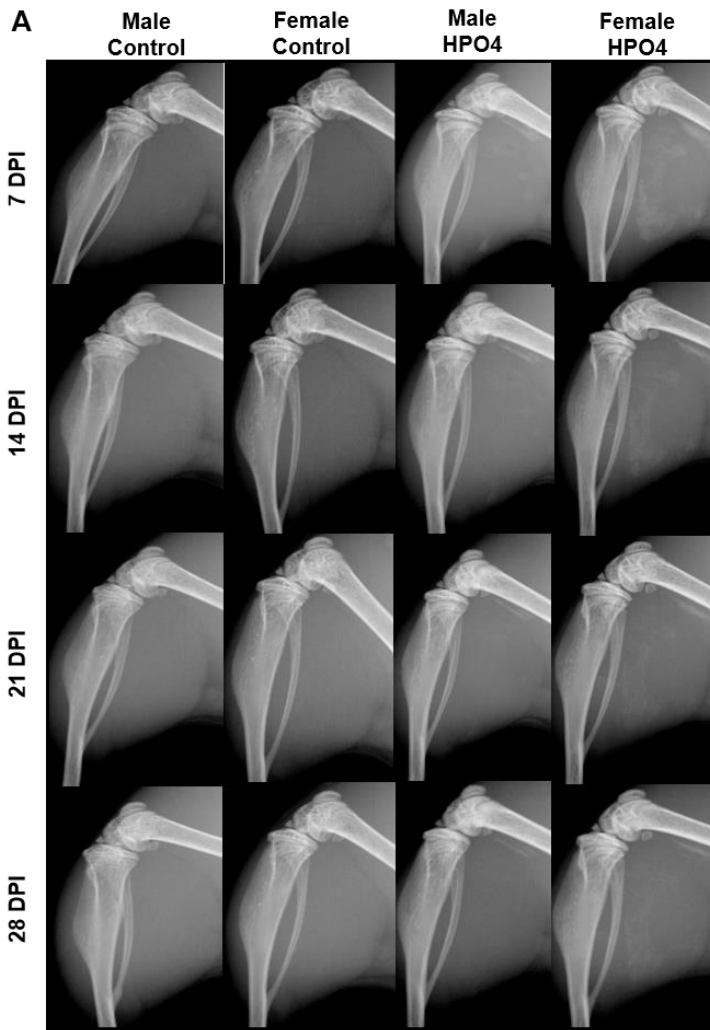
Beginning at three weeks of age, male and female mice at the time of weening (3 weeks of age) were placed on either on a control diet (0.7% inorganic phosphate) or a high phosphate diet (1.7% inorganic phosphate) for the entirety of study. At 6 weeks of age, our previously described focal skeletal muscle injury was applied to the mice fed either the high phosphate or control diet. Mice were then assessed weekly by radiographic analysis and STiCSS quantification for the formation of dystrophic calcification. At the time of sacrifice, injured skeletal muscle tissue was obtained for  $\mu$ CT and histological analysis.

### *Results*

#### *Administration of a High Phosphate Diet Is Sufficient to Promote Skeletal Muscle Calcification Following a Focal Injury*

Following a focal muscle injury, radiographic analysis at 7 DPI detected a significantly greater amount of skeletal muscle dystrophic calcification within the gastrocnemius and soleus muscles of mice fed a high phosphate diet as compared to the control diet (Figure 65 and Table 19). Furthermore, we observed no significant differences in the amount of

skeletal muscle calcification following injury between males and females within each experimental group (Table 19).



**Figure 65: High Phosphate Diet Alone is Sufficient to Predispose Skeletal Muscle to**



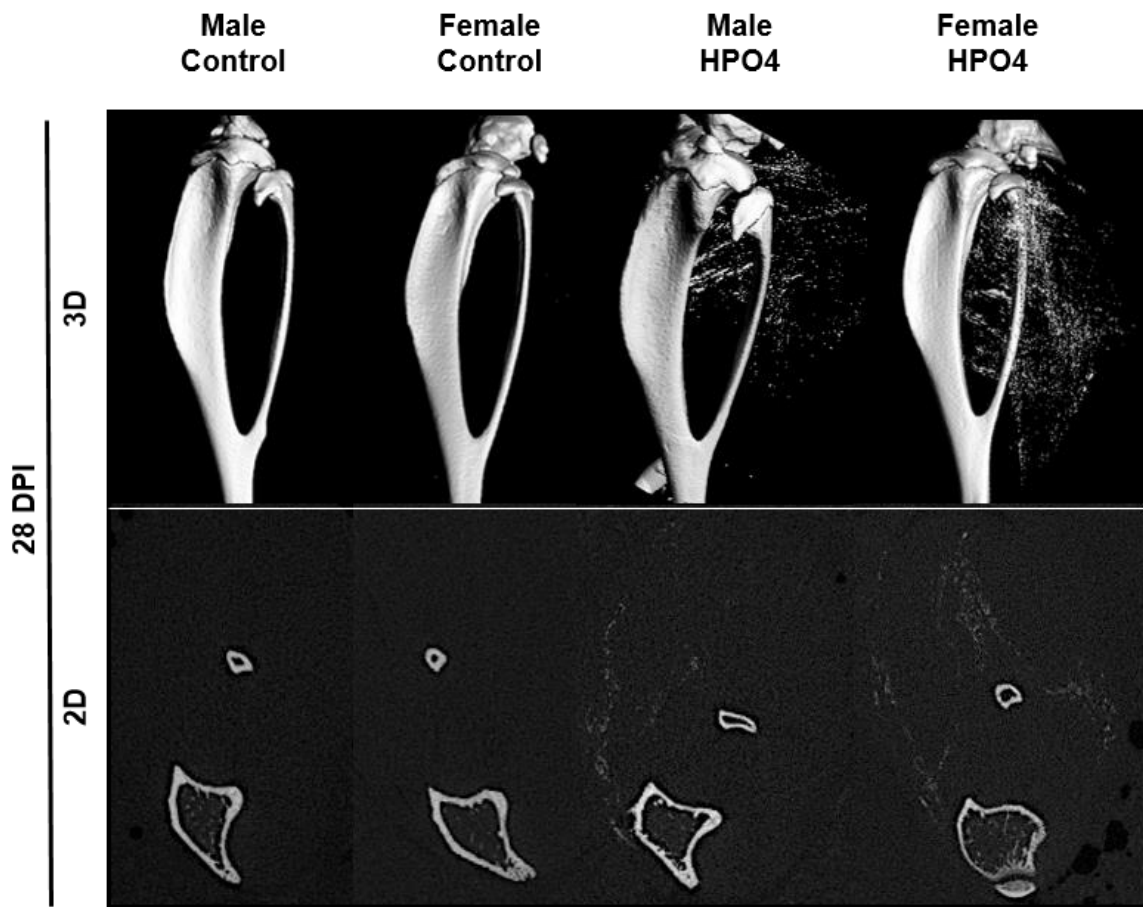
**Dystrophic Calcification Following Focal Injury.** Beginning at 7DPI, dystrophic calcification formation was assessed in WT C57BL/6J mice fed either control diet (0.7% phosphate) or a high phosphate diet (1.7% phosphate). A) Longitudinal radiographic analysis of male and female mice beginning at 7 DPI. B) Corresponding longitudinal STiCSS score per individual animal.

**Table 19: Statistical Analysis of STiCSS Values of Mice fed different diets at 28 Days Post Injury.** N represents total number of individual samples analyzed (left and right leg considered as individual samples); n represents the number of mice per group. Statistical analysis between groups was performed using a non-parametric Mann-Whitney test.

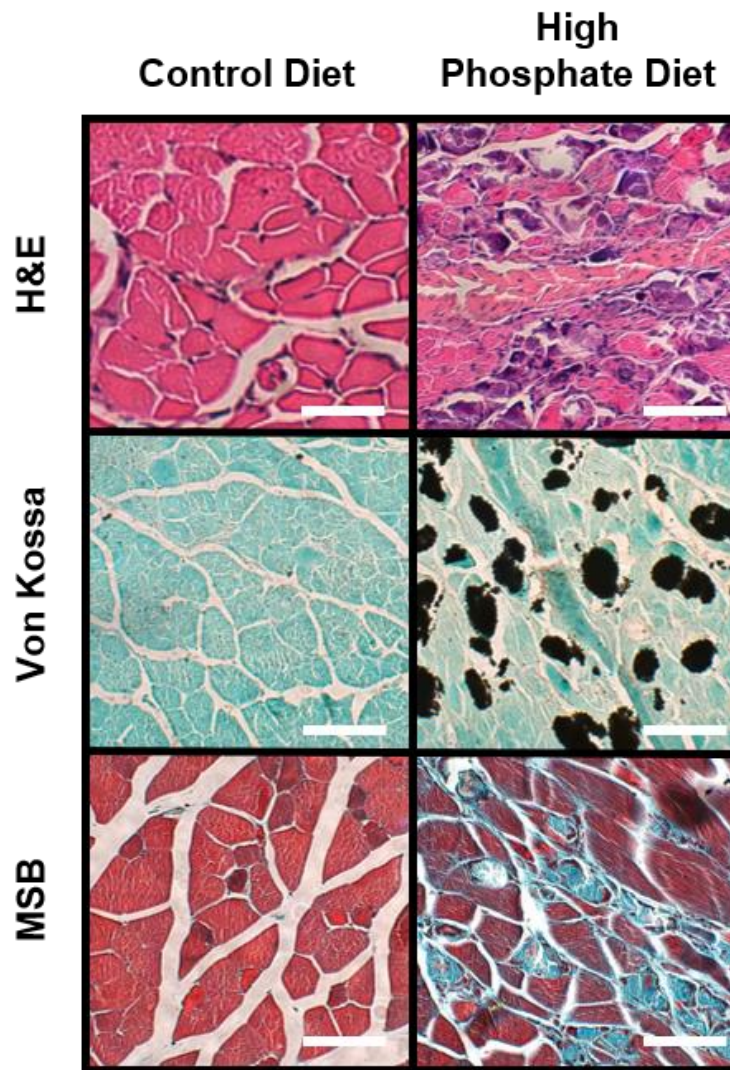
<b>STiCSS Score</b>	<b>Control Diet</b>		<b>High Phosphate Diet</b>	
	<b>N</b>	<b>%</b>	<b>N</b>	<b>%</b>
0	18	100	17	42.5
1	0	0	12	30.0
2	0	0	7	17.5
3	0	0	3	7.5
4	0	0	1	2.5
<b>N (n)</b>	18 (9 mice)		40 (20 mice)	
<b>Median STiCSS</b>	0		1	
<b>Statistics</b>	p<0.001, ***			

When assessed by longitudinal radiographic analysis, we observed a progressive decrease in the amount of diet induced skeletal muscle calcification through 28 DPI (Figure 65), indicating that while predisposed to dystrophic calcification formation, the biological regression mechanism responsible for removing calcified/damaged tissues from injured tissues is still viable. While diminished, 2D and 3D  $\mu$ CT analysis still detected marked dystrophic calcification at 28 DPI in mice fed a high phosphate diet as compared to those

fed a standard phosphate diet (Figure 66). Histological analysis of injured skeletal muscle at 28 DPI confirms previous radiological findings of dystrophic calcification formation. While redressable, the formation of dystrophic calcification has a prolonged effect on skeletal muscle regeneration at 28 DPI compared to mice fed a control diet (Figure 67) highlighted by the formation of fibrosis, as indicated by MSB staining, within areas of damaged tissue.



**Figure 66: Microcomputed tomography Assessment of Dystrophic Calcification at 28 DPI.**



**Figure 67: Diet-induced Dystrophic Calcification Impairs Sarcomere Regeneration and Promotes Fibrosis.** Tissue samples were isolated and processed from mice fed control (0.7% inorganic phosphate) or high phosphate diet (1.7% inorganic phosphate) at 28 DPI. Following the administration of a high phosphate diet, marked calcification, as measured by H&E and von kossa staining, was observed. Furthermore, MSB staining indicated marked areas of tissue fibrosis present in injured tissues of mice fed a high phosphate diet. Images presented are representative.  $N \geq 3$  mice per diet group. Scale bar represents 100um

### *Conclusion*

Taken together, these results demonstrate that high phosphate diet alone is sufficient to predispose skeletal muscle to dystrophic calcification formation following injury. This model represents how a change in the physiologic balance by increasing a promoting factor (inorganic phosphate) through diet, has the ability to outweigh the skeletal muscle protection mechanisms, resulting in dystrophic calcification formation. Importantly, in this model we also observed regression of the dystrophic calcification over 28 DPI, measured by radiographic analysis. This suggests that the biological mechanisms responsible for regression of dystrophic calcification are still intact, allowing the dystrophic calcification which formed to be removed over time.

Therefore, this model would allow us to test our overarching hypothesis that the development of dystrophic calcification within damaged tissues is sufficient to support an osteoinductive microenvironment capable of forming HO following injury. However, in this model we did observe variability in the degree of dystrophic calcification in damaged skeletal muscle between animals. This finding may be a product of not being able to control the consumption of high phosphate food between animals, therefore going forward we also examined additional genetic models where soft tissue protection mechanisms are reduced to predispose to dystrophic calcification formation following injury in hopes of developing a more reliable model of dystrophic calcification formation.

### Soft Tissue Protection Mechanisms

Given the high circulating concentrations of calcium and phosphate, soft tissue such as

skeletal muscle, the cardiovascular system, the skin, and the renal system employ specialized biological mechanisms to prevent the formation of dystrophic calcification following injury. Plasmin, as discussed previously in Article 6 & 9, was found to be a potent protector of skeletal muscle calcification, yet the molecular mechanisms by which this protection is achieved remains unknown.

Osteopontin (OPN), a highly negatively charged extracellular matrix protein, has likewise been demonstrated to possess potent anti-mineralization properties as a result of its flexible structure, acidic protein motifs, and high negative charge[258, 305]. Additionally, when genetically reduced in a murine model, loss of OPN resulted in the formation of dystrophic calcification within damaged muscle [306, 307]. Clinically, OPN is also found to be up regulated at sites of pathologic dystrophic calcification, presumably in response to the aberrant mineralization it is responsible for inhibiting [308, 309]. Therefore, we aimed to recapitulate these preclinical results in our lab to assess whether OPN deficient mice may offer a reliable model of dystrophic calcification, yet we were unable to consistently reproduce the previously results. We found that, unlike the consistency seen in plasminogen deficient mice, OPN deficient animals did not reliably develop dystrophic calcification as measured by radiographic analysis. Therefore, given that we possessed much stronger and more reliable targets, we discontinued our investigations into OPN as a model system at this time.

Pyrophosphate (PPi), another well-defined anti-mineralization molecule, has been demonstrated to protect soft tissues such as skin and cardiovascular system from the

formation of aberrant calcification. However, until studies conducted in our lab, little was known about the role of PPi in protecting skeletal muscle from aberrant calcification. Briefly, we found that like other soft tissue, PPi protected skeletal muscle from aberrant calcification following injury, such that when PPi was reduced, we observed reliable formation of dystrophic calcification following injury (See Article 10). Going forward to examine the hypothesis that development of dystrophic calcification within damaged tissues is sufficient to support an osteoinductive microenvironment capable of forming HO following injury, we utilized a genetic mouse model with reduced circulating levels of pyrophosphate. These studies are discussed in detail in Article 10. Below, we will first discuss the scientific premise of PPi as a potent anti-mineralization mechanism for soft tissues such as skeletal muscle.

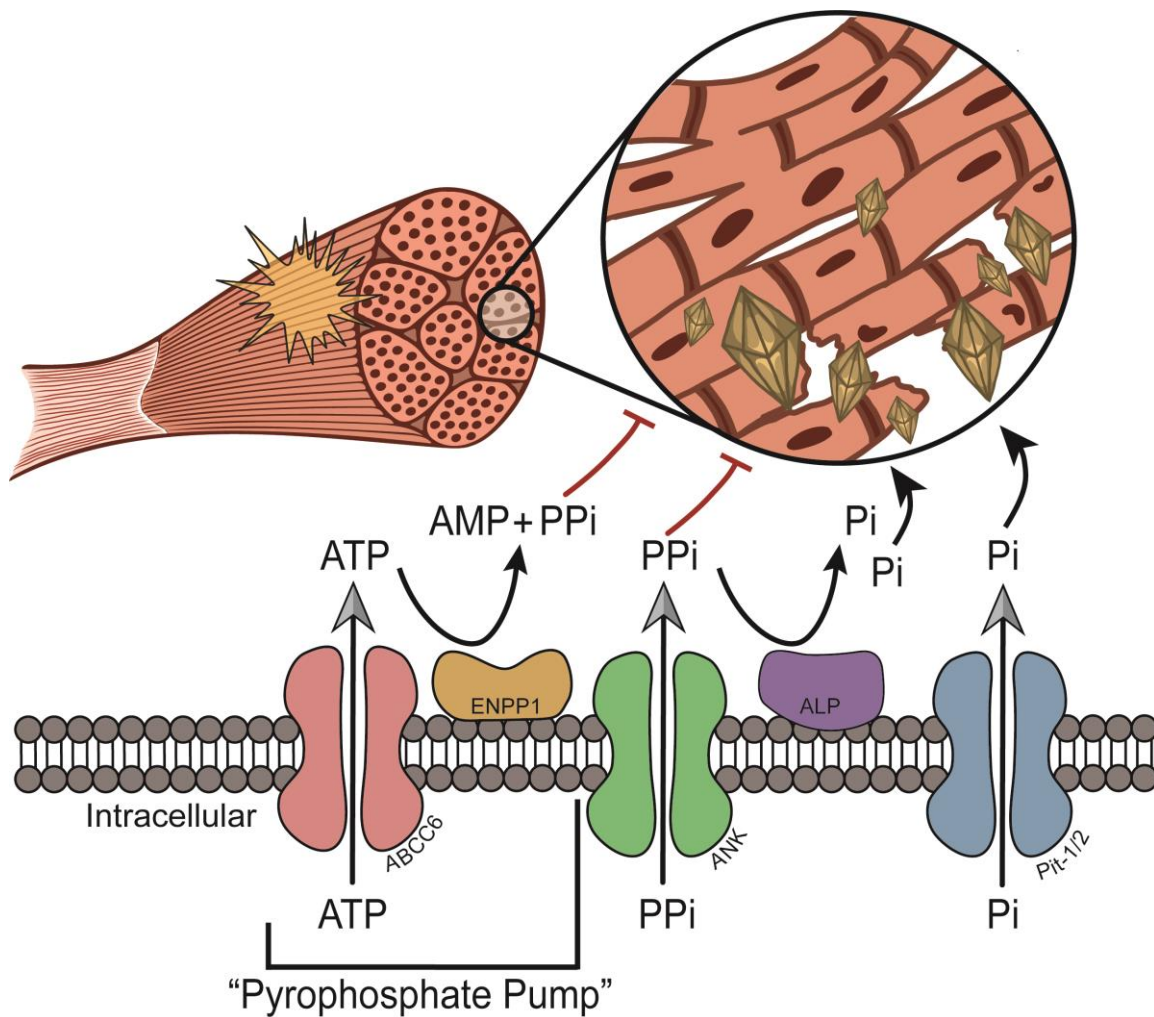
#### *Pyrophosphate: History, Production, And Mechanism of Action*

In 1961, a key observation was made by Dr. Bill Neuman and Dr. Herbert Fleisch. They observed that the body was super-saturated with respect to calcium phosphate and that the addition of collagen could act as a nucleating agent for the deposition of hydroxyapatite crystals *in vitro* [206, 207]. As such, they hypothesized that all tissues could calcify were it not for the presence of an inhibitor within body fluids. As early as 1930, trace amounts of PPi were known to act as a water softener by inhibiting the crystallization of calcium salts; yet it was not until 1962 that this same molecule was demonstrated to be present in biological fluids [310]. Over the next ten years, numerous studies would elucidate the concept of PPi as a “biological water softener” that prevents calcification in soft tissues such as the skin, kidney, and smooth muscle, while also regulating bone mineralization

[311, 312].

Although PPI was identified in the 1960s, it was not until the last 10 years that the mechanism and protein systems behind PPI regulation were identified. The PPI system is comprised of a group of proteins that work independently to tightly regulate PPI at various locations within the body to inhibit the formation of aberrant mineralization in soft tissues, yet allow for proper mineralization and formation of bone (**Figure 68**)[313-315]. This highly regulated balance is critical, such that too much PPI, as seen in patients with hypophosphatasia (TNAP mutation), can result in poor bone mineralization and growth [316-318], whereas too little PPI is considered to be the potential underlying cause of soft tissue calcification disorders such as Pseudoxanthoma elasticum (ABCC6 mutation) [319-321] and generalized arterial calcification of infancy (ENPP1 mutation) [322-325], among others (**Table 20**).

Although PPI has been clearly demonstrated to be integral to prevent calcification in soft tissues such as the skin, kidney, and cardiac muscle, little information prior to our studies was available about the role of PPI in muscle protection. Utilizing mice deficient in *Abcc6*, previously demonstrated to possess reduced levels of PPI, we examined the role of PPI for protecting skeletal muscle from DC following injury. Briefly, as stated above, we found that like other soft tissue, PPI protected skeletal muscle from aberrant calcification following injury.



**Figure 68: Protein components of the Pyrophosphate Pump:** Molecular components of pyrophosphate (PPi) production within the hepatocytes to the extracellular circulation as it pertains to the hypothesized regulation of skeletal muscle calcification. ABCC6- ATP-binding cassette C sub family, member 6; ENPP1-nucleotide pyrophosphatase; ANK- ANKH inorganic pyrophosphate transport regulator; ALP- alkaline phosphatase (also known as tissue nonspecific alkaline phosphatase, TNAP). Molecules: ATP- adenosine triphosphate; AMP- adenosine monophosphate; PPi- pyrophosphate; Pi- inorganic phosphate.



**Table 20: Human Diseases Associated with Mutations in the Pyrophosphate Pump that Result in Aberrant Mineralization**

Human Disease	Phenotype	Gene/Protein Mutation
<b>Mutations Resulting in Increased Mineralization</b>		
PXE	Mineralization of skin, eyes, and cardiovascular system	<i>ABCC6</i> , ATP-Binding Cassette Subfamily, Member 6
GACI	Arterial calcification and joint and spine ossification	<i>ENPP1</i> , nucleotide pyrophosphatase; <i>ABCC6</i> , ATP-Binding Cassette Subfamily, Member 6
CPPD	Deposition of crystals of calcium pyrophosphate dihydrate, Chondrocalcinosis, cartilage calcification	<i>ANKH</i> , ANKH Inorganic Pyrophosphate Transport Regulator
<b>Mutations resulting in Decreased Mineralization</b>		
Hypophosphatasia	Defective bone mineralization as a result of increased P <sub>i</sub> levels	<b>Inactive:</b> <i>ALPL</i> , Alkaline Phosphatase <b>Over-active:</b> <i>ANKH</i> , ANKH Inorganic Pyrophosphate Transport Regulator; <i>ENPP1</i> , Nucleotide Pyrophosphatase;
ARHR2	Defective bone mineralization, slow bone growth, and hypophosphatemia	<i>ENPP1</i> , Nucleotide Pyrophosphatase;

PXE, pseudoxanthoma elasticum; GACI, Generalized arterial calcification of infancy; CPPD, calcium pyrophosphate dihydrate deposition disease; ARHR2, autosomal recessive hypophosphatemic rickets-2.

Article 10: Trauma-Induced Nanohydroxyapatite Deposition in Skeletal Muscle is Sufficient to Drive Heterotopic Ossification

*Stephanie N. Moore-Lotridge*<sup>1,4</sup>, Qiaoli Li<sup>6</sup>, Breanne H.Y. Gibson<sup>1,4</sup>, Joseph T. Martin<sup>5</sup>, Gregory D. Hawley<sup>1</sup>, Thomas H. Arnold<sup>1,3</sup>, Masanori Saito<sup>1</sup>, Sami Tannouri<sup>6</sup>, Herbert S. Schwartz<sup>1</sup>, Richard J. Gumina, Justin M.M. Cates<sup>2</sup>, Jouni Uitto<sup>6</sup>, & Jonathan G. Schoenecker<sup>1,2,3,4,\*</sup>

Vanderbilt University Medical Center, <sup>1</sup>Department of Orthopaedics and Rehabilitation, <sup>2</sup>Department of Pathology Microbiology and Immunology, <sup>3</sup>Department of Pediatrics

Vanderbilt University, <sup>4</sup> Department of Pharmacology, <sup>5</sup>College of Arts and Science

Thomas Jefferson University, <sup>6</sup>Department of Dermatology and Cutaneous Biology, Sidney Kimmel Medical College

\*To whom correspondence should be directed:

*Submitted September 2018 for Publication in Calcified Tissue International*

## *Introduction*

Heterotopic ossification (HO) is the formation of bone within injured soft tissues such as skeletal muscle or tendons. In addition to imposing pain from chronic inflammation and tissue deformation, peri-articular HO restricts joint mobility and limb function thus precluding activities of daily living [326, 327]. While reports vary, HO is a significant problem in the civilian population, particularly following severe injury. For example, up to 25% of traumatic acetabular fractures, 20% of spinal cord injuries, and 11% of brain injuries have been reported to be complicated by HO development [328-330]. The incidence of HO dramatically rises in military related injuries, such that HO affected up to 65% of the severe wartime extremity injuries during the Afghanistan and Iraqi conflicts [331]. Although of great significance to both the civilian and military population, the pathophysiology of HO remains poorly understood and consequently, current treatments are suboptimal. Thus, studies aimed at defining the pathophysiology of HO to develop novel therapeutic strategies, especially following severe injuries in military populations, are essential.

The majority of soft tissue injuries experienced by patients do not form HO, rather they repair fully to the original tissues form. Failure of tissue repair typically results in fibrosis, devoid of bone. Yet, following traumatic-injuries, a subset of patients develops HO. As an explanation to this phenomenon, Chalmers *et. al.* proposed in 1975 that soft-tissue injury was a prerequisite of developing HO, and additional predisposing factors that favor ossification within the injured soft tissues environment were available to support bone formation [202]. In support of this theory, it was identified in 2006 that patients and

animals with fibrodysplasia ossificans progressive (FOP), a genetically-driven form of HO, possess gain-of-function mutations in the Type 1 bone morphogenic protein (BMP) receptor, which favors cellular transformation within injured soft tissue towards an osteoblast lineage [332, 333]. Although these mutations have been demonstrated to be the causative factor in FOP, genome wide association studies have failed to correlate mutations in the BMP signaling pathways with the greater majority of trauma-induced HO [204], suggesting that, in non-FOP cases, alternative predisposing pro-ossification factors may be responsible.

The primary mechanism by which chondrocytes and osteoblasts, two pro-ossification cells, initiate bone mineralization is by stimulating the formation and accumulation of nanohydroxyapatite crystals upon collagen X and collagen I within their extracellular environment [5]. Importantly, calcium and phosphate circulate at near-saturating concentrations [334] thereby favoring the formation of nanohydroxyapatite by these pro-ossification cells [335]. While these ionic concentrations are ideal for maintaining bone integrity, soft-tissue and homeostatic environments are simultaneously exposed to these saturating conditions; thus if a nucleating matrix is available, crystal formation will progress [334, 335].

Given the pathologic implications of hardened or mineralized soft tissues, the body possess a myriad of factors that either prevent or dissolve nanohydroxyapatite [259, 319, 335-349]. One of the most well described soft tissue protection mechanisms is the production of pyrophosphate (PPi), a potent anti-mineralization molecule, produced primarily from

the cleavage of adenosine triphosphate (ATP) [320, 350]. Thus, in accordance with Chalmers' theory [202], we surmise that if a predisposing ossification factor such as nanohydroxyapatite was not regulated within soft tissues, its deposition could mimic the bone environment and favor ossification. From this scientific premise, we hypothesized that, as an alternative to a gain-of-function of an ossification gene (as seen in FOP), a loss-of-function mutation in the molecular mechanisms that protect soft tissues from nanohydroxyapatite formation may also be sufficient to support HO following soft tissue injury.

To test this hypothesis, we investigated the fate of skeletal muscle following injury in a murine model of a rare calcification disorder, pseudoxanthoma elasticum (PXE, incidence of 1:50,000). PXE occurs due to biallelic null mutations primarily in *Abcc6* (ATP binding cassette sub family C, member 6), an ATP transporter produced in the liver responsible for moving ATP from the intracellular space to the extracellular environment where it is cleaved by ENPP1 (ectonucleotide pyrophosphatase/phosphodiesterase 1) to produce AMP and PPi, a potent inhibitor of nanohydroxyapatite formation. As such, patients and animals with PXE have diminished PPi and develop progressive deposits of nanohydroxyapatite within the skin, cardiovascular system, and retinas [319, 320, 350-354]. Yet, the role of *Abcc6* in preventing nanohydroxyapatite and HO in skeletal muscle following injury is unknown. Here, we investigated two related hypotheses: 1) to determine if a loss of *Abcc6* promotes nanohydroxyapatite deposition within injured muscle following injury and 2) if so, whether nanohydroxyapatite deposition in the injured muscle environment is sufficient to promote HO.

### *Study Specific Methods and Materials: Operational Definitions of Soft Tissue Calcification*

The following operational definitions will be utilized throughout in reference to various forms of calcification within skeletal muscle, delineated by their unique morphological properties. 1) Dystrophic calcification will be used broadly to describe deposits of amorphous calcium phosphate crystals within soft tissues. 2) Nano-hydroxyapatite is a sub-classification of dystrophic calcification that will be utilized to describe calcium phosphate deposits that are both i) within the nanometer range and ii) the molecular composition of hydroxyapatite. 3) HO is defined as bone formation in soft tissue, characterized by the presence of woven bone, hematopoietic marrow, and/or the presence of rimming osteoblasts.

### *Murine Model of Skeletal Muscle Calcification: Animal Husbandry*

All animal procedures were approved by the Vanderbilt University IACUC (M1600225) and performed in accordance with the ethical standards of the institution. *Abcc6*<sup>+/+</sup>, *Abcc6*<sup>+/-</sup>, and *Abcc6*<sup>-/-</sup> mice were housed within Vanderbilt University Medical Center under a 12-hour light/dark cycle with free access to food and water. All studies were conducted in 6-week-old animals on a C57BL/6J background fed a standard chow diet. Equal numbers of male and female animals were included in each cohort. Welfare related assessments were carried out prior to and throughout all experiments by trained personnel at Vanderbilt University and Vanderbilt University Medical Center. This article does not contain any studies with human participants performed by any of the authors.

### *Murine Cardiotoxin-Induced Muscle Injury Model*

Following adequate anesthesia with isoflurane, focal muscle injury was induced via intramuscular injection of 40 $\mu$ L of 10nM cardiotoxin (Accurate Chemical and Scientific Corp, Westbury, NY) into the posterior compartment of the lower leg using a lateral approach with a 28.5G, 0.5ml, insulin syringe as previously described [292, 298]. Both the right and left posterior compartment muscles of the lower extremity were injured and analyzed by radiography for the presence of skeletal muscle calcification.

### *Output Analysis and Quantification of Skeletal Muscle Calcification: Radiographic Analysis*

Beginning 7 days post injury (DPI) and continuing through sacrifice, digital radiographs (Faxitron, Tucson, AZ) of the lower extremity were acquired. Following adequate anesthesia, mice were placed in the prone position with hips in abduction, allowing for external rotation of the leg by placing the tibia in a reproducible lateral position. Single plane lateral radiographic images were collected at an exposure of 4 seconds at 35 kV and saved as a DICOM (.dcm) files for image processing and quantification.

### *Soft Tissue Calcification Scoring System (STiCSS) Quantification*

As previously described in Article 7, the STiCSS is a previously validated ordinal grading system developed by our lab to quantify the extent of soft tissue calcification within the posterior compartment muscle of the lower extremity longitudinally by serial radiographic analysis [298]. Briefly, the operational definitions of each score are based on the percentage area of soft tissue calcification observed in the posterior compartment of the

lower extremity: 0 (0%), 1 (1-25%), 2 (25-49%), 3 (50-75%) and 4 (>75%).

#### *μCT Analysis*

μCT images of the injured hind limbs were acquired following sacrifice at 55kVp, 145μA, 200ms integration, 500 projections per 180° rotation, with a 20μm isotropic voxel size (μCT40, Scanco Medical AG, Bassersdorf, Switzerland). After reconstruction, a volume of interest comprising the region of soft tissue calcification within the posterior compartment of the lower extremity was selected as previously described [292]. Mineralized tissue within the volume of interest was segmented from soft tissue using a threshold of 220 per thousand (or 450.7mgHA/cm<sup>3</sup>), a Gaussian noise filter of 0.2, and support of 1.

#### *Histological Analysis*

Injured hind limbs were fixed in 10% neutral-buffered formalin for 24 to 72 hours. All samples were processed in graded series of ethanol, cleared, and embedded in paraffin prior to sectioning. 6μm sections were cut and stained as described below.

**Hematoxylin and Eosin (H/E) Staining:** Deparaffinized sections were stained in Gills 3 hematoxylin solution for 5 min. Slides were rinsed in tap water for 10 min followed by eosin staining for 2 min. Slides were then dehydrated and cleared in xylene before mounting with Permount. Histological quantification of skeletal muscle damage was assessed by light microscopy at 200X magnification (Axio imager a1, ZEISS; Oberkochen, Germany) as previously described [292]. At least 3 mice were analyzed per group, with >2 sections per mouse and >4 images per section (i.e. minimum of 24 images per group).



Briefly, skeletal muscle damage was evaluated in a blinded manner by counting 1) 'damaged sarcomeres' identified by hypereosinophilic sarcoplasm and centrally-located nuclei, 2) 'calcified sarcomeres' identified by dense basophilic staining for hematoxylin, and 3) histologically normal sarcomeres. These groups were then expressed as a percentage of total muscle fibers within 200X magnification field.

Von Kossa Staining for Calcification: Deparaffinized sections were rinsed with distilled water and exposed to 1% AgNO<sub>3</sub> solution under UV light for 30 min. Slides were counterstained with Fast Green for 5 min, dehydrated, and cleared in xylene before mounting with Permount.

Martius Scarlet Blue (MSB) Staining: Following deparaffinization, staining was performed per standard protocols to assess for fibrin and collagen deposition within damaged tissues. Briefly, deparaffinized sections were rinsed with tap water and stained with Wiegert's Hematoxylin for 5 minutes. Slides were then rinsed, differentiated in 1% acid alcohol for 15 seconds, rinsed again in tap water, and cleared in several changes of 95% ethanol. Next, slides were placed into working Martius yellow solution for 2 minutes, rinsed, and stained with Crystal Ponceau 6R for 10 minutes. Slides were then differentiated in 15 phosphotungstic Acid for 5 minutes, washed, and finally stained with methyl blue solution for 5 minutes prior to dehydration through graded ethanol, clearing with xylene, and mounting with Permount.

Immunohistochemical (IHC) Staining of F4/80+ Cells: IHC for F4/80+ cells indicative of

monocyte lineage was performed per standard protocols in a core facility (Vanderbilt Translational Pathology Shared Resource; [www.mc.vanderbilt.edu/tpsr](http://www.mc.vanderbilt.edu/tpsr)). % Area of positive F4/80 staining was quantified by ImageJ through the use of the IHC toolkit freely provided.

#### *Energy Dispersive X-Ray Analysis*

Sections of muscle were analyzed using energy dispersive X-ray (EDS) analysis and topographic mapping. Paraffin sections were mounted onto carbon carriers, imaged, and analyzed for elemental composition with a FEI 600 Quanta FEG scanning electron microscope (FEI Company, Eindhoven, The Netherlands) fitted with an Octane Super SDD EDS detector (EDAX, Sandy, UT, USA). X-ray topographic (RADAR) maps of calcium and phosphorus were acquired using Spirit software version 1.07.05 (Princeton Gamma-Tech, Rocky Hill, NJ, USA). EDS spectra and topographic maps were collected for 60.8 and 717.5 s (80 frames), respectively.

#### *Macrophage Depletion*

Depletion of macrophages was accomplished through intravenous administration of 200  $\mu$ L of clodronate or PBS filled (control) liposomes (Liposoma, Amsterdam, The Netherlands) with a 28.5G, 0.5ml, insulin syringe weekly beginning at the time of injury until sacrifice[355, 356].

#### *Transition Electron Microscopy to Visualize Macrophage Mediate Dystrophic Calcification Regression*

Specimens were processed for transition electron microscopy (TEM) and imaged in the Vanderbilt Cell Imaging Shared Resource-Research Electron Microscopy facility.

**Embedding:** Samples were fixed in 2.5% glutaraldehyde in 0.1M cacodylate buffer, pH7.4 at room temperature (RT) 1 hour then transferred to 4°C, overnight. Samples were washed in 0.1M cacodylate buffer, and then incubated 1 hour in 1% osmium tetroxide at RT then washed with 0.1M cacodylate buffer. Subsequently, samples were dehydrated through a graded ethanol series and then 3 exchanges of 100% ethanol. Next, samples were incubated for 5-minutes in 100% ethanol and propylene oxide (PO) followed by 2 exchanges of pure PO. Samples were then infiltrated with 25% Epon 812 resin and 75% PO for 30 minutes at RT. Next, samples were infiltrated with Epon 812 resin and PO [1:1] for 1 hour at RT then overnight at RT. Next day, the samples went through a [3:1] (resin: PO) exchange for 3-4 hours, and then incubated with pure epoxy resin overnight. Samples were then incubated in two more changes of pure epoxy resin then allowed to polymerize at 60°C for 48 hours.

**Sectioning and Imaging:** 70-80nm ultra-thin sections were cut and collected on 200-mesh copper grids and post-stained with 2% uranyl acetate and then with Reynold's lead citrate. Samples were subsequently imaged on the Philips/FEI Tecnai T12 electron microscope at various magnifications.

#### *Statistics and Data Handling*

STiCSS scores between the indicated cohorts were compared using the non-parametric Mann-Whitney or Kruskal-Wallis test with correction for multiple comparisons (Dunn's

multiple comparisons test) as previously validated [298]. Error bars represent median with interquartile range. Quantification and statistical analysis of skeletal muscle healing was assessed with a Kruskal-Wallis test with correction for multiple comparisons. P values reported are corrected for multiple comparisons. Statistical analyses were performed in GraphPad Prism (v6, GraphPad Software, La Jolla, CA) with  $\alpha=0.05$ , two-sided testing was applied. Number of mice (N) per group and number of limbs assessed (n) is reported in the designated figure or figure legend.

#### *Sample Size*

Calculation for sample size was based upon previously published investigations [292, 298]. Previously, we determined that 3 mice per groups were necessary to detect a 100% change in soft tissue calcification quantified by radiographic analysis between experimental and wild type animals. Therefore, all studies were conducted with an excess of 3 mice per group.

#### *Data Collection & Inclusion*

Data from all animal experiments was collected at either 7, 14, or 28 days post injury as indicated within the figures or figure legends. During these experiments, no animals experience adverse consequences necessitating their removal from the study; therefore, no additional endpoints were assessed. The selected endpoints were previously established, prior to this investigation, with the approval of our animal use protocols. All radiographic data collected was quantified and included within this manuscript. No animals were excluded from the study. Histological results were conducted on a minimum of 3 mice per

group, with the image included representing the mean response observed.

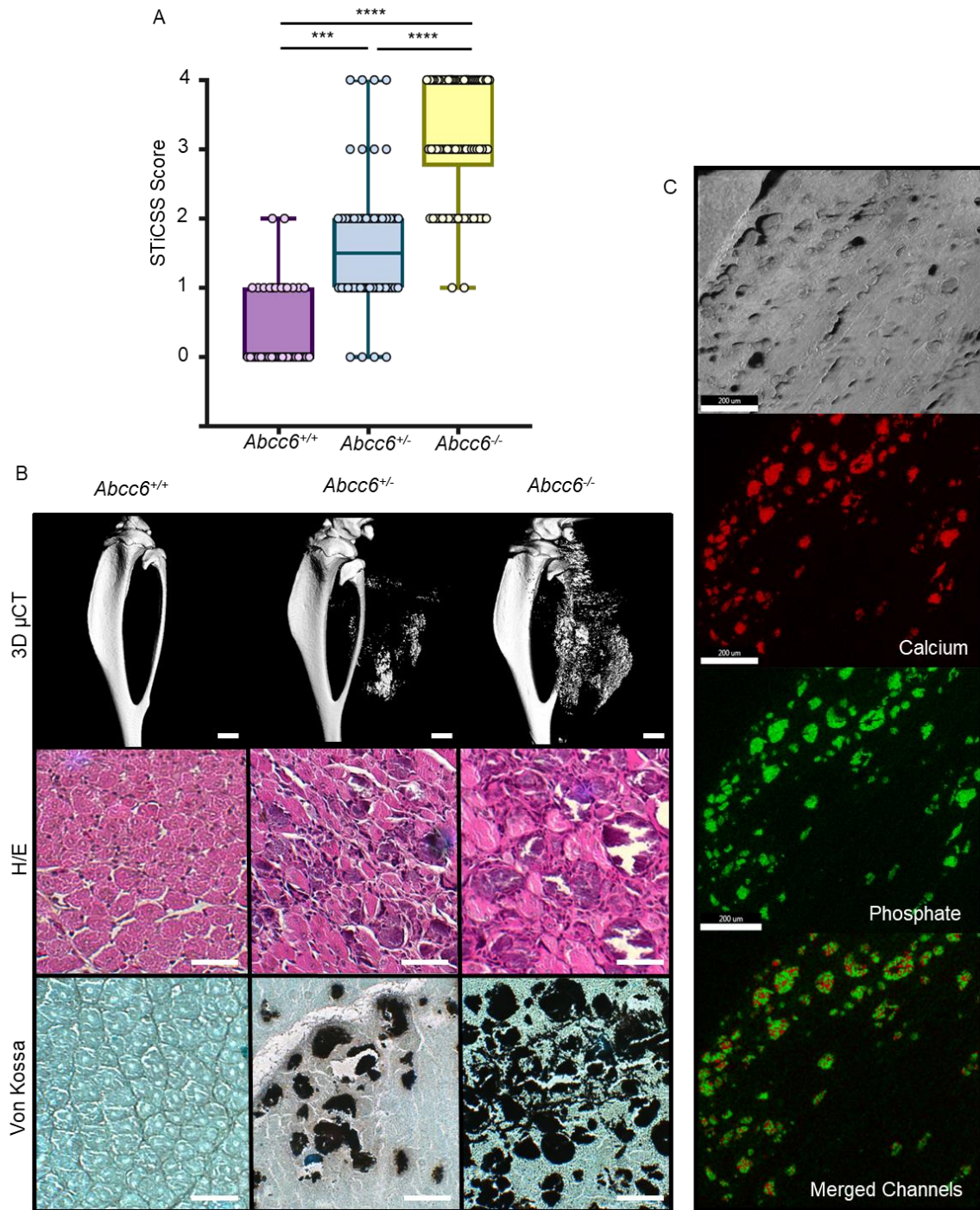
#### *Randomization & Blinding*

Once genotyped, all male and female mice from a single litter were randomly assigned to an experimental or treatment group. Mice of different genotypes or treatment group were mixed within each cage. Individuals quantifying weekly radiographic images for the amount of soft tissue calcification were blinded to the genotype or experimental group of the animals. Furthermore, histologic slides were blinded prior to quantification of skeletal muscle regeneration. For studies conducted on high phosphate diet, mice were randomly assigned to each diet groups at the time of weening. However due to the clear color difference in food, we were not able to blind the diet groups to the investigators obtaining weekly radiographs. Yet, radiographs were quantified by a separate party in a blinded manner.

## *Results*

### *Loss of ABCC6 Predisposes Skeletal Muscle to Nanohydroxyapatite Deposition Following Injury*

Utilizing mice with either partial (*Abcc6*<sup>+/-</sup>) or complete (*Abcc6*<sup>-/-</sup>) genetic reduction of ABCC6, we observed a gene-dependent predisposition for dystrophic calcification within the injured skeletal muscle at 7 DPI as measured by radiographic analysis and  $\mu$ CT (Figure 69A&B, Table 21). Further analysis by energy dispersive x ray (EDS) and histologic analysis demonstrated that the dystrophic calcification present within damaged skeletal muscle was in the nanometer range and possessed both inorganic calcium and phosphate with an average calcium/phosphate atomic ratio of 1.67 $\pm$  0.2, indicative of nanohydroxyapatite (Figure 69C). Together, these results demonstrate that loss of ABCC6 is sufficient to predispose skeletal muscle, like other soft tissues, to the deposition of nanohydroxyapatite following injury.



**Figure 69: Loss of ABCC6 Predisposes Skeletal Muscle to Nanohydroxyapatite deposition at 7DPI.** A) WT (*Abcc6*<sup>+/+</sup>), heterozygous (*Abcc6*<sup>+/-</sup>), and homozygous (*Abcc6*<sup>-/-</sup>) mice were assessed for calcification at the site of skeletal muscle injury by radiographic analysis and subsequent STiCSS quantification at 7 DPI. See Table 2 for

detailed analysis of the genotypes and N.  $p < 0.001$ , \*\*\*;  $p < 0.0001$ , \*\*\*\*. Statistical analysis between groups was performed using a non-parametric Mann-Whitney test. B) Representative 3D  $\mu$ CT reconstructions and histological analysis of skeletal muscle calcification within the injured gastrocnemius and soleus muscles at 7 DPI. Scale bar represents 100 $\mu$ m.  $n \geq 3$  mice per genotype. C) Energy dispersive x-ray (EDS) analysis of dystrophic calcification nodules within damaged ABCC6 deficient skeletal muscle at 14 DPI. Topographic mapping demonstrated marked co-localization of calcium and phosphate with an average calcium/phosphate atomic ratio of  $1.67 \pm 0.2$ , indicative of hydroxyapatite. Analysis was conducted following random sampling of 5 distinct spots per tissue section. Scale bar represents 200 $\mu$ M, thereby indicating nanohydroxyapatite.

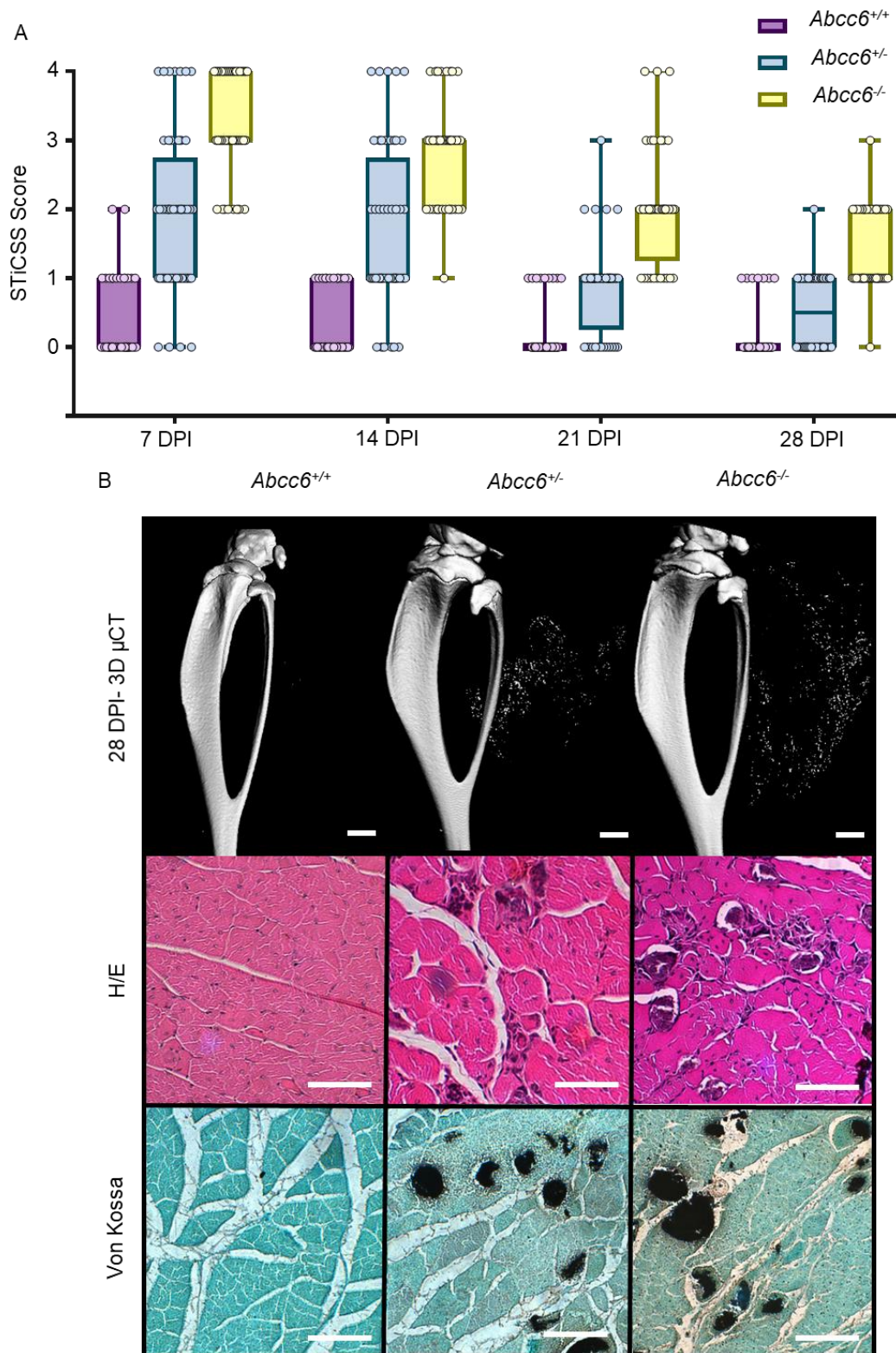
**Table 21: Quantification of Skeletal Muscle Calcification in ABCC6 Deficient Mice at 7DPI.** N represents total number of individual samples analyzed, with the left and right leg acting as individual samples. n represents total number of mice per group. Equal number of male and females were used in each genotype.

STiCSS Score	ABCC6 <sup>+/+</sup>		ABCC6 <sup>+/-</sup>		ABCC6 <sup>-/-</sup>	
	N	%	N	%	N	%
0	43	67.2	4	7.7	0	0
1	20	31.3	22	42.3	2	2.3
2	1	1.5	18	34.6	19	22.1
3	0	0	4	7.7	23	26.7
4	0	0	4	7.7	42	48.9
<b>N (n)</b>	64 (32 mice)		52 (26 mice)		86 (43 mice)	
<b>Median</b>	0.0		1.5		3.0	



*Nano-Hydroxyapatite Deposited in Skeletal Muscle Following Injury is Reversible*

Given the above findings, we next examined the second hypothesis that nanohydroxyapatite deposited within skeletal muscle following injury would be sufficient to promote HO. Longitudinal radiographic analysis of *Abcc6*-deficient mice demonstrated robust nanohydroxyapatite depositing within injured tissues at 7 DPI that progressively decreased in both *Abcc6*<sup>+/-</sup> and *Abcc6*<sup>-/-</sup> mice over 28 DPI (Figure 70A). Histological quantification of damaged skeletal muscle at 7 and 28 DPI in *Abcc6*<sup>+/+</sup>, *Abcc6*<sup>+/-</sup>, and *Abcc6*<sup>-/-</sup> demonstrated comparable initial levels of injury between cohorts, given the comparable percentage of histologically normal sarcomeres, and confirmed the decrease of nanohydroxyapatite in *Abcc6*<sup>+/-</sup> and *Abcc6*<sup>-/-</sup> between 7 to 28 DPI (Figure 70B & Table 22). Taken together, while loss of ABCC6 is sufficient to predispose skeletal muscle to nanohydroxyapatite deposition at 7 DPI, the mineral deposited was progressively removed from the damaged skeletal muscle and therefore was insufficient to promote ossification.



**Figure 70: Nanohydroxyapatite deposition in ABCC6 Deficient Mice is Degraded Over 28 DPI.** Beginning at 7DPI, *Abcc6*<sup>+/+</sup>, *Abcc6*<sup>+/-</sup>, or *Abcc6*<sup>-/-</sup> animals were A)

assessed weekly by radiographic analysis through 28 DPI and quantified by the STiCCS, to reveal progressive resolution of nanohydroxyapatite from damaged skeletal muscle. B) 3D  $\mu$ CT and histologic analysis at 28 DPI demonstrates reduced nanohydroxyapatite deposition compared to results seen in 7 DPI. H/E staining was utilized to assess sarcomere morphology and regeneration quantified in Table 3, Von Kossa Staining was used to visualize calcification. Scale bar represents 100 $\mu$ m.  $n \geq 3$  mice per genotype.

**Table 22: Histological Quantification of Skeletal Muscle Calcification and Regeneration at 7 and 28 DPI.** Detailed histological analysis of *Abcc6*<sup>+/+</sup>, *Abcc6*<sup>+/-</sup>, and *Abcc6*<sup>-/-</sup> mice at 7 and 28 DPI. N= number of individual analyzed per time point, mixed between male and females. 4 sections per mouse and 4 images per section were analyzed as outline in the materials and methods section.

Genotype (Timepoint)	N=	% Histologically		Calcified or Damaged Sarcomeres
		Normal Sarcomeres	Regenerating Sarcomeres	
ABCC6 <sup>+/+</sup> 7 DPI	8	26.53 $\pm$ 15.31 <sup>a</sup>	72.40 $\pm$ 15.30	1.07 $\pm$ 1.92
ABCC6 <sup>+/-</sup> 7 DPI	8	18.81 $\pm$ 11.51 <sup>a</sup>	56.92 $\pm$ 15.95	24.27 $\pm$ 15.24 <sup>d,e</sup>
ABCC6 <sup>-/-</sup> 7 DPI	11	18.50 $\pm$ 13.71 <sup>a</sup>	43.44 $\pm$ 11.07 <sup>c</sup>	38.06 $\pm$ 15.84 <sup>f</sup>
ABCC6 <sup>+/+</sup> 28 DPI	6	42.20 $\pm$ 17.67 <sup>b</sup>	57.45 $\pm$ 18.18	0.35 $\pm$ 0.86 <sup>g</sup>
ABCC6 <sup>+/-</sup> 28 DPI	13	39.37 $\pm$ 16.81 <sup>b</sup>	54.78 $\pm$ 16.85	5.82 $\pm$ 3.64 <sup>h</sup>
ABCC6 <sup>-/-</sup> 28 DPI	13	31.47 $\pm$ 10.53 <sup>b</sup>	51.78 $\pm$ 11.78	16.75 $\pm$ 4.89 <sup>i</sup>

a: non-significant difference between groups,  $p > 0.05$

b: non-significant difference between groups,  $p > 0.05$

c: *Abcc6*<sup>+/+</sup> vs *Abcc6*<sup>-/-</sup>, \*\*,  $p = 0.001$

d: *Abcc6*<sup>+/+</sup> vs *Abcc6*<sup>+/-</sup>, \*\*\*,  $p = 0.0001$

e: *Abcc6*<sup>+/-</sup> vs *Abcc6*<sup>-/-</sup>, \*,  $p = 0.028$

f: *Abcc6*<sup>+/+</sup> vs *Abcc6*<sup>-/-</sup>, \*\*\*\*,  $p < 0.0001$

g: *Abcc6*<sup>+/+</sup> 7 vs 28 DPI, non-significant difference,  $p > 0.05$

h: *Abcc6*<sup>+/-</sup> 7 vs 28 DPI, \*\*\*,  $p = 0.0007$

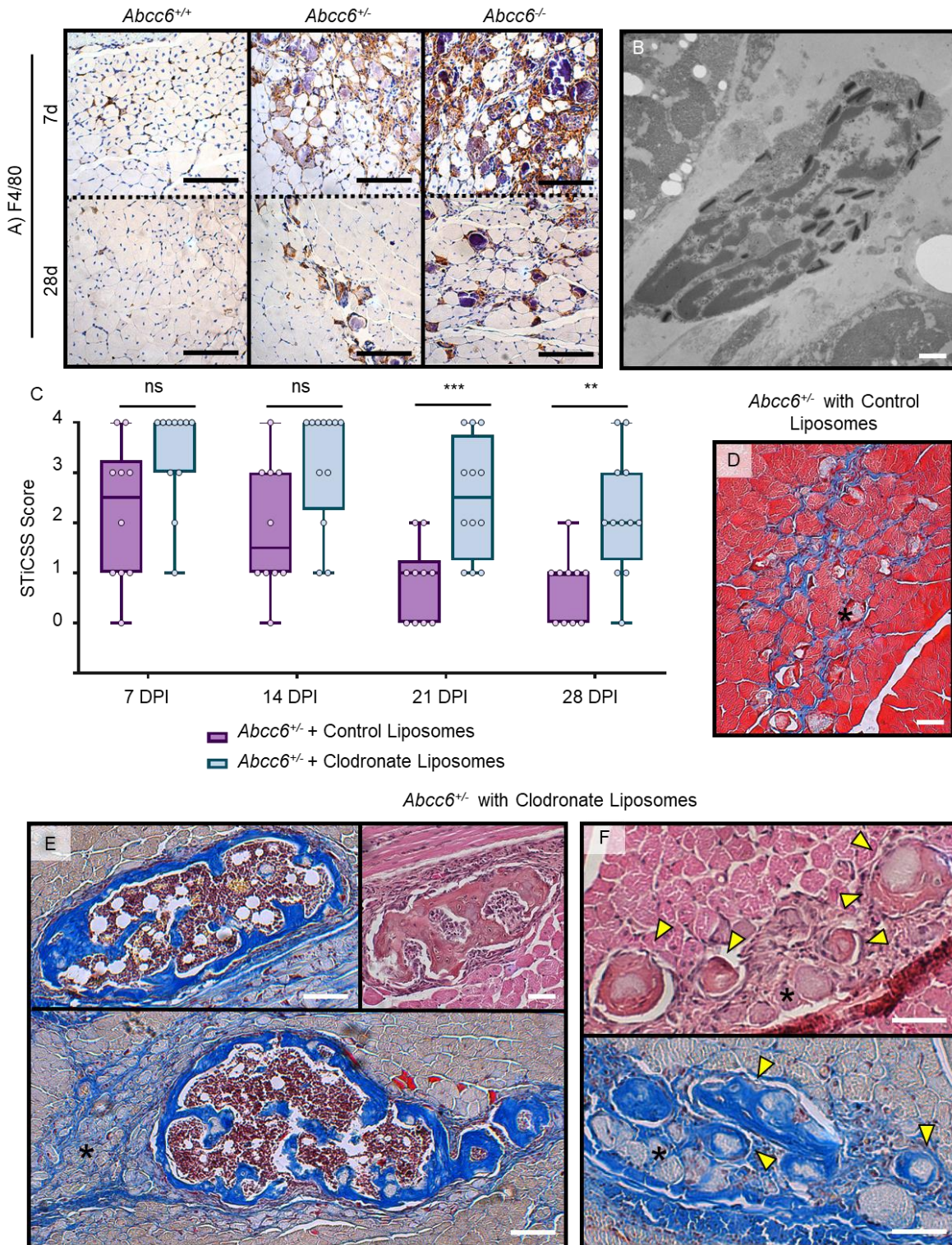
i: *Abcc6*<sup>-/-</sup> 7 vs 28 DPI, \*\*\*\*,  $p < 0.0001$

### *Macrophages Mediate Nano-Hydroxyapatite Resorption from Damaged Skeletal Muscle*

Given the progressive decrease in nan-hydroxyapatite from damaged skeletal muscle over 28 DPI, we next investigated 1) the mechanisms by which nanohydroxyapatite was degraded and 2) the pathologic consequence of impaired nanohydroxyapatite degradation on skeletal muscle healing.

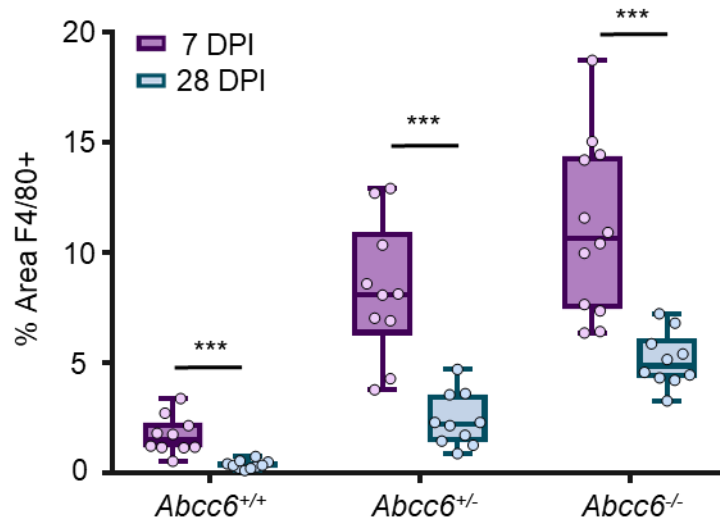
Previously, macrophages have been suggested to assist in the resorption of calcification in vitro and within the cardiovascular system, yet it is unknown what role macrophage play in regression of nanohydroxyapatite deposited in skeletal muscle. Here, histological analysis of *Abcc6*<sup>+/-</sup> and *Abcc6*<sup>-/-</sup> injured skeletal muscle demonstrated foci of nanohydroxyapatite surrounded by a cellular inflammatory infiltrate consisting of F4/80+ macrophages/monocytes. This infiltrate was present at 7 DPI and persisted through 28 DPI, where it was largely focused around the remaining sites of nanohydroxyapatite (**Figure 71A**). When quantified, the % area of positive F4/80 staining increased in a gene-dependently at both 7 and 28 DPI (**Figure 72**), aligning with the gene dependent levels of calcification observed previously by radiographic and histologic analysis (**Figure 69 & 70**). Transition electron microscopy of injured skeletal muscle revealed macrophages adjacent to damaged sarcomeres containing dense encapsulated granules, indicative of resorbed nanohydroxyapatite (**Figure 71B**). Furthermore, when macrophages were inhibited in either *Abcc6*<sup>+/-</sup> or *Abcc6*<sup>-/-</sup> deficient animals via liposome-targeted clodronate administration, we observed significant inhibition of nanohydroxyapatite resorption through 28 DPI compared to control treated animals (**Figure 71 C&D**). Taken together, these data suggest that macrophages are present within damaged tissues and are

participating in the resorption of nanohydroxyapatite from damaged skeletal muscle.



**Figure 71: Macrophage-mediated Resolution of Nanohydroxyapatite Prevents**

**Maturation to HO.** A) Immunohistochemical stain for F4/80+ cells at 7 and 28 DPI in injure skeletal muscle from *Abcc6*<sup>+/+</sup>, *Abcc6*<sup>+/-</sup>, or *Abcc6*<sup>-/-</sup> mice. B) Transition electron microscope image of a macrophage containing phagocytosed nanohydroxyapatite. Scale bar represent 500nm. C) Longitudinal STiCSS analysis of *Abcc6*<sup>+/-</sup> treated with either control (PBS) or clodronate filled liposomes beginning at the time of injury. N<sub>≥</sub>5 mice per group. Nanohydroxyapatite was not observed in *Abcc6*<sup>+/+</sup> mice treated with either control or clodronate filled liposomes, N<sub>≥</sub>4 mice per group. Data not shown. p<0.01, \*\*, p<0.001, \*\*\* D) MSB histological analysis at 28 DPI of *Abcc6*<sup>+/-</sup> mice treated with control liposomes. E&F) Histological analysis of *Abcc6*<sup>+/-</sup> mice treated with clodronate-containing liposomes indicating the presence of mature HO (E, MSB and H/E) characterized by the presence of woven bone, blue staining (MSB) indicative of collagen deposition, and central hematopoiesis. Regions of persistent nanohydroxyapatite (black asterisks), and regions that appear to be nanohydroxyapatite maturing to ossified lesions (F-Yellow arrows, MSB and H/E) were also observed. Scale bar represents 100μm.



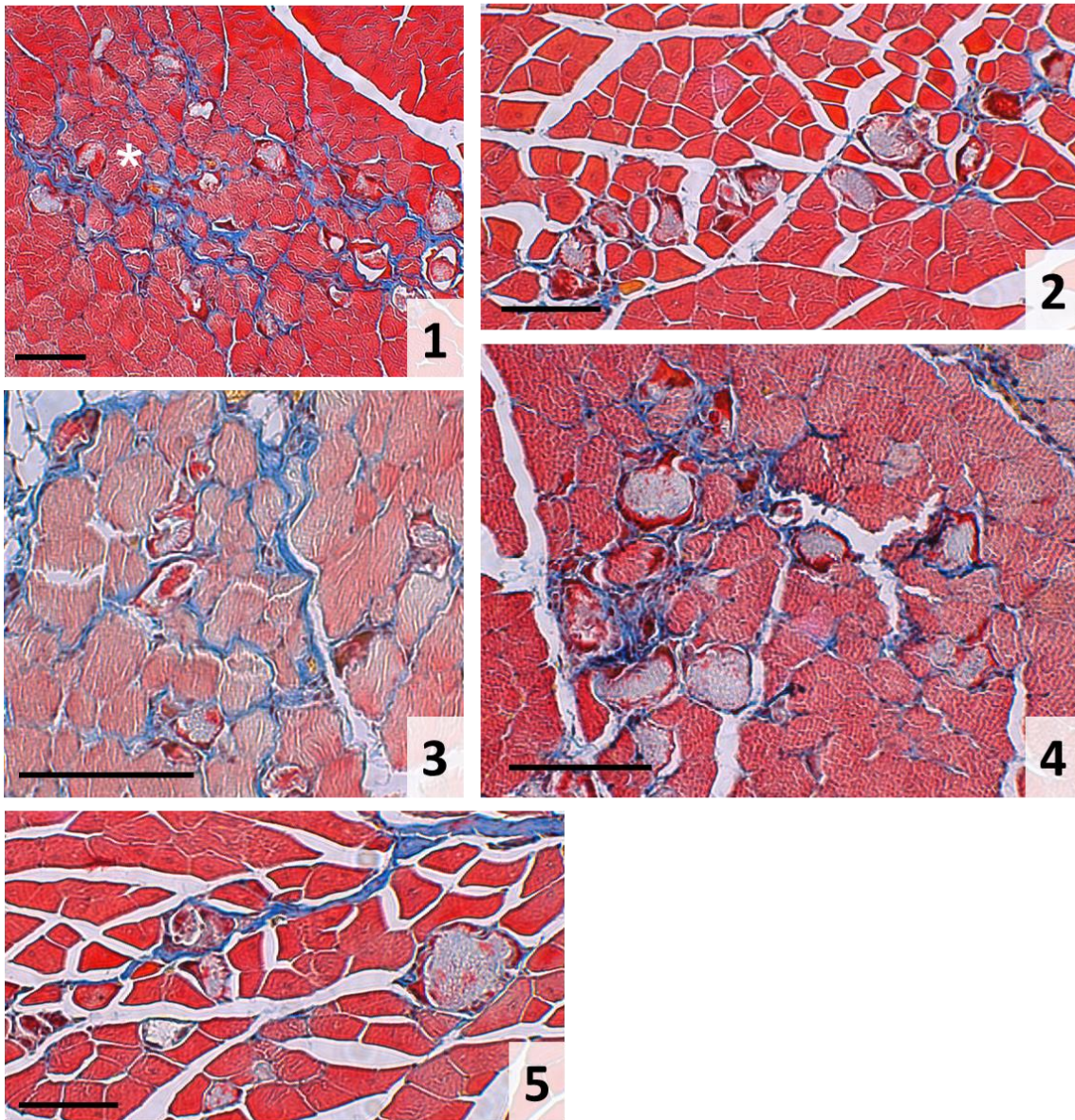
**Figure 72: Quantification of F4/80+ Staining in Damaged Skeletal Muscle at 7 and 28 Days post Injury.** Quantification of F4/80+ IHC demonstrated significantly greater % area

of positive staining in homozygous null mice (*Abcc6*<sup>-/-</sup>) compare to heterozygous (*Abcc6*<sup>+/-</sup>) or WT animals at both 7 and 28 days post injury, aligning with the previously reported elevation in skeletal muscle calcification. All P values have been adjusted for multiplicity testing (Sidak's multiple comparison testing). *Abcc6*<sup>-/-</sup> vs *Abcc6*<sup>+/-</sup>: 7d, \*, p=0.015; 28d, \*, p=0.0264. *Abcc6*<sup>+/-</sup> vs *Abcc6*<sup>+/+</sup>: 7d, \*\*\*, p<0.001; 28d, ns, p=0.145. *Abcc6*<sup>-/-</sup> vs *Abcc6*<sup>+/+</sup>: 7d, \*\*\*, p<0.001; 28d, \*\*\*, p<0.001. Furthermore, aligning with the regression of calcification observed between 7 and 28 days post injury, we likewise observed a statistically significant reduction in the F4/80+ staining between 7 and 28 days in all genotypes. \*\*\*, p<0.001. N≥10 images quantified of individual injury locations per cohort.

#### *Pathologic Consequence of Impaired Nanohydroxyapatite Resorption*

Histological analysis of *Abcc6*<sup>+/-</sup> tissue at 28 DPI demonstrated that while both cohorts of mice developed nanohydroxyapatite, in mice lacking macrophage-mediated resorption, nanohydroxyapatite was persistent in 5/5 mice and sufficient to support HO in 4/5 mice analyzed, characterized by the presence of woven bone and central hematopoiesis (Figure 71D&E, Figure 73 & 74). Detailed assessment of these regions demonstrated small focal areas morphologically akin to HO as well as regions that appear to be nanohydroxyapatite transitioning to ossified lesions (Figure 71F- Yellow arrows). Together, these data suggest that 1) macrophages are an essential cellular mediator, capable of regressing nanohydroxyapatite from damaged skeletal muscle, and 2) if macrophages are inhibited, persistent nanohydroxyapatite within damaged tissues is sufficient to predispose damaged skeletal muscle to HO formation.

*Abcc6*<sup>+/-</sup> with Control Liposomes

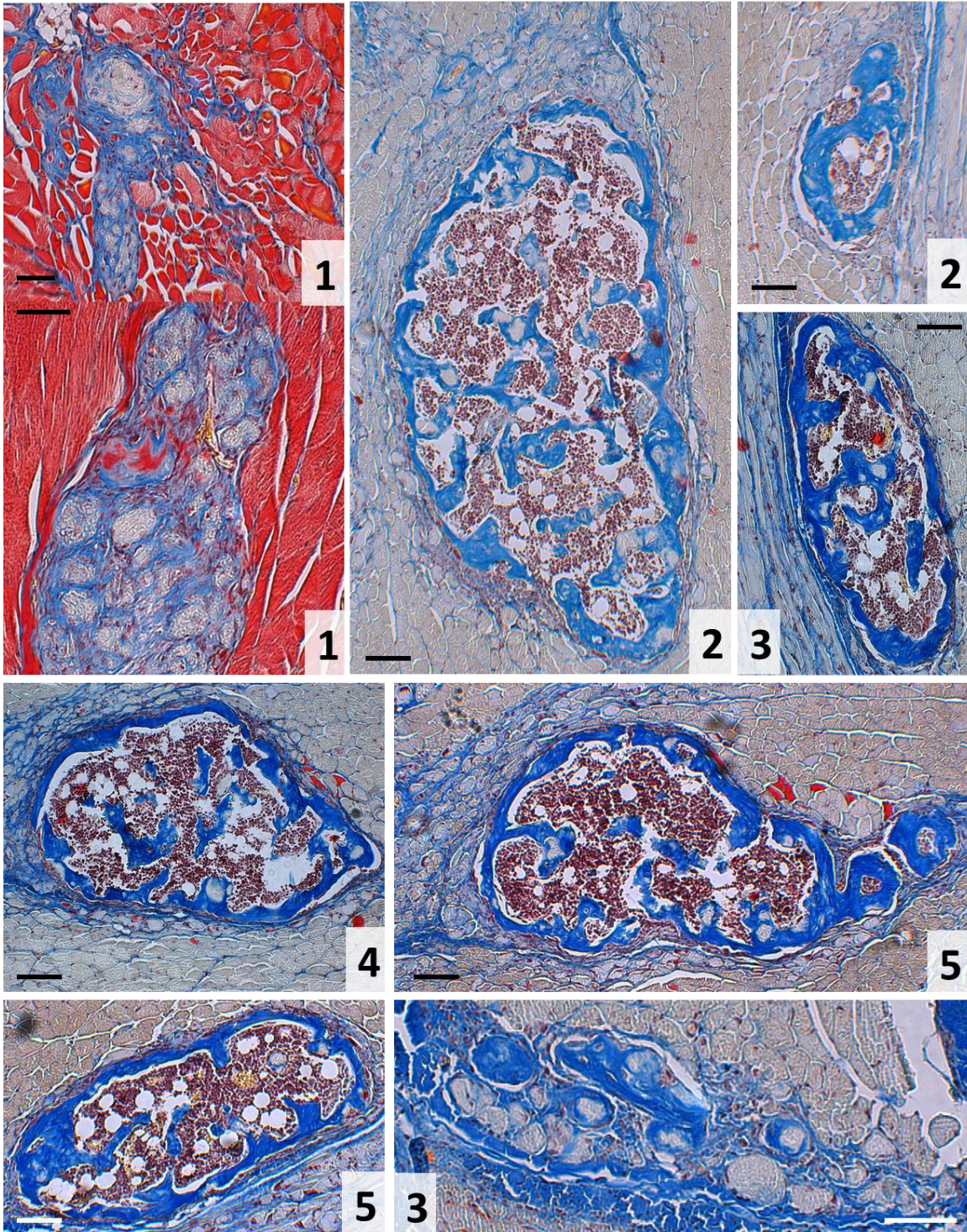


**Figure 73: Histological sampling of *Abcc6* heterozygous mice treated with control (PBS-filled) liposomes.** Histological samples stained with MSB at 28 days post injury in 5 individual mice. Number at the bottom of the image indicates the individual mouse the image was obtain from. Sections demonstrate variable levels of residual dystrophic calcification surrounded by fibrotic tissue indicated by blue staining within skeletal muscle. Phenotype was observed in 5/5 mice. No mouse demonstrated heterotopic ossification.



Scale bar represents 100µm.

*Abcc6*<sup>+/-</sup> with Clodronate Liposomes

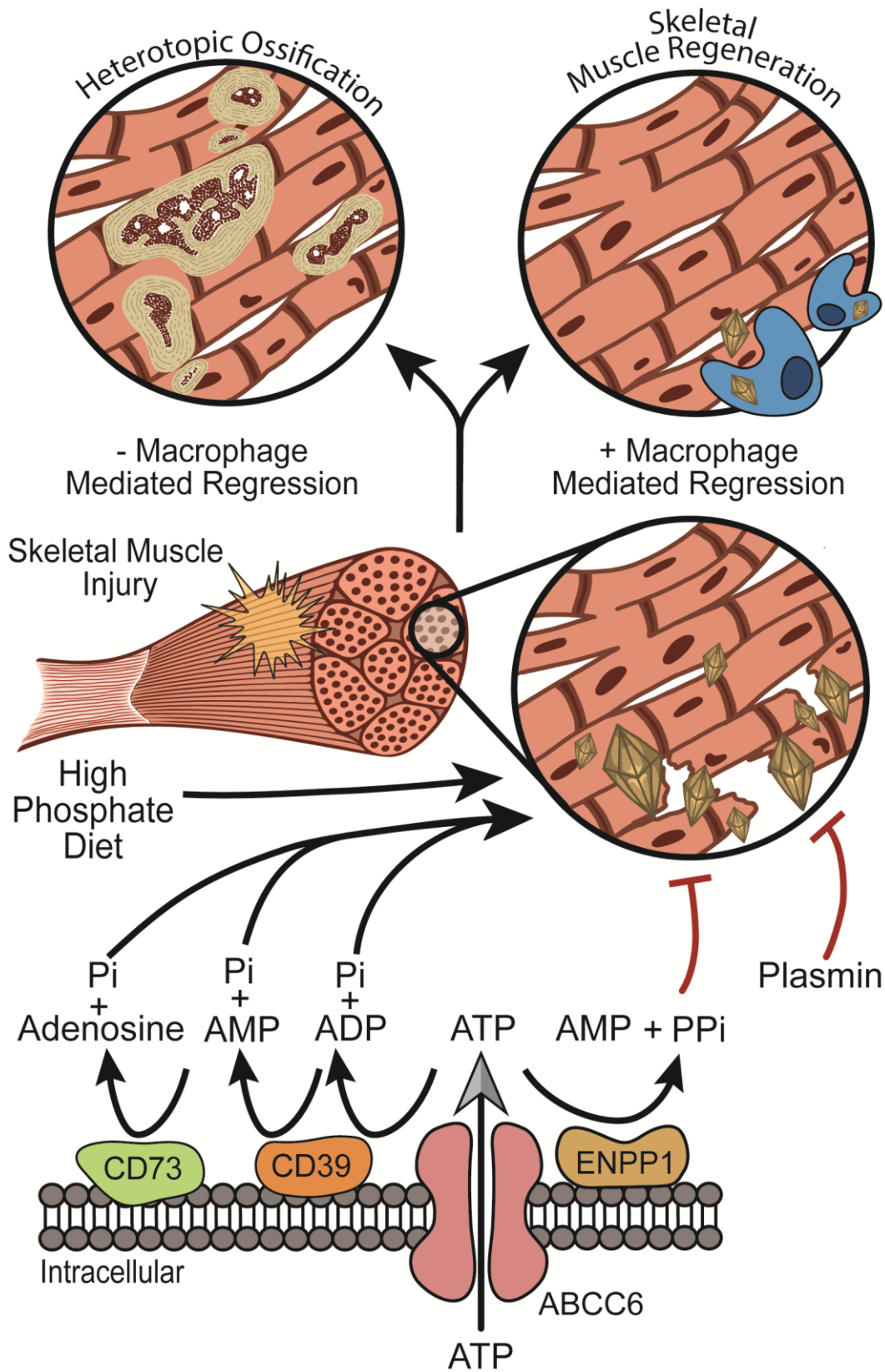


**Figure 74: Histological sampling of *Abcc6* heterozygous mice treated with clodronate**

**filled liposomes.** Histological samples stained with MSB at 28 days post injury in 5 individual mice. Number at the bottom of the image indicates the individual mouse the image was obtain from. Sections demonstrate heterotopic ossificaiton in 4/5 mice examined (mice 2-5) with one mouse demonstrating significant regions of dystrophic calcification, but no morphologically detectable heterotopic ossificaiton (mouse 1). Regions of heterotopic ossificaiton were variable in size, yet all possessed marked bone formation with central hematopoiesis. Scale bar represents 100 $\mu$ m.

### *Discussion & Conclusions*

Since proposed by Chalmers in 1975 [202], the theory that HO requires a pro-ossification stimulus within an injured soft-tissue environment has been maintained. This theory supported the search for gain-of-function mutations in soft-tissues, such as those found in the BMP pathway (i.e. FOP), responsible for cellular transformation of soft tissue cells into bone forming cells. Here, we demonstrate that a loss-of-function mutation in the cellular machinery designed to protect soft-tissue from nanohydroxyapatite deposition is an additional mechanism through which HO can form following soft tissue injury. Interestingly, we observed that as a contingency plan to the primary soft tissue protection mechanisms, macrophages efficiently resorbed nanohydroxyapatite immediately prior to myogenesis. In the absence of both synergistic soft tissue protection mechanisms (loss of both *Abcc6* and macrophage resorption), HO ensued. These findings support a potential additional paradigm in HO; that HO can result from insufficient protection against nanohydroxyapatite with a subsequent failure of macrophage-mediated resorption (Figure 75).



**Figure 75: The “Two Hit” Mechanism of HO Formation:** Taken together with previous

studies [292], our results suggest that nanohydroxyapatite can deposit within skeletal muscle following injury if one of the skeletal muscle protection mechanisms (i.e. ABCC6 or Plasmin) are insufficient or if the balance is shifted in favor of ossification by the administration of a high phosphate diet (Chapter 2). Fortunately, the body possesses a secondary macrophage-mediated clean-up crew to regress nanohydroxyapatite from damaged tissues; thereby resolving the predisposing factors to HO formation. Together, these two lines of defense are critical for preventing nanohydroxyapatite deposition within damaged tissues and its subsequent maturation to HO. These findings suggest a new paradigm for HO formation in which HO can result from insufficient protection against nanohydroxyapatite with a failure of macrophage-mediated regression.

Nanohydroxyapatite deposition within soft tissues can occur from a variety of risk factors, including both genetic and environmental (i.e. high phosphate diet) sources [259, 319, 335-349]. Here, we observed for the first time that genetic loss of *Abcc6* lead to robust deposition of nanohydroxyapatite within damaged muscle. These findings support a potential role for *Abcc6* in preventing aberrant mineralization in skeletal muscle, much akin to its activity in other soft tissues such as the skin, kidney, and cardiovascular system [313, 319, 345, 357-359]. Furthermore, while homozygous null mutations in *Abcc6* have been linked to rare calcification disorders, such as PXE, we observed that even a partial loss (*Abcc6*<sup>+/-</sup>) was sufficient to predispose skeletal muscle to nano-hydroxyapatite deposition following injury. While loss-of-function mutations of *Abcc6* such as is those seen in PXE are rare (1:50,000), an estimated 1:150-1:300 individuals are carriers for pathologic mutations in *Abcc6* [360]. Our results do not suggest that all individuals with

either partial and biallelic pathologic mutations in *Abcc6* will develop HO, they rather suggest that these individuals may be at risk for the formation nanohydroxyapatite within damaged soft tissue; which may predispose damaged skeletal muscle to ossification if persistent. Furthermore, considering that severely injured patients prone to HO formation have been reported independently to experience both deposits of dystrophic calcification and failure of macrophage function [70, 361-367], these findings together demonstrate the plausibility for this new loss-of-function paradigm of HO.

The molecular mechanisms through which ABCC6 prevents mineralized of soft tissues are not completely understood. Various groups have provided evidence that alteration to either adenosine [368-371] and/or pyrophosphate production [319, 320, 372] are responsible for the aberrant calcification observed in ABCC6 deficient animal models and patients with PXE. While *Abcc6* deficient animals develop robust skeletal muscle calcification, preliminary studies utilizing animals deficient in either CD73 or CD39, two critical components of adenosine production, demonstrated minimal skeletal calcification skin to wildtype animals following injury. These findings suggest that reduced adenosine production [373] does not predispose skeletal muscle to nanohydroxyapatite deposition. Therefore, given the numerous reports of reduced circulating PPI levels in patients with PXE and ABCC6 deficient mice [320, 352-354] and recent reports of successful administration of oral PPI to inhibit connective tissue calcification in an ABCC6-deficient murine model [374], these results together suggest that PPI production and its presence in circulation may be responsible for protecting skeletal muscle from calcification following injury. As pyrophosphate levels were not directly measured in this study, further

biochemical and enzymatic investigations will be necessary to confirm PPI direct role in protecting skeletal muscle from trauma-induced calcification.

Regardless of the mechanism, the loss of Abcc6 resulted in robust deposition of nanohydroxyapatite in the injured muscle. However, against our hypothesis, the presence of nanohydroxyapatite did not result in HO. Instead, we observed that macrophages resorb the injury-induced nanohydroxyapatite and muscle repair ensues. The essential role of macrophages in this process is highlighted by our experiments in which macrophages were eliminated using liposome-clodronate. In these experiments, not only did the nanohydroxyapatite deposition persist, but ossification ensued.

These findings are transformative in regards to the role of macrophages in HO. The presence of macrophages and inflammation within damaged skeletal muscle has long been observed, both clinically and in basic science investigations. Although debated, currently, macrophages are thought to be a driving factor of HO pathophysiology. For example, in murine models of FOP, it has been demonstrated that depletion of macrophages reduce HO in this model by ~50% [375]. Furthermore, in a preclinical model of neurological HO it was observed that ablation of macrophages reduced the size of HO by 90% [376]. Therefore, while macrophages have been demonstrated to be essential for tissue repair, they dichotomously can promote the inflammatory state, as observed in prior HO studies and conditions such as rheumatoid arthritis. Therefore, when we began our investigations, we recognized that macrophages may or may not be beneficial for proper tissue repair following the deposition of nanohydroxyapatite. Through using the same techniques of

macrophage ablation of prior HO studies, our results clearly demonstrated that the macrophages stimulated by injury and nanohydroxyapatite deposition function positively to rid tissues of dystrophic calcification, thereby prevent subsequent HO.

While prior results seem contradictory to our findings, neither of these previous models have been demonstrated to progress through a nanohydroxyapatite precursor. Therefore, we propose that role of macrophages in HO is variable and rather may be dependent upon the state of the calcification the macrophage encounter within the damaged tissue. In support of this theory, prior reports have demonstrated that macrophage-mediated regression of calcification is size and composition dependent. If in the nanometer range, macrophages can effectively phagocytose small hydroxyapatite crystals, such as those found in dystrophic calcification lesions; yet, if particles grow beyond 10 $\mu$ m, they become difficult for a single macrophage to phagocytose [335, 377]. Like size, the composition of calcification greatly impacts the macrophage phenotype and phagocytosis abilities. If the organic components of bone are present (i.e. collagen fibrils), macrophage binding and subsequent phagocytosis is inhibited [378]. Moreover, recent investigations by Villa-Bellosta *et. al.* has demonstrated *in vitro* that macrophages in the presence of high levels of phosphate adopt a M2 like phenotype and expresses elevated anti-mineralization activity dependent upon PPI production [379, 380]. Aligning these finding with our *in vivo* observations, we propose that when the macrophages encounter nanohydroxyapatite deposits within the injured skeletal muscle, the M2 like macrophages (or reparative macrophages) can respond to this calcium-phosphate rich environment, and adjust their phenotype to promote anti-mineralization activity and clearance of the calcific deposits. To

investigate this hypothesis, further investigation into the phenotype of macrophages surrounding the nanohydroxyapatite deposits is warranted. Together, these findings demonstrated that the role of macrophages in HO is potentially more dichotomous than previously believed, thus caution should be raised when considering therapeutics aimed at inhibiting macrophages for treating HO, prior to determining whether the macrophages is a driver or protector for HO in that particular pathologic state.

Previously, our laboratory demonstrated that plasmin (a powerful reparative protease) like ABCC6, protects skeletal muscle from the formation of dystrophic calcification following injury [292] (Article 6). Yet, plasmin has many additional roles during tissue repair, one of which is promotion of macrophage activity and migration. As such, in plasminogen deficient mice, we previously observed the formation of dystrophic calcification which persisted over 28 DPI and developed in HO. This observation provided the foundation for the theory that dystrophic calcification and HO, rather than being dichotomous pathologies, may rather be part of the same pathologic continuum. However, given plasmin's variable roles in tissue repair, we necessitated an additional model to isolate specific steps of the pathologic continuum. The studies presented within represent the use of ABCC6 as a directed model to examine the pathologic continuum of dystrophic calcification to HO. Aligning with the results observed in plasmin deficient animals, utilizing an isolated model, we found that the formation of dystrophic calcification, if persistent due to reduced macrophage-mediated regression, is sufficient to drive HO.

In summary, these foundational studies reveal a potential new paradigm in HO, where



persistent nanohydroxyapatite within damaged skeletal muscle as a result of a loss-of-function mutation, in conjunction with a failure of macrophage mediated resorption, is sufficient to support HO. If found to be clinically valid, this paradigm suggests that rather than being dichotomous pathologies, nanohydroxyapatite formation and HO may be part of the same pathologic continuum; thus providing a novel therapeutic advantage given that nanohydroxyapatite, unlike mature bone, can be resorbed from the damaged tissues. Furthermore, as current treatment regimens for HO, such as prophylactic drugs and radiation therapy, are focused on preventing bone formation, they likewise target physiologic bone leading to adverse effects on bone regeneration and bone health [235, 248-250]. Yet, by placing nanohydroxyapatite and HO on a pathologic continuum, this expands the number of potential pharmacologic strategies available by applying early therapeutic interventions aimed at nanohydroxyapatite in lieu of mature bone. Furthermore, early intervention at the nanohydroxyapatite level potentially allows for improved preservation of physiologic bone formation.

### Chapter 2 Summary

Here, using our novel model of dystrophic calcification formation, independent of alterations to monocyte/macrophage function or BMP, we examined the hypothesis that persistent dystrophic calcification within damaged tissue is sufficient to form an osteoinductive tissue environment sufficient to support cellular transformation and the subsequent formation of trauma-induced HO. Through this investigation, we demonstrated that the body has two lines of defense against the formation of an osteoinductive tissue environment: 1) skeletal muscle protection mechanisms like PPi and 2) macrophage

mediated clean-up of dystrophic calcification from damaged tissue. Importantly, we found if both steps are inhibited (i.e. “two hit model”), persistent dystrophic calcification is sufficient to promote the formation of HO through a chondrocyte intermediate. These findings support our initial hypothesis, thereby redefining the possible pathophysiology of trauma-induced HO formation and elucidating numerous additional therapeutic targets.

Taken together with the results of Article 6 above, we have identified three potential therapeutic targeting points to potentially prevent soft tissue calcification: 1) plasmin pathway, 2) pyrophosphate pathway, or 3) enhancement of macrophage function to regress dystrophic calcification. Importantly, when examining each of these therapies, we must also consider their impact on physiologic bone formation. This consideration becomes increasingly important when we consider trauma-induced HO as many of these patients may be suffering from concomitant fractures that necessitate physiologic bone formation at the same time we are aiming to prevent soft tissue calcification. These possible therapeutic advancements are discussed in detail in Chapter 3.

## **CHAPTER 3:**

### **Therapeutic Modulation of Trauma-Induced HO**

#### Current Practice

Given that the pathophysiology of trauma-induced HO is undefined, the development of effective therapeutics aimed at preventing or regressing trauma-induced HO have been, to date, largely unsuccessful. Specifically, current preventative and therapeutic methods, such as NSAID, radiotherapy, or surgical removal have been well studied yet are either ineffective, expensive, or have intolerable side effect profiles [224-226, 253]. Specifically, chronic NSAID use has been suggested to reduce the progression of HO through inhibition of cyclooxygenase, but patient compliance is poor and side effects (such as gastrointestinal bleeding) can be life threatening. Radiation therapy is theorized to inhibit differentiation of mesenchymal stem cells into osteoblasts, yet this treatment cannot be used effectively for patients after major trauma. When these pharmacological treatments are unsuccessful, patients possessing HO must undergo surgical resection of the aberrant mineralization. As surgical resection of HO is akin to reinjuring the affected soft tissues, HO frequently recurs following surgery if not properly timed or prophylaxed [331, 381, 382].

When these treatments are unsuccessful, chronic pain from intractable HO can become a burden on patient's morbidity. Therefore, investigating pharmaceutical treatments that are safe, inexpensive, and efficacious at preventing HO following a traumatic injury are essential to decrease the need for surgery and the burden of chronic pain. Furthermore,

given that HO forms following a traumatic injury, the ideal therapeutic would likewise not alter physiologic bone healing.

Within this chapter, we discuss two therapeutic strategies currently under investigation for prevention of HO: 1) the use of bisphosphonates and 2) BMP antagonists. As a bisphosphonate is simply a non-hydrolyzable pyrophosphate analog, application of this therapy aligns well with our findings. As such, we will examine bisphosphonate administration in our animal models, as well as experimental therapeutics aimed at improving plasmin activity and/or macrophage function as an alternative strategy to prevent the formation of dystrophic calcification and subsequently HO.

#### Bisphosphonate Treatment for the Prevention of HO

Bisphosphonates, a non-hydrolysable analog of PPI, are a powerful family of pharmaceuticals utilized by clinicians for more than 40 years to treat osteoporosis [313].

The pharmaceutical application of bisphosphonates is largely based on their ability to act as effective inhibitors of the HMG-CoA reductase pathway resulting in pleiotropic effects on cellular function, most notably attenuating osteoclast activity and reducing these cells' ability to resorb bone [383]. Therefore, one of the most common clinical applications of bisphosphonates is for the treatment of osteoporosis. However, bisphosphonates, like their parent compound PPI, also directly inhibit calcium and phosphate aggregation to prevent aberrant mineralization. In fact, application of the anti-mineralization properties of bisphosphonates precedes all others as they were first employed to “soften” public water

supplies in the 1800s thereby preventing calcification of pipes. Thus, in addition to preventing osteoporosis, the clinical application of bisphosphonates includes the prevention of aberrant calcium and phosphate aggregation in soft tissue. This latter effect, aligning well with our finding in Article 10, makes them uniquely suited for preventing trauma-induced HO.

#### *Current Supportive Clinical Investigations*

Bisphosphonates, formerly called diphosphonates, were first trialed in the treatment of HO in the 1970's [384]. Given their antimineralization function, they have since been trialed to prevent HO in patients who experience burns, traumatic brain injury, spinal cord injury, and following total hip replacements[385-388]. Through an extensive literature review, we identified 22 clinical studies where bisphosphonates were used as the primary HO treatment or prophylaxis [386, 387, 389-409]. However, six of those studies had clear inconsistencies in the patient populations, timing of treatment initiation, initiating dose, maintenance dose, route of administration, and duration of drug use. The remaining 16 studies consisted of a mixture of prospective cohort studies, retrospective cohort studies, and cases series. Eighteen of the 22 studies concluded favoring the use of bisphosphonates to prevent HO, 2 studies produced inconclusive results and 2 studies rejected the use of bisphosphonates (Table 23)

**Table 23: Review of Bisphosphonate Use for Treatment of HO.**

<b>Author, Year</b>	<b>Injury type</b>	<b>Study Type</b>	<b>N</b>	<b>Treatment</b>	<b>Dose</b>	<b>Timing</b>	<b>Duration</b>	<b>Outcome</b>
<b>Spielman, 1983</b>	BI	Cohort	20	Etidronate	20mg/kg/day 1st 3 months and 10 mg/kg/day for last 3 months	2-7 DPI	6 months	+
<b>Banavoc, 1993</b>	SCI	PCT	38	Etidronate	300mg (IV) daily for 3–5 days and 20 mg orally for 6 months.	<1 week PI	6 months	+
<b>Garland, 1983</b>	HO after SCI	Case Series	14	Etidronate	20mg/kg/day First two weeks 10mg/kg/day for 2 years	Mean 26 DPI	Mean 14 months	~
<b>Banavoc, 1997</b>	SCI	PCT	46	Etidronate	300mg/day IV for 3 days Oral 20 mg/kg/day for 6 months	Mean 27 DPI	6 months	+
<b>Banavoc, 2000</b>	SCI	Case Series	40	Etidronate	300mg/day IV for 3 days Oral 20 mg/kg/day for 6 months	unknown	6 months	+
<b>Fuller, 2005</b>	BI- HO Knee Excision	Case Series	17	Etidronate	20 mg/kg for 2 months	unknown	2 months	+
<b>Moore, 1993</b>	BI- HO Elbow and Knee Excision	Case Series	17	Etidronate	10mg/kg body weight per day for 3 months	Post-op	3 months	+

<b>Schuetz, 2005</b>	SCI- HO Excision	Case Series	5	Pamidronate	IV- 120 mg in the first 12 h and subsequent reduction to 75-60-30-15 mg/12 h over a period of 10-14 days.	Post-op	10-14 days	+
<b>Kolessar, 1996</b>	BI- HO Excision	Case Series	17	Etidronate/ Indomethacin	Indomethacin (75 mg/day) + Etidronate (20mg/kg/day) mg/kg/ day	Post-op	3 months	+
<b>Subbarao, 1987</b>	SCI- HO Excision	Case Series	5	Etidronate	20 mg/kg body weight preoperatively for 10–14 days- 10 mg/kg body weight post-operatively for at least 3 months	Post-op	3 months	+
<b>Stover, 1976</b>	SCI	RCT (treatment/ placebo)	149	Etidronate	20 mg/kg/day for two weeks, then 10 mg/kg/day for ten weeks	20-121 DPI Mean 57 DPI	12 weeks	+
<b>Ono, 1988</b>	SCI	RCT (treatment/ placebo)	80	Etidronate	1000mg once daily	Unknown	12 weeks	+

<b>Bijvoet, 1974</b>	THR	RCT (treatment/ No treatment)	44	Etidronate	20 mg per kg per day (All start 6 weeks before surgery- 7pts ended 6 weeks after surgery 13 pts ended 12 weeks after surgery)	6 weeks prior	12-18 weeks	+
<b>Finerman, 1977</b>	THR	RCT (treatment/ placebo)	99	Etidronate	20 mg/kg/day for 1 month pre-op and 3 months post- op	1 month pre-op	4 months	+
<b>Thomas, 1985</b>	THR	Prospective cohort	177	Etidronate	10 mg/kg/day 2-4 weeks pre- op and 3 months post- op for early patients; 20 mg/kg/day 2-4 weeks pre-op and 3 months post-op for later patients	2-4 wk pre-op	2-4 weeks pre-op + 3 months post op	-
<b>Yutani, 1995</b>	THR	RCT (treatment/ no treatment)	77	Etidronate	600-1000mg daily	<2 weeks before surgery	12 weeks	+
<b>Shafer, 2008</b>	Burn	RCR	57	Etidronate	600mg daily from admission to discharge	on admission	Mean 39 days	-



					(mean duration 39 days)			
<b>Tepperman, 1984</b>	Burn	Case Report	1	Etidronate	20mg/kg/day first month, 10mg/kg/day for 11 months	<1 week PI	1 year	~
<b>Peters, 1990</b>	Burn- HO excision	Case Report	1	Etidronate	20mg/kg/day first month, 10mg/kg/day for 11 months	<1 week PI	1 year	+
<b>Lippin, 1994</b>	Burn	Case Report	1	Etidronate	2mg/kg/day for 1 month 10mg/kg/day after	<1week PI	Lost to follow up	+
<b>Biering- Sorensen, 1993</b>	BI- HO Excision	Case Series	2	Etidronate/ Indomethacin	20 mg/kg/day 2 weeks pre surgery to 3 months post surgery; 10 mg/kg/day 4th month;5 mg/kg/day 5th month given indomethacin 25 mg twice daily, from 2 weeks prior to surgery to 6 weeks post surgery.	2 month pre-op	7 months	+
<b>Freed, 1982</b>	SCI	Cohort	52	Etidronate	3-6 months of treatment, variable	variable	variable	+

### *Limitation to Bisphosphonate Therapy for Treating HO*

Given these results, while some studies provided promising evidence for use of bisphosphonates in preventing HO following a traumatic injury, the current literature base overall is difficult to decipher given the variability of dosing strategies, type of bisphosphonate administered, the type of injury experienced by patients, and the variable timing of administration. In order to clearly decipher the effects of bisphosphonates for preventing trauma-induced HO, each of these factors would need to be standardized, which can be extraordinarily difficult to do in a clinical population. For example, in the prior studies highlighted in Table 25, several were confounded as they compared HO development in patients with preexisting HO or at high risk of developing HO, against patients with a lower risk of HO. Other studies had poor follow-up, and some focused on the radiographic presence of ectopic bone while others documented range of motion, inflammation, and pain.

While regulating these variables in clinical trials would be very challenging, through employing an animal model of trauma-induced HO that appropriately recapitulate the clinical condition, many of these variables can be controlled, and the data collected from the model can be standardized. As such, our lab and others have been working to develop clinically relevant models, to test therapies such as bisphosphonates. These models will be discussed in detail within Chapter 3.

Furthermore, given that bisphosphonates can inhibit bone resorption, which is a critical stage of both normal bone development and fracture healing, various bisphosphonates have

been examined clinically and in preclinical animal models regarding their influence in fracture repair. In preclinical models, bisphosphonate administration is associated with both increased fracture callus size and a delay in callus remodeling, but not with a delay in the formation of a fracture callus (Table 24). In clinical studies, short term bisphosphonates administration does not appear to have a positive or negative effect on fracture healing. However, long term administration studies have suggested that bisphosphonate may negatively influence fracture healing [410]. Therefore, in addition to testing their efficacy in preventing trauma induced HO, we must also simultaneously consider their impact on fracture healing. To assess both of these factors simultaneously, we have developed murine models of trauma induced calcification (genetic- plasminogen, ABCC6, etc; environmental- high phosphate diet; and traumatic injury- burn model) that can be combined with our model of fracture repair to assess the simultaneous effects of bisphosphates of pathologic and physiologic bone formation.

First, I will highlight our investigations of bisphosphonate administration for the prevention of dystrophic calcification and subsequently HO in our models of trauma induced calcification. From this foundation, we will next discuss their localization and physiologic effects when administered at different times post injury in a combined model of fracture repair and skeletal muscle calcification (Article 11).

**Table 24: Literature Review of Bisphosphonate use in Fracture Healing**

Author, Year	Animal Model	Stabilized or Unstabilized	Treatment	Administration Parameters	Analysis Time Point	<i>Effect on Fracture Healing</i>		
						Fracture Union	Callus Size	Callus Remodeling
<b>Hyvonen et al., 1994</b>	Rat, 16 week old Sprague Dawley Female	Closed Femur fracture (unstable)	Clodronate	0, 3, 10, 30 mg/kg Clodronate S.C Daily (Possibly beginning at time of injury)	1, 2, 3, 4, 8, 12, and 22 weeks post fracture	No Change	No Change (measure histologically)	Inhibited Remodeling (histological Analysis)
<b>Nyman et al., 1993</b>	Male (Adult) Albino-Original Rat	Bilateral Tibial Fracture with Fixation	Clodronate	50mg/kg S.C weekly beginning at the time of Fx	1, 2, 3, 4, 5, and 8 weeks post fx	No change	No change in area but increased weight	No change
<b>Koivukangas et al., 2003</b>	Female 3 month old Sprague Dawley Rats	Tibial fracture with intramedullary nailing	Clodronate	2mg/kg of 10 mg/kg S.C. twice a weeks for 24 weeks and then continuing past fracture for either 4 or 8 weeks	4 and 8 weeks post injury	No Change	Increased Callus size	N/A
<b>Nyman et al., 1996</b>	Male Albino-Original rats (Adult)	Tibial double osteotomy with fixation	Clodronate	Daily S.C for 6 weeks	6 weeks post fracture	No Change	Increased Callus	Delayed mineralization of bone matrix and inhibited

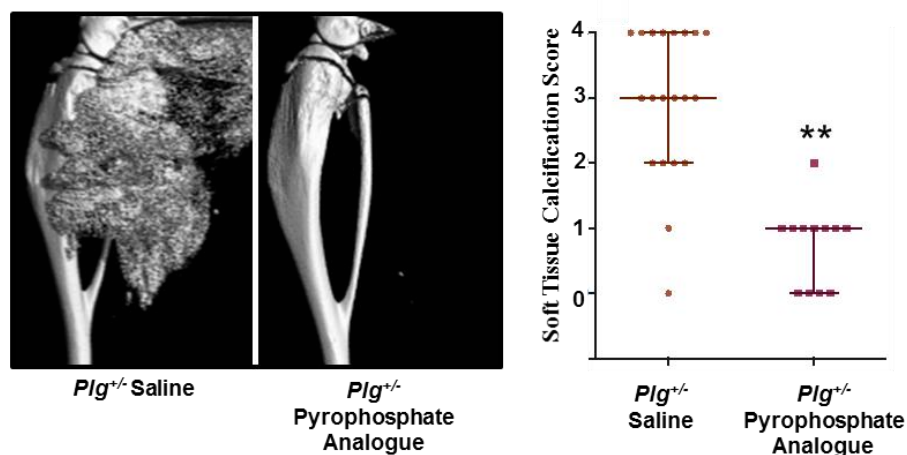
							osteoblast differentiation		
<b>Madsen et al., 1998</b>	Male 12 week Wistar Rats	12 old	Tibial Fracture stabilized by intramedullary nailing	Clodronate	Administered daily for 28 days before and after Fx (10mg/kg/d)	4 weeks	N/A	No Change	N/A
<b>Tarvainen et al., 1994</b>	Female Osteopenic Rat		Closed femur fracture, Stabilized	Clodronate	10/mg/kg/ day S.C beginning one day following injury and continuing throughout study	2, 4, 8, and 12 weeks post fracture	Impaired Union	Increased Callus	Delayed remodeling
<b>Peter et al., 1996</b>	Male and Female Mature Beagle Dogs		transvers mid- diaphyseal fracture of the radius, stabilized by splinting	Alendronate	2mg/kg/day for 9weeks before fracture, 16 weeks after fracture or both for a total of 25 weeks	16 weeks following Fx	No Change	Larger Callus in dogs that received drug during healing period	Impaired Remodeling but no effect on bone formation or mineralization
<b>Li et al., 2001</b>	Female Sprague Dawley rats, 6 week old		Femur fracture and fixed with intramedullary wires	Incadronate	Inject three times per week of either 10ug/lg or 100ug/kg two weeks before Fx and then either stopped	2 weeks and 4 weeks after fracture	N/A	Increased Callus at 4 weeks post Fracture	Resorption Decreased (change in osteoclast number)

						or continued through study				
<b>Li et al., 1999</b>	Female Sprague Dawley Rat, 6 week old	Femur fracture and fixed with intramedullary wires	Incadron	ate	10ug/kg or 100 ug/kg two times a week for two week before injury. Treatment was either then stopped or continued	6 and 16 weeks post fracture	Impaired at 6 week no change at 16 weeks	Larger Callus both 6 and 16 weeks	Delayed remodeling in pretreatment group but reach similar levels at 16 weeks	
<b>Lenahan et al., 1985</b>	Female Mature Bengal Dogs,	Radial Fracture, Stabilized with plaster splint	Etidronic Acid		S.C 0.2, 0.5, 5.0 mg/kg/day for 20weeks. On drug 8 weeks before fx	12 weeks following Fx	Impaired at high dose (5.0mg/kg/d)	N/A	Disrupted Remodeling at high dose	
<b>Amanat et al., 2005</b>	Wistar Rat, 12 week old males	Femur Open Osteotomy Fixed with K wire	Pamidronate		Bolus; 3mg/kg time surgery Local Administration via coating K wire with 0.1mg/kg or 1.0 mg/kg	S.C at post osteotomy or y	6 week	Impaired union in 3/10 high local dose group	Increased Volume in all groups	Delayed Remodeling
<b>Amanat et al., 2007</b>	Male Wistar Rat 8-9 Weeks old	Close Femur Fracture Model, Fixed with K wire	Carbon-14 Labeled Zoladronic Acid		Local Injected to fracture gap at surgery (0.01 mg/kg) or systemic of	6 week post Fx	N/A	Increased callus volume (largest with 2w	delayed remodeling at 6w	

					(0.1mg/kg) IV at the time of fracture, 1w post or 2w post		post dose0			
<b>Greiner et al., 2009</b>	5 month old Sprague Dawley Rat (unknown Male or Female)	Tibia Fracture Stabilized with k wire	Zoledronic Acid	Local Administration on coated Implant (k wire)	6 weeks and 12 weeks post fracture	Increased Bridging at 6 weeks	Increased at both 6 and 12 weeks	Delayed at 6 weeks, same at 12 weeks		
<b>McDonald et al., 2008</b>	Male Wistar Rat, 9 weeks of age	Femur; Stabilized	Zoledronic Acid	Bolus; 0.1mg/kg or 5 Weekly Doses; 0.02 mg/kg	6 and 26 weeks post fracture	No Change	Increase; Increase	No Change; delayed in weekly doses		
<b>Menzdorf et al., 2016</b>	Female Wistar Rat (unknown age)	Femur; Stabilized	Pamidronate	Local Administration on Collagen Matrix; 0.6 mg/kg	14 days or 28 days post fracture	N/A	Slight Increase; Increase	N/A		

### *Bisphosphonate Administration to Prevent Skeletal Muscle Calcification*

Within Article 6, we demonstrated that plasminogen is a critical skeletal muscle protection mechanism against trauma-induced calcification. Given our findings in Article 10 of pyrophosphate likewise protecting skeletal muscle from calcification following injury, and the support of numerous bisphosphonate studies being investigated clinically, we investigated if administration of zoledronic acid prior to injury was sufficient to protect plasminogen deficient mice from skeletal muscle calcification following injury (Figure 76). Through these experiments, we observed that if administered prior to injury, the bisphosphonate zoledronic acid (pyrophosphate analogue) was sufficient to significantly reduce the amount of skeletal calcification in plasminogen heterozygous mice by 7 days post injury. By 28 DPI, when analyzed by histological analysis, 0/5 mice treated with the bisphosphonate possessed HO within their injured tissue, yet in saline treated plasminogen heterozygous mice, 5/6 mice demonstrated marked HO (\*,  $P < 0.05$ )



**Figure 76: Bisphosphonate Treatment Prevents Soft Tissue Calcification in the Setting of Plasmin Deficiency and Muscle Injury.**  $\mu$ CT reconstructions and STiCSS Scores of lower limb of CTX-injured *Plg*<sup>+/-</sup> mouse pretreated with bisphosphonates

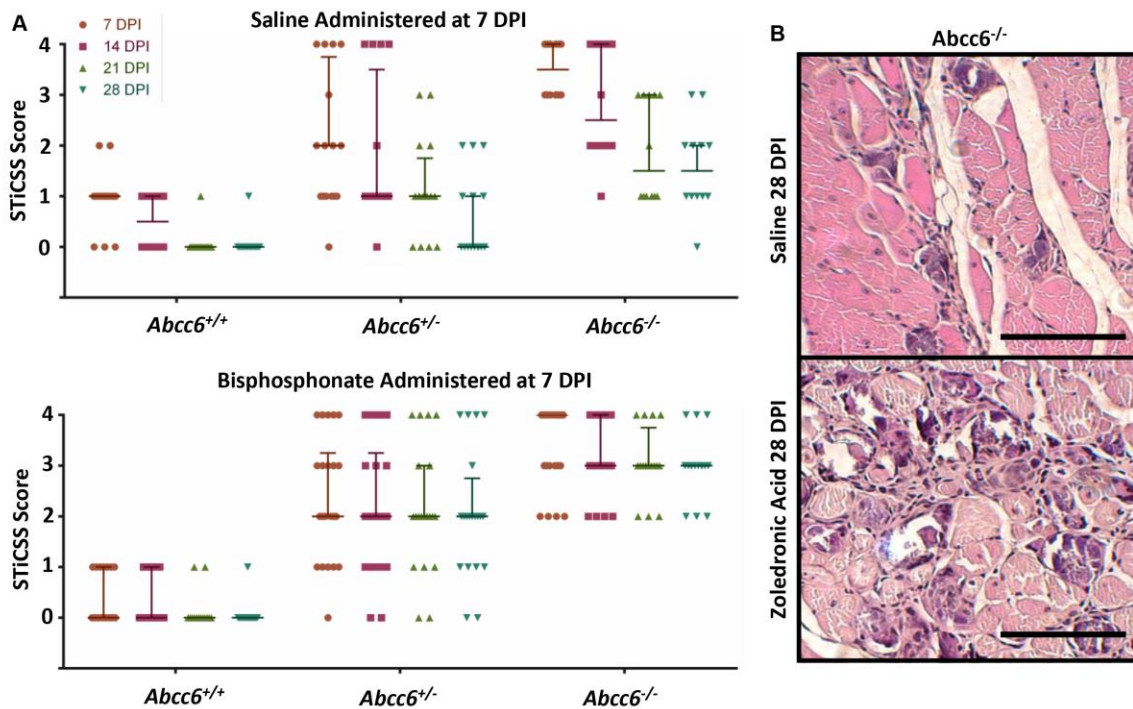


(pyrophosphate analogue) demonstrated marked reduction of soft tissue calcification compared to controls 7 DPI. Medians and interquartile ranges are shown. ( $N \geq 12$ ; \*\*  $P < .001$ , Mann-Whitney test; see Supplemental Table-5 for further statistical evaluation).

Building upon these successful results, we likewise assessed the effectiveness of administering zoledronic acid to mice deficient in ABCC6, and presumably pyrophosphate. Through these studies we investigated both the administration of bisphosphonates prior to injury (Figure 77) as well as at 7 DPI when calcification was already radiographically evident (Figure 78). When administered prior to injury, we observed only a mild decrease in the amount of calcification at 7DPI in ABCC6 heterozygous and homozygous knockout animals. While the type, timing, and amount of bisphosphonate administered was the same between Figures 77 and 78, we observed more effective reduction in plasminogen heterozygous mice treated with bisphosphonates. I hypothesize this difference may be in response to the remaining available mechanisms. In plasminogen heterozygous mice, half the activity of plasmin, as well as in theory the complete pyrophosphate system is still intact. Therefore, when bisphosphonates are administered, it may supersaturate the pyrophosphate system in conjunction with partial plasmin activity. Alternatively, in the ABCC6 deficient animals, while the plasminogen system is in theory still intact, the pyrophosphate system is either partially or completely diminished. As such, bisphosphonate administration is not sufficient to raise this activity to a supersaturated level, as in the plasminogen deficient mice, and therefore we observed only a partial rescue.



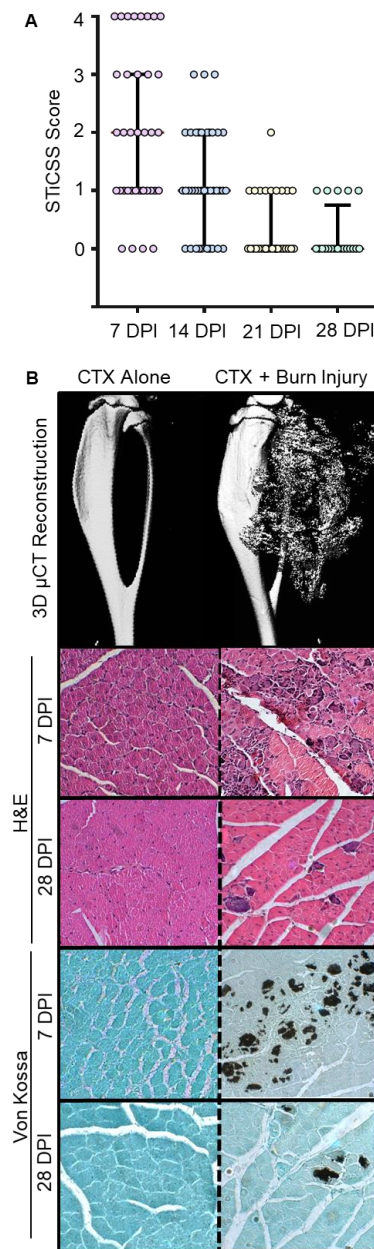
Next, we assessed the effects of bisphosphonates if they were administered at 7 DPI, once calcification was already radiographically evident (Figure 78). Previously, in *in vitro* experiments, bisphosphonates had been demonstrated to stabilize calcification through arresting the growth of calcific deposits yet simultaneously impairing their cellular-mediated regression. Aligning with these prior investigations, when administered to either ABCC6 heterozygous or homozygous knockout animals, we observed marked inhibition of dystrophic regression through 28 DPI. Interestingly though, while the calcification was present for an extended time in the damaged tissue, unlike the finding of Article 10, we did not observe the maturation of dystrophic calcification to HO. These results suggest that bisphosphonate administration once dystrophic calcification is present within damaged tissues can indeed stabilize the crystal and impair skeletal muscle regeneration, yet this persistent calcification is inhibited from ossifying to form HO (Figure 78).



**Figure 78: Bisphosphonate Administration Stabilized Dystrophic Calcification and Impedes Regression.** A) Longitudinal STiCSS analysis of mice treated with either saline or a bisphosphonate (zoledronic acid, 200 ug/kg) weekly beginning at 7DPI demonstrated marked inhibition of skeletal muscle calcification regression over 28 DPI. B) H/E histological analysis of *Abcc6*<sup>-/-</sup> mice at 28 DPI with or without bisphosphonate treatment. Scale bar represents 100um.

Finally, in addition to testing the use of bisphosphonate in our genetic models of trauma-induced skeletal muscle calcification, we likewise investigated their application in our traumatic injury model of burn. In this mouse model, we inflict a 20% total body surface area burn to the dorsum of the mouse in conjunction with a focal muscle injury to the lower extremity to direct skeletal muscle calcification. This mode was developed to recapitulate the clinical scenario of burn patients developing HO

following injury (Figure 76). Specifically, by 7 days post the combined burn and skeletal muscle injury, we observed marked skeletal muscle calcification in wild type C57/BL6 mice which progressively regressed over 28 DPI. Importantly, when a skeletal muscle injury is applied to wildtype mice, independent of the burn, we do not observe any skeletal muscle calcification (Figure 79)

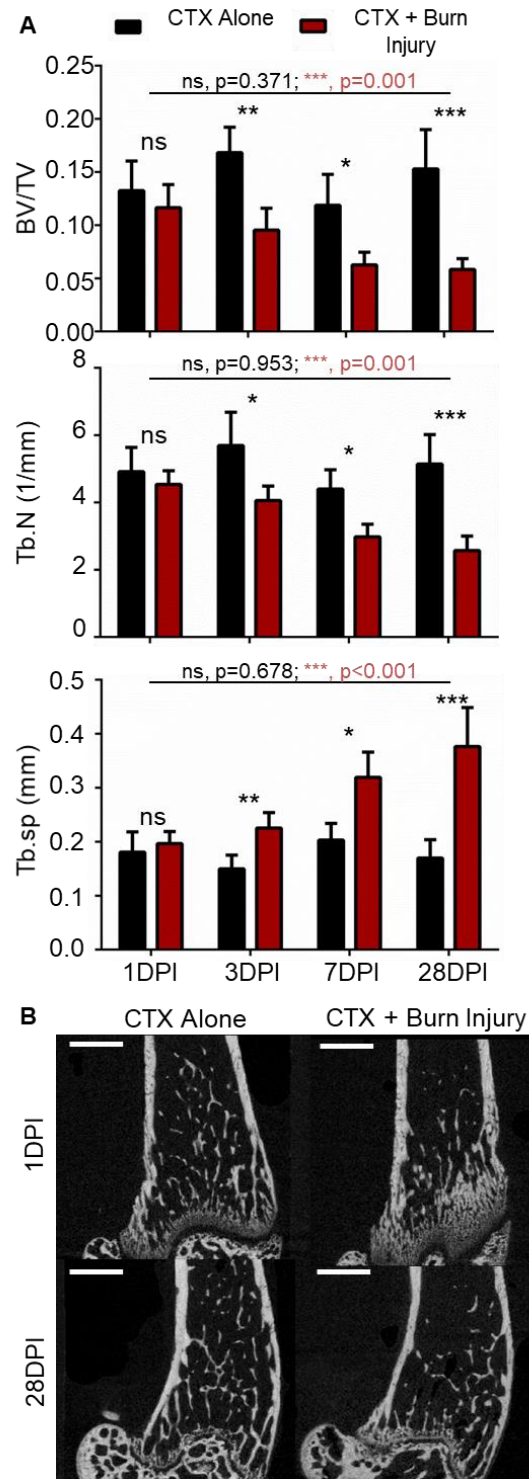


**Figure 79: Burn-induced Skeletal Muscle Calcification Model.** Following a

combined burn and skeletal muscle injury, we observed marked skeletal muscle calcification at 7DPI that progressively regressed by 28 DPI as evident by radiographic (A) and histological analysis (B).

Furthermore, in this model, we were likewise able to detect burn induced osteoporosis (Figure 80). While thermal injury causes a variety of systemic derangements clinically, one of the more paradoxical clinical observations is the dysregulation of mineralization, in which patients can experience both a loss of mineralization from the skeleton (burn-induced osteoporosis) and a gain of mineralization in soft tissues such as the skin and skeletal muscle (HO) [411, 412]. Together, dysregulation of mineralization following a severe burn significantly impacts patient outcomes given that burn-induced osteoporosis increases the potential for fragility fractures, delays rehabilitation, and also increases mortality from prolonged hospital stays. Likewise, the development of aberrant calcification within soft tissues such as skeletal muscle can result in pain, joint dysfunction, and in severe cases, necessitate amputation of the effected limb.

Despite observing both bone loss and soft tissue calcification following thermal injury clinically, few studies have explored the association between these two complications[412]. As such, observation that our murine model of burn injury experience both of these complications in a temporally related manner open the possibility for future investigations elucidating whether these two pathologies are indeed related (Figure 80).

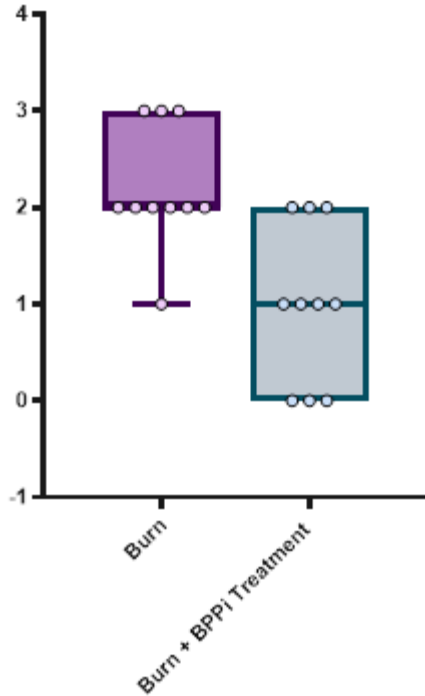


**Figure 80: Following burn injury, mice experience detectable burn induced osteoporosis within 3 days post injury. In mice receiving a combined dorsal burn**

and focal skeletal muscle injury, we observed marked bone loss characterized by a decrease in bone volume/ total volume (BV/TV; CTX Alone (N=5)-  $0.168 \pm 0.024$ ; Burn + CTX (N=6)-  $0.095 \pm 0.021$ ), trabecular number (Tb.N (1/mm); CTX Alone (N=5)-  $5.69 \pm 0.994$ ; Burn + CTX (N=6)-  $4.06 \pm 0.430$ ), and a corresponding increase in trabecular space (Tb.Sp (mm); CTX Alone (N=5)-  $0.150 \pm 0.026$ ; Burn + CTX (N=6)-  $0.225 \pm 0.029$ ) beginning at 3 DPI. Further analysis at 7 and 28 DPI indicated progressive bone loss of the distal femur in mice that received a combined burn and focal skeletal muscle injury, yet no significant change bone in mice receiving only a focal skeletal muscle injury.

Given the phenocopied nature of our murine model of burn injury to the clinical scenario, we aimed to investigate if the administration of bisphosphonates, specifically zoledronic acid, was effective at preventing skeletal muscle calcification and/or trauma induced osteoporosis (Figure 81 and Figure 82). When administered prior to injury, akin to the results observed in plasminogen and ABCC6 deficient mice, we observed a significant reduction in the amount of calcification at 7DPI (\*\*,  $p=0.005$ ) (Figure 82).



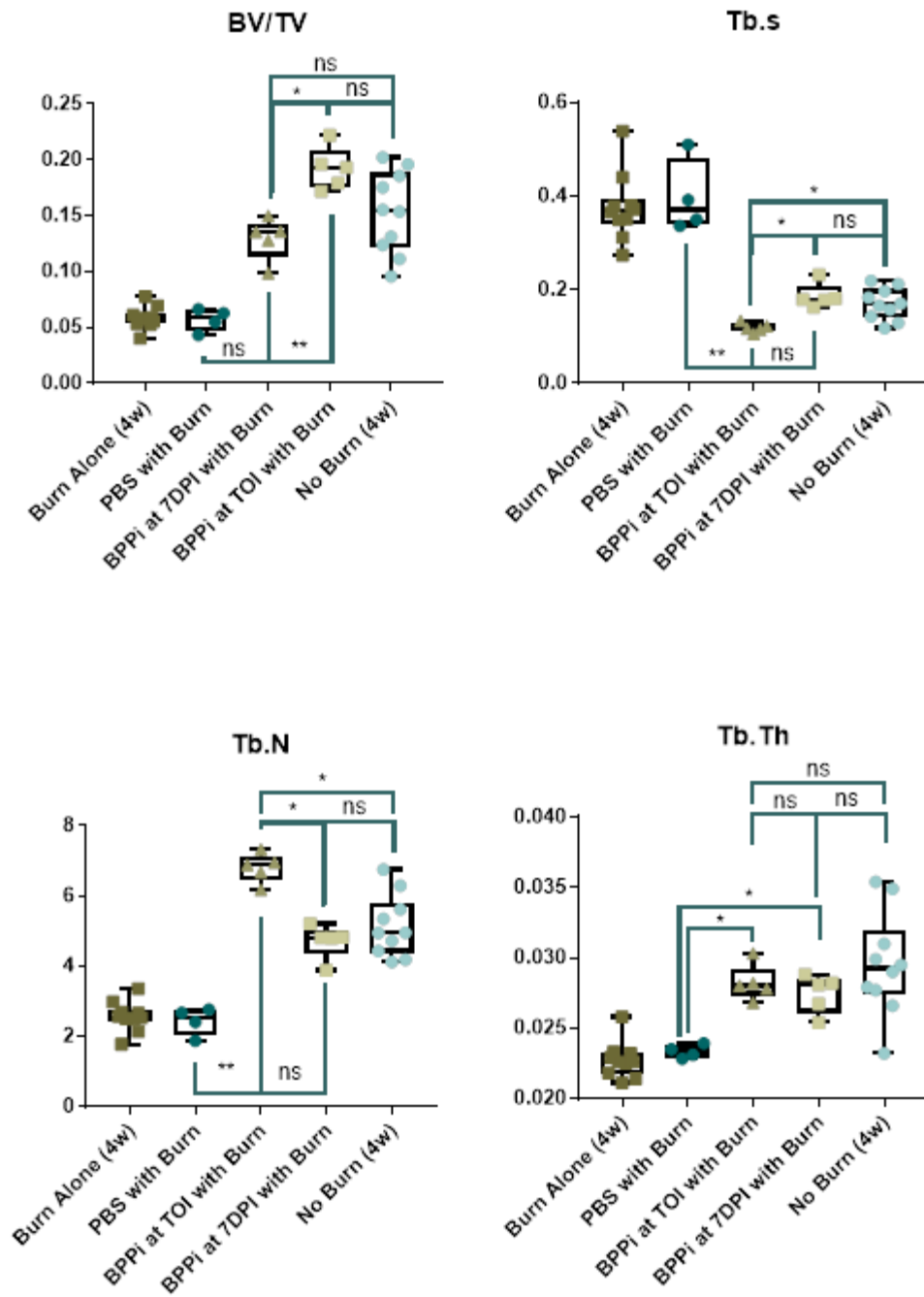


**Figure 81: Bisphosphonate administration prior to burn injury effectively reduced skeletal muscle calcification present at 7 DPI.** In our combined burn + skeletal muscle injury model, when zoledronic acid (200mg/kg, weekly) was administered prophylactically beginning two weeks prior to injury, we observed a significant reduction in the development of skeletal muscle calcification at 7 DPI as measured by radiographic analysis.

When assessed for its ability to reduce trauma induced osteoporosis, bisphosphonates were administered to our combined burn + skeletal muscle injury model either at the time of injury or at 7 DPI. These time points were selected due to their clinical relevance, as while effective, prophylactic administration of bisphosphonates may only be useful in conditions of elective surgery, such as a total hip replacement, and not for traumatic injury which are unexpected. Through  $\mu$ CT analysis of the distal

femurs, we observed that bisphosphonate administration at either the time of injury or at 7 DPI positively influence the bone structure, resulting in increased BV/TV ratio, decreased trabecular space (Tb.S.), increase in trabecular number (Tb.N.), and an increase in trabecular thickness (Tb.Th) (Figure 82).

Taken together with our prior results, these findings suggest the bisphosphonates may serve as an effective therapeutic to prevent skeletal muscle calcification if administered immediately following injury; yet bisphosphonate administration may negatively influence dystrophic calcification regression if administered once calcification is radiographically evident. Alternatively, we observed an improvement in bone structure following the burn injury independent of the timing of administration. These results demonstrate the importance of timing for bisphosphonate administration. Given that bisphosphonates preferentially localize to areas of active bone formation, it has long been hypothesized by physicians that the timing of bisphosphate administration following traumatic injury will greatly impact their therapeutic effectiveness. The results presented to this point align well with this hypothesis, yet further investigation in Article 11, where we combined our skeletal muscle injury model, fracture model, and bisphosphonate administration together, specifically demonstrates how the timing of bisphosphonate administration following injury greatly influences the drug's localization as effect on both prevention of skeletal muscle calcification and fracture repair.



**Figure 82: Administration of bisphosphonates improved the osteoporotic phenotype observed in mice following a burn injury to levels comparable of non-burned animals.** When zoledronic acid (200mg/kg) was administered either at the

time of injury (TOI) or at 7 DPI we observed improvement in the bone parameters akin to non-burned levels (BV/TV, Tb.S, Tb.N, Tb.Th) at 28 days post injury compared to vehicle treated burned animals. \*  $p < 0.05$ , \*\*  $p < 0.01$ . ns= non-significant.

Article 11: Temporal-Spatial Localization of Bisphosphonates in a Combined Musculoskeletal Injury Model

Masanori Saito<sup>^</sup>, **Stephanie N. Moore-Lotridge**<sup>^</sup>, J. Patton Robinette, Satoru Egawa, Breanne HY. Gibson, Yael Ihejirika, Sasidhar Uppuganti, Jeffrey S Nyman, & Jonathan G Schoenecker\*

\*To whom correspondence should be directed

<sup>^</sup>indicated that the authors contributed equally

*Manuscript preparation in progress*

*Introduction*

As discussed above, bisphosphonates bind with high affinity to newly forming hydroxyapatite[383, 413]. It is therefore hypothesized that the anatomic distribution of bisphosphonates will rapidly change during fracture repair; thereby altering the biology of fracture repair and the systemic therapeutic benefit of the medication. Because of this, many physicians and surgeons question the appropriate time to start bisphosphonate therapy after fractures or osteotomies associated with surgical procedures.

Currently, there are no guidelines that stipulate an appropriate time to begin bisphosphonate therapy after a fracture, though many anecdotal reports from both practicing endocrinologists and orthopaedic surgeons suggest a waiting period of two

to six weeks following fracture, due to a loss of the systemic therapeutic benefit. Aligning with this strategy, prior studies showed that treatment of hip fracture patients with intravenous bisphosphonate within 2 weeks post fracture, negated the benefit in mortality and fracture reduction compared to patients who received bisphosphonate between 3 and 12 weeks post fracture due to the hypothesized tropism of the bisphosphonate for the healing fracture site rather than systemic bone [414-416]. Yet, no prior study has been able to directly visualize the tropism of the bisphosphonate molecule for the fracture site instead of the systemic bony skeleton, nor have any prior studies directly examined the effects of bisphosphonate administration at different time points relative to time of fracture fixation on size of the fracture callus, fracture callus remodeling, and time to fracture union.

The question of appropriate bisphosphonate timing becomes even more difficult in the setting of traumatic injury. Aside from trauma-induced fractures, traumatic events such as severe burn, blast, neurologic injury, or major orthopaedic procedures can induce soft tissue calcification at the time of injury. Though primarily utilized as anti-resorption therapy since their introduction to the market in the late 1960s, the first studies on bisphosphonates were focused primarily on the anti-mineralization properties of the drug. Therefore, bisphosphonates have also been suggested as a therapeutic option for the treatment of soft tissue calcification (Table 23).

Similar to fracture healing, bisphosphonates are also hypothesized to have temporal and spatial tropism that can affect soft tissue calcification, such that, if administered

once soft tissue calcification is present, the drug can bind and stabilize the formed hydroxyapatite crystal, thus preventing soft tissue calcification regression. Like fracture healing above, no prior studies have investigated the temporal-spatial tropism of bisphosphonates in regards to soft tissue calcification and subsequent regression following traumatic injury; therefore currently, no clinical guidelines exist for bisphosphonate use in patients at risk for soft tissue calcification.

Given the dichotomous need following traumatic fracture to both mineralize the site of the healing fracture, yet simultaneously regress the calcification present in soft tissues to allow for proper healing, we developed a novel murine model of concurrent fracture and soft tissue calcification. With this model, we assessed the temporal-spatial tropism of bisphosphonates at different time points relative to time of injury and subsequent longitudinal effects on fracture healing and regression of soft tissue calcification concurrently.

### *Methods*

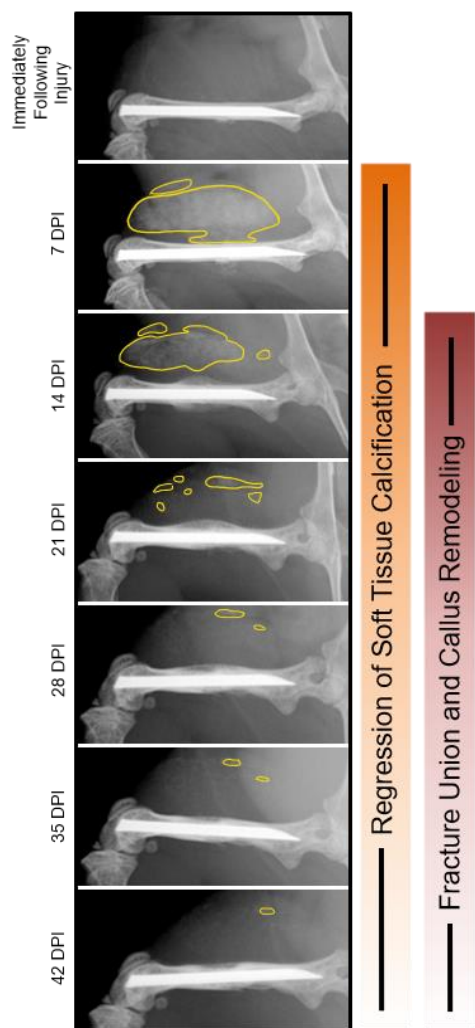
All animal procedures in this protocol were approved by the Vanderbilt Institutional Animal Care and Use Committee (M1600231 and M1600225). Male 6-week-old BALB/cJ mice were purchased directly from The Jackson Laboratory (Bar Harbor, ME) for use in these studies. BALB/cJ mice were selected for these experiments given their previously described predisposition to soft tissue calcification following injury.

### *Combined Murine Fracture + Cardiotoxin Skeletal Muscle Injury*

At 8 weeks of age, male BALB/c mice received a cardiotoxin muscle injury followed by a transverse midshaft femur fracture [29, 253, 298]. Briefly, mice were anesthetized with Isoflurane, the fur overlying the medial thigh was removed, and the skin was prepped with betadine prior to making a 10 mm long incision overlying the midshaft of the femur. Once exposed, a cardiotoxin-induced skeletal muscle injury was induced in the quadriceps by injecting 40uL of 10um cardiotoxin (Accurate Chemical and Scientific Corp, Westbury, NY). Following cardiotoxin injury, a transverse femur fracture was induced and fixed with a 23-gauge needle [29]. The incision was then closed with 4-0 nylon sutures and mice were provided analgesia every 12 hours for 3 days post-surgery.

Longitudinal analysis by radiographic imaging was utilized to assess both soft tissue calcification and fracture healing. Figure 83 demonstrates the standard longitudinal course of fracture healing and regression of soft tissue calcification observed in this model.





**Figure 83: Standard Fracture Healing and Soft Tissue Calcification in murine combined injury model.** Longitudinal radiographic analysis was utilized weekly beginning at the time of injury to assess the temporal pattern for fracture healing and regression of soft tissue calcification following injury in our combined model. *Fracture Healing:* Beginning at 14 DPI, a radiographically opaque fracture callus was observed. By 21 DPI, marked calcification of the callus had begun, resulting in bony union which remodeled over 42 DPI. *Soft Tissue Calcification Regression:* Following skeletal muscle injury, we observed marked soft tissue calcification within the

quadriceps musculature at 7DPI (yellow outline). Through serial radiographic imaging, we observed progressive regression of the soft tissue calcification over 42 DPI with minimal calcification present by 28 DPI.

#### *Therapeutic Administration*

Zoledronic Acid (ZOL), a nitrogen containing bisphosphonate, was administered subcutaneously at 200 ug/kg/week. Bisphosphonates were administered using either a continuous weekly dose or a single dose strategy. Sterile saline was administered at equal volume/weight as a vehicle control.

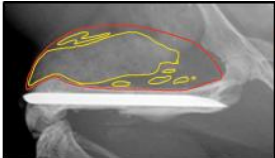

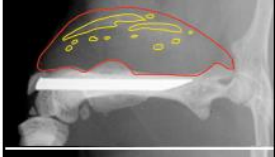
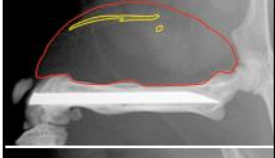

Continuous dosing strategy: ZOL was administered weekly either 1) beginning 7 days prior to injury and at the TOI, or 2) beginning at 7 DPI and continuing through 42 days post injury. Single dose strategy: Single doses of ZOL were administered beginning at 7, 14, 21, 28, or 35 days post injury.

#### *Experimental Outputs: Radiographic Analysis*

Digital radiographic imaging was utilized longitudinally to assess both fracture healing and skeletal muscle calcification. Following adequate anesthesia, mice were placed in the prone position with hips in abduction, allowing for external rotation of the limb and reproducible placement of the injured femur at a 90 degree angle to the tibia. Single plane radiographic images were collected at an exposure of 4 seconds at 35kV (Faxitron LX 60) and saved as DICOM (.dcm) files for image quantification of either the skeletal muscle calcification or the fracture healing.

*Modified Soft Tissue Calcification Scoring System Scale*

The soft tissue calcification scoring system (STiCSS) is an ordinal scoring system previously developed by our lab to longitudinally quantify skeletal muscle calcification from digital radiographic images (Article 7). This ordinal scoring system, which was first designed for use in the gastrocnemius and soleus muscles, was modified for use in the quadriceps (Figure 84). The modified STiCSS was used throughout to longitudinally quantify skeletal muscle mineralization of the quadriceps adjacent to the transverse femur fracture.

4		Greater than 75% Mineralization of the Quadriceps
3		50-74% Mineralization of the Quadriceps
2		25-49% Mineralization of the Quadriceps
1		Less than 25% Mineralization of the Quadriceps
0		No Mineralization of the Quadriceps

**Figure 84: Modified Soft Tissue Calcification Scoring System for use in Quadriceps.** Images represent an ordinal scale from 0-4, with “4” representing robust

mineralization of greater or equal to 75% of the visible quadriceps area becoming mineralized, “3” representing 50-74% mineralization of the visible quadriceps, “2” represent 25-49% mineralization of the visible quadriceps, “1” representing less than 25% mineralization of the quadriceps, and 0 representing no visible mineralization within the quadriceps.

### *Quantification of Fracture Healing*

Fracture healing is a series of events in which soft and hard tissue calluses and revascularization occur dynamically. While, many methodologies have been proposed to quantify fracture healing in animal models, here we utilized a previously validated scaling system (Article 8), using plain digital radiographs that align with changes in soft to hard tissue callus during fracture repair.

### *Fracture Healing Scoring System*

Fracture healing was monitored using radiographic analysis and a validated scoring system based on bone formation, fracture union, and callus remodeling from 7 to 42 days post-fixation. Briefly, each criteria was scored as either “0” indicating “does not meet the criteria” (i.e. not present/visible on the radiograph) or “1” indicating that the criteria was met and is present by radiographic analysis. Operational definitions for each criteria point are as follows: 1) Bone Formation; 0 point: no apparent hard tissue callus formation, 1 point: apparent hard tissue callus formation. 2) Bone Union; 0: an existence of no mineralization between hard tissue calluses, 1: continuity of mineralization. 3) Bone Remodeling; 0: no apparent shrinkage in the size of hard

tissue callus compared to maximum size of hard tissue callus, 1: apparent shrinkage in the size of hard tissue callus compared to maximum size of hard tissue callus. This scoring criterion was employed for both the superior (area 1) and inferior sides (area 2) of the femur resulting in a maximum score of 6 and a minimum score of 0 per image. We computed the inter-observer errors of the fracture healing scoring system and found that, using the Landis and Koch criteria, examiners were in moderate to almost perfect agreement (Kappa= 0.5437 to 0.8388) at all time points assessed (Table 25).

**Table 25: Analysis of inter-observer variation between 7 independent observers.**

Observers were found to be in moderate to almost perfect agreement by Landis and Koch criteria at all time points assessed (Kappa= 0.5437 to 0.8388).

Supplemental Table 5: Interobserver Error Kappa Statistics							
Observer	A	B	C	D	E	F	G
A		0.738	0.631	0.619	0.839	0.651	0.766
B			0.587	0.545	0.779	0.556	0.678
C				0.544	0.686	0.659	0.645
D					0.559	0.525	0.544
E						0.679	0.779
F							0.762
G							

### *Histological Analysis*

Following sacrifice at the designated time point, samples were fixed with 10% neutral buffered formalin for a minimum of 4 days and decalcified with 0.1M EDTA until the

bone was no longer radiographically evident (~7 days). Samples were then transferred to 70% ethanol and processed in graded series of ethanol, cleared, and embedded into paraffin prior to sectioning. 6um sections were made either in the transverse or sagittal plane and prepared for staining.

Hematoxylin and Eosin (H&E) staining was performed according to standard protocols. Briefly, sections were deparaffinized, stained in Gills 3 hematoxylin solution for 10 minutes, rinsed in tap water for 10 minutes, and differentiated with 1% acid alcohol for 10-15 seconds. Slides were then immediately rinsed in running tap water for 10 minutes and dehydrated in 70% and 95% ethanol for three minutes each. Finally, slides were stained with eosin for 3 minutes, dehydrated, and cleared in xylene before mounting with Permount.

Safranin Orange/ Fast Green (Safranin-O) staining was performed according to standard protocols. Briefly, sections were deparaffinized, rehydrated in tap water, and placed in freshly filtered working Weigert's hematoxylin solution for 10 minutes. Slides were then immediately washed in running tap water for 10 minutes and placed in 0.1% Fast Green solution for 5 minutes. Slides were then rinsed quickly in 1% acetic acid for 10-15 seconds, placed in 0.1% Safranin-O solution for 5 minutes, dehydrated, and cleared in xylene prior to mounting with Permount.

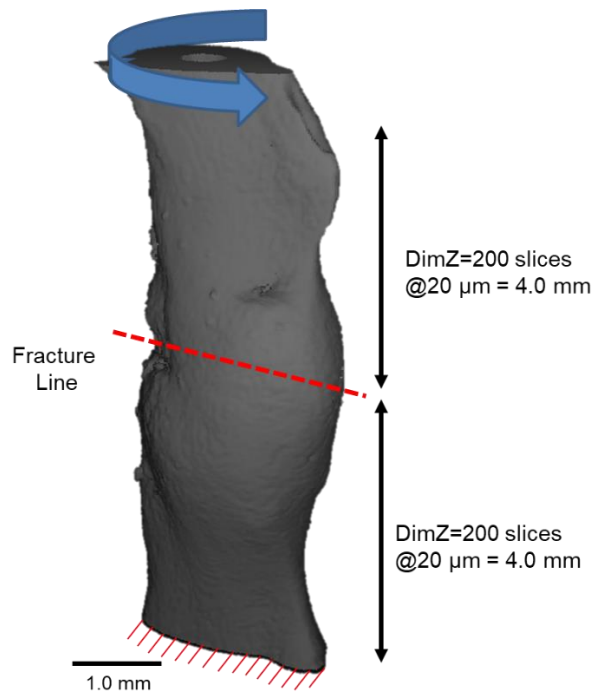
#### *Microcomputed Tomography ( $\mu$ CT) Analysis*

$\mu$ CT images were acquired ( $\mu$ CT40, Scanco Medical AG, Bassersdorf, Switzerland) of

injured hind-limbs or microfilled tissues at 55kVp, 145uA, 200ms integration, 500 projections per 180° rotation with a 20 µm isotropic voxel size following sacrifice. After reconstruction, the volume of interest including the injured femur and surrounding skeletal muscle tissue was selected. Mineralized tissue was segmented from soft tissue using a threshold of 220 per thousand (or 450.7mgHA/cm<sup>3</sup>), a Gaussian noise filter of 0.2, and support of 1.

#### *Finite Element Analysis (FEA)*

FEA was utilized to predict the stability of the fracture callus in-silica. Briefly, µCT images were converted to finite element models (voxel-to-element) for an elastic FEA solver using built-in code (FE-software v1.13) from Scanco Medical AG. After ensuring that each fracture callus was aligned in the z-direction (i.e. along the anatomical long axis), the distal most end of the 3D fracture callus model was constrained to be rigid while proximal end of the femur was prescribed a unit force vector resulting in rotation about the z axis. The boundary conditions (i.e. critical volume and strain deformation of the elements and nodes for von-Mises equivalent strain) in the FEA solver then calculated the predicted failure moment and torsional rigidity (Figure 85).



**Figure 85:  $\mu$ CT-FEA of Fracture Callus on femur mid-shaft.** FEA problem statement utilized- 53; Prescribed unit torque around the z dir. Displacements of nodes located at the face  $z=Z_{\min}$  are suppressed in all directions. At the face  $z=Z_{\max}$  nodal forces are applied which results in a force vector at an orientation that rotates around the center with a magnitude that increases linearly with the distance from this center.

#### *Fluorescent Imaging of Bisphosphonate Localization*

To assess bisphosphonate localization, OsteoSense 800 (NEV11105, PerkinElmer, Shelton, CT), an NIR-labeled, targeted fluorescent bisphosphonate was used. 24 hours before imaging, mice were injected intraperitoneally with 2 nmols of OsteoSense 800 in a total volume of 100 $\mu$ L. A Pearl small animal imaging system and image studio software (LI-COR Biotechnology, Lincoln, NE) were utilized to measure fluorescence at an excitation wavelength of 780 nm and an emission wavelength of 805nm following sacrifice.



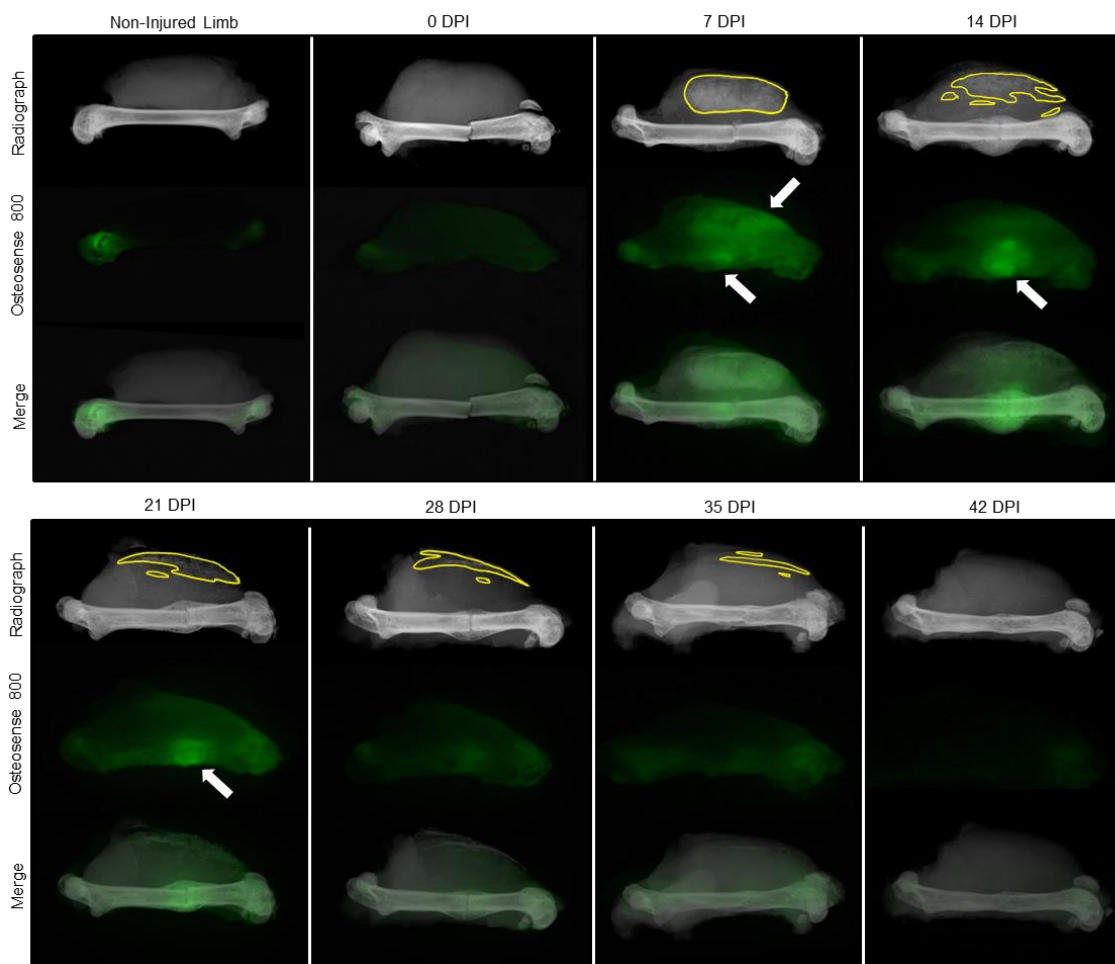
### *Statistical Analysis*

Modified STiCSS scores were statistically evaluate between groups longitudinally using an ordinary two-way ANOVA with a Tukey's multiple comparison test. Likewise, Y-Scale scores between groups over time were statistically evaluated using an ordinary two-way ANOVA with a Tukey's multiple comparison test. Functional testing of fractures at 42 days following injury were evaluated by a non-parametric ANOVA (Kruskal-Wallis Test) with a Dunn's test for multiple comparisons against a control group. P values reported are adjusted for multiplicity. For all analysis, alpha = 0.05. All statistical analysis was performed in GraphPad V6.

### *Results: Temporal Localization of Bisphosphonate Following Combined Fracture and Skeletal Muscle Injury*

Using a murine model of combined fracture and skeletal muscle injury, we first analyzed the temporal localization of bisphosphonates to either calcified soft tissue or the fracture site. Through the use of a fluorescently labeled bisphosphonate, we observed marked bisphosphonate localization to the physis in non-injured limbs, as anticipated. Immediately following the combined fracture and skeletal muscle injury, we observed little to no localization of the bisphosphonate to either the soft tissue or fracture site; yet, when administered and assessed at 7 days post injury (DPI), marked fluorescent signal was observed at both the fracture site and within the mineralized soft tissue (Figure 86, white arrows). Analysis at 14 and 21 DPI demonstrated marked bisphosphonate localization to the fracture callus, but reduced localization to calcified skeletal muscle aligning with its degradation. Finally, analysis at 28, 35, or 42 DPI

demonstrated reduced localization of bisphosphonate at both the fracture callus and the remaining skeletal muscle calcification compared to 7 DPI.

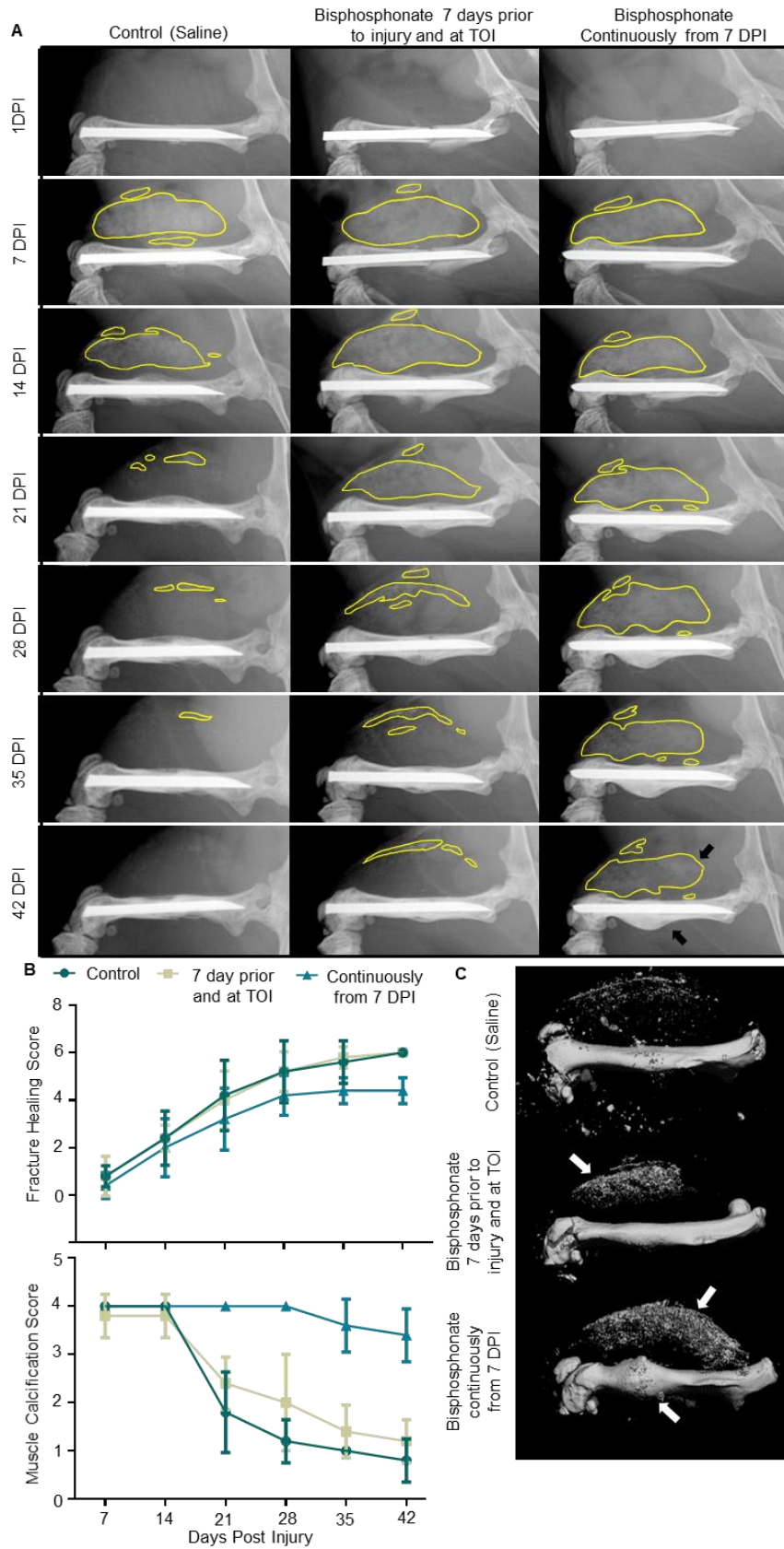


**Figure 86: Temporal Assessment of Bisphosphonate Localization Following Combined Fracture and Skeletal Muscle Injury.** To assess the temporal-spatial tropism of bisphosphonates following injury, a fluorescently labeled bisphosphonate (osteosense800) was administered at various days post injury. White arrows indicate focal localization of bisphosphonate to skeletal muscle calcification (7DPI) and/or fracture site (7, 14, 21 DPI). Yellow outline indicated skeletal muscle calcification.

*Impact of Continuous Bisphosphonate Dosing Following Combined Fracture and Skeletal Muscle Injury*

Given the temporal-spatial localization of bisphosphonates, we next assessed the physiologic effects of bisphosphonate administration on fracture healing and regression of skeletal muscle calcification utilizing two independent dosing strategies. Mice received either 1) bisphosphonate 7 days prior to injury and at the time of injury (TOI), 2) bisphosphonate weekly beginning at 7 days post injury through 42 DPI, or 3) saline as a vehicle control.

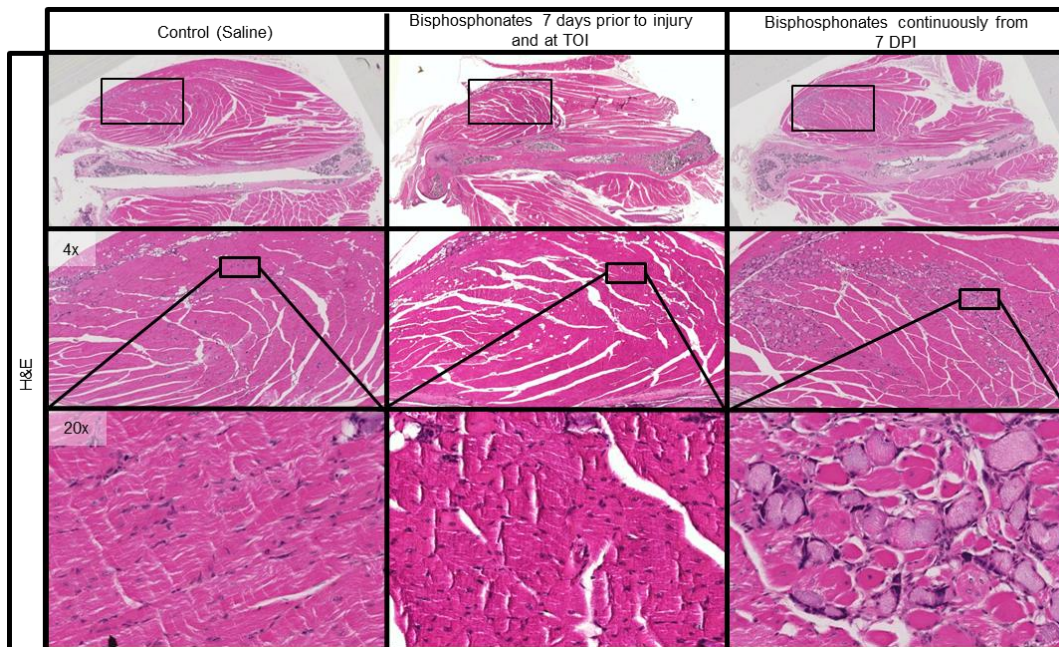
In comparing control mice to those administered bisphosphonates 7 days prior to injury and at the time of injury, we observed comparable fracture healing and a minimal, though not statistically significant, change in the regression of soft tissue calcification (Figure 87, Table 26 & 27). Alternatively, when comparing control mice to those who received bisphosphonates weekly beginning at 7 DPI through 42 DPI, we observed significant changes in fracture healing at 42 DPF characterized by reduced hard callus remodeling ( $p=0.018$ ). Furthermore, we also observed a marked reduction in soft tissue calcification regression in mice who received ZOL weekly beginning at 7 DPI, resulting in substantial calcification present within damaged tissues by 42 DPI, as measured by radiographic,  $\mu$ CT imaging (Figure 84, Table 26 & 27), and histological analysis (Figure 88).



**Figure 87: Continuous Bisphosphonate Dosing Following Combined Fracture and Skeletal Muscle Injury Delays Fracture Repair and Regression of Soft Tissue Calcification.** A) Representative longitudinal radiographic analysis of mice administered saline (n=16), bisphosphonates beginning 7 days prior to injury and at the TOI (n=5), or bisphosphonates beginning 7 DPI and continuing weekly until 42 DPI (n=5). Yellow outline indicates soft tissue calcification within the quadriceps. Black arrow highlights delay in fracture remodeling and regression of soft tissue calcification in mice administered bisphosphonates beginning at 7 DPI through 42 DPI. B) Quantification of fracture healing and skeletal muscle calcification longitudinally. Please see Table 23 and 27 for statistical analysis between groups at each time point. C) 3D  $\mu$ CT reconstruction of fractured femur and adjacent soft tissue calcification of the quadriceps. White arrows indicate marked residual soft tissue calcification and delay in fracture callus remodeling at 42 DPI.

<b>Table 26: Y-Scale Statistical Analysis</b>			
	<b>Saline vs Bisphosphonates 7 days prior to injury and at TOI</b>	<b>Saline vs Bisphosphonates continuously from 7 DPI</b>	<b>Bisphosphonates 7 days prior to Injury and at TOI vs Bisphosphonate continuously from 7 DPI</b>
	<i>Significance</i>	<i>Significance</i>	<i>Significance</i>
<b>7 DPI</b>	ns; p>0.999	ns; p>0.999	ns; p>0.999
<b>14 DPI</b>	ns; p>0.999	ns; p>0.999	ns; p>0.999
<b>21 DPI</b>	ns; p>0.999	ns; p=0.244	ns; p=0.485
<b>28 DPI</b>	ns; p>0.999	ns; p=0.244	ns; p=0.244
<b>35 DPI</b>	ns; p>0.999	ns; p=0.112	*; p=0.047
<b>42 DPI</b>	ns; p>0.999	*; p=0.018	*; p=0.018

<b>Table 27: STiCSS Score Statistical Analysis</b>			
	<b>Saline vs Bisphosphonates 7 days prior to injury and at TOI</b>	<b>Saline vs Bisphosphonates continuously from 7 DPI</b>	<b>Bisphosphonates 7 days prior to Injury and at TOI vs Bisphosphonate continuously from 7 DPI</b>
	<i>Significance</i>	<i>Significance</i>	<i>Significance</i>
<b>7 DPI</b>	ns; p>0.999	ns; p>0.999	ns; p>0.999
<b>14 DPI</b>	ns; p>0.999	ns; p>0.999	ns; p>0.999
<b>21 DPI</b>	ns; p=0.136	***; p<0.001	***; p<0.001
<b>28 DPI</b>	*; p=0.025	***; p<0.001	***; p<0.001
<b>35 DPI</b>	ns; p=0.535	***; p<0.001	***; p<0.001
<b>42 DPI</b>	ns; p=0.535	***; p<0.001	***; p<0.001



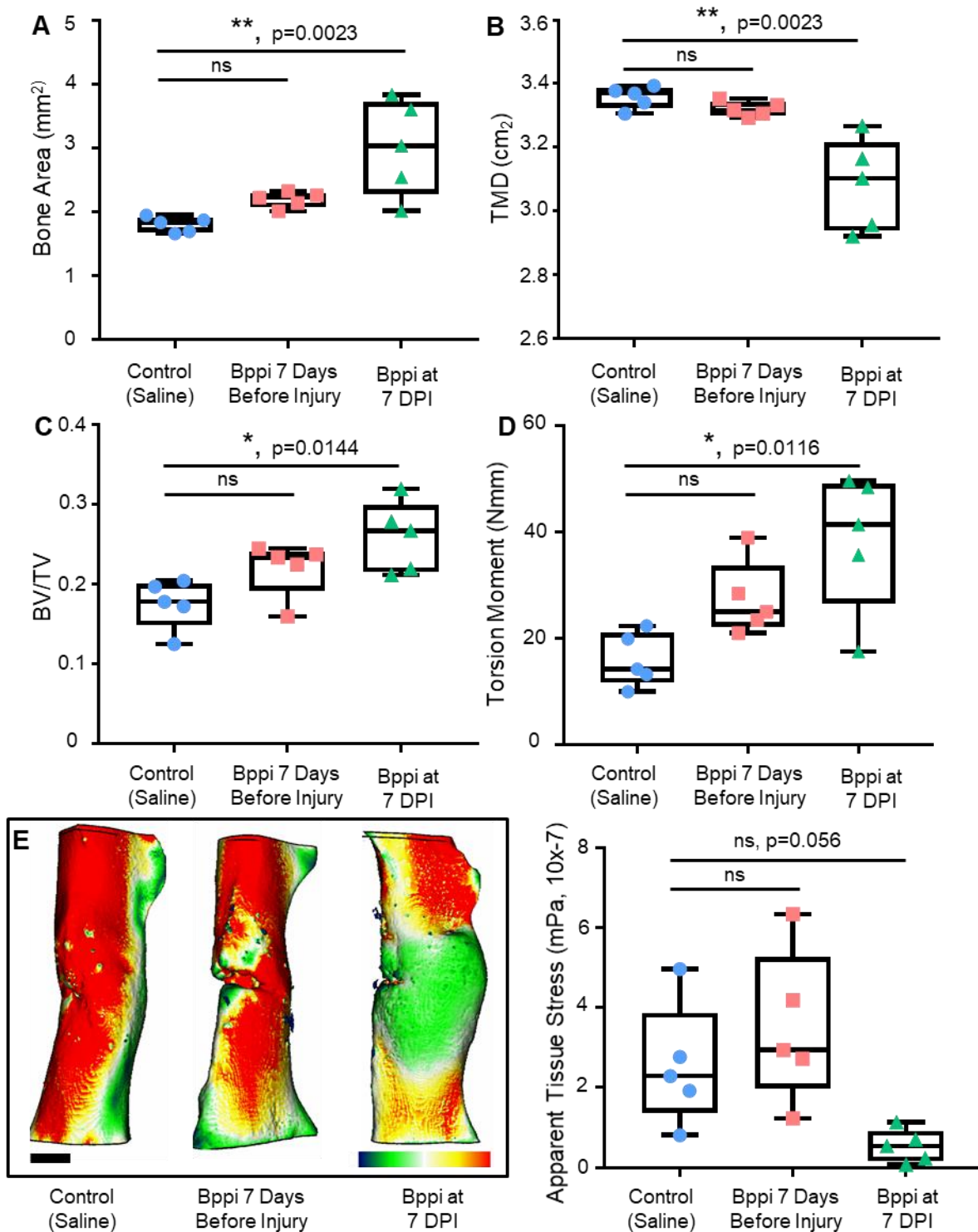
**Figure 88: Histological analysis of injured quadriceps at 42 DPI.** Marked nodules of dystrophic calcification are still observed at 42 DPI in within the damaged skeletal muscle of mice administered bisphosphonates beginning 7 DPI and continuing weekly through 42 DPI.

Given the impairment of fracture callus remodeling observed by radiographic analysis and  $\mu$ CT reconstruction, we next assessed the structural and biomechanical properties the fracture callus between cohorts. Through evaluation with  $\mu$ CT, we confirmed an increased in fracture callus size at 42 DPI in mice treated with bisphosphonates beginning at 7 DPI compared to saline control ( $p=0.0023$ , Figure 89A & Figure 90) and observed a corresponding significant decrease in tissue mineral density (TMD,  $p=0.0023$ , Figure 89B), and an increase in in the bone volume to total volume ratio (BV/TV,  $p=0.0144$ , Figure 89C). Taken together, these results suggest that bisphosphonate treatment at 7 DPI lead to in a larger, less dense, fracture callus by 42 DPI. Through application of finite element analysis, we observed that mice treated with bisphosphonates beginning at 7 DPI also possess a higher predicted failure moment (Torsion Moment,  $p=0.0116$ ), aligning with the callus being larger in this cohort. Yet when considering the apparent tissue stress able to be withstood before breaking, while the callus was larger, mice treated with bisphosphonates at 7 DPI possessed a markedly lower apparent tissue stress level then control treated animals, trending towards statistical significance.

Taken together, these data suggest that while bisphosphonate administration prior to injury possess a minimal effect on fracture callus structure, bone remodeling, and soft tissue calcification regression, continuous administration of bisphosphates beginning at 7 DPI greatly impairs soft tissue calcification regression and bone remodeling post-union, leading to weaker bone surrounding the fracture site at 42 DPI. Going forward, since continuous dosing of bisphosphonates beyond 7DPI altered fracture remodeling

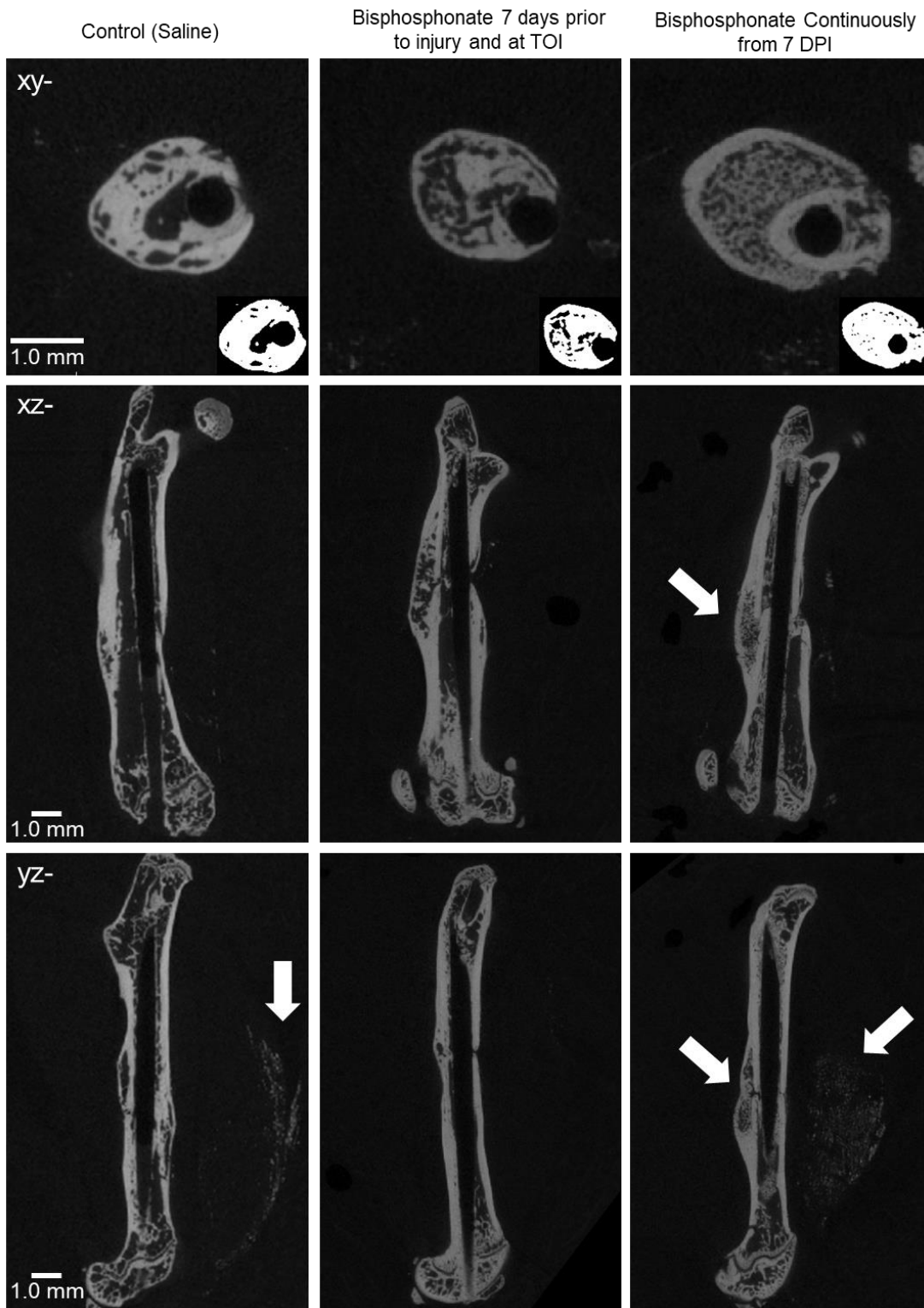
and soft tissue calcification regression, we next utilized single dosing at 7, 14, 21, 28, and 35 DPI to investigate the effect of bisphosphonates in a narrower therapeutic window.





**Figure 89: Structural and Biomechanical Properties of Healing Fractures Following Continuous Bisphosphonate Dosing.** At 42 DPI, fractured femurs were

isolated from mice and assessed for A) fracture callus size as measured by total bone area ( $\text{mm}^2$ ), B) tissue mineral density (TMD,  $\text{cm}^2$ ), and C) Bone Volume to Total Volume (BV/TV). Finite element analysis for the scanned fractured femurs was applied assuming a force of 10Gpa, a failure strain of  $7000\mu\epsilon$ , and a failure volume of 20%. D) Predicted failure moment assuming a single material increases in a positive correlation with callus size ( $R^2=0.803$ ). E) 3D reconstructions and quantification of apparent tissue strain in the -zz axis. \*,  $p\leq 0.05$ ; \*\*,  $p\leq 0.01$ ; \*\*\*,  $p\leq 0.001$ . Bppi= Bisphosphonat



**Figure 90: Two Dimensional Images of Fracture Femur at 42 DPI.** Images obtained following  $\mu$ CT imaging of two dimensional planes of section. Arrows

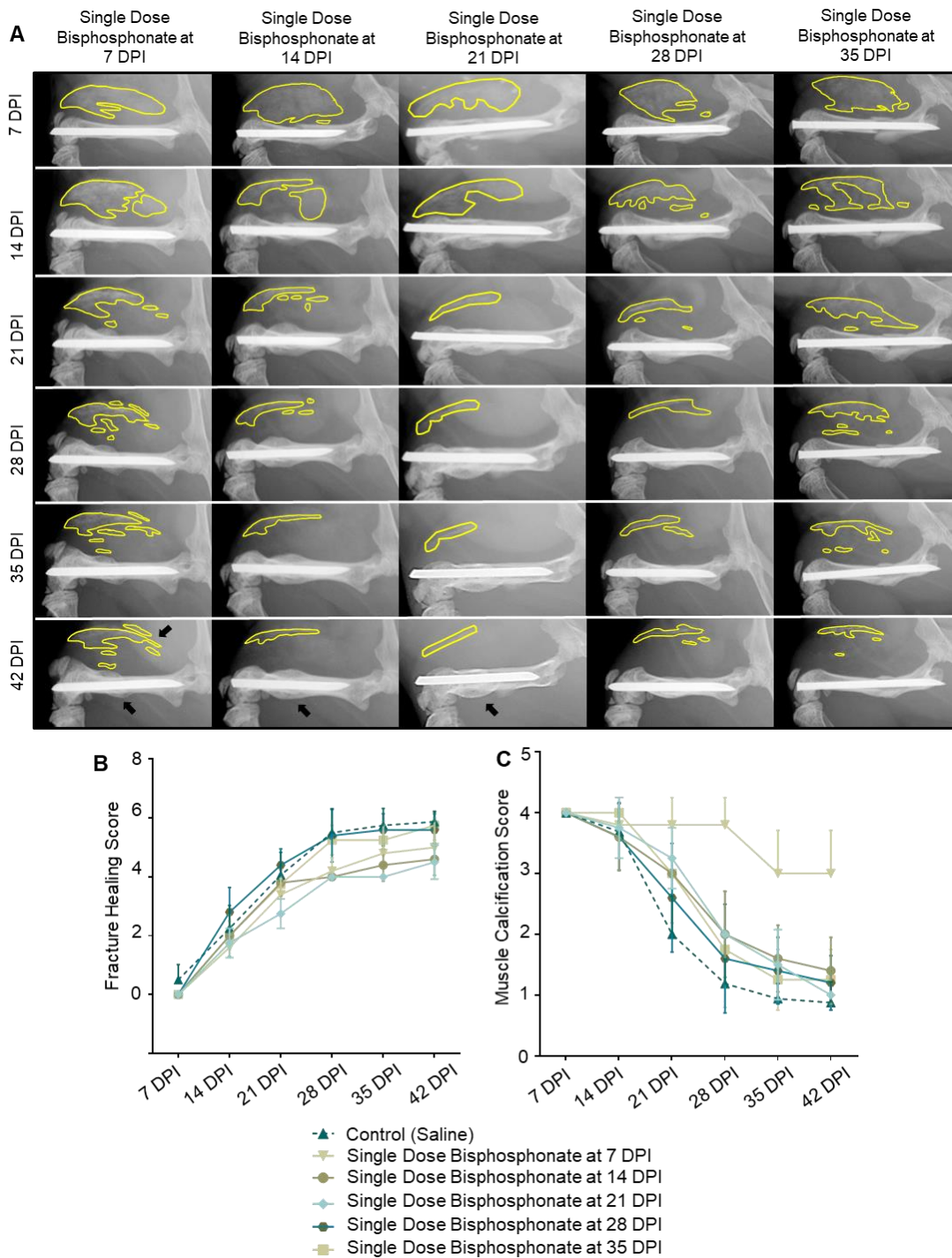
indicate the detection of calcified skeletal muscle, as previously visualize in 3D reconstructions (Figure 82C) and enlarged fracture callus as quantified in Figure 86A. Images are representative of the cohort. Scale bare = 1.0mm

### *Single Bisphosphonate Dosing Following Combined Fracture and Skeletal Muscle Injury*

Using a single does bisphosphonate administration, we further analyzed the temporal-spatial localization of bisphosphonates and the effects on fracture healing and soft tissue calcification regression, through a narrower, one-week therapeutic windows. A single dose of bisphosphonate was administered at 7, 14, 21, 28, or 35 days post injury and mice were longitudinally assessed for fracture healing and soft tissue calcification regression.

Aligning with the temporal-spatial localization of labeled bisphosphonate following injury (Figure 83), we found that single dose of bisphosphonates at 7 DPI markedly impaired both fracture callus remodeling and regression of soft tissue calcification to a comparable degree seen with continuous dosing previously. When bisphosphonate was administered at 14 or 21 DPI, we observed a similar impairment of fracture callus remodeling though limited impairment of soft tissue calcification degradation which was nonsignificant by 42 days post injury. Finally, when at administered at 28 or 35 DPI, we observed no significant impairment in fracture callus remodeling and limited impairment of soft tissue calcification degradation (Figure 91, Tables 28 & 29). Taken together, these data suggest that starting bisphosphonate administration after 28 DPI

will not impact fracture callus remodeling or soft tissue calcification regression, while earlier administration will impact one or both of these processes.



**Figure 91: Single Dose Bisphosphonate Dosing Following Combined Fracture**

**and Skeletal Muscle Injury.** A) Representative longitudinal radiographic analysis of mice administered a single dose of bisphosphonates at 7, 14, 21, 28, or 35 DPI (N= 5, 5, 4, 5, 4 respectively). Yellow outline indicates soft tissue calcification within the quadriceps. Black arrow highlights delay in fracture remodeling and regression of soft tissue calcification. B) Quantification of fracture healing and C) skeletal muscle calcification longitudinally. Please see Table 28 and 29 for statistical analysis between groups at each time point.

CHAPTER 3

<b>Table 28: Y-Scale Statistical Analysis</b>					
	<b>Saline vs Single Dose Bisphosphonate at 7 DPI</b>	<b>Saline vs Single Dose Bisphosphonate at 14 DPI</b>	<b>Saline vs Single Dose Bisphosphonate at 21 DPI</b>	<b>Saline vs Single Dose Bisphosphonate at 28 DPI</b>	<b>Saline vs Single Dose Bisphosphonate at 35 DPI</b>
<b>7 DPI</b>	ns; p=0.440	ns; p=0.440	ns; p=0.536	ns; p=0.440	ns; p=0.536
<b>14 DPI</b>	ns; p=0.176	ns; p=0.936	ns; p=0.536	ns; p=0.336	ns; p=0.955
<b>21 DPI</b>	ns; p=0.161	ns; p=0.922	***, p<0.001	ns; p=0.806	ns; p=0.891
<b>28 DPI</b>	***, p<0.001	***, p<0.001	***, p<0.001	ns; p=0.999	ns; p=0.955
<b>35 DPI</b>	*, P=0.012	***, p<0.001	***, p<0.001	ns; p=0.993	ns; p=0.536
<b>42 DPI</b>	*, P=0.028	***, p<0.001	***, p<0.001	ns; p=0.907	ns; p=0.998

<b>Table 29: STICSS Score Statistical Analysis</b>					
	<b>Saline vs Single Dose Bisphosphonate at 7 DPI</b>	<b>Saline vs Single Dose Bisphosphonate at 14 DPI</b>	<b>Saline vs Single Dose Bisphosphonate at 21 DPI</b>	<b>Saline vs Single Dose Bisphosphonate at 28 DPI</b>	<b>Saline vs Single Dose Bisphosphonate at 35 DPI</b>
<b>7 DPI</b>	ns; p>0.999	ns; p>0.999	ns; p>0.999	ns; p>0.999	ns; p>0.999
<b>14 DPI</b>	ns; p=0.994	ns; p=0.998	ns; p=0.999	ns; p=0.998	ns; p=0.749
<b>21 DPI</b>	***, p<0.001	***, p<0.001	***, p<0.001	ns; p=0.071	**, p=0.001
<b>28 DPI</b>	***, p<0.001	**, p=0.005	*, p=0.013	ns; p=0.385	ns; p=0.167
<b>35 DPI</b>	***, p<0.001	*, p=0.035	ns; p=0.167	ns; p=0.263	ns; p=0.749
<b>42 DPI</b>	***, p<0.001	ns; p=0.137	ns; p=0.993	ns; p=0.639	ns; p=0.583

### Section Summary: Bisphosphonates

Through these studies, we identified using our combined injury model, that bisphosphonate localization and therapeutic effect does indeed alter in respect to when the drug is administered following injury. While we did not observe a significant decrease in the skeletal muscle calcification following injury with pretreatment of bisphosphonates, we did observe impaired regression dystrophic calcification if bisphosphonates were administered at 7 DPI. These results aligned with the results observed in ABCC6 deficient mice above.

Interestingly, dependent upon the time of administration and bisphosphonate localization, we observed differing effects on fracture repair. Specifically, if administered at the point where the hard tissue callus is forming, we observed marked localization of the bisphosphonate to the site of injury and a related impairment of callus remodeling through 42 DPI.

Taken together with the individual assessments of the bisphosphonate's effect on the prevent soft tissue calcification above, we have demonstrated that the timing of administration post injury and the model utilized can alter the conclusion drawn about bisphosphates effectiveness and impact on fracture repair. These dichotomous results align with the variable results of prior studies (Table 25 and 26), thereby demonstrating the difficulty in assessing whether bisphosphonate administration is an effective therapeutic for preventing trauma induced calcification.



### *Future Directions*

Building upon these results, we have established the necessary combinatory animal models to effectively test different type of bisphosphonates, varying doses of bisphosphonates, and the effects of the drug, dependent upon the model examined. To this point, we have investigated a single variable of time of administration, in a single type and dose of bisphosphonate (zoledronic acid). Considering the other therapeutic variables, going forward we have the foundation for numerous additional studies to identify the ideal bisphosphonate regime for prevention of soft tissue calcification and to avoid impairment of fracture healing. This discussion will be expanded upon in in Chapter 4 in future directions.

### **BMP Antagonists for The Treatment Of HO**

In addition to bisphosphonates administration, another pharmacologic approach currently being developed to reduce trauma-induced HO is through inhibiting BMP signaling. However, one disadvantage of this strategy is that BMP signaling is crucial for fracture repair and union [46, 248]. As a consequence, any pharmacologic strategy that targets the BMP pathway will increase the likelihood of impacting fracture repair and union. Thus, considering physiologic bone formation, I hypothesize that this therapy will ultimately not be effective for treating trauma-induced HO given the potential combinatory nature of the injury.

Therefore, beyond these current therapies, our laboratory has begun investigations into

potential novel therapeutic interventions, guided by our finding detailed above. Specifically, given that plasmin activity is essential for both fracture repair and prevention of skeletal muscle calcification, this suggests that, unlike current treatments for HO which ultimately sacrifice physiologic bone health for prevention of pathologic calcification, targeting plasmin activity represents a therapeutic strategy that would be beneficial to prevent HO yet simultaneously support physiologic bone formation. As such, we have been investigating how enhancement of plasmin activity may be therapeutically advantageous to treat trauma-induced skeletal muscle calcification.

### **Therapeutic Modulation of Plasmin to Prevent HO**

Through preliminary experiments, we have examined the ability to enhance plasmin activity through therapeutically targeting its primary biological inhibitor, alpha 2 antiplasmin (a2AP) with a targeted antisense oligonucleotide (ASO). This therapeutic strategy has allowed us to target a2AP specifically, to an effective level with limited impact on liver toxicity (Table 30).

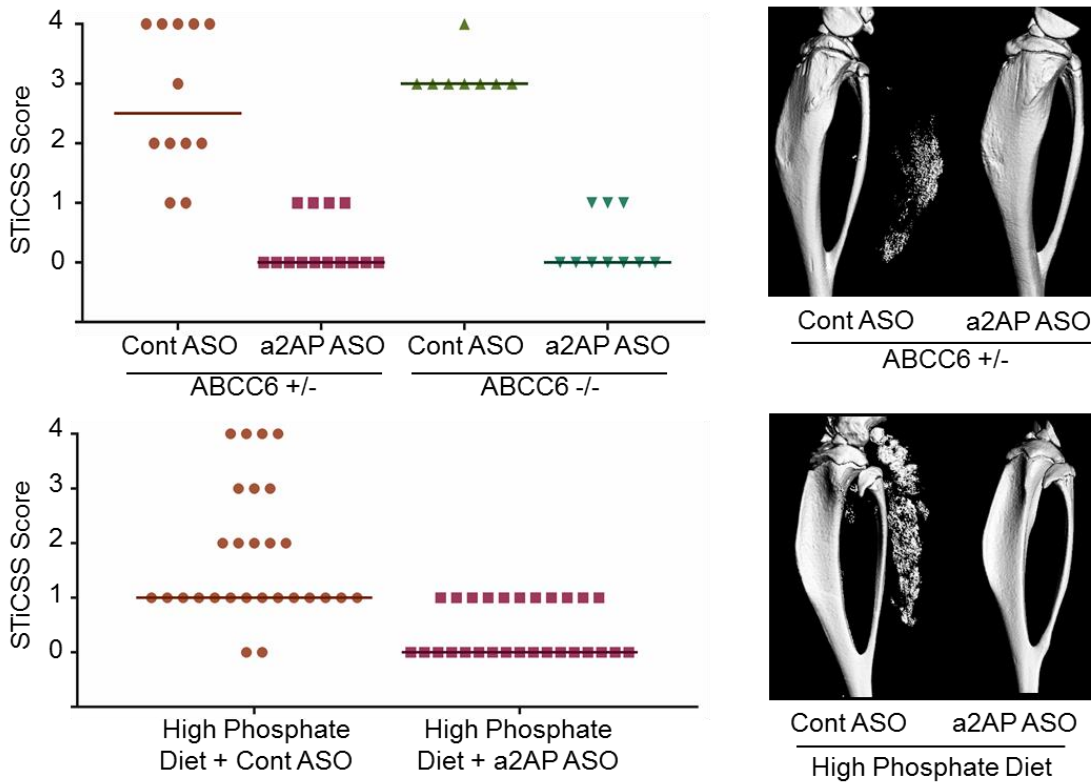
<b>Antisense Oligonucleotide</b>	<b>Percent Hepatic mRNA Knockdown</b>	<b>AST</b>	<b>ALT</b>
<b>Alpha 2-antiplasmin inhibitor</b>	86.5 (+/- 7%)	191.5 (+/- 88.6)	83.3 (+/- 14.3)

**Table 30: Quantitation of percent  $\alpha$ 2AP mRNA knockdown in the livers of WT mice after receiving 100mg/kg/week of the respective ASO for 2 weeks. Since**

hepatotoxicity can negatively affect hepatic protein synthesis, AST and ALT levels (U/L) were also determined (normal range of mouse AST, 54-298 U/L; ALT, 17-77 U/L).

When applied to partially plasminogen deficient mice (Plg<sup>+/-</sup>), we observed a rescue of plasminogen activity, which correlated with reduce dystrophic calcification formation compare to control ASO treated animals. These experiments are outlined in detail in Article 6, Figure 50-52.

Given the success of enhancing plasminogen through a2AP ASO administration, we next examined where enhancement of plasmin activity can be supersaturated in an animal model predisposed to dystrophic calcification formation, independent of changes in plasmin activity. Therefore, we administered a2AP or control ASO to either ABCC6 deficient more of mice fed a high phosphate diet prior to injury (Figure 89). Through these experiments we observed marked reduction in dystrophic calcification, demonstrating that plasmin can be further activated beyond its native state to reduce dystrophic calcification. Through further experiments, the molecular mechanisms through which a2AP ASO elicits these effects, specifically determining if they are through the macrophage or skeletal muscle specific mechanisms, will be investigated. Please see Chapter 4 for further discussion of these investigations.



**Figure 92: Enhancement of Plasmin Activity Prior to Injury Prevents Dystrophic Calcification.** In both ABCC6 deficient animals and those fed a high phosphate diet, we found that enhancement of plasmin activity by administration of an a2AP ASO effectively inhibited DC formation following injury, compared to mice treated with a control ASO.

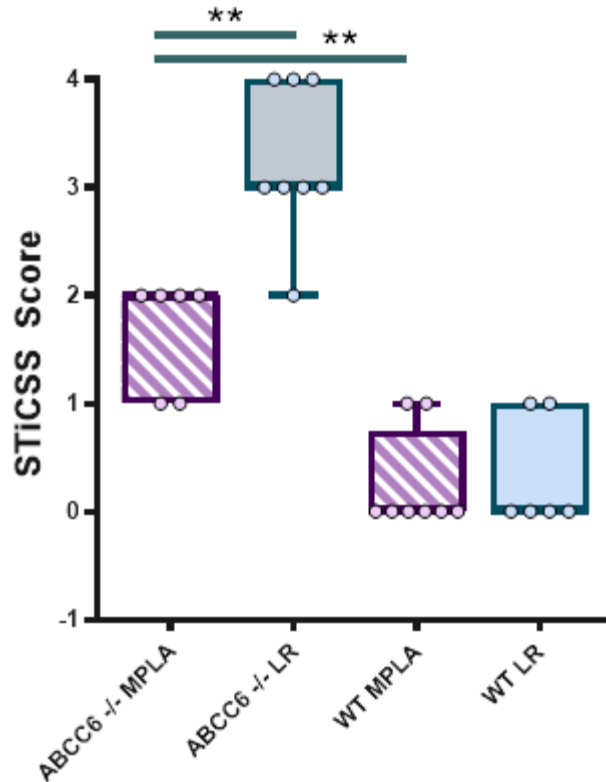
To this point, we have discussed in detail, current and experimental therapeutics aimed at modulating either the pyrophosphate pathway through administering a bisphosphonate or modulation of the plasmin pathway by targeting a2AP, plasmin's main physiological inhibitor. While bisphosphonate administration, depending upon the timing of administration as demonstrated in Article 11, may negatively impact fracture repair, we hypothesize that plasmin activation will positively influence

physiologic bone formation, given its essential role in both skeletal muscle regeneration and fracture repair. However, overactivation of plasmin may be a double edged sword when considering conditions such as infection or cancer. For example, plasmin is utilized by many bacteria, as well as cancer cells, to drive their dissemination. For example, *staphylococcus aureus* utilized fibrin matrices to develop abscesses within the body where they are protected from the host immune system. Once the bacteria reach quorum, they then utilize plasmin activity to break out of their fibrin encased abscess and disseminate throughout the body. Similar processes are likewise used by an even greater bacterial villain to the orthopaedic community, necrotizing fasciitis. Further details of the pathologic mechanisms of necrotizing fasciitis and how it over activates plasmin to drive the pathogenic spread through facial planes is discussed in Article 12, found within the Appendix I. Taken together, it is with caution that I suggest overactivation of plasmin as a cure all therapeutic. Rather, while it may be highly beneficial for multiple facets of musculoskeletal repair, it likewise may be very damaging in conditions of infection. As such, to test these interactions, our lab is currently beginning investigations utilizing preclinical models of infection where we have observed fibrin histologically surrounding the bacterial burdens. Through these models, we aim to examine the pathologic effect of plasmin over activation (a2AP ASO), loss of plasminogen (PLG ASO), loss of fibrin (FIB ASO) on the course of abscess formation, bacterial dissemination, and morbidity.

Finally, given our recent findings that macrophages are essential for regressing dystrophic calcification for the damaged skeletal muscle, we have recently begun

investigations into therapeutic mechanisms aimed at activating the macrophage to promote regression of dystrophic calcification from damaged tissue, thus preventing its maturation to HO. Through studies conducted by Dr. Edward Sherwood's laboratory at Vanderbilt University, it has been demonstrated that administering monophosphoryl lipid A (MPLA) to mice prior to bacterial infection, effectively augments the innate host immune system to confer greater resistance [417]. Through drill down investigations published this year, it was demonstrated that MPLA drives resistance to infection by reprogramming the macrophage's metabolism, promoting pathogen clearance [418]. Guided by these findings, we examined whether MPLA administration immediately prior to skeletal muscle injury in a predisposed murine line such as ABCC6, would prevent dystrophic calcification or support enhanced regression compared to control treated animals.

When applied in the same dosing strategy as Dr. Sherwood's groups work, we observed at 7 DPI a significant decrease in the amount of calcification between MPLA and vehicle control (Lactated ringers, LR) treated animals; however, these levels were not to that of WT mice (Figure 93). From this data, it looks promising that enhancement of macrophage activity may be effective at reducing dystrophic calcification from damaged skeletal muscle. Further longitudinal investigations are necessary to investigate the optimal timing of therapeutic administration and whether the effects we are observing are due to a greater regression and/or a reduction in the initial amount of dystrophic calcification formed.



**Figure 93: Enhancement of Macrophages Reduces Dystrophic Calcification at 7 DPI.** Administration of monophosphoryl lipid A (MPLA) to enhance macrophages, results in decreased dystrophic calcification at 7DPI in ABCC6 heterozygous knockout animals (ABCC6 +/-) as measured by radiographic analysis (\*\*,  $p < 0.01$ ). Each point represents an individual leg analyzed.

In addition to MPLA as a therapeutic to improve macrophage function, given that plasmin likewise activates macrophage migration and activity, it is plausible that the success of the a2AP ASO treatment may in part be due to enhanced macrophage function. Going forward, a detailed line of investigation is warranted into the mechanisms through which plasmin activity may be eliciting its effects, taking

primary prevention of dystrophic calcification, the ability to enhance macrophages, as well as its ability to promote ossification as observed in fracture healing.

### **Chapter 3 Summary**

Through this chapter, we have discussed in detail currently utilized pharmacologic and novel experimental therapies aimed at preventing skeletal muscle calcification, specifically HO. As noted previously, when considering therapeutics aimed at treating trauma-induced HO, it is essential to consider both pathologic and physiologic bone formation. As such the ideal therapeutic would be one that prevent mineralization of soft tissues, while simultaneously preserving or promoting physiological mineralization within the skeleton.

Aligning with this goal, I have highlighted in detail above the pros and cons of bisphosphonate and plasmin targeted therapies as they pertain to both pathologic and physiologic bone formation. Through the use of preclinical animal models of both soft tissue calcification and fracture injury and repair, I am hopeful that detailed investigations will be plausible going forward to examine the optimal timing, dose, and form of therapeutic necessary to direct biomineralization following a traumatic injury.



## **CHAPTER 4:**

### **Future Directions**

Within this chapter, I will discuss some of the future directions of the work outlined within my dissertation, specifically highlighting new investigations surrounding physiologic bone formation and investigations into the detailed pathophysiology of pathologic soft tissue calcification. Furthermore, in this chapter I will discuss the clinical implications this work may have going forward.

#### Physiologic Bone Formation: Fracture Repair

In Chapter 1, I highlighted the foundations of bone biology and the molecular mechanisms at play during fracture repair that are essential for resolving excessive interfragmentary strain to allow for subsequent vascularity and ossification to ensue.

As fracture healing is a temporal process, organized into stages of healing which cannot progress until the prior stage has been completed, we cannot only consider ossification or bony union when assessing fracture repair. Rather in preclinical models assessing fracture repair, one must consider the matrix production, cellular activity, strain, vascularity, and ossification to gather a complete picture of fracture repair. As such clinically, while radiographic analysis is the primary means by which fracture healing is assessed, it is important to note that this imaging method only accounts for ossification, the last step of the fracture healing cascade. Therefore, if a physician observed a reduction in ossification, this pathology could be a result of an alteration to

any of the prior stages such as excessive strain, reduced cellular availability, impaired matrix production, or impaired vascularity.

Thus, a coordinated effort would be needed both clinically and through basic science research to better assess the root of impaired fracture healing to bring about customized treatments for each patient. Specifically, in the clinical realm, physicians would require a quantifiable measure of strain, vascularity, and cellular activity or matrix production during the fracture healing process to identify which phase of the APR the patient is currently undergoing. Once identified, directed therapeutic interventions for each of the potential stages of fracture repair would be necessary to assist in the advancement to the next phase of fracture repair. This is where directed basic science investigations aimed at designing therapeutics to promote the varying stages of fracture repair would be necessary to harness and promote the biological processes necessary.

Hopefully, innovative efforts will lead to the development of devices and therapeutic interventions capable of creating the perfect biological and biomechanical environment for every fracture. Therefore, one day, even in the most severe of cases, customized fracture treatment may be possible, leading us to expect nothing less than ideal and timely fracture repair.

## Bone Grafting

In Chapter 1, building upon my foundational knowledge of bone biology and bone formation, I highlighted a study in which we utilized this knowledge to inform us of a potential novel alternative to bone grafting: use of the hypertrophic chondrocyte. This line of investigation is of great interest to our laboratory given that the rate of spinal fusion increased 137% between 1998 and 2008, up to 135 per 100,000 adults annually [126]. The expense of spinal fusion has also increased, with the average hospital bill for each surgery rising over \$34,000 and with the annual aggregate hospital charges up to \$33.9 billion in 2008, surpassing all other elective procedures [126, 419].

Over 200,000 of these operations are performed each year, with a majority involving various bone graft options to facilitate bone generation [129]. Failed fusion results in increased patient morbidity, cost, and often revision surgery [420, 421]. Indeed, reoperation rates can be as high as 20% following lumbar fusion with the majority of revision spine operations being performed for non-union [422, 423]. In the effort to achieve successful spinal fusion, various grafts and graft substitutes have been developed, with varying rates of success [422, 424]. Thus, there is a clear need for novel grafting alternatives.

Through our studies, we observed that implantation of hypertrophic chondrocytes was sufficient to support bone formation and the fusion of the lumbar spine in a murine model (Article 3). However, the question still remains- how can we obtain large enough quantities of hypertrophic chondrocytes to translate this novel grafting method

clinically?

Through collaboration with Dr. Jason McCarthy, we have begun to answer such a question. While culturing large quantities of chondrocytes and getting them to transition to a hypertrophic state *in vitro* may be plausible, these conditions have yet to be established and, moreover, this method would be difficult to translate to clinical use as “off the shelf” availability would not be available. Furthermore, this method also begs the question as to where the initial source of chondrocytes would come from and would they need to be patient derived to reduce the possibility of xenobiologic rejection. Therefore, to overcome these challenges, we propose the possibility of making a “synthetic” hypertrophic chondrocyte by packaging nanoparticles with the essential components released by a hypertrophic chondrocyte to promote bone, specifically BMP, VEGF, nanohydroxyapatite, and alkaline phosphatase to reduce the bodies innate soft tissue protection mechanisms. Going forward, together with our collaborators at Vanderbilt, we are proposing to characterize the proteins produced by the hypertrophic chondrocyte, and with Dr. McCarthy’s skill in chemistry and nanomaterial synthesis, develop synthetic hypertrophic chondrocytes to be examined in our mouse model of spinal fusion or our large segment defect model as a means to promote bone formation.

#### Pathologic Bone Formation: Drilling Down on The Macrophage

Through our work assessing the mechanisms by which skeletal muscle protects itself from dystrophic calcification and subsequent HO formation, we developed the “two

hit” mechanism of HO formation. Specifically, while nanohydroxyapatite can deposit within skeletal muscle following injury, fortunately, the body possesses a secondary macrophage-mediated clean-up crew to regress nanohydroxyapatite from damaged tissues; thereby resolving the predisposing factors to HO formation. Interestingly, the idea that macrophages prevent HO is divergent from much of the literature suggesting that macrophages are rather a driver of the inflammatory state within damaged tissues and promote the maturation of HO. As discussed above, I believe the macrophages we are assessing are a different population than those previously examined to promote the maturation of HO. Rather, I propose that we are looking at an earlier population of macrophages responsible for regressing damaged tissue, debris, as well as calcification from soft tissues following injury.

Going forward, further phenotyping experiments of the macrophages surrounding dystrophic lesions in ABCC6 deficient mice is warranted. Ultimately, I hope to compare these populations of macrophages at different time points as the calcification is regressed following injury as well as to WT macrophages. I hypothesize we will find similar results to that of Villa-Bellosta *et. al.* who demonstrated *in vitro* that macrophages in the presence of high levels of phosphate adopt a M2 like phenotype and express elevated anti-mineralization activity dependent upon PPI production [379, 380]. In our ABCC6 deficient animals, though not reported I am interested to see if macrophages from these animals possess reduced PPI production, as is seen in the liver and circulation, or if the PPI production at the macrophage level is independent.

In addition to phenotyping the type of macrophage responsible for dystrophic calcification regression, identifying the mechanisms through which the macrophage is activated, migrates into the damaged tissue area, and recognizes dystrophic calcification as a material to be phagocytosed all warrant investigations. Specifically, through previous investigations, it has been suggested that plasmin is essential for macrophage entrance into the damaged tissue, and that when overactivated by administration of a2AP ASO, the initial levels of dystrophic calcification is reduced in multiple models. These data, taken with our two hit hypothesis, suggest that plasmin activation of macrophages is an essential component to their regression of dystrophic calcification. Going forward I would like to i) examine the mechanism by which plasmin activates the macrophage, potentially through urokinase plasminogen activator, ii) examine if plasmin signaling to the macrophage alters its phenotype or ability to phagocytose crystal, and finally iii) determine if activation of plasmin through a2AP ASO administration is sufficient to expedite the regression of dystrophic calcification from damaged tissues.

#### The Transition of Dystrophic Calcification to HO

Through our examination, we observed in two separate studies that the persistence of dystrophic calcification within skeletal muscle was sufficient to drive HO: however, to this point we know very little about the middle of this biological process. Going forward in future studies, we would like to determine the mechanism, molecular signaling, and intermediate steps that are taking place as DC matures to form HO.

Questions to be answered include:

- Are the cells surrounding the dystrophic calcification going through a chondrocytic intermediate to support HO?
- Are the cells surrounding the dystrophic calcification gathering an osteoblastic like phenotype and then simply utilizing the excess calcium and phosphate as a seed crystal to form HO?
- What matrices are being produced? Do the matrices of HO match those of physiologic bone? Are there any differences that we could exploit to target therapies to HO and away from normal bone?
- Where are the bone forming cells originating or differentiating from? Are they from pericytes or an alternative mesenchymal stem cell?
- Is the calcium and phosphate in the dystrophic calcification being transferred to bone or are these new calcium and phosphate stores?
- Where does the calcium and phosphate in dystrophic calcification arise from (see next section)?
- What molecular signaling is occurring to promote the maturation of dystrophic calcification to HO? Is SOX-9 (osteoblast marker), Aggrecan (chondrocyte marker), or other (unknown) expressed in the transitioning tissue areas?
- If present once the transition from dystrophic calcification to HO begins, do the macrophages take on a different phenotype that supports ossification, aligning with prior studies in patients with FOP?
- Once the transition from dystrophic calcification to HO begins, can it be

reversed? Can cells be pushed back to support myogenic lineages over osteogenic lineages?

- Is plasmin activity necessary for the maturation of dystrophic calcification to HO as it is needed in fracture healing for ossification to ensue? What role is it playing?
- Does the amount of movement or strain within the muscle alter the maturation of dystrophic calcification to HO (the process of ossification) as it does in fracture healing? Could increasing strain be used to stop the maturation of dystrophic calcification to HO?

Through the use of specialized cellular lineage tracing animals recently obtained from collaborators, many of these questions are within reach. With the foundation of my dissertation work, many of the experimental animal models needed to answer these questions and the measures of dystrophic calcification and HO have been validated. Now all we need is time...well... and grant funding!

#### Within the Sarcomere- How Is Dystrophic Calcification Born?

Following injury, dystrophic calcification can form within damaged skeletal muscle, yet the mechanisms of this process at a cellular level are just beginning to be deciphered. Taken from reports of normal physiologic bone formation, it has been suggested by many studies that the mitochondria are an essential mediator, packager, and exporter of dense calcium and phosphate granules from the inside of the cell to the extracellular space. This export not only protects the cells from oversaturation of ions



that can be extremely inhibitory to cellular signaling, it also allows the exported and packaged calcium and phosphate granules to act as seed crystals to support further biomineralization.

Yet the question stands: why in wild type animals following injury, do the majority of sarcomeres not become mineralized, yet when plasminogen or ABCC6/pyrophosphate is lost, the sarcomeres lose their ability regulate calcium and phosphate, resulting in cell death and dystrophic calcification? This question highlights how little we know currently about plasminogen's and ABCC6/pyrophosphate's role at a cellular level. Furthermore, through preliminary studies in our laboratory, we have observed that plasminogen flocks to sites of tissue injury. As such, this raises the following questions:

- Why does plasminogen flock to a damaged tissue? What impact does it have on cellular response to injury? What cell type or types is it binding to? Does it selectively bind to cells based on their level of damage?
- What cellular receptor is plasminogen interacting with following injury? What impact does this have on cellular signaling in response to injury?
- Does plasmin become activated at the site of injury to elicit its effects? What activator is responsible (uPA, tPA or both)?
- Is pyrophosphate produced locally by injured soft tissues to prevent aberrant calcification or does all pyrophosphate come to injury tissue through circulation after being produced in the liver?
- Does pyrophosphate in the extracellular space signal impact intracellular

events? Do pyrophosphate levels alter cellular signaling? Do pyrophosphate levels build up in damaged tissues?

- Does ABCC6 play a different role within damaged tissues to regulate the response to injury beyond pyrophosphate production?
- Given that ABCC6 deficient tissues have been previously demonstrated to possess morphologically perturbed mitochondria, is this why ABCC6 deficient mice do not manage mineral appropriately following injury?
- What role does ABCC6 have on mitochondrial structure and function?
- Are the mitochondria the primary cellular component responsible for regulating calcium, phosphate, and mineralization following injury? What signaling occurs to alert the mitochondria to damage? Does plasmin communicate with the mitochondria?

To examine many of these questions, *in vitro* examination will be necessary through utilizing either C2C12 cell culture (myocyte lineage) or muscle explant and primary culture from genetically modulated animals. *In vitro* experiments will allow for a higher throughput analysis of the molecular mechanisms at play and will allow for detailed measures of mitochondria function, cellular calcification status, and cellular signaling pathways under different experimental conditions with greater resolution.

### **What Do These Findings Mean Clinically?**

Taken together, much of my dissertation work has been focused on defining the

pathophysiology of trauma-induced calcification. Through utilizing cues from prior investigations and long-standing tenants of bone biology, we demonstrated in a murine model that dystrophic calcification, independent of its inciting source, if persistent can promote HO. Importantly, dystrophic calcification, or the deposition of amorphous calcium and phosphate within soft tissue is commonly observed clinically following injury, but many times does not impact the patient and resolves over time. Considering independently that traumatic injury associated with HO formation (burn, blast, traumatic brain injuries, etc.) have been associated with reduced macrophage function, it is plausible that these two clinical events could occur in the same patient population and potentially lead to HO formation.

While plausible, many prospective studies will be necessary to corroborate our findings clinically. One major challenge is that dystrophic calcification, unlike HO, many times does not cause patients discomfort and therefore will go undetected. Thus, in order to correlate a dystrophic precursor with HO formation, we would necessitate a prospective longitudinal study where patients at risk for HO formation, ideally those who had already experiences HO (thus putting them at higher risk for recurrence), would be assessed by radiographic analysis and biopsy at multiple time points following injury to assess the state of calcification. While this study would take a considerable amount of time and cost to conduct, as an alternative strategy we are currently collecting patient biopsies, both retrospectively and prospectively, of patients with HO. Through looking at these samples histologically, we are attempting to find examples of patients that possess both HO lesions and dystrophic calcification lesions

within the same histologic section, thereby giving further evidence that the transition of dystrophic calcification to HO is plausible.

Through my thesis work, we have likewise identified essential soft tissue protection mechanisms (plasminogen and ABCC6/pyrophosphate) that inhibit pathologic calcification. Through our plasminogen-based investigations, we utilized both genetic and pharmacologic reduction of plasminogen; however, complete plasminogen deficiencies in humans are incredibly rare. Yet, recent investigations by our laboratory, in collaboration with the Burn Unit at Vanderbilt University Medical Center, has demonstrated that patients who experience a severe burn injury possess decreased levels of plasminogen at their time of admission that correlated with their severity of injury. Going forward, we aim to correlate plasminogen levels to other forms of trauma beyond burn injuries and begin to assess longitudinally if a patient's plasminogen level correlates with adverse consequences in survival or repair.

Considering our ABCC6-based investigation, unlike plasminogen, genetic abnormalities in *Abcc6* do exist in patients with a condition known as pseudoxanthoma elasticum (PXE). While loss-of-function mutations of *Abcc6* such as is those seen in PXE are rare (1:50,000), an estimated 1:150-1:300 individuals are carriers for pathologic mutations in *Abcc6* [360]. Therefore, while our results do not suggest that all individuals with either partial and biallelic pathologic mutations in *Abcc6* will develop HO, they rather suggest that these individuals may be at risk for the formation dystrophic calcification within damaged soft tissue. Given i) the frequency of partial

mutations of *Abcc6* and that ii) our studies were the first to demonstrate a pathologic consequence of even a partial loss of ABCC6, going forward, I would like to prospectively assess individuals with confirmed HO, for mutations in the ABCC6 gene. If confirmed, these studies may open the potential for ABCC6-genetic status to be considered a risk factor for HO formation.

Considering patients with PXE, while we observed dystrophic calcification in the ABCC6 animal model following injury, the calcification was sufficiently regressed over 28 days. As PXE is a progressive calcific disease affecting soft tissues such as the eyes, skin, and cardiovascular system, these results together raise many questions. Specifically:

- Why does the calcification formed in PXE patient not regress?

Our hypothesis from assessing many historical articles and comparing our murine results is that the areas affected in PXE are largely immune privileged areas where macrophages do not enter, such as the eye. Therefore, we anticipate that all soft tissues in the mice are at risk for calcification, however the macrophages can manage this calcification on many of the tissues, but are unable to reach other tissues, resulting in the build up of pathologic calcification.

- What about calcification of the skin? If immune cells can enter the tissue why does the calcification continue to build up?

My hypothesis currently is that the calcification experiences in the skin is a progressive condition that the macrophages are continually cleaning up. However, while macrophages can enter the skin, we observe the calcification in PXE patients surrounding elastic fibers. Therefore, further work investigating if the location of these pathologic deposits is indicative of altered macrophage phagocytosis of mineralization is warranted. Furthermore, given that we see areas of calcification forming in patients with PXE in regions of the greatest movement (neck, axillary, etc.), it is plausible that these regions experience microdamage to the tissue, thereby supporting continual damage and calcification of the tissue. Further studies are necessary to determine if the lesions within PXE patients are static or if they turn over.

If found that the calcific lesions in PXE, primarily those in the skin, do turn over, this opens the possibility for therapeutics aimed at enhancing macrophage function in combination with those limiting new dystrophic calcification; thereby effectively resolving the pathologic mineralization. However, in areas where immune cells cannot reach, such as the eye, we do not currently possess a therapeutic strategy to reverse the calcification, but rather would need to focus on blocking the progression of the disease.

Going forward, I am excited to see where these findings lead us. I hope one day we will be applying a universal theory of fracture repair, such that advancements will make it possible to customize fracture repair to the patients, thus lowering the risk for non-union. I hope one day we will utilize our knowledge of bone biology to design

synthetic hypertrophic chondrocytes to promote bone formation to improve spine fusions and long segment defects. Finally, I hope we will be able to define the pathophysiology of trauma-induced HO and identify therapeutic strategies that will effectively limit soft tissue calcification in traumatically injured patients as well as those suffering genetic diseases such as PXE.

Considering again the quote by Dr. Atul Gawande, in his book entitled *Being Mortal*,

*“Even as our bones and teeth soften, the rest of our body hardens. Blood vessels, joints, the muscle and valves of the heart, and even the lungs pick up substantial deposits of calcium and turn stiff... As we age, it is as if the calcium seeps out of our skeleton and into our tissues.”*

I hope what I have learned in my thesis work will be the first steps to regulating biomineralization as we age. While we hope never to experience a traumatic injury, one inevitable factor of life is that we age. Therefore, many individuals (our friends, family, and colleagues), will likely experience the loss of mineral from their skeleton and its reemergence in soft tissue. I hope through our work in the laboratory, that one day we will have the ability to block the mineral transition associated with aging, thereby preserving bone and soft tissue to their youthful functions.

## APPENDIX I:

### Article 12: Necrotizing Fasciitis: Coagulopathy, Adrenal Insufficiency, and Nosocomial Transmission

Deke M. Blum<sup>d,^</sup>, Alexander A. Hysong<sup>d,^</sup>, Samuel L. Posey<sup>d,^</sup>, Michael A. Benvenuti<sup>a</sup>, Teresa A. Benvenuti<sup>a</sup>, Thomas J. An<sup>a</sup>, Megan E. Johnson<sup>a,e</sup>, Gregory A. Mencio<sup>a,h</sup>, William T. Obremskey<sup>a</sup>, **Stephanie N. Moore-Lotridge<sup>a,c</sup>**, and Jonathan G. Schoenecker<sup>a,b,c,e,\*</sup>

<sup>a</sup>Department of Orthopaedics and Rehabilitation, Vanderbilt University Medical Center.

<sup>b</sup>Department of Pathology, Microbiology, and Immunology, Vanderbilt University Medical Center.

<sup>c</sup>Department of Pharmacology, Vanderbilt University

<sup>d</sup>Vanderbilt University School of Medicine

<sup>e</sup>Department of Pediatrics, Vanderbilt University Medical Center

<sup>f</sup>Center for Bone Biology, Vanderbilt University Medical Center

\*To whom correspondence should be directed

<sup>^</sup>Indicated that authors contributed equally

*In preparation for Submission*



## Abstract

Necrotizing fasciitis carries a mortality rate of over 25 percent, making it one of the most serious infections of the musculoskeletal system. Medical therapies for necrotizing fasciitis are scarce, and novel pharmacologic treatments are needed. In this case series, we present 3 cases of necrotizing fasciitis to highlight the danger and potential benefit of treating coagulopathy and adrenal insufficiency in this condition. Retrospective chart review was conducted, and an account of hospital course, vital signs, laboratory values, surgical treatment, and medical therapy for each patient was documented. All 3 patients developed consumptive coagulopathy and adrenal insufficiency, and only the 2 patients who received aggressive coagulation and adrenal support survived. In necrotizing fasciitis, the body employs several mechanisms to prevent the spread of pathogens, including the formation of fibrin/platelet webs at involved sites. These webs act as physical barriers to trap pathogens and prevent dissemination. The bacteria that cause necrotizing fasciitis possess virulence factors that dysregulate coagulation and fibrinolysis to evade these barriers. Causative pathogens of necrotizing fasciitis also express superantigens that trigger excessive inflammation. Dysregulation of coagulation and fibrinolysis combined with the effect of superantigens results in a hyperinflammatory, hypercoagulable, and hyperfibrinolytic state that can lead to disseminated intravascular coagulation (DIC) and adrenal insufficiency. We believe the development of coagulopathy and adrenal insufficiency in necrotizing fasciitis are signs of severe disease, and targeted medical therapies directed at these complications may have potential to improve outcomes.

## Introduction

Necrotizing fasciitis has an annual incidence of 3 to 5 cases per 100,000 population, but carries a mortality rate of 29%, making it one of the most serious infections of the musculoskeletal system [425]. Low incidence and high mortality make necrotizing fasciitis a difficult disease to treat and study. As such, current management is largely based on historical practice patterns with rapid recognition and surgical debridement being widely accepted as paramount for survival; however, validated medical therapies are scarce, and novel pharmacologic treatments are needed. A thorough understanding of the pathophysiology of necrotizing fasciitis is required to identify potential targets for therapeutic intervention. Here, we examined the pathophysiology of necrotizing fasciitis with a focus on the causative pathogens' ability to manipulate the coagulation and fibrinolytic systems to evade the body's protective containment mechanisms [426]. In the setting of necrotizing fasciitis, manipulation of the fibrinolytic system can lead to the development of a consumptive coagulopathy and subsequent depletion of fibrin, platelets, and various other coagulation factors, increasing the risk of complications such as septic shock, DIC, adrenal insufficiency, and eventually death [427]. In this case series, we present three cases that highlight these dangers and examine the hypothesis that, in patients with necrotizing fasciitis, addressing coagulopathy and corticosteroid insufficiency with targeted medical therapies may improve outcomes. Additionally, one of the cases represents an example of nosocomial transmission to an orthopaedic surgeon, which highlights the importance of healthcare providers wearing an N-95 respirator when treating this patient population.

### *Historical Perspective*

As the “Father of Medicine,” Hippocrates was perhaps the first physician to describe necrotizing fasciitis as “malignant cases of erysipelas, some from a known exciting cause and some not. Many died, and many suffered pain in the throat...the erysipelas would quickly spread widely in all directions...Flesh, sinews and bones fell away in large quantities” [428]. This classic description of necrotizing fasciitis hints that transmission can occur from direct contact as well as from patients with pharyngitis. It also describes the rapid and invasive nature of necrotizing fasciitis. In the 19<sup>th</sup> century, Dr. Joseph Jones (a surgeon during the American Civil War) depicted necrotizing fasciitis with chilling detail and impressive accuracy. In his published scientific findings from 1871, Dr. Jones describes necrotizing fasciitis as having, “no quality of pus except its fluidity and color...the muscles could be seen as nicely dissected as if prepared for class demonstration by the anatomist’s knife” [429]. These descriptions are consistent with the classic finding of liquefactive necrosis (akin to "dishwater fluid") in necrotizing fasciitis and display the difficulty that the body has containing the infection. Despite our increased understanding of this pathology, necrotizing fasciitis continues to present therapeutic and surgical challenges to modern day physicians.

### Patient 1

A 17-month-old female presented to a regional hospital with fever, nausea, vomiting, and diarrhea. Physical exam and laboratory values at presentation were unremarkable. The patient was discharged home with supportive care for a presumptive diagnosis of

“the flu.” The patient’s fever persisted over the next 3 days, and on the third day her arm was noted to be swollen with dark discoloration of her fingers and bloody yellow discharge from her antecubital fossa. The patient presented to her primary care physician (PCP) who immediately referred her to the emergency department (ED).

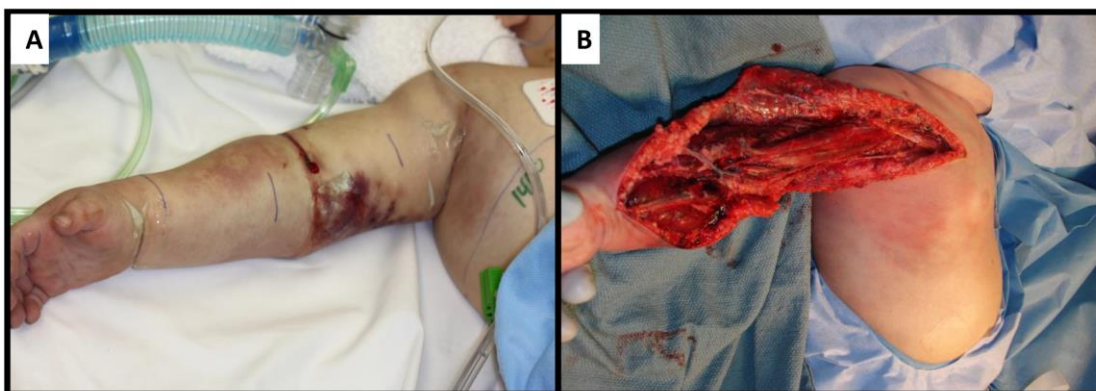
Upon arrival to the ED, she was found to be febrile to 101°F and tachycardic. Physical exam revealed a grossly swollen right arm that was mottled, cool to the touch, and exquisitely painful. Radial and ulnar pulses were absent in the right extremity, but doppler ultrasound did reveal a right brachial pulse. Heparin was administered for suspected thrombosis; however, it was discontinued when the patient was found to have a platelet count of 27,000/ $\mu$ l. Due to concern for sepsis the patient was started on vancomycin and ceftriaxone and was transferred to a tertiary care hospital.

Upon arrival to the second hospital, she was intermittently hypotensive to the 60s mm/Hg systolic and displayed signs of respiratory fatigue. She received a bolus of IV saline, which normalized her blood pressure. However, she had continued respiratory distress and was subsequently intubated.

Once stable, she remained normotensive in the ED without pressure support. Her fever increased to 102.5°F, and her coagulopathy worsened with a PT-INR of 1.9 in addition to a persistently low platelet count. To correct her coagulopathy, she was administered vitamin K, fresh frozen plasma, and packed blood cells. Subsequent

blood work displayed an improved PT-INR at 1.6, though platelets remained low at 20,000/ $\mu$ l.

During this time, orthopaedics diagnosed the patient with compartment syndrome and had high concern for necrotizing fasciitis. The patient was taken to the OR for immediate fasciotomy, fascial biopsy, irrigation, and debridement (Figure 94).

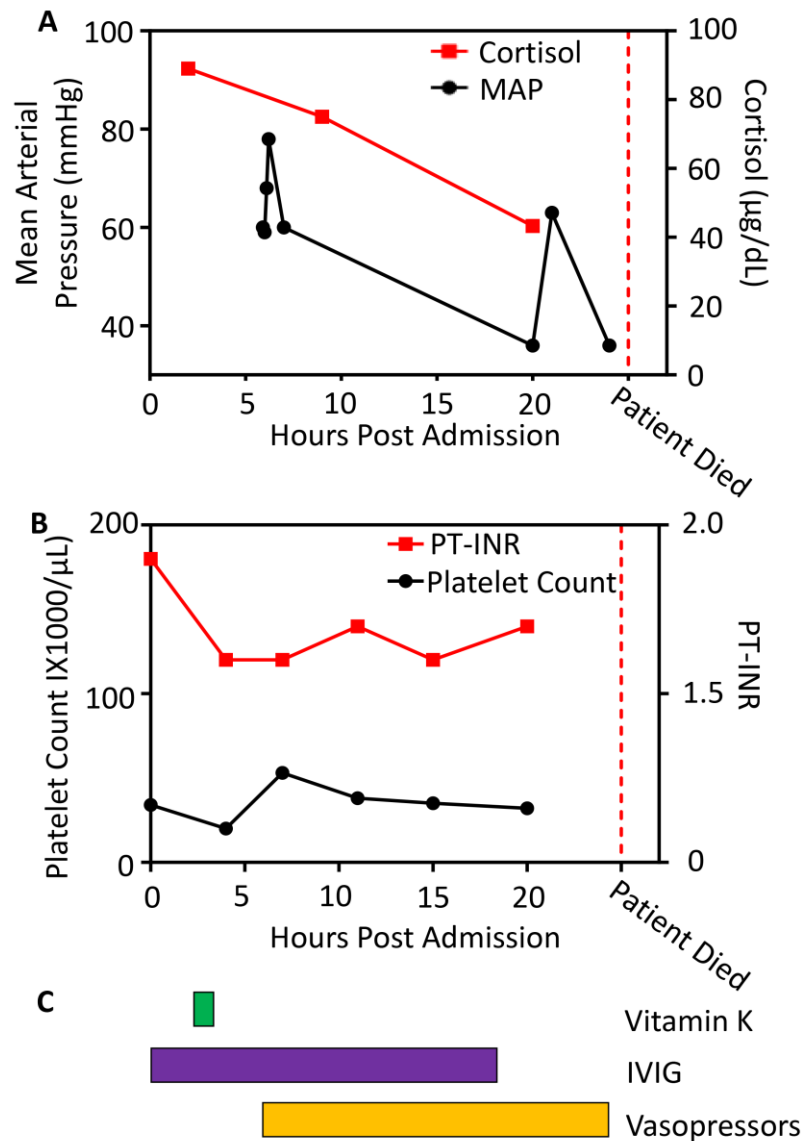


**Figure 94: Patient 1's right upper extremity.** A) Appearance of patient 1's arm on presentation with characteristic findings of necrotizing fasciitis: erysipelas, swelling, discharge, and mottling. B) Intraoperative findings in necrotizing fasciitis. Rapid dissemination of bacteria and liquefactive necrosis beneath fascial planes results in well dissected muscular compartments independent of the surgeon's knife.

In the OR, the surgical team explored the right upper extremity to a margin of uninvolved tissue on the anterior chest. Fascial biopsy confirmed the diagnosis of necrotizing fasciitis. Of note, the patient required multiple rounds of calcium and blood products to maintain adequate perfusion pressures throughout the procedure.

After the fasciotomy, the vascular status of the patient's arm improved, and her right radial pulse returned. The incisions were left open for a repeat debridement the following morning.

Initially, the patient was normotensive upon admission to the ICU, and the team serially monitored serum cortisol to assess for the development of corticosteroid insufficiency. Fresh frozen plasma and blood products were continued to achieve a target PT-INR of <1.3 and platelet count of >30,000/ $\mu$ l (a second dose of vitamin K was ordered but not administered). Antibiotics (clindamycin, vancomycin, penicillin G, and ceftriaxone) were continued and IVIG was added to attenuate her inflammatory response. Serial labs revealed a persistently low platelet count, an increased PT-INR to 1.7, and a progressively declining cortisol level (from 89  $\mu$ g/dL at 3:45 p.m. to 55.6  $\mu$ g/dL at 4:15 a.m. the next day) (Figure 95).



**Figure 95: Patient 1 Laboratory Values.** Vital signs and major coagulation labs were taken during treatment and premortem for patient 1, illustrating the downward course of her disease and attempted efforts at resuscitation. A) During the course of her infection, her serum cortisol (red line) trended steadily downward along with her mean arterial pressures (black line). B) Patient 1's PT-INR (red line) started high at 1.9 and remained elevated above 1.6 for the duration of her disease course. Patient #1's platelet count (black line) was also depressed below 70,000/ $\mu$ L throughout her

hospitalization. C) The patient unfortunately expired 26 hours after admission despite treatment with Vitamin K (green), IVIG (purple), and vasopressors (yellow).

The patient remained hemodynamically stable without the use of vasopressors throughout the night but became hypotensive in the early morning. The decision was made to begin dopamine for pressure support. Repeat evaluation by the orthopaedic surgery team revealed a similar exam without spread of the infection, and they proceeded with the planned debridement. The procedure was completed without complication and intraoperative fascial biopsy displayed no evidence of infection.

However, shortly after the debridement, the patient developed abdominal distension concerning for abdominal compartment syndrome. She quickly decompensated and was taken for emergent exploratory laparotomy. Her abdomen was opened, and a silo was placed. After surgery, chest compressions were required for over an hour due to pulseless electrical activity. A rhythm was eventually obtained; however, the patient's blood pressure remained persistently low despite resuscitative efforts. After 3 hours, the patient's parents requested that all lifesaving medical treatment be stopped, and the patient expired.

Autopsy revealed that the cause of death was severe sepsis with disseminated intravascular coagulation (DIC). Pertinent findings included bilateral subarachnoid hemorrhages, gram-positive cocci in the antecubital fossa and bilateral lungs, and widespread petechiae on the gastrointestinal mucosa. Labs shortly before death



revealed a random serum total cortisol of 43.3 µg/dL (drawn at 9:30 am), PT-INR of 1.7, and platelet count of 32,000/µl, and blood and soft tissue cultures revealed Group A streptococcus.

Patient 2:

A previously healthy 12-year-old girl presented to the ED three days after falling and scraping her left knee. Over the course of day, the patient's knee became erythematous, painful, and swollen. She developed a subjective fever, rigors, and emesis. Three days after the initial injury, she presented to her PCP who immediately referred her to the local tertiary care center's ED.

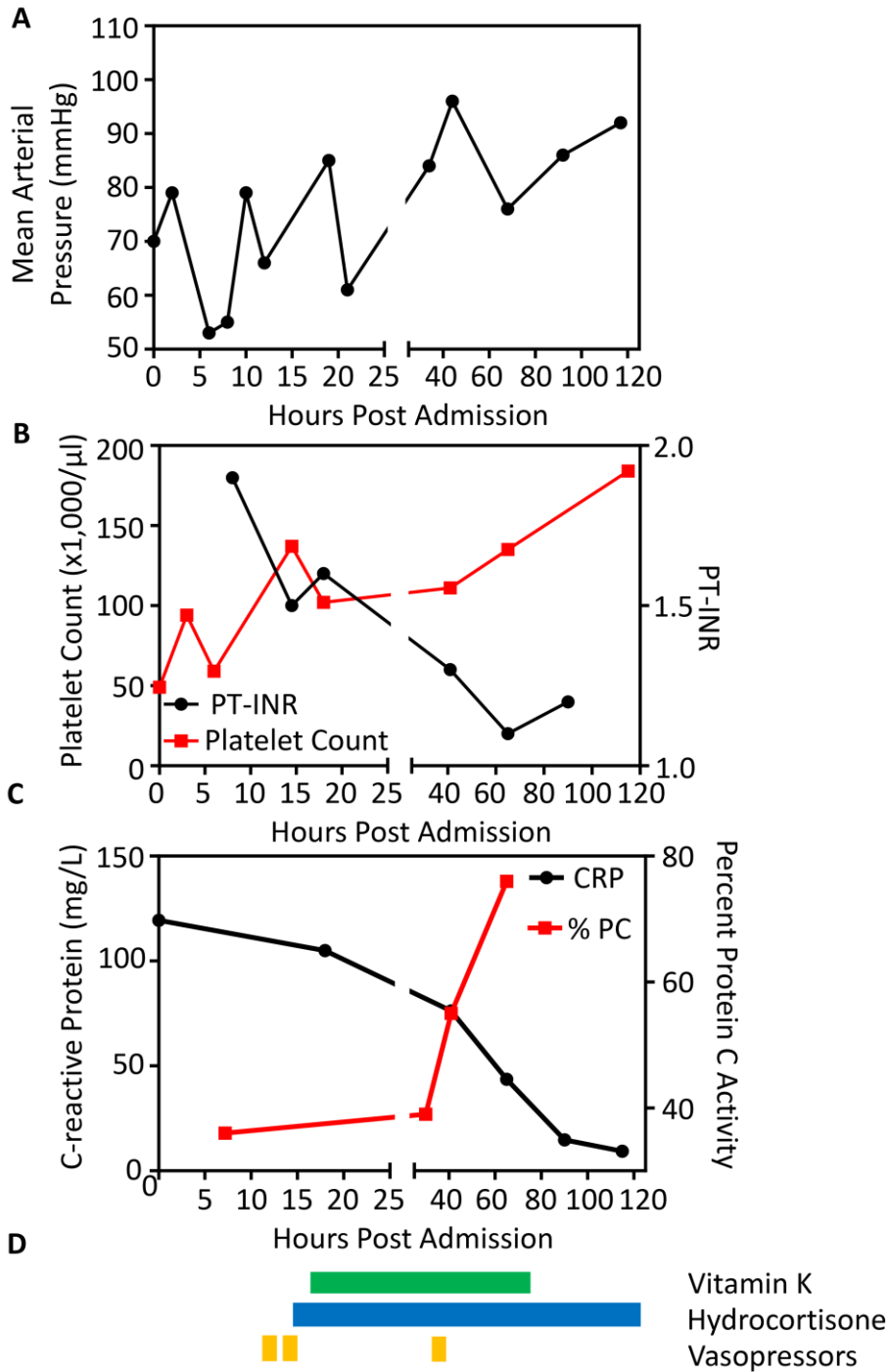
In the ED, she was found to be febrile to 102.7°F with severe pain radiating from her left knee to her groin on ambulation. An x-ray of the knee was consistent with soft tissue swelling. Infectious and inflammatory labs were drawn. While waiting for results, the patient became acutely hypotensive to the 90s/30s mm/Hg and developed an erythroderma type rash. IV normal saline and epinephrine were administered to normalize and maintain her blood pressure. In addition, vancomycin and clindamycin were initiated out of concern for sepsis. The patient was transferred to the critical care unit. Notable lab results from presentation including a platelet count of 49,000/µl and C-reactive protein (CRP) of 119.4 mg/L.

During this time, orthopaedics evaluated the patient. Due to concern for necrotizing fasciitis, the patient underwent irrigation, debridement, and fascial biopsies of the left

knee. Biopsies confirmed the diagnosis of necrotizing fasciitis. The effected tissue was removed to a point of negative margins.

Postoperatively, the patient was started on high-dose hydrocortisone with a loading dose of 160 mg followed by 10 doses of 20 mg q6h (random serum total cortisol prior to the procedure was 7.4 µg/dL) and penicillin G for potential group A streptococcus (GAS). Coagulation labs were drawn and revealed an elevated PT-INR of 1.9, an elevated fibrinogen of 480 mg/dL, low protein C activity (36%), normal protein S activity, and an elevated D-dimer at 2.38µg/ml. Given low protein C activity, there was concern for a persistent consumptive coagulopathy, and vitamin K was administered for a total of 3 doses throughout her stay.

Following initiation of these therapies, the patient was successfully weaned from pressor support. Her PT-INR, Protein C, D-dimer, Fibrinogen, CRP, and platelets all gradually returned to normal (Figure 96). She returned to the operating room two more times for additional debridement and eventual closure. Steroids were weaned and discontinued. She was discharged home in stable condition on Day 6 with clindamycin monotherapy. Four months following discharge, her only complication was intermittent knee pain.



**Figure 96: Patient 2 Laboratory Values.** A) Patient 2 presented with vasopressor resistant hypotension and B) a major coagulopathy: low platelet count (49,000/ $\mu$ L), low protein C activity (37%), and elevated INR (1.9). C) Patient 2's active systemic inflammatory response is demonstrated by the CRP curve, with a peak at 120 mg/L.

D) Throughout the course of the hospitalization, Patient 2's condition gradually improved with systemic support via administration of vitamin K (green), hydrocortisone (blue), and vasopressors (yellow) shown below the laboratory trends.

### Patient 3

A previously healthy 47-year-old orthopaedic trauma surgeon presented to the hospital ten days after operating on a patient with severe lower extremity GAS necrotizing fasciitis. During the operation, all personnel in the operating room wore standard protective equipment, including surgical masks. The surgeon suffered a bovie strike to left middle finger that was promptly washed out and dressed. Otherwise, the operation was completed without complication.

The surgeon was asymptomatic for the week following the surgery, but on Day 8 he developed fatigue, malaise, subjective fevers and chills. Subsequently, he noted erythema and swelling in the third and fourth web spaces of his right foot (which were chronically affected by tinea pedis). This progressed to involve his entire lower extremity to the medial thigh. Upon admission, he had MRI findings consistent with cellulitis and lymphangitis in the right lower extremity and was admitted for IV antibiotics (vancomycin and piperacillin/tazobactam). Notable initial vital signs and laboratory results included a mean arterial pressure (MAP) of 66 mm/Hg, CRP of 284 mg/L, PT-INR 1.5, and a platelet count of 234,000/ $\mu$ l.

The surgeon's clinical condition continued to worsen, with progressive swelling and severe pain in his right lower extremity. On hospital Day 2, he developed hypotension to the 60s mm/Hg systolic and required volume resuscitation and vasopressors. In addition, he received red blood cell and fresh frozen plasma transfusions. Blood cultures were drawn and returned positive for GAS. Genetic typing revealed the same strain found in the patient previously operated on by the surgeon. On hospital Day 3, the surgeon displayed signs of toxic shock syndrome and multi-organ failure (MOF) with acute respiratory distress syndrome (ARDS), which required intubation. Subsequently, he was taken to the OR for debridement. In the OR, the skin, subcutaneous tissue, and muscle of the right thigh were viable, but fascial necrosis was present. On hospital Day 4, he was taken to the OR for a second debridement, which revealed progression of the necrosis. Labs continued to display MOF with severe coagulopathy. Platelets dropped to a trough of 63,000/ $\mu$ l, and PT-INR was elevated to 1.6. Random total serum cortisol was found to be 18  $\mu$ g/dL and IV dexamethasone was started at that time. On hospital Day 5, the surgeon's condition began to improve. The lower extremity erythema began to resolve, and there was resolution of his ARDS. On hospital Day 6, platelet count began to improve, rising to 100,000/ $\mu$ l. On hospital Day 7, platelets rose to 203,000/ $\mu$ l, and a wound vacuum was placed over the right medial thigh. The surgeon was extubated on hospital Day 9 and discharged home on hospital Day 12. Seven days after discharge, he underwent delayed primary closure of the medial thigh wound. He has since returned to full practice as an orthopaedic trauma surgeon.

Of note, the surgeon was not the only individual who suffered GAS infection following participation in the necrotizing fasciitis debridement. A resident that was present for the case developed severe strep pharyngitis three days after the operation, presumed to be from inhalation of the infectious organism. Subsequent culture of Patient 3's throat revealed GAS colonization, suggesting that he became an asymptomatic carrier of the pathogen following exposure in the operating room.

### Discussion

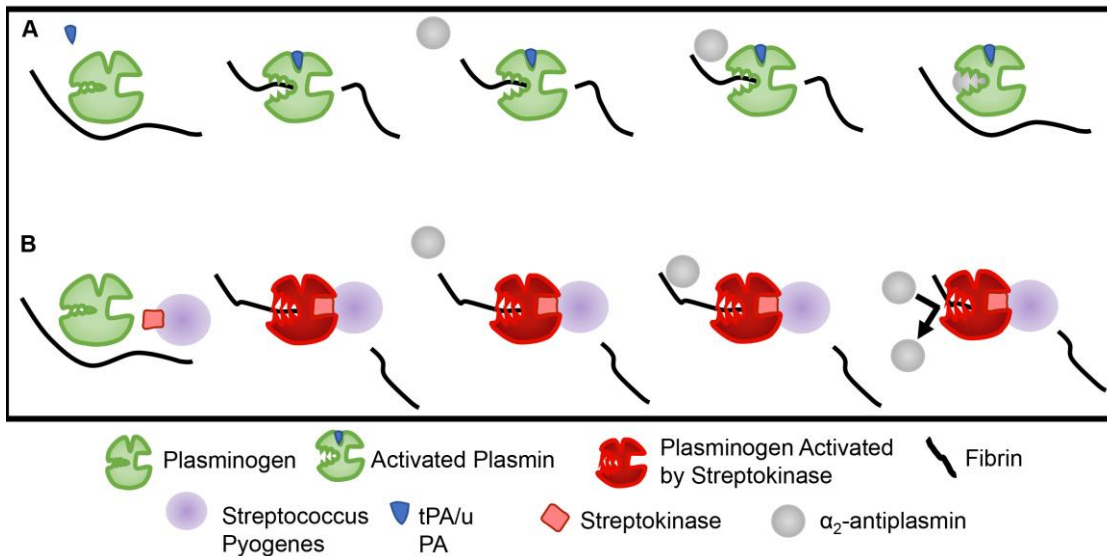
Due to low incidence and rapid progression, necrotizing fasciitis is a difficult disease process to treat. Currently, diagnosis and treatment are largely based on historical practice patterns and logical inference. However, it is not common practice to use the coagulation and hypothalamic-pituitary-adrenal (HPA) axis to monitor illness severity [15, 430]. These three cases suggest that developing a coagulopathy and corticosteroid insufficiency in necrotizing fasciitis are signs of severe disease, potentially indicative of a poor prognosis. Additionally, they suggest that efforts should be made to address these complications with targeted therapeutic interventions. To justify these novel approaches, we will explore the pathophysiology of necrotizing fasciitis.

### *Pathophysiology*

Under physiologic conditions, the elements of the musculoskeletal system are separated into distinct anatomical compartments by fascia and other matrix tissues. Tissue damage due to infection, such as in necrotizing fasciitis, causes disruption of these anatomic compartments and predisposes to the spread of infection into and

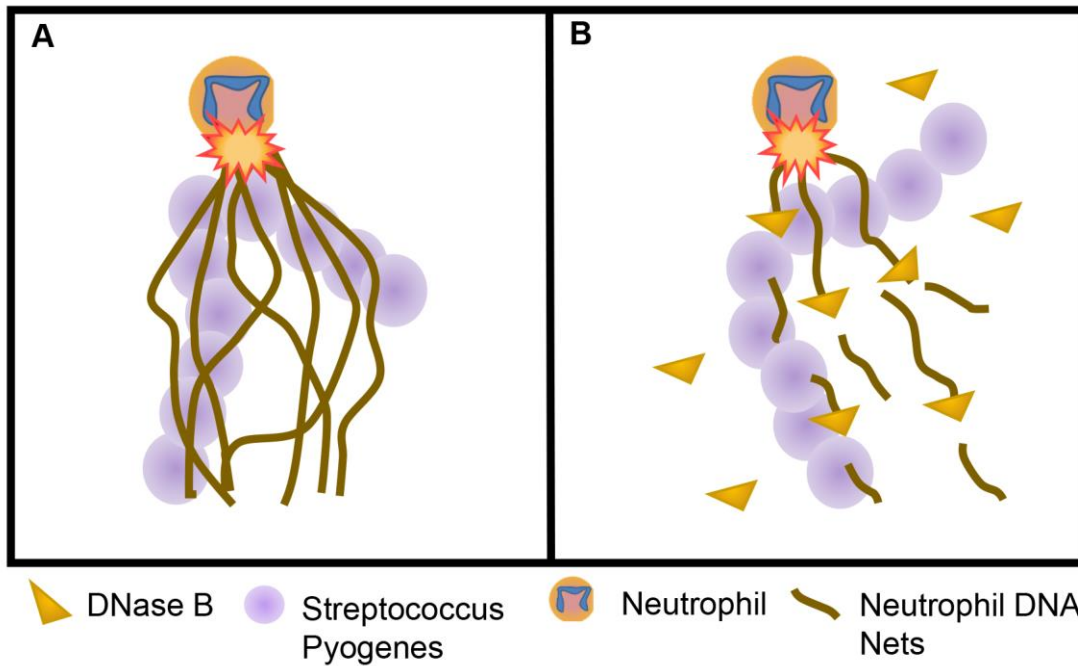
through adjacent tissues[427]. To combat this, the body employs several mechanisms to contain and prevent the spread of pathogens. First, in response to infection, the body activates the acute phase response and releases procoagulant factors that lead to the formation of a fibrin/platelet web at the site of infection [431, 432]. This web acts as a physical barrier to trap pathogens and prevent dissemination. In addition, neutrophils are attracted to the site of infection and create neutrophil extracellular traps, which consist of extracellular DNA fibers that also act as a physical barrier to trap pathogens [433, 434]. The bacteria that cause necrotizing fasciitis possess virulence factors that hijack these protective mechanisms and instead use them to evade host immune responses.

*S. pyogenes*, the most common cause of necrotizing fasciitis, is an excellent model for demonstrating how pathogens hijack and evade the body's protective containment mechanisms [435]. *S. pyogenes* expresses the virulence factor streptokinase, which constitutively activates plasmin and consequently fibrinolysis [432, 436]. Plasmin bound to streptokinase is resistant to deactivation and thus prevents formation of the fibrin/platelet web at the site of infection, allowing *S. pyogenes* to spread through tissues and along fascial planes (Figure 97) [437, 438]. Furthermore, *S. pyogenes* also expresses DNase B, which is an enzyme that cleaves DNA and prevents formation of neutrophil extracellular traps (Figure 98) [439]. This also allows *S. pyogenes* to disseminate through tissues (Figure 99).

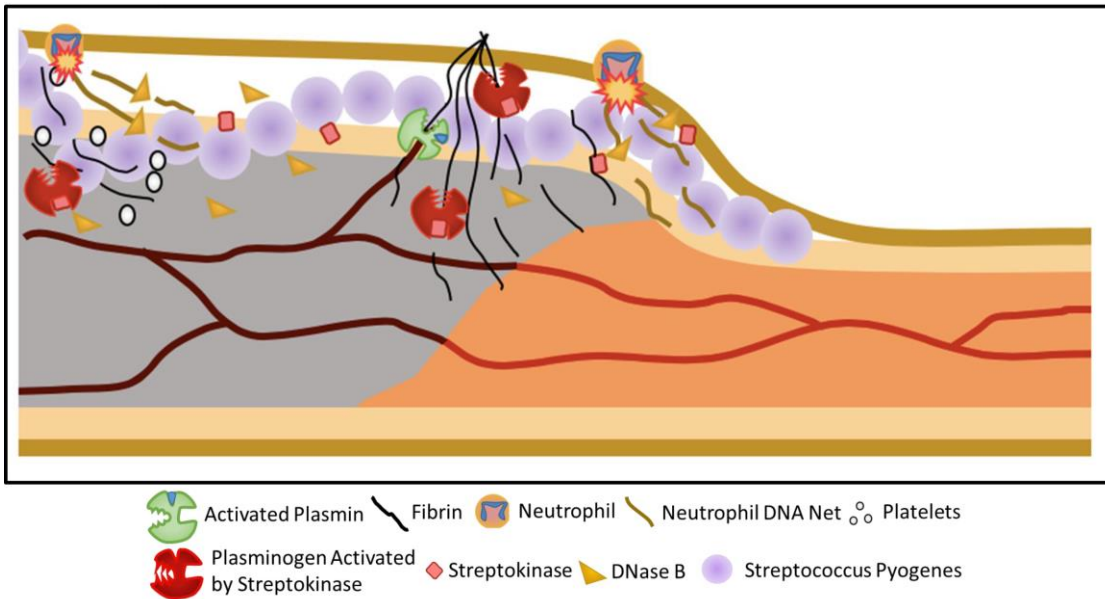


**Figure 97: Plasmin Activation.** A) Under physiologic conditions, the body employs tight control over fibrinolysis. Plasminogen is converted into its active form, plasmin, by either tPA(tissue plasminogen activator) or uPA (urokinase-type plasminogen activator). Once activated it can breakdown fibrin. After plasmin has completed its job, the body expresses proteins like  $\alpha_2$ -antiplasmin which bind plasmin and inhibit further fibrinolysis. B) In the setting of necrotizing fasciitis, strep expresses streptokinase which activates plasminogen independent of tPA/uPA. This plasminogen activated by streptokinase cannot be inhibited by the body's regulatory mechanisms. This allows the strep bacteria to rapidly degrade clots that the body develops to contain it.





**Figure 98: Containment of Bacteria by DNA Webs.** A) One way body attempts to contain the spread of bacteria is through the release of "DNA webs" by neutrophils. B) Virulent strains of strep express the virulence factor DNase B, which allows it to degrade the DNA webs and further evade containment.

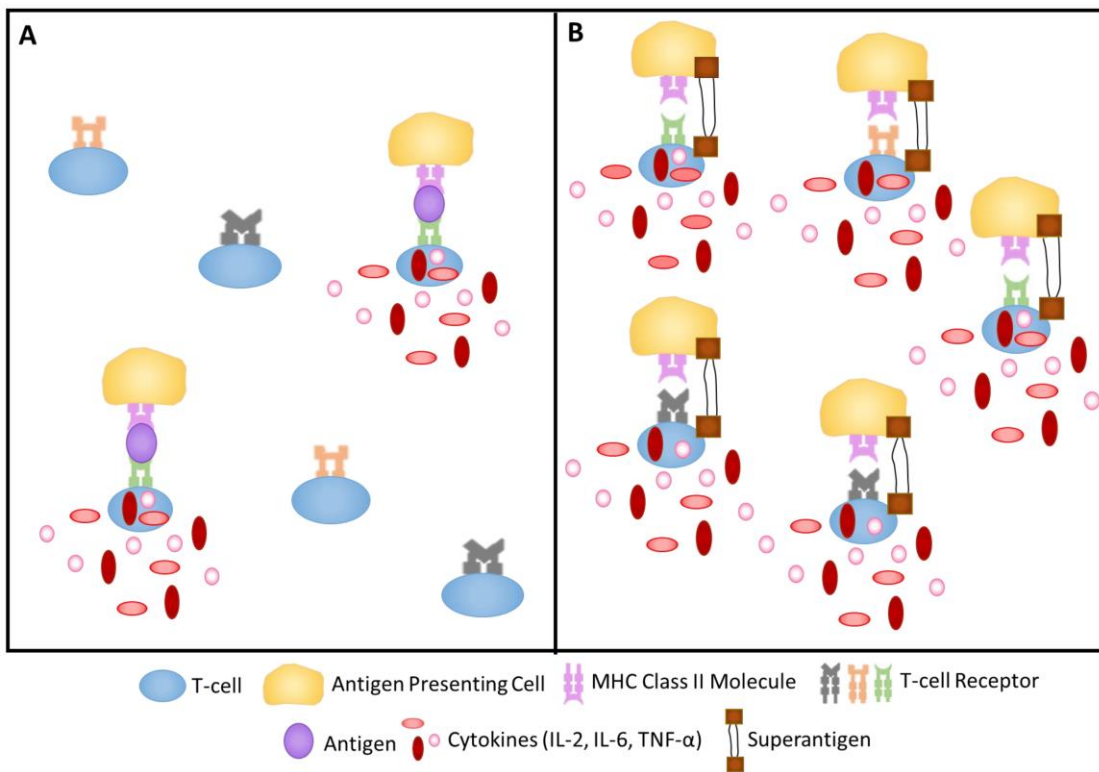


**Figure 99: Fascial Spreading.** The strep responsible for necrotizing fasciitis expresses large quantities of virulence factors like streptokinase and DNase B, which allow it to evade containment and rapidly spread under fascial planes. The body's repetitive and unsuccessful attempts to contain the bacteria contributes the consumption of clotting factors that often occurs in the setting of necrotizing fasciitis.

*S. aureus* is another pathogen that can hijack the body's containment mechanisms and cause necrotizing fasciitis. Unlike *S. pyogenes*, which activates plasmin to prevent trapping by the fibrin web, *S. aureus* expresses the virulence factors coagulase and von Willebrand binding protein (vWBP) to initially activate fibrin formation [440-443]. This abnormal activation of coagulation leads to the formation of a fibrin web that protects the bacteria and prevents host immune cells from clearing the infection, resulting in abscess formation. When the abscess reaches quorum (necessary pathogen density), *S. aureus* expresses the virulence factor staphylokinase, which similarly to streptokinase, activates plasmin to promote fibrinolysis and abscess rupture, leading to

dissemination[444]. Virulence factors such as streptokinase, DNase B, and staphylokinase destroy fibrin and DNA webs and lead to the characteristic finding of “dishwater fluid” instead of fibrinous pus during surgical debridement of necrotizing fasciitis. In the setting of inappropriate fibrinolysis, coagulation is continually activated in an ineffective attempt to contain the infection, leading to consumption of clotting factors and a coagulopathy [445].

In addition to possessing virulence factors that aid in evasion of the host immune system, causative pathogens of necrotizing fasciitis often express superantigens that can trigger excessive T cell activation and an exuberant inflammatory response [446]. Superantigens are a family of proteins that bind MHC class II molecules without first going through the conventional pathways of antigen processing and presentation by antigen presenting cells. This allows superantigens to bind MHC class II molecules as intact proteins at sites other than the peptide binding groove. By bypassing MHC-restricted antigen processing in this manner, superantigens can activate an abnormally large fraction of host T cells (up to 25%) and lead to an excessive inflammatory response resulting in septic shock (Figures 100 A&B). Specific examples of superantigens include streptococcal superantigen (SSA, expressed by *S. pyogenes*) and toxic shock syndrome toxin (TSST, expressed by *S. aureus*).



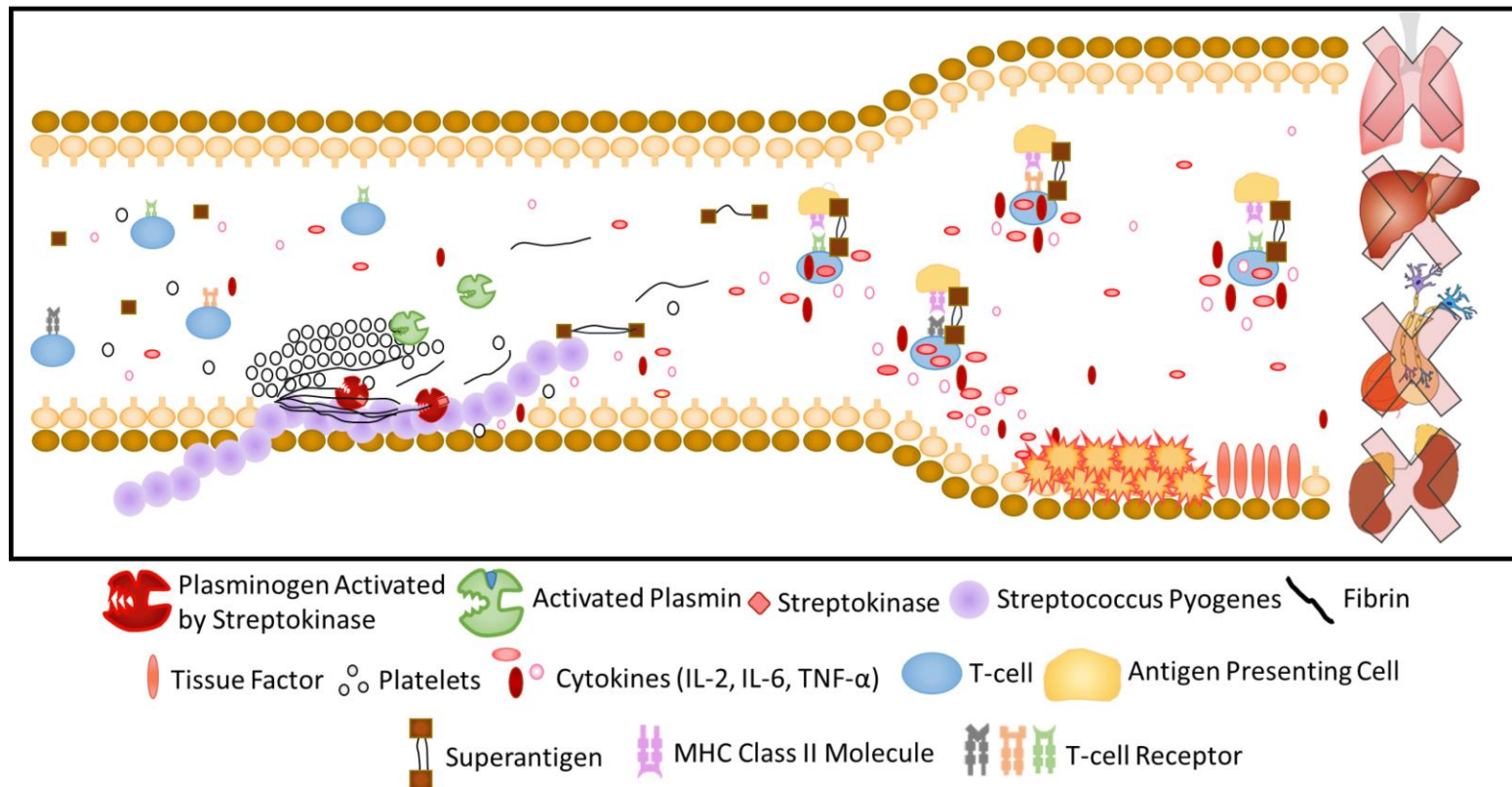
**Figure 100: Release of Superantigens.** A) In the body's normal response to infection, MHC II mediated presentation of antigens to T-cells results in the release of cytokines and bolsters the immune response. B) In the setting of necrotizing fasciitis, virulent strains of strep release superantigens that are able to aberrantly activate T-cells in the absence of bacterial antigens. This results in a massive release of cytokines and an excessive inflammatory response.

Other organisms, in addition to *S. pyogenes* and *S. aureus*, can cause necrotizing fasciitis as well. *P. aeruginosa* and *E. coli* can also manipulate the plasminogen-plasmin system to evade containment and disseminate through tissues [447, 448]. Because these pathogens also manipulate the fibrinolytic system, they often lead to consumption of clotting factors. This dysregulation of fibrinolysis and coagulation, in

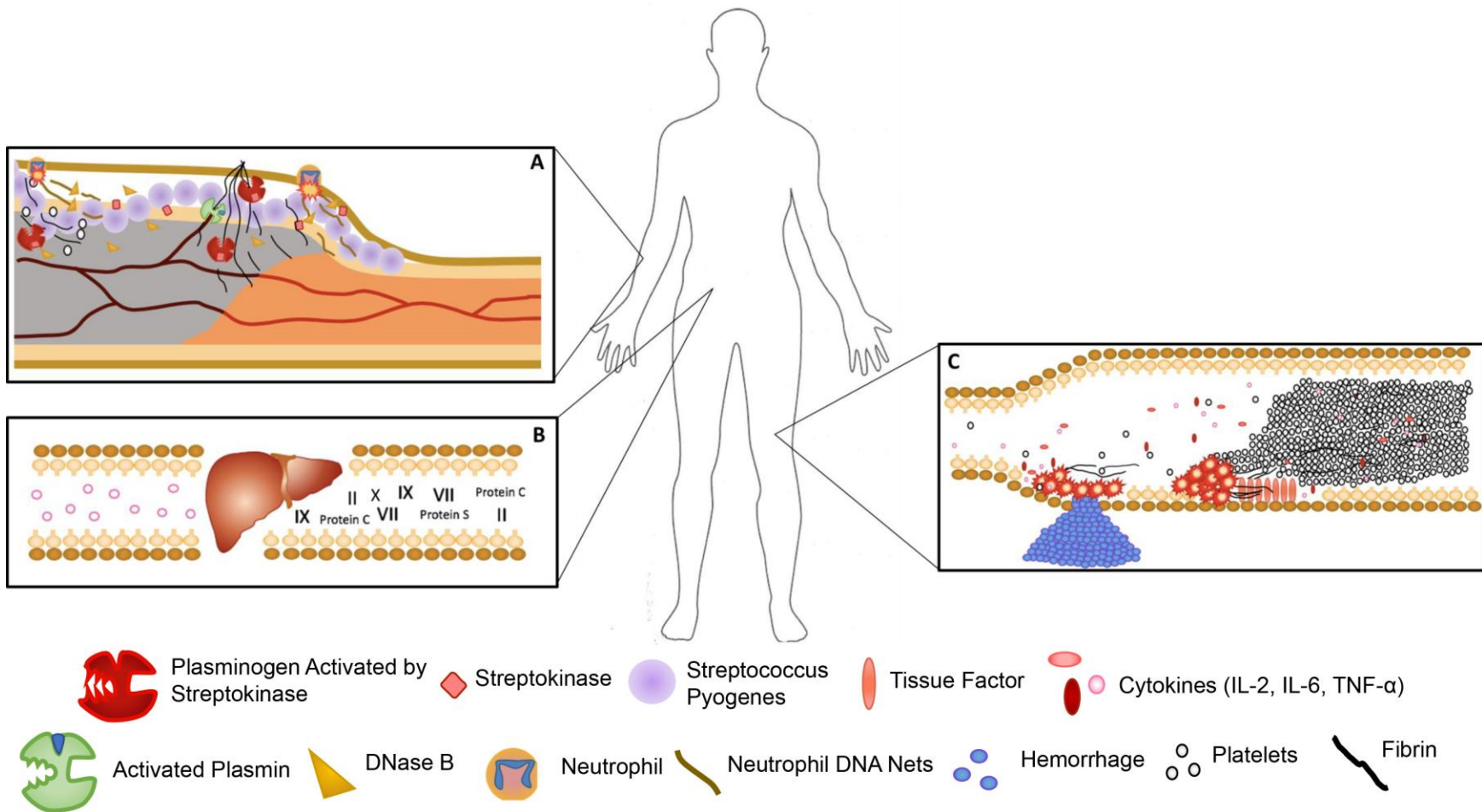
combination with excessive activation of T cells by superantigens, results in a hyperinflammatory, hypercoagulable, and hyperfibrinolytic state that can lead to several severe complications. Two such examples include multiorgan failure and septic shock, which are the main causes of mortality in necrotizing fasciitis[449].

### *Coagulation Therapies*

In the context of necrotizing fasciitis, we believe that morbidity and mortality can be improved by replenishing the factors that are commonly depleted in DIC and septic shock (Figure 101 & 102). The most depleted factors are coagulant proteins as made evident by the PT-INR of 1.9 and 1.7 in both pediatric cases and the adult case, respectively. This coagulopathic state and thrombocytopenia contribute to the commonly observed petechiae and mucosal bleeding.



**Figure 101: Development of Toxic Shock.** Superantigens produced by strep result in a massive release of cytokines (like TNF- $\alpha$ ) into the systemic circulation. These cytokines have a number of detrimental effects including significant vasodilation, disruption of the vascular endothelium, and hypercoagulability (i.e. increased clotting factor production via the liver and upregulated expression of tissue factor on the vascular endothelium). These systemic effects contribute to the septic shock and multi-organ failure that is often the cause of death in patients with necrotizing fasciitis.



**Figure 102: Diffuse Intravascular Coagulation (DIC) Following Necrotizing Fasciitis.**

A) Representative image of strep at the site of infection using its virulence to spread under the fascia. As it spreads, strep repetitively breaks down the body's attempts to contain it with fibrin-platelet clots. This process contributes to a massive consumption of clotting factors and the development of the coagulopathy that occurs in necrotizing fasciitis. In reality, this consumption does not occur exclusively at the site of infection, but rather as the infection progresses, the systemic vascular damage incited by inflammation activates coagulation and further exacerbates the depletion of clotting factors. B) In response to the cytokines released at the site of infection (namely IL-6), the liver produces thousands of acute phase reactant proteins. Included in these thousands of proteins are the vitamin K dependent clotting factors (II, VII, IX, X)/Anti-clotting factors (Protein C/S). In necrotizing fasciitis, these factors are continually produced due to rapid tissue destruction and severe inflammation. Eventually, the body begins to diminish the resources it needs to produce these factors (i.e. vitamin K). As a result, the activity of these factors begins to decrease starting with those that have the shortest half-lives (Protein C has the shortest of half-life of all the vitamin k dependent factors). C) As a result of the massive consumption of clotting factors, production of clotting factors, systemic inflammatory response, and cytokine mediated vascular changes, patients with necrotizing fasciitis often develop DIC. DIC is a concomitant state of hypercoagulability and hypocoagulability. For example, patients in DIC may develop thromboses in the microvasculature of the kidneys while at the same hemorrhaging into the skin, brain, and intestines (as was documented in Patient 1's autopsy).



Although less obvious, both procoagulant and anti-coagulant factors are depleted in severe infection, resulting in a simultaneous hyper- and hypo-coagulable state. Levels of activated Protein C, an anti-coagulant, are decreased in severe infection, and reduced activity of Protein C has been associated with poorer outcomes in infection [450]. In fact, patient 2 presented with 36% of normal protein C activity, which contributed to both her shock and coagulopathy. Replenishing this factor alone, however, has been associated with increased bleeding thereby leaving physicians without any proven therapeutic options for supplementing protein C [451].

A number of potential therapeutics can be used to replenish coagulation proteins and treat hypo-coagulability, such as fresh frozen plasma. However, fresh frozen plasma has an effective INR of 1.6, so its role in treating patients with necrotizing fasciitis is limited unless severe coagulopathy is present [452]. In the case of the patients presented here with INRs of 1.9, a large volume of plasma would be necessary to have a significant effect on the prothrombin time. By contrast, vitamin K can be used for treatment of hyper- and hypo-coagulability and is administered in more manageable doses. Because many procoagulant and anticoagulant factors require vitamin K for production, some physicians have begun using this treatment to help patients synthesize deficient factors in the setting of infection [453-455] . In patient 2, activated protein C activity and the prothrombin time were both abnormal, suggesting that there was a potential therapeutic benefit for vitamin K. While both patients were treated with vitamin K, patient 2 received three doses compared to the single dose given to patient 1. The PT-INR fell towards the normal range with treatment in patient

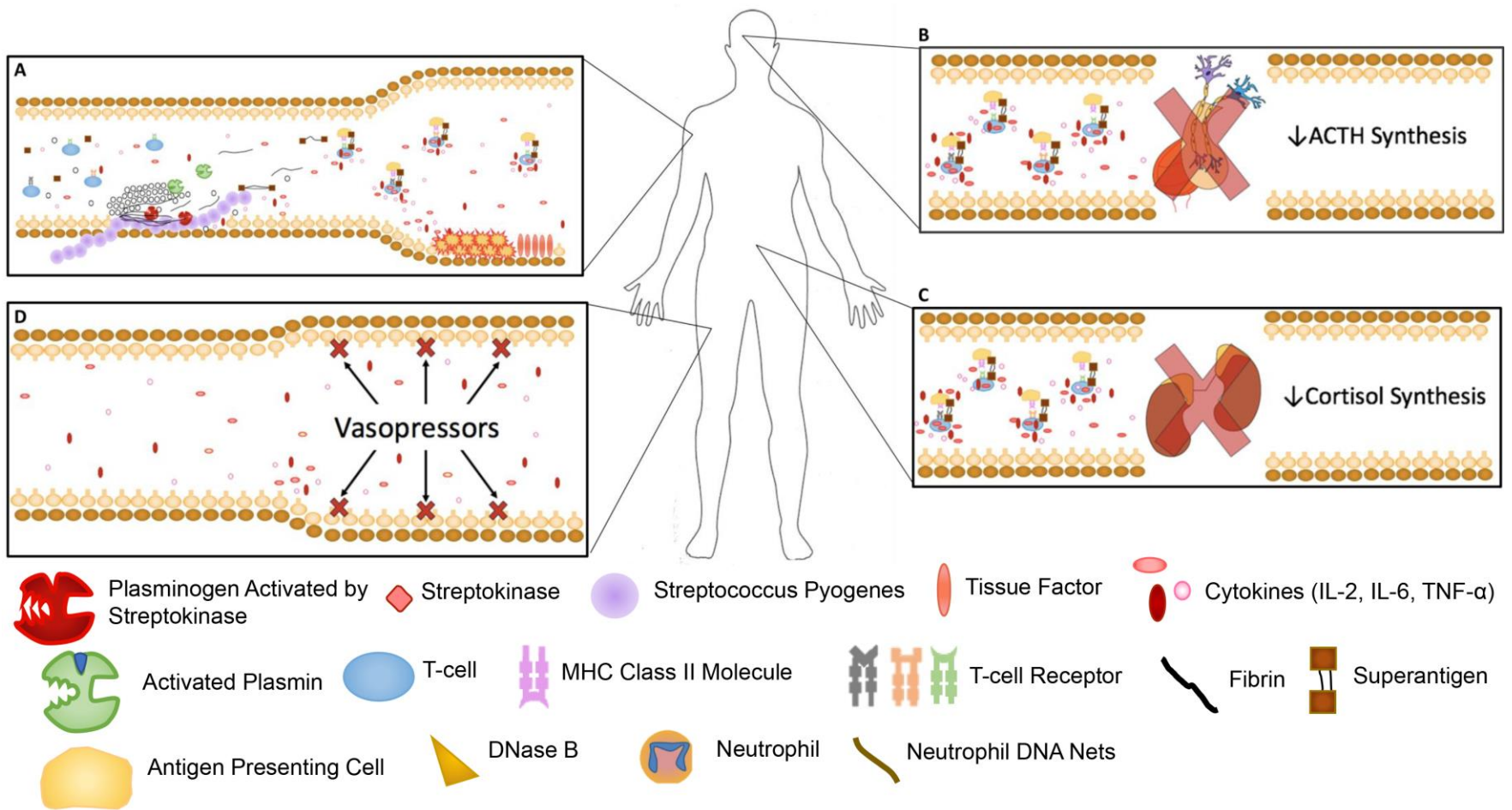
2, but there are many other factors that may have contributed to this improvement, including effective surgical intervention. In the authors' opinion, the morbidity of septic shock and the potential benefits (with minimal side effects) of vitamin K make its administration worthwhile in cases of severe disease. Furthermore, the replacement of platelets via transfusion should also be considered as they are an integral component of the initial containment aspect of the acute phase response, and their depletion is associated with poor outcomes [456].

### *Corticosteroid Insufficiency*

It is well known that systemic illness results in activation of the HPA axis and elevated plasma cortisol concentrations [457, 458]. However, the optimum cortisol response to various insults remains unclear, and there have been many studies that have found both excessively elevated or decreased plasma cortisol levels to be associated with increased mortality in severe infection [459, 460]. Furthermore, the use of corticosteroids to treat severe infection and septic shock remains controversial in terms of efficacy, with previous studies such as the CORTICUS trial showing no mortality benefit for patients with septic shock. However, newer larger trials such as the APROCCHSS trial have found a significant mortality benefit with no adverse effects [460, 461]. In this case series, patients 1 and 2 both displayed concerning plasma cortisol patterns. Patient 1 had a very high cortisol of 89  $\mu\text{g/dL}$  that declined in the setting of worsening illness, and patient 2 had a low random serum total cortisol of 7.4  $\mu\text{g/dL}$ . However, of the two patients, only patient 2 received treatment with corticosteroids, and only patient 2 survived. Based on these cases, as well as the

results of new studies such as the APROCCHSS trial, we believe that early recognition and treatment of corticosteroid insufficiency in the setting of necrotizing fasciitis may improve outcomes.

Additionally, it has been recently recognized that critically ill patients often develop a condition known as critical-illness related corticosteroid insufficiency (CIRCI), defined in 2008 as inadequate cellular cortisol activity for the severity of the patient's illness [462]. The pathophysiology of CIRCI is complex and multifactorial, involving alterations in the adrenal synthesis of cortisol, impaired synthesis of adrenocorticotropic hormone (ACTH), altered cortisol metabolism, and target tissue resistance to cortisol [463]. In addition, hemorrhage of the hypothalamus, pituitary, and/or adrenal glands in the setting of critical illness may result in CIRCI (Figure 103). In patients with severe conditions such as necrotizing fasciitis, CIRCI allows for an overwhelming inflammatory response with many potential complications.



**Figure 103: Critical-Illness Related Corticosteroid Insufficiency (CIRCI) Following Necrotizing Fasciitis.** A) Representative image of strep superantigens leading to the aberrant release of cytokines. These cytokines disseminate systemically causing hyperinflammation contributes to vasodilatation, tissue damage, and hypercoagulability.

B) Hypothalamic/pituitary dysfunction secondary to impaired protein synthesis, hemorrhage, and/or infarction may contribute to CIRCI by reducing the production of ACTH, which in turn results in less cortisol production by the adrenal glands. C) Adrenal gland dysfunction secondary to decreased ACTH production by the pituitary, impaired cortisol synthesis, hemorrhage, and/or infarction may contribute to CIRCI by direct loss of corticosteroid production. D) This state of relative corticosteroid insufficiency/resistance in conjunction with the vasodilation of toxic shock results in vasopressor resistant hypotension. If not corrected, end organ damage caused by hypoperfusion can contribute to the mortality of necrotizing fasciitis.

CIRCI can be difficult to diagnose, and there is no single test that is reliable for making the diagnosis. However, current guidelines recommend that a random plasma cortisol of  $< 10 \mu\text{g/dL}$  or a delta cortisol  $< 9 \mu\text{g/dL}$  60 minutes after administration of  $250 \mu\text{g}$  cosyntropin may be used to make the diagnosis[464]. For treatment of CIRCI, current guidelines recommend administering IV hydrocortisone 400 mg/day for 3 days in adult patients with fluid and vasopressor resistant septic shock. There are no current guidelines for the management of CIRCI specifically in the setting of necrotizing fasciitis. There are also no guidelines for management of CIRCI in pediatric patients, though the Surviving Sepsis Campaign 2012 guidelines recommend using hydrocortisone  $50 \text{ mg/m}^2/24\text{hrs}$  to treat children with fluid and catecholamine resistant septic shock and suspected or confirmed adrenal insufficiency [465]. Given the lack of guidelines, we recommend monitoring serum total cortisol levels in cases of necrotizing fasciitis and initiating corticosteroid therapy in patients that meet criteria

for CIRCI or who display a sharp decline in cortisol levels with increasing illness severity.

#### *Appropriate Protective Equipment*

While we have used these case reports to emphasize the importance of rapid surgical debridement, reversal of the coagulopathy, and treatment of adrenal dysfunction in patients with necrotizing fasciitis, we also want to highlight the importance of appropriate protective equipment for healthcare workers treating this condition. The most common cause of necrotizing fasciitis, group A streptococcus, is a highly contagious organism that is transmitted readily via respiratory droplets as well as through physical contact [466]. Previously, it was believed that contact precautions and the use of standard surgical masks would provide adequate protection from GAS colonization and infection [467]. However, recent case studies have revealed that excessive exposure to open wounds infected by GAS can act as a potent source of aerosolized transmission to healthcare workers despite the use of standard protective equipment [467, 468]. Understandably, surgeons who debride patients affected with GAS necrotizing fasciitis have the highest risk for being inoculated [468].

We believe this is potentially how patient 3 developed necrotizing fasciitis, as both he and the resident were inoculated by GAS following the operation. However, unlike the resident who developed severe GAS pharyngitis, patient 3 may have remained an asymptomatic carrier. Following his colonization, the patient could have transmitted the infectious organism from his oropharynx to his right foot web spaces through skin

affected by chronic tinea pedis (i.e. scratching his foot with his hand after wiping his mouth). This explanation is in contrast to the spread of infection from his bovie strike. And while the bovie was a possible source, it is strange that his upper extremity was completely unaffected by the infection.

One potential approach for surgeons and other healthcare workers to protect their oropharynx from GAS colonization while treating necrotizing fasciitis cases is with the use of an N-95 respirator. This is particularly true when working near open wounds in this patient population within 48 hours of the initiation of antibiotic therapy [468].

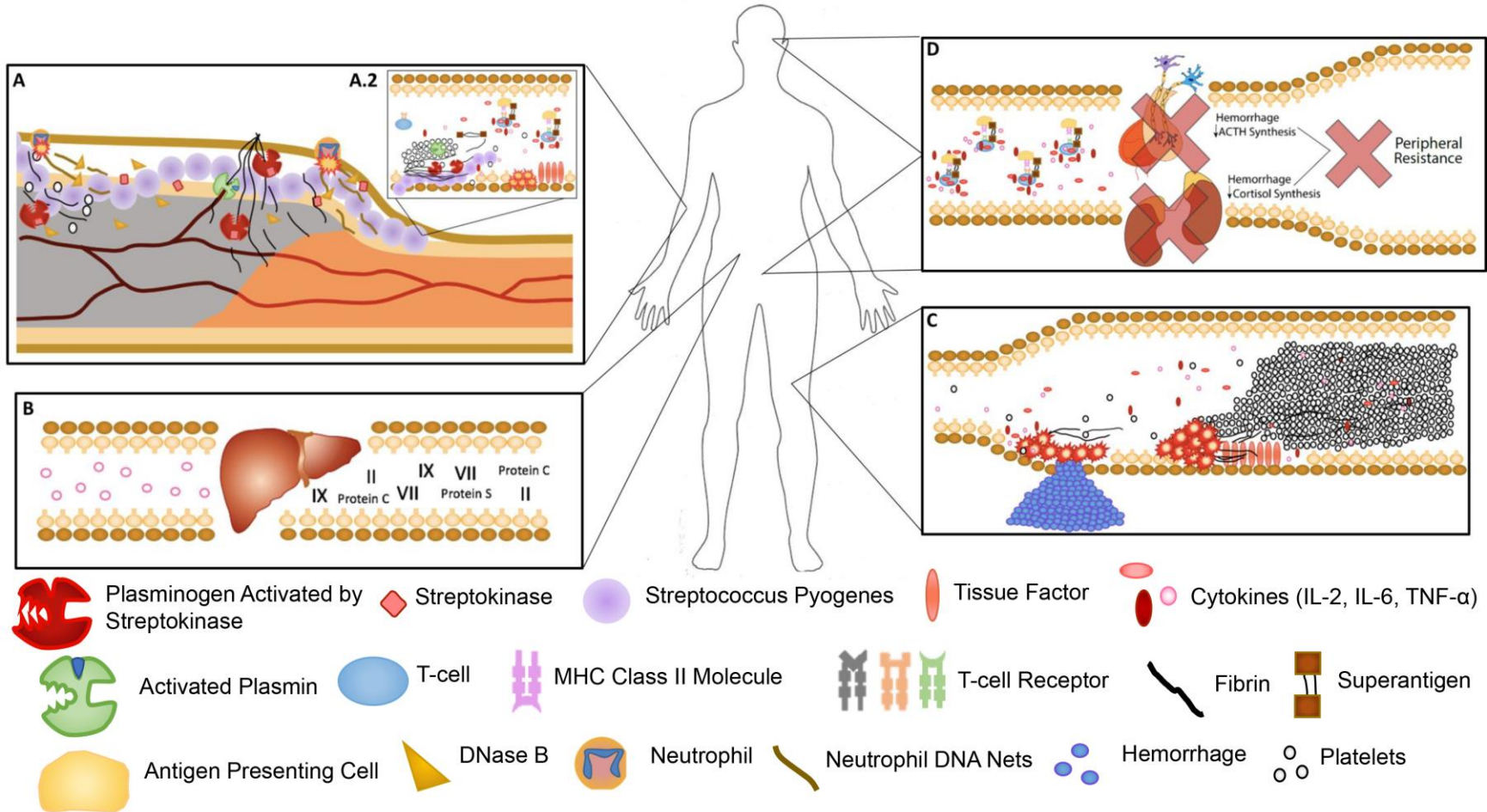
### Conclusion

The severe and rapidly progressive nature of necrotizing fasciitis is a direct result of the causative pathogens' ability to avoid containment and induce an exuberant inflammatory response. The three patients presented in this case study demonstrate that this breach of containment results in a critical condition that must be addressed as quickly and effectively as possible.

While no definitive conclusions on how to best monitor or treat necrotizing fasciitis can be drawn from this case series, given that this was not a randomized control trial, it is of the authors' opinion that certain measures should be taken to both improve patient mortality and healthcare provider safety. With regards to patients afflicted with necrotizing fasciitis, we believe that a consumptive coagulopathy (low platelets,

elevated PT-INR, and low protein C/S) is indicative of the infectious organism continuously breaking down the host's attempts at containment. In addition, we believe that patients exhibiting signs of vasopressor-resistant hypotension in the setting of rapidly declining or low (<10) random serum total cortisol levels are experiencing CIRCI (Figure 103). Taken together, consumptive coagulopathy and adrenal insufficiency in a patient with necrotizing fasciitis should be viewed as signs that a patient's clinical condition is deteriorating. Furthermore, these cases suggest addressing these two systems directly may improve patient outcomes (Figure 104).





**Figure 104: Summary of Necrotizing Fasciitis Pathophysiology.** None of the processes described are mutually exclusive, but rather they occur together throughout the progression of necrotizing fasciitis. Local spread of the infection (A) results in rapid tissue damage and consumption of clotting factors. As the infection spreads,

bacteria release of superantigens into the vasculature resulting in massive cytokine production (A.2). The local activation of the fibrinolytic system in addition to the hypercoagulable state incited by inflammation, results in both the overconsumption and production (B) of clotting factors, which contributes to DIC (C). At the same time, the massive inflammation caused by local tissue destruction and super antigen release can result in a state of relative corticosteroid insufficiency (D). This insufficiency further exacerbates the hypotension experienced by the patients in toxic shock. All together, these processes make necrotizing fasciitis an extremely dangerous disease process.

Finally, with regards to the healthcare professionals treating necrotizing fasciitis, we strongly encourage that they take extreme protective measures. In both the time of Hippocrates and the modern-day OR, it is apparent that there is potential for aerosolized transmission of virulent organisms that can cause necrotizing fasciitis. Thus, we recommend the use of an N-95 respirator during surgery to protect against colonization of the oropharynx.

## REFERENCES

1. Sophia Fox, A.J., A. Bedi, and S.A. Rodeo, *The basic science of articular cartilage: structure, composition, and function*. Sports Health, 2009. **1**(6): p. 461-8.
2. Akkiraju, H. and A. Nohe, *Role of Chondrocytes in Cartilage Formation, Progression of Osteoarthritis and Cartilage Regeneration*. J Dev Biol, 2015. **3**(4): p. 177-192.
3. Eyre, D., *Collagen of articular cartilage*. Arthritis Res, 2002. **4**(1): p. 30-5.
4. Anderson, H.C., *Electron microscopic studies of induced cartilage development and calcification*. J Cell Biol, 1967. **35**(1): p. 81-101.
5. Boonrungsiman, S., et al., *The role of intracellular calcium phosphate in osteoblast-mediated bone apatite formation*. Proc Natl Acad Sci U S A, 2012. **109**(35): p. 14170-5.
6. Anderson, H.C., *Molecular biology of matrix vesicles*. Clin Orthop Relat Res, 1995(314): p. 266-80.
7. Ham, A.W. and D.H. Cormack, *Ham's histology*. Histology. 1987, Philadelphia: Lippincott. xiv, 732 p.
8. Golub, E.E., *Role of matrix vesicles in biomineralization*. Biochim Biophys Acta, 2009. **1790**(12): p. 1592-8.
9. Cui, L., et al., *Characterisation of matrix vesicles in skeletal and soft tissue mineralisation*. Bone, 2016. **87**: p. 147-58.
10. Komori, T., *Functions of the osteocyte network in the regulation of bone mass*. Cell Tissue Res, 2013. **352**(2): p. 191-8.

11. Raggatt, L.J. and N.C. Partridge, *Cellular and molecular mechanisms of bone remodeling*. J Biol Chem, 2010. **285**(33): p. 25103-8.
12. Feng, X. and J.M. McDonald, *Disorders of bone remodeling*. Annu Rev Pathol, 2011. **6**: p. 121-45.
13. Andersson, G. and A.A.o.O. Surgeons, *United States Bone and Joint Initiative: The Burden of Musculoskeletal Diseases in the United States (BMUS), 2014*. Rosemont, IL. 2015.
14. <*The Burden of Musculoskeletal Diseases in the United States (BMUS) 3rd Edition (Dated 4-29-2015).pdf*>.
15. Benvenuti, M., et al., *Double-Edged Sword*. Orthopedic Clinics, 2017. **48**(2): p. 181-197.
16. An, T.J., et al., *Similar Clinical Severity and Outcomes for Methicillin-Resistant and Methicillin-Susceptible Staphylococcus aureus Pediatric Musculoskeletal Infections*. Open Forum Infectious Diseases, 2017. **4**(1): p. ofx013-ofx013.
17. Loi, F., et al., *Inflammation, Fracture and Bone Repair*. Bone, 2016. **86**: p. 119-130.
18. Carano, R.A. and E.H. Filvaroff, *Angiogenesis and bone repair*. Drug Discov Today, 2003. **8**(21): p. 980-9.
19. Geris, L., et al., *Angiogenesis in bone fracture healing: a bioregulatory model*. J Theor Biol, 2008. **251**(1): p. 137-58.
20. Cowin, S.C. and L. Cardoso, *Blood and interstitial flow in the hierarchical pore space architecture of bone tissue*. J Biomech, 2015. **48**(5): p. 842-54.

21. Filipowska, J., et al., *The role of vasculature in bone development, regeneration and proper systemic functioning*. *Angiogenesis*, 2017. **20**(3): p. 291-302.
22. Lieurance, R., J.B. Benjamin, and W.D. Rappaport, *Blood loss and transfusion in patients with isolated femur fractures*. *J Orthop Trauma*, 1992. **6**(2): p. 175-9.
23. Clarke, R., E. Topley, and C.T. Flear, *Assessment of blood-loss in civilian trauma*. *Lancet*, 1955. **268**(6865): p. 629-38.
24. Hoff, P., et al., *Human immune cells' behavior and survival under bioenergetically restricted conditions in an in vitro fracture hematoma model*. *Cell Mol Immunol*, 2013. **10**(2): p. 151-8.
25. Johnson, B.A., M.R. Amancharla, and B.R. Merk, *Dislocation of the proximal tibiofibular joint in association with a tibial shaft fracture: two case reports and a literature review*. *Am J Orthop (Belle Mead NJ)*, 2007. **36**(8): p. 439-41.
26. Stalker, T.J., et al., *Hierarchical organization in the hemostatic response and its relationship to the platelet-signaling network*. *Blood*, 2013. **121**(10): p. 1875-85.
27. Welsh, J.D., et al., *Hierarchical organization of the hemostatic response to penetrating injuries in the mouse macrovasculature*. *J Thromb Haemost*, 2017. **15**(3): p. 526-537.
28. Yuasa, M., et al., *The temporal and spatial development of vascularity in a healing displaced fracture*. *Bone*, 2014. **67**: p. 208-21.

29. Yuasa, M., et al., *Fibrinolysis is essential for fracture repair and prevention of heterotopic ossification*. J Clin Invest, 2015. **125**(8): p. 3117-31.
30. Krautgartner, W.D., et al., *Fibrin mimics neutrophil extracellular traps in SEM*. Ultrastruct Pathol, 2010. **34**(4): p. 226-31.
31. Bastian, O., et al., *Systemic inflammation and fracture healing*. J Leukoc Biol, 2011. **89**(5): p. 669-73.
32. Hurst, S.M., et al., *Il-6 and its soluble receptor orchestrate a temporal switch in the pattern of leukocyte recruitment seen during acute inflammation*. Immunity, 2001. **14**(6): p. 705-14.
33. O'Keefe, R.J., *Fibrinolysis as a Target to Enhance Fracture Healing*. N Engl J Med, 2015. **373**(18): p. 1776-8.
34. Marsell, R. and T.A. Einhorn, *The biology of fracture healing*. Injury, 2011. **42**(6): p. 551-5.
35. Mangialardi, G., A. Cordaro, and P. Madeddu, *The bone marrow pericyte: an orchestrator of vascular niche*. Regenerative Medicine, 2016. **11**(8): p. 883-895.
36. Matthews, B.G., et al., *Analysis of  $\alpha$ SMA-Labeled Progenitor Cell Commitment Identifies Notch Signaling as an Important Pathway in Fracture Healing*. Journal of bone and mineral research : the official journal of the American Society for Bone and Mineral Research, 2014. **29**(5): p. 1283-1294.
37. Roberts, S.J., et al., *Uncovering the periosteum for skeletal regeneration: the stem cell that lies beneath*. Bone, 2015. **70**: p. 10-8.

38. Dy, P., et al., *Sox9 directs hypertrophic maturation and blocks osteoblast differentiation of growth plate chondrocytes*. *Developmental cell*, 2012. **22**(3): p. 597-609.
39. Hirao, M., et al., *Oxygen tension regulates chondrocyte differentiation and function during endochondral ossification*. *J Biol Chem*, 2006. **281**(41): p. 31079-92.
40. Woods, A., G. Wang, and F. Beier, *Regulation of chondrocyte differentiation by the actin cytoskeleton and adhesive interactions*. *J Cell Physiol*, 2007. **213**(1): p. 1-8.
41. Claes, L.E. and C.A. Heigele, *Magnitudes of local stress and strain along bony surfaces predict the course and type of fracture healing*. *J Biomech*, 1999. **32**(3): p. 255-66.
42. Augat, P., et al., *Mechanics and mechano-biology of fracture healing in normal and osteoporotic bone*. *Osteoporosis international : a journal established as result of cooperation between the European Foundation for Osteoporosis and the National Osteoporosis Foundation of the USA*, 2005. **16 Suppl 2**: p. S36-43.
43. Miller, G.J., L.C. Gerstenfeld, and E.F. Morgan, *Mechanical microenvironments and protein expression associated with formation of different skeletal tissues during bone healing*. *Biomechanics and modeling in mechanobiology*, 2015. **14**(6): p. 1239-1253.
44. Bleuel, J., et al., *Effects of cyclic tensile strain on chondrocyte metabolism: a systematic review*. *PLoS One*, 2015. **10**(3): p. e0119816.

45. Anderson, H.C., R. Garimella, and S.E. Tague, *The role of matrix vesicles in growth plate development and biomineralization*. Front Biosci, 2005. **10**: p. 822-37.
46. Yu, Y.Y., et al., *Immunolocalization of BMPs, BMP antagonists, receptors, and effectors during fracture repair*. Bone, 2010. **46**(3): p. 841-51.
47. Gerber, H.P., et al., *VEGF couples hypertrophic cartilage remodeling, ossification and angiogenesis during endochondral bone formation*. Nat Med, 1999. **5**(6): p. 623-8.
48. Gerstenfeld, L.C., et al., *Chondrocytes provide morphogenic signals that selectively induce osteogenic differentiation of mesenchymal stem cells*. J Bone Miner Res, 2002. **17**(2): p. 221-30.
49. Deckers, M.M., et al., *Bone morphogenetic proteins stimulate angiogenesis through osteoblast-derived vascular endothelial growth factor A*. Endocrinology, 2002. **143**(4): p. 1545-53.
50. Wei, J., et al., *Glucose Uptake and Runx2 Synergize to Orchestrate Osteoblast Differentiation and Bone Formation*. Cell, 2015. **161**(7): p. 1576-1591.
51. Trueta, J. and V.P. Amato, *The vascular contribution to osteogenesis. III. Changes in the growth cartilage caused by experimentally induced ischaemia*. The Journal of bone and joint surgery. British volume, 1960. **42-B**: p. 571-87.
52. Brighton, C.T. and R.M. Hunt, *Early histologic and ultrastructural changes in microvessels of periosteal callus*. J Orthop Trauma, 1997. **11**(4): p. 244-53.
53. Diaz-Flores, L., Jr., et al., *Cell sources for cartilage repair; contribution of the mesenchymal perivascular niche*. Front Biosci (Schol Ed), 2012. **4**: p. 1275-94.



54. Zhou, X., et al., *Chondrocytes transdifferentiate into osteoblasts in endochondral bone during development, postnatal growth and fracture healing in mice*. PLoS Genet, 2014. **10**(12): p. e1004820.
55. Hu, D.P., et al., *Cartilage to bone transformation during fracture healing is coordinated by the invading vasculature and induction of the core pluripotency genes*. Development, 2017. **144**(2): p. 221-234.
56. Maes, C., et al., *Osteoblast Precursors, but Not Mature Osteoblasts, Move into Developing and Fractured Bones along with Invading Blood Vessels*. Developmental cell, 2010. **19**(2): p. 329-344.
57. Hu, K. and B.R. Olsen, *Osteoblast-derived VEGF regulates osteoblast differentiation and bone formation during bone repair*. The Journal of Clinical Investigation, 2016. **126**(2): p. 509-526.
58. Hu, K. and B.R. Olsen, *The roles of vascular endothelial growth factor in bone repair and regeneration*. Bone, 2016. **91**: p. 30-8.
59. Kolodny, A., *Periosteal Blood Supply and Healing Fractures*. J Bone Joint Surg Am, 1923. **5**: p. 698-711.
60. Trueta, J. and A.X. Cavadias, *Vascular changes caused by the Kuntscher type of nailing; an experimental study in the rabbit*. The Journal of bone and joint surgery. British volume, 1955. **37-B**(3): p. 492-505.
61. Trueta, J. and J.D. Morgan, *The vascular contribution to osteogenesis. I. Studies by the injection method*. The Journal of bone and joint surgery. British volume, 1960. **42-B**: p. 97-109.

62. Trueta, J. and K. Little, *The vascular contribution to osteogenesis. II. Studies with the electron microscope*. The Journal of bone and joint surgery. British volume, 1960. **42-B**: p. 367-76.
63. Trueta, J., *Appraisal of the vascular factor in the healing of fractures of the femoral neck*. The Journal of bone and joint surgery. British volume, 1957. **39-B(1)**: p. 3-5.
64. Rhinelander, F.W., *Tibial blood supply in relation to fracture healing*. Clinical orthopaedics and related research, 1974(105): p. 34-81.
65. Rhinelander, F.W., *The normal microcirculation of diaphyseal cortex and its response to fracture*. J Bone Joint Surg Am, 1968. **50(4)**: p. 784-800.
66. Rhinelander, F.W. and R. Baragry, *Microangiography in bone healing. I. Undisplaced closed fractures*. J Bone Joint Surg Am, 1962. **44-A**: p. 1273-98.
67. Akiyama, H., et al., *The transcription factor Sox9 has essential roles in successive steps of the chondrocyte differentiation pathway and is required for expression of Sox5 and Sox6*. Genes Dev, 2002. **16(21)**: p. 2813-28.
68. Bi, W., et al., *Sox9 is required for cartilage formation*. Nat Genet, 1999. **22(1)**: p. 85-9.
69. Mayr-Wohlfart, U., et al., *Vascular endothelial growth factor stimulates chemotactic migration of primary human osteoblasts*. Bone, 2002. **30(3)**: p. 472-7.
70. Wang, Y., et al., *The hypoxia-inducible factor alpha pathway couples angiogenesis to osteogenesis during skeletal development*. The Journal of clinical investigation, 2007. **117(6)**: p. 1616-26.

71. Duda, G.N., et al., *Mechanical boundary conditions of fracture healing: borderline indications in the treatment of unreamed tibial nailing*. J Biomech, 2001. **34**(5): p. 639-50.
72. Cheal, E.J., et al., *Role of interfragmentary strain in fracture healing: ovine model of a healing osteotomy*. J Orthop Res, 1991. **9**(1): p. 131-42.
73. Morgan, E.F., et al., *Correlations between local strains and tissue phenotypes in an experimental model of skeletal healing*. J Biomech, 2010. **43**(12): p. 2418-24.
74. Perren, S.M., *The concept of biological plating using the limited contact-dynamic compression plate (LC-DCP). Scientific background, design and application*. Injury, 1991. **22 Suppl 1**: p. 1-41.
75. Uthoff, H.K., P. Poitras, and D.S. Backman, *Internal plate fixation of fractures: short history and recent developments*. Journal of Orthopaedic Science, 2006. **11**(2): p. 118-126.
76. Uthoff, H.K. and M.A. Finnegan, *The role of rigidity in fracture fixation. An overview*. Arch Orthop Trauma Surg, 1984. **102**(3): p. 163-6.
77. Gardner, M.J., et al., *In Vivo Cyclic Axial Compression Affects Bone Healing in the Mouse Tibia*. Journal of orthopaedic research : official publication of the Orthopaedic Research Society, 2006. **24**(8): p. 1679-1686.
78. Goodship, A.E. and J. Kenwright, *The influence of induced micromovement upon the healing of experimental tibial fractures*. J Bone Joint Surg Br, 1985. **67**(4): p. 650-5.

79. Goodship, A.E., J.L. Cunningham, and J. Kenwright, *Strain rate and timing of stimulation in mechanical modulation of fracture healing*. Clin Orthop Relat Res, 1998(355 Suppl): p. S105-15.
80. Schell, H., et al., *The course of bone healing is influenced by the initial shear fixation stability*. J Orthop Res, 2005. **23**(5): p. 1022-8.
81. Klein, P., et al., *The initial phase of fracture healing is specifically sensitive to mechanical conditions*. J Orthop Res, 2003. **21**(4): p. 662-9.
82. Park, S.H., et al., *The influence of active shear or compressive motion on fracture-healing*. J Bone Joint Surg Am, 1998. **80**(6): p. 868-78.
83. Mehta, M., et al., *Influences of age and mechanical stability on volume, microstructure, and mineralization of the fracture callus during bone healing: is osteoclast activity the key to age-related impaired healing?* Bone, 2010. **47**(2): p. 219-28.
84. Perren, S.M., *Evolution of the internal fixation of long bone fractures. The scientific basis of biological internal fixation: choosing a new balance between stability and biology*. J Bone Joint Surg Br, 2002. **84**(8): p. 1093-110.
85. Kubiak, E.N., et al., *The evolution of locked plates*. J Bone Joint Surg Am, 2006. **88 Suppl 4**: p. 189-200.
86. Yu, Y.Y., et al., *Bone morphogenetic protein 2 stimulates endochondral ossification by regulating periosteal cell fate during bone repair*. Bone, 2010. **47**(1): p. 65-73.
87. Hak, D.J., et al., *Delayed union and nonunions: epidemiology, clinical issues, and financial aspects*. Injury, 2014. **45 Suppl 2**: p. S3-7.

88. Colnot, C., et al., *Distinguishing the contributions of the perichondrium, cartilage, and vascular endothelium to skeletal development*. *Dev Biol*, 2004. **269**(1): p. 55-69.
89. Knothe Tate, M.L., et al., *Testing of a new one-stage bone-transport surgical procedure exploiting the periosteum for the repair of long-bone defects*. *J Bone Joint Surg Am*, 2007. **89**(2): p. 307-16.
90. Colnot, C., X. Zhang, and M.L. Knothe Tate, *Current insights on the regenerative potential of the periosteum: molecular, cellular, and endogenous engineering approaches*. *J Orthop Res*, 2012. **30**(12): p. 1869-78.
91. Antabak, A., et al., *Reducing damage to the periosteal capillary network caused by internal fixation plating: An experimental study*. *Injury*, 2015. **46 Suppl 6**: p. S18-20.
92. Schmal, H., et al., *Flexible fixation and fracture healing: do locked plating 'internal fixators' resemble external fixators?* *J Orthop Trauma*, 2011. **25 Suppl 1**: p. S15-20.
93. Pfeifer, R., R. Sellei, and H.C. Pape, *The biology of intramedullary reaming*. *Injury*, 2010. **41 Suppl 2**: p. S4-8.
94. Donegan, D.J., et al., *Intramedullary Nailing of Tibial Shaft Fractures: Size Matters*. *J Orthop Trauma*, 2016. **30**(7): p. 377-80.
95. Study to Prospectively Evaluate Reamed Intramedullary Nails in Patients with Tibial Fractures, I., et al., *Randomized trial of reamed and unreamed intramedullary nailing of tibial shaft fractures*. *J Bone Joint Surg Am*, 2008. **90**(12): p. 2567-78.

96. Investigators, S., et al., *Study to prospectively evaluate reamed intramedullary nails in patients with tibial fractures (S.P.R.I.N.T.): study rationale and design*. BMC Musculoskelet Disord, 2008. **9**: p. 91.
97. Chapman, M.W., *The effect of reamed and nonreamed intramedullary nailing on fracture healing*. Clin Orthop Relat Res, 1998(355 Suppl): p. S230-8.
98. Schemitsch, E.H., et al., *Prognostic Factors for Predicting Outcomes After Intramedullary Nailing of the Tibia*. The Journal of Bone and Joint Surgery. American volume, 2012. **94**(19): p. 1786-1793.
99. Omerovic, D., F. Lazovic, and A. Hadzimehmedagic, *Static or Dynamic Intramedullary Nailing of Femur and Tibia*. Medical Archives, 2015. **69**(2): p. 110-113.
100. Alho, A., K. Stromsoe, and A. Ekeland, *Locked intramedullary nailing of femoral shaft fractures*. J Trauma, 1991. **31**(1): p. 49-59.
101. Watson, J.T. and R.W. Sanders, *Controlled Compression Nailing for At Risk Humeral Shaft Fractures*. Journal of Orthopaedic Trauma, 2017. **31**(6 Suppl): p. S25-S28.
102. Takahara, S., et al., *Human pseudoarthrosis tissue contains cells with osteogenic potential*. Injury, 2016. **47**: p. 1184-1190.
103. Einhorn, T.A., *Current concepts review enhancement of fracture-healing*. The Journal of Bone and Joint Surgery 1995. **77-A**: p. 940-956.
104. Pountos, I., et al., *Fracture non-union: Can biomarkers predict outcome?* Injury, 2013. **44**: p. 1725-1732.

105. Rupp, M., et al., *Diaphyseal long bone nonunions — types, aetiology, economics, and treatment recommendations*, in *International Orthopaedics*. 2017. p. 1-12.
106. Lu, C., et al., *Ischemia leads to delayed union during fracture healing: A mouse model*. *Journal of Orthopaedic Research*, 2007. **25**: p. 51-61.
107. Davis, K.M., et al., *Muscle-bone interactions during fracture healing*, in *Journal of Musculoskeletal Neuronal Interactions*. 2015. p. 1-9.
108. Bhandari, M., et al., *Randomized trial of reamed and unreamed intramedullary nailing of tibial shaft fractures*. *Journal of Bone and Joint Surgery - Series A*, 2008.
109. Miller, G.J., L.C. Gerstenfeld, and E.F. Morgan, *Mechanical microenvironments and protein expression associated with formation of different skeletal tissues during bone healing*. *Biomechanics and Modeling in Mechanobiology*, 2015. **14**: p. 1239-1253.
110. Carter, D.R., et al., *Mechanobiology of skeletal regeneration*. *Clinical orthopaedics and related research*, 1998: p. S41-55.
111. Glatt, V., C.H. Evans, and K. Tetsworth, *A concert between biology and biomechanics: The influence of the mechanical environment on bone healing*, in *Frontiers in Physiology*. 2017.
112. Zuscik, M.J., et al., *Regulation of chondrogenesis and chondrocyte differentiation by stress*, in *Journal of Clinical Investigation*. 2008. p. 429-438.
113. Chapman, M.W., *The effect of reamed and nonreamed intramedullary nailing on fracture healing*, in *Clinical Orthopaedics and Related Research*. 1998.

114. Wehner, T., et al., *Optimization of intramedullary nailing by numerical simulation of fracture healing*. J Orthop Res, 2012.
115. Omerovic, D., F. Lazovic, and A. Hadzimehmedagic, *Static or dynamic intramedullary nailing of femur and tibia*. Medical archives (Sarajevo, Bosnia and Herzegovina), 2015.
116. Alho, A., et al., *Slotted versus non-slotted locked intramedullary nailing for femoral shaft fractures*. Archives of Orthopaedic and Trauma Surgery, 1992.
117. Hiltunen, A., et al., *Retarded chondrogenesis in transgenic mice with a type II collagen defect results in fracture healing abnormalities*. Developmental Dynamics, 1994. **200**: p. 340-349.
118. Marsell, R. and T.A. Einhorn, *The biology of fracture healing*, in *Injury*. 2011. p. 551-555.
119. Loi, F., et al., *Inflammation, fracture and bone repair*, in *Bone*. 2016. p. 119-130.
120. Carano, R.A.D. and E.H. Filvaroff, *Angiogenesis and bone repair*, in *Drug Discovery Today*. 2003. p. 980-989.
121. Geris, L., et al., *Angiogenesis in bone fracture healing: A bioregulatory model*. Journal of Theoretical Biology, 2008. **251**: p. 137-158.
122. Yuasa, M., et al., *Unexpected timely fracture union in matrix metalloproteinase 9 deficient mice*. PloS one, 2018. **13**: p. 1-12.
123. Cole, H.A., et al., *Differential development of the distal and proximal femoral epiphysis and physis in mice*. Bone, 2013. **52**(1): p. 337-46.



124. O'Neill, K.R., et al., *Micro-computed tomography assessment of the progression of fracture healing in mice*. Bone, 2012.
125. Green, E., J.D. Lubahn, and J. Evans, *Risk factors, treatment, and outcomes associated with nonunion of the midshaft humerus fracture*. Journal of surgical orthopaedic advances, 2005. **14**: p. 64-72.
126. Rajaei, S.S., et al., *Spinal fusion in the United States: analysis of trends from 1998 to 2008*. Spine (Phila Pa 1976), 2012. **37**(1): p. 67-76.
127. Rajaei, S.S., L.E. Kanim, and H.W. Bae, *National trends in revision spinal fusion in the USA: patient characteristics and complications*. Bone Joint J, 2014. **96-b**(6): p. 807-16.
128. Grabowski, G. and C.A. Cornett, *Bone graft and bone graft substitutes in spine surgery: current concepts and controversies*, in *J Am Acad Orthop Surg*. 2013: United States. p. 51-60.
129. Boden, S.D., *Overview of the biology of lumbar spine fusion and principles for selecting a bone graft substitute*. Spine (Phila Pa 1976), 2002. **27**(16 Suppl 1): p. S26-31.
130. Fischer, C.R., et al., *A systematic review of comparative studies on bone graft alternatives for common spine fusion procedures*. Eur Spine J, 2013. **22**(6): p. 1423-35.
131. Burchardt, H., *The biology of bone graft repair*. Clin Orthop Relat Res, 1983(174): p. 28-42.
132. Almubarak, S., et al., *Tissue engineering strategies for promoting vascularized bone regeneration*. Bone, 2016. **83**: p. 197-209.

133. Boden, S.D., J.H. Schimandle, and W.C. Hutton, *An experimental lumbar intertransverse process spinal fusion model. Radiographic, histologic, and biomechanical healing characteristics*. Spine (Phila Pa 1976), 1995. **20**(4): p. 412-20.
134. Thompson, Z., et al., *A model for intramembranous ossification during fracture healing*. J Orthop Res, 2002. **20**(5): p. 1091-8.
135. Mackie, E.J., et al., *Endochondral ossification: how cartilage is converted into bone in the developing skeleton*. Int J Biochem Cell Biol, 2008. **40**(1): p. 46-62.
136. Brown, C.W., T.J. Orme, and H.D. Richardson, *The rate of pseudarthrosis (surgical nonunion) in patients who are smokers and patients who are nonsmokers: a comparison study*. Spine (Phila Pa 1976), 1986. **11**(9): p. 942-3.
137. Araldi, E. and E. Schipani, *Hypoxia, HIFs and bone development*. Bone, 2010. **47**(2): p. 190-6.
138. Fiedler, J., et al., *BMP-2, BMP-4, and PDGF-bb stimulate chemotactic migration of primary human mesenchymal progenitor cells*. J Cell Biochem, 2002. **87**(3): p. 305-12.
139. Landis, J.R. and G.G. Koch, *The measurement of observer agreement for categorical data*. Biometrics, 1977. **33**(1): p. 159-74.
140. Vaccaro, A.R., et al., *Bone grafting alternatives in spinal surgery*. Spine J, 2002. **2**(3): p. 206-15.
141. Boden, S.D., *Clinical application of the BMPs*. J Bone Joint Surg Am, 2001. **83-A Suppl 1**(Pt 2): p. S161.

142. Ferrara, N., H.P. Gerber, and J. LeCouter, *The biology of VEGF and its receptors*. Nat Med, 2003. **9**(6): p. 669-76.
143. Montesano, R., et al., *Basic fibroblast growth factor induces angiogenesis in vitro*. Proc Natl Acad Sci U S A, 1986. **83**(19): p. 7297-301.
144. Sheehy, E.J., et al., *Engineering osteochondral constructs through spatial regulation of endochondral ossification*. Acta Biomater, 2013. **9**(3): p. 5484-92.
145. Thompson, E.M., et al., *Recapitulating endochondral ossification: a promising route to in vivo bone regeneration*. J Tissue Eng Regen Med, 2015. **9**(8): p. 889-902.
146. Gerstenfeld, L.C., et al., *Fracture healing as a post-natal developmental process: Molecular, spatial, and temporal aspects of its regulation*. Journal of Cellular Biochemistry, 2003. **88**: p. 873-884.
147. Bahney, C.S., et al., *Stem cell-derived endochondral cartilage stimulates bone healing by tissue transformation*. J Bone Miner Res, 2014. **29**(5): p. 1269-82.
148. Kim, S.J. and S. Sabharwal, *Risk factors for venous thromboembolism in hospitalized children and adolescents: a systemic review and pooled analysis*. Journal of pediatric orthopedics. Part B, 2014. **23**(4): p. 389-93.
149. Sandoval, J.A., et al., *Incidence, risk factors, and treatment patterns for deep venous thrombosis in hospitalized children: an increasing population at risk*. Journal of vascular surgery, 2008. **47**(4): p. 837-43.

150. Raffini, L., et al., *Dramatic increase in venous thromboembolism in children's hospitals in the United States from 2001 to 2007*. *Pediatrics*, 2009. **124**(4): p. 1001-8.
151. Arlikar, S.J., et al., *Development of a new risk score for hospital-associated venous thromboembolism in critically-ill children not undergoing cardiothoracic surgery*. *Thrombosis research*, 2015. **136**(4): p. 717-22.
152. Mantadakis, E., et al., *Deep venous thrombosis in children with musculoskeletal infections: the clinical evidence*. *International journal of infectious diseases : IJID : official publication of the International Society for Infectious Diseases*, 2012. **16**(4): p. e236-43.
153. Hollmig, S.T., et al., *Deep venous thrombosis associated with osteomyelitis in children*. *The Journal of bone and joint surgery. American volume*, 2007. **89**(7): p. 1517-23.
154. LePage, A.A., E.P. Hess, and R.M. Schears, *Septic thrombophlebitis with acute osteomyelitis in adolescent children: a report of two cases and review of the literature*. *International journal of emergency medicine*, 2008. **1**(2): p. 155-9.
155. Gorenstein, A., et al., *The pivotal role of deep vein thrombophlebitis in the development of acute disseminated staphylococcal disease in children*. *Pediatrics*, 2000. **106**(6): p. E87.
156. Cirillo, P., et al., *C-reactive protein induces tissue factor expression and promotes smooth muscle and endothelial cell proliferation*. *Cardiovascular research*, 2005. **68**(1): p. 47-55.

157. Mold, C., H. Gewurz, and T.W. Du Clos, *Regulation of complement activation by C-reactive protein*. Immunopharmacology, 1999. **42**(1-3): p. 23-30.
158. Wu, J., et al., *C-reactive protein enhances tissue factor expression by vascular smooth muscle cells: mechanisms and in vivo significance*. Arteriosclerosis, thrombosis, and vascular biology, 2008. **28**(4): p. 698-704.
159. Ji, Y., et al., *C-reactive protein induces expression of tissue factor and plasminogen activator inhibitor-1 and promotes fibrin accumulation in vein grafts*. Journal of thrombosis and haemostasis : JTH, 2014. **12**(10): p. 1667-77.
160. Stutz, C.M., et al., *Coagulopathies in orthopaedics: links to inflammation and the potential of individualizing treatment strategies*. Journal of orthopaedic trauma, 2013. **27**(4): p. 236-41.
161. Mignemi, M.E., et al., *A Novel Classification System Based on Dissemination of Musculoskeletal Infection is Predictive of Hospital Outcomes*. Journal of pediatric orthopedics, 2016.
162. Povoas, P., *C-reactive protein: a valuable marker of sepsis*. Intensive care medicine, 2002. **28**(3): p. 235-43.
163. Unkila-Kallio, L., M.J. Kallio, and H. Peltola, *The usefulness of C-reactive protein levels in the identification of concurrent septic arthritis in children who have acute hematogenous osteomyelitis. A comparison with the usefulness of the erythrocyte sedimentation rate and the white blood-cell count*. The Journal of bone and joint surgery. American volume, 1994. **76**(6): p. 848-53.
164. Copley, L.A., et al., *A proposed scoring system for assessment of severity of illness in pediatric acute hematogenous osteomyelitis using objective clinical*

- and laboratory findings*. The Pediatric infectious disease journal, 2014. **33**(1): p. 35-41.
165. Martin, A.C., et al., *Predictors of Outcome in Pediatric Osteomyelitis: Five Years Experience in a Single Tertiary Center*. The Pediatric infectious disease journal, 2016. **35**(4): p. 387-91.
166. Wolberg, A.S., et al., *Procoagulant activity in hemostasis and thrombosis: Virchow's triad revisited*. Anesth Analg, 2012. **114**(2): p. 275-85.
167. Battinelli, E.M., A. Marshall, and J.M. Connors, *The role of thrombophilia in pregnancy*. Thrombosis, 2013. **2013**: p. 516420.
168. Caine, G.J., et al., *The hypercoagulable state of malignancy: pathogenesis and current debate*. Neoplasia, 2002. **4**(6): p. 465-73.
169. Khan, S. and J.D. Dickerman, *Hereditary thrombophilia*. Thromb J, 2006. **4**: p. 15.
170. Agnelli, G., *Prevention of venous thromboembolism in surgical patients*. Circulation, 2004. **110**(24 Suppl 1): p. IV4-12.
171. Allen, K.S., E. Sawheny, and G.T. Kinasewitz, *Anticoagulant modulation of inflammation in severe sepsis*. World J Crit Care Med, 2015. **4**(2): p. 105-15.
172. Freedman, K.B., et al., *A meta-analysis of thromboembolic prophylaxis following elective total hip arthroplasty*. J Bone Joint Surg Am, 2000. **82-A**(7): p. 929-38.
173. Kroger, K., et al., *Risk factors for venous thromboembolic events in cancer patients*. Ann Oncol, 2006. **17**(2): p. 297-303.

174. Chan, A.K., et al., *Venous thrombosis in children*, in *Journal of Thrombosis and Haemostasis*. 2003. p. 1443-1455.
175. Kumar, D.R., et al., *Virchow's contribution to the understanding of thrombosis and cellular biology*. *Clinical Medicine and Research*, 2010. **8**: p. 168-172.
176. Team., M.V.P.B. *Cincinnati Children's Hospital Medical Center: Best Evidence Statement Venous Thromboembolism (VTE) Prophylaxis in Children and Adolescents*. 2014; Available from:  
<https://www.cincinnatichildrens.org/service/j/anderson-center/evidence-based-care/recommendations>.
177. Cox, M., et al., *Non-Catheter-related Venous Thromboembolism in Children: Imaging Review from Head to Toe*. *RadioGraphics*, 2017. **37**: p. 1753-1774.
178. Chan, A.K.C. and P. Monagle, *Updates in thrombosis in pediatrics: where are we after 20 years?* *Hematology / the Education Program of the American Society of Hematology*. American Society of Hematology. Education Program, 2012. **2012**: p. 439-43.
179. Jaffray, J., M. Bauman, and P. Massicotte, *The Impact of Central Venous Catheters on Pediatric Venous Thromboembolism*. *Frontiers in Pediatrics*, 2017. **5**: p. 5.
180. Jung, H.L., *Venous thromboembolism in children and adolescents*. *Blood research*, 2016. **51**: p. 149-151.
181. Cayley, W.E., *Preventing deep vein thrombosis in hospital inpatients*, in *British Medical Journal*. 2007, BMJ Publishing Group. p. 147-151.

182. Radulescu, V., *Management of venous thrombosis in the pediatric patient*. Pediatric Health, Medicine and Therapeutics, 2015. **Volume 6**: p. 111.
183. Azu, M.C., et al., *Venous thromboembolic events in pediatric trauma patients: is prophylaxis necessary?* J Trauma, 2005. **59**: p. 1345-1349.
184. Candrilli, S.D., R. Balkrishnan, and S.H. O'Brien, *Effect of injury severity on the incidence and utilization-related outcomes of venous thromboembolism in pediatric trauma inpatients\**. Pediatric Critical Care Medicine, 2009. **10**: p. 554-557.
185. Beck, C., et al., *Incidence and risk factors of catheter-related deep vein thrombosis in a pediatric intensive care unit: a prospective study*. The Journal of Pediatrics, 1998. **133**: p. 237-241.
186. Higginson, R.A., et al., *Incidence and risk factors associated with venous thrombotic events in pediatric intensive care unit patients\**. Pediatric Critical Care Medicine, 2011. **12**: p. 628-634.
187. Massicotte, P., et al., *An open-label randomized controlled trial of low molecular weight heparin for the prevention of central venous line-related thrombotic complications in children: The PROTEKT trial*. Thrombosis Research, 2003. **109**: p. 101-108.
188. Cohen, J., *Weighted kappa: nominal scale agreement with provision for scaled disagreement or partial credit*. Psychological bulletin, 1968. **70**(4): p. 213-20.
189. Takemoto, C.M., et al., *Hospital-associated venous thromboembolism in children: Incidence and clinical characteristics*. Journal of Pediatrics, 2014. **164**: p. 332-338.



190. Jaffray, J. and G. Young, *Developmental hemostasis. clinical implications from the fetus to the adolescent.*, in *Pediatric Clinics of North America*. 2013. p. 1407-1417.
191. Toulon, P., *Developmental hemostasis: laboratory and clinical implications*, in *International Journal of Laboratory Hematology*. 2016. p. 66-77.
192. Hanslik, A., et al., *Incidence and diagnosis of thrombosis in children with short-term central venous lines of the upper venous system*. *Pediatrics*, 2008. **122**: p. 1284-1291.
193. Aksu, K., A. Donmez, and G. Keser, *Inflammation-induced thrombosis: mechanisms, disease associations and management*. *Current pharmaceutical design*, 2012. **18**: p. 1478-93.
194. Jagers, J. and J.H. Lawson, *Coagulopathy and Inflammation in Neonatal Heart Surgery: Mechanisms and Strategies*. *Annals of Thoracic Surgery*, 2006. **81**: p. S2360-S2366.
195. Monagle, P., *Thrombosis in children with BT shunts, Glenns and Fontans*, in *Progress in Pediatric Cardiology*. 2005, Elsevier. p. 17-21.
196. Silvey, M. and L.R. Brandão, *Risk Factors, Prophylaxis, and Treatment of Venous Thromboembolism in Congenital Heart Disease Patients*. *Frontiers in Pediatrics*, 2017. **5**: p. 146.
197. Weber, C.F., M. Klages, and K. Zacharowski, *Perioperative coagulation management during cardiac surgery*. *Curr Opin Anaesthesiol*, 2013. **26**(1): p. 60-4.

198. Vidal, E., et al., *Central venous catheter-related thrombosis and thromboprophylaxis in children: a systematic review and meta-analysis*. *Journal of Thrombosis and Haemostasis*, 2014. **12**: p. 1096-1109.
199. Moore, S.N., S.B. Tanner, and J.G. Schoenecker, *Bisphosphonates: from softening water to treating PXE*. *Cell Cycle*, 2015. **14**(9): p. 1354-5.
200. Gawande, A., *Being Mortal: Medicine and What Matters in the End*. 2014, New York, New York: Metropolitan Books.
201. Eisenstein, N., S. Stapley, and L. Grover, *Post-Traumatic Heterotopic Ossification: An Old Problem in Need of New Solutions*. *J Orthop Res*, 2018. **36**(4): p. 1061-1068.
202. Chalmers, J., D.H. Gray, and J. Rush, *Observations on the induction of bone in soft tissues*. *J Bone Joint Surg Br*, 1975. **57**(1): p. 36-45.
203. Kaplan, F.S., et al., *Classic and Atypical FOP Phenotypes are Caused by Mutations in the BMP Type I Receptor ACVRI*. *Human mutation*, 2009. **30**(3): p. 379-390.
204. Mitchell, E.J., et al., *The genetics of heterotopic ossification: insight into the bone remodeling pathway*. *J Orthop Trauma*, 2010. **24**(9): p. 530-3.
205. Black, A.S. and I.O. Kanat, *A review of soft tissue calcifications*. *J Foot Surg*, 1985. **24**(4): p. 243-50.
206. Fleish, H. and W.F. Neuman, *Mechanisms of calcification: role of collagen, polyphosphates, and phosphatase*. *Am J Physiol*, 1961. **200**: p. 1296-300.

207. Fleisch, H., J. Maerki, and R.G. Russell, *Effect of pyrophosphate on dissolution of hydroxyapatite and its possible importance in calcium homeostasis*. Proc Soc Exp Biol Med, 1966. **122**(2): p. 317-20.
208. Gillman, T., R.A. Grant, and M. Hathorn, *Histochemical and chemical studies of calciferol-induced vascular injuries*. Br J Exp Pathol, 1960. **41**: p. 1-18.
209. Goodman, R.M., et al., *Pseudoxanthoma Elasticum: A Clinical and Histopathological Study*. Medicine (Baltimore), 1963. **42**: p. 297-334.
210. Yuan, H., et al., *Osteoinduction by calcium phosphate biomaterials*. J Mater Sci Mater Med, 1998. **9**(12): p. 723-6.
211. Ripamonti, U., *Osteoinduction in porous hydroxyapatite implanted in heterotopic sites of different animal models*. Biomaterials, 1996. **17**(1): p. 31-5.
212. Le Nihouannen, D., et al., *Ectopic bone formation by microporous calcium phosphate ceramic particles in sheep muscles*. Bone, 2005. **36**(6): p. 1086-93.
213. Baker, B.F., et al., *2'-O-(2-Methoxy)ethyl-modified anti-intercellular adhesion molecule 1 (ICAM-1) oligonucleotides selectively increase the ICAM-1 mRNA level and inhibit formation of the ICAM-1 translation initiation complex in human umbilical vein endothelial cells*. J Biol Chem, 1997. **272**(18): p. 11994-2000.
214. O'Connor, J.P., *Animal models of heterotopic ossification*. Clin Orthop Relat Res, 1998(346): p. 71-80.
215. Anthonissen, J., et al., *A new small-animal model for the study of acquired heterotopic ossification after hip surgery*. Acta Orthop Traumatol Turc, 2015. **49**(2): p. 197-202.

216. Peterson, J.R., et al., *Direct Mouse Trauma/Burn Model of Heterotopic Ossification*. J Vis Exp, 2015(102): p. e52880.
217. Czerwinska, A.M., et al., *Mouse gastrocnemius muscle regeneration after mechanical or cardiotoxin injury*. Folia Histochem Cytobiol, 2012. **50**(1): p. 144-53.
218. Couteaux, R., J.C. Mira, and A. d'Albis, *Regeneration of muscles after cardiotoxin injury. I. Cytological aspects*. Biol Cell, 1988. **62**(2): p. 171-82.
219. Shimono, K., et al., *Potent Inhibition of Heterotopic Ossification by Nuclear Retinoic Acid Receptor  $\gamma$  Agonists*. Nature medicine, 2011. **17**(4): p. 454-460.
220. Kan, L., et al., *Dysregulation of local stem/progenitor cells as a common cellular mechanism for heterotopic ossification*. Stem Cells, 2009. **27**(1): p. 150-6.
221. Bohannon, J., et al., *Dendritic cell modification of neutrophil responses to infection after burn injury*. Journal of immunology (Baltimore, Md. : 1950), 2010. **185**(5): p. 2847-2853.
222. Toliver-Kinsky, T.E., et al., *Enhancement of dendritic cell production by fms-like tyrosine kinase-3 ligand increases the resistance of mice to a burn wound infection*. J Immunol, 2005. **174**(1): p. 404-10.
223. Cohen, J., *Weighted kappa: nominal scale agreement with provision for scaled disagreement or partial credit*. Psychol Bull, 1968. **70**(4): p. 213-20.
224. Seegenschmiedt, M.H., et al., *Prevention of heterotopic ossification about the hip: final results of two randomized trials in 410 patients using either*

- preoperative or postoperative radiation therapy. Int J Radiat Oncol Biol Phys*, 1997. **39**(1): p. 161-71.
225. Seegenschmiedt, M.H., et al., *Prevention of heterotopic ossification (HO) after total hip replacement: randomized high versus low dose radiotherapy. Radiother Oncol*, 1993. **26**(3): p. 271-4.
226. Parkinson, J.R., C.M. Evarts, and L.F. Hubbard, *Radiation therapy in the prevention of heterotopic ossification after total hip arthroplasty. Hip*, 1982: p. 211-27.
227. Ayers, D.C., V.D. Pellegrini, Jr., and C.M. Evarts, *Prevention of heterotopic ossification in high-risk patients by radiation therapy. Clin Orthop Relat Res*, 1991(263): p. 87-93.
228. Klinck, R.J., G.M. Campbell, and S.K. Boyd, *Radiation effects on bone architecture in mice and rats resulting from in vivo micro-computed tomography scanning. Med Eng Phys*, 2008. **30**(7): p. 888-95.
229. Flick, M.J., X. Du, and J.L. Degen, *Fibrin(ogen)-alpha M beta 2 interactions regulate leukocyte function and innate immunity in vivo. Exp Biol Med (Maywood)*, 2004. **229**(11): p. 1105-10.
230. Deconinck, N. and B. Dan, *Pathophysiology of duchenne muscular dystrophy: current hypotheses. Pediatr Neurol*, 2007. **36**(1): p. 1-7.
231. Suelves, M., et al., *uPA deficiency exacerbates muscular dystrophy in MDX mice. J Cell Biol*, 2007. **178**(6): p. 1039-51.
232. Lounev, V.Y., et al., *Identification of progenitor cells that contribute to heterotopic skeletogenesis. J Bone Joint Surg Am*, 2009. **91**(3): p. 652-63.

233. Romer, J., et al., *Impaired wound healing in mice with a disrupted plasminogen gene*. Nat Med, 1996. **2**(3): p. 287-92.
234. Cole, H.A., et al., *Fibrin accumulation secondary to loss of plasmin-mediated fibrinolysis drives inflammatory osteoporosis in mice*. Arthritis Rheumatol, 2014. **66**(8): p. 2222-33.
235. Li, J., et al., *Concentration of bisphosphonate (incadronate) in callus area and its effects on fracture healing in rats*. J Bone Miner Res, 2000. **15**(10): p. 2042-51.
236. Lluis, F., et al., *Urokinase-dependent plasminogen activation is required for efficient skeletal muscle regeneration in vivo*. Blood, 2001. **97**(6): p. 1703-11.
237. Suelves, M., et al., *Plasmin activity is required for myogenesis in vitro and skeletal muscle regeneration in vivo*. Blood, 2002. **99**(8): p. 2835-44.
238. Urist, M.R., R.J. DeLange, and G.A. Finerman, *Bone cell differentiation and growth factors*. Science, 1983. **220**(4598): p. 680-6.
239. Douglas, T.E., et al., *Enzymatically induced mineralization of platelet-rich fibrin*. J Biomed Mater Res A, 2012. **100**(5): p. 1335-46.
240. Bugge, T.H., et al., *Loss of fibrinogen rescues mice from the pleiotropic effects of plasminogen deficiency*. Cell, 1996. **87**(4): p. 709-19.
241. Vidal, B., et al., *Amelioration of Duchenne muscular dystrophy in mdx mice by elimination of matrix-associated fibrin-driven inflammation coupled to the alphaMbeta2 leukocyte integrin receptor*. Hum Mol Genet, 2012. **21**(9): p. 1989-2004.

242. Kanno, Y., et al., *Lack of alpha2-antiplasmin improves cutaneous wound healing via over-released vascular endothelial growth factor-induced angiogenesis in wound lesions*. J Thromb Haemost, 2006. **4**(7): p. 1602-10.
243. Khalil, N., et al., *Plasmin regulates the activation of cell-associated latent TGF-beta 1 secreted by rat alveolar macrophages after in vivo bleomycin injury*. Am J Respir Cell Mol Biol, 1996. **15**(2): p. 252-9.
244. Ploplis, V.A., et al., *Plasminogen deficiency differentially affects recruitment of inflammatory cell populations in mice*. Blood, 1998. **91**(6): p. 2005-9.
245. Roth, D., et al., *Plasmin modulates vascular endothelial growth factor-A-mediated angiogenesis during wound repair*. Am J Pathol, 2006. **168**(2): p. 670-84.
246. Schoenecker, J., et al., *2010 Young Investigator Award winner: Therapeutic aprotinin stimulates osteoblast proliferation but inhibits differentiation and bone matrix mineralization*. Spine (Phila Pa 1976), 2010. **35**(9): p. 1008-16.
247. Eren, M., et al., *PAI-1-regulated extracellular proteolysis governs senescence and survival in Klotho mice*. Proc Natl Acad Sci U S A, 2014. **111**(19): p. 7090-5.
248. Tsuji, K., et al., *BMP2 activity, although dispensable for bone formation, is required for the initiation of fracture healing*. Nat Genet, 2006. **38**(12): p. 1424-9.
249. Cooley, L.M. and R.J. Goss, *The effects of transplantation and x-irradiation on the repair of fractured bones*. Am J Anat, 1958. **102**(2): p. 167-81.

250. De Luca, F., et al., *Retinoic acid is a potent regulator of growth plate chondrogenesis*. *Endocrinology*, 2000. **141**(1): p. 346-53.
251. Lewis, C.A., et al., *Inhibition of limb chondrogenesis in vitro by vitamin A: alterations in cell surface characteristics*. *Dev Biol*, 1978. **64**(1): p. 31-47.
252. Standeven, A.M., et al., *Retinoid-induced epiphyseal plate closure in guinea pigs*. *Fundam Appl Toxicol*, 1996. **34**(1): p. 91-8.
253. Mignemi, N.A., et al., *Plasmin Prevents Dystrophic Calcification after Muscle Injury*. *J Bone Miner Res*, 2016.
254. Cohen, M.J., et al., *Critical role of activated protein C in early coagulopathy and later organ failure, infection and death in trauma patients*. *Ann Surg*, 2012. **255**(2): p. 379-85.
255. Enderson, B.L., et al., *Fibrinolysis in multisystem trauma patients*. *J Trauma*, 1991. **31**(9): p. 1240-6.
256. Sorensen, J.V., *Levels of fibrinolytic activators and inhibitors in plasma after severe trauma*. *Blood Coagul Fibrinolysis*, 1994. **5**(1): p. 43-9.
257. Zouaoui Boudjeltia, K., et al., *Relationship between CRP and hypofibrinolysis: Is this a possible mechanism to explain the association between CRP and outcome in critically ill patients?* *Thromb J*, 2004. **2**(1): p. 7.
258. Christensen, B., et al., *Osteopontin is cleaved at multiple sites close to its integrin-binding motifs in milk and is a novel substrate for plasmin and cathepsin D*. *J Biol Chem*, 2010. **285**(11): p. 7929-37.
259. Steitz, S.A., et al., *Osteopontin inhibits mineral deposition and promotes regression of ectopic calcification*. *Am J Pathol*, 2002. **161**(6): p. 2035-46.



260. Colnot, C., et al., *Altered fracture repair in the absence of MMP9*. Development, 2003. **130**(17): p. 4123-33.
261. Benvenuti, M., et al., *Double-Edged Sword: Musculoskeletal Infection Provoked Acute Phase Response in Children*. The Orthopedic clinics of North America, 2017. **48**(2): p. 181-197.
262. Yuasa, M., et al., *Fibrinolysis is essential for fracture repair and prevention of heterotopic ossification*. The Journal of clinical investigation, 2015. **125**(8): p. 3117-31.
263. Baramova, E.N., et al., *Involvement of PA/plasmin system in the processing of pro-MMP-9 and in the second step of pro-MMP-2 activation*. FEBS letters, 1997. **405**(2): p. 157-62.
264. Coussens, L.M., et al., *MMP-9 supplied by bone marrow-derived cells contributes to skin carcinogenesis*. Cell, 2000. **103**(3): p. 481-90.
265. O'Neill, K.R., et al., *Micro-computed tomography assessment of the progression of fracture healing in mice*. Bone, 2012. **50**(6): p. 1357-67.
266. Mohseni, M.A., et al., *AO tubular external fixation vs. unreamed intramedullary nailing in open grade IIIA-IIIB tibial shaft fractures: a single-center randomized clinical trial*. Pakistan journal of biological sciences : PJBS, 2011. **14**(8): p. 490-5.
267. Klein, P., et al., *Comparison of unreamed nailing and external fixation of tibial diastases--mechanical conditions during healing and biological outcome*. Journal of orthopaedic research : official publication of the Orthopaedic Research Society, 2004. **22**(5): p. 1072-8.

268. Park, S.H., K.M. O'Connor, and H. McKellop, *Interaction between active motion and exogenous transforming growth factor Beta during tibial fracture repair*. Journal of orthopaedic trauma, 2003. **17**(1): p. 2-10.
269. Claes, L.E., et al., *Effects of mechanical factors on the fracture healing process*. Clinical orthopaedics and related research, 1998(355 Suppl): p. S132-47.
270. Miclau, T., et al., *Effects of delayed stabilization on fracture healing*. Journal of orthopaedic research : official publication of the Orthopaedic Research Society, 2007. **25**(12): p. 1552-8.
271. Tay, B.K., et al., *Histochemical and molecular analyses of distraction osteogenesis in a mouse model*. Journal of orthopaedic research : official publication of the Orthopaedic Research Society, 1998. **16**(5): p. 636-42.
272. Hiltunen, A., E. Vuorio, and H.T. Aro, *A standardized experimental fracture in the mouse tibia*. Journal of orthopaedic research : official publication of the Orthopaedic Research Society, 1993. **11**(2): p. 305-12.
273. Hallock, G.G., M.M. Anous, and B.C. Sheridan, *The surgical anatomy of the principal nutrient vessel of the tibia*. Plastic and reconstructive surgery, 1993. **92**(1): p. 49-54.
274. Laing, P.G., *The blood supply of the femoral shaft; an anatomical study*. The Journal of bone and joint surgery. British volume, 1953. **35-B**(3): p. 462-6.
275. Chalidis, B.E., et al., *Reamed interlocking intramedullary nailing for the treatment of tibial diaphyseal fractures and aseptic nonunions. Can we expect*

- an optimum result?* Strategies in trauma and limb reconstruction, 2009. **4**(2): p. 89-94.
276. Gradl, G., *Intramedullary nailing of long bone fractures: sixty years of evolution but what the future holds?* Injury, 2014. **45 Suppl 1**: p. S1-2.
277. Lu, C., et al., *Effect of age on vascularization during fracture repair.* Journal of orthopaedic research : official publication of the Orthopaedic Research Society, 2008. **26**(10): p. 1384-9.
278. Roth, D., et al., *Plasmin modulates vascular endothelial growth factor-A-mediated angiogenesis during wound repair.* The American journal of pathology, 2006. **168**(2): p. 670-84.
279. Agarwal, S., S. Loder, and B. Levi, *Heterotopic Ossification Following Upper Extremity Injury.* Hand Clin, 2017. **33**(2): p. 363-373.
280. Morrey, B.F., L.J. Askew, and E.Y. Chao, *A biomechanical study of normal functional elbow motion.* J Bone Joint Surg Am, 1981. **63**(6): p. 872-7.
281. Evans, P.J., et al., *Prevention and treatment of elbow stiffness.* The Journal of hand surgery, 2009. **34**(4): p. 769-78.
282. Josefsson, P.O., O. Johnell, and C.F. Gentz, *Long-term sequelae of simple dislocation of the elbow.* The Journal of bone and joint surgery. American volume, 1984. **66**(6): p. 927-30.
283. Weiss, A.P. and K. Sachar, *Soft tissue contractures about the elbow.* Hand clinics, 1994. **10**(3): p. 439-51.

284. Brinsden, M.D., A.J. Carr, and J.L. Rees, *Post-traumatic flexion contractures of the elbow: Operative treatment via the limited lateral approach*. J Orthop Surg Res, 2008. **3**: p. 39.
285. Seth, M.K. and J.K. Khurana, *Bony ankylosis of the elbow after burns*. J Bone Joint Surg Br, 1985. **67**(5): p. 747-9.
286. Garland, D.E. and R.M. O'Hollaren, *Fractures and dislocations about the elbow in the head-injured adult*. Clin Orthop Relat Res, 1982(168): p. 38-41.
287. Djurickovic, S., et al., *Range of motion and complications after postburn heterotopic bone excision about the elbow*. J Trauma, 1996. **41**(5): p. 825-30.
288. Moore, E.E., et al., *Postinjury fibrinolysis shutdown: Rationale for selective tranexamic acid*. J Trauma Acute Care Surg, 2015. **78**(6 Suppl 1): p. S65-9.
289. Schochl, H., et al., *Trauma-associated hyperfibrinolysis*. Hamostaseologie, 2012. **32**(1): p. 22-7.
290. Raza, I., et al., *The incidence and magnitude of fibrinolytic activation in trauma patients*. J Thromb Haemost, 2013. **11**(2): p. 307-14.
291. Sulniute, R., et al., *Plasminogen is a critical regulator of cutaneous wound healing*. Thromb Haemost, 2016. **115**(5): p. 1001-9.
292. Mignemi, N.A., et al., *Plasmin Prevents Dystrophic Calcification After Muscle Injury*. J Bone Miner Res, 2017. **32**(2): p. 294-308.
293. Schafer, B.M., et al., *Plasminogen activation in healing human wounds*. Am J Pathol, 1994. **144**(6): p. 1269-80.

294. Mansat, P., B. Morrey, and R. Hotchkiss, *Extrinsic contracture: " the column procedure," lateral and medial capsular releases*. *The elbow and its disorders*, 2000.
295. King, G.J. and K.J. Faber, *Posttraumatic elbow stiffness*. *Orthopedic Clinics*, 2000. **31**(1): p. 129-143.
296. Gibson, B., et al., *The Consumption of Plasminogen Following Severe Burn and Its Implications in Muscle Calcification*. *The FASEB Journal*, 2017. **31**(1\_supplement): p. 390.4-390.4.
297. Amaro, E., et al., *Abstract P20: Severe Injury Leads to Plasmin Consumption Below a Critical Threshold Required to Heal Soft Tissue Injury*. *Plastic and Reconstructive Surgery – Global Open*, 2017. **5**(4S): p. 115-116.
298. Moore, S.N., et al., *Validation of a Radiography-Based Quantification Designed to Longitudinally Monitor Soft Tissue Calcification in Skeletal Muscle*. *PLoS One*, 2016. **11**(7): p. e0159624.
299. Garry, G.A., M.L. Antony, and D.J. Garry, *Cardiotoxin Induced Injury and Skeletal Muscle Regeneration*. *Methods Mol Biol*, 2016. **1460**: p. 61-71.
300. Yee, J.A., et al., *Plasminogen-dependent activation of latent transforming growth factor beta (TGF beta) by growing cultures of osteoblast-like cells*. *J Cell Physiol*, 1993. **157**(3): p. 528-34.
301. Ploplis, V.A., et al., *Effects of disruption of the plasminogen gene on thrombosis, growth, and health in mice*. *Circulation*, 1995. **92**(9): p. 2585-93.
302. Dunham, C.L., et al., *Pronation-Supination Motion Is Altered in a Rat Model of Post-Traumatic Elbow Contracture*. *J Biomech Eng*, 2017. **139**(7).

303. Dunham, C.L., et al., *Persistent motion loss after free joint mobilization in a rat model of post-traumatic elbow contracture*. J Shoulder Elbow Surg, 2017. **26**(4): p. 611-618.
304. Lake, S.P., et al., *Development and use of an animal model to study post-traumatic stiffness and contracture of the elbow*. J Orthop Res, 2016. **34**(2): p. 354-64.
305. Christensen, B. and E.S. Sørensen, *Structure, function and nutritional potential of milk osteopontin*. International Dairy Journal, 2016. **57**: p. 1-6.
306. Wada, T., et al., *Calcification of vascular smooth muscle cell cultures: inhibition by osteopontin*. Circulation Research, 1999. **84**(2): p. 166-178.
307. Zhao, Y., et al., *Characterization of dystrophic calcification induced in mice by cardiotoxin*. Calcified tissue international, 2009. **85**(3): p. 267-275.
308. Denhardt, D.T., et al., *Osteopontin as a means to cope with environmental insults: regulation of inflammation, tissue remodeling, and cell survival*. The Journal of clinical investigation, 2001. **107**(9): p. 1055-1061.
309. Jiménez-Corona, A.E., et al., *Osteopontin upregulation in atherogenesis is associated with cellular oxidative stress triggered by the activation of scavenger receptors*. Archives of medical research, 2012. **43**(2): p. 102-111.
310. Fleisch, H. and S. Bisaz, *Isolation from urine of pyrophosphate, a calcification inhibitor*. American Journal of Physiology-Legacy Content, 1962. **203**(4): p. 671-675.

311. Alfrey, A.C. and L.S. Ibels, *Role of phosphate and pyrophosphate in soft tissue calcification*, in *Homeostasis of Phosphate and Other Minerals*. 1978, Springer. p. 187-193.
312. Gabbiani, G., M. Jacqmin, and R. Richard, *Soft-tissue calcification induced by rare earth metals and its prevention by sodium pyrophosphate*. *British journal of pharmacology and chemotherapy*, 1966. **27**(1): p. 1-9.
313. Russell, R.G., *Bisphosphonates: the first 40 years*. *Bone*, 2011. **49**(1): p. 2-19.
314. Abhishek, A. and M. Doherty, *Pathophysiology of articular chondrocalcinosis--role of ANKH*. *Nat Rev Rheumatol*, 2011. **7**(2): p. 96-104.
315. Terkeltaub, R.A., *Inorganic pyrophosphate generation and disposition in pathophysiology*. *Am J Physiol Cell Physiol*, 2001. **281**(1): p. C1-C11.
316. Russell, R.G., *Excretion of Inorganic Pyrophosphate in Hypophosphatasia*. *Lancet*, 1965. **2**(7410): p. 461-4.
317. Fraser, D., *Hypophosphatasia*. *Am J Med*, 1957. **22**(5): p. 730-46.
318. Rathbun, J.C., *Hypophosphatasia; a new developmental anomaly*. *Am J Dis Child*, 1948. **75**(6): p. 822-31.
319. Dabisch-Ruthe, M., et al., *Pyrophosphates as a major inhibitor of matrix calcification in Pseudoxanthoma elasticum*. *J Dermatol Sci*, 2014. **75**(2): p. 109-20.
320. Jansen, R.S., et al., *ABCC6-mediated ATP secretion by the liver is the main source of the mineralization inhibitor inorganic pyrophosphate in the systemic circulation-brief report*. *Arterioscler Thromb Vasc Biol*, 2014. **34**(9): p. 1985-9.

321. Jansen, R.S., et al., *ABCC6 prevents ectopic mineralization seen in pseudoxanthoma elasticum by inducing cellular nucleotide release*. Proc Natl Acad Sci U S A, 2013. **110**(50): p. 20206-11.
322. Nitschke, Y., et al., *Generalized arterial calcification of infancy and pseudoxanthoma elasticum can be caused by mutations in either ENPP1 or ABCC6*. Am J Hum Genet, 2012. **90**(1): p. 25-39.
323. Nitschke, Y. and F. Rutsch, *Genetics in arterial calcification: lessons learned from rare diseases*. Trends Cardiovasc Med, 2012. **22**(6): p. 145-9.
324. Nitschke, Y. and F. Rutsch, *Generalized arterial calcification of infancy and pseudoxanthoma elasticum: two sides of the same coin*. Front Genet, 2012. **3**: p. 302.
325. Rutsch, F., et al., *Hypophosphatemia, hyperphosphaturia, and bisphosphonate treatment are associated with survival beyond infancy in generalized arterial calcification of infancy*. Circ Cardiovasc Genet, 2008. **1**(2): p. 133-40.
326. Ranganathan, K., et al., *Heterotopic Ossification: Basic-Science Principles and Clinical Correlates*. J Bone Joint Surg Am, 2015. **97**(13): p. 1101-11.
327. Nauth, A., et al., *Heterotopic ossification in orthopaedic trauma*. J Orthop Trauma, 2012. **26**(12): p. 684-8.
328. Garland, D.E., *Clinical observations on fractures and heterotopic ossification in the spinal cord and traumatic brain injured populations*. Clin Orthop Relat Res, 1988(233): p. 86-101.
329. Giannoudis, P.V., et al., *Operative treatment of displaced fractures of the acetabulum. A meta-analysis*. J Bone Joint Surg Br, 2005. **87**(1): p. 2-9.



330. Dey, D., et al., *The traumatic bone: trauma-induced heterotopic ossification*. Transl Res, 2017. **186**: p. 95-111.
331. Forsberg, J.A., et al., *Heterotopic ossification in high-energy wartime extremity injuries: prevalence and risk factors*. J Bone Joint Surg Am, 2009. **91**(5): p. 1084-91.
332. Kaplan, F.S., et al., *Classic and atypical fibrodysplasia ossificans progressiva (FOP) phenotypes are caused by mutations in the bone morphogenetic protein (BMP) type I receptor ACVRI*. Hum Mutat, 2009. **30**(3): p. 379-90.
333. Shore, E.M. and F.S. Kaplan, *Role of altered signal transduction in heterotopic ossification and fibrodysplasia ossificans progressiva*. Curr Osteoporos Rep, 2011. **9**(2): p. 83-8.
334. Moore, S.N., S.B. Tanner, and J.G. Schoenecker, *Bisphosphonates: from softening water to treating PXE*. Cell Cycle, 2015. **14**(9): p. 1354-1355.
335. Jahnen-Dechent, W., et al., *Mineral chaperones: a role for fetuin-A and osteopontin in the inhibition and regression of pathologic calcification*. J Mol Med (Berl), 2008. **86**(4): p. 379-89.
336. Brylka, L. and W. Jahnen-Dechent, *The role of fetuin-A in physiological and pathological mineralization*. Calcif Tissue Int, 2013. **93**(4): p. 355-64.
337. Cuervo, L.A., J.C. Pita, and D.S. Howell, *Ultramicroanalysis of pH, p CO<sub>2</sub> and carbonic anhydrase activity at calcifying sites in cartilage*. Calcif Tissue Res, 1971. **7**(3): p. 220-31.
338. Giachelli, C.M., *Inducers and inhibitors of biomineralization: lessons from pathological calcification*. Orthod Craniofac Res, 2005. **8**(4): p. 229-31.

339. Hendig, D., et al., *Role of serum fetuin-A, a major inhibitor of systemic calcification, in pseudoxanthoma elasticum*. Clin Chem, 2006. **52**(2): p. 227-34.
340. Hendig, D., et al., *The local calcification inhibitor matrix Gla protein in pseudoxanthoma elasticum*. Clin Biochem, 2008. **41**(6): p. 407-12.
341. Jahnen-Dechent, W., et al., *Fetuin-A regulation of calcified matrix metabolism*. Circ Res, 2011. **108**(12): p. 1494-509.
342. Jahnen-Dechent, W., et al., *Cloning and targeted deletion of the mouse fetuin gene*. J Biol Chem, 1997. **272**(50): p. 31496-503.
343. Jiang, Q., Q. Li, and J. Uitto, *Aberrant mineralization of connective tissues in a mouse model of pseudoxanthoma elasticum: systemic and local regulatory factors*. J Invest Dermatol, 2007. **127**(6): p. 1392-402.
344. Li, Q., et al., *Juxta-articular joint-capsule mineralization in CD73 deficient mice: similarities to patients with NT5E mutations*. Cell Cycle, 2014. **13**(16): p. 2609-15.
345. Li, Q. and J. Uitto, *Mineralization/anti-mineralization networks in the skin and vascular connective tissues*. Am J Pathol, 2013. **183**(1): p. 10-8.
346. Schafer, C., et al., *The serum protein alpha 2-Heremans-Schmid glycoprotein/fetuin-A is a systemically acting inhibitor of ectopic calcification*. J Clin Invest, 2003. **112**(3): p. 357-66.
347. Sly, W.S., et al., *Carbonic anhydrase II deficiency in 12 families with the autosomal recessive syndrome of osteopetrosis with renal tubular acidosis and cerebral calcification*. N Engl J Med, 1985. **313**(3): p. 139-45.

348. Westenfeld, R., et al., *Fetuin-A (AHSG) prevents extraosseous calcification induced by uraemia and phosphate challenge in mice*. *Nephrol Dial Transplant*, 2007. **22**(6): p. 1537-46.
349. Yuan, Q., et al., *Increased osteopontin contributes to inhibition of bone mineralization in FGF23-deficient mice*. *J Bone Miner Res*, 2014. **29**(3): p. 693-704.
350. Dabisch-Ruthe, M., et al., *Variants in genes encoding pyrophosphate metabolizing enzymes are associated with Pseudoxanthoma elasticum*. *Clinical Biochemistry*, 2014. **47**(15): p. 60-67.
351. Li, Q., et al., *A novel animal model for pseudoxanthoma elasticum: the KK/HlJ mouse*. *Am J Pathol*, 2012. **181**(4): p. 1190-6.
352. Jiang, Q., et al., *Parabiotic heterogenetic pairing of Abcc6<sup>-/-</sup>/Rag1<sup>-/-</sup> mice and their wild-type counterparts halts ectopic mineralization in a murine model of pseudoxanthoma elasticum*. *Am J Pathol*, 2010. **176**(4): p. 1855-62.
353. Li, Q., et al., *Abcc6 Knockout Rat Model Highlights the Role of Liver in PPI Homeostasis in Pseudoxanthoma Elasticum*. *J Invest Dermatol*, 2017. **137**(5): p. 1025-1032.
354. Ziegler, S.G., et al., *Ectopic calcification in pseudoxanthoma elasticum responds to inhibition of tissue-nonspecific alkaline phosphatase*. *Sci Transl Med*, 2017. **9**(393).
355. van Rooijen, N., *Liposomes for targeting of antigens and drugs: immunoadjuvant activity and liposome-mediated depletion of macrophages*. *J Drug Target*, 2008. **16**(7): p. 529-34.

356. van Rooijen, N., J. Bakker, and A. Sanders, *Transient suppression of macrophage functions by liposome-encapsulated drugs*. Trends Biotechnol, 1997. **15**(5): p. 178-85.
357. Fleisch, H. and S. Bisaz, *Isolation from urine of pyrophosphate, a calcification inhibitor*. Am J Physiol, 1962. **203**: p. 671-5.
358. Russell, R.G. and A. Hodgkinson, *The urinary excretion of inorganic pyrophosphate by normal subjects and patients with renal calculus*. Clin Sci, 1966. **31**(1): p. 51-62.
359. Barker, L.M., et al., *Studies on mechanisms of calcification. I. Properties of urinary derivatives which inhibit cartilage calcification. II. Electron microscopic observations of the effect of inhibitors in crystal formation*. Johns Hopkins Med J, 1970. **127**(1): p. 2-22.
360. Uitto, J., et al., *Pseudoxanthoma elasticum: progress in diagnostics and research towards treatment : Summary of the 2010 PXE International Research Meeting*. Am J Med Genet A, 2011. **155A**(7): p. 1517-26.
361. Hiemstra, P.S., *Altered macrophage function in chronic obstructive pulmonary disease*. Ann Am Thorac Soc, 2013. **10 Suppl**: p. S180-5.
362. Bories, G., et al., *Impaired alternative macrophage differentiation of peripheral blood mononuclear cells from obese subjects*. Diab Vasc Dis Res, 2012. **9**(3): p. 189-95.
363. Liang, Z., et al., *Impaired macrophage phagocytosis of bacteria in severe asthma*. Respir Res, 2014. **15**: p. 72.

364. Fernandez-Boyanapalli, R., et al., *Impaired phagocytosis of apoptotic cells by macrophages in chronic granulomatous disease is reversed by IFN-gamma in a nitric oxide-dependent manner*. J Immunol, 2010. **185**(7): p. 4030-41.
365. Schrijvers, D.M., et al., *Phagocytosis of apoptotic cells by macrophages is impaired in atherosclerosis*. Arterioscler Thromb Vasc Biol, 2005. **25**(6): p. 1256-61.
366. Kobayashi, M., et al., *An Increase in the Susceptibility of Burned Patients to Infectious Complications Due to Impaired Production of Macrophage Inflammatory Protein 1 $\alpha$* . The Journal of Immunology, 2002. **169**(8): p. 4460-4466.
367. Herlihy, J.P., et al., *Impaired alveolar macrophage function in smoke inhalation injury*. J Cell Physiol, 1995. **163**(1): p. 1-8.
368. Markello, T.C., et al., *Vascular pathology of medial arterial calcifications in NT5E deficiency: implications for the role of adenosine in pseudoxanthoma elasticum*. Mol Genet Metab, 2011. **103**(1): p. 44-50.
369. Szabó, Z., et al., *ABCC6 does not transport adenosine &#x2014; Relevance to pathomechanism of pseudoxanthoma elasticum*. Molecular Genetics and Metabolism, 2011. **104**(3): p. 421.
370. Leftheriotis, G., et al., *Reply to the article of C. Markello et al. entitled "Vascular pathology of medial arterial calcifications in NT5E deficiency: Implications for the role of adenosine in pseudoxanthoma elasticum"*. Mol Genet Metab, 2011. **103**(2): p. 199-200.

371. Markello, T.C., et al., *Reply to Professor Leftheriotis et al.* Mol Genet Metab, 2011. **103**(3): p. 305.
372. Zhao, J., et al., *Plasma PPI Deficiency Is the Major, but Not the Exclusive, Cause of Ectopic Mineralization in an Abcc6(-/-) Mouse Model of PXE.* J Invest Dermatol, 2017. **137**(11): p. 2336-2343.
373. Yegutkin, G.G., et al., *Altered purinergic signaling in CD73-deficient mice inhibits tumor progression.* Eur J Immunol, 2011. **41**(5): p. 1231-41.
374. Dedinszki, D., et al., *Oral administration of pyrophosphate inhibits connective tissue calcification.* EMBO Mol Med, 2017. **9**(11): p. 1463-1470.
375. Convente, M.R., et al., *Depletion of Mast Cells and Macrophages Impairs Heterotopic Ossification in an Acvr1(R206H) Mouse Model of Fibrodysplasia Ossificans Progressiva.* J Bone Miner Res, 2018. **33**(2): p. 269-282.
376. Genet, F., et al., *Neurological heterotopic ossification following spinal cord injury is triggered by macrophage-mediated inflammation in muscle.* J Pathol, 2015. **236**(2): p. 229-40.
377. Milde, R., et al., *Multinucleated Giant Cells Are Specialized for Complement-Mediated Phagocytosis and Large Target Destruction.* Cell Rep, 2015. **13**(9): p. 1937-48.
378. Chambers, T.J., *Phagocytic recognition of bone by macrophages.* J Pathol, 1981. **135**(1): p. 1-7.
379. Villa-Bellosta, R., M.R. Hamczyk, and V. Andres, *Alternatively activated macrophages exhibit an anticalcifying activity dependent on extracellular*

- ATP/pyrophosphate metabolism*. Am J Physiol Cell Physiol, 2016. **310**(10): p. C788-99.
380. Villa-Bellosta, R., M.R. Hamczyk, and V. Andres, *Novel phosphate-activated macrophages prevent ectopic calcification by increasing extracellular ATP and pyrophosphate*. PLoS One, 2017. **12**(3): p. e0174998.
381. Forsberg, J.A., et al., *Burned to the bone*. Sci Transl Med, 2014. **6**(255): p. 255fs37.
382. Forsberg, J.A. and B.K. Potter, *Heterotopic ossification in wartime wounds*. J Surg Orthop Adv, 2010. **19**(1): p. 54-61.
383. Russell, R.G.G., *Bisphosphonates: the first 40 years*. Bone, 2011. **49**: p. 2-19.
384. Fleisch, H., *Bisphosphonates: a new class of drugs in diseases of bone and calcium metabolism*, in *Bisphosphonates and tumor osteolysis*. 1989, Springer. p. 1-28.
385. Mavrogenis, A.F., P.N. Soucacos, and P.J. Papagelopoulos, *Heterotopic ossification revisited*. Orthopedics, 2011. **34**(3): p. 177-177.
386. Schuetz, P., et al., *Amino-bisphosphonates in heterotopic ossification: first experience in five consecutive cases*. Spinal Cord, 2005. **43**(10): p. 604.
387. Shafer, D.M., et al., *The use of eidronate disodium in the prevention of heterotopic ossification in burn patients*. Burns, 2008. **34**(3): p. 355-360.
388. Sullivan, M., et al., *Heterotopic ossification after central nervous system trauma: a current review*. Bone & joint research, 2013. **2**(3): p. 51-57.

389. Aubut, J.-A.L., et al., *A Comparison of Heterotopic Ossification Treatment within the Traumatic Brain and Spinal Cord Injured Population: An Evidence Based Systematic Review*. NeuroRehabilitation, 2011. **28**(2): p. 151-160.
390. Banovac, K., *The effect of etidronate on late development of heterotopic ossification after spinal cord injury*. The journal of spinal cord medicine, 2000. **23**(1): p. 40-44.
391. Banovac, K. and F. Gonzalez, *Evaluation and management of heterotopic ossification in patients with spinal cord injury*. Spinal Cord, 1997. **35**(3): p. 158.
392. Biering-Sørensen, F. and E. Tøndevold, *Indomethacin and disodium etidronate for the prevention of recurrence of heterotopic ossification after surgical resection. Two case reports*. Spinal Cord, 1993. **31**(8): p. 513.
393. Bijvoet, O., et al., *Effect of a diphosphonate on para-articular ossification after total hip replacement*. Acta Orthopaedica Scandinavica, 1974. **45**(6): p. 926-934.
394. Finerman, G. *ROLE OF DIPHOSPHONATE ON HETEROTOPIC OSSIFICATION AFTER TOTAL HIP ARTHROPLASTY*. in *JOURNAL OF BONE AND JOINT SURGERY-BRITISH VOLUME*. 1977. BRITISH EDITORIAL SOC BONE JOINT SURGERY 22 BUCKINGHAM STREET, LONDON, ENGLAND WC2N 6ET.
395. Finerman, G.A., et al. *Role of diphosphonate (EHDP) in the prevention of heterotopic ossification after total hip arthroplasty: a preliminary report*. in



*The hip: proceedings of the fifth open scientific meeting of The Hip Society.*

1977. CV Mosby, St. Louis.

396. Fitzsimmons, A.S., et al., *Radial nerve injury associated with traumatic myositis ossificans in a brain injured patient.* Archives of physical medicine and rehabilitation, 1993. **74**(7): p. 770-773.
397. Fuller, D.A., A. Mark, and M.A.E. Keenan, *Excision of heterotopic ossification from the knee: a functional outcome study.* Clinical orthopaedics and related research, 2005. **438**: p. 197-203.
398. Garland, D.E., et al., *Diphosphonate treatment for heterotopic ossification in spinal cord injury patients.* Clinical orthopaedics and related research, 1983(176): p. 197-200.
399. Kolessar, D.J., S.D. Katz, and M.A. Keenan, *Functional outcome following surgical resection of heterotopic ossification in patients with brain injury.* The Journal of Head Trauma Rehabilitation, 1996. **11**(4): p. 78-87.
400. Lippin, Y., et al., *Vocal cords dysfunction resulting from heterotopic ossification in a patient with burns.* The Journal of burn care & rehabilitation, 1994. **15**(2): p. 169-173.
401. Ono, K., et al., *A double-blind study of EHDP on heterotopic ossification after spinal cord injury using placebo.* Rinsho Hyoka, 1988. **16**: p. 581-615.16581.
402. Peters, W., *Heterotopic ossification: can early surgery be performed, with a positive bone scan?* The Journal of burn care & rehabilitation, 1990. **11**(4): p. 318-321.

403. Spielman, G., T. Gennarelli, and C. Rogers, *Disodium etidronate: its role in preventing heterotopic ossification in severe head injury*. Archives of physical medicine and rehabilitation, 1983. **64**(11): p. 539-542.
404. Stover, S.L., H.R. Hahn, and J.M. Miller, *Disodium etidronate in the prevention of heterotopic ossification following spinal cord injury (preliminary report)*. Spinal Cord, 1976. **14**(2): p. 146.
405. Stover, S.L. and K. Niemann, *Disodium etidronate in the prevention of postoperative recurrence of heterotopic ossification in spinal-cord injury patients*. The Journal of bone and joint surgery. American volume, 1976. **58**(5): p. 683-688.
406. Subbarao, J.V., B. Nemchausky, and M. Gratzner, *Resection of heterotopic ossification and Didronel therapy—regaining wheelchair independence in the spinal cord injured patient*. The Journal of The American Paraplegia Society, 1987. **10**(1): p. 3-7.
407. Tepperman, P.S., et al., *Heterotopic ossification in burns*. The Journal of Burn Care & Rehabilitation, 1984. **5**(4): p. 283-287.
408. Thomas, B. and H. Amstutz, *Results of the administration of diphosphonate for the prevention of heterotopic ossification after total hip arthroplasty*. The Journal of bone and joint surgery. American volume, 1985. **67**(3): p. 400-403.
409. Yutani, Y., et al., *Clinical effect of etidronate disodium (EHDP) on heterotopic ossification following total hip arthroplasty*. Osaka city medical journal, 1995. **41**(2): p. 63-73.

410. Kates, S.L. and C.L. Ackert-Bicknell, *How do bisphosphonates affect fracture healing?* Injury, 2016. **47 Suppl 1**: p. S65-8.
411. Muschitz, G.K., et al., *Long-Term Effects of Severe Burn Injury on Bone Turnover and Microarchitecture.* Journal of Bone and Mineral Research, 2017. **32**(12): p. 2381-2393.
412. Rinkinen, J., et al., *The systemic effect of burn injury and trauma on muscle and bone mass and Composition.* Plastic and reconstructive surgery, 2015. **136**(5): p. 612e.
413. Russell, R.G. and H. Fleisch, *Pyrophosphate, phosphonates and pyrophosphatases in the regulation of calcification and calcium homeostasis.* Proc R Soc Med, 1970. **63**(9): p. 876.
414. Bukata, S.V., *Systemic administration of pharmacological agents and bone repair: what can we expect.* Injury, 2011. **42**(6): p. 605-608.
415. Lyles, K.W., et al., *Zoledronic acid and clinical fractures and mortality after hip fracture.* New England Journal of Medicine, 2007. **357**(18): p. 1799-1809.
416. Schilcher, J., K. Michaëlsson, and P. Aspenberg, *Bisphosphonate use and atypical fractures of the femoral shaft.* New England Journal of Medicine, 2011. **364**(18): p. 1728-1737.
417. Romero, C.D., et al., *The Toll-like receptor 4 agonist monophosphoryl lipid a augments innate host resistance to systemic bacterial infection.* Infect Immun, 2011. **79**(9): p. 3576-87.

418. Fensterheim, B.A., et al., *The TLR4 Agonist Monophosphoryl Lipid A Drives Broad Resistance to Infection via Dynamic Reprogramming of Macrophage Metabolism*. *J Immunol*, 2018. **200**(11): p. 3777-3789.
419. Deyo, R.A., A. Nachemson, and S.K. Mirza, *Spinal-fusion surgery - the case for restraint*, in *N Engl J Med*. 2004: United States. p. 722-6.
420. Kornblum, M.B., et al., *Degenerative lumbar spondylolisthesis with spinal stenosis: a prospective long-term study comparing fusion and pseudarthrosis*, in *Spine (Phila Pa 1976)*. 2004: United States. p. 726-33; discussion 733-4.
421. Schofferman, J., et al., *Failed back surgery: etiology and diagnostic evaluation*, in *Spine J*. 2003: United States. p. 400-3.
422. Dimar, J.R., 2nd, et al., *Two-year fusion and clinical outcomes in 224 patients treated with a single-level instrumented posterolateral fusion with iliac crest bone graft*, in *Spine J*. 2009: United States. p. 880-5.
423. Martin, B.I., et al., *Reoperation rates following lumbar spine surgery and the influence of spinal fusion procedures*, in *Spine (Phila Pa 1976)*. 2007: United States. p. 382-7.
424. Kang, J., et al., *Grafton and local bone have comparable outcomes to iliac crest bone in instrumented single-level lumbar fusions*. *Spine (Phila Pa 1976)*, 2012. **37**(12): p. 1083-91.
425. Stevens, D.L. and A.E. Bryant, *Necrotizing Soft-Tissue Infections*. *N Engl J Med*, 2017. **377**(23): p. 2253-2265.

426. Reglinski, M. and S. Sriskandan, *The contribution of group A streptococcal virulence determinants to the pathogenesis of sepsis*. *Virulence*, 2014. **5**(1): p. 127-136.
427. An, T.J., et al., *Pediatric Musculoskeletal Infection: Hijacking the Acute-Phase Response*. *JBJS Rev*, 2016. **4**(9).
428. Hippocrates, *De Morbis Popularibus, EPIDEMICS III*. 1868: Harvard University Press.
429. Jones, J., *Investigations upin the nature, causes, and treatments of hospital gangrene, as it prevailed in the Confederate armies, 1861-1865*. 1871, New York: Surg Mem War Rebellion.
430. Copley, L.A., et al., *A proposed scoring system for assessment of severity of illness in pediatric acute hematogenous osteomyelitis using objective clinical and laboratory findings*. *Pediatr Infect Dis J*, 2014. **33**(1): p. 35-41.
431. Esmon, C.T., J. Xu, and F. Lupu, *Innate immunity and coagulation*. *Journal of Thrombosis and Haemostasis*, 2011. **9**: p. 182-188.
432. Loof, T.G., C. Deicke, and E. Medina, *The role of coagulation/fibrinolysis during Streptococcus pyogenes infection*. *Frontiers in cellular and infection microbiology*, 2014. **4**: p. 128.
433. Brinkmann, V., et al., *Neutrophil extracellular traps kill bacteria*. *science*, 2004. **303**(5663): p. 1532-1535.
434. Fuchs, T.A., et al., *Novel cell death program leads to neutrophil extracellular traps*. *The Journal of cell biology*, 2007. **176**(2): p. 231-241.

435. Khamnuan, P., et al., *Necrotizing fasciitis: epidemiology and clinical predictors for amputation*. International journal of general medicine, 2015. **8**: p. 195.
436. Verhamme, I., P. Panizzi, and P. Bock, *Pathogen activators of plasminogen*. Journal of Thrombosis and Haemostasis, 2015. **13**: p. S106-S114.
437. Aisina, R., et al., *Streptokinase and staphylokinase: differences in the kinetics and mechanism of their interaction with plasminogen, inhibitors, and fibrin*. Russian Journal of Bioorganic Chemistry, 2015. **41**(5): p. 506-517.
438. Huish, S., C. Thelwell, and C. Longstaff, *Activity regulation by fibrinogen and fibrin of streptokinase from streptococcus pyogenes*. PloS one, 2017. **12**(1): p. e0170936.
439. Buchanan, J.T., et al., *DNase expression allows the pathogen group A Streptococcus to escape killing in neutrophil extracellular traps*. Current Biology, 2006. **16**(4): p. 396-400.
440. Crosby, H.A., J. Kwiecinski, and A.R. Horswill, *Staphylococcus aureus Aggregation and Coagulation Mechanisms, and Their Function in Host-Pathogen Interactions*, in *Advances in applied microbiology*. 2016, Elsevier. p. 1-41.
441. Friedrich, R., et al., *Staphylocoagulase is a prototype for the mechanism of cofactor-induced zymogen activation*. Nature, 2003. **425**(6957): p. 535.
442. Kroh, H.K., P. Panizzi, and P.E. Bock, *Von Willebrand factor-binding protein is a hysteretic conformational activator of prothrombin*. Proceedings of the National Academy of Sciences, 2009. **106**(19): p. 7786-7791.

443. Panizzi, P., et al., *The staphylocoagulase family of zymogen activator and adhesion proteins*. Cellular and Molecular Life Sciences CMLS, 2004. **61**(22): p. 2793-2798.
444. Peetermans, M., et al., *Plasminogen activation by staphylokinase enhances local spreading of S. aureus in skin infections*. BMC microbiology, 2014. **14**(1): p. 310.
445. Gafter-Gvili, A., et al. *Thrombocytopenia in Staphylococcus aureus bacteremia: risk factors and prognostic importance*. in *Mayo Clinic Proceedings*. 2011. Elsevier.
446. Llewelyn, M. and J. Cohen, *Superantigens: microbial agents that corrupt immunity*. The Lancet infectious diseases, 2002. **2**(3): p. 156-162.
447. da Silva, C.I.M.F., et al., *Binding of plasminogen to Pseudomonas aeruginosa results in formation of surface-associated plasmin and enhanced bacterial invasiveness*. Microbial pathogenesis, 2004. **36**(2): p. 59-66.
448. Lahteenmaki, K., et al., *Immobilization of plasminogen on Escherichia coli flagella*. FEMS Microbiology Letters, 1993. **106**(3): p. 309-314.
449. Jabbour, G., et al., *Pattern and predictors of mortality in necrotizing fasciitis patients in a single tertiary hospital*. World Journal of Emergency Surgery, 2016. **11**(1): p. 40.
450. Fourrier, F., et al., *Septic shock, multiple organ failure, and disseminated intravascular coagulation: compared patterns of antithrombin III, protein C, and protein S deficiencies*. Chest, 1992. **101**(3): p. 816-823.

451. Hollander, J.E., *Drotrecogin alfa (activated) in septic shock*. The New England journal of medicine, 2012. **367**(10): p. 968; author reply 969.
452. Sharma, A.K., M. Sharma, and M.A. Refaai, *Looking Beyond INR of 1.5 and Fresh Frozen Plasma in Liver Disease*. Cardiovascular and interventional radiology, 2016. **39**(12): p. 1795.
453. Levi, M., E. de Jonge, and T. van der Poll, *Plasma and plasma components in the management of disseminated intravascular coagulation*. Best practice & research Clinical haematology, 2006. **19**(1): p. 127-142.
454. Mignemi, M.E., N.W. Langdon, and J.G. Schoenecker, *Vitamin K-Dependent Coagulopathy in Pediatric Osteomyelitis: A Case Report*. JBJS Case Connect, 2013. **3**(1): p. e21.
455. Lin, J.-J., et al., *Bullous impetigo: a rare presentation in fulminant streptococcal toxic shock syndrome*. Pediatric emergency care, 2007. **23**(5): p. 318-320.
456. Warner, P., et al., *Thrombocytopenia in the pediatric burn patient*. Journal of Burn Care & Research, 2011. **32**(3): p. 410-414.
457. Chrousos, G.P., *The hypothalamic–pituitary–adrenal axis and immune-mediated inflammation*. New England Journal of Medicine, 1995. **332**(20): p. 1351-1363.
458. Schroeder, S., et al., *The hypothalamic-pituitary-adrenal axis of patients with severe sepsis: altered response to corticotropin-releasing hormone*. Critical care medicine, 2001. **29**(2): p. 310-316.



459. Annane, D., *The role of ACTH and corticosteroids for sepsis and septic shock: an update*. *Frontiers in endocrinology*, 2016. **7**: p. 70.
460. Sprung, C.L., et al., *Hydrocortisone therapy for patients with septic shock*. *New England Journal of Medicine*, 2008. **358**(2): p. 111.
461. Annane, D., et al., *Hydrocortisone plus fludrocortisone for adults with septic shock*. *New England Journal of Medicine*, 2018. **378**(9): p. 809-818.
462. Marik, P.E., et al., *Recommendations for the diagnosis and management of corticosteroid insufficiency in critically ill adult patients: consensus statements from an international task force by the American College of Critical Care Medicine*. *Critical care medicine*, 2008. **36**(6): p. 1937-1949.
463. Annane, D., et al., *Critical illness-related corticosteroid insufficiency (CIRCI): a narrative review from a Multispecialty Task Force of the Society of Critical Care Medicine (SCCM) and the European Society of Intensive Care Medicine (ESICM)*. *Intensive care medicine*, 2017: p. 1-12.
464. Annane, D., et al., *Guidelines for the diagnosis and management of critical illness-related corticosteroid insufficiency (CIRCI) in critically ill patients (Part I): Society of Critical Care Medicine (SCCM) and European Society of Intensive Care Medicine (ESICM) 2017*. *Intensive care medicine*, 2017. **43**(12): p. 1751-1763.
465. Dellinger, R.P., et al., *Surviving Sepsis Campaign: international guidelines for management of severe sepsis and septic shock, 2012*. *Intensive care medicine*, 2013. **39**(2): p. 165-228.

466. Brouwer, S., et al., *Streptococcus pyogenes* adhesion and colonization. FEBS letters, 2016. **590**(21): p. 3739-3757.
467. Lacy, M.D. and K. Horn, *Nosocomial transmission of invasive group a streptococcus from patient to health care worker*. Clinical infectious diseases, 2009. **49**(3): p. 354-357.
468. Chandler, R.E., et al., *Transmission of group A Streptococcus limited to healthcare workers with exposure in the operating room*. Infection Control & Hospital Epidemiology, 2006. **27**(11): p. 1159-1163.